

Modeling and
Energy Consumption
with
Parallel and Series
VAV Terminal Units
with ECM and PSC Motors

Fourth Edition

An ASHRAE Topical Compilation

Expanded to Include New Research



ISBN 978-1-939200-51-8

© 2014, 2015, 2016 ASHRAE
1791 Tullie Circle, NE
Atlanta, GA 30329
www.ashrae.org

All rights reserved.

**This collection of papers reflects ASHRAE Research co-sponsored by
ASHRAE Technical Committee 5.3, Room Air Distribution,
and ASHRAE Technical Committee 7.7, Testing and Balancing.**

The collection was compiled by Eugene W. (Gus) Faris.

Project Monitoring Committee Members

The following members of the Project Monitoring Committees are gratefully acknowledged.

Floyd Blackwell

Dan Int-Hout

Jerry Sipes

Douglas Fetters

David John

Jack Stegall

Gaylon Richardson

Investigators

John Bryant

Michael A. Davis

Dennis O'Neal

ASHRAE is a registered trademark in the U.S. Patent and Trademark Office, owned by the American Society of Heating, Refrigerating and Air-Conditioning Engineers, Inc.

ASHRAE has compiled this publication with care, but ASHRAE has not investigated, and ASHRAE expressly disclaims any duty to investigate, any product, service, process, procedure, design, or the like that may be described herein. The appearance of any technical data or editorial material in this publication does not constitute endorsement, warranty, or guaranty by ASHRAE of any product, service, process, procedure, design, or the like. ASHRAE does not warrant that the information in the publication is free of errors, and ASHRAE does not necessarily agree with any statement or opinion in this publication. The entire risk of the use of any information in this publication is assumed by the user.

No part of this publication may be reproduced without permission in writing from ASHRAE, except by a reviewer who may quote brief passages or reproduce illustrations in a review with appropriate credit, nor may any part of this publication be reproduced, stored in a retrieval system, or transmitted in any way or by any means—electronic, photocopying, recording, or other—without permission in writing from ASHRAE. Requests for permission should be submitted at www.ashrae.org/permissions.

ASHRAE STAFF SPECIAL PUBLICATIONS

Mark S. Owen, *Editor/Group Manager of Handbook and Special Publications*
Cindy Sheffield Michaels, *Managing Editor*
James Madison Walker, *Managing Editor of Standards*
Sarah Boyle, *Assistant Editor*
Lauren Ramsdell, *Assistant Editor*
Michshell Phillips, *Editorial Coordinator*

PUBLISHER

W. Stephen Comstock

Introduction

Since fan-powered variable-air-volume (VAV) terminal units were introduced to the marketplace, proponents of both parallel and series types have argued about which provides a system with the highest energy efficiency.* ASHRAE/AHRI research was undertaken to define the operation of each type and investigate the issue. Descriptions of the findings are described in the first six papers included in this collection. Additional research was undertaken by a consortium of terminal unit manufacturers, motor manufacturers, and Texas A&M University to evaluate motor types (electrically commutated motors vs. permanent split capacitor motors) and their associated effects in both terminal unit designs. All of this second research was donated to AHRI and ASHRAE to get the information into the public domain. Since the original research was completed, 13 papers have been written describing the processes and the results. Two of them—“Performance of Series Fan-Powered Terminal Units with Electronically Commutated Motors” and “Modeling the Performance of ECM and SCR Parallel Fan-Powered Terminal Units in Single-Duct VAV Systems”—won the Crosby Field Award for the highest-rated paper presented at a Technical Session, Symposium, or Poster Session for an ASHRAE Society year.

At this point, AHRI has begun modeling research and the papers are focusing on energy modeling and how to get the research data into a format that programs such as the U.S. Department of Energy’s *EnergyPlus* and other proprietary models can use. Getting the research into the hands of those who can use it to better design occupied spaces and those modelers who can accurately predict energy usage has been difficult. Many different models are in use today, and none of them accurately use all the variables that were evaluated and found to be significant in the research.

This collection contains the published papers that describe the processes, the tests, and the outcomes and gives the reader insight into the research and the results. It also introduces the problems of getting research into current energy models and the current solution to those problems. There are plans for many additional papers as we continue to model the different types of terminal units, comparing energy consumption between them. Hopefully, this collection will continue to grow as the research continues.

* *ASHRAE Handbook—HVAC Systems and Equipment* provides detailed descriptions of parallel and series units and *ASHRAE Handbook—HVAC Applications* provides descriptions of the different characteristics of the units.

Contents

Performance of VAV Fan-Powered Terminal Units: Experimental Setup and Methodology

James C. Furr, Dennis L. O’Neal, Michael A. Davis, John A. Bryant, Andrew Cramlet

Performance of VAV Parallel Fan-Powered Terminal Units: Experimental Results and Models

James C. Furr, Dennis L. O’Neal, Michael A. Davis, John A. Bryant, Andrew Cramlet

Performance of VAV Series Fan-Powered Terminal Units: Experimental Results and Models

James C. Furr, Dennis L. O’Neal, Michael A. Davis, John A. Bryant, Andrew Cramlet

Experimental Verification of a Three Zone VAV System Model Operating with Fan Powered Terminal Units

John A. Bryant, Michael A. Davis, Dennis L. O’Neal, Andrew Cramlet

Modeling the Performance of Single-Duct VAV Systems that use Fan Powered Terminal Units

Michael A. Davis, John A. Bryant, Dennis L. O’Neal, Andrew Cramlet

***Reflections on ARI/ASHRAE Research Project RP-1292,
Comparison of the Total Energy Consumption of Series versus Parallel Fan Powered VAV Terminal Units***

Eugene W. (Gus) Faris

Excerpt: Spreadsheet Tutorial from ASHRAE RP-1292

Michael Davis, John A. Bryant, Dennis L. O’Neal, Aaron Hervey, Andrew Cramlet

***Energy Use Comparison for Series vs. Parallel Fan Powered Terminal Units
in a Single Duct Variable Air Volume System***

John Bryant, Michael Davis, Dennis O’Neal

***Performance of VAV Fan Powered Terminal Units:
An Evaluation of Operational Control Strategies for Series vs. Parallel Units***

John Bryant, PhD, PE Dennis O’Neal, PhD, PE Michael Davis

Performance of Series Fan-Powered Terminal Units with Electronically Commutated Motors

Jacob L. Edmondson, Dennis L. O’Neal, John A. Bryant, Michael A. Davis

Performance of Parallel Fan-Powered Terminal Units with Electronically Commutated Motors

Jacob L. Edmondson, Dennis L. O’Neal, John A. Bryant, Michael A. Davis

***Modeling the Performance of ECM and SCR Series Fan-Powered Terminal Units
in Single-Duct VAV Systems***

Michael A. Davis, John A. Bryant, Dennis L. O’Neal

***Modeling the Performance of ECM and SCR Parallel Fan-Powered Terminal Units
in Single-Duct VAV Systems***

Michael A. Davis, John A. Bryant, Dennis L. O’Neal

Comparison of Performance Characteristics of SCR and ECM Controlled Series Fan Powered Terminal Units

Dennis L. O'Neal, Jacob L. Edmondson, Peng "Solomon" Yin

Characterizing Airflow and Power of VAV Series Fan-Powered Terminal Units from Component Data—Part I

Peng Yin, Dennis L. O'Neal

Characterizing Airflow and Power of VAV Series Fan-Powered Terminal Units from Component Data—Part II

Peng Yin, Dennis L. O'Neal

Modeling Fan-Powered Terminal Unit Fan/Motor Combinations Controlled by Silicon Controlled Rectifiers

Dennis L. O'Neal, Douglas D. Ingram, Carl L. Reid

A Simplified Model of the Fan/Motor Performance of Fan-Powered Terminal Units that Use Electronically Commutated Motors

Dennis L. O'Neal, Carl L. Reid, Douglas D. Ingram

Development of Models to Simulate the Part-Load Performance of Oversized ECM Fan-Powered Terminal Units

Dennis L. O'Neal

In-Situ Fan Differential Pressure Rise for a Series VAV-Fan-Powered Terminal Unit with SCR Control

John A. Bryant, Stephen J. Bryant

Characterizing the Performance of Fixed-Airflow Series Fan-Powered Terminal Units Using a Mass and Energy Balance Approach

Carl L. Reid, Dennis L. O'Neal, Peng Yin

Using a Mass and Energy Balance Approach to Model the Performance of Parallel Fan-Powered Terminal Units with Fixed-Airflow Fans

Peng Yin, Carl L. Reid, Dennis L. O'Neal

Performance of VAV Fan-Powered Terminal Units: Experimental Setup and Methodology

James C. Furr

Dennis L. O'Neal, PhD, PE

Michael A. Davis

Fellow ASHRAE

John A. Bryant, PhD, PE

Andrew Cramlet

Member ASHRAE

Student Member ASHRAE

ABSTRACT

This paper is the first of three papers on the development of experimental performance models of variable air volume fan powered terminal units. Tests were conducted on both parallel and series fan powered terminal units. Data from these tests were used to develop empirical models of airflow, power, and leakage of both parallel and series fan power terminal units. These models are suitable for use in annual energy use models of variable air volume systems in commercial buildings. This paper provides a description of the experimental apparatus, the terminal units, and measurements for airflow and power. Both 8 in. (203 mm) and 12 in. (304 mm) primary air inlet terminal units from three manufacturers were evaluated.

INTRODUCTION

Variable Air Volume (VAV) systems maintain comfort conditions by varying the volume of primary air delivered to a space. A VAV system (Figure 1) often consists of a central air handling unit (AHU), where air is cooled by cooling coils (Wendes 1994). This air, referred to as primary air, is sent through a single-duct supply system to VAV terminal units by the supply fan. Each terminal unit is ducted to air outlets, usually serving two or more offices or an open area. VAV terminal units that include a fan to improve circulation within a zone are called fan powered terminal units. These terminal units can draw in air from the plenum area and mix it with primary air from the central Air Handling Unit (AHU) to maintain comfort conditions in the occupied space.

There are two configurations for fan powered terminal units: series and parallel. The fan can be in the path of the primary airflow (Figure 2). This configuration is called a fan

powered series terminal unit. The controller will modulate the terminal unit damper in response to the control signals from the thermostat and air velocity sensor. The fans on these terminal units output a constant amount of air that does not vary with load because the downstream pressure is constant (Alexander and Int-Hout 1998). As a result, when the primary air damper closes, more plenum air is induced and recirculated into the space. When the signal from the inlet air velocity sensor indicates that the primary airflow has reached a predetermined minimum (because of ventilation requirements), the damper will not close any more. If the space is still too cold, electric or hot water supplemental heat can be used to meet the thermostat setpoint.

When the fan is outside the primary airflow, the configuration is called a fan powered parallel terminal unit (Figure 3). During operation, the fan for a parallel terminal unit cycles on and off. During periods of maximum cooling, the fan is off. A backdraft damper prevents cold air from blowing backwards through the fan. The terminal unit primary air damper modulates the airflow to maintain the space temperature setpoint. An inlet air velocity sensor within the primary air stream allows the unit controller to maintain a consistent volume of airflow to the zone depending on the temperature setpoint. When the primary airflow drops below a specified amount, the controller activates the fan. At this point, the terminal unit mixes primary air with air being drawn in from the plenum. Electric or hot water supplementary heat can be used for additional heating. Depending on the control scheme, the controller can continue to reduce primary air to the conditioned space by adjusting the damper.

In the field, the fan on a VAV terminal unit often must be fine tuned (test and balancing) to provide the airflow output for

James C. Furr is a Thermal Management Engineer at Lockheed Martin, Fort Worth, TX. Dennis L. O'Neal is Holdredge/Paul Professor and Head and Andrew Cramlet is a student at the Department of Mechanical Engineering, Texas A&M University, College Station, TX. Michael A. Davis is a Research Engineer and John A. Bryant is a Visiting Associate Professor, Department of Mechanical Engineering, Texas A&M University Qatar, Doha, Qatar.

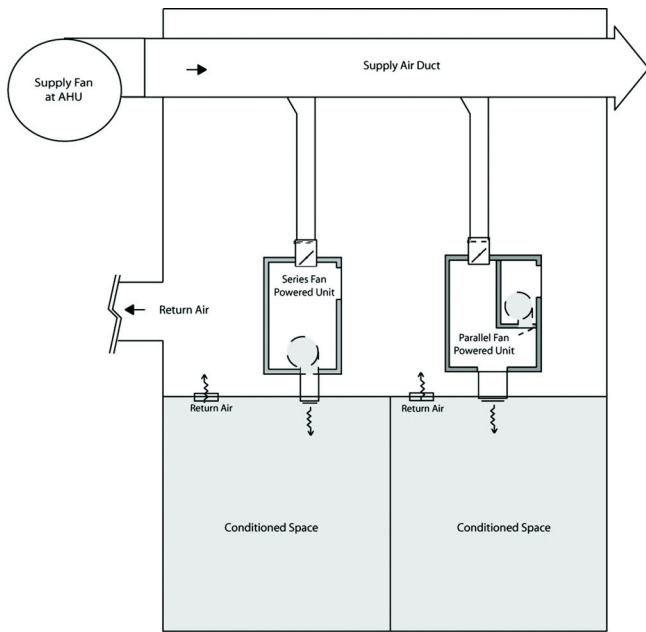


Figure 1 A typical variable air volume system (adapted from Chen and Demster 1996).

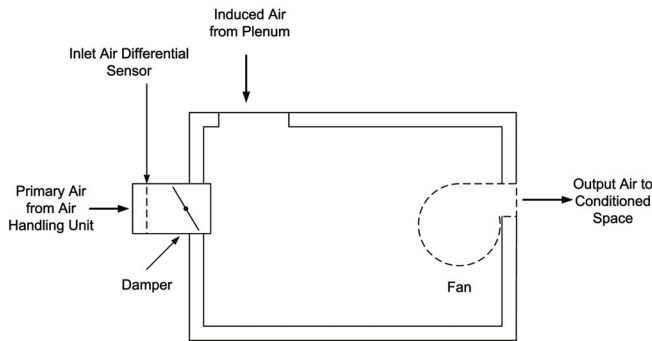


Figure 2 Generic series variable air volume fan powered terminal unit.

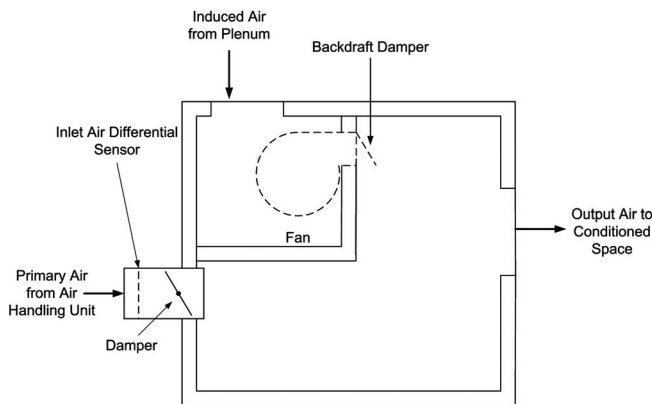


Figure 3 Generic parallel variable air volume fan powered terminal unit.

the specific space's needs. For these cases, the fan in both series and parallel fan powered terminal units is equipped with a speed controller known as a silicon-controlled rectifier (SCR). For a typical unit in the field, the SCR is controlled by a setscrew or knob and is usually adjusted only once when the VAV system is initially balanced.

Current energy codes show a preference for parallel over series terminal units. For example, when following the energy cost budget method in ASHRAE Standard 90.1 (2004), parallel fan powered terminal units are prescribed for VAV systems. Series terminal units are not mentioned. In design guidelines published by the California Energy Commission, Hydeman et al. (2003) states that "series fan powered terminal units should be avoided, with the exception of a few specific applications." This recommendation is supported with reference to the low combined efficiencies of the small terminal unit fans and motors. Energy use of the terminal units is treated separately from the supply fans rather than treating them as a system. While the fans on series VAV terminal units are in constant operation, there is potential for energy savings because the static pressure of the supply fan can be set lower than with parallel terminal unit systems.

Elleson (1993) conducted a field study of cold air distribution systems with series and parallel fan powered terminal units in two separate buildings. Results from computer simulations provided a comparison between series and parallel systems for both cold air and conventional air distribution systems. For both cold air and conventional systems, the results showed that the total fan power consumption, combining the power of the supply fan and terminal units' fans, was greater for series terminal unit systems. The simulations included a reduced supply static pressure for series units of 0.25 in. w.g. (62 Pa) less than the parallel units' design static pressure.

An energy study sponsored by the California Energy Commission included a comparison of parallel and series terminal units operating in perimeter zones (Kolderup et al., 2003). The study was based on running a simulation with DOE 2.2 (1998) and took into account the reduced static pressure of the main supply fan in series systems. The main supply fan static pressure was reduced from 4.0 to 3.67 in. w.g. (996 to 914 Pa) for the series systems. The findings concluded that, for the case studied, a parallel system would use 9% less energy than a series system.

Both studies used the simplified built-in functions of their HVAC simulation software to model the fan powered terminal units. These functions ignore effects of air leakage, fan variable speed controller on power consumption, and design differences, such as the type of primary air or backdraft dampers. As a result, these built in functions did not fully describe the characteristics of typical fan powered terminal units. Additionally, there was no experimental evidence to support the simplified functions.

There is a need to develop a better understanding of systems using parallel and series fan powered VAV terminal

units. To model a system properly, it is important to be able to characterize the individual terminal units. To date, there has been little work in this area. Khoo et al. (1998) developed non-linear models for three standard VAV terminal units without fans. This study concluded that the damper-only approximations of VAV terminal units used in some HVAC simulation packages were not accurate representations of terminal units. The work by Khoo et al. was the only research found on modeling VAV terminal units.

The primary goal for this research was the development of empirical models of power and airflow output for parallel and series fan powered terminal units at typical operating pressures. An experimental setup was developed and used to test fan powered terminal units from three manufacturers. An experimental protocol was developed and used for all tests. This paper (first of three) describes the experimental apparatus, the fan powered terminal units, and the test procedure. Experimental results and the empirical models for airflow, power, and leakage for the parallel and airflow and power for the series fan powered terminal units are presented in second (Furr, et al 2008a) and third (Furr, et al 2008b) papers, respectively.

EXPERIMENTAL APPARATUS

This section describes the experimental apparatus, which included the fan powered terminal units, the equipment to measure airflow, the equipment to measure power, and the data acquisition system

Fan Powered Terminal Units

Fan powered terminal units were obtained from three manufacturers. These consisted of both series and parallel units with 8 in. (203 mm) and 12 in. (304 mm) primary air inlets, resulting in a total of twelve units. A naming convention of A, B, and C was used to differentiate between the three manufacturers. Units were identified as S (series) or P (parallel), followed by the inlet size in inches, and then the manufacturer's identification. For example, the 8 in. (203 mm) parallel terminal unit from manufacturer B was designated unit P8B.

The terminal units were selected so that the units in one set would be similar in airflow output to those in the other two sets. Specifications were given to the manufacturers to meet this criterion (Table 1). All of the unit fans were powered with single phase, 277 AC voltage. However, there were small differences between the terminal units. These included the rated power of the terminal unit fan, the style of the primary airflow damper, and the style of the backdraft damper. These differences in the box design resulted in different unit performances across the three manufacturers.

In the series terminal units, the primary air inlet had either a butterfly damper, with a single rotated blade, or an opposing-blade style, where two blades operated in unison. Series group C used the opposing-blade dampers. Series groups A and B

were equipped with butterfly dampers. In all of the parallel units, the butterfly style primary air damper was used.

A major difference between the parallel terminal units was the style of the backdraft damper. Parallel groups B and C used a gravity-operated damper (Figure 4). During cooling mode, when the fan was off, the damper naturally closed. Approximately 1/8 in. (3.18 mm) thick foam along the edges of the damper formed a loose seal when it closed. The pressure inside the terminal unit would assist in pushing the damper closed against this foam. When the terminal unit fan turned on, the damper opened due to the output pressure of the fan

Parallel group A utilized a primary air-operated backdraft damper (Figure 5). A metal extension attached to the damper and protruded into the primary air stream. When the fan was off during cooling mode, the primary air pushed against the damper extension to push the damper closed. When the fan turned on, the damper opened due to the output airflow of the fan. Unlike parallel groups B and C, the parallel terminal units from group A did not have the foam seal along the backdraft damper edges.

Other significant differences among the parallel terminal units were the location of some box features, such as the plenum air inlet and the backdraft damper (Figures 6 through 8). Parallel groups A and C had backdraft dampers located in the primary air stream, as opposed to parallel group B, where the terminal unit fan was oriented facing the unit outlet and out of the primary airstream. Parallel groups A and B had the induced air port located parallel to the primary inlet. In parallel group C, the induced air port was located on the side of the terminal unit. Table 2 summarizes the specifications for each of the parallel fan powered VAV units tested.

Another design configuration difference among the series terminal units was the placement of the induced air inlet (Figures 9 and 10). Series groups A and B were very similar in that the induced air port was parallel to the primary air port. Series group C had the induced air port located on the side of the box. Table 3 summarizes the specifications of the series terminal units.

Airflow Measurement

The experimental setup was located in an open, unconditioned area where the space temperature varied from 70 °F (24 °C) to 95 °F (35 °C). The relative humidity varied from 23% to 52%. The test setup (Figure 11) was constructed in accordance with the guidelines for testing fan powered terminal units as specified in ANSI/ASHRAE Standard 130, (1996). Two blowers, controlled by variable speed drives (VSDs), were used to adjust the static pressures upstream and downstream of the terminal units. Unconditioned air was used for primary and induced air. The mixing efficiency of the primary and induced air was not analyzed.

Two airflow chambers, a Figure 15 and a Figure 12 (ANSI/AMCA Standard 210, (1999)), were used to measure the terminal unit primary air and output air. The differential pressure across the airflow nozzles, chamber static pressure,

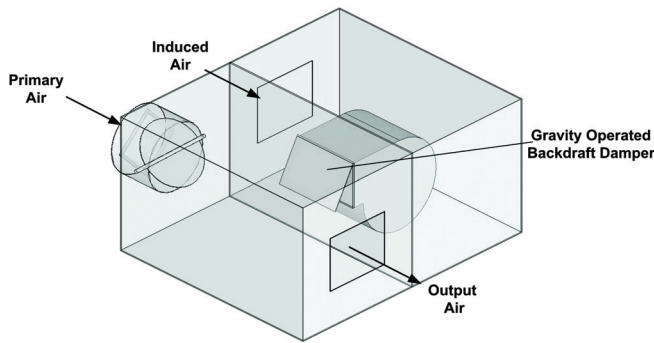


Figure 4 Terminal unit with gravity operated backdraft damper.

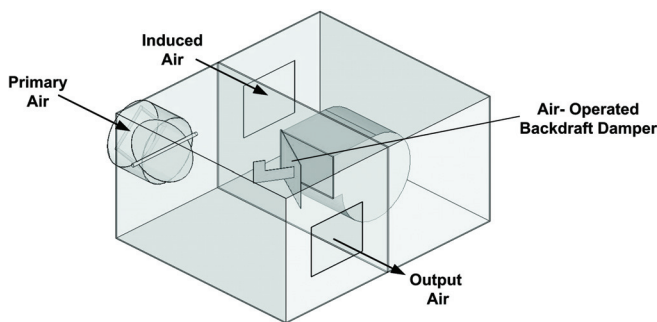


Figure 5 Terminal unit with air-operated backdraft damper.

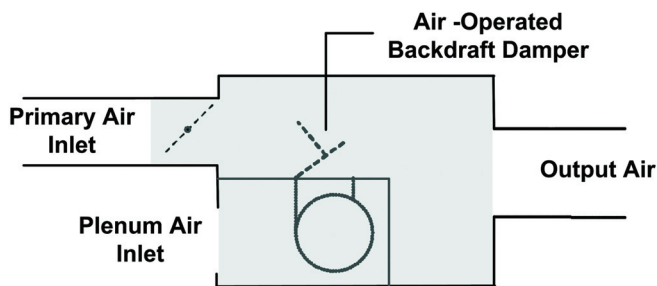


Figure 6 Plan view of group A parallel terminal units.

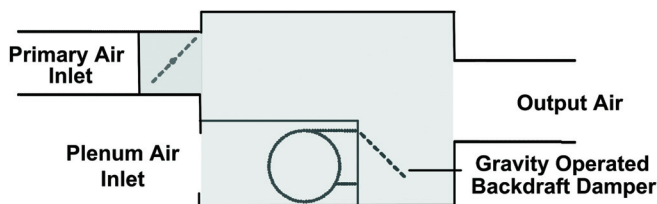


Figure 7 Plan view of group B parallel terminal units.

air temperature, and relative humidity were used to determine the airflow rate through each chamber. The density of the air was assumed to be constant for airflow calculations through both the Figure 12 and 15 chambers. Temperature in the Figure

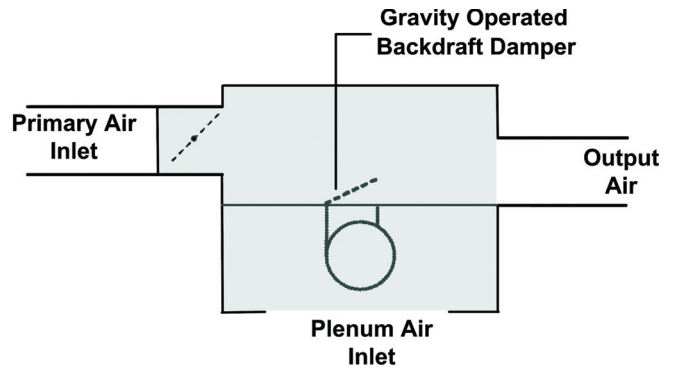


Figure 8 Plan view of group C parallel terminal units.

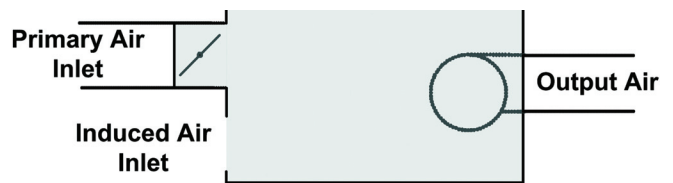


Figure 9 Plan view of groups A and B series terminal units.

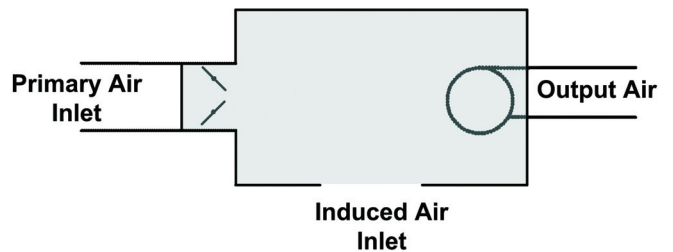


Figure 10 Plan view of group C series terminal units.

12 chamber could be up to 2 °F (1.2 °C) higher than the measurement taken at the Figure 15 chamber. However, the effect on density calculations due to this slight change in temperature was less than 1%. Because of the changes in temperature and humidity on days that the tests were conducted, the volumetric airflow quantities were converted to an airflow at standard density of 0.075 lb/ft³ (1.20 kg/m³), to allow for comparison between terminal units.

The combination humidity/temperature transmitter had a stated accuracy of ±2% RH and ±0.7 °F (±0.4 °C). The upstream and downstream static pressures, differential pressures across the flow nozzles, chamber static pressures, and inlet air velocity sensor pressure were measured using 4-20 mA pressure transducers, each with an accuracy of ±0.25% of their full-scale output. The transducers were sized as specified in Table 4.

The upstream and downstream static pressures, P_{up} and P_{down} , are two important variables in the characterization of the fan powered terminal units. The measurement locations for

Table 1. General Specifications for Terminal Units

Terminal Unit	Maximum Fan Airflow, cfm (m ³ /s)	Maximum Terminal Unit Output, cfm (m ³ /s)
8 in. (203 mm) Series	700 (0.330)	700 (0.330)
12 in. (304 mm) Series	1500 (0.708)	1500(0.708)
8 in. (203 mm) Parallel	500 (0.236)	700 (0.330)
12 in. (304 mm) Parallel	1050 (0.496)	1500 (0.708)

Table 2. Specifications of Parallel Terminal Units

Size	Terminal Unit	Fan Rated Hp (W)	Primary Air Damper Type	Backdraft Damper Style	Location Of Backdraft Damper
8 in. (203 mm)	P8A	1/10 (75)	Butterfly	Primary Airflow Operated	In primary air stream
	P8B	1/6 (124)	Butterfly	Gravity Operated	Out of primary air stream
	P8C	1/4 (187)	Butterfly	Gravity Operated	In primary air stream
12 in. (304 mm)	P12A	1/2 (373)	Butterfly	Primary Airflow Operated	In primary air stream
	P12B	1/4 (187)	Butterfly	Gravity Operated	Out of primary air stream
	P12C	1/2 (373)	Butterfly	Gravity Operated	In primary air stream

Table 3. Specifications of Series Terminal Units

Size	Terminal Unit	Fan Rated hp (W)	Primary Air Damper type	Location of Induced Air Port
8 in. (203 mm)	S8A	1/4 (187)	Butterfly	Parallel to Primary Inlet
	S8B	1/4 (187)	Butterfly	Parallel to Primary Inlet
	S8C	1/4 (187)	Opposing Blade	Side
12 in. (304 mm)	S12A	1/2 (373)	Butterfly	Parallel to Primary Inlet
	S12B	1/3 (249)	Butterfly	Parallel to Primary Inlet
	S12C	1/2 (373)	Opposing Blade	Side

these values were specified in ANSI/ASHRAE Standard 130, (1996). The upstream static pressure used the average of four taps, 90° apart, located 1.5 equivalent diameters upstream of the VAV terminal unit. The downstream static pressure was taken similarly, located 2.5 equivalent diameters downstream of the VAV terminal unit.

In this test setup, the Figure 15 chamber measured the amount of primary airflow, $Q_{primary}$, and the Figure 12 chamber measured terminal unit output, Q_{out} . If air densities are assumed equal, a mass balance can be expressed in terms of volumetric flows (Equation 1 and Figure 12). $Q_{induced}$ was the amount of airflow through the terminal unit fan. $Q_{leakage}$ was

the amount of air leaking from sheet metal seams of the unit and along the backdraft damper when the fan was off. The direction of air leakage is assumed to be out of the terminal unit.

$$Q_{primary} + Q_{induced} = Q_{out} + Q_{leakage} \quad (1)$$

$Q_{leakage}$ was assumed to be small in value relative to the other terms in Equation 1 for parallel terminal unit. $Q_{induced}$ was then calculated as the difference between Q_{out} and $Q_{primary}$. This was done because it was difficult to measure the air leakage directly. During testing it was determined that assum-

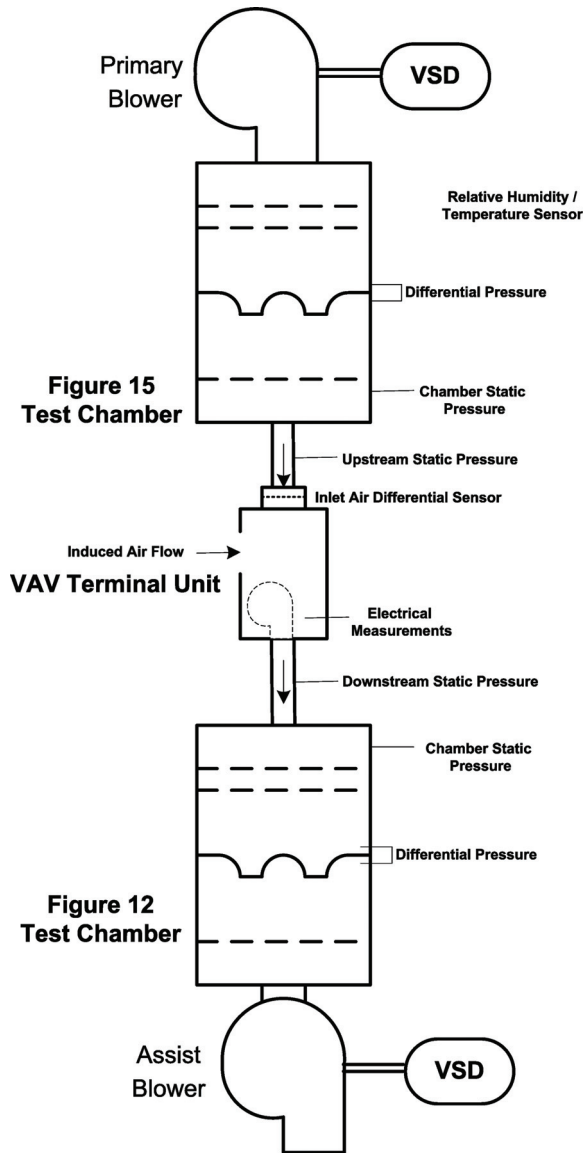


Figure 11 Schematic of experimental test setup.

ing negligible air leakage was reasonable for all of the terminal units except one.

The two airflow chambers were connected in series, without a terminal unit, to verify that the two provided similar results for airflow measurements. The measured error between the two flow chambers averaged 3.2% for airflows ranging from 280 (7.9) to 1821(5.16) cfm (m^3/s).

Power Measurement

The data for instantaneous current and voltage entering the VAV terminal unit fan motor were obtained at 1320 Hz and saved for a duration of six seconds, allowing for current and voltage waveforms to be produced. The current was measured using a 5 Amp current transducer with a full-scale accuracy of $\pm 1\%$, and installed on the 277 V wiring for the fan motor. The

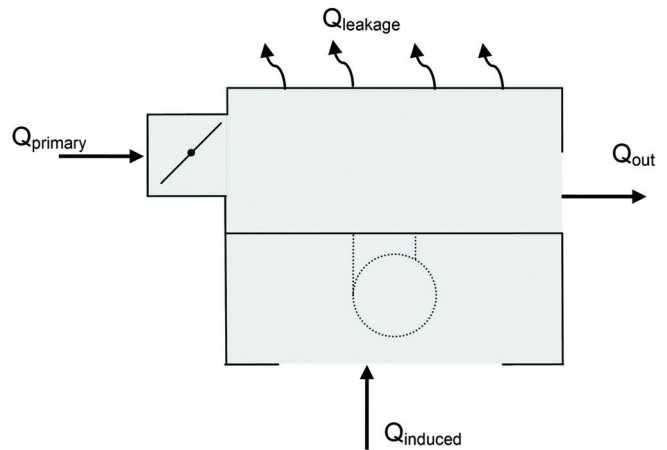


Figure 12 Volumetric airflow balance of a terminal unit.

voltage was measured at the +277 V wiring between the output of the SCR and the fan motor. RMS of current and voltage were calculated for each voltage/current cycle, and then averaged across the 360 cycles. Power was determined using V_{RMS} and I_{RMS} .

EXPERIMENTAL PROCEDURE

A factorial design was employed for testing the VAV terminal units. In this case, there were two separate dependent variables that were of interest; Q_{fan} , the airflow through the fan, and $Power_{fan}$, the power consumption of the terminal unit fan. The independent variables were:

1. The static pressure upstream of the terminal unit, P_{up} ,
2. The static pressure downstream of the terminal unit, P_{down} ,
3. The speed of the terminal unit fan controlled by the SCR, as represented by the RMS average voltage to the unit,
4. The position of the terminal unit's damper, and
5. The control pressure from the flow sensor, P_{iav} . This variable was directly affected by the position of the damper and the upstream static pressure.

Before testing a unit, each of the independent variables was assigned a set of specific values. The number of levels for each of the variables and their values are shown in Table 5. The values for the levels differed across VAV terminal units because the maximum and minimum values for certain variables differed across units. The maximum and minimum values for the SCR voltage were determined by adjusting the SCR setscrew completely in both directions. The maximum value for the damper setting was defined as when the damper was horizontal, or fully open and minimum was defined as when the damper was closed. The levels for downstream static pressure varied from 0.1 to 0.5 in w.g. (25 to 125 Pa). The levels for upstream static pressure varied depending on the test being run.

Table 4. Pressure Transducer Sizing

Point Name	Transducer Size
Differential Pressure Across Nozzles, Fig 12	0-6 in. w.g.(0 – 1.5 kPa)
Differential Pressure Across Nozzles, Fig 15	0-6 in. w.g. (0-1.5 kPa)
Chamber Static Pressure, Fig 12	0-10 in. w.g. (0-2.5 kPa)
Chamber Static Pressure, Fig 15	0-10 in. w.g. (0-2.5 kPa)
Upstream Static Pressure	0-2 in. w.g. (0-0.5 kPa)
Downstream Static Pressure	0-2 in. w.g. (0-0.5 kPa)
Inlet air velocity Sensor Pressure	0-2 in. w.g. (0-0.5 kPa)

Table 5. Test Variable Levels

Independent Variable	Number of Levels	Values
Upstream Static Pressure	3	varied from 0.3 to 2 in. w.g. (75 to 498 Pa)
Downstream Static Pressure	3	0.1, 0.25, 0.5 in. w.g (25, 62, 125 Pa)
SCR Voltage (Fan Speed)	4	Equally spaced
Damper Position	4	Equally spaced

The characterization of a terminal unit consisted of several tests. These tests were conducted for each combination of damper and SCR settings. In every test, data for each combination of upstream and downstream static pressure levels were obtained. This process was a full-factorial design because data points for all combinations of independent variables were obtained. The sequence of these tests usually consisted of running the tests for all of the SCR speeds at a single damper position, adjusting the damper to the next position, and continuing the sequence.

Before starting a test, the damper and SCR were manually adjusted to the desired positions according to the test being run. Throughout a test, the damper and SCR would remain in the same position. During a test, the data acquisition system allowed the user to adjust the VSD's on the upstream and downstream blowers to meet desired conditions for a test point.

The upstream static pressure was first adjusted to the smaller of the following: the point where the primary airflow was approximately 5% greater than the terminal unit's specified maximum or 2 in. w.g. (498 Pa). This pressure was designated as the maximum level for the upstream static pressure variable. The minimum upstream static pressure setting was determined by the downstream pressure. It could not be lower than the downstream static pressure because primary air would flow backwards into the terminal unit. Each test had three minimum level upstream static pressures. These minimums were selected to be approximately 0.25 in. w.g (60 Pa) greater than the corresponding downstream static pressure, except in cases where damper position caused insufficient primary airflow. For each downstream static pressure, a third

point was obtained for the upstream static pressure approximately halfway between the corresponding minimum and maximum. This procedure resulted in three data points for each downstream static pressure level, and nine points per test.

The upstream and downstream blowers were manually adjusted to the desired conditions for a specific data point. After static pressures reached steady state, data were acquired

DATA ACQUISITION SYSTEM

A computer data acquisition system was used to obtain, process, and store data. This system consisted of a personal computer, two separate data acquisition cards, and the termination blocks for all signal wires.

An eight channel, sixteen-bit sample-and-hold data card was used to measure instantaneous current and voltage. The simultaneous sample and hold prevented any introduction of error due to phase shift between the voltage and current signals. The elimination of phase shift allowed for accurate determination of the power factor for the VAV unit fans. The analog inputs had a resolution of 16 bits.

The other data acquisition card was an eight channel card, with two analog outputs to control the variable speed drives on the test setup assist blowers. The resolution of the analog inputs on this card was 12 bits.

SUMMARY

This paper is the first of three papers. Tests were conducted on six parallel and six series variable air volume fan powered terminal units. Both 8 in. (203 mm) and 12 in. (304 mm) primary air inlet terminal units from three manufacturers were evaluated. This paper provides a description of the

twelve fan powered terminal units, the experimental apparatus, the test procedure, and the data acquisition system.

ACKNOWLEDGMENTS

This work was a part of a project funded by ASHRAE under RP-1292 and we would like to thank the project monitoring subcommittee of TC 5.3 and the manufacturers they represent for their support during the project. Several manufacturers donated terminal units for use in this study. Through cooperative ventures such as these, ASHRAE research funding can be utilized to the fullest. We appreciate the contributions from these industry leaders.

NOMENCLATURE

P_{down}	=	downstream static pressure, in. w.g
P_{iaV}	=	pressure across inlet air velocity flow sensor, in. w.g.
P_{unit}	=	static pressure inside terminal unit, in. w.g.
P_{up}	=	upstream static pressure, in. w.g.
$\text{Power}_{\text{fan}}$	=	power consumption of terminal unit fan, W
Q_{fan}	=	amount of airflow through terminal unit fan, cfm
Q_{induced}	=	amount of airflow induced from plenum, cfm
Q_{leakage}	=	amount of airflow leaking from a terminal unit, cfm
Q_{out}	=	amount of parallel terminal unit airflow output, cfm
Q_{primary}	=	amount of primary airflow, cfm
V	=	RMS average of SCR voltage output, V

REFERENCES

Alexander, J. and D. Int-Hout. 1998. Assuring zone IAQ. White paper. Titus. Retrieved Sept. 15, 2005 http://www.titus-hvac.com/tech_papers.asp.

AMCA. 1999. ANSI/AMCA standard 210-99, Laboratory methods of testing fans for aerodynamic performance rating. Arlington Heights, IL: Air Movement and Control Association.

ASHRAE. 1996. ANSI/ASHRAE standard 130, Methods of testing for rating ducted air terminal units. Atlanta: American Society of Heating, Refrigerating and Air-Conditioning Engineers, Inc.

ASHRAE. 2001. ASHRAE fundamentals handbook. Atlanta: American Society of Heating, Refrigerating and Air-Conditioning Engineers, Inc.

ASHRAE. 2004. ANSI/ASHRAE standard 90.1-2004, Energy standard for buildings except low-rise residential buildings. Atlanta: American Society of Heating, Refrigerating and Air-Conditioning Engineers, Inc.

Chen, S.Y.S., and S.J. Demster. 1996. Variable air volume systems for environmental quality. New York: McGraw-Hill.

DOE 2.2: Building Energy Use and Cost Analysis Software. 1998. Lawrence Berkeley National Laboratory at the University of California and James J. Hirsch & Associates.

Elleson, J.S. 1993. Energy use of fan-powered mixing boxes with cold air distribution. ASHRAE Transactions 99(1):1349-1358.

Furr, J., O'Neal, D.L., Davis, M. A., Bryant, J.A., and Cramlet, A. 2008a. Performance of VAV fan powered parallel terminal units: experimental results and models, ASHRAE Transactions, submitted for review.

Furr, J., O'Neal, D.L., Davis, M. A., Bryant, J.A., and Cramlet, A. 2008b. Performance of VAV fan powered series terminal units: experimental results and models, ASHRAE Transactions, submitted for review.

Hydeman, M., S. Taylor, and J. Stein. 2003. Advanced variable air volume system design guide. Integrated energy systems: productivity and building science. San Francisco: California Energy Commission.

Khoo, I., G.J. Levermore, and K.M. Letherman. 1998. Variable-air-volume terminal units I: steady state models. Building Services Engineering Research & Technology 19(3):155-162.

Kolderup, E., T. Hong, M. Hydeman, S. Taylor, and J. Stein. 2003. Integrated design of large commercial HVAC systems. Integrated energy systems: productivity and building science. San Francisco: California Energy Commission.

Performance of VAV Parallel Fan-Powered Terminal Units: Experimental Results and Models

James C. Furr

Dennis L. O'Neal, PhD, PE

Michael A. Davis

Fellow ASHRAE

John A. Bryant, PhD, PE

Andrew Cramlet

Member ASHRAE

Student Member ASHRAE

ABSTRACT

Empirical models of airflow output, power consumption, and primary airflow were developed for parallel fan powered variable air volume terminal units at typical operating pressures. Both 8 in. (203 mm) and 12 in. (304 mm) primary air inlet terminal units from three manufacturers were evaluated. Generalized models were developed from the experimental data with coefficients varying by size and manufacturer.

Fan power and airflow data were collected at downstream static pressures over a range from 0.1 to 0.5 in. w.g. (25 to 125 Pa). Upstream static pressures ranged from 0.1 to 2.0 in. w.g. (25 to 498 Pa). Data were collected at four primary air damper positions and at four terminal unit fan speeds. Model variables included the RMS voltage entering the terminal unit fan, the inlet air differential sensor pressure, and the downstream static pressure. A model was also developed to quantify air leakage when the unit fan was off.

In all but one of the VAV terminal units, the resulting models of airflow and power had R^2 values greater than 0.90. For the exception, excessive air leakage from the unit appeared to limit the ability of the airflow and power models to capture the variation in the experimental data. These performance models can be used in HVAC simulation programs to model parallel fan powered VAV systems.

INTRODUCTION

Variable Air Volume (VAV) systems maintain comfort conditions by varying the volume of primary air that is delivered to a space. A VAV system often consists of a central air handling unit (AHU), where air is cooled by cooling coils (Wendes 1994). This air, referred to as primary air, is sent through a single-duct supply system to VAV terminal units by

the supply fan. Each terminal unit is ducted to air outlets, usually serving two or more offices or an open area. VAV terminal units that include a fan to improve circulation within a zone are called fan powered terminal units. These terminal units can draw in warm air from the plenum area and mix it with primary air from the central Air Handling Unit (AHU) to maintain comfort conditions in the occupied space.

When the fan in a VAV fan powered terminal unit is outside the primary airflow, the configuration is called a parallel terminal unit. During operation, the fan for a parallel terminal unit cycles on and off. During periods of maximum cooling, the fan is off. A backdraft damper prevents cold air from blowing backwards through the fan. The terminal unit primary air damper modulates the airflow to maintain the space temperature setpoint. An inlet air differential sensor within the primary air stream allows the unit controller to maintain a consistent volume of airflow to the zone depending on the temperature setpoint. When the primary airflow drops below a specified amount, the controller activates the fan. At this point, the terminal unit mixes primary air with air being drawn in from the plenum. Electric or hot water supplemental heat can be used for additional heating. Depending on the control scheme, the controller can continue to reduce primary air to the conditioned space by adjusting the damper.

There is a need to develop a better understanding of systems using parallel and series fan powered terminal units. To model a VAV system properly in a commercial building energy use model, it is important to be able to characterize the individual terminal units.

This paper is the second of three papers that describe the development of experimental models of VAV fan powered terminal units. The first paper (Furr et al. 2008a) described the

James C. Furr is a thermal management engineer with Lockheed Martin, Fort Worth, TX. **Dennis L. O'Neal** is Holdredge/Paul Professor and Head, Department of Mechanical Engineering, Texas A&M University, College Station, TX. **Michael A. Davis** is a research engineer with and **John A. Bryant** is a visiting associate professor in the Department of Mechanical Engineering, Texas A&M University Qatar, Doha, Qatar. **Andrew Cramlet** is a research assistant, Department of Mechanical Engineering, Texas A&M University, College Station, Texas.

experimental setup and methodology used to measure the performance of parallel and series fan powered units. The third paper (Furr et al. 2008b) describes the measured results and models developed for series fan powered terminal units. In this paper, the performance of six parallel fan powered terminal units from three manufacturers (labeled A, B, and C) is measured and models developed from the data. These units included three 8 in. (203 mm) and three 12 in. (304 mm) units. An 8 in. (203 mm) unit from manufacturer A has the designation P8A. One from manufacturer B that is 12 in. (304 mm) is P12B, etc. As described in the first paper (Furr et al. 2008a), there were small differences between the terminal units that included the rated power of the terminal unit fan, the style of the primary airflow damper, and the style of the backdraft damper. Statistical analyses of experimental data were performed and used to develop generalized models that can be applied to the different manufacturers' terminal units. The empirical models were developed for units from three manufacturers and two sizes to obtain representative samples of fan power terminal units installed into the field. In addition to the models of airflow output and energy consumption, a model was developed to characterize the air leakage that occurred in the parallel terminal units when unit fan was off.

RESULTS AND MODELS

One goal of this research was to determine if a single generalized model could be used for all terminal units tested for a given size. Because of design differences in the units, performance varied dramatically. Thus, no single model could be used to describe a given size unit. However, the models that were developed had the same form, but used different coefficients for the different sizes and manufacturers.

Variables were first identified that were expected to be significant in explaining fan airflow and power. Models were then developed by determining the most statistically influential independent variables using multiple linear and non-linear regression techniques. For the multiple linear regression, the variable with the largest F statistic was added first. Statistically significant variables were continually added to the model provided their respective F statistic was above 4.0. Between each step, models were compared against each other according to their adjusted coefficient of determination, R^2_{adj} (Neter et al. 1996).

In developing the models for the parallel units, several variables were considered: the SCR voltage, P_{iad} , P_{dwn} , P_{up} , and $Q_{primary}$. The models for all of the parallel terminal units were compared against each other. Any differences in terms included in the airflow or power models were investigated in an effort to create a single form model that would be applicable to all of the terminal units.

Leakage Model

During the cooling mode, the terminal unit fan is off and the backdraft damper was supposed to prevent any air from circulating backwards through the fan. For this case, the airflow output downstream of the terminal unit should have been equal

to the inlet primary airflow. However, it was discovered that air leakage occurred at the backdraft damper and through the sheet metal seams of the terminal unit. A leakage model was developed to quantify the amount of air leakage from the terminal units.

The primary factor that was expected to influence air leakage was the pressure inside the terminal unit. Because there was no physical obstruction at the outlet of the terminal units, the static pressure inside the terminal units was assumed to be very close in value to the downstream static pressure. Therefore, the downstream static pressure was used as a proxy for the pressure inside the box and was expected to be the most significant variable in the leakage model.

Initial analysis of the data confirmed that the downstream static pressure played a significant role in air leakage. Air leakage increased with an increase in downstream static pressure for the 8 in. (203 mm) and 12 in. (304 mm) units (Figures 1 and 2). The response between air leakage and downstream

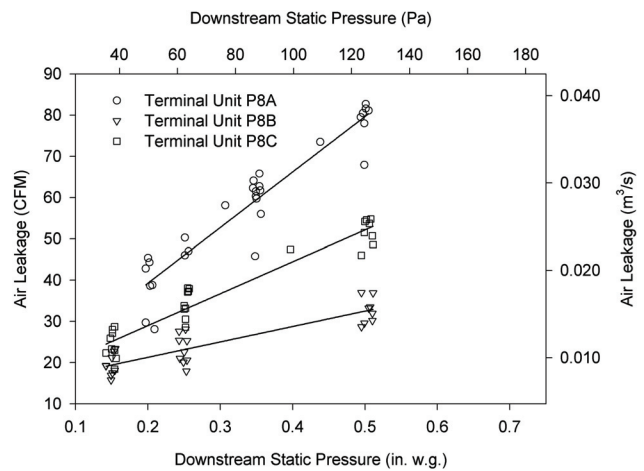


Figure 1 Air leakage for 8 in. (203 mm) inlet parallel terminal units.

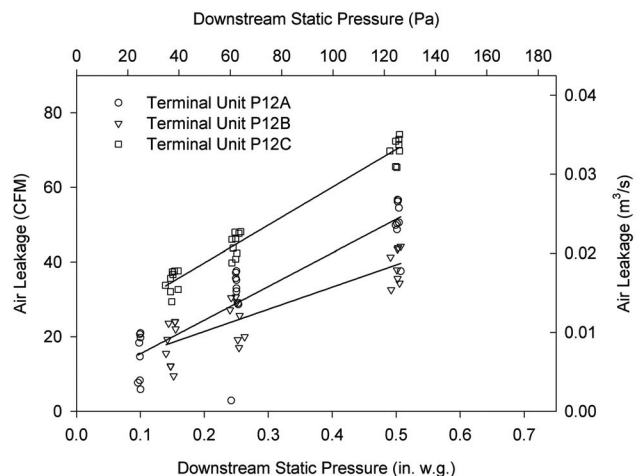


Figure 2 Air leakage for 12 in. (304 mm) inlet parallel terminal units.

static pressure was very similar among the six terminal units. However, terminal unit P8A showed more scatter than the other units.

Air leakage occurred either through the sheet metal seams of the terminal units or at the backdraft damper. The leakage at the seams was affected mainly by the static pressure inside the terminal unit. The primary air velocity across the damper was expected to influence the leakage around the backdraft damper. Terminal units from group A utilized the primary air-operated backdraft damper. A change in primary air would have an effect on the operation of this damper. In the terminal units from groups B and C, the backdraft dampers were gravity operated, and primary air velocity was expected to have a lesser effect, or possibly no effect on leakage. The pressure at the inlet air differential sensor, P_{iad} , was approximately linear (Appendix) with respect to the primary airflow entering the terminal over the ranges studied in this paper. P_{iad} was used to approximate the influence of primary air velocity.

A leakage model using only P_{dwn} was developed for parallel terminal unit P8C with a resulting R^2_{adj} of 0.917. Upon further analysis of the F-statistics, another model using P_{dwn} and P_{iad} as explanatory variables was developed and the R^2_{adj} improved to 0.970. Similar results were found for all of the group A and C units. The results indicate that primary airflow, as represented by P_{iad} , played a statistically significant role in the air leakage from the terminal units.

Similar analysis was conducted for unit P8B. The P_{iad} term failed the F-statistic test ($F = 1.3 < 4.0$), did not improve the R^2_{adj} statistic from 0.767, and was not included in the model. The backdraft damper was not located in the primary airstream for this unit as it was for group A and C units.

The P12B terminal unit, with the backdraft damper out of the primary airstream, did not respond in the same way. The addition of the P_{iad} variable (with an F statistic of 87.6) increased the R^2_{adj} statistic from 0.7398 to 0.9454 which indicated that P_{iad} should be included in the model. While the two group B units had the same backdraft damper configuration, the larger terminal unit had air dynamics acting on the backdraft damper that did not occur in the smaller terminal unit. More investigation would need to be conducted regarding the air dynamics within the terminal units.

Air leakage was found to be dependent on P_{dwn} , and P_{iad} (Equation 1). Table 1 provides the coefficients for each of the terminal units. In this model, the P_{dwn} term accounts for the

Table 1. Coefficients for the Leakage Model

Name	C_1 , cfm	C_2 , cfm/ $\sqrt{V^2}$	C_3 , cfm/in. w.g.	R^2_{adj}
P8A	23.15	101.70	-12.31	0.937
P8B	13.8	37.41	0	0.767
P8C	16.86	77.55	-10.76	0.970
P12A	14.4	97.94	-37.9	0.858
P12B	17.83	58.26	-27.16	0.945
P12C	22.30	100.83	-15.02	0.989

effect of the internal terminal unit pressure on leakage, while P_{iad} accounts for the effects of primary air on the backdraft damper.

$$Q_{leakage} = C_1 + C_2 P_{dwn} + C_3 P_{iad} \quad (1)$$

Airflow Model

This model quantified the amount of airflow going through a terminal unit fan during the heating mode when the fan was on. The fans on each of the terminal units were centrifugal, forward-curved style fans. The model for these fans were expected to follow typical fan curves and the fan laws (ASHRAE 2001).

The SCR settings of the fans were a variable in the model that had to be quantified first. Each SCR setting corresponded to a different fan speed. A simple experiment was conducted to determine the relationship between the SCR setting and the speed of the fan. A tachometer was instrumented to terminal unit P8A and at several different voltage settings, the RPM of the fan was measured. During this testing, the upstream and downstream static pressures were held constant to eliminate the effects of pressure on the fan speed. A quadratic equation was fitted to the data for unit P8A (Figure 3) and had an R^2 of 0.999.

This test was conducted on two other terminal units, P12B and P8C, which resulted in R^2 values of 0.994 and 0.997, respectively. Because of the high R^2 values for the variety of groups and sizes, it was assumed that a general quadratic relationship would remain true for all of the terminal units even if their coefficients differed.

A linear relationship between airflow and fan speed was expected (ASHRAE, 2001). Because a quadratic equation had been used to show the relationship between SCR voltage and fan speed, it was assumed that a different equation of the same form could be used for the relationship between SCR voltage and fan airflow.

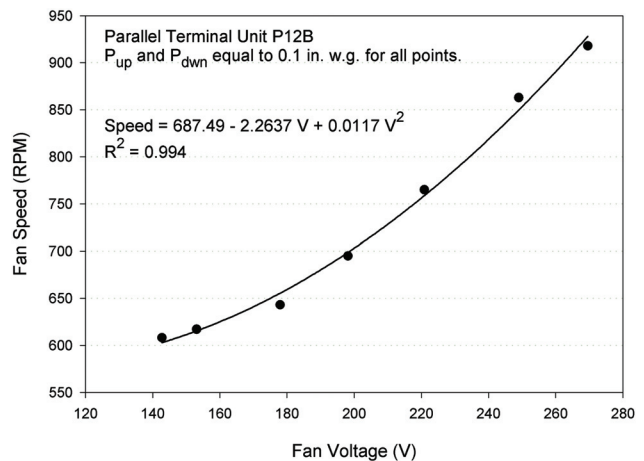


Figure 3 Effect of SCR voltage on fan speed for parallel terminal unit P8A.

From an understanding of fan curves and the fan laws, the only other factor that should influence the fan output would be the pressure across the fan. For all parallel terminal units tested, the pressure on the front side of the fan was atmospheric. The pressure at the fan output was assumed to be approximately equal to the downstream static pressure. Therefore, this pressure would have the other significant influence on the terminal fan capacity. The results typical for the terminal units of groups B and C confirm the effect on fan airflow due to the downstream static pressure and the SCR voltage (Figure 4).

The results from group A (Figures 5 and 6) differed with that of groups B and C. Two reasons possibly explain this difference in results. First, parallel terminal unit P8A appeared to have significant air leakage. Second, both terminal units had a different style backdraft damper that could have affected the fan performance.

Parallel unit P8A leaked more air than any of the other units (Figure 1). Additionally, the coefficient, C_2 , of the leakage model for P8A was the highest of the 8 in. (203 mm) units (Table 1). This part of the model estimates the leakage related to the internal static pressure of the terminal unit. It would be

expected that a terminal unit with greater leakage would have a model that gave more weight towards P_{dwn} . The leakage model for P8A displayed this characteristic, confirming the leakage that occurred when the unit fan was off.

At higher downstream static pressures, the P8A unit fan had little net airflow and was negative at the higher downstream pressures for the lowest SCR voltage setting (Figure 5). Because Q_{fan} was not directly measured but was determined by taking the difference between Q_{out} and $Q_{primary}$. The calculation assumed that the leakage was negligible. The negative values on the figure show that at downstream static pressures above 0.5 in w.g. (75 Pa) and lowest SCR voltage setting, the leakage was equal to or greater than the primary airflow output of the terminal unit:

$$Q_{fan} = (Q_{out} - Q_{primary}) + Q_{leakage} \quad (2)$$

The second reason for the distinctive results from the units of group A was possibly the style of the backdraft damper. This damper used an extension to allow primary air to force it closed. It was expected that while the primary fan was on, an increase in the amount of primary air would push the damper further closed, resulting in a decrease in output of the terminal unit fan. P_{iad} was added as an explanatory variable to the parallel airflow model to account for this effect of the backdraft damper. Only the units from group A utilized this extra variable. Analysis of the F statistics for P_{iad} confirmed that it was an insignificant variable for groups B and C, which did not have that style backdraft damper.

For the gravity-operated backdraft damper units, groups B and C, the airflow was not affected by the amount of primary air input to the terminal unit. The airflow model (Equation 3) for these terminal units was a function of SCR voltage and downstream static pressure. Table 2 provides the coefficients for the groups B and C parallel terminal units.

$$Q_{fan} = C_1 + C_2V + C_3V^2 + C_4P_{dwn} \quad (3)$$

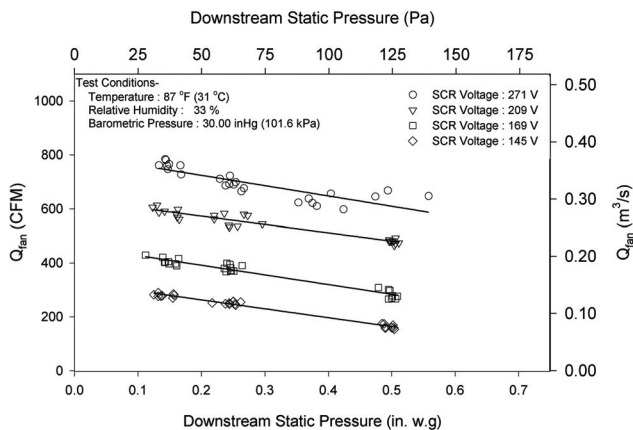


Figure 4 Fan airflow for parallel terminal unit P8B.

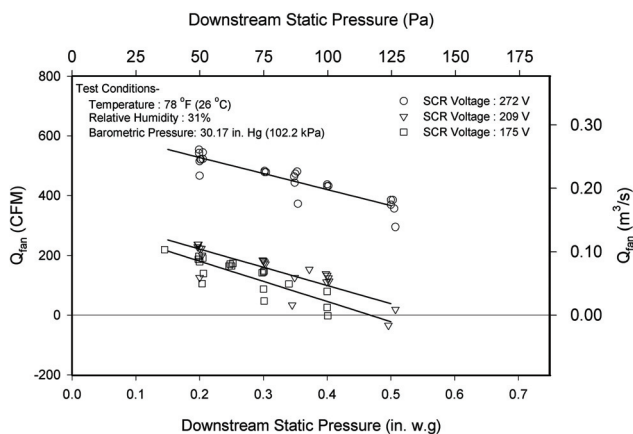


Figure 5 Fan airflow for parallel terminal unit P8A.

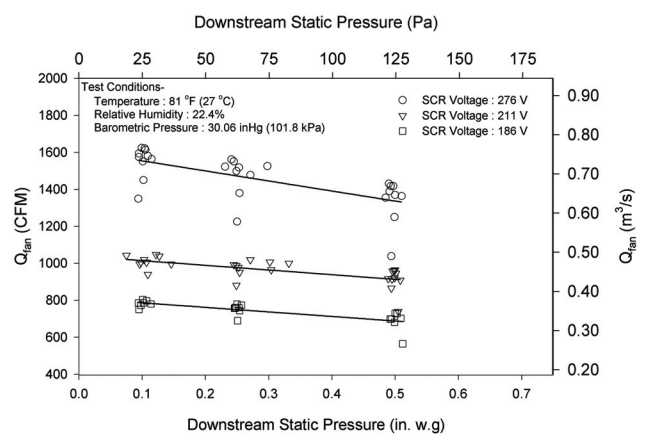


Figure 6 Fan airflow for parallel terminal unit P12A.

Table 2. Airflow Model Coefficients for Terminal Units with a Gravity-Operated Backdraft Damper

Name	C_1 , cfm	C_2 , cfm/ V	C_3 , cfm/ V^2	C_4 , cfm/in. w.g.	R^2_{adj}
P8B	-988.5	11.85	-0.0197	-303.0	0.990
P8C	-1725	19.79	-0.0328	-564.4	0.991
P12B	-1143	13.56	-0.0131	-364.8	0.998
P12C	-2142.9	26.36	-0.0396	-1920.9	0.931

Table 3. Airflow Model Coefficients for Terminal Units with a Primary Air-Operated Backdraft Damper

Name	C_1 , cfm	C_2 , cfm/ V	C_3 , cfm/ V^2	C_4 , cfm/in. w.g.	C_5 , cfm/in. w.g.	R^2_{adj}
P8A	-233.2	3.37	-0.023	-917.3	-229.1	0.808
P12A	-1567.3	16.98	-0.0199	-407.4	-360.2	0.978

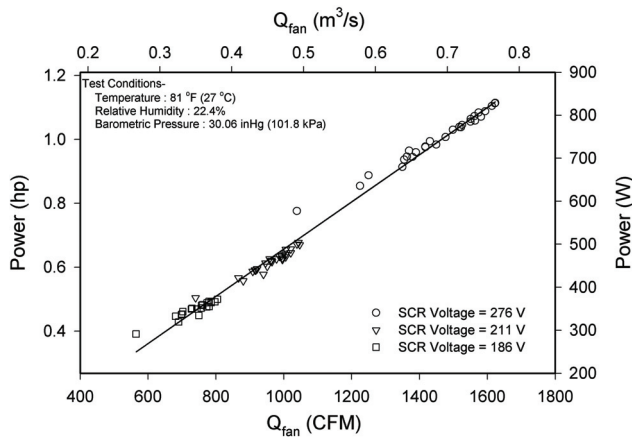


Figure 7 Fan power for parallel terminal unit P12A.

The airflow model for the primary air-operated backdraft damper terminal units (Equation 4) had the same form as the airflow model already presented, except that P_{iad} was added as a variable to include the effect of primary air interacting with the backdraft damper. Table 3 provides the coefficients for this model.

$$Q_{fan} = C_1 + C_2V + C_3V^2 + C_4P_{dwn} + C_5P_{iav} \quad (4)$$

Fan Power Model

Data analysis of the power curves for each of the terminal unit fans revealed a common characteristic. In each of the terminal units, except parallel terminal unit P8A, there appeared to be a nearly linear relationship between power and airflow. Figure 7 shows an example of data for P12A. The data for power versus fan airflow for terminal unit P8A was different (Figure 8). While the data were linear over two ranges, the overall plot was non-linear.

Terminal units with minimal leakage, such as parallel terminal unit P12A (Figure 7), allow the direct relationship between fan capacity and power to be depicted in a single

Table 4. Model Coefficients for Parallel Terminal Unit Fan Power Model

Name	C_1 , W	C_2 , W/ V^2	C_3 , W/ V	C_4 , W/in. w.g.	C_5 , W/in. w.g.	R^2_{adj}
P8A	345	0.00862	-2.92	-72.5	-30.7	0.973
P8B	-258	-0.00600	3.65	-82.3	0	0.989
P8C	-363	-0.00880	5.18	-145	0	0.990
P12A	-631	-0.0039	6.22	-142	0	0.956
P12B	-403	-0.00515	5.15	-128.7	0	0.996
P12C	-622	-0.0159	9.48	-638	0	0.923

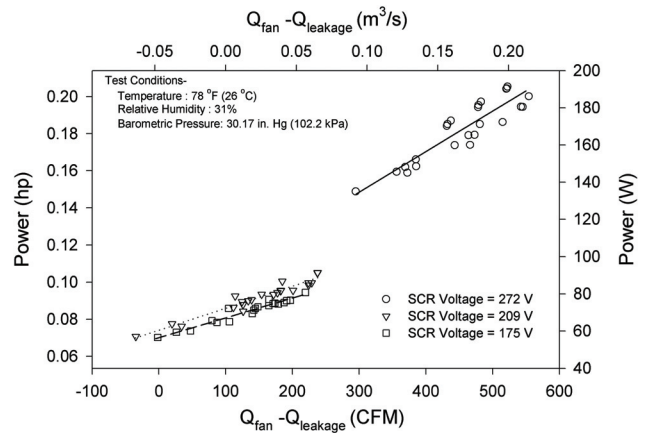


Figure 8 Fan power for parallel terminal unit P8A.

graph. However, because parallel terminal unit P8A has been shown to have significant leakage, Figure 8 does not depict the relationship between the fan airflow and power. Rather, it illustrates the relationship between $(Q_{fan} - Q_{leakage})$ and the fan power. For this terminal unit, it was expected that the model for power would need to include a term to account for terminal unit leakage.

Because of the linear relationship between airflow and power for parallel terminal units, the model developed for power maintained the same form as the model for airflow. Equation 5 is the model that was developed for the power consumption of the fan in parallel terminal units. Table 4 provides the coefficients for each of the terminal units.

$$Power_{fan} = C_1 + C_2V^2 + C_3V + C_4P_{dwn} + C_5P_{iav} \quad (5)$$

Primary Airflow Model

The primary airflow as a function of differential pressure across the terminal units is needed in predicting the upstream static pressure under various operating conditions when applying the above models in an energy simulation program. The equations developed above for the parallel terminal unit allow prediction of the induced air flow when the fan was turned on when various quantities of primary air was moving through the box. These equations express the fan flow as a function of the SCR voltage, the downstream static pressure, and the amount of primary air flowing through the box. These

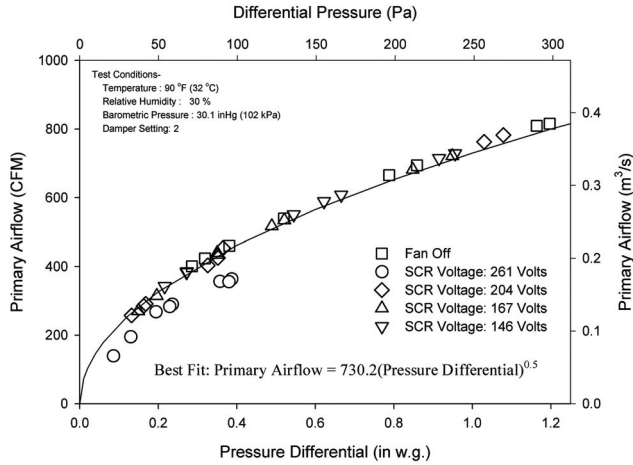


Figure 9 Primary airflow for terminal unit P8C at damper setting of 23 degrees.

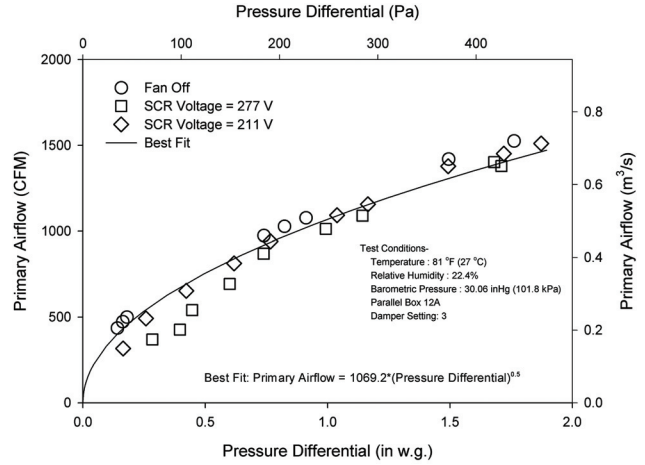


Figure 10 Primary airflow for terminal unit P12A at damper setting of 42 degrees.

equations did not include any variables that would allow for direct estimation of the upstream static pressure as it corresponded to the operation of the terminal unit either with or without the operation of the fan.

Initially, it was assumed that the primary air flow rate would be a function of damper setting (degrees), SCR setting (voltage), and the pressure differential across the terminal unit. Data from several terminal units were analyzed and it was found that the data showed little dependence on SCR. Figures 9 and 10 show the primary airflow for terminal unit P8C for a damper setting of 23 and 42°, respectively. For the typical box with a butterfly damper, a damper setting of 0° was a damper set at full open position and one at 90° at full close position. For all tests, the range of the damper was set at 4 to 5 positions to cover the complete range of movement for the damper. P8C was run for 4 SCR voltage settings and with the fan off while P12A was run for 2 SCR voltage settings and with the fan off. Most of the data fall right along a parabolic curve where the primary airflow ($Q_{primary}$) is a function of the square root of the pressure differential (DP) across the terminal unit multiplied by a constant, K :

$$Q_{primary} = KDP^{0.5} \quad (6)$$

Equation 6 indicates that the primary airflow of the terminal unit is proportional to the square root of the pressure differential across the terminal unit for a given damper setting. Also, if there is no pressure differential across the unit, there will be no flow. The fact that the primary airflow showed little dependence on the SCR Voltage meant the model of primary airflow could be simplified to include only damper setting, S , and pressure differential across the terminal unit, DP, as independent variables. The data for P8C and P12A were analyzed and a variety of forms of the model evaluated. The final form of the model relating the primary airflow to the damper setting (S , in degrees) and pressure differential was:

$$Q_{primary} = C_1(1 + C_2S + C_3S^2)(DP)^{0.5} \quad (7)$$

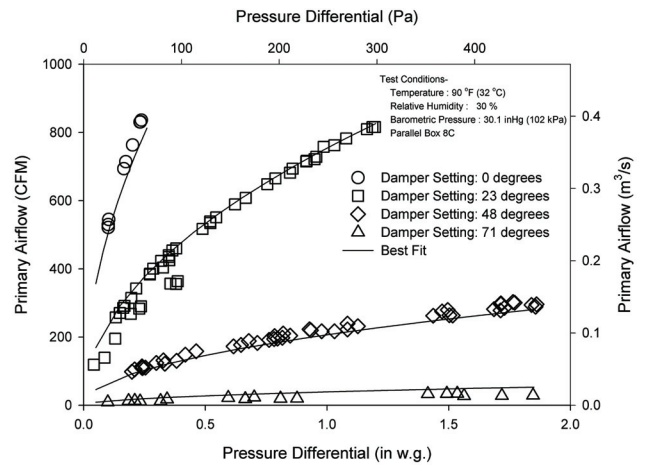


Figure 11 Primary airflow for terminal unit P8C.

Table 5. Model Coefficients for Primary Airflow in Parallel Fan Powered Terminal Units

Name	C_1	C_2	C_3	R^2
P8A	1362.9	-0.0202	9.87E-05	0.924
P8B	1935.0	-0.0248	1.61E-04	0.981
P8C	1593.8	-0.0273	1.91E-04	0.981
P12A	7425.1	-0.0307	2.45E-04	0.935
P12B	5781.2	-0.0280	2.04E-04	0.893
P12C	1838.4	-0.0120	1.63E-05	0.637

Table 5 provides the coefficients for Equation 7 for the six parallel fan powered terminal units. Figures 11 and 12 show samples of the data and model (Equation 7) plotted together for P8C and P12A, respectively. All three of the eight inch units and P12A provided high R^2 values (above 0.9). The primary airflow data for P12C showed more scatter, resulting in a much lower R^2 values.

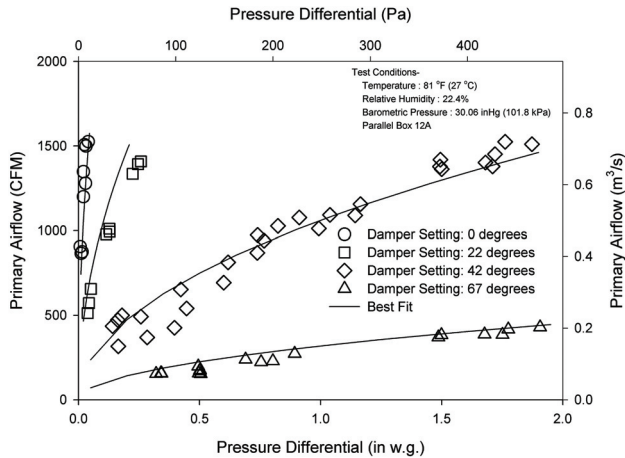


Figure 12 Primary airflow for terminal unit P12A.

SUMMARY AND CONCLUSIONS

Characterizing the performance of parallel terminal VAV units required four models: a leakage, airflow, power consumption model, and a primary airflow model. The leakage model was required because the units leaked through seams and backdraft damper when the fan was off. The R^2_{adj} statistics for the leakage model indicated that four of the six terminal units had models that accounted for at least 95% of the variation in the leakage measurements. The other two terminal units had models that accounted for 77 and 86% of the variation in the leakage measurements. Leakage was generally small with the exception of one unit (P8A).

A second model characterized the fan airflow. The statistics for the parallel airflow model indicated that five of the six units had models that accounted for at least 93% of the variation in fan airflow. The sixth terminal unit appeared to have significant leakage when the fan was on, resulting in a model with an R^2 value of 0.81. Because of the other high values of R^2 (all above 0.90), the parallel airflow model appears to be adequate for characterizing airflow in these units.

The third model for the parallel terminal units characterized the power consumption of the terminal unit fan. The statistics for the parallel power model showed that all terminal unit models explained at least 91% of the variation in power. The terminal unit with the lowest R^2 value was P8A, which was the unit that had the greatest air leakage. As with the airflow model, leakage increased scatter in the model results.

The fourth model characterized the primary airflow as a function of damper setting and pressure differential across the terminal unit. While the model was non-linear, it was something of a surprise that the flow regressed well with the square root of the pressure differential across the terminal unit at a given damper setting and showed no dependence on SCR.

The construction quality of these terminal units could be an item of concern. These units were obtained from several manufacturers and in different sizes in an effort to get a broad sample of units typically installed in the field. However, this

sample of six terminal units resulted in one (P8A) that would be expected to perform poorly in the field, particularly under higher downstream static pressures. Air leakage from parallel terminal units can be interpreted as lost energy to the plenum space. This leakage can also result in control issues because the terminal unit controller adjusts the primary air damper position in order to provide a certain quantity of primary air, depending on the thermostat control signal. However, if a portion of this primary air is not being delivered to the space containing the thermostat, there is potential for control instability.

The leakage from the other terminal units when the terminal unit fan was off was strongly dependent upon the downstream static pressure. At a fixed downstream static pressure, the unit would leak the same amount of air, regardless of the amount of primary being delivered to the unit. At lower primary air flow rates and high downstream static pressures, leakage could be as high as 10%.

The terminal unit models developed in this study should provide researchers with accurate models that can be incorporated into building energy simulation tools to model the energy use of VAV systems with multiple terminal units. A user would need to “balance” the terminal units in the building simulation model. An SCR voltage would be assigned to each terminal unit to set the fan airflow. For the calculations for all simulations, these voltages would remain the same. The other variables in the VAV terminal unit models would then be applied in the simulation program. The downstream and upstream static pressures will be applied from the simulation calculations. For each step/iteration, most simulations calculate the primary airflow required to meet the space load. The inlet air differential pressure can be calculated using these primary airflow values and the Table A-1 in the appendix.

When using these models as a tool to predict performance, it is important to note that extrapolation of data points outside the range of experimentally determined values is not recommended. The response of the dependent variables, airflow and power, was statistically determined within the ranges of independent variables.

ACKNOWLEDGMENTS

This work was a part of a project funded by ASHRAE under RP-1292 and we would like to thank the project monitoring subcommittee of TC 5.3 and the manufacturers they represent for their support during the project. Several manufacturers donated terminal units for use in this study. Through cooperative ventures such as these, ASHRAE research funding can be utilized to the fullest. We appreciate the contributions from these industry leaders.

NOMENCLATURE

DP	=	pressure differential across the terminal unit, in. w.g.
P_{dwn}	=	downstream static pressure, in. w.g.
P_{iad}	=	pressure across inlet air differential flow sensor, in. w.g.

- P_{unit} = static pressure inside terminal unit, in. w.g.
- P_{up} = upstream static pressure, in. w.g.
- $Power_{fan}$ = power consumption of terminal unit fan, W
- Q_{fan} = amount of airflow through terminal unit fan, cfm
- $Q_{induced}$ = amount of airflow induced from plenum, cfm
- $Q_{leakage}$ = amount of airflow leaking from a terminal unit, cfm
- Q_{out} = amount of parallel terminal unit airflow output, cfm
- $Q_{primary}$ = amount of primary airflow, cfm
- S = damper setting, degrees (°)
- V = RMS average of SCR voltage output, V

REFERENCES

- ASHRAE. 2001. *ASHRAE Handbook—Fundamentals*. Atlanta: American Society of Heating, Refrigerating and Air-Conditioning Engineers, Inc.
- Furr, J., D.L. O’Neal, M. Davis, J. Bryant, and A. Cramlet. 2008a. Performance of VAV fan powered terminal units: experimental setup and methodology. *ASHRAE Transactions*, submitted for review.
- Furr, J., D.L. O’Neal, M. Davis., J. Bryant, and A. Cramlet. 2008b. Performance of VAV fan powered terminal units: experimental results and models for parallel units. *ASHRAE Transactions*, submitted for review.

Neter, J., M.H. Kutner, C.J. Nachtsheim, and W. Wasserman. 1996. *Applied linear regression models*. Chicago: Irwin, Inc.

Wendes, H. 1994. *Variable air volume manual*. Lilburn, GA: The Fairmont Press, Inc.

APPENDIX

The relationship between inlet air differential pressure and primary air entering the terminal unit can be approximated as linear over the ranges used in this study. This linear approximation is presented in Equation A.1, with the coefficients for each terminal unit presented in Table A-1.

$$P_{iad} = C_1 + C_2 Q_{primary} \quad (A.1)$$

Table A-1. Coefficients for Inlet Air Differential Sensor Approximation

Name	C_1 , in. w.g.	C_2 , in. w.g./cfm
P8A	-0.190	0.00109
P8B	-0.130	0.000749
P8C	-0.149	0.000816
P12A	-0.168	0.000438
P12B	-0.0991	0.000277
P12C	-0.109	0.000279

Performance of VAV Series Fan-Powered Terminal Units: Experimental Results and Models

James C. Furr

Dennis L. O'Neal, PhD, PE

Michael A. Davis

Fellow ASHRAE

John A. Bryant, PhD, PE

Andrew Cramlet

Member ASHRAE

Student Member ASHRAE

ABSTRACT

Empirical models of airflow output and power consumption were developed for series fan powered variable air volume terminal units at typical operating pressures. Terminal units with 8 in. (203 mm) and 12 in. (304 mm) primary air inlets from three different manufacturers were evaluated. Generalized models were developed from the experimental data with coefficients varying by size and manufacturer.

Fan power and airflow data were collected at downstream static pressures of 0.25 w.g. (63 Pa). Upstream static pressures ranged from 0.1 to 2.0 in w.g. (25 to 498 Pa). Data were collected at four different primary air damper positions and at four terminal unit fan speeds. Model variables included the RMS voltage entering the terminal unit fan, the inlet air differential sensor pressure, and the upstream static pressure.

In all but one of the VAV terminal units, the resulting models of airflow and power had R^2 values greater than 0.98. For the remaining unit, a faulty motor had been installed and shipped in the unit which prevented proper operation of the SCR. These models can be applied to HVAC simulation programs to model series fan powered VAV systems.

INTRODUCTION

Variable Air Volume (VAV) systems maintain comfort conditions by varying the volume of primary air that is delivered to a space. VAV terminal units that include a fan to improve circulation within a zone are called fan powered terminal units. These terminal units can draw in return air from the plenum space and mix it with primary air from the central Air Handling Unit (AHU).

When the fan is in the path of the primary airflow, the configuration is called a series terminal unit (Figure 1). During

normal operations, the terminal unit fan usually remains on except during un-occupied times in the zone. The controller will modulate the terminal unit damper in response to the control signals from the thermostat and the inlet air differential sensor. The inlet air differential sensor within the primary airstream allows the controller to maintain a consistent volume of airflow to the zone depending on the temperature setpoint.

The fans on these terminal units output a constant amount of air that does not vary with load because the downstream pressure is constant (Alexander and Int-Hout 1998). As a result, when the primary air damper closes, more plenum air is induced and recirculated into the space. When the signal from the air velocity sensor indicates that the primary airflow has reached a predetermined minimum (because of ventilation requirements), the damper will not close any more. If the space is still too cold, electric or hot water supplemental heat can be used to meet the thermostat setpoint. To allow for various fan airflows, the units are typically equipped with a silicon controlled rectifier (SCR) fan speed controller.

There is a need to develop a better understanding of systems using parallel and series fan powered VAV terminal units. To model a system properly, it is important to be able to characterize the individual terminal units. To date, there has been little work in this area.

The primary goal for this research was the development of empirical models of power and airflow output for series fan powered terminal units at typical operating pressures. Three manufacturers (labeled A, B, and C) provided series terminal units for this work. An experimental setup was developed and used to test the fan powered terminal units. An experimental protocol was developed and used for all tests. Statistical analyses of experimental data were performed and used to develop

James C. Furr is a thermal management engineer with Lockheed Martin, Fort Worth, Texas. **Dennis L. O'Neal** is Holdredge/Paul Professor and Head and **Andrew Cramlet** is a research assistant, Department of Mechanical Engineering, Texas A&M University, College Station, Texas. **Michael A. Davis** is a research engineer with and **John A. Bryant** is a visiting associate professor in the Department of Mechanical Engineering, Texas A&M University Qatar, Doha Qatar.

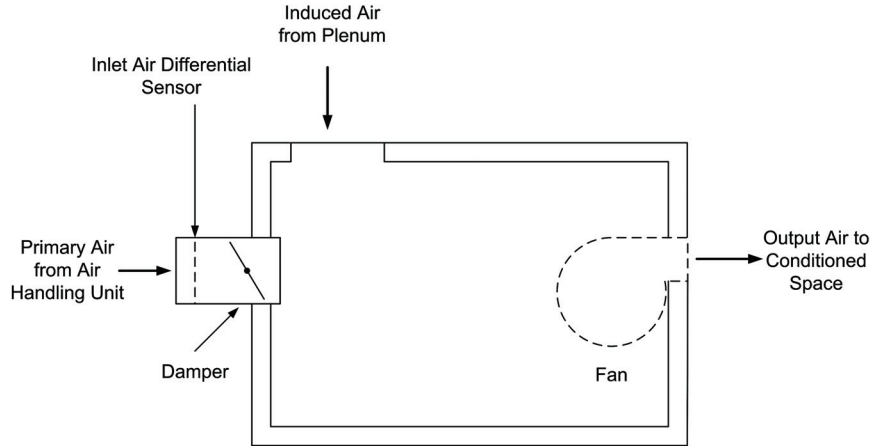


Figure 1 Series VAV fan-powered terminal unit.

generalized models that can be applied to the different manufacturers' terminal units. The units included three 8 in. (203 mm) and three 12 in. (304 mm) units. Manufacturer's A 8 in. unit had the designation S8A, manufacturer's B 12 in. unit was S12B, etc.

This paper is the third of three papers that describe the development of experimentally based models of VAV fan powered terminal units. The first paper (Furr et al. 2008a) described the experimental setup and methodology used to measure the performance of parallel and series fan powered units. That paper also described the small differences between the terminal units that included the rated power of the terminal unit fan, the style of the primary airflow damper, and the style of the backdraft damper. In the second paper (Furr et al. 2008b), the performance of six parallel fan powered terminal units from three manufacturers was measured and characterized.

DATA ANALYSIS METHODOLOGY

One goal of this research was to determine if a single generalized model could be used for all the series terminal units tested for a given size. Because of design differences in the units, the performances of the same sized units varied dramatically. Thus, no single model could be used to describe a given size unit. The models had the same form, but used different coefficients for the different sizes and manufacturers.

Variables were first identified that were expected to be significant in explaining fan airflow and power. Models were then developed by determining the most statistically influential independent variables using the F statistic. The variable with the largest F statistic was added first. This method of adding terms to the model was continued until no other variables added were significant, defined as when the variables' F statistic was below 4.0. Between each step, models were compared against each other according to their adjusted coefficient of determination, R^2_{adj} (Neter et al. 1996).

In developing the models for the series units, several variables were considered: the SCR voltage, inlet air differential pressure (P_{iad}), upstream pressure (P_{up}), and primary airflow

($Q_{primary}$). The models for all of the series terminal units were compared against each other. Any differences in terms included in the airflow or power models were investigated in an effort to create a single form model that would be applicable to all of the terminal units.

RESULTS AND MODELS

Fan Terminal Unit Airflow

The fans on the series units used centrifugal, forward-curved style fans. These fans were expected to follow typical fan curves and fan laws (ASHRAE 2001). The SCR voltage, upstream static pressure, and inlet air differential pressure were expected to be variables that could influence the capacity of the terminal unit fan.

SCR setting was a variable in the model that had to be quantified. Each SCR setting corresponded to a different fan speed. A simple experiment was conducted to determine the relationship between SCR setting and the speed of the fan. A tachometer was instrumented to an 8 in. (203 mm) parallel fan terminal unit from manufacturer A. Because the same motors and SCRs were used with the parallel and series terminal units, it was assumed that the relationship between SCR setting and fan speed would be the same for fans in both the series and parallel units. It would have been preferred to test the series units' fans, to verify this assumption. However, given that the fan in a series unit is inside the terminal unit, it would have been difficult to ensure a constant pressure difference across the fan so that the relationship between fan speed and SCR setting could have measured.

At several different voltage settings, the RPM of the fan was measured. During this testing, the upstream and downstream static pressures were maintained constant to eliminate the effects of pressure on the fan speed. A quadratic equation was fit to the data (Figure 2) and had a R^2 value of 0.999.

This test was conducted on two other terminal units, parallel terminal units P12B and P8C, which resulted in R^2 values of 0.994 and 0.997, respectively. Because of the high R^2

values for the variety of groups and sizes, it was assumed that a general quadratic relationship would remain true for all of the terminal units.

According to the fan laws, there should be a linear relationship between airflow and fan speed (ASHRAE 2001). Because a quadratic equation had been used to show the relationship between SCR voltage and fan speed, it was assumed that an equation of the same form could be used for the relationship between SCR voltage and fan airflow.

After this relationship was established, the other factors that were considered in the modeling of the air output of the fan were the pressures immediately upstream and downstream of the fan. Because the downstream static pressure was maintained at the same value for all tests, it was not used explicitly as an explanatory variable for the model. Another pressure that could influence the airflow output of the unit fan would be the pressure inside the terminal unit, immediately upstream of the fan, P_{unit} (Figure 3).

During normal operation, some air was always induced into the terminal unit. Thus, the static pressure within the series terminal unit was always sub-atmospheric but the pressure was not measured. In planning for the experiments, there did not appear to be a good way to instrument the terminal unit to measure this pressure accurately. After statistical analysis, it was determined that the pressure that the inlet air differential pressure, P_{iad} , was a suitable variable to include in the model

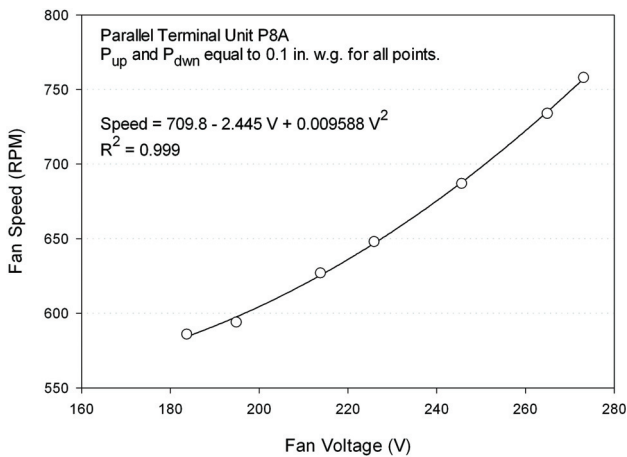


Figure 2 Effect of SCR voltage on fan speed for parallel terminal unit P8A.

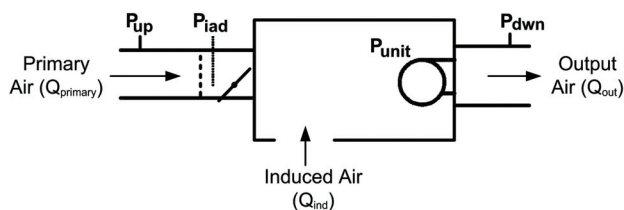


Figure 3 Series VAV fan-powered terminal unit with pressure measurement locations.

to estimate the influence of the internal terminal unit static pressure. For example, when an airflow model using V , V^2 , P_{iad} , and P_{up} was regressed for the series terminal unit S8C, the resulting F statistics for P_{iad} and P_{up} were 160 and 15, respectively. Because both F values were greater than 4.0 both variables could have been used in the model. However, the model using only V , V^2 , and P_{iad} for the S8C terminal unit obtained an R^2_{adj} value of 0.989. This model was deemed sufficient and in an attempt to maintain model simplicity, the variable P_{up} was not included in the airflow models for the series units. The resulting model for predicting the airflow in series terminal units was a function of the SCR voltage and the inlet air differential pressure.

Five of the six series terminal units had very similar results for outlet airflow as a function of inlet air differential pressure. Two samples are shown in Figures 4 and 5 for terminal units S8A and S12C, respectively. The gentle slopes of the lines indicate that airflow was only slightly dependent on P_{iad} . These results support the premise, found in literature (Alexander and Int-Hout 1998), that variations of upstream duct pressure, primary airflow, and damper position have little

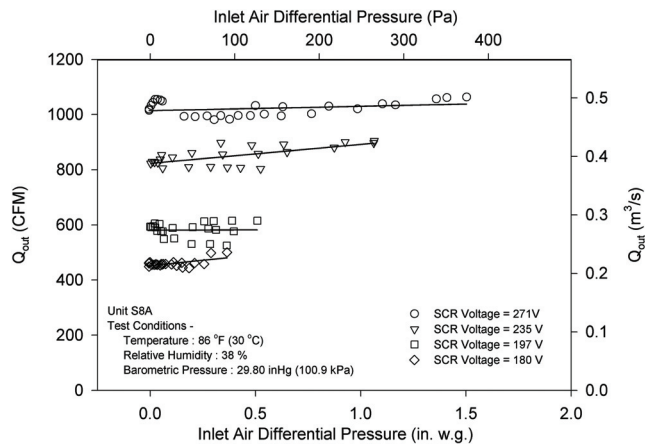


Figure 4 Fan airflow for series terminal unit S8A.

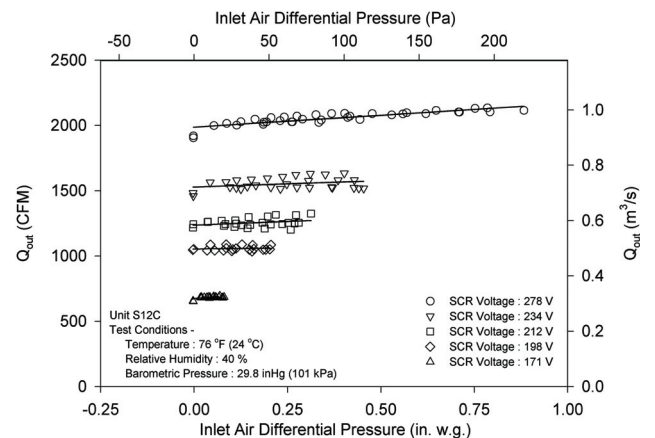


Figure 5 Fan airflow for series terminal unit S12C.

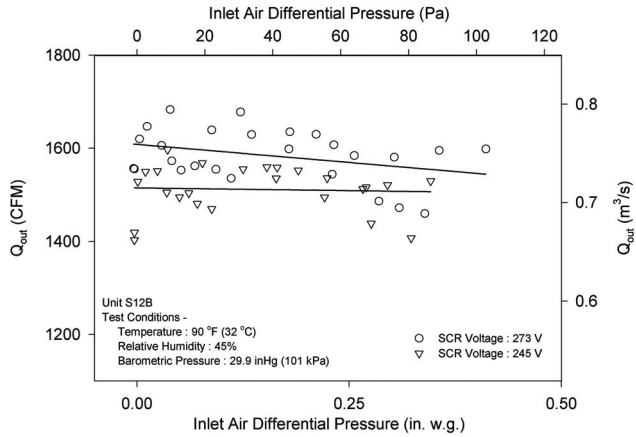


Figure 6 Fan airflow for series terminal unit S12B.

Table 1. Airflow Model Coefficients for Series Terminal Units

Name	C_1 , cfm	C_2 , cfm/ V^2	C_3 , cfm/ V	C_4 , cfm/in. w.g.	R^2_{adj}
S8A	-1776	-0.0228	16.49	0.0036	0.989
S8B	-1705	-0.0254	18.15	-0.0448	0.994
S8C	-1310	-0.0183	13.94	0.0677	0.997
S12A	-778.5	0.0091	6.918	0.0394	0.993
S12C	-1903	-0.0105	16.78	0.0812	0.990

Table 2. Airflow Model Coefficients for Series Terminal Unit S12B

Name	C_5 , cfm	C_6 , cfm/ V^2	C_7 , cfm/ V	C_8 , cfm/in. w.g.	R^2_{adj}
S12B	-925.7	2.68	-55.8	-293.2	0.688

effect on the pressure inside a series terminal unit, resulting in a fairly constant airflow. After a series terminal unit has been balanced for airflow, the air output of the series terminal unit should be relatively constant despite changes in the upstream conditions.

The airflow results from series terminal unit S12B showed much more scatter than the results from the other terminal units (Figure 6). After trouble shooting the unit and discussions with the manufacturer of this unit, the disparity was due to an incorrect fan motor installed and shipped in the unit. This motor prevented the SCR from working correctly: the full range of SCR settings on this unit only resulted in a difference of 30 V as compared to differences of over 100 V in the other units. The result was that there was no discernable distinction in airflow output for different SCR settings.

Analysis of the data from unit S12B showed that the quadratic relationship between the SCR voltage and fan output was not evident. After initially developing models that included V^2 and V , the F statistics were 0.04 and 0.22, respec-

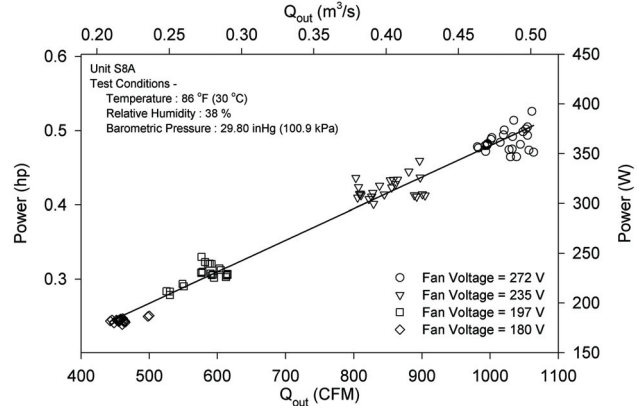


Figure 7 Fan power for series terminal unit S8A.

tively. A model developed using only V resulted in an F statistic of 34. Inclusion of the squared term was never significant. This was probably due to the SCR/motor combination not behaving as the ones in the other terminal units that were tested.

The fan terminal unit output airflow model in series fan terminal units is shown in Equation 1. The coefficients for each unit are presented in Table 1.

$$Q_{out} = C_1 + C_2 \cdot V^2 + C_3 \cdot V + C_4 \cdot P_{iad} \quad (1)$$

Equation 2 is the model to characterize series terminal unit S12B, which was determined to have a faulty motor. In this model, V captures the small effect that SCR setting has on the airflow output. P_{up} and P_{iad} were both included in this model, because their F values in the model were 88 and 83. Table 2 provides the coefficients for the model of this terminal unit.

$$Q_{out} = C_5 + C_6 \cdot V + C_7 \cdot P_{up} + C_8 \cdot P_{iad} \quad (2)$$

Power Model

Data analysis of the power data for each of the terminal unit fans revealed a common characteristic. In each of the units, there appears to be a linear response between power and fan airflow. Figures 7 and 8 show data for S8A and S12C, respectively. Because of this linearity, the resulting model to predict power maintained the same form as the model for fan airflow, and was a function of the SCR voltage and the inlet air differential pressure.

As mentioned in the previous section, terminal unit S12B produced inconsistent data from the others, possibly because of a malfunctioning SCR. Those results provided little difference in the airflow for the various SCR settings. In the analysis of the power data for this terminal unit (Figure 9), there was also little difference in power for the various SCR settings.

The fan power model for series fan terminal units, Equation 3, was a function of the SCR voltage and the inlet air

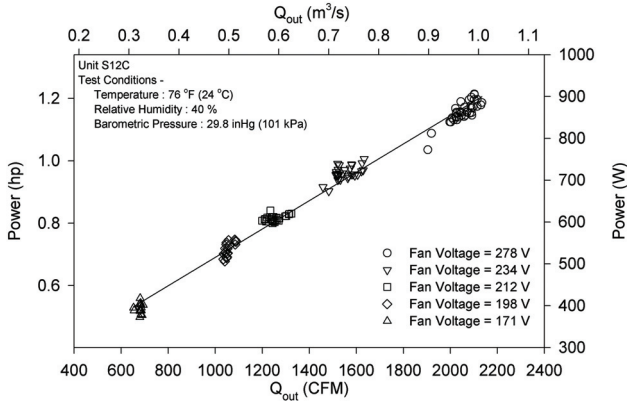


Figure 8 Fan power for series terminal unit S12C.

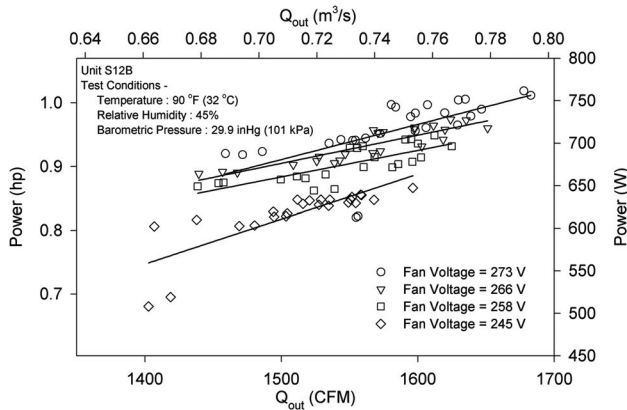


Figure 9 Fan power for series terminal unit S12B.

differential pressure. The coefficients for the various sizes and groups are presented in Table 3.

$$Power_{fan} = C_1 + C_2 \cdot V^2 + C_3 \cdot V + C_4 \cdot P_{iad} \quad (3)$$

Primary Airflow Model

As with the parallel terminal units, prediction of the primary airflow as a function of differential pressure across the units is needed to predict the upstream static pressure under a range of operating conditions for energy modeling purposes. The equations developed above allow prediction of the unit's outlet airflow and power. These equations did not include any variables that would allow for direct estimation of the upstream static pressure for operation of the terminal unit either with or without the operation of the fan.

The performance of the series terminal units was similar to that of the parallel units. The primary airflow showed little dependence on SCR voltage, but did vary with damper setting, S (in degrees), and pressure differential (DP) across the terminal unit. Sample plots of primary airflow for terminal units S8B and S12C are shown in Figures 10 and 11, respectively.

Table 3. Model Coefficients for Series Fan Power Model

Name	C_1 , W	C_2 , w/v ²	C_3 , w/v	C_4 , w/in. w.g.	R^2_{adj}
S8A	-732.7	-0.0114	7.13	-2.12	0.989
S8B	-595.7	-0.0111	6.96	-13.25	0.983
S8C	-455.5	-0.00817	5.32	1.91	0.994
S12A	-269.4	0.00854	1.80	19.05	0.997
S12B	125.9	0.00534	0.736	-16.36	0.870
S12C	-917.0	-0.0129	9.86	97.73	0.990

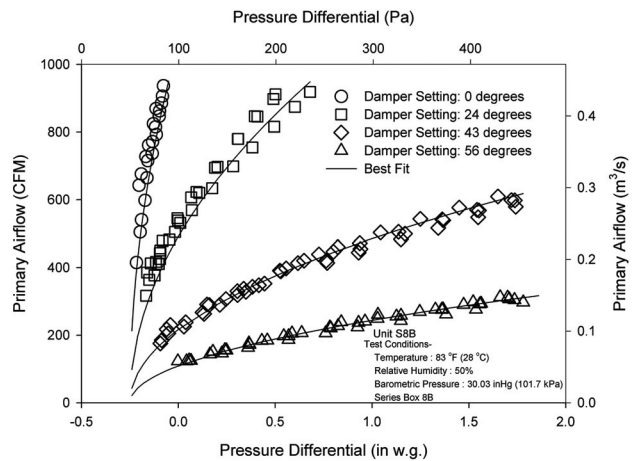


Figure 10 Primary airflow as a function of inlet damper setting and pressure differential across the S8B terminal unit.

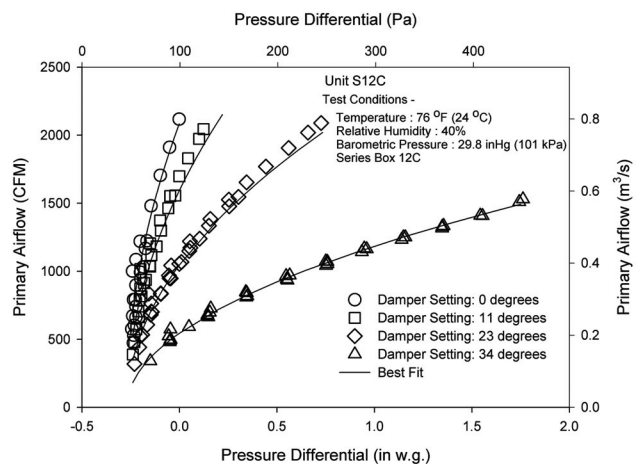


Figure 11 Primary airflow as a function of inlet damper setting and pressure differential across the S12C terminal unit.

Both figures showed that the primary airflow varied with approximately the square root of the pressure differential across the terminal unit at a given damper setting.

Table 4. Model Coefficients for Primary Airflow in Series Terminal Units

Name	C ₁	C ₂	C ₃	R ²
S8A	1644	-0.019	8.46E-05	0.970
S8B	2126	-0.025	0.00	0.987
S8C	2136	-0.032	0.00	0.920
S12A	4349	-0.022	0.00	0.963
S12B	5902	-0.031	0.00	0.934
S12C	4021	-0.019	9.5E-05	0.964

For the series units, zero flow was at approximately -0.25 in. water (62 Pa). The data from the series terminal units were fit to a similar model to that of the parallel, except the pressure differential term (DP) had to be offset so the flow would be zero for negative DP. The offset that provided the best correlations was a value of 0.27 in. water (67 Pa). The equation that was fit to the primary airflow is shown in Equation 4. Table 4 provides the coefficients and R-Squared values for the six series terminal units. All units had R-Squared values above 0.9.

$$Q_{primary} = C_1(1 + C_2^*S + C_3^*S^2)^*(DP + 0.27)^{0.5} \quad (4)$$

SUMMARY AND CONCLUSIONS

Characterizing the performance of series terminal VAV units required developing models for the primary and output airflow and the fan power. Comparison of the statistics for the airflow model shows that it accounts for 99% of the variation in airflow for five of the six terminal units. The exception was series terminal unit S12B. In this case, it was not possible to develop a model that could adequately describe the response to the airflow variable. The model did not account for 31% of the variation in the data. This variation appeared to be the result of a faulty fan motor.

The power model had R²_{adj} statistics greater than 98% for five of the six terminal units. The lowest R²_{adj} value of 0.870 was for the series S12B terminal unit, which also had the lowest R²_{adj} for the airflow model. This is the same unit which had the lowest of the six R²_{adj} values in the airflow model, mentioned above.

These units were obtained from several manufacturers and in different sizes in an effort to get a “snapshot” of units typically installed in the field. Unfortunately, this sample of six terminal units had one unit (S12B) that would be expected to perform poorly in the field because of problems with its fan motor. The terminal unit models developed in this study should provide researchers with accurate models that can be incorporated into building energy simulation tools to model the energy use of VAV systems with multiple terminal units. An analyst would need to “balance” the terminal units in the building simulation model. A SCR voltage would be assigned to each terminal unit to set the fan airflow. For the calculations for all simulations, these voltages would remain the same. The

other variables in the VAV terminal unit models would then be applied in the simulation program. The downstream and upstream static pressures will be applied from the simulation calculations. For each step-iteration, most simulations calculate the primary airflow required to meet the space load. The inlet air differential pressure can be calculated using these primary airflow values and the Table A-1 in the appendix.

When using these models as a tool to predict performance, it is important to note that extrapolation of data points outside the range of experimentally determined values is not recommended. The response of the dependent variables, airflow and power, was only statistically determined within the ranges of independent variables.

ACKNOWLEDGMENTS

This work was a part of a project funded by ASHRAE under RP-1292. We would like to thank the project monitoring subcommittee of TC 5.3 for their suggestions and advice throughout the duration of this project. We would also like to thank the three manufacturers who provided the terminal units for this project.

NOMENCLATURE

P_{dwn}	=	downstream static pressure, in. w.g
P_{iad}	=	pressure across the inlet air differential flow sensor, in. w.g.
P_{unit}	=	static pressure inside terminal unit, in. w.g.
P_{up}	=	upstream static pressure, in. w.g.
$Power_{fan}$	=	power consumption of terminal unit fan, W
$Q_{induced}$	=	amount of airflow induced from plenum, CFM
Q_{out}	=	amount of terminal unit airflow output, CFM
$Q_{primary}$	=	amount of primary airflow, CFM
S	=	damper setting, degrees
V	=	RMS average of SCR voltage output, V

REFERENCES

- Alexander, J. and D. Int-Hout. 1998. Assuring zone IAQ. White paper. Titus. Retrieved Sept. 15, 2005. http://www.titus-hvac.com/tech_papers.asp.
- ASHRAE. 2001. *ASHRAE Handbook—Fundamentals*.
- Furr, J., D.L. O’Neal, M. Davis., J. Bryant, and A. Cramlet. 2008a. Performance of VAV fan powered terminal units: experimental setup and methodology. *ASHRAE Transactions*, submitted for review.
- Furr, J., D.L. O’Neal, M. Davis., J. Bryant, and A. Cramlet. 2008b. Performance of VAV fan powered terminal units: experimental results and models for parallel units. *ASHRAE Transactions*, submitted for review.
- Neter, J., M.H. Kutner, C.J. Nachtsheim, and W. Wasserman. 1996. *Applied linear regression models*. Chicago: Irwin, Inc.

APPENDIX

For this study, the relationship between the inlet air differential pressure and the amount of primary air entering the terminal unit was assumed to be linear over the ranges measured. This linear approximation is presented in Equation A.1, with the coefficients for each terminal unit presented in Table A-1.

$$P_{iad} = C_1 + C_2 \cdot Q_{primary} \quad (A.1)$$

Table A-1. Coefficients for Inlet Air Differential Sensor for Equation (A.1)

Name	C_1 [in. w.g.]	C_2 [in. w.g./CFM]
S8A	-0.204	0.00111
S8B	-0.140	0.000776
S8C	-0.183	0.000922
S12A	-0.162	0.000409
S12B	-0.129	0.000306
S12C	-0.158	0.000351

Experimental Verification of a Three Zone VAV System Model Operating with Fan Powered Terminal Units

John A. Bryant, PhD, PE
Member ASHRAE

Dennis L. O'Neal, PhD, PE
Fellow ASHRAE

Michael A. Davis
Associate Member ASHRAE

Andrew Cramlet

This paper is based on findings resulting from ASHRAE Research Project RP-1292.

ABSTRACT

This paper outlines the methodology used to represent and verify a simplified engineering model of a VAV system with fan powered terminal units serving a three zone building. The building loads were generated for five weather diverse locations in the United States and normalized for peak and zone conditions. Experimental results from a previous study were used to build models of the individual fan powered terminal units. The resulting system model was verified against results from an experimental test stand. A test stand was configured to allow simultaneous testing of up to three manufacturer's fan powered terminal units. Typical 8 inch (200 mm) and 12 inch (300 mm) terminal units were evaluated. Results from the test stand verified the model predicted values. The predicted results were well within experimental measurement uncertainty. The verified model provides the engineering community with a tool to expand existing VAV system simulation and energy analysis capabilities.

INTRODUCTION

Variable Air Volume (VAV) systems maintain comfort by varying the amount of primary air delivered to conditioned zones in a building. Primary components for VAV systems typically include a fan and cooling coil that supply pressurized and conditioned air to the primary distribution ductwork. This fan is referred to as the "primary" fan and the conditioned air is the "primary" air. A VAV terminal unit regulates the amount of primary air supplied to the zone in response to zone cooling or heating loads.

This study focused on the operation of a Single Duct Variable Air Volume (SDVAV) system using Fan Powered Terminal Units (FPTU). Figure 1 shows a SDVAV system using FPTUs serving five zones in a building. The primary fan pressurizes the duct system and controls static pressure supplied at each FPTU. Static pressure control for the primary fan is typically governed by the zone with the greatest need for cooling (zone cooling load).

There are two common fan powered terminal units - Series and Parallel. Both of these FPTU types have small fans built into the terminal unit. When the terminal unit fan is operating it draws air from the zone return air plenum and supplies the space with a mixture of cool primary and warm plenum (return) air.

Series FPTUs have a small internal fan that works in series with the primary system fan. Conversely, the parallel FPTU has its fan arranged to operate parallel to the primary fan. The control of either of these units is different too. Series units typically run continuously, supplying a constant volume of air to the space. Even if the primary VAV inlet valve to the FPTU is at minimum, the series unit still delivers a fixed volume of air. Minimum inlet valve setting also corresponds to minimum cooling load or initiation of heating mode. A series FPTU will first use warmer plenum air for heating through an induction port built into the unit. If additional heat is needed for the zone, an electric or hot water reheat coil at the discharge of the FPTU will be activated. The parallel FPTU fan operates only if the zone it serves needs heat. In heating mode, the parallel FPTU first draws warmer air from the return plenum and if the zone controller continues to need heat, reheat (either electric or hot water) can be added to the airstream.

John A. Bryant is an associate professor in the Mechanical Engineering Program and **Michael A. Davis** is a research engineer at the Texas A&M University at Qatar. **Dennis L. O'Neal** is a professor and head of the Mechanical Engineering Department and **Andrew Cramlet** completed graduate studies in the Mechanical Engineering Department at Texas A&M University in College Station, TX.

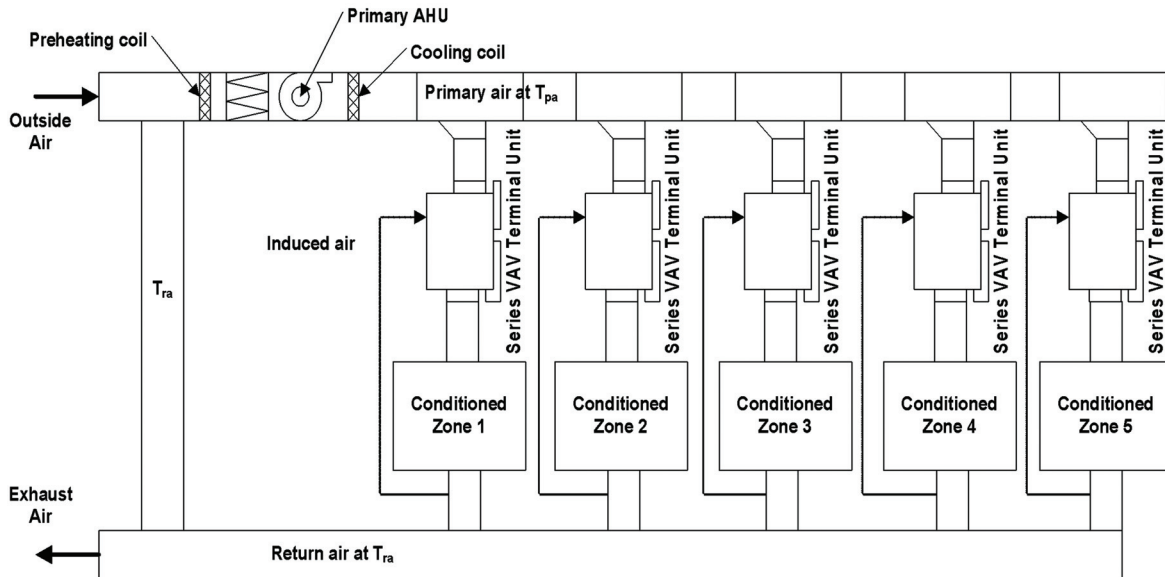


Figure 1 Diagram of a five zone single duct VAV system using fan-powered terminal units.

Experimental work on FPTUs resulted in the development of characteristic performance models for airflow, power, and pressure drop through the FPTU (Furr et al. 2008).

This paper will focus on the methodology used to model a three zone VAV system operating in a building and the comparison of that model with experimental results from laboratory testing of a complete three zone VAV system operating with fan powered terminal units.

MODEL RATIONALE

For this study, VAV FPTUs were supplied from three different manufacturers. The FPTU sizes and ratings were selected by the manufacturers to represent the most common units typically used in current VAV system design. The manufacturers supplied one 8 inch (203 mm) and one 12 inch (305 mm) size in each of the series and parallel FPTUs. A three-zone VAV system configuration evolved from this selection of FPTUs because incorporating more zones would only have duplicated the use of a particular FPTU model.

Figure 2 shows the layout of a generic three zone office building model used to generate heating and cooling load data. The development and application of the building model will be described in the following section.

The building model consisted of commonly defined zones with exterior exposures covering a range of loads resulting from weather and solar effects. To match the three zone VAV system configuration, the North, South, East, and West zones were combined into North – East and South – West zones. The interior, or core zone, would be dominated by internal thermal loads. The building was a single story rectangular structure with a footprint of 122.5 x 122.5 ft (37.3 x 37.3 m). The perimeter zones had 1,612 ft² (149.8 m²) of floor area and 50% glass

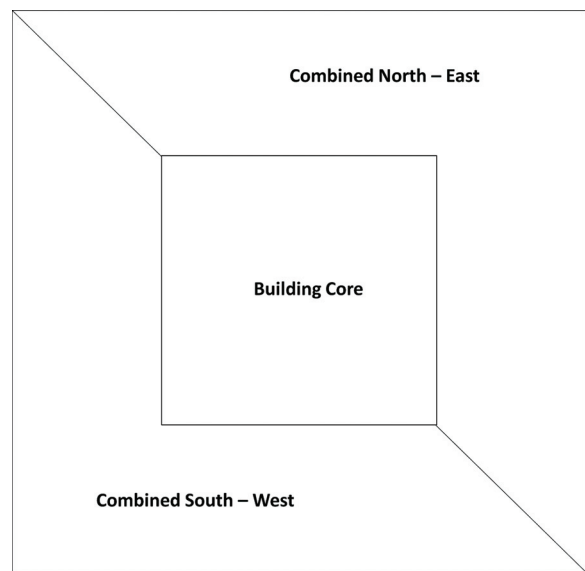


Figure 2 Diagram of the building floor plan used as the basis for the DOE-2 loads model.

walls while the core zone had 8,556 ft² (794.9 m²). The perimeter zones had walls with a U-Factor of 0.46 Btu/hr/°F/ft² (2.6 W/m²/°C) and a solar heat gain coefficient of 26%. The wall insulation was R-13 (2.6 m²K/W) and the roof insulation was R-15 (2.64 m²K/W). The cooling loads due to people in the building were calculated using a factor of 275 ft² (25.5 m²) per person. The lighting and equipment loads were 1.3 W/ft² and 0.75 W/ft² (14 W/m² and 8.1 W/m²) respectively.

The building was operated on a typical office schedule for the entire year. Hourly sensible and latent space loads were calculated for all zones for the entire 8,760 hours in a year using TMY weather data for five locations: Chicago, Houston, New York, Phoenix and San Francisco (NREL 1995). These climates were chosen because of the variety in range of peak summer and winter ambient temperatures, the range of latent loads during the cooling months, and number of hours in cooling or heating mode during the year.

Figure 3 shows the numbers of hours at an average temperature over the course of a year for each city. Each city shows that a significant number of hours in the year are at temperatures other than peak heating or cooling temperatures. The large variation in high and low temperatures, time spent at given temperatures (cooling or heating loads), and span of temperature extremes are evident for these cities. A building “moved” to each of these geographical locations would have significantly different heating and cooling load profiles. The load variations represented with these locations would permit complete characterization of the three zone VAV model under different operating conditions.

NORMALIZING THE LOADS

For comparisons to be made between the VAV systems with either series or parallel FPTUs, it was necessary that the system be subjected to the same cooling and heating load profiles. The space loads generated by the building model did not exactly match the capacities of the series or the parallel fan powered terminal units in either the 8 inch (200 mm) or 12 inch (300 mm) sizes. Each size/manufacturer had different primary air flow characteristics and as such had different rated cooling capacities. If a system designer were to select the proper FPTUs for a system operating in Houston, different units would likely have to be selected to operate for the same system operating in Phoenix or New York. To facilitate comparison of

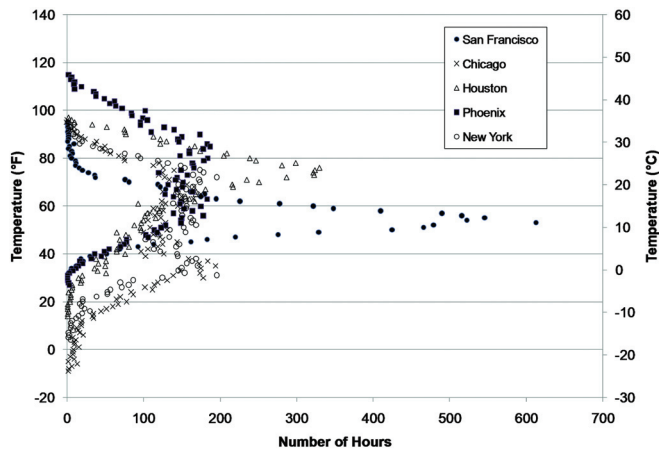


Figure 3 Number of hours at each temperature for five locations used to generate building load data.

VAV systems in this study, the VAV system had to be able to “move” from one city to another.

Hourly cooling and heating loads for the three zone building were used to build load profiles for each zone at each city location. Hourly load profiles as a fraction of the peak load for a given hour and location were obtained by normalizing each zone load as shown in Equation 1,

$$\text{Normalized Load}_{\text{hr } 10, \text{ New York}} = \frac{\text{Peak Load}_{\text{hr } 10, \text{ New York}}}{\text{Peak Load}_{\text{New York}}} \quad (1)$$

Figure 4 shows a 24 hour normalized load profile for the South – West zone for each of the cities. Using the normalized profiles, a zone load could be scaled to the peak cooling capacity of the VAV terminal unit that was selected to handle a particular zone.

This technique allowed modeling of the operation of the facility at various geographic weather locations while maintaining the peak cooling loads within the capacity of the selected FPTU. This method also eliminated any bias in the simulation results if the VAV terminal units were either over or undersized when moved to different geographic locations.

THREE ZONE BUILDING MODEL

A three zone model was used for both the engineering model and experimental portion of this study. The load calculation process for each of the zones was as follows:

1. Add the hourly sensible and latent load from each zone and average the respective loads.
2. Repeat the first step for all hours during the year.
3. Divide all hourly values by the maximum value to normalize the load profile for the entire year (using Equation 1).

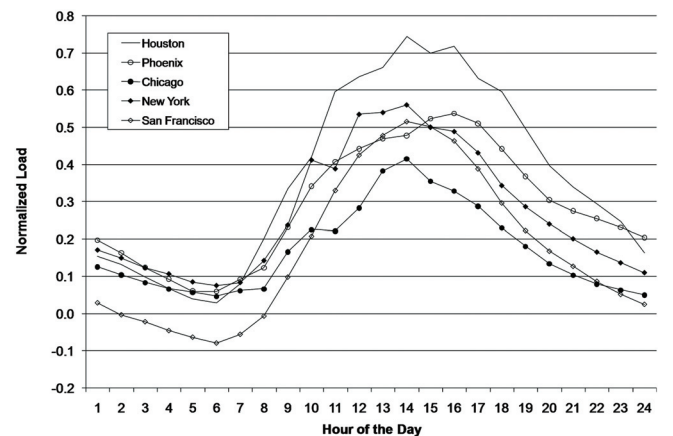


Figure 4 Normalized load profiles for the south – west zone at five different city locations.

The combined loads for the three zone model were calculated only for the Houston location because of the high percentage of yearly operating hours in the cooling mode with high coincident latent load relative to the other geographical locations.

THREE ZONE TESTING POINTS

The Houston load data were reviewed and specific times during the year were selected as the operating points to be used with the experimental apparatus to verify the three zone model. The Houston data showed distinct variation in cooling and heating loads during the course of the year for the combined South/West and Core zone. Transitional periods where the interior space loads shift from predominantly cooling/heating to heating/cooling are also present in the Houston South/West zone data. This type of load profile causes a VAV system to switch from cooling to heating in a relatively short time span. This system behavior was important to include in the VAV system model and in the verification testing. As expected for an office building, the Houston Core zone was very consistent in load and was predominantly cooling year-round.

PRIMARY SYSTEM AND FPTU MODELS

The three zone system model was used to predict the operation of a VAV system and to develop a matrix of test points for the experimental setup. The experimentally measured values would then be compared to the predicted (model) values. This verification process ensured that the engineering system model could closely predict values obtained from a system operating under the same conditions. If the system model and the measured values did not agree, then adjustments could be made to the model to correct any calculation errors or improper assumptions.

Figure 5 shows a model flow diagram of a three zone single duct VAV system model using fan powered terminal units. Energy and mass balances were the primary engineering tool used to build the VAV system model. The system simulation procedure began with the calculation of the zone level conditions (Conditioned Space). Once the zone calculations were completed, the Return Air calculations were performed. The Mixed Air conditions after the introduction of Fresh Air were evaluated next and then the Preheat Coil conditions for the Primary Fan were calculated. Following the Primary Fan, the entering and leaving Cooling Coil conditions were calculated. The properties of the air leaving the primary Cooling Coil were assumed to be the same as the primary air entering the VAV terminal unit. The engineering model was designed to mimic the behavior of a three zone VAV system. It had to predict the upstream static pressure, down stream static pressure, primary air flow, and induced air flow for a known space load at the FPTU as well as total VAV system response to these zone loads.

The VAV FPTU inlet valve position also had to be predicted by the model for a given set of duct conditions. It would not have been possible to verify the accuracy of the engineering model unless the upstream static pressure and the flow associated with the VAV valve position were accurately modeled. The details of the calculation procedures describing the VAV valve position control as well as all other primary VAV system calculations may be found in Davis et al. (2009).

THREE ZONE TEST STAND

A three zone system was designed and constructed to support an air distribution system consisting of three VAV zones. The model, as previously described, had been used to develop the testing points for use in the experimental test stand. A diagram of the system is shown in Figure 6. The diagram shows the test stand with a primary air plenum supplying air to three separately controllable duct systems which in turn, served three zones.

The sheet metal plenum supplying primary air to the three zones was connected to the primary air plenum of an 80-ton (281 kW) packaged rooftop air conditioner. The main fan for the packaged rooftop unit served as the primary supply air fan for the test stand.

Each of the three zones was connected to the primary air plenum with round sheet metal ducts. A butterfly damper was located at the connection point between the primary air

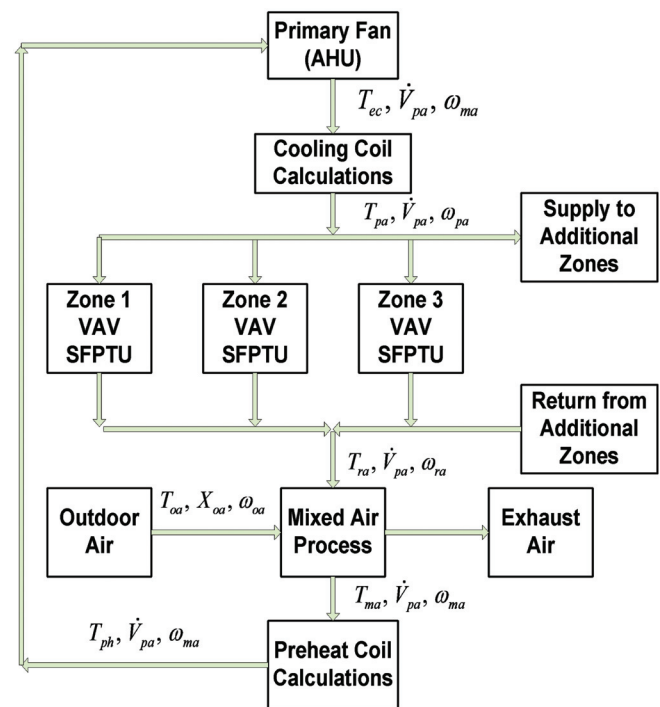


Figure 5 Block diagram of a three zone single duct VAV system using fan powered terminal units.

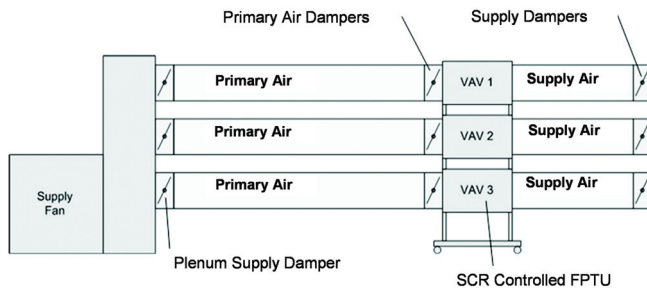


Figure 6 Diagram of the three zone test stand.

plenum and the zone primary air duct. This damper was used to control the upstream static pressure supplied to each zone.

The supply duct consisted of rectangular sheet metal terminated at a supply register with an integrated opposed blade damper that was used to control the downstream static pressure. The speed of the terminal unit fans was controlled by adjusting a silicon controlled rectifier (SCR). Another actuator was used to adjust the SCR potentiometer to set the fan motor speed.

The entire setup was controlled by an off-the-shelf control system of a type typically used in building control applications. The operator of the test stand adjusted the actuator settings of each of the zones by issuing commands directly through the control system console. When a test was conducted, the actuators at each position in the test stand were set to control values pre-determined by the three zone model. Figure 7 shows the completed test stand.

THREE ZONE TEST MATRIX

A test matrix was developed that identified the critical test conditions for peak cooling and heating loads as well as moderate operating conditions expected in the spring and summer. The matrix supplied operational points for use in the experimental three zone system test stand. Normalized hourly load profiles were used to develop a test plan for the various FPTU sizes. The four daily profiles selected for testing were January 4, April 5, July 6, and September 28. These profiles were considered most likely to result in the operation of the VAV terminal units over their full range. The final normalized total hourly graph for these dates in Houston is shown in Figure 8.

After the operating load points were selected, the settings to be used for the test stand were determined for the FPTUs. The units were set up based on the peak cooling capacity of the terminal unit and the peak cooling load of the zone. Using the normalized loads that had been scaled to the capacity of the terminal unit, the test stand settings were established using the three zone series terminal unit model.

Table 1 shows the test stand control system and duct settings for each hour selected as a test point. The unit designa-

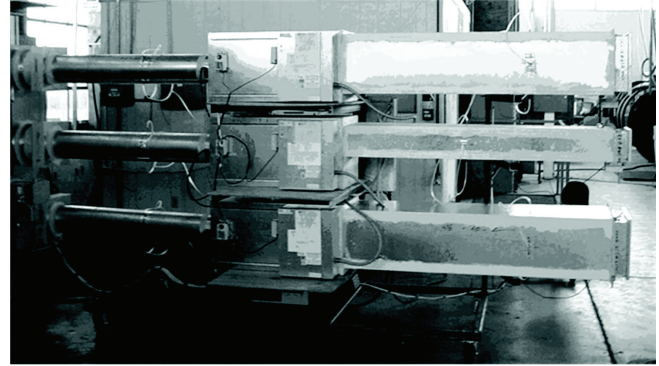


Figure 7 Completed test stand with three series FPTUs mounted for evaluation.

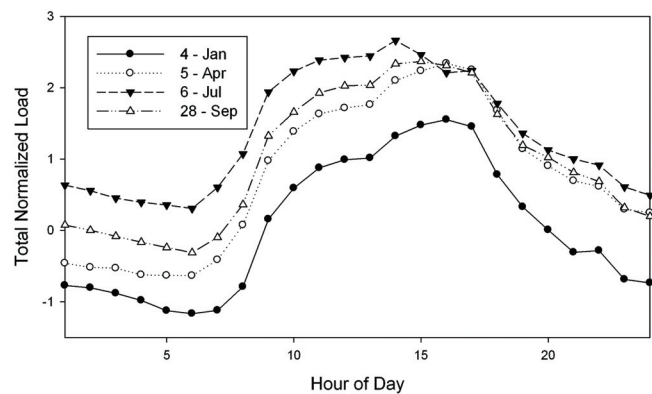


Figure 8 Hourly normalized daily load profiles selected from annual loads.

nation “S12C, S12B, and S8C” refer to a series FPTU from manufacturers B and C, and in 12 and 8 inch (200 and 300 mm) sizes. Note that the values shown in Table 1 are “predicted” values. That is, these are the values that resulted from the three zone engineering model evaluated at the specified zone conditions.

For example, the model predicts that for the load and system to be satisfied at 10am in the morning on July 6 in Zone 2 using FPTU S12B, primary static pressure must be 0.10 in.wg (24.9 Pa), the primary air damper control voltage must be 3.7 Vdc, the SCR control voltage is set at 277 Vac, and the downstream static has to be 0.25 in.wg (62.2 Pa).

The test stand was operated at the conditions outlined as shown in Table 1 to replicate the model parameters. The resulting discharge air temperature, FPTU power, and downstream static pressure data were recorded for comparison to the engineering model. This testing sequence was repeated for three other seasonal representative loads as shown in Figure 8.

**Table 1. FPTU Test Stand Settings for a July 6 Operating Profile—
Downstream Static held at 0.25 in. w.g. (62.2 Pa) and SCR held at 277 Vac**

Hour	Zone 1 – S12C		Zone 2 – S12B		Zone 3 – S8C	
	Primary Static, in.w.g. (Pa)	Primary Air Damper, Vdc	Primary Static, in.w.g. (Pa)	Primary Air Damper, Vdc	Primary Static, in.w.g. (Pa)	Primary Air Damper, Vdc
8	0.10 (24.9)	3.672	0.10 (24.9)	4.4	0.10 (24.9)	7.1
9	0.10 (24.9)	2.188	0.10 (24.9)	4.4	0.10 (24.9)	7.1
10	0.10 (24.9)	1.406	0.10 (24.9)	3.7	0.10 (24.9)	6.5
15	0.14 (34.9)	0.313	0.14 (34.9)	3.2	0.14 (34.9)	3.4
16	0.15 (37.4)	0.273	0.15 (37.4)	3.3	0.15 (37.4)	3.2
17	0.10 (24.9)	2.813	0.10 (24.9)	3.6	0.10 (24.9)	3.6

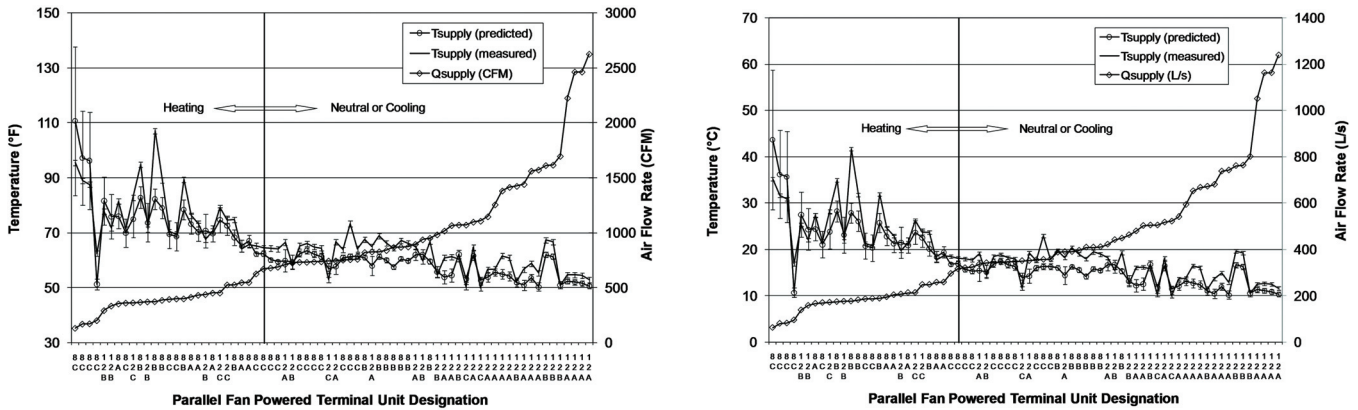


Figure 9 Parallel VAV FPTU supply temperature data and airflow relationship for model vs. experimental operation: (a) traditional units and (b) SI units.

THREE ZONE MODEL VERIFICATION AND RESULTS

The data gathered using the three zone test stand were used to perform the verification analysis of the three zone engineering model. Measured values of upstream static pressure, downstream static pressure, FPTU flow sensor pressure, primary air damper position, and SCR voltage were used in the three zone engineering model to generate a predicted supply air temperature (T_{supply}). The predicted supply air temperatures were then compared to the actual measured supply temperatures from the test stand. Figures 9a and 9b show test data for parallel VAV FPTUs where data are shown from low to high airflow rates against predicted and measured T_{supply} . This figure shows that the uncertainty in the predicted T_{supply} is quite high for these units when they are operating at low airflow or primarily heating (low airflow) conditions. Throughout the “neutral” or cooling range of operation the test stand data agrees very with the engineering model predicted supply temperatures with uncertainty bands in the predicted

temperature often overlapping the measured quantity. A detailed development of the uncertainty in the model predicted supply temperatures is given in Appendix A. The predicted supply temperature from the FPTU into a given zone is a function of the plenum supply temperature, zone room temperature, primary air flow into the FPTU, FPTU fan flow, and fan power used at the FPTU. Each of these have an associated uncertainty that show in the total propagated uncertainty for T_{supply} . The test stand T_{supply} measurement was an absolute measurement with an uncertainty of $\pm 0.7^\circ\text{F}$ ($\pm 0.4^\circ\text{C}$).

SUMMARY AND CONCLUSIONS

Figure 10 shows the data grouped for the Parallel FPTU type and manufacturers that were used in this study. The largest spread in the model’s T_{supply} uncertainty occurred only at high supply air temperatures which are typically at the unit’s lowest airflow rates.

This is an expected result as uncertainty in airflow measurements increases with decreasing airflow (uncertainty

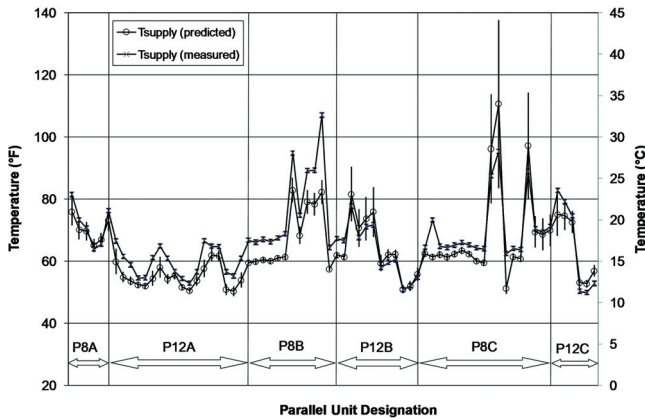


Figure 10 Predicted vs. measured supply temperatures for parallel VAV terminal units.

equations in Appendix A show a dominant airflow term in the denominator). As stated earlier, a typical VAV system only operates at design conditions a few hours out of the entire year. That type of operation is also the only time the system would be at maximum airflow. The majority of operation for these systems is somewhere in-between the maximum and minimum airflow for the FPTU.

The results shown in Figure 11 confirms the validity of the model. The percentage error was calculated between $T_{supply, measured}$ and $T_{supply, predicted}$ for the range of tested air flow rates. The average percentage error was +4.5%. That is, the model under predicts the T_{supply} by about 4.5% compared to actual laboratory measurements.

The slight positive bias in the percentage error could be because of the constant value used for the specific heat of air in the model energy calculations (Davis et al 2009).

A Student-t test assuming equal variances was conducted on the T_{supply} model and experimental data to verify the claim that the model is not statistically different from the experimental temperature values. The results of the Student-t test showed that at an alpha of 0.05, the Null Hypothesis was valid. That is, that there was no statistical difference between the two temperature data sets. Similar results were found for the Series units used in this study.

These results provided verification of the VAV FPTU model described in this paper and the basic three zone VAV model can now be expanded and more complex systems modeled with a high degree of confidence.

ACKNOWLEDGMENTS

This work was a part of a project funded by ASHRAE under RP-1292 and we would like to thank the project monitoring subcommittee of TC 5.3 and the manufacturers they represent for their support during the project. Several manufacturers donated terminal units for use in this study. Through cooperative ventures such as these, ASHRAE research fund-

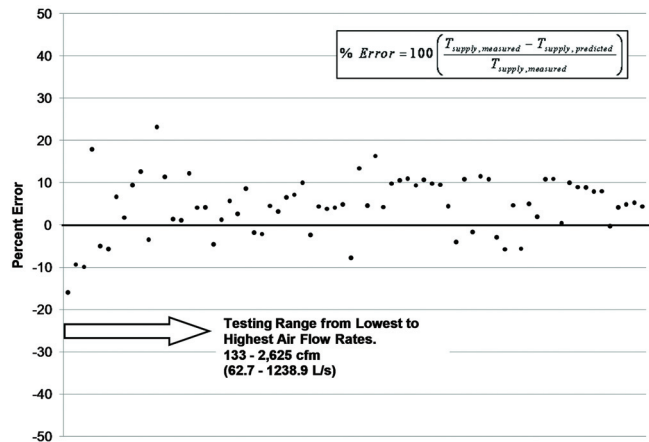


Figure 11 Percentage error for measured vs. predicted supply air temperatures.

ing can be utilized to the fullest. We appreciate the contributions from these industry leaders.

REFERENCES

- ASHRAE. 1996. *ANSI/ASHRAE Standard 130, Methods of Testing for Rating Ducted Air Terminal Units*. Atlanta: American Society of Heating, Refrigerating and Air-Conditioning Engineers, Inc.
- Davis, M., Bryant, J., and O’Neal, D.L. 2009. Modeling the Performance of Single-Duct VAV Systems that use Fan Powered Terminal Units (RP-1292). *ASHRAE Transactions* 115(1).
- Furr, J., O’Neal, D.L., Davis, M., Bryant, J., and Cramlet, A. 2008. Performance of VAV Parallel Fan-Powered Terminal Units: Experimental Results and Models (RP-1292). *ASHRAE Transactions* 115(1).
- NREL. 1995. User’s Manual for TMY2s (Typical Meteorological Years), NREL/SP-463-7668, and TMY2s, Typical Meteorological Years Derived from the 1961-1990 National Solar Radiation Data Base. Golden, CO: National Renewable Energy Laboratory.

APPENDIX A

For a FPTU in the fan “on” condition, Equation A1 gives an expression for the Supply Temperature (T_{supply})

$$T_{Supply} = \frac{Q_P T_P + Q_F T_R + \frac{3.412 P_{Fan}}{1.08}}{Q_P + Q_F} \quad (A1)$$

Equation A2 is the uncertainty (see Kline et al. 1953) in the Supply Temperature (T_{supply}) following from Equation A1 for an FPTU in the fan “on” condition:

$$uT_s = \left[\left(\left(\frac{T_P}{Q_P + Q_F} - \frac{Q_P T_P + Q_F T_R + 3.16 P_{Fan}}{(Q_P + Q_F)^2} \right) uQ_P \right)^2 + \left(\frac{Q_P}{Q_P + Q_F} uT_P \right)^2 + \left(\left(\frac{T_R}{Q_P + Q_F} - \frac{Q_P T_P + Q_F T_R + 3.16 P_{Fan}}{(Q_P + Q_F)^2} \right) uQ_F \right)^2 + \left(\frac{Q_F}{Q_P + Q_F} uT_R \right)^2 + \left(\frac{3.16}{Q_P + Q_F} uP_{Fan} \right)^2 \right]^{1/2} \quad (A2)$$

- uT_s = uncertainty in estimated supply temperature
 T_P = measured plenum supply temperature (also referred to as T_{supply})
 uT_P = uncertainty in plenum supply temperature (assumed to be $\pm 0.7F$)
 T_R = measured room temperature
 uT_R = uncertainty in room temperature (assumed to be $\pm 0.7F$)
 Q_P = measured Primary air flow rate into the FPTU
 Q_F = measured Fan air flow rate
 P_{Fan} = power used by the FPTU fan motor
 uQ_P = uncertainty in primary air flow, see equation (A4)
 uQ_F = uncertainty in FPTU fan air flow

Total propagated uncertainty would then be expressed as $T_s \pm uT_s$.

The expression for when the FPTU is in the fan "off" condition is given as

$$T_s = T_P + \frac{3.412 P_{Htr}}{1.08 Q_S} \quad (A3)$$

Propagated uncertainty in T_{supply} for this case is given by

$$uT_s = \left[(uT_P)^2 + \left(\frac{3.16 uP_{Htr}}{Q_S} \right)^2 + \left(\frac{3.16 P_{Htr} uQ_S}{Q_S^2} \right)^2 \right]^{1/2} \quad (A4)$$

A previous study generated correlating equations for use with the parallel fan powered terminal units used in this study (Furr 2007). Uncertainty for the flow in these units was estimated using these correlations and, depending on the unit, the uncertainty equation is as follows.

$$uQ_P = \left[\left((C1(1 + C2 \times S + C3 \times S^2)(P_{up} - P_{dn})^{1/2}) uDmpr \right)^2 + \left(\left(0.5 C1 \left(\frac{1 + C2 \times S + C3 \times S^2}{(P_{up} - P_{dn})^{1/2}} \right) \right) uP_{up} \right)^2 + \left(\left(-0.5 C1 \left(\frac{1 + C2 \times S + C3 \times S^2}{(P_{up} - P_{dn})^{1/2}} \right) \right) uP_{dn} \right)^2 \right]^{1/2} \quad (A5)$$

$Dmpr$ is the damper setting (in degrees), $uDmpr$ is the uncertainty in the damper setting (assumed as ± 5 degrees), and uP_{up} and uP_{dn} are the uncertainty in the upstream and downstream static pressures. The coefficients $C1$, $C2$, and $C3$ depend on which box is being used. Those coefficients are given in Table A1.

APPENDIX A REFERENCES

- Kline, S. J., and F. A. McClintock. 1953. Describing Uncertainties in Single-Sample Experiments. *Mech. Eng.*, p. 3.
- Furr, J., D.L. O'Neal, M. Davis, J. Bryant, and A. Cramlet. 2007. Performance of VAV Parallel Fan-Powered Terminal Units: Experimental Results and Models (RP-1292). *ASHRAE Transactions*.

Table A1. Coefficients for Parallel FPTUs from Flow Correlations (Furr 2007)

Box	C1	C2	C3
P8A	1,362.9	-2.020E-02	9.870E-05
P8B	1,935.0	-2.480E-02	1.910E-04
P8C	1,593.8	-2.730E-02	1.910E-04
P12A	7,425.1	-3.070E-02	2.450E-04
P12B	5,781.2	-2.770E-02	2.040E-04
P12C	1838.4	-1.160E-02	1.630E-05

Modeling the Performance of Single-Duct VAV Systems that use Fan Powered Terminal Units

Michael A. Davis
Associate Member ASHRAE

John A. Bryant, PhD, PE
Member ASHRAE

Dennis L. O'Neal, PhD, PE
Fellow ASHRAE

Andrew Cramlet

This paper is based on findings resulting from ASHRAE Research Project RP-1292.

ABSTRACT

Variable Air Volume (VAV) systems are commonly used to maintain space comfort in commercial buildings. Single-Duct VAV (SDVAV) systems often use Fan-Powered Terminal Units (FPTU) to control the amount of conditioned air that is delivered to a zone to maintain space conditions. A model was developed to evaluate the operation of a SDVAV system using Series and/or Fan Powered Terminal Units. The procedure used to model the system is described in this paper as are the equations used to model all non-zone level components in the system. The SDVAV system model was verified in the laboratory using a test stand that supported the operation of a three zone system using both series and parallel FPTU. The test stand was set up to mimic the operating points as predicted by the model. System operation was measured and then compared to the predicted values. The details of the model verification are described in another paper.

INTRODUCTION

The purpose of this study was to model the operation of the Single Duct Variable Air Volume (SDVAV) systems that used Fan-Powered Terminal Units (FPTU). The objective of this paper is to describe the system model and to serve as a reference for other papers that detail the operation of the system when series or parallel type fan powered terminal units are used.

Variable Air Volume (VAV) systems maintain zone comfort by varying the amount of primary air that is delivered to conditioned spaces. The central cooling system includes a fan and cooling coil that supply pressurized and conditioned

air to the primary distribution ducts. The central fan is usually referred to as the primary fan while the air that is conditioned by the cooling coil is referred to as primary air. Primary air is supplied to the conditioned space by a VAV terminal unit that regulates the amount of primary air supplied to the zone.

Figure 1 shows a SDVAV system using five FPTU. For this project, a three zone system model was developed and used to determine a matrix of test points that were then used to perform laboratory verification of the model. After the three zone model was verified it was expanded to five zones and used to evaluate the operation of a building at five different weather locations around the United States. The three zone and five zone models used the same methodology for all calculations with the exception of error corrections that were made as a result of the laboratory verification process. The verification of the model is described in a related paper (Bryant et al. 2009).

SYSTEM MODEL OVERVIEW

The system simulation procedure began with the calculation of zone level conditions followed by the return air calculations, the introduction of fresh air, pre-heat coil process and finally the primary fan and cooling coil calculations. The zone level calculations were dependent upon the type of FPTU installed in the zone. For the purpose of describing the system model, the zone level calculations will be treated as a "black-box" model that provides known values for the parameters related to the operation of the conditioned space. Using the known space parameters, the rest of the system calculations may be performed.

Michael A. Davis is a research engineer with and **John A. Bryant** is an associate professor in the Mechanical Engineering Program at Texas A&M University at Qatar. **Dennis L. O'Neal** is a professor in and head of and **Andrew Cramlet** is a graduate student in the Mechanical Engineering Department at Texas A&M University, College Station, TX.

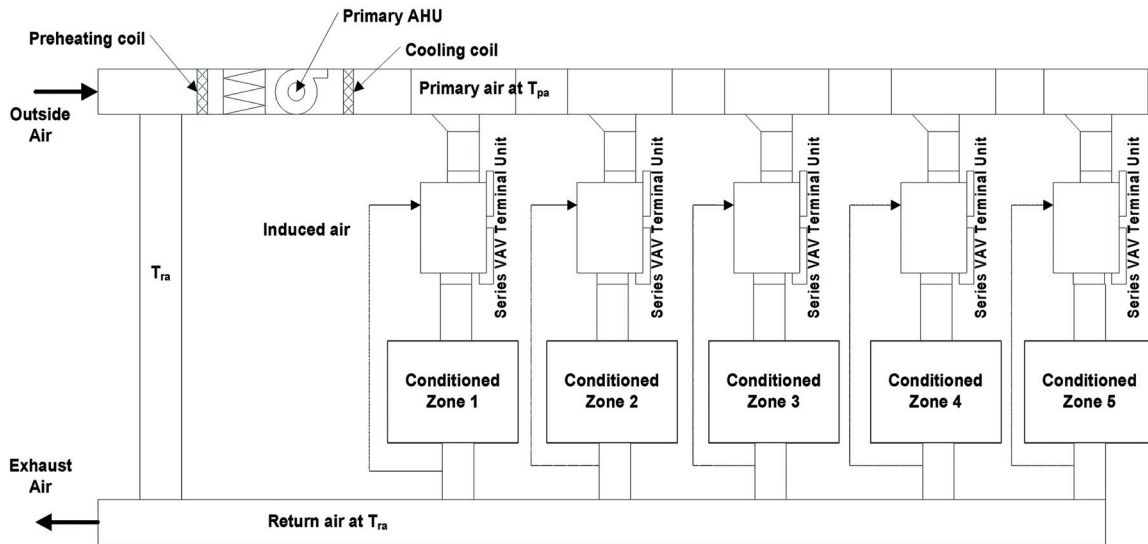


Figure 1 Block diagram of the five zone single duct VAV system using fan-powered terminal units.

After the zone-level return air calculations were completed, the mixed return-air conditions were calculated following the introduction of fresh air. Next, the air properties leaving the pre-heat coil were estimated and entering and leaving conditions for the primary fan were calculated. The properties of the air leaving the primary cooling coil were assumed to be the same as the primary air entering the SFPTU. At each step along the flow path, the temperature and moisture content of the air were calculated. In the cases where air streams were mixed, the mixed air properties were calculated.

Figure 2 shows a flow diagram that identifies the calculation sequence used in the simulation program. The following sections detail the calculation procedures used in the model.

It was not required that the inlet flow valve position at each FPTU be predicted accurately by the model for a given set of duct conditions. The calculation procedure covered below assumed that the VAV valve would adjust as required to meet space conditions. This assumption was verified during laboratory tests and found to be reasonable. The model description will begin with the zone level calculations.

ZONE CALCULATIONS

The zone calculations were performed based on the type of FPTU installed in the zone. To be able to predict the behavior of the system, this model had to accurately predict upstream static pressure and primary air flow requirements for known space loads.

The parameters determined by the zone level calculations consisted of the following:

1. The amount of primary air required by the zone - this included any air that had to be supplied to make up for leakage from the FPTU and between the FPTU and the space.

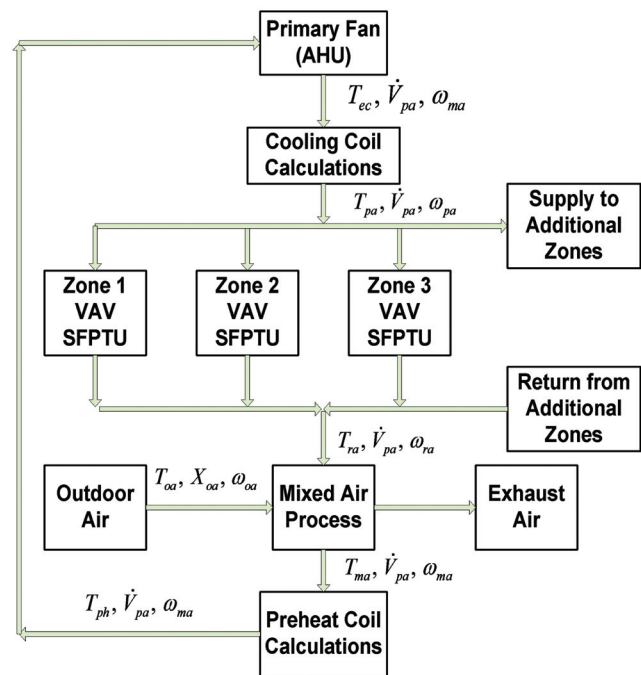


Figure 2 SDVAV System Flow Chart.

2. Any heat required to maintain space conditions including reheat for over cooling and space heating.
3. The upstream static pressure required by the primary fan.
4. The temperature of the return air from the zone.

RETURN AIR

Temperature, absolute humidity, and flow rate of the return air at the zone level were determined by the model based on the FPTU type and the zone sensible and latent loads. The

properties for the system return air were evaluated by performing an energy and mass balance on the return air duct. Equation 1 was used to calculate the return air mixed air temperature and was based on an energy balance of the return air stream (ASHRAE 2005).

$$T_{ra} = \frac{\sum_{i=1}^n \dot{V}_i T_i}{\sum_{i=1}^n \dot{V}_i} \quad (1)$$

Similarly, Equation 2 was used to calculate the mixed return air humidity ratio based on a mass balance of the return air duct.

$$\omega_{ra} = \frac{\sum_{i=1}^n \omega_i \dot{V}_i}{\sum_{i=1}^n \dot{V}_i} \quad (2)$$

EXHAUST/FRESH AIR

The properties of the mixed air after the exhaust of some return air and introduction of fresh air were based on energy and mass balances similar to the calculations for the air streams entering the return system from the zones.

The mixed air temperature after the exhaust/fresh air intake was calculated using Equation 3.

$$T_{ma} = XT_{oa} + (1-X)T_{ra} \quad (3)$$

In Equation 3, the fraction of air introduced into the return air system is the same as the fraction of the return air that was exhausted from the system. The humidity ratio of the mixed air stream after the exhaust and fresh air intake was calculated using Equation 4:

$$\omega_{ma} = X\omega_{oa} + (1-X)\omega_{ra} \quad (4)$$

PRE-HEAT COIL

The return air entered the pre-heat coil as mixed air after fresh outside air was introduced into the system. If the temperature of the mixed air was too low after the introduction of the outside air, then heat was added. The required amount of heat was determined using equation 5. If the temperature of the return air was above the minimum entering air temperature for the primary fan, then no heat was added and the air entering the fan was the same as the mixed air temperature. The humidity ratio did not change as the air passed through the pre-heat coil.

$$Q_{ph} = 1.08\dot{V}(T_{min} - T_{ma}) \quad (5)$$

PRIMARY FAN

The increase in the temperature of the air as it passed through the fan was calculated from Equation 6 where the value of Q was the work done on the air by the fan. The heat added to the air (Q) was calculated using Equation 8 which was developed from manufacturer's literature.

$$T_{ec} = T_{ma} + \frac{Q_{fan}}{1.08\dot{V}} \quad (6)$$

Equation 7 is a fan model that was developed from manufacturer's data for primary fan air flow as a function of the fan speed in RPM and static pressure. Coefficients used in this equation are given in Table 1.

The fan speed was determined first from the required combination of air flow and primary static pressure. The required air flow was the total primary air required to serve all of the zones. The primary static pressure was the highest static pressure that was required to serve any one of the zones.

$$\dot{V} = a_1 + a_2P + a_3P^2 + a_4S + a_5S^2 + a_6PS + a_7P^2S^2 \quad (7)$$

The model also included facilities for setting the primary static pressure to either a specific value, a minimum value, or to a base value. The minimum static pressure setting would not allow the primary static pressure to drop below the specified value. The base value parameter was used to establish a base primary static pressure to which the highest zone static pressure was added. The minimum and base static pressures were

Table 1. Coefficients for Equation 7

	Coefficient	English Units	Coefficient	SI Units
a_1	-1227.76	ft ³ /min	-252.2	m ³ /min
a_2	-1610.45	ft ³ /min-in. w.g.	-410.2	m ³ /min-Pa
a_3	3.047	ft ³ /min-(in.w.g.) ²	0.25	m ³ /min-Pa ²
a_4	3.786	ft ³ /min-rpm	0.610	m ³ /min-rpm
a_5	-0.00017	ft ³ /min-rpm ²	-0.000003	m ³ /min-rpm ²
a_6	0.302	ft ³ /min-in.w.g.-rpm	0.013	m ³ /min-Pa-rpm
a_7	-9.8E-07	ft ³ /min-(in.w.g.-rpm) ²	-1.7E-09	m ³ /min-(Pa-rpm) ²

used to model losses through the primary coil as well as filters and primary duct pressure drops. The specific static pressure setting was used to model systems that maintain a constant primary static pressure.

Equation 8 was then used to calculate the amount of power consumed by the fan using Equation 7 iteratively to solve for the required fan speed.

$$Q_{fan} = 746 \left(\frac{S}{1631} \right)^2 \left(\frac{1}{\text{efficiency}} \right) \quad (8)$$

PRIMARY COOLING COIL

The temperature of the air entering the cooling coil was calculated by adding the temperature rise across the fan to the temperature of the air leaving the pre-heat coil. The sensible cooling load at the cooling coil was calculated using Equation 9.

$$Q_{ccsen} = 1.08 \dot{V} (T_{ec} - T_{pa}) \quad (9)$$

The latent load on the primary cooling coil was calculated using Equation 10.

$$Q_{cclat} = 4840 \dot{V} (\omega_{ma} - \omega_{pa}) \quad (10)$$

4840 = conversion factor with units of $\text{Btu} \cdot \text{min} \cdot \text{lb}_{\text{air}} / \text{ft}^3 \cdot \text{hr} \cdot \text{lb}_{\text{water}}$. The S.I. equivalent is $46.05 \text{ kW} \cdot \text{min} \cdot \text{kg}_{\text{air}} / \text{m}^3 \cdot \text{kg}_{\text{water}}$

The total load on the cooling coil was the sum of the sensible and latent loads.

COOLING PLANT MODEL

The cooling plant was modeled as a simplified DX cooling system where the efficiency (EER) decreased linearly as a function of the increase in the outdoor temperature. A starting EER was based on 95°F (35°C) outdoor temperature and for every 10°F (18°C) that the temperature was over 95°F (35°C), the EER dropped by 1 point. The EER used for the model was an input to the model spreadsheet and was not related to any specific piece of equipment or manufacturer.

MODEL VERIFICATION

The model verification is detailed in another paper (Bryant et al. 2009) and will only be covered briefly in this paper. A three zone system test stand was designed and constructed to support an air distribution system consisting of three SDVAV zones. The test stand was built with a primary air plenum supplying air to three separately controllable duct systems which served as the three zones. Measurements were taken of the primary, induced, and supply air stream temperatures. Additional measurements consisted of the primary and induced air relative humidity, upstream, downstream and flow sensor static pressure, silicon controlled rectifier (SCR) voltage, terminal unit fan power, and the power supplied to a duct heater that was installed in the supply air streams for each

zone. Conditioned air was supplied to the primary air plenum and room air was available to the induction ports. The air flow rates and pressures were controlled with actuators that modulated control dampers. The amount of primary air that passed through the terminal unit was controlled by an actuator that opened and closed a damper located in the primary inlet port of the terminal units. The speed of each terminal unit fan was adjusted by an actuator attached to a voltage controller.

RESULTS

After the model accuracy was laboratory verified, it was used to evaluate the performance of SDVAV systems with both series and parallel FPTU. The model showed that the energy exchanges in the system occurred in four key processes: 1) zone operation, 2) primary cooling coil, 3) primary fan, and 4) introduction of fresh air. The model showed that the operation of the zones had a significant impact on the operation of the primary fan. The processes related to the energy interactions at the primary coil and during the introduction of fresh air were not studied in detail as a part of this project.

The processes related to the zone operation were the primary focus of this study but the zone operation had such a significant impact on the system that the operation of the primary fan had to be included in the study of the FPTU. Figure 3 shows the primary air flow rate of typical parallel and series FPTU as a function of space loads handled by the FPTU.

Figure 3 shows the primary air flow rate as a function of the zone sensible load for Series and Parallel FPTU. This figure also shows the minimum air flow rate required to meet the space sensible load. As the zone load changes the primary air flow varies from maximum to minimum. The minimum flow rate for the FPTU was set at 20% of maximum. Once the space load dropped below 20% of the maximum load, the primary air flow rate was maintained at 20% of the maximum flow rate.

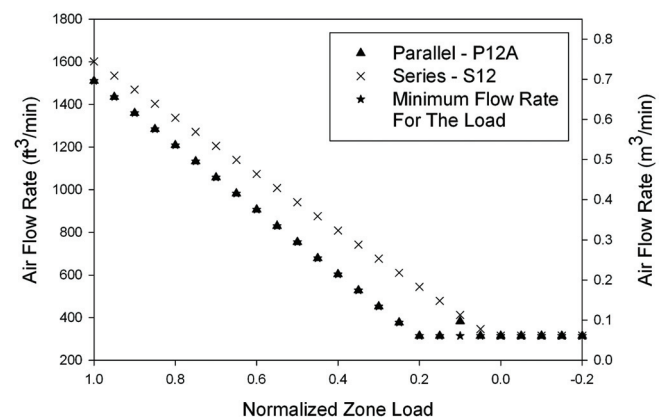


Figure 3 Characteristic primary air flow rates for series and parallel FPTUs.

Primary air leakage was common for all of the parallel FPTU tested in the laboratory. The flow rate for the parallel FPTU shown in Figure 3 did not include any leakage which is why the parallel units performed similarly to the theoretical minimum required air flow rate. The leakage from the parallel units was from the seams of the pressurized mixing chamber as well as from the back-draft damper. The leakage of parallel FPTU is discussed in detail in another paper that describes the zone model used with the system model (Davis et al., 2009). The series FPTU did not leak but it is a very realistic possibility that if a building management system is not properly tuned, more supply air can be driven into the mixing chamber than the FPTU fan can supply to the space. With the over pressurized condition, the series FPTU would use more air at part load conditions than shown in Figure 3.

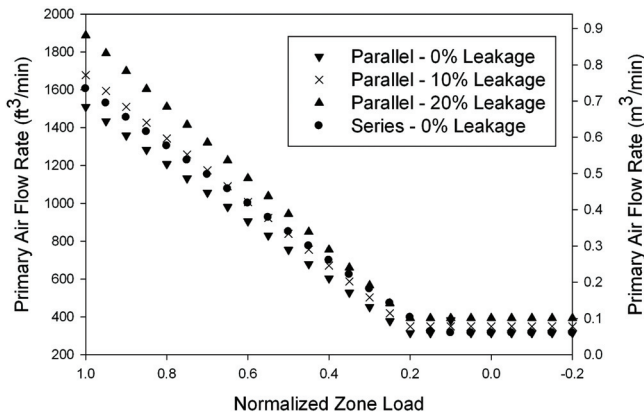


Figure 4 Primary air flow rates for parallel FPTUs with leakage.

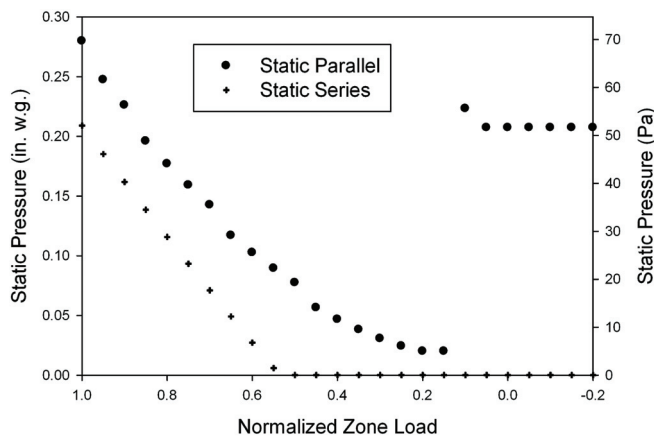


Figure 5 Primary static pressure as a function of zone sensible load for series and parallel FPTUs.

Figure 4 shows the primary air flow rate as a function of zone sensible load for parallel FPTU with leakage rates of 0%, 10%, and 20%. Figure 4 also includes the primary air flow rate for a series FPTU. The primary air flow rate increases for all operating conditions when parallel units leak. Figure 4 also shows that the primary air requirements for a parallel FPTU with a leakage rate higher than 10% is equal to or greater than the primary air required for a series FPTU where the air flow rate is not higher than the terminal unit fan operating point.

Figure 5 shows the primary static pressure as a function of zone sensible load for both series and parallel FPTU. The parallel FPTU shown in Figure 5 had a leakage rate of 0%. This figure shows that the primary static pressure requirements for the series FPTU is always lower than the primary static pressure required for the parallel FPTU. It also shows that when the zone sensible load reduces to the point that the parallel FPTU fan is activated, the primary static pressure is forced to increase in order to maintain minimum primary air flow rate. The impact on the system is that the system primary static pressure is increased and all air flow through the system must be moved against the higher static pressure. The result is that the maximum static pressure required by any of the zones is the minimum static pressure that has to be supplied by the primary fan.

Figure 6 shows the primary static pressure as a function of zone sensible load for parallel FPTU with leakage rates of 0%, 10% and 20%. Figure 6 also includes the primary static pressure for a series FPTU. This shows that the increased primary air flow required as a result of the leakage rate from the parallel FPTU results in an increase in the primary air static pressure. The leakage rate also impacts the primary static pressure required at minimum load when the parallel unit fan is activated. Figure 6 shows that for all operating conditions, the primary static pressure required by the series FPTU is lower than the pressure required by the parallel units.

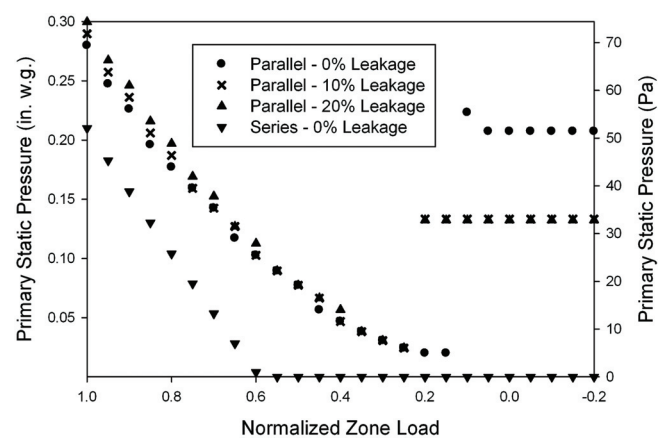


Figure 6 Primary static pressure as a function of zone sensible loads for parallel FPTUs with leakage.

SUMMARY AND CONCLUSIONS

This paper had two objectives: 1) describe the system model, 2) serve as a reference for the papers that describe the zone models and the impact on the system from the type of FPTU used in the zone.

The model description detailed the performance calculations for components used in a typical SDVAV system with FPTU. The calculations started with the zone loads and proceeded through the entire system until the air properties were known for all air streams in the system.

The model was verified by using it to predict duct conditions and control point settings for a variety of operating points that were then replicated in an experimental test rig. A laboratory test stand was built and operated using this matrix of test points determined with the SDVAV model with FPTU (Bryant et al. 2009). At each test point, the supply temperature predicted by the SDVAV model was compared with the actual data from the test stand. The measured supply temperatures were found to agree with the predicted supply temperatures within the uncertainty of the experimental measurements thus verifying the accuracy of the model over the full operating range of the SDVAV FPTU system model. For a complete description of the uncertainty analysis, please refer to Bryant et al. 2009.

The impact on the primary fan because of leakage from the parallel FPTU has a negative impact on the performance of air conditioning systems that use these type terminal units. The impact on the primary fan at minimum loads due to the activation of the terminal fans has a negative impact on the operation of the systems that use parallel FPTU. It cannot be concluded from the data presented in this paper that either the series or parallel based systems are the “best” system to use in a given application. The performance of both systems are compared in related papers.

ACKNOWLEDGEMENTS

This work was part of a project funded by ASHRAE under RP-1292 and we would like to thank the project monitoring subcommittee of TC 5.3 and the manufacturers they represent for their support during the project. Several manufacturers donated terminal units for use in this study. Through cooperative ventures such as these, ASHRAE research funding can be utilized to the fullest. We appreciate the contributions from these industry leaders.

NOMENCLATURE

$a_1 - a_7$ = coefficients used in Equation 7
 P = primary fan static pressure, in. w.g. (Pa)

Q_{cclat} = latent cooling coil load, Btu/hr (W)
 Q_{ccsen} = sensible cooling coil load, Btu/hr (W)
 Q_{fan} = primary fan power, Btu/hr (W)
 Q_{ph} = sensible energy added at preheating coil, Btu/hr (W)
 S = fan speed, RPM
 T_{ec} = temperature of the air entering the coil, °F (°C)
 T_i = temperature of the air returned from zone i , °F (°C)
 T_{ma} = mixed air temperature before it enters the terminal unit fan, °F (°C)
 T_{min} = minimum temperature leaving preheat coil, °F (°C)
 T_{oa} = temperature of the outside air, °F (°C)
 T_{pa} = temperature of the primary air, °F (°C)
 T_{ra} = temperature of the return air, °F (°C)
 \dot{V} = volumetric air flow rate, ft³/min (m³/min)
 \dot{V}_i = volumetric air flow rate, ft³/min (m³/min) of the i^{th} zone
 ω_i = humidity ratio of the i^{th} zone return air, lb_{moisture}/lb_{air} (kg_{moisture}/kg_{air})
 ω_{ma} = mixed air humidity ratio, lb_{moisture}/lb_{air} (kg_{moisture}/kg_{air})
 ω_{oa} = humidity ratio of the outside air - lb_{moisture}/lb_{air} (kg_{moisture}/kg_{air})
 ω_{ra} = return air humidity ratio, lb_{moisture}/lb_{air} (kg_{moisture}/kg_{air})
 ω_{pa} = primary air humidity ratio, lb_{moisture}/lb_{air} (kg_{moisture}/kg_{air})
 X = mass fraction of fresh air added to the return air, expressed as a fraction

REFERENCES

- ASHRAE. 2005. ASHRAE Handbook – Fundamentals, Chapter 30, Atlanta: American Society of Heating, Refrigerating and Air-Conditioning Engineers, Inc.
 Bryant, J., Davis, M.A., O’Neal, D.L., and Cramlett, A.: “Experimental Verification of a Three Zone VAV System Model Operating with Fan Powered Terminal Units (RP-1292)”, ASHRAE Transactions 08, in publication.

BIBLIOGRAPHY

- ASHRAE. 1996. *ANSI/ASHRAE Standard 130, Methods of testing for rating ducted air terminal units*. Atlanta: American Society of Heating, Refrigerating and Air-Conditioning Engineers, Inc.
 McQuiston and Parker, *Heating, Ventilating, and Air Conditioning*, 5th ed., 2005

Reflections on ARI/ASHRAE Research Project RP-1292, Comparison of the Total Energy Consumption of Series versus Parallel Fan Powered VAV Terminal Units

Eugene W. (Gus) Faris
Member ASHRAE

This paper is based on findings resulting from ASHRAE Research Project RP-1292.

IMPORTANT POINTS FROM THE EXECUTIVE SUMMARY

The first phase of the project generated voluminous data that were used to develop mathematical models of each of the units being tested and modeled. There were 12 units total – two series and two parallel from each of three manufacturers. One series and one parallel from each manufacturer were sized for a small zone, and one other series and one other parallel from each manufacturer were sized for a large zone. Consequently, each manufacturer supplied equipment for both parallel and series to study both a representative small and large zone. The zone sizes were picked by the Project Monitoring Subcommittee (PMS). The three manufacturers were chosen to represent the largest possible cross section of equipment available in the market today.

Each unit was placed on a test stand and operated at different inlet and outlet static pressures as well as at different airflows. Every component was mathematically modeled and equations were written to describe the operation over the entire operating range of the unit. Once the models were developed, a test stand was built to accommodate 3 boxes at one time. The units were mounted to this test stand in groups and the models that had been developed were tested under field simulated applications that would resemble real field operations. The purpose of this test was to verify that the mathematical models generated earlier would prove to be accurate under real world conditions when the units were grouped like they would be with a duct system. Rather than making manual adjustments and charting data through the operating ranges of the equipment, these tests were conducted under various

settings for upstream static pressure, downstream static pressure, airflow, damper positions and SCR settings for the motors. Then the damper positions, pressure drops, fan settings and electrical data were checked to determine if the predicted results from the earlier models were confirmed. There were few differences, but where differences did occur, the models were updated.

The second phase of the project took the mathematical models that had been verified and inserted that operating data into workbooks that represent the performance of a system with 5 zones that have been equipped with series or parallel units. Each workbook consists of several spreadsheets. Each spreadsheet describes one of the models that were developed. The spreadsheets, all working together within a workbook, simulate the operation of a building. The zones for this building are interior, north, east, south and west. At that point, the workbooks were expanded to simulate building performance using only the fan powered VAV terminal unit selection as a variant during different times of the year and in different locations. The purpose being to simulate operating costs for each type of unit so that a comparison could be made. DOE 2 data and performance were used as input data for the simulations.

The spreadsheets were designed so that certain sections could be turned on or off. This allows the user to not only simulate a building performance, but also to evaluate the effect on total energy consumption caused by any individual component. The return air heat gain can be turned off or set to any percentage thus simulating interior floors and top floors or single story buildings. The air handler fan energy can be turned off making the air movement through the ducts magical, or the terminal unit fans can be turned off making the air movement

Eugene W. (Gus) Faris is the director of engineering at Nailor Industries, Inc., Houston, TX.

through the terminal units magical. These are useful as evaluation tools to allow examination of the effects caused by individual components within the system. These magical options were not part of the original research plan, but as the PMS began to realize that preconceived notions about the operational characteristics of the equipment were going to contradict conventional expectations, they needed additional evaluation tools to better understand the results.

The intent was to make models that were averages of all three different units by each of the three manufacturers. This proved to be problematic in that the units were distinctly different in some ways. Representative models were arrived at that are believed to be representative of the market place, but it was not a straightforward deduction.

Finally, the program for the comparison work was written and conclusions began filtering out. There were some issues that were viewed as inconsistent by either the PMS or the

researchers. Each time this occurred, more study was needed and another meeting was called. Inlet static pressure on the parallel units was an issue, but not as large as was anticipated by the PMS. The leakage on the parallel units was a larger issue than anticipated by the PMS. Set points on the SCR motor speed controllers had to be evaluated. There were others, but these are the largest.

THE TEST STAND

If additional research is done, it would be nice to do it on a much grander scale. An entire building or at least multiple floors within a building might cause additional issues to reveal themselves that are hidden from our view due to averaging within the system. The cost for instrumentation alone would be problematic, but maybe something could be worked out.

FINDINGS

When embarking on a research project, the first requirement is to clear your mind of preconceived notions and prepare to evaluate the results based on the experiments. That does not mean to throw out your past experience. That is a valuable asset as you plan and go through your research. Researchers are researchers. The PMS was entirely made up of people familiar with applied units and job site experience. There were areas of expertise that did not overlap, and they led to some really fun discussions. These issues surfaced mostly at the final stages of the project. See Figures 1 through 3.

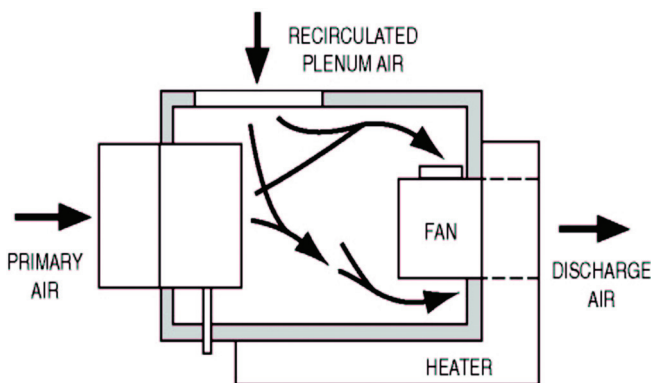


Figure 1 Series flow terminal configuration.

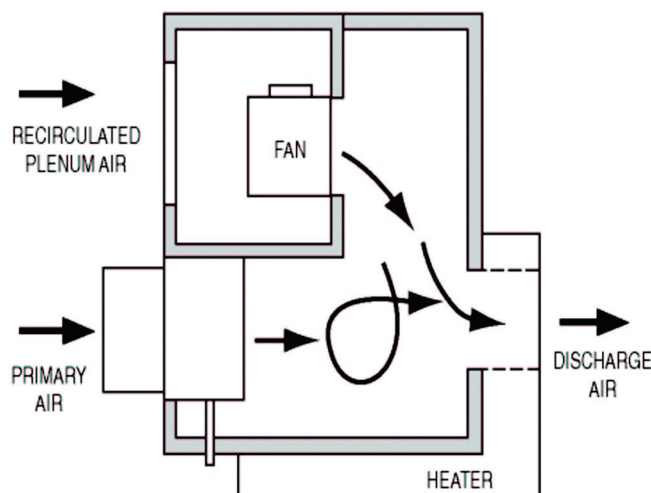
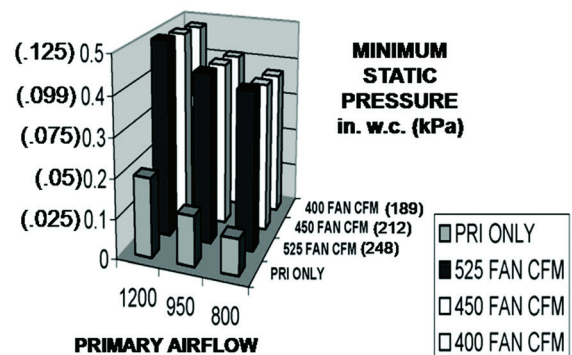


Figure 2 Parallel flow terminal configuration.

STATIC PRESSURE COMPARISON - SIZE 2



	CFM (l/s)			
	1200 (566)	950 (448)	800 (378)	in. w.c. (kPa)
PRI ONLY	0.2 (.05)	0.125 (.03)	0.09 (.02)	
525 FAN CFM	0.5 (.12)	0.43 (.11)	0.4 (.10)	
450 FAN CFM	0.49 (.12)	0.42 (.10)	0.38 (.09)	
400 FAN CFM	0.48 (.12)	0.41 (.10)	0.37 (.09)	

Figure 3 Static pressure comparisons at different primary airflows and fan settings for a parallel fan powered terminal unit.

INLET STATIC PRESSURE

Inlet Static pressure requirements was one of the issues that seemed to be a sticking factor. The PMS members' experience was that the parallel units needed quite a bit more than the series units. The researchers had their mathematical model, and the verification tests seemed to vindicate them rather than the PMS.

The PMS members were all in the industry before electronic controls were used. We are all familiar with the practice of defining critical paths and setting static pressure based on a sensor somewhere along that particular duct run. That process causes the entire duct system to be operated at a static pressure that services one duct run during all conditions affecting the building. Today, ASHRAE 90.1 recognizes that the critical path is not static, but rather it is dynamic and varies depending on the conditions both inside and outside of the building. Recognizing this, ASHRAE Standard 90.1, paragraph 6.3.3.2.3 requires that the duct static pressure on systems with direct digital control of individual zone boxes reporting to the central control panel be reset to cause at least one VAV damper to operate at a nearly completely open position under all operating conditions. This can be a huge energy savings practice in the building. But important to 1292-RP is that the real difference between the parallel and series units was used in the comparison, not differences that are imposed because of controls limitations in measuring static in the duct system. It was not as large as has been used in practice, and that provided a great deal of discussion as we worked our way through the findings. With pneumatic controls or systems that are not capable of dynamic reset, the practice has been to identify a critical zone and set the static in that duct run to be maintained at either 0.75 in. wg for series units or 1.5 in. wg for parallel units. The real difference found during the research was less.

MOTOR HEAT

The heat generated by the motors on both series and parallel units will raise the ambient air temperature by 1 to 3° F (.56 to 1.7° C). This was a much larger issue on the series units than the PMS members had anticipated. As the units are turned down from the full cooling mode, this heat is still being put into the airstream. Since we are not at full cooling and consequently not taxing the chiller or chilled water system, we tend to ignore this in real life applications. This is wrong, because the motor heat load is fairly constant. As the zone load decreases, the motor load, being constant, becomes a larger percentage of the instantaneous zone load and consequently becomes a larger percentage of energy use for the zone. Table 1 shows how each unit is affected by the motor heat.

LEAKAGE

Leakage became another issue that in the past has been mostly ignored, but is, in reality, a much larger issue than we anticipated. In fact, it is the largest single issue next to the operating schedule. Neither series nor parallel units have sealed panels and the parallel unit has a back draft damper designed

Table 1. Comparison of Motor Heat Issues

Parallel Unit	Series Unit
• Motor heat only present when motor is running	• Motor heat present all the time
• Motor runs during dead-band mode	• Motor heat adds to heat load at part load conditions
• Motor runs during heating mode	• Motor heat add is constant and bigger part of total load at part load conditions

to stop leakage of cold air to the plenum when the fan is not running. Leakage occurs all the time in both models. However, in the parallel unit, the casing is pressurized from the primary inlet to the back draft damper compared to the return air plenum; in the series unit, the casing is nearly neutral at all operating conditions compared to the return air plenum. There are other differences. The parallel unit is positive compared to the return air plenum, so leakage is cold primary air moving outward on the parallel unit, and it is always a bad thing. Leakage on the series unit, even though the difference is very small, is negative, and it is plenum air moving inward on the series unit. Since the series unit is always inducing some air, except at full cooling when there is no leakage and since the leakage is the same air being induced through the induction port, the leakage is not an issue. The parallel unit experiences the lowest internal pressure at near minimum primary damper position when the fan is off. It experiences the highest internal pressure when the fan is running or when in full cooling mode depending on the fan airflow setpoint. Conversely, the series unit experiences the most neutral pressure when the primary airflow is at maximum and the highest when the unit is in dead-band or heating mode. As stated above, leakage at deadband is of no consequence because it is simply part of the induced air. Consequently leakage on the series unit is inconsequential, whereas leakage in the parallel unit is a huge issue as cooling air is recirculated back to the air handler bypassing the occupied space. Overall cooling air must be increased to get the space needs to the room while the leaked air short circuits back to the air handler. Table 2 shows how leakage affects both units.

ENERGY USE

Of particular interest in this body of research is that, as forceful and dramatic as the arguments over energy use for these two unit types were, they proved to be about equal, albeit for very different reasons. The series unit motor heat was more than expected, and the central fan energy savings were less. The parallel unit leakage was more than expected, and the central fan energy was higher, but less than expected. Table 3 shows how energy use is affected by both units.

CONCLUSIONS

The plan was to help decide how to

- build better buildings,

- create better environments, and
- capitalize on new and existing technologies,

focusing on how best to apply new technologies. These new technologies include:

- dedicated outdoor air systems
- lower coil and discharge air temperatures
- ECM motors

The ECM motors were a later addition to the research program. Since they were not included in the original project, a second research program was planned to investigate the motor options. It is pretty straight forward to expect energy savings in excess of 50% on series units operating at typical conditions and employing the ECM motors; however, nobody knows what the results will be with parallel units until the research is done.

SO WHICH ONE DO WE USE?

Every job needs to be evaluated based on local issues and occupant needs. Some local codes such as the ability to go to full shut-off of the primary damper may allow benefits for the parallel unit, but even in this case, the leakage needs to be accounted for. If the area has very short heating seasons as well, maybe a single duct reheat unit is the best choice rather than a parallel unit. Even though outside the scope of this research, the issue of fan cycling and associated noise has to be considered as well. This can be a huge noise issue. So in general, the issues listed in Table 4 dictate the selection.

REFERENCE

ASHRAE. ARI/ASHRAE Research Project 1292 Comparison of the Total Energy Consumption of Series vs. Parallel Fan Powered VAV Terminal Units. Final Report, American Society of Heating, Refrigerating and Air-Conditioning Engineers, Inc., Atlanta, GA

(www.ashrae.org/research) and Air-Conditioning and Refrigeration Institute, Arlington, VA (www.arti-research.org/21cr_completed.php).

Table 2. Comparison of Leakage Issues

Parallel Unit	Series Unit
• Positive internal casing pressure	• Neutral internal casing pressure
• Primary air leaks outward bypassing the zone	• Plenum air leaks inward replacing plenum air pulled into the induction port
• Highest leakage at full cooling	• Lowest leakage at full cooling
• Typical leakage is between 5 and 20%	• Typical leakage not measured
• All bypassed primary air must be replaced by additional primary air to satisfy the zone requirements	• No effect to energy
• At full load, the unit may be undersized	• No effect

Table 3. Comparison of Energy Use

Parallel Unit	Series Unit
• Uses 17% less energy than series unit with 0% leakage	• Uses 5.5% less energy than parallel unit with 20% leakage
• Uses 3-4% less energy than series unit with 10% leakage	
• Maximum leakage can be in excess of 30%	
• Typical leakage is between 5 and 20%	• Units are equal in energy use for all practical purposes

Table 4. Issues to Evaluate when Selecting a Terminal Unit Type

Issue	Parallel	Series
Low temperature air	poor control	available option
Dedicated outdoor air supply	poor control	available option
First cost	increased	unchanged
Operating costs	increased	unchanged
90.1 requirement to count motor horsepower	no	yes
Increased air handler hp	yes	no
Noise levels	variable	constant
Comfort levels	variable	constant
62.1 allows credit for recirculated air reducing outdoor air requirements	no	yes
Potential savings with ECM motors	no	yes

Comparison of the Total Energy Consumption of
Series versus Parallel Fan Powered VAV Terminal Units

Spreadsheet Tutorial

ASHRAE Project 1292-RP:

Comparison of the Total Energy Consumption of
Series versus Parallel Fan Powered VAV Terminal Units

Submitted by

Michael Davis

John A. Bryant

Dennis L. O'Neal

Aaron Hervey

Andrew Cramlet

Energy Systems Laboratory

Texas A&M University

College Station, Texas 77843

Aug 18, 2007

Table of Contents

Table of Contents	ii
List of Figures.....	iii
CHAPTER 1	1
<i>Introduction</i>	<i>1</i>
VAV Systems	1
CHAPTER 2	3
<i>Workbook Organization.....</i>	<i>3</i>
Introduction.....	3
Normalized Loads.....	3
System.....	7
parallel Zone - Core/North/East/South/West	15
Series Zones - Core / North / East / South / West.....	19
CHAPTER 3.....	23
<i>Running The Simulation</i>	<i>23</i>
Introduction.....	23
Building Description.....	23
Setup THE Normalized Loads.....	24
Setup THE System Inputs.....	25
Perform The Calculations	26
Review the Results.....	27

List of Figures

Figure 1.1. Single Duct VAV System with Non-Fan Powered VAV Terminal Units.....	1
Figure 1.2. Single Duct VAV System with Fan-Powered VAV Terminal Units.....	2
Figure 2.1. The “From The Model” section of the Normalized Loads spreadsheet.....	5
Figure 2.2. The “Normalized Load Profiles” section of the “Normalized Loads” spreadsheet.....	5
Figure 2.3. The “Normalized Load Values” section of the “Normalized Loads” spreadsheet.....	6
Figure 2.4. The System spreadsheet with the inputs and outputs sections highlighted.....	8
Figure 2.5. The “System Settings” section of the System spreadsheet.....	9
Figure 2.6. “Zone Setting” input section in the System spreadsheet.....	11
Figure 2.7. “Primary Fan Coefficients” input section in the System spreadsheet.....	11
Figure 2.8. The “Simulation Summary” section of the System spreadsheet.....	12
Figure 2.9. The “Outdoor Air Properties” input section of the System spreadsheet.....	13
Figure 2.10. The “System Operation - Parallel” section in the System spreadsheet.....	13
Figure 2.11. The “System Energy Consumption” section for the parallel system model.....	14
Figure 2.12. The “System Operation – Series” section of the System spreadsheet.....	14
Figure 2.13. The series model “System Energy Consumption” section of the spreadsheet.....	15
Figure 2.14 shows the “Box Settings At Peak Loads” for the parallel zones.....	16
Figure 2.15. The “Simulation” section of the zone spreadsheet.....	17
Figure 2.16. The model input section for the parallel terminal units.....	18
Figure 2.17. “Zone Operation” output section of the zone level spreadsheets.....	18
Figure 2.18 shows the “Box Settings At Peak Loads” for the parallel zones.....	20
Figure 2.19. The “Simulation” section of the zone spreadsheet.....	21
Figure 2.20. The model input section for the series terminal units.....	22
Figure 2.21. “Zone Operation” output section of the zone level spreadsheets.....	22
Figure 3.1. Diagram of the Floor Plan of the Building Used as the Basis for the DOE-2 Loads Model.....	24
Figure 3.2. The hourly loads values from the DOE 2 simulation.....	25

CHAPTER 1

Introduction

VAV SYSTEMS

There are two types of VAV systems that are relevant to this project – Single Duct VAV (SDVAV) using standard VAV terminal units and Single Duct VAV using Fan-Powered Terminal Units (FPTU). Figure 1.1 shows a SDVAV system using a typical VAV unit. Figure 1.2 shows a typical SDVAV system using a FPTU. There are two basic types of fan powered terminal units consisting of series and parallel fan arrangements.

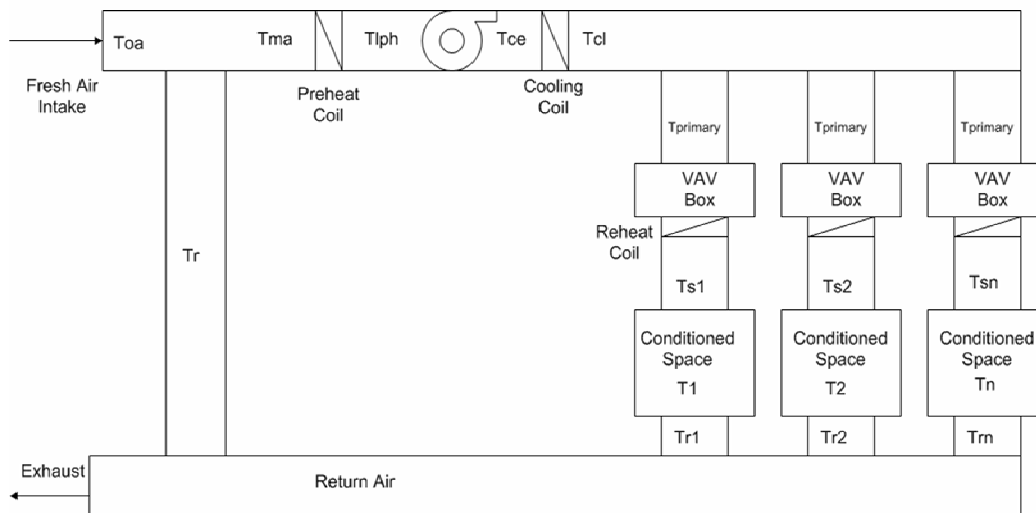


Figure 1.1. Single Duct VAV System with Non-Fan Powered VAV Terminal Units.

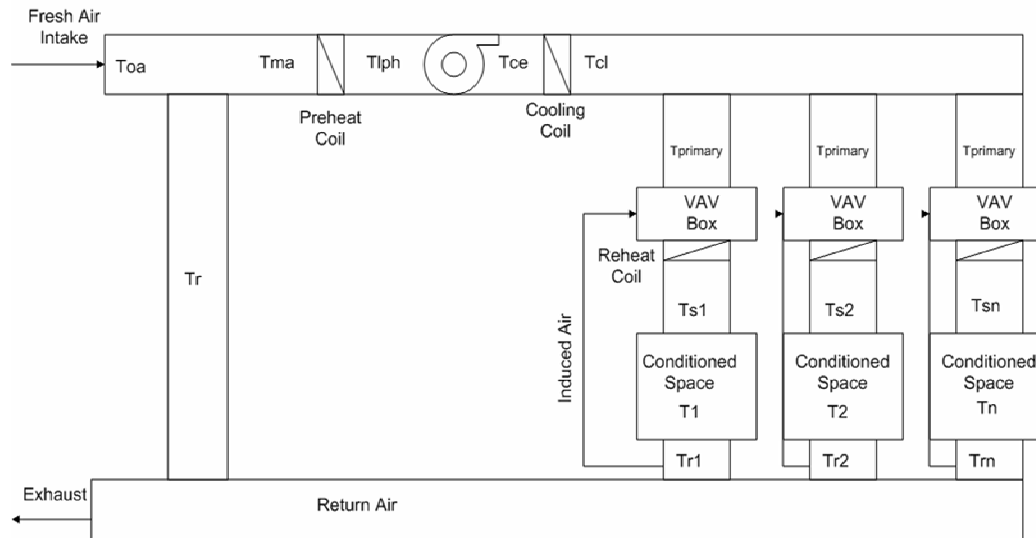


Figure 1.2. Single Duct VAV System with Fan-Powered VAV Terminal Units.

SDVAV systems maintain space conditions by varying the amount of supply air to the space in proportion to the change in the space load. The advantage of the SDVAV system is that a multi-zone system can maintain space comfort conditions at part-load conditions even when a variety of zone load profiles are handled simultaneously by a single primary system. Other advantages over constant volume systems include cost of operations and better zone control.

The disadvantage of a SDVAV system is that when the space loads drop below minimum flow conditions, heat has to be added to the supply air in order to maintain space conditions even before a true heating load exists in the space. The overcooling of a space and the subsequent heating is an inefficiency that can significantly offset the savings resulting from the use of a VAV system.

The single-duct VAV system using fan-powered terminal units can operate without auxiliary heating over a greater range of low-load conditions for a given space. Both the series and the parallel based units mix return air with the supply air at low-load conditions. The introduction of the return air at low load conditions allows the system to delay the use of supplementary heating until the zone requires more heat than can be supplied by the return air operating as first stage heating for most applications.

CHAPTER 2

Workbook Organization

INTRODUCTION

The five zone model for the series and parallel systems were developed as a single excel workbook that consists of twelve spreadsheets. In addition to the twelve spreadsheets, Visual Basic macros embedded in the workbook perform the complex calculations that require the equations developed during the Phase I work. The twelve spreadsheets consist of the following:

1. Normalized Loads – spreadsheet that generates the hourly normalized loads.
2. System – contains all of the inputs and outputs for both series and parallel systems.
3. Core – contains the inputs and outputs for the parallel Core zone.
4. North – contains the inputs and outputs for the parallel North zone.
5. East – contains the inputs and outputs for the parallel East zone.
6. South – contains the inputs and outputs for the parallel South zone.
7. West – contains the inputs and outputs for the parallel West zone.
8. Core Series – contains the inputs and outputs for the series Core zone.
9. North Series – contains the inputs and outputs for the series North zone.
10. East Series – contains the inputs and outputs for the series East zone.
11. South Series – contains the inputs and outputs for the series South zone.
12. West Series – contains the inputs and outputs for the series West zone.

The organization of each spreadsheet will be described in the sections below.

NORMALIZED LOADS

The “Normalized Loads” spreadsheet is used to generate a normalized load profile from the hourly load values obtained from some other program. For this project the hourly loads were generated using the DOE2.1 program. The user of the spreadsheet can generate the hourly loads using any program or method that they consider to be reliable. The objective behind the normalized load generation is to size the loads the VAV terminal unit capacity

The Normalized Loads spreadsheet is organized into four main sections:

1. Time
2. From The Model
3. Normalized Load Profiles
4. Normalized Load Values

The Time section contains a single column with the first two rows consisting of titles. The first row contains the title of the columns and is labeled “Time.” The second row contains the title of the values of items in the columns adjacent to the first column and is titled “Max Values ->.” This means that the items in columns that are in the spreadsheet horizontally across the spreadsheet are the maximum values of the items listed in the columns below the max value row. This will be explained with an example in the next section.

The values in the time columns that are below the title rows consist of the repeated hourly values for the year. The column consists of 0:00 through 23:00 repeated for 365 days. This column serves as a label that identifies the time of day for the 8760 hours contained in an hourly simulation. The first hour represents the time period from midnight on Jan 1st to 1:00 am on January 1st whereas the last hour in the column represents the time period of 11:00 pm to midnight (12:00 am) on December 31st.

The “From the Model” section contains the inputs of the hourly loads for the five zones which consist of the core zone and the four perimeter zones. The input values are typed directly into the appropriate cells. Each zone has inputs for the sensible and the latent hourly loads. Figure 2.1 shows the “From The Model” section of the Normalized Loads spreadsheet. The first column in the figure shows the time column and the “Max Values->” label in the time column identifies the maximum values of each column. The maximum value is the largest value listed in the column. For example, in the “Core Zone” there are two columns labeled Sensible (Btu/hr) and Latent (Btu/hr) respectively. The Sensible column contains the sensible loads for the core zone and loads are in British Thermal Units per hour (Btu/hr). The value shown in the first row (which is parallel to the Max Value label) is the maximum value that is listed in any hour in the column. The maximum value is found using the Excel function Max with the cell range being from the first “0:00” to the last “23:00” hour.

The “From the Model” section contains five subsections labeled “Core Zone”, “South perimeter”, “East Perimeter”, “West Perimeter” and “North Perimeter.” Each subsection has two columns for the loads and they are labeled “Sensible” and “Latent.” The columns titles are followed by the units of the values that are to be entered into the columns. For this project the units are Btu/hr.

Time	From The Model									
	Core zone		South perimeter		East Perimeter		West Perimeter		North Perimeter	
	Sensible Btu/hr	Latent Btu/hr								
Max Values->	47776.89	4581.48	39069.56	863.42	37502.77	863.42	45401.01	863.42	32099.96	863.42
0:00	3624.24	0	-14317.97	0	-14718.95	0	-14946.03	0	-15237.14	0
1:00	2342.36	0	-17156.69	0	-17512.92	0	-17659.46	0	-17918.51	0
2:00	1227.13	0	-18146	0	-18455.79	0	-18673.25	0	-18898.54	0
3:00	256.88	0	-18851.72	0	-19121.24	0	-19245.49	0	-19441.49	0
4:00	-587.24	0	-19071.33	0	-19305.81	0	-19142.09	0	-19312.61	0
5:00	-1321.62	0	-20403.36	0	-20607.36	0	-20942.18	0	-21090.53	0
6:00	1543	0	-20303.08	0	-20743.44	0	-20430.31	0	-20823.23	0
7:00	8836.12	482.26	-17737.07	90.89	-17524.54	90.89	-18684.47	90.89	-19083.43	90.89
8:00	30850.85	964.52	-11797.01	181.77	-12161.06	181.77	-12770.79	181.77	-13491.28	181.77
9:00	37125.23	4581.48	-9414.95	863.42	-10161.85	863.42	-10371.6	863.42	-11254.37	863.42
10:00	39433.8	4581.48	-8491.26	863.42	-8676.46	863.42	-8604.07	863.42	-8766.26	863.42
11:00	38846.67	2170.18	-5144.38	408.99	-6654.56	408.99	-6560.17	408.99	-7524.01	408.99
12:00	36932.43	2170.18	-5281.81	408.99	-6437.93	408.99	-5857.02	408.99	-6187.86	408.99
13:00	44091.45	4581.48	-1008.62	863.42	-2847.92	863.42	-2454.24	863.42	-3368	863.42
14:00	45494.41	4581.48	-606.33	863.42	-2227.05	863.42	-1649.98	863.42	-2655.45	863.42
15:00	46714.98	4581.48	-1130.01	863.42	-2364.6	863.42	-1282.83	863.42	-2139.1	863.42
16:00	47776.89	4581.48	-1092.78	863.42	-2489.62	863.42	-1686.18	863.42	-2783.1	863.42
17:00	34686.59	4581.48	-4966.88	863.42	-6277.23	863.42	-5519.09	863.42	-6528.15	863.42
18:00	23817.91	1446.78	-7254.42	272.66	-8671.37	272.66	-7729.44	272.66	-8889.72	272.66
19:00	21504.63	482.26	-7961.69	90.89	-9332.27	90.89	-8374.99	90.89	-9522.23	90.89
20:00	16828.59	482.26	-9618	90.89	-10217.09	90.89	-9302.92	90.89	-9705.21	90.89
21:00	15485.72	482.26	-9310.43	90.89	-10445.38	90.89	-9589.11	90.89	-10552.61	90.89
22:00	6791.24	0	-12234.71	0	-12725.48	0	-11681.66	0	-12023.09	0
23:00	5097.66	0	-11629.01	0	-12669.65	0	-11795.21	0	-12704.84	0

Figure 2.1. The “From The Model” section of the Normalized Loads spreadsheet..

Normalized Load Profiles									
Core zone		South perimeter		East Perimeter		West Perimeter		North Perimeter	
Sensible Btu/hr	Latent Btu/hr	Sensible Btu/hr	Latent Btu/hr	Sensible Btu/hr	Latent Btu/hr	Sensible Btu/hr	Latent Btu/hr	Sensible Btu/hr	Latent Btu/hr
0.075858	0	-0.366474	0	-0.392476	0	-0.3292	0	-0.474678	0
0.049027	0	-0.439132	0	-0.466977	0	-0.388966	0	-0.55821	0
0.025685	0	-0.464454	0	-0.492118	0	-0.411296	0	-0.58874	0
0.005377	0	-0.482517	0	-0.509862	0	-0.4239	0	-0.605655	0
-0.012291	0	-0.488138	0	-0.514784	0	-0.421623	0	-0.60164	0
-0.027662	0	-0.522232	0	-0.549489	0	-0.461271	0	-0.657027	0

Figure 2.2. The “Normalized Load Profiles” section of the “Normalized Loads” spreadsheet.

Figure 2.2 shows the “Normalized Load Profiles” section of the “Normalized Loads” spreadsheet. The values in the “Normalized Load Profiles” section of the spreadsheet are derived from the hourly values in the “From The Model” section of the spreadsheet and the maximum value found at the top of the loads columns in the “From The Model” section of the spreadsheet. The value shown in each cell in the “Normalized Load Profiles” is calculated by dividing the hourly load value in the “From The Model “ section by the maximum value listed in the appropriate column. For example, for hour 0:00 in Figure 2.1 the Core Zone sensible load value from the model is shown as 3,624.24 Btu/hr. The maximum value which is shown at the top of the same column is 47,776.89 Btu/hr. The value for the Core Zone Sensible Load in the “Normalized Load Profiles” section for hour 0:00 is 0.075858 and is unit less. The value is derived as follows: $0.075858 = 3624.24/47776.89$. The spreadsheet shows the calculation as accurate to two decimal places for the maximum value of 47,776.24. The actual accuracy and therefore the proper number of significant digits to be used in the simulation is the responsibility of the user.

Normalized Load Values									
Core zone		South perimeter		East Perimeter		West Perimeter		North Perimeter	
Sensible	Latent	Sensible	Latent	Sensible	Latent	Sensible	Latent	Sensible	Latent
Btu/hr	Btu/hr	Btu/hr	Btu/hr	Btu/hr	Btu/hr	Btu/hr	Btu/hr	Btu/hr	Btu/hr
37510	8799	37510	8799	37510	8799	37510	8799	37510	8799
2845	0	-13746	0	-14722	0	-12348	0	-17805	0
1839	0	-16472	0	-17516	0	-14590	0	-20938	0
963	0	-17422	0	-18459	0	-15428	0	-22084	0
202	0	-18099	0	-19125	0	-15900	0	-22718	0
-461	0	-18310	0	-19310	0	-15815	0	-22568	0
-1038	0	-19589	0	-20611	0	-17302	0	-24645	0

Figure 2.3. The “Normalized Load Values” section of the “Normalized Loads” spreadsheet.

Figure 2.3 shows the “Normalized Load Values” section of the spreadsheet. The values contained in this section of the spreadsheet are the hourly loads that will be handled by the zone as cooling and heating loads when the simulation is performed. This section of the spreadsheet has five subsections that contain two columns each. The five subsections consist of the “Core Zone”, “South Perimeter”, “East Perimeter”, “West Perimeter”, and “North Perimeter.” Each subsection contains two columns that consist of the hourly sensible and latent loads in Btu/hr. The first value in each column is the maximum cooling load value that will be experienced by the zone during the year. The maximum value is a user entry and the maximum cooling capacity

of the VAV terminal unit. The maximum value should be calculated from the maximum air flow that can be supplied by the VAV terminal minus any fan energy that has to be handled by the terminal unit. The values in the “Normalized Load Values” section of the spreadsheet are derived by multiplying the maximum value in the “Normalized Load Values” section of the spreadsheet by the hourly value in the “Normalized Load Profiles” section of the spreadsheet for the corresponding column and hour. For example, in Figure 2.3 the maximum values shown in the Core Zone Sensible Loads column is 37,510 Btu/hr. The load value for hour “0:00” shown in the “Sensible” column of the “Core Zone” subsection of the “Normalized Load Values” section of the spreadsheet is shown in Figure 2.3 as 2,845 Btu/hr. The corresponding value in the “Normalized Load Profiles” section is shown in Figure 2.2 as 0.075858. The hour 0:00 value shown in the “Core Zone” “Sensible” column in Figure 2.3 was calculated as $2,845 \text{ Btu/hr} = 0.075858 (\text{Btu/hr} / \text{Btu/hr}) \times 37,510 \text{ Btu/hr}$.

SYSTEM

The “System” spreadsheet contains the inputs and outputs for the “System” level calculations. Figure 2.4 shows the System spreadsheet with the inputs and outputs highlighted. The spreadsheet is divided into several sections that are for inputs and two sections that are for outputs. The output section of the spreadsheet contains the results of the system level calculations that are based on the results from the zone level calculations. The system level calculations are performed using cell relations and cell-based equations. The inputs sections of the spreadsheet are used by the zone level calculations to perform the hourly zone level calculations. The inputs are located in the system spreadsheet in order to ensure that all zones use the same parameters when the zone level calculations are performed.

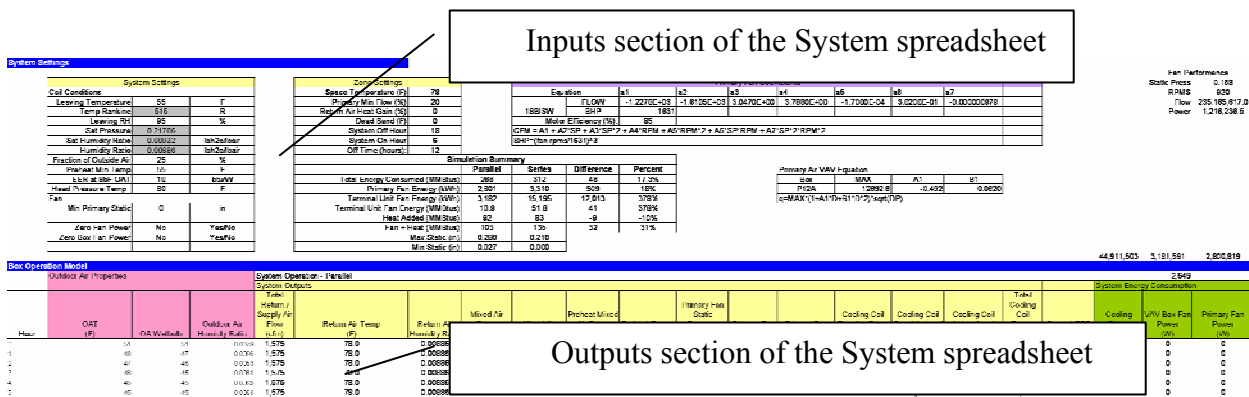


Figure 2.4. The System spreadsheet with the inputs and outputs sections highlighted.

The System spreadsheet is not very complex but it has a lot of cells that use the output of other cells to perform their calculations. As a result of all of the cell interactions, the System spreadsheet can take a long time to perform a complete recalculation when other spreadsheet cell values change. To reduce the impact of cell interactions the user will need to turn on and turn off the automatic update feature in Excel. The following chapters that show how to perform a simulation will highlight when to turn on/off the automatic recalculations.

The input sections of the System spreadsheet consist of data entry cells for the primary fan, the Zones, and the system. Each input section will be covered in the next few paragraphs and then the outputs for the parallel and series systems will be covered.

Figure 2.5 shows the “System Settings” section of the spreadsheet. The data entry fields are white while the gray fields are derived values and are shown so that the user can verify their values.

System Settings		
Coil Conditions		
Leaving Temperature	55	F
Temp Rankine	515	R
Leaving RH	95	%
Sat Pressure	0.21706	
Sat Humidity Ratio	0.00932	lbh2o/lbair
Humidity Ratio	0.00886	lbh2o/lbair
Fraction of Outside Air	25	%
Preheat Min Temp	55	F
EER at 95F OAT	10	btu/W
Head Pressure Temp	80	F
Fan		
Min Primary Static	0	in
Zero Fan Power	No	Yes/No
Zero Box Fan Power	No	Yes/No

Figure 2.5. The “System Settings” section of the System spreadsheet.

The inputs in the “System Settings” cells are used to set the primary air cooling coil conditions, control the amount of outside air used, trigger the pre-heating coil if required, and control the primary and terminal unit fan power status. The spreadsheet assumes that the system plant (the chiller) has the capacity needed to maintain the specified conditions. The inputs consist of the following data:

1. Leaving Temperature. The leaving temperature in degrees F for the cooling coil. The spreadsheet assumes that the primary plant (chiller) has the capacity to maintain the leaving coil conditions.
2. Leaving RH. The percent Relative Humidity (RH) of the primary when it leaves the cooling coil. The system assumes that dehumidification has occurred and that humidity ratio is for air at 95% RH when it exits the coil. When the calculations are performed in the spreadsheet, if the entering coil humidity ratio is lower than the leaving humidity ratio then the energy consumption associated with the dehumidification is set to zero.
3. Fraction of Outside Air. The percent of outside introduced into the system. The model assumes that the system is balanced and exhaust air volume is the same as the fresh air.
4. Preheat Min Temp. The ventilation air is introduced after the exhaust air has been expelled but before the preheat coil. When the return air is mixed with the outside air a mixed air temperature prior to the reheat coil is calculated. If the mixed air temperature is below the value in this field, then the air is heated to this value by the preheat coil.

5. EER at 95F OAT. This value is the nominal rated Energy Efficiency Ratio at 95F outside air conditions. The EER is used to calculate the energy consumed by the cooling system after the hourly total load on the primary coil has been calculated. The EER is adjusted as a function of the outside air temperature based on the following:

$$EER(OAT) = EER_{95F} - (OAT - 95F)/10 \quad (1)$$

Where EER = Energy Efficiency Ratio (BTUH/Watt)

OAT = Outdoor Air Temperature in degrees F.

EER_{95} = EER at 95F

For example, if the EER at 95F is 10, then at 85F the EER would be $11 = 10 - (85 - 95)/10$.

6. Head pressure Temp. This field is not used but was added for future expansion of the model.
7. Fan Min Primary Static Pressure. The primary fan static pressure setting which is the minimum static pressure that the primary has to overcome to move the air into the primary air ducts. The pressure drops through the VAV terminal units is added on top of this pressure setting.
8. Zero Fan Power. This input toggles the primary fan power calculation. When this value is set to “Yes”, the primary fan does not use power to move the air through the system. This input was added to be able to evaluate the sensitivity of the model to the primary fan power consumption. The normal setting for this value is “No.”
9. Zero Box power. This input toggles the VAV terminal unit fan power calculation. When this value is set to “Yes”, the terminal unit fan does not use power to move the air through the zone when the terminal unit fan is turned on. This input was added to be able to evaluate the sensitivity of the model to the terminal unit fan power consumption. The normal setting for this value is “No.”

Zone Settings	
Space Temperature (F)	78
Primary Min Flow (%)	20
Return Air Heat Gain (%)	0
Dead Band (F)	0
System Off Hour	18
System On Hour	6
Off Time (hours):	12

Figure 2.6. “Zone Setting” input section in the System spreadsheet.

Figure 2.6 shows the “Zone Settings” section of the System spreadsheet. The zone settings are used by each zone to control the zone space temperature, minimum primary air flow, return air heat gain, etc. The data was placed as an entry field in the System spreadsheet so that all of the zones would reference the same control parameters. This was done to reduce the errors associated with multiple entry points. The zone spreadsheets also have the same entry fields but the data is pulled from the system fields using cell relations within Excel. The user can override the System inputs at the zone level inputs.

Primary Fan Coefficients								
Equation	a1	a2	a3	a4	a5	a6	a7	
18BISW	FLOW	-1.2278E+03	-1.6105E+03	3.0470E+00	3.7860E+00	-1.7000E-04	3.0200E-01	-0.000000979
	BHP	1631						
	Motor Efficiency (%):	85						
CFM = A1 + A2*SP + A3*SP^2 + A4*RPM + A5*RPM^2 + A6*SP*RPM + A7*SP^2*RPM^2								
BHP=(fan rpms/1631)^3								

Figure 2.7. “Primary Fan Coefficients” input section in the System spreadsheet.

Figure 2.7 shows the “Primary Fan Coefficients” input section in the System spreadsheet. The primary fan has two main sections of data for coefficients: 1. Flow, 2. Brake Horsepower (BHP). The Flow inputs represent the coefficients of the equation that is used to calculate the primary fan air flow rate as a function of primary static pressure (SP) and primary fan speed (RPM). The equation is shown in Figure 2.7 immediately below the motor efficiency input. The equation calculates the air flow rate in CFM. Below the CFM equation the equation for the BHP is shown. The power used by the primary fan is the BHP of the fan divided by the motor efficiency which is an input located below BHP entry fields.

Simulation Summary				
	Parallel	Series	Difference	Percent
Total Energy Consumed (MMBtus)	266	312	46	17.3%
Primary Fan Energy (kWh)	2,801	3,310	509	18%
Terminal Unit Fan Energy (kWh)	3,182	15,195	12,013	378%
Terminal Unit Fan Energy (MMBtus)	10.9	51.8	41	378%
Heat Added (MMBtus)	92	83	-9	-10%
Fan + Heat (MMBtus)	103	135	32	31%
Max Static (in)	0.280	0.210		
Min Static (in)	0.027	0.000		

Figure 2.8. The “Simulation Summary” section of the System spreadsheet.

Figure 2.8 shows the “Simulation Summary” section of the System spreadsheet. The “Simulation Summary” section of the spreadsheet is an output only set of data fields. This table is provided as a summarization of the final results of the spreadsheet calculations. The values in this table are derived by cell relationships that collect data from the system level calculations.

Figure 2.9 shows the input fields for the ambient conditions used by the simulation. The first column shows the hour of the day starting at midnight on January 1st. The second column is the Outdoor Air Temperature (OAT) in degrees F. The third column is the outdoor Air Wet-Bulb in degrees F. the fourth column is the Outdoor Air Humidity Ratio in pounds of water per pound of dry air. The outdoor air properties section is an input section. Before a simulation is done, the Outdoor Air Properties section must be populated with the weather data for the climate that is being modeled. The ambient air conditions are used to calculate the mixed air temperature and moisture content of the return air after the fresh air has been introduced into the system immediately prior to the primary air pre-heat coil.

Outdoor Air Properties				
Hour	OAT (F)	OA Wetbulb		Outdoor Air Humidity Ratio
0		51	51	0.0079
1		48	47	0.0066
2		47	46	0.0063
3		46	45	0.0061
4		45	45	0.0063
5		45	45	0.0063
6		44	44	0.0061
7		44	44	0.0061
8		47	46	0.0063
9		48	47	0.0066
10		50	49	0.0071
11		52	51	0.0077
12		53	52	0.008
13		54	53	0.0083
14		55	54	0.0086
15		56	55	0.009

Figure 2.9. The “Outdoor Air Properties” input section of the System spreadsheet.

Figure 2.10 shows the “System Operation – Parallel” section of the System spreadsheet. The system operation is the output summary for all five zones. There is a “System Operation” section for both the series and the parallel system models. The values in the “System operation” section are self-explanatory and are either a summarization of the values in the zones or they are cell relationships that take the values in other cells and use them as inputs for macros. The user should modify the contents of the cells in the “System Operation” section of the spreadsheet. Modification of the cells will destroy the relations that are used to perform the calculations and will cause the results to be wrong.

System Operation - Parallel														
System Outputs														
Total Return / Supply Air Flow (cfm)	Return Air Temp (F)	Return Air Humidity Ratio	Mixed Air Temp (F)	Mixed Air Humidity Ratio	Preheat Mixed Air Temp (F)	Preheat Energy (Btu/s)	Primary Fan Static Pressure (in)	Primary Fan Speed (rpm)	Primary Fan Power (W)	Cooling Coil Entering Temp (F)	Cooling Coil Sensible Load (Btu/s)	Cooling Coil Latent Load (Btu/s)	Total Cooling Coil Energy (Btu/h)	Current EER
1,575	78.0	0.00886	71.3	0.00862	71.3	0.000	0.134	820.00	111.5	71.5	28,024	0	28,024	11.5
1,575	78.0	0.00886	70.5	0.00829	70.5	0.000	0.134	820.00	111.5	70.7	26,748	0	26,748	11.5
1,575	78.0	0.00886	70.3	0.00822	70.3	0.000	0.134	820.00	111.5	70.5	26,322	0	26,322	11.5
1,575	78.0	0.00886	70.0	0.00817	70.0	0.000	0.134	820.00	111.5	70.2	25,897	0	25,897	11.5
1,575	78.0	0.00886	69.8	0.00822	69.8	0.000	0.134	820.00	111.5	70.0	25,472	0	25,472	11.5
1,575	78.0	0.00886	69.8	0.00822	69.8	0.000	0.134	820.00	111.5	70.0	25,472	0	25,472	11.5
1,575	78.0	0.00886	69.5	0.00817	69.5	0.000	0.134	820.00	111.5	69.7	25,047	0	25,047	11.5
1,591	78.0	0.00946	69.5	0.00862	69.5	0.000	0.137	830.00	115.7	69.7	25,307	0	25,307	11.5
2,236	78.0	0.00971	70.3	0.00886	70.3	0.000	0.134	1,010.00	208.4	70.5	37,524	28	37,552	11.5
2,453	78.0	0.01259	70.5	0.01110	70.5	0.000	0.169	1,080.00	254.8	70.8	41,606	26,347	67,953	11.5
2,596	78.0	0.01248	71.0	0.01114	71.0	0.000	0.187	1,110.00	278.8	71.3	44,255	27,884	71,819	11.5
2,488	78.0	0.01059	71.5	0.00987	71.5	0.000	0.182	1,100.00	269.2	71.8	45,253	12,143	57,396	11.5
2,427	78.0	0.01083	71.8	0.00987	71.8	0.000	0.167	1,080.00	254.8	72.1	44,781	13,109	57,890	11.5
2,654	78.0	0.01228	72.0	0.01129	72.0	0.000	0.236	1,170.00	324.0	72.4	49,827	31,204	81,030	11.5
2,698	78.0	0.01223	72.3	0.01132	72.3	0.000	0.248	1,190.00	340.9	72.6	51,427	32,153	83,580	11.5
2,737	78.0	0.01218	72.5	0.01138	72.5	0.000	0.260	1,200.00	349.5	72.9	52,914	33,466	86,380	11.5

Figure 2.10. The “System Operation - Parallel” section in the System spreadsheet.

Figure 2.11 shows the “System Energy Consumption” section for the parallel zones. Both the series and the parallel models have a “System Energy Consumption” section which is located

next to the “System Operation” section for both series and parallel system models. The data in the cells in the “System Energy Consumption” section is derived from the hourly data generated by the system model. The user should not modify the contents of the “System Energy Consumption” section of the spreadsheet. This is an output only section.

System Energy Consumption					
Cooling Power (W)	VAV Box Fan Power (W)	Primary Fan Power (W)	Total Power (W)	Total Heating (btus)	Total Energy Consumed (btus)
0	0	0	0	0	0
0	0	0	0	0	0
0	0	0	0	0	0
0	0	0	0	0	0
0	0	0	0	0	0
0	0	0	0	0	0
2,178	1,743	112	4,032	113,418	127,176
2,201	1,742	116	4,059	98,835	112,684
3,265	1,394	208	4,868	76,347	92,957
5,909	1,394	255	7,558	67,465	93,253
6,254	1,394	277	7,925	60,725	87,764
4,991	1,394	269	6,654	52,349	75,054
5,034	1,394	255	6,683	50,122	72,924
7,046	1,394	324	8,764	36,322	66,226
7,268	1,394	341	9,003	33,818	64,536
7,511	1,394	350	9,255	33,551	65,130

Figure 2.11. The “System Energy Consumption” section for the parallel system model.

Figure 2.12 shows the “System Operation – Series” section of the System spreadsheet. This section of the spreadsheet is used to perform the system level calculations for the series model. The user should not modify this section of the spreadsheet as it will cause errors to be introduced into the calculations.

System Operation - Series														
System Outputs														
Total Return / Supply Air Flow (cfm)	Return Air Temp (F)	Return Air Humidity Ratio	Mixed Air Temp (F)	Mixed Air Humidity Ratio	Preheat Mixed Air Temp (F)	Preheat Energy (btus)	Primary Fan Static Pressure (in)	Primary Fan Speed (rpm)	Primary Fan Power (W)	Cooling Coil Entering Temp (F)	Cooling Coil Sensible Load (btus)	Cooling Coil Latent Load (btu)	Total Cooling Coil Energy (btu)	Current EER (btu/W)
1,577	78.0	0.00886	71.3	0.00862	71.3	0.000	0.000	770.00	92.3	71.4	27,991	0	27,991	11.5
1,577	78.0	0.00886	70.5	0.00829	70.5	0.000	0.000	770.00	92.3	70.7	26,713	0	26,713	11.5
1,577	78.0	0.00886	70.3	0.00822	70.3	0.000	0.000	770.00	92.3	70.4	26,288	0	26,288	11.5
1,577	78.0	0.00886	70.0	0.00817	70.0	0.000	0.000	770.00	92.3	70.2	25,862	0	25,862	11.5
1,577	78.0	0.00886	69.8	0.00822	69.8	0.000	0.000	770.00	92.3	69.9	25,436	0	25,436	11.5
1,577	78.0	0.00886	69.8	0.00822	69.8	0.000	0.000	770.00	92.3	69.9	25,436	0	25,436	11.5
1,577	78.0	0.00886	69.5	0.00817	69.5	0.000	0.000	770.00	92.3	69.7	25,010	0	25,010	11.5
1,636	78.0	0.00944	69.5	0.00861	69.5	0.000	0.000	790.00	99.7	69.7	25,959	0	25,959	11.5
2,332	78.0	0.00968	70.3	0.00883	70.3	0.000	0.026	1,000.00	202.3	70.5	39,094	0	39,094	11.5
2,530	78.0	0.01245	70.5	0.01099	70.5	0.000	0.092	1,080.00	254.8	70.8	43,223	26,083	69,306	11.5
2,603	78.0	0.01235	71.0	0.01104	71.0	0.000	0.118	1,110.00	276.6	71.3	45,925	27,458	73,383	11.5
2,584	78.0	0.01052	71.5	0.00982	71.5	0.000	0.111	1,100.00	269.2	71.8	46,974	12,008	58,982	11.5
2,524	78.0	0.01056	71.8	0.00992	71.8	0.000	0.090	1,080.00	254.8	72.1	46,528	13,009	59,537	11.5
2,750	78.0	0.01216	72.0	0.01120	72.0	0.000	0.169	1,170.00	324.0	72.4	51,600	31,139	82,739	11.5
2,795	78.0	0.01211	72.3	0.01123	72.3	0.000	0.184	1,190.00	340.9	72.6	53,226	32,123	85,349	11.5
2,833	78.0	0.01207	72.5	0.01130	72.5	0.000	0.186	1,210.00	358.4	72.9	54,770	33,482	88,252	11.5

Figure 2.12. The “System Operation – Series” section of the System spreadsheet.

System Energy Consumption					
Cooling Power (W)	VAV Box Fan Power (W)	Primary Fan Power (W)	Total Power (W)	Total Heating (btus)	Total Energy Consumed (btus)
0	0	0	0	0	0
0	0	0	0	0	0
0	0	0	0	0	0
0	0	0	0	0	0
0	0	0	0	0	0
0	0	0	0	0	0
2,175	3,469	92	5,736	107,600	127,173
2,257	3,469	100	5,826	94,181	114,060
3,400	3,469	202	7,071	71,693	95,819
6,027	3,469	255	9,751	62,811	96,080
6,381	3,469	277	10,127	56,071	90,623
5,129	3,469	269	8,867	47,695	77,950
5,177	3,469	255	8,901	45,468	75,838
7,195	3,469	324	10,988	31,668	69,158
7,422	3,469	341	11,232	29,164	67,486
7,674	3,469	358	11,502	28,897	68,141

Figure 2.13. The series model “System Energy Consumption” section of the spreadsheet.

Figure 2.13 shows that the “System Energy Consumption” section for the series system model is the same as for the parallel model and contains the hourly results of the calculations for the series system model. This section is located next to the “System Operation – Series” section of the spreadsheet and is an output only section.

PARALLEL ZONE - CORE/NORTH/EAST/SOUTH/WEST

The parallel model has built in support for five zones that use parallel VAV terminal units. The example model uses the same size terminal units from the same manufacturer for all five zones. Different terminal units – size and manufacturer – can be used provided the user scales the loads to the capabilities of the terminal unit that will be used in the model.

The five zones supported by the model consist of the Core zone plus four perimeter zones – North, East, South, and West. The spreadsheet for the parallel zone is identical for all five zones – that is the inputs and outputs are identical. For the case of the example, the same parallel fan powered terminal unit is used for all five zones so the inputs are identical. The outputs are based on the inputs and the hourly loads so even with the same FPTU in all five zones, the outputs vary with the loads.

The parallel zone spreadsheet has four sections that consist of the “Box Settings at Peak Loads”, “Simulation”, “Zone VAV Box Coefficients” and “Box Operation Model.” Each section will be described in the following paragraphs.

Figure 2.14 shows the “Box Settings At Peak Loads” for the parallel zones. All parallel zones have the same inputs for this section. Before a simulation is performed, the user adjusts

the inputs in this section to adjust the operation of the terminal unit to match design conditions for the zone.

Box Settings At Peak Loads	
Core	Zone Data
Box Data	
Box Type	P12
Upstream Static	0.30
Downstream Static	0.25
DP	0.05
Damper Setting	0.00
Primary Max Flow	1575
Downstream K	0.1008
Primary Min Setting	20
Primary Min Flow	315
Sens Cooling at Min Flow	7825
SCR Setup	
P Flow Sensor	-0.0076
Max Flow	1575
Dwn Static When On	0.141
SCR Setting (V)	159
On Flow (75% Max)	787
Estimated Fan Power	360
Sen Fan Load	1228
Net Sens Cooling At Min Flow	6597
Leakage Factor	10
Loads At Peak	
Total Load	46309
SHR at Peak	0.81
Sensible Peak	37510
Latent Peak	8799
Return Air Gain Rate	0
Return Air Gain	0
Zone Space Settings	
Space Temperature	78
Dead Band Setting	0
Primary Air	
Temp	55
RH	95
Humidity Ratio	0.0089

Figure 2.14 shows the “Box Settings At Peak Loads” for the parallel zones.

The data entry fields for this section of the spreadsheet are as follows:

1. Upstream Static (inches of water).
2. Downstream Static (inches of water).
3. Damper Setting.
4. Primary Min Setting.
5. SCR Setting (V).
6. Leakage Factor (%).
7. Space Temperature (F).
8. RH (%).
9. Humidity Ratio (lbs H₂O / lb Dry Air).

The inputs in Figure 2.14 are fields that are either white, green, or yellow. The white fields are straight inputs at the zone level. The grey fields are outputs that are derived from the inputs. The green fields are inputs that are pulled from the “Normalized Loads” spreadsheet using cell relations. The yellow fields are inputs that are pulled from the “System” spreadsheet using cell relations. The data in the green and yellow fields can be entered manually at the zone level but keep in mind that manual data entry will destroy the cell relationships that link the system level inputs to the zone level settings.

Figure 2.15 shows the “Simulation” section of the zone spreadsheet. The Simulation inputs consist of the following:

1. Start Row. The initial row used in the calculation process.
2. Qty. The number of hours to for which to perform the calculations.

Simulation	
Start Row	64
End Row	8823
Qty	8760

Perform Calcs

Figure 2.15. The “Simulation” section of the zone spreadsheet.

The Simulation section controls the zone level calculations. The zone level calculations are too complex to be able to reliably use cell relations for the calculations. The zone level calculations were put into a series of Visual Basic macros that were embedded in the workbook. The “Perform Calcs” button initiates the calculation process and activates the control algorithm that works through all of the hourly calculations one row at a time. The algorithm starts at the row entered into the “Start Row” field and continues for the number of row listed in the “Qty” field. The “End Row” field is a calculated value.

Figure 2.16 shows the input fields that contain the terminal unit performance coefficients. The terminal units are modeled with three questions and therefore there are three sets of input. The first equation is titled “Primary Flow” and is used to model the primary air flow through the fan powered terminal unit. The second equation is used to calculate the amount of air that flows through the terminal unit fan. The total amount of air supplied to a zone is a combination of the primary air flow and the fan air flow. The third equation models the power used by the terminal unit fan.

Primary Flow						
Box	C1	C2	C3			
P12A	7425.1	-0.0307	0.000245			
$q = \text{MAX}(1 + A1 * D + B1 * D^2) * \text{sqrt}(DP)$						
Fan Flow						
Box	MAX	c1	c2	c3	c4	c5
P12	2000.0	0	-0.0001	0.0000	-0.2020	-0.102
			v	v^2	pdwn	prake
$y = c1 + c2 * V^2 + C3 * V + c4 * P_{\text{downstream}} + c5 * \text{FlowPressure}$						
Fan Power						
Box	MAX	c1	c2	c3	c4	c5
P12	900.0	0	0.0004	0.0000	-0.1580	0.0000
$y = c1 + c2 * V^2 + C3 * V + c4 * P_{\text{downstream}} + c5 * \text{FlowPressure}$						
Primary Flow vs. P _{sensor}						
Box						
P12	1.0	2	3.0000	4.0000	5.0000	
$P = C1 + C2 * \text{Flow}(cfm)$						

Figure 2.16. The model input section for the parallel terminal units.

Figure 2.17 shows the outputs that result from the hourly calculations. The columns of data titled “Space Sensible load (Btu/hr)” and “Space latent Load (Btu/hr)” are inputs that are pulled from the “Normalized Loads” spreadsheet using cell relations. The user can override these values but should be aware that manual data entry into these fields will result in the destruction of the cell relations.

Zone Operation													
Zone Data													
Hour	Space Sensible Load (btu/hr)	Space Latent Load (btu/hr)	Primary Air Flow (cfm)	Box Fan Air Flow (cfm)	Supply Air Flow (cfm)	Box Fan Power (W)	Zone Return Air Temp (F)	Zone Supply Temp (F)	Zone Required Supply Temp (F)	Heat Added to Meet Load (btu/hr)	Zone Upstream Static (in)	Zone Downstream Static (in)	
1/1/1999 0:00	2,845	0	315	794	1109	349	78.0	72.5	75.6	3,790	0.1341	0.1241	
1/1/1999 1:00	1,839	0	315	794	1109	349	78.0	72.5	76.5	-1,796	0.1341	0.1241	
1/1/1999 2:00	963	0	315	794	1109	349	78.0	72.5	77.2	5,672	0.1341	0.1241	
1/1/1999 3:00	202	0	315	794	1109	349	78.0	72.5	77.8	6,434	0.1341	0.1241	
1/1/1999 4:00	-461	0	315	794	1109	349	78.0	72.5	78.4	7,098	0.1341	0.1241	
1/1/1999 5:00	-1,038	0	315	794	1109	349	78.0	72.5	78.9	7,673	0.1341	0.1241	
1/1/1999 6:00	1,211	0	315	794	1109	349	78.0	72.5	77.0	5,424	0.1341	0.1241	
1/1/1999 7:00	6,937	926	331	791	1422	348	78.0	72.2	72.3	0	0.1369	0.1269	
1/1/1999 8:00	24,221	1,852	975	0	975	0	78.0	55.0	55.0	0	0.1158	0.0958	
1/1/1999 9:00	29,147	8,799	1173	0	1173	0	78.0	55.0	55.0	0	0.1687	0.1387	
1/1/1999 10:00	30,960	8,799	1246	0	1246	0	78.0	55.0	55.0	0	0.1865	0.1565	
1/1/1999 11:00	30,499	4,168	1228	0	1228	0	78.0	55.0	55.0	0	0.1819	0.1519	
1/1/1999 12:00	28,996	4,168	1167	0	1167	0	78.0	55.0	55.0	0	0.1673	0.1373	
1/1/1999 13:00	34,617	8,799	1384	0	1384	0	78.0	55.0	55.0	0	0.2367	0.1967	
1/1/1999 14:00	35,718	8,799	1438	0	1438	0	78.0	55.0	55.0	0	0.2484	0.2084	

Figure 2.17. “Zone Operation” output section of the zone level spreadsheets.

SERIES ZONES - CORE / NORTH / EAST / SOUTH / WEST

The series model has built in support for five zones that use series VAV terminal units. The example model uses the same size terminal units from the same manufacturer for all five zones. Different terminal units – size and manufacturer – can be used provided the user scales the loads to the capabilities of the terminal unit that will be used in the model.

The five zones supported by the model consist of the Core zone plus four perimeter zones – North, East, South, and West. The spreadsheet for the series zone is identical for all five zones – that is the inputs and outputs are identical. For the case of the example, the same series fan powered terminal unit is used for all five zones so the inputs are identical. The outputs are based on the inputs and the hourly loads so even with the same FPTU in all five zones, the outputs vary with the loads.

The series zone spreadsheet has four sections that consist of the “Box Settings at Peak Loads”, “Simulation”, “Zone VAV Box Coefficients” and “Box Operation Model.” Each section will be described in the following paragraphs.

Figure 2.18 shows the “Box Settings At Peak Loads” for the series zones. All parallel zones have the same inputs for this section. Before a simulation is performed, the user adjusts the inputs in this section to adjust the operation of the terminal unit to match design conditions for the zone.

The data entry fields for this section of the spreadsheet are as follows:

1. SCR Setting.
2. Primary Max Upstream (static pressure in inches of water).
3. Damper Setting.
4. Primary Min Setting (static pressure in inches of water).
5. Sensible Peak (cooling load in Btu/hr).
6. Latent Peak (cooling load in Btu/hr).
7. Return Air Gain Rate (percent of peak load)
8. Return Air Gain (Btu/hr).
9. Space Temperature (F).
10. Primary Air Temperature (F).
11. Primary Air RH (%).
12. Primary Air Humidity Ratio (lbs H₂O / lb Dry Air).

Box Settings At Peak Loads	
Core Series	Zone 1
Box Data	
SCR Setting	242
Supply Flow	1574
Calc Pflow sens	0.471
Primary Max Upstream	0.2
Damper Setting	1
Primary Max Flow	1577
Primary Min Setting	20
Primary Min Flow	315
Box Fan Power	694
Fan Delta-T	1.39
Return Air Temp	78.0
Loads At Peak	
Total Load	46309
SHR at Peak	0.81
Sensible Peak	37510
Latent Peak	8799
Return Air Gain Rate	0
Return Air Gain	0
Zone Space Settings	
Space Temperature	78
Primary Air	
Temp	55
RH	95
Humidity Ratio	0.0089

Figure 2.18 shows the “Box Settings At Peak Loads” for the parallel zones.

The inputs in Figure 2.18 are fields that are white, green, or yellow. The white fields are straight inputs at the zone level. The grey fields are outputs that are derived from the inputs. The green fields are inputs that are pulled from the “Normalized Loads” spreadsheet using cell relations. The yellow fields are inputs that are pulled from the “System” spreadsheet using cell relations. The data in the green and yellow fields can be entered manually at the zone level but keep in mind that manual data entry will destroy the cell relationships that link the system level inputs to the zone level settings.

Figure 2.19 shows the “Simulation” section of the zone spreadsheet. The Simulation inputs consist of the following:

1. Start Row. The initial row used in the calculation process.
2. Qty. The number of hours to for which to perform the calculations.

Simulation	
Start Row	64
End Row	8823
Qty	8760

Perform Calcs

Figure 2.19. The “Simulation” section of the zone spreadsheet.

The Simulation section controls the zone level calculations. The zone level calculations are too complex to be able to reliably use cell relations for the calculations. The zone level calculations were put into a series of Visual Basic macros that were embedded in the workbook. The “Perform Calcs” button initiates the calculation process and activates the control algorithm that works through all hourly calculations one row at a time. The algorithm starts at the row entered into the “Start Row” field and continues for the number of row listed in the “Qty” field. The “End Row” field is a calculated value.

Figure 2.20 shows the input fields that contain the terminal unit performance coefficients. The terminal units are modeled with three equations and therefore there are three sets of input. The first equation is titled “Primary Flow” and is used to model the primary air flow through the fan powered terminal unit. The second equation is used to calculate the amount of air that flows through the terminal unit fan. The total amount of air supplied to a zone is a combination of the primary air flow and the fan air flow. The third equation models the power used by the terminal unit fan.

VAV Box Coefficients										
Primary Flow										
Box	MAX	a1	a2	a3	a4	a5	a6	a7	a8	a9
S12	2052	-0.0045	1.891	-0.3785	0.001069	0.00000427	0.0004	-0.022535	-0.0016	2.92E-07
Flow=MAX*(a1+a2*p+a3*p^2+a4*v+a5*v^2+a6*d+a7*d^2+a8*p*v*d+a9*p^2*v^2*d^2)										
Fan Flow										
Box	MAX	c1	c2	c3	c4	c5				
S12	2065	-0.681043882	-2.336E-07	0.006019274	3.07E-05	0.000				
cfm = MAX*(c1+c2*v^2+C3*v+c4*FlowPressure)										
Fan Power										
Box	MAX	c1	c2	c3	c4	c5				
S12	900.000	-0.6354	-0.000002	0.006	0.062	0.0000				
Watts = MAX*(c1+c2*v^2+C3*v+c4*FlowPressure)										
Primary Flow vs. Psensor										
Box	1	2	3	4	5					
S12	-0.160	0.000400								

Figure 2.20. The model input section for the series terminal units.

Figure 2.21 shows the outputs that result from the hourly calculations. The columns of data titled “Space Sensible load (Btu/hr)” and “Space latent Load (Btu/hr)” are inputs that are pulled from the “Normalized Loads” spreadsheet using cell relations. The user can over ride these values but should be aware that manual data entry into these fields will result in the destruction of the cell relations.

Zone Operation										
Zone 1										
Hour	Space Sensible Load (btu/hr)	Space Latent Load (btus/hr)	Required Supply Temp Ts (F)	Required Before Fan Mixed Air Temp Tvavm	Primary Airflow (cfm)	Induced Air Flow (cfm)	Actual Before Fan Temp Before Heat Added (F)	Space Heating Required (btus)	Min Upstream Static (in)	
1/1/1999 0:00	2,845	0	76.33	74.94	315	1,258	73.39	2,627	0.0001	
1/1/1999 1:00	1,839	0	76.92	75.53	315	1,258	73.39	3,633	0.0001	
1/1/1999 2:00	963	0	77.43	76.04	315	1,258	73.39	4,509	0.0001	
1/1/1999 3:00	202	0	77.88	76.49	315	1,258	73.39	5,270	0.0001	
1/1/1999 4:00	-461	0	78.27	76.88	315	1,258	73.39	5,933	0.0001	
1/1/1999 5:00	-1,038	0	78.61	77.22	315	1,258	73.39	6,510	0.0001	
1/1/1999 6:00	1,211	0	77.29	75.90	315	1,258	73.39	4,261	0.0001	
1/1/1999 7:00	6,937	926	73.92	72.53	374	1,199	72.53	0	0.0001	
1/1/1999 8:00	24,221	1,852	63.75	62.36	1,070	503	62.36	0	0.0263	
1/1/1999 9:00	29,147	8,799	60.85	59.46	1,289	305	59.46	0	0.0924	
1/1/1999 10:00	30,960	8,799	59.78	58.39	1,341	232	58.39	0	0.1177	
1/1/1999 11:00	30,499	4,168	60.06	58.67	1,323	251	58.67	0	0.1109	
1/1/1999 12:00	28,996	4,168	60.94	59.55	1,262	311	59.55	0	0.0905	
1/1/1999 13:00	34,617	8,799	57.63	56.24	1,489	85	56.24	0	0.1687	
1/1/1999 14:00	35,718	8,799	56.98	55.59	1,533	41	55.59	0	0.1842	

Figure 2.21. “Zone Operation” output section of the zone level spreadsheets.

CHAPTER 3

Running The Simulation

INTRODUCTION

A building model was used to form the basis of the operation of the system level models. Early in the project, it was decided to use the DOE-2 building simulation program. This software is widely used to model building heating and cooling loads and was used in this project to develop the hourly loads used for the system simulations. The project goal was to develop a five zone system model and this required that a five zone building model be developed. A generic five zone building model was designed with North, East, South, West and Core zone types. These zone exposures cover the primary loads created through the influence of external weather and solar effects. The interior, or Core zone, would be dominated by internal loads. These zone types represent most zone types encountered in applications that used single duct VAV systems based on either series or parallel fan powered terminal units. The inputs for the generic building were used to develop this tutorial.

BUILDING DESCRIPTION

Figure 3.1 shows a diagram of the five zone building layout. The building was a rectangular structure that had a footprint of 122.5 ft x 122.5 ft (37.3 m x 37.3 m). The perimeter zones had 1,612 ft² (149.8 m²) while the core zone had 8,556 ft² (794.9 m²).

The perimeter zones had walls that were 50% glass with a window U-Factor of 0.46 Btu/hr/F°/ft² and a solar heat gain coefficient of 26%. The wall insulation was R-13 while the roof insulation was R-15. The cooling loads due to people in the building were calculated using a factor of 275 ft² (25.5 m²) per person. The Lighting and equipment loads were 1.3 Watt/ft² and 0.75 Watt/ft² (14 Watt/m² and 8.1 Watt/m²) respectively.

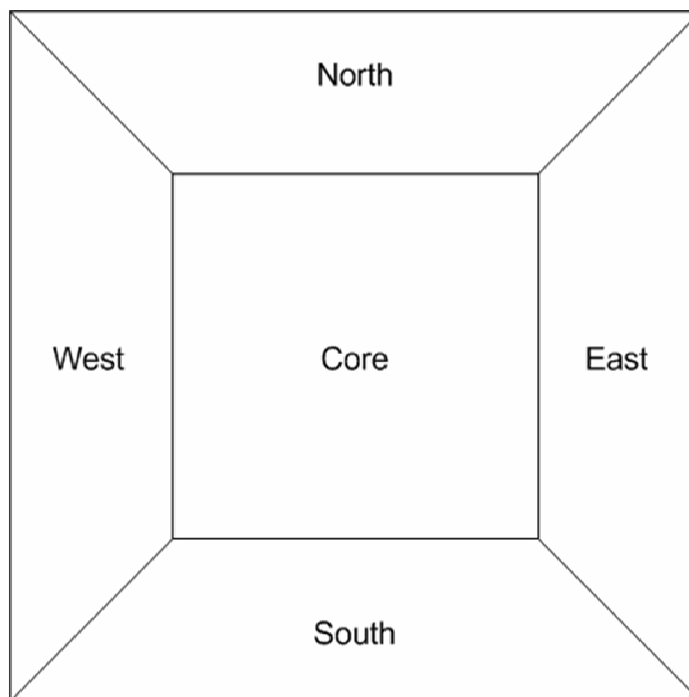


Figure 3.1. Diagram of the Floor Plan of the Building Used as the Basis for the DOE-2 Loads Model.

The building was operated on a typical office schedule for the entire year and the normal holidays encountered in the U.S. were not included in the operating schedule. The hourly cooling/heating loads were generated using the TMY weather data set for the five locations of Chicago, Houston, New York, Phoenix and San Francisco. The hourly loads were generated for all five building zones for each of the five geographic locations. Hourly sensible and latent space loads were calculated for all zones for the entire 8,760 hours in a year.

After the space loads for each climate were generated, they were exported to an Excel spreadsheet. The hourly data used to generate the hourly loads were also loaded into a separate Excel workbook with each set of weather data loaded into a separate worksheet. The hourly weather data consisted of a time stamp (as included in the TMY data set), the outdoor ambient dry-bulb temperature, and the outdoor ambient humidity ratio.

SETUP THE NORMALIZED LOADS

The output from the DOE simulation was loaded into a spreadsheet and organized as shown in Figure 3.2. The original data layout from the output from DOE2 was used as the basis for the

development of the normalization spreadsheet. To enter the loads into this spreadsheet for use the user should first make sure that the automatic update feature is turned on.

Time	Core zone		South perimeter		East Perimeter		West Perimeter		North Perimeter	
	Sensible	Latent	Sensible	Latent	Sensible	Latent	Sensible	Latent	Sensible	Latent
	Btu/hr	Btu/hr	Btu/hr	Btu/hr	Btu/hr	Btu/hr	Btu/hr	Btu/hr	Btu/hr	Btu/hr
Max Values->	47776.89	4581.48	39069.56	863.42	37502.77	863.42	45401.01	863.42	32099.96	863.42
0:00	3624.24	0	-14317.97	0	-14718.95	0	-14946.03	0	-15237.14	0
1:00	2342.36	0	-17156.69	0	-17512.92	0	-17659.46	0	-17918.51	0
2:00	1227.13	0	-18146	0	-18455.79	0	-18673.25	0	-18898.54	0
3:00	256.88	0	-18851.72	0	-19121.24	0	-19245.49	0	-19441.49	0
4:00	-587.24	0	-19071.33	0	-19305.81	0	-19142.09	0	-19312.61	0
5:00	-1321.62	0	-20403.36	0	-20607.36	0	-20942.18	0	-21090.53	0
6:00	1543	0	-20303.08	0	-20743.44	0	-20430.31	0	-20823.23	0
7:00	8836.12	482.26	-17737.07	90.89	-17524.54	90.89	-18684.47	90.89	-19083.43	90.89

Figure 3.2. The hourly loads values from the DOE 2 simulation.

The automatic update feature can be found using the Excel help system and will not be explained here. After the hourly data has been arranged into a spreadsheet in the proper format and the automatic update feature has been enabled, the user will copy the data from the source spreadsheet and paste it into the “From The Model” section of the “Normalized Loads” spreadsheet. After the hourly values have been copied into the loads spreadsheet, the normalized load values will automatically be calculated. The user will need to edit the Max Value for the loads in the “Normalized Loads” section of the spreadsheet to scale the hourly loads to the desired peak load for the terminal units used in the zone models.

SETUP THE SYSTEM INPUTS

After the normalized loads have been generated, the user will need to select the “System” tab to display the “System” spreadsheet. Before entering data into the “System” spreadsheet inputs the user should verify that the “Automatic Update” feature is turned on.

After the automatic update feature has been activated the user may proceed to edit the system inputs. After the system inputs have been adjusted to the desired values the user should tab through the zone screens to verify that any zone level data inputs were properly transferred to each zone. All zones should be checked by the user.

Once the “System Settings” and the “Zone Settings” have been updated and the zones checked for proper updates, the user may proceed to the zone level calculations.

PERFORM THE CALCULATIONS

The zone level calculations can be performed after the system settings have been completed. Each zone should be processed completely before the user proceeds to another zone. The user should start the zone level calculations with the Core parallel zone and then proceed one at a time through all of the parallel zones. After the parallel zone calculations have been completed, the user should start with the “Core Series” zone and work through the series zones one at a time.

Each zone should be processed using the following sequence of events:

1. Verify that the Automatic Update feature in Excel has been TURNED ON.
2. Edit the “Zone VAV Box Coefficients” if required. The proper coefficients must be in place before the box settings are modified because the box settings use the equations for calculating some of the parameters used by the simulation.
3. Edit the “Box Settings At Peak Loads” to ensure the desired operation of the fan powered terminal unit at peak cooling load and at minimum flow conditions. Once the “Box Settings At Peak Loads” are at the desired values proceed to the next step.
4. Edit the “Simulation” section of the spreadsheet. After the start row and the quantity have been entered, the end row should update to a new value. Verify that the start and end rows are the proper values and when they are, proceed to the next step.
5. Repeat steps 2 – 4 for all zones.
6. Set the “Automatic Update” feature to OFF. Once the “Automatic Update” feature has been set to manual calculations, proceed to the next step.
7. Go to the parallel Core zone and initiate the zone level calculation by pressing the “Perform Calcs” button located under the Qty entry field. The button will stay down until the zone calculations are complete. On a 2.1 GHz machine this process takes about 80 seconds.
8. Repeat step 7 for all zones. After all zone calculations have been completed go to the next step.
9. Go to the “System” spreadsheet.
10. Use the Excel menus and TURN ON the automatic update feature and then press the “Calc Now (F9)” button shown on the Tools->Options screen. The options screen will

close and the zone level calculations will begin. The zone level calculations will take several minutes on a 2.1 GHz machine. If your computer is slower, it will take longer.

11. Repeat step 10. Repeat step 10 because Excel does not always keep proper track of the cell interactions.

REVIEW THE RESULTS

The results of the calculations will be listed in the zone and system level spreadsheets.

AB-10-C019

Energy Use Comparison for Series vs. Parallel Fan Powered Terminal Units in a Single Duct Variable Air Volume System

John Bryant, PhD, PE

Member ASHRAE

Michael Davis

Associate Member ASHRAE

Dennis O'Neal, PhD, PE

Fellow ASHRAE

ABSTRACT

Previous papers under RP 1292 presented engineering models and experimental verification of those models for series and parallel VAV fan powered terminal units. This paper presents the results from the research in terms of power consumption for series vs. parallel fan powered terminal units (FPTU). Each system type was simulated in a base configuration for Houston, Texas and six different scenarios were simulated for comparison. The primary case was expanded to cover other geographic/weather locations which confirmed this trend. Previous results from RP-1292 showed that parallel FPTU have a leakage rate of up to 20% of primary air. When this leakage is included in the simulation the series FPTU fare much better. If 20% parallel leakage is assumed, the series system consumes 6% less energy than the parallel system.

INTRODUCTION

Previous papers have described the configuration, engineering model, and experimental verification of the model for a Single Duct Variable Air Volume (SDVAV) system that used Fan Powered Terminal Units (FPTU) (Davis, et al. 2009, Bryant, et al. 2009). The focus of the study was on the use of Series and Parallel FPTU as applied in common configurations in the field. The objective of this paper is to summarize the results of the simulated operation of the five zone model and compare the energy consumption of the series based five zone system to the parallel based five zone system. A five zone system model was used to predict the operation of a typical commercial building operating for one year for both series and parallel FPTU at five different geographical locations around the United States. (Davis, et al. 2009).

Results presented here cover the base case operating conditions and use Houston, Texas weather data and cooling and heating loads for the analysis. The system model used a variety operating parameters that determined the operation of the system. The base case was followed by a sensitivity analysis that consisted of

John Bryant is an associate professor in the Mechanical Engineering Program, Texas A&M University at Qatar. **Michael Davis** is Director of Laboratories for New York University at Abu Dhabi. **Dennis O'Neal** is Professor and Head of the Mechanical Engineering Department. Texas A&M University, College Station, Texas

modified base case operation using Houston cooling and heating loads and weather data. The objective of the sensitivity analysis was to understand the operation of the model at various system operating conditions that may be encountered in real buildings. The case variations in these results include the following:

Base case with Houston loads and weather.

1. Base case with 10% primary air leakage rate (parallel).
2. Base case with 20% primary air leakage rate (parallel).
3. Differences using different manufacturer's parallel FPTU.
4. No-power terminal unit fans.
5. A 15% return air heat gain at the zone level.

BASE CASE

The base case settings were intended to mimic the theoretical best case operating patterns of most buildings that use FPTU. The return heat gain setting was set to zero to mimic the operation of a system installed in a space below a conditioned space. The primary fan minimum static pressure was set to 0.0 in.w.g. (0.0 Pa) thus primary energy power consumption was based only on the static pressure requirements of the FPTU. The leakage rate for the parallel units was set to zero to mimic perfect back-draft damper operation and perfect manufacturing of the FPTU. Leakage was not included for series units since the only part of the series unit that is under positive pressure is the outlet from the fan to the supply duct. Any leakage from the supply duct for either type of unit was assumed to be the same for both systems. The operating schedule was set to have the system turn on at 6:00 a.m. and off at 6:00 p.m. which is common to the operation of commercial buildings. A weekend schedule was not modeled.

The model allowed for the use of a "Zero FPTU Fan Power" setting. This setting allowed the model to calculate the terminal unit fan power for all zones and estimate the amount of heat added to the zones as a result or ignore the heat energy penalty generated by the FPTU fan. When "Zero FPTU Fan Power" was enabled, the FPTU fans acted as "zero-power" devices and allowed the model to move air at the FPTU using no power and thus, did not introduce heat into the zones.

A similar function was included in the model for the primary fan. The "Zero Primary Fan Power" setting (on or off) caused the primary fan to use power (on) or not (off) when it moved the primary air through the system. When "Zero Primary Fan Power" was enabled, the primary fan still moved air through the system but it did not consume power. This feature allowed the impact of the primary fan on system energy consumption to be studied.

Table 1 shows the summary of the base case results for the five zone system model as simulated for the Houston location. The total energy consumed by the series system was 17.3% higher than the energy consumed by the parallel system for this base case. The table shows that the primary fan used 18% more energy for the series system than for the parallel system. It is commonly believed that a primary fan would use less energy serving a series system than it would for a parallel system. This is because in the series system the primary fan does not have to work against as much static pressure as it does in a parallel system. In effect, the

series FPTU “helps” the primary fan deliver air to the required zone. The results of the base case simulation show this is not the case.

Table 1. Annual Total Single Zone VAV Base Simulation Results for the Houston Location.

	Parallel (kWh)	Series (kWh)	Percent Difference
Total System Energy Use	77,957	91,438	17.3%
Primary Fan Energy	2,801	3,310	18%
Terminal Unit Fan Energy	3,182	15,195	378%
Thermal Energy Added	26,962	24,324	-10%
Terminal Unit Fan + Aux Heat Energy	30,186	39,564	31%
Max. Static Pressure (in. w.g., (Pa))	0.280 (69.7)	0.210 (52.3)	
Min. Static Pressure (in. w.g., (Pa))	0.027 (6.7)	0.00	

The primary fan energy use was higher for the series system because the series system required more primary air flow during cooling conditions. The series FPTU using a generic fan model, required 2,200 Btu (694 W) as shown in Table 2. The “Input Values” used in this table were the result of laboratory testing and development of a generalized model for a series FPTU (Bryant, et al. 2009).

Table 2. Base Case Series FPTU Peak Load Settings for a Single Duct, Five Zone VAV System Simulation for Houston.

Core, Series	Zone 1
Series FPTU Input Data	
SCR Setting (V_{ac})	242
Zone Supply Air (cfm (l/s))	1,574 (743)
Primary Upstream Static Pressure (in. w.g. (Pa))	0.2 (49.8)
FPTU Inlet Valve Setting	1
Primary Air Minimum Flow setting (cfm (l/s))	20 (9.4)
Series FPTU Calculated Values	
Flow Sensor Differential Pressure (in. w.g. (Pa))	0.47 (117)
Primary Maximum Air Flow (cfm (l/s))	1,577 (744)
Primary Minimum Air Flow (cfm (l/s))	315 (149)
Series Fan Power (Btuh (W))	2,200 (694)

After these values were set for a particular simulation case, the model would generate the “Calculated Values” portion of the table. The total power consumption of the terminal unit fans for the five zone series system was 11,840 Btu/hr (3,470 W) or an additional cooling load of approximately one ton (thermal). This cooling load required additional primary air flow of 477 cfm (225 l/s) as shown in Equation 1,

$$AirFlow = \frac{11,840 \text{ Btu/hr}}{1.08 \times (T_{setpoint} - T_{primary})} = \frac{11,840 \text{ Btu/hr}}{1.08 \times (78 - 55)} = 477 \text{ cfm} \quad (1)$$

Because of this extra heat load in the zones, the primary fan had to supply an

extra 477 cfm (225 l/s) at the highest peak zone static pressure requirement.

At the peak load for the zone, primary air would experience a temperature rise of approximately 1.4°F (0.8°C) as it passed through the series FPTU fans. The temperature increase across the FPTU fans thus represented a 6% loss in cooling capacity at peak loads. When the space load is less than the peak, the loss in cooling capacity is even greater.

The total primary air flow rate for the series system at design peak was 7,604 cfm (3,589 l/s). The parallel system peak flow rate occurred at the same time and was 7,129 cfm (3,364 l/s). There was a difference of 475 cfm (224 l/s) between the series and parallel system flow rate at the peak load. The simulations also showed that the series unit consistently required less upstream static pressure than a parallel unit under similar conditions. It is the extra thermal load from the FPTU fans that account for the difference in performance between the two systems.

CASE 1 - PARALLEL 10% PRIMARY LEAKAGE RATE

Case 1 consisted of modifying the base case to allow for leakage from parallel FPTU. 10% leakage for this first case was included in the parallel terminal unit models because a significant amount of leakage was measured during the laboratory characterization of parallel terminal units (Furr, et al. 2008b).

The leakage rates measured varied from one manufacturer to another as well as from one unit size to another between manufacturers (Furr, et al. 2008b). Because of these differences, a leakage rate could not be determined for the units that could be considered as the "right" amount for any given analysis. Since only one terminal unit was provided from each manufacturer for the two sizes that were tested, it was not possible to determine a generic leakage rate equation that could be applied with a reasonable degree of confidence when modeling the operation of the parallel system.

Table 3 shows the summary of the 10% leakage case results for the five zone system model. The "Case 1" simulation that generated the results shown in this table was performed for the Houston location. Table 3 shows the annual totals for the series and parallel five zone models for total energy consumption, primary fan energy consumption, terminal unit fan energy consumption, and thermal energy added to maintain space temperature.

The series based FPTU system consumed only 6.7% more total annual energy than the parallel FPTU system. Under the base case scenario, series FPTU system energy consumption was 17.3% higher than the parallel FPTU system. With 10% leakage annual energy consumption for the parallel FPTU system increased by 7,620 kWh while series energy consumption remained unchanged.

This result was expected because leakage was included only for the parallel units and this is reflected in the added energy use by the Primary fan in the parallel system. With Primary air leaking into the plenum space instead of being delivered to the load in the space, the Primary fan has to provide even more air to meet the load. A 10% leakage rate resulted in about a 10% increase in the energy consumption for the parallel system compared to the base case.

Table 3. Simulation Summary for the Houston Location with 10% Primary Air Leakage for Parallel FPTU.

	Parallel Case 1	Parallel Base	Series Case 1	Series Base	Case 1 Diff	%Diff
Total Annual Energy (kWh)	85,577	77,957	91,438	91,438	5,861	6.7%
Primary Fan Energy (kWh)	3,635	2,801	3,310	3,310	-325	-9%
FPTU Fan Energy (kWh)	3,183	3,182	15,195	15,195	12,012	377%
Thermal Energy Added (kWh)	32,273	26,962	24,325	24,325	-7,948	25%
FPTU Fan + Thermal (kWh)	35,456	30,186	39,520	39,520	4,064	12%

CASE 2 - PARALLEL 20% PRIMARY LEAKAGE RATE

Case 2 consisted of modifying the Houston base case such that primary air leakage rate for the parallel FPTU was 20%. Table 4 shows the summary of the 20% leakage case results for the five zone system model. The table shows the annual energy totals for the series and parallel five zone models for total energy consumption, primary fan energy consumption, FPTU fan energy consumption, and thermal energy added to maintain space temperature. The total annual energy consumed by the series FPTU system was 3.3% lower than the energy consumed by the parallel system with 20% leakage. Again, referring to the base case, the series FPTU system energy consumption had been 17.3% greater than for the parallel FPTU system.

For the case of 20% primary leakage, energy consumption increased by 16,705 kWh for the parallel FPTU system while the series FPTU energy consumption remained unchanged. This is a 21% increase in energy consumption compared to the base Parallel FPTU system.

Table 4. Simulation Summary for the Houston Location with 20% Primary Air Leakage for Parallel FPTU.

	Parallel Case 2	Parallel Base	Series Case 2	Series Base	Case 2 Diff.	% Diff.
Total Annual Energy (kWh)	94,662	77,957	91,438	91,438	-3,224	-3.3%
Primary Fan Energy (kWh)	4,927	2,801	3,310	3,310	-1,617	-33%
FPTU Fan Energy (kWh)	3,184	3,182	15,195	15,195	12,011	377%
Thermal Energy Added (kWh)	37,513	26,962	24,325	24,325	-13,188	35%
FPTU Fan + Thermal kWh)	40,697	30,186	39,520	39,520	-1,177	-3%

The penalty for parallel FPTU unit leakage appears to exhibit a linear relationship with increased energy consumption. Over the past several years, energy codes have addressed the problem of supply air duct leakage, but not the terminal units themselves. The results of this project demonstrate that leakage at the parallel FPTU should not be ignored.

CASE 3 - SENSITIVITY TO PARALLEL FPTU MANUFACTURER

Table 5 presents a summary of results from the base case using a P12A parallel FPTU and running the simulation with a different parallel FPTU designated as a P12C. This table shows that the change in the parallel FPTU system annual energy

use was not significant with a difference of just 1.1 percent. This was not considered significant and the analyses for the remainder of the simulations used the P12A FPTU.

Results of this sensitivity simulation did highlight the primary difference between these parallel FPTU systems. The P12C FPTU required significantly higher static pressure at peak and at minimum loads as compared to P12A. Even though these model results show increases of 325 and 250% respectively, there is minimal impact on the annual energy use. However, there are implications for the primary fan selection and control strategies for this unit.

Table 5. Simulation Results Replacing Parallel FPTU Terminal Unit Models in Base Case.

	Parallel P12C	Parallel Base P12A	P12C - A Diff.	Percent Diff.
Total Annual Energy Use (kWh)	78,836	77,957	879	1.1%
Primary Fan Energy Use (kWh)	3,552	2,801	751	26.8%
Terminal Unit Fan Energy (kWh)	3,223	3,182	41	1.3%
Thermal Energy Added (kWh)	26,962	26,962	0	0.0%
FPTU Fan + Thermal Energy (kWh)	30,185	30,144	41	1.3%

Table 6 shows a summary of the simulation results using the parallel P12C FPTU model including a 20% primary air leakage rate. The table shows that the change of 2.2% in the parallel system annual energy use was not significant compared to the P12A. Though total annual energy use was not significantly different between the P12A and P12C parallel FPTU with 20% leakage, the change in upstream static pressure required to operate P12C with 20% leakage was significant. As in the base case, this additional pressure requirement doesn't affect annual energy use very much, but the impact on primary fan selection and control would be different depending on specific manufacturer supplying the parallel FPTU for a given project.

Table 6. Simulation Results for the P12C Compared to the P12A FPTU Model with 20% leakage.

	Parallel P12C	Case 2 P12A	P12C - A Diff.	Percent Diff.
Total Annual Energy Use (kWh)	96,713	94,662	2,051	2.2%
Primary Fan Energy Use (kWh)	6,497	4,927	1,570	32%
Terminal Unit Fan Energy (kWh)	3,186	3,184	2	0.0%
Thermal Energy Added (kWh)	37,513	37,513	0	0.0%
FPTU Fan + Thermal (kWh)	40,699	40,697	41	0.0%

CASE 4 - "ZERO POWER" FPTU FANS

A special simulation run consisting of allowing the terminal unit fans to operate without consuming power was performed. With this setting, the operation of the series and the parallel FPTU systems were held the same as in the base case except that the terminal unit fans consumed zero power. All other base case parameters were left unchanged.

The results shown in Table 7 reveal that the annual energy use for both systems is essentially the same. The slightly higher value for the parallel FPTU system is because of the greater static pressure requirement of that system versus the series system.

Primary air requirements are shown to be essentially the same for both systems. As opposed to the base case, this simulation eliminates the thermal energy penalty that was demonstrated with Equation (1) and as would be expected, the primary fan energy for both systems is about equal. This case shows that power consumption in the series FPTU fans is the primary reason for increased energy consumption compared to a parallel FPTU system.

Table 7. Simulation Results for the Houston Location Using "Zero Power" FPTU Fans.

	Parallel (kWh)	Series (kWh)	% Difference
Total System Energy Use	77,752	77,547	-0.3%
Primary Fan Energy	2,797	2,611	-7%
Terminal Unit Fan Energy	0	0	NA
Thermal Energy Added	30,186	30,186	0%

CASE 5 - RETURN AIR HEAT GAIN

The base case was run using no return air heat gain, a common assumption for a zone sandwiched between two conditioned zones in a building. This case was run assuming that the zone was located below an insulated roof subject to a 15% return air heat gain. All other parameters remained the same as the base case. Results for this case are shown in Table 8.

Table 8. Simulation Results at Houston Location With 15% Return Air Heat Gain.

	Parallel (kWh)	Series (kWh)	% Difference
Total System Energy Use	75,612	90,852	20.1%
Primary Fan Energy	2,854	3,897	36.5%
Terminal Unit Fan Energy	3,175	15,195	379%
Thermal Energy Added	18,170	15,533	-17%

Total annual energy use actually dropped, relative to the base case, for both systems though the series FPTU system still has higher energy consumption. The parallel FPTU system cooling energy increased by 14% and auxiliary heat energy use dropped by 33% compared to the base case.

Auxiliary heat energy consumption dropped by 36% for the series FPTU system while energy use for cooling increased 16%. These are very similar for the parallel system. As with the base case however, the series FPTU system has the FPTU fan energy and the complicating effect of the additional amount of primary air required to offset the thermal energy added to the zone supply air by the FPTU fans. This is an energy penalty that cannot be avoided with a series FPTU system.

SUMMARY AND CONCLUSIONS

For all cases presented in this paper, except when allowing for primary air

leakage in parallel FPTU, a parallel FPTU system consistently uses less energy than a comparable series FPTU system. Unlike parallel FPTU, series FPTU do not operate under positive pressure and therefore they do not exhibit primary air leakage. The problem of leakage in parallel FPTU should not be ignored when simulating VAV systems with FPTU. Leakage, at some base level, was present in all parallel FPTU units tested as part of this research (Furr, et al. 2008b). The absolute amount of primary air leakage was dependent upon manufacturer and static pressure downstream of the FPTU. Rates varied from single digit up to 20% of the primary air being supplied to the FPTU. So, although Case 2 might seem high at 20% primary air leakage, it was within the range of values found for the three manufacturer's FPTU used in this study. This problem calls for further study to quantify the extent of leakage in newly manufactured parallel FPTU and impact of many existing parallel FPTU systems still in operation.

However, in all other cases studied and presented in this paper, the parallel FPTU VAV system uses less energy than the series FPTU system and the primary reason are the series FPTU fans. There is no way to avoid the fact that these fans run continuously while the system is in operation and they generate a thermal load that is delivered directly to the zone being served by that unit. This thermal load is ultimately picked up by the cooling system and shows as additional energy at the primary fan.

A relatively new addition to the FPTU systems is the use of electronically commutated motors (ECM). All FPTU used in this study used permanent split capacitor motors (PSC) controlled at the FPTU by an SCR controller adjusted at a specific speed. If ECMs are used to replace the PSC motors in series FPTU, the overall energy use of the cases presented here would be expected to decrease.

ACKNOWLEDGEMENTS

This work was a part of a project funded by ASHRAE under RP-1292 and the authors would like to thank the project monitoring subcommittee of TC 5.3 and the manufacturers they represent for their support during the project. Several manufacturers donated terminal units for use in this study. Through cooperative ventures such as these, ASHRAE research funding can be utilized to the fullest. We appreciate the contributions from these industry leaders.

REFERENCES

- Bryant, J., Davis, M., O'Neal, D.O., and Cramlett, A., 2009. Experimental Verification of a Three Zone VAV System Model Operating with Fan Powered Terminal Units (RP-1292), *ASHRAE Transactions* 115 (1).
- Davis, M., Bryant, J., and O'Neal, D.L., 2009. Modeling the Performance of Single-Duct VAV Systems that use Fan Powered Terminal Units (RP-1292). *ASHRAE Transactions* 115 (1).
- Furr, J., O'Neal, D.O., Davis, M., Bryant, J., and Cramlett, A., 2008a. Performance of VAV Fan Powered Terminal Units: Experimental Setup and Methodology. *ASHRAE Transactions* 114(1).
- Furr, J., O'Neal, D.O., Davis, M., Bryant, J., and Cramlett, A., 2008b. Performance of VAV Fan Powered Terminal Units: Experimental Results and Models for Parallel Units. *ASHRAE Transactions* 114(1).

AB-10-C020

Performance of VAV Fan Powered Terminal Units: An Evaluation of Operational Control Strategies for Series vs. Parallel Units

John Bryant, PhD, PE

Member ASHRAE

Dennis O'Neal, PhD, PE

Fellow ASHRAE

Michael Davis

Associate Member ASHRAE

ABSTRACT

Previous papers under RP 1292 presented engineering models and experimental verification of those models for series and parallel VAV fan powered terminal units. Terminal units with 8 in. (203 mm) and 12 in. (304 mm) primary air inlets from three different manufacturers were evaluated under this research project. This paper presents the results from the research in terms of operational control strategies for series vs. parallel fan powered terminal units. Each system type was operated in a simulation that varied geographic location in five regions of the United States and under several different control strategies. Results show that, depending on system loads, system control, and operational settings, the VAV control strategy can have a significant impact on operations, comfort conditions, and energy consumption. Conventional control strategies are likely going to lead to underperforming systems and a resulting increase in energy consumption. Improvements to conventional control strategies are also presented and discussed in this paper.

INTRODUCTION

Previous papers have described the configuration, engineering model, and experimental verification of the model for a Single Duct Variable Air Volume (SDVAV) system that used Fan Powered Terminal Units (FPTU) (Davis, et al. 2009, Bryant, et al. 2009). The focus of the original study under RP-1292 was on the use of Series and Parallel FPTU as applied in common configurations in the field. This paper is a companion to a paper that compares the energy use of series vs. parallel FPTU VAV systems (Bryant, et al. 2010). The objective of this paper is to summarize the results of the model operation of the five zone system and compare the energy consumption of the series to the parallel based five zone system when under various control strategies. The five zone system model was used to predict the operation of a typical commercial building operating for one year for both series and parallel fan powered terminal units at five different geographical locations around the United States (Davis, et al. 2009).

John Bryant is an Associate professor with the Mechanical Engineering Program, Texas A&M University at Qatar. **Dennis O'Neal** is Head and Professor in the Department of Mechanical Engineering, Texas A&M University, College Station, Texas. **Michael Davis** is Director of Laboratories, New York University at Abu Dhabi.

Results presented here cover a base case operating condition and use with Houston, Texas weather data. The model was then run for systems in Phoenix, San Francisco, Chicago, and New York. The system model used a variety of operating parameters that determined the operation of the system. The base case was followed by a sensitivity analysis that consisted of modified base case operation using Houston cooling and heating loads and weather data. The objective of the sensitivity analysis was to understand the operation of the model at various system operating conditions that may be encountered in real buildings. The case variations in these results include the following:

Base case with Houston loads and weather.

1. Minimum static pressure.
2. Constant static pressure.
3. 24 hour operation.

BASE CASE

The base case settings were intended to mimic the theoretical best case operating patterns of most buildings that use fan powered terminal units. The return heat gain setting was set to zero to mimic the operation of a system installed in a space below a conditioned space. The primary fan minimum static pressure was set to 0.0 in.w.g. (0.0 Pa). Thus primary energy power consumption was based only on the static pressure requirements of the FPTU. The leakage rate for the parallel units was set to zero to mimic perfect back-draft damper operation and perfect manufacturing of the FPTU. Leakage was not included for series units since the only part of the series unit that is under positive pressure is the outlet from the fan to the supply duct. Any leakage from the supply duct for either type of unit was assumed to be the same for both systems. The operating schedule was set to have the system turn on at 6:00 a.m. and off at 6:00 p.m. which is common to the operation of commercial buildings. A weekend schedule was not modeled.

The model allowed for the use of a "Zero FPTU Fan Power" setting where the terminal unit fan power for all zones was estimated, but the amount of heat energy added to the zones from the FPTU fans was ignored. When "Zero FPTU Fan Power" was enabled, the FPTU fans acted as "zero-power" devices and allowed the model to move air at the FPTU using no power and thus, did not introduce heat into the zones.

A similar function was included in the model for the primary fan. The "Zero Primary Fan Power" setting (on or off) caused the primary fan to use power (on) or not (off) when it moved the primary air through the system. When "Zero Primary Fan Power" was enabled, the primary fan still moved air through the system but it did not consume power. This feature allowed an estimation of the impact of the primary fan on system energy consumption.

Table 1 shows the summary of the base case results for the five zone system model as simulated for the Houston location. The total energy consumed by the series system was 17.3% higher than the energy consumed by the parallel system for this base case. The table shows that the primary fan used 18% more energy for the series system than for the parallel system. While the primary fan in the series

system had a smaller operating static pressure than did the primary fan in the parallel system, the primary fan energy use was higher for the series system because it required more primary air flow during cooling conditions. Table 2 shows the FPTU fan model required 2,200 (694 W) and other input data which were developed from previous tests (Bryant, et al. 2009).

Table 1. Annual Total Single Zone VAV Base Simulation Results for the Houston Location.

	Parallel (kWh)	Series (kWh)	Percent Difference
Total System Energy Use	77,957	91,438	17.3%
Primary Fan Energy	2,801	3,310	18%
Terminal Unit Fan Energy	3,182	15,195	378%
Thermal Energy Added	26,962	24,324	-10%
Terminal Unit Fan + Aux Heat Energy	30,186	39,564	31%
Max. Static Pressure (in. w.g., (Pa))	0.280 (69.7)	0.210 (52.3)	
Min. Static Pressure (in. w.g., (Pa))	0.027 (6.7)	0.00	

Table 2. Base Case Series FPTU Peak Load Settings for a Single Duct, Five Zone VAV System Simulation for Houston.

Core, Series	Zone 1
Series FPTU Input Data	
SCR Setting (V_{ac})	242
Zone Supply Air (cfm (l/s))	1,574 (743)
Primary Upstream Static Pressure (in. w.g. (Pa))	0.2 (49.8)
FPTU Inlet Valve Setting	1
Primary Air Minimum Flow setting (cfm (l/s))	20 (9.4)
Series FPTU Calculated Values	
Flow Sensor Differential Pressure (in. w.g. (Pa))	0.47 (117)
Primary Maximum Air Flow (cfm (l/s))	1,577 (744)
Primary Minimum Air Flow (cfm (l/s))	315 (149)
Series Fan Power (Btuh (W))	2,200 (694)

The model generated the "Calculated Values" portion of Table 2. The total power consumption of the terminal unit fans for the five zone series system was 11,840 Btu/hr (3,470 W) or an additional cooling load of approximately one ton (thermal). This cooling load required additional primary air flow of 477 cfm (225 l/s) as shown in Equation 1,

$$AirFlow = \frac{11,840 \text{ Btu/hr}}{1.08 \times (T_{setpoint} - T_{primary})} = \frac{11,840 \text{ Btu/hr}}{1.08 \times (78 - 55)} = 477 \text{ cfm} \quad (1)$$

Because of this extra heat load in the zones, the primary fan had to supply an extra 477 cfm (225 l/s) at the highest peak zone static pressure requirement.

At the peak load for the zone, primary air would experience a temperature rise of approximately 1.4°F (0.8°C) as it passed through the series FPTU fans. The

temperature increase across the FPTU fans thus represented a 6% loss in cooling capacity at peak loads. When the space load is less than the peak, the loss in cooling capacity is even greater.

The total primary air flow rate for the series system at design peak was 7,604 cfm (3,589 l/s). The parallel system peak flow rate occurred at the same time and was 7,129 cfm (3,364 l/s). There was a difference of 475 cfm (224 l/s) between the series and parallel system flow rate at the peak load. The simulations also showed that the series unit consistently required less upstream static pressure than a parallel unit under similar conditions. It is the extra thermal load from the FPTU fans that account for the difference in performance between the two systems.

Figure 1 shows the characteristics of the primary static pressure requirements for series and parallel FPTU on the peak load day for the Houston location. As expected, the series unit requires less upstream static pressure than a parallel unit under similar conditions. This is further evidence that it is the thermal load from the series FPTU fans that causes the performance difference between the two systems.

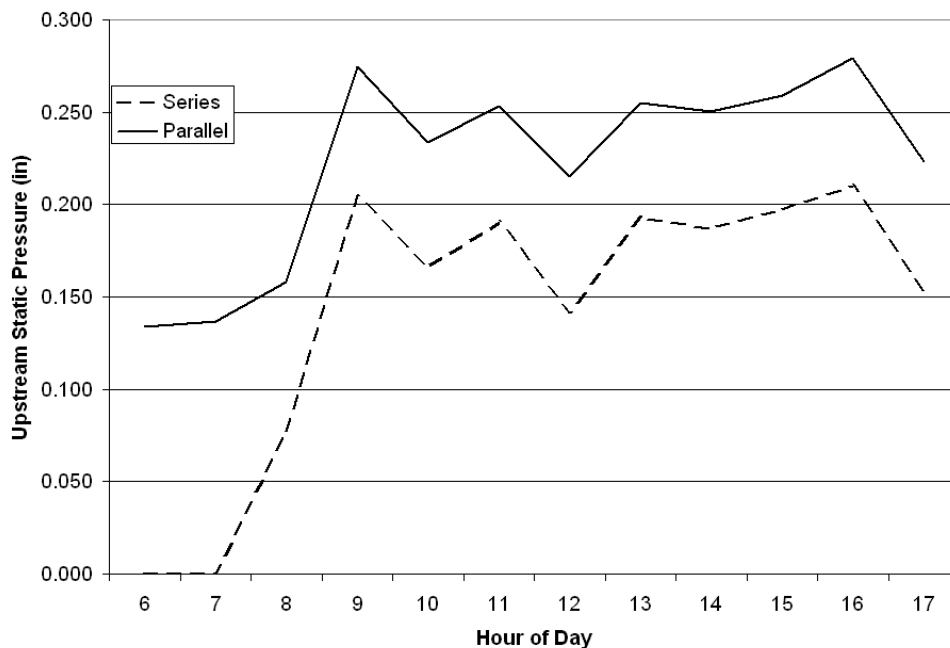


Figure 1. Primary Static Pressure for Series and Parallel FPTU on the Peak Cooling Day, Houston Base Case.

CASE 1 - MINIMUM STATIC PRESSURE

Case 1 consisted of modifying the base case setting so that the primary fan operated at a minimum static pressure of 1.5 in. wg. (373.6 Pa). With this setting, the upstream static pressure for any operating hour was set to a minimum of 1.5 in. wg. (373.6 Pa) plus the upstream static pressure required by the

terminal unit to create the required primary air flow. For example, if the minimum required upstream static pressure for the terminal unit was 0.28 in. wg. (69.7 Pa), the primary fan static pressure was calculated to be 1.78 in. wg. (443.4 Pa). The primary fan power was then calculated using that static pressure and the total flow rate required to supply all zones. Under the base case simulation scenario, the upstream static pressure was allowed to "float" and match the required static pressure depending on which zone had the greatest need. All other base case parameters were left unchanged.

Table 3 shows the summary of this case for the five zone system model. These results are for simulation using weather and load data for the Houston location. The table shows the annual totals for the series and parallel five zone models for total energy consumption, primary fan energy consumption, terminal unit fan energy consumption, heat added to maintain space temperature, the maximum upstream static pressure required to supply air to the zone, and the minimum upstream static pressure required to supply air to the zone.

Table 3. Simulation Summary for the Houston Location with a Minimum Primary Static Pressure of 1.5 in. w.g. (373.6 Pa).

	Parallel Case 1	Parallel Base	Series Case 1	Series Base	Case 1 Diff	%Diff Case 1
Total Annual Energy (kWh)	82,060	77,957	95,834	91,438	13,774	16.8%
Primary Fan Energy (kWh)	6,044	2,801	6,774	3,310	730	12.1%
FPTU Fan Energy (kWh)	3,182	3,182	15,195	15,195	12,012	378%
Thermal Energy Added (kWh)	26,962	26,962	24,325	24,325	-2,637	-10%
FPTU Fan + Thermal (kWh)	30,186	30,186	39,520	39,520	4,064	31%
Maximum Static Pressure (in. w.g. (Pa))	1.780 (443.4)	0.280 (69.7)	1.710 (425.9)	0.210 (52.3)		
Minimum Static Pressure (in. w.g. (Pa))	1.527 (380.4)	0.027 (6.7)	1.500 (373.6)	0.000		

The total energy consumed by the series system was 16.8% higher than the energy consumed by the parallel system. The parallel system used a total of 82,060 kWh for the year while the series system consumed 95,834 kWh.

Table 3 shows that the primary fan used more energy for both systems when compared to their base cases. The series FPTU system still uses more energy than does the parallel system. The reasons for higher energy consumption by the primary fan for the series system compared to the fan for the parallel system were documented with the base case.

For this case, the extra fan energy used by the series primary fan over the parallel primary fan was 730 Watts while for the base case, the series system primary fan energy used 509 Watts more than the parallel system primary fan. At a fixed minimum static pressure requirement of 1.5 in.wg. (373.6 Pa) the primary fan power for the parallel system fan increased by 3,243 Watts and the primary fan power for the series system increased by 3,464 Watts. This was expected because the same primary air flow rate is required and under this scenario it has to be delivered against a higher pressure minimum static pressure. The extra cooling

capacity required to handle the loads from the series FPTU fans was still needed in addition to the higher primary fan static pressure. The primary fan energy differential increased because the same 477 CFM (225 l/s) has to work against 1.5 in. wg. (373.6 Pa) of additional static pressure.

CASE 2 - CONSTANT STATIC PRESSURE

Case 2 consisted of modifying the base case setting by setting and maintaining a constant static pressure of 1.5 in. wg. (373.6 Pa) for the primary fan. For example, if the minimum required upstream static pressure for the terminal unit was 0.28 in. wg. (69.5 Pa), the primary fan static pressure would remain at 1.5 in. wg. (373.6 Pa). The primary fan power was then calculated at the 1.5 in. wg. (373.6 Pa) static pressure and the total flow rate required to supply all zones for each hour. As with Case 1, this control strategy is compared to the base case simulation where the upstream static pressure was allowed to "float" and match the required static pressure depending on which zone had the greatest need. All other base case parameters were left unchanged.

Table 4 shows the summary of the "Case 2" results for the five zone system model. The simulation that generated the results shown in this table was for the Houston location. This table shows the annual totals for the series and parallel five zone models for total energy consumption, primary fan energy consumptions, terminal unit fan energy consumption, heat added to maintain space temperature, the maximum upstream static pressure required to supply air to the zone, and the minimum upstream static pressure required to supply air to the zone.

Table 4. Simulation Summary for the Houston Location with Constant Primary Static Pressure of 1.5 in. w.g. (373.6 Pa).

	Parallel Case 2	Parallel Base	Series Case 2	Series Base	Case 1 Diff	%Diff Case 1
Total Annual Energy (kWh)	81,473	77,957	95,541	91,438	14,068	17.2%
Primary Fan Energy (kWh)	5,566	2,801	6,501	3,310	-325	16.8%
FPTU Fan Energy (kWh)	3,182	3,182	15,195	15,195	12,012	378%
Thermal Energy Added (kWh)	26,962	26,962	24,325	24,325	-2,637	-10%
FPTU Fan + Thermal (kWh)	30,144	30,144	39,520	39,520	9,376	31%
Maximum Static Pressure (in. w.g. (Pa))	1.500 (373.6)	0.280 (69.7)	1.500 (373.6)	0.210 (52.3)		
Minimum Static Pressure (in. w.g. (Pa))	1.500 (373.6)	0.027 (6.7)	1.500 (373.6)	0.000		

The total energy used by the series FPTU system was 17.2% higher than the energy consumed by the parallel FPTU system. The parallel system consumed a total of 81,473 kWh for the year while the series system consumed 95,541 kWh.

Table 4 shows that the primary fan used more energy for the series FPTU system than for the parallel FPTU system. The reasons for higher energy consumption by the primary fan for the series system compared to the fan for the parallel system were documented with the base case.

For "Case 2" the additional annual energy used by the series primary fan over

the parallel primary fan was 935 kWh. This compares to the base case where the series system primary fan used 509 kWh more than the parallel system primary fan. With a constant static pressure requirement of 1.5 in. wg. (373.6 Pa), the primary fan power for the parallel system increased by 2,765 kWh and the primary fan power for the series system increased by 3,191 Watts compared to the base cases. This was because the same primary air flow rate is required and it has to be moved against a constant static pressure instead of adjusting to the zone with maximum demand. The extra cooling capacity required to handle the thermal loads from the series FPTU fans was still required with the higher primary fan static pressure.

For both systems, using either a minimum static or constant static pressure causes greater energy use. Allowing the system to control static pressure on demand from the zone with the greatest load assures a better match of primary fan power to system needs.

CASE 3 - 24 HOUR OPERATION

The base case simulation was operated on a 12 hour schedule, on at 6 a.m. and off at 6 p.m. with no separate weekend schedule. This is a common on-off control schedule for commercial buildings. Case 3 allows both systems to run on a 24 hour schedule for all days of the week. Though not a typical operational scheme, the case was run to see if parallel systems might be "penalized" by increased energy use because of operation during more of the heating hours of the year (parallel FPTU fan running).

Table 5 shows a summary of the total energy consumption for all five geographic locations for the series and the parallel FPTU single duct VAV system with a five zone operation. For all cases, the series FPTU system consumes more energy than the parallel system. For most cases the series terminal units consume about 10% more energy than the parallel systems when operating under the same conditions.

Table 5. Total Annual VAV Single Duct FPTU System Energy Use Summary for Five Geographic Locations in the U.S. Under 24 Hour Operation.

	Parallel (kWh)	Series (kWh)	%Diff
Houston	162,361	175,945	8%
Phoenix	137,157	150,638	10%
Chicago	145,949	158,844	9%
New York	137,157	150,638	10%
San Francisco	126,900	139,795	10%

SUMMARY AND CONCLUSIONS

For all cases presented in this paper, a parallel FPTU system consistently used less energy than a comparable series FPTU system. Two very commonly used static pressure control strategies were simulated, establishing a minimum and a constant primary static pressure in the ductwork serving the FPTU VAV system. When these cases were compared to an FPTU VAV system operating in response to maximum zone cooling demand, the result was increased energy use. There were no benefits to operating systems in this manner. Both FPTU types, parallel or series, had a

minimum static pressure requirement that was much below an artificial minimum/constant setpoint of 1.5 in. w.g. (373.6 Pa). There was a significant energy penalty when operating these devices above their static pressure needs.

The 24 hour operation was simulated because the parallel system would normally thought to be at a disadvantage in this condition. It was thought that the additional energy needs in the heating mode would show an increased FPTU fan energy use for a parallel system. However, the simulation showed that the series system still uses more energy under this scenario.

All of the results in this analysis assumed that there was no significant leakage in the parallel FPTUs. As demonstrated in some of the measured data in Furr, et al (2008), leakage can be significant in some parallel systems. As a consequence, the differences in energy use between series and parallel systems as the amount of leakage increases in parallel systems (Davis, et al 2009).

A relatively new addition to FPTU systems is the use of electronically commutated motors (ECM). All FPTU used in this study used permanent split capacitor motors (PSC) controlled at the FPTU by an SCR controller adjusted at a specific speed. If ECMs are used to replace the PSC motors in series FPTU, the overall energy use of the cases presented here would be expected to decrease. Further, if VAV control of the ECM in series FPTU is enabled, even more energy savings should be possible in those systems.

ACKNOWLEDGEMENTS

This work was a part of a project funded by ASHRAE under RP-1292 and the authors would like to thank the project monitoring subcommittee of TC 5.3 and the manufacturers they represent for their support during the project. Several manufacturers donated terminal units for use in this study. Through cooperative ventures such as these, ASHRAE research funding can be utilized to the fullest. We appreciate the contributions from these industry leaders.

REFERENCES

- Bryant, J., Davis, M., O'Neal, D.O., and Cramlett, A., 2009. Experimental Verification of a Three Zone VAV System Model Operating with Fan Powered Terminal Units (RP-1292), *ASHRAE Transactions* 115 (1).
- Bryant, J., Davis, M., O'Neal, D.L., 2010. Energy Use Comparison for Series vs. Parallel Fan Powered Terminal Units in a Single Duct Variable Air Volume System, *In Review for ASHRAE Conference, Summer, 2010*.
- Davis, M., Bryant, J., and O'Neal, D.L., 2009. Modeling the Performance of Single-Duct VAV Systems that use Fan Powered Terminal Units (RP-1292). *ASHRAE Transactions* 115 (1).
- Furr, J., O'Neal, D.L., Davis, M., Bryant, J. and Cramlet, A. 2008. Performance of VAV Fan Powered Terminal Units: Experimental Results and Models for Parallel Units (RP-1292). *ASHRAE Transactions* 114 (1).

ML-11-036

Performance of Series Fan-Powered Terminal Units with Electronically Commutated Motors

Jacob L. Edmondson
Associate Member ASHRAE

John A. Bryant, PhD, PE
Member ASHRAE

Dennis L. O'Neal, PhD, PE
Fellow ASHRAE

Michael A. Davis, PhD
Member ASHRAE

ABSTRACT

Semi-empirical models were developed for fan airflow output, fan power consumption, and primary airflow for series fan-powered variable-air-volume terminal units with electronically commutated motors. Eight series terminal units with either 8 in. (203 mm) or 12 in. (304 mm) primary inlets from three terminal unit manufacturers and two motor manufacturers were evaluated.

Fan power and airflow data were collected at a downstream static pressure of 0.25 in. w.g. (62.3 Pa). Upstream static (primary air) pressures were varied from 0.0 to 2.0 in. w.g. (0 to 498 Pa). Data were collected at four primary inlet damper positions and at four fan motor settings. Model variables included primary air inlet damper position, fan motor input setting, the air inlet differential sensor pressure, and the upstream (primary air) and downstream (supply air) static pressures.

All of the resulting fan power and airflow models had R^2 values greater than 0.895. The models for the fan airflow output and fan power had R^2 values greater than 0.968. The models developed in this paper can be used in HVAC simulation programs to estimate the energy use and potential savings of series fan-powered terminal units with electronically commutated motors.

INTRODUCTION

Variable-air-volume (VAV) systems maintain space conditions by varying the volume of conditioned air delivered to a space. A VAV system typically consists of several components starting at a central air handler unit (AHU), where cooling coils cool and dehumidify the primary air. This conditioned air, referred to as primary air, is delivered by the

AHU central supply fan through a single-duct supply system to VAV terminal units. These terminal units are ducted to air outlets usually serving multiple offices or open areas in a building. Terminal units with a fan are called fan-powered terminal units (FPTU) and offer several advantages over terminal units without fans (ASHRAE 2008). FPTUs provide better mixing of the air induced from the plenum space with the primary air and allow the downstream air pressure to be increased to service rooms that might be short of air. Because the fan in the FPTU can be operated independently of the primary air handler, perimeter zones can be heated during unoccupied hours (ASHRAE 2008).

When the fan in a VAV fan-powered terminal unit is in series with the primary air (Figure 1), the unit is referred to as a series fan-powered terminal unit. In series units, the terminal unit fan must be in operation for air to be delivered to the space. The primary air inlet damper modulates the amount of primary

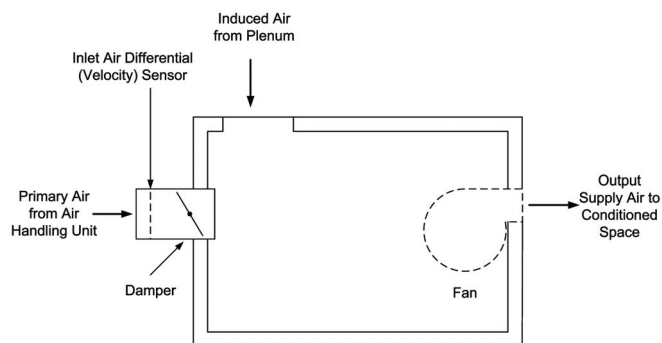


Figure 1 Simplified diagram of a series fan-powered terminal unit.

Jacob L. Edmondson is a mechanical engineer, E.I.T., with Goetting and Associates, San Antonio, TX. **Dennis L. O'Neal** is Holdredge/Paul Professor and head of the Department of Mechanical Engineering, Texas A&M University, College Station, TX. **John A. Bryant** is an associate professor at Texas A&M University at Qatar, Doha, Qatar. **Michael A. Davis** is the director of laboratories at New York University Abu Dhabi, Abu Dhabi, United Arab Emirates.

air delivered to the space to maintain the temperature setpoint. The inlet air velocity sensor provides data on the primary airflow supplied to the series unit. Electric resistance or hot water coils (not shown in Figure 1) can be used to provide supplemental terminal reheat. Because the fan in a series FPTU is in series with the primary air handler, the air pressure for the primary air can be decreased compared to operation with a parallel FPTU (ASHRAE 2008).

It is important to be able to characterize individual terminal units to properly model a VAV system in a building energy use simulation. Complete system models based on measured performance data of fan-powered terminal units have only recently been made available for use in building simulation programs by Furr et al. (2008a; 2008b), who developed performance models for parallel and series fan-powered terminal units that had silicon-controlled rectifier (SCR) fan motors. Manufacturers also sell FPTUs with newer electronically commutated motors (ECMs). Because ECMs allow the FPTU to vary fan airflow by changing fan motor speed in response to changes in zone loads in a building, FPTUs with ECMs are expected to use less energy than older style SCR FPTUs. This paper includes performance data on eight FPTUs that cover two duct sizes, three manufacturers, and two ECM manufacturers.

Experimental Setup and Procedure

Furr et al. (2008c) described in detail the experimental setup and methodology used to test and characterize the performance of series and parallel SCR-controlled fan-powered terminal units. A brief description of the setup and test procedure is provided here. The basic test setup used for airflow measurements in this study is shown in Figure 2. Airflow was controlled and measured using nozzle airflow chambers (AMCA 1999) located both upstream and downstream of the FPTU. Each chamber had a booster fan controlled by a variable speed drive (VSD). Nozzle combinations differed between each chamber and were selected by the

operator. As the cumulative nozzle diameter was increased, less pressure was required to attain the same volumetric airflow through the chamber.

The two airflow chambers and FPTU were connected with sheet-metal ductwork. The length of this duct followed the specifications outlined in ASHRAE Standard 130 (2006). Tests were also done with only ductwork connected between the two airflow chambers to compare the airflow measurements between the two chambers. For the airflow ranges used for this study, the two chambers agreed within $\pm 3\%$.

Airflow quantities were calculated using the techniques found in AMCA Standard 210 (1999). The upstream airflow chamber was used to measure the primary air into the FPTU. Airflow values were adjusted to standard temperature and pressure conditions to compensate for environmental changes in the laboratory during the days of data collection. Induced airflow into the FPTU was calculated as the difference of the airflow measured with the upstream and downstream airflow chambers.

ASHRAE Standard 130 (2006) also dictated that the static pressure measurements be located specific distances (2.5 duct diameters downstream and 1 duct diameter upstream) from the FPTU. Static pressures were averaged across the respective cross-sections both upstream and downstream of the terminal unit.

FPTUs typically share three common elements. Incoming primary air is received via an inlet duct with an inlet air velocity pressure (P_{iav}) sensor, which is a multi-point device that averages pressure over four locations across the duct. A second common element is a mechanical damper which regulates the flow rate of primary air and helps set the pressure differential across the entire terminal unit. Dampers typically come in either butterfly or opposing blade configurations. Modulation of these dampers is typically achieved using an electrically controlled actuator with a 0 to 10 VDC range that provides for operation from fully open to fully closed. The third common element is the fan, whose location inside the

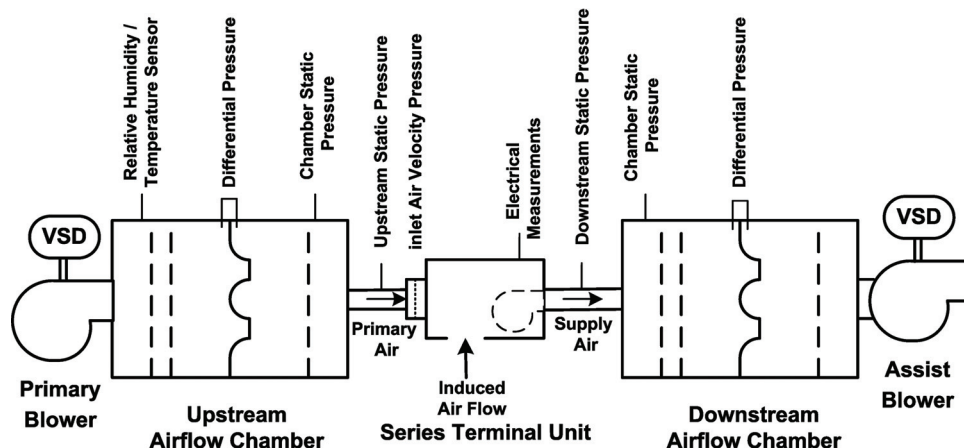


Figure 2 Airflow test apparatus including FPTU and airflow chambers.

terminal unit varies by manufacturer. Parallel FPTUs also have a backdraft damper that is used to prevent air from leaking in through the induction port when the FPTU fan is not running.

Electrical performance data were recorded with a power quality analyzer. Current transformers rated for 0–5A were selected and had a ±1% full scale accuracy. The current transformers were applied to both the power and neutral wires of the single-phase 277 VAC input. The simultaneously measured and recorded data included, but were not limited to: real and apparent power, RMS voltage (V_{RMS}) and current (I_{RMS}), associated harmonics, and total harmonic distortion. The data files were cached in the power quality analyzer's internal memory and then transferred to a personal computer.

A factorial test matrix spanning several independent variables was established for the FPTU designs to adequately span the expected range of operation in the field. Table 1 shows the independent variables and their ranges for this study.

The damper position, D , varied for the respective FPTU designs. Orientation was controlled using a damper actuator with a 0 to 10 VDC input that could vary the damper position between 100% fully open and fully closed. The fully closed condition was not included in the test matrix because this damper position would have produced no primary airflow, regardless of upstream pressure. The three manufacturers that provided terminal units for this study were designated as manufacturer A, B, and C. Two inlet sizes were evaluated: 8 in. (203 mm) and 12 in. (304 mm). Each terminal unit was labeled according to primary air inlet size and manufacturer. For example, an 8 in. (203 mm) terminal unit from manufacturer A was labeled as ECM_S8A. Manufacturer C provided units with ECM motors from two motor manufacturers. These terminal units were also differentiated by brand of ECM motor, either M1 or M2. Thus, a 12 in. (304 mm) terminal unit with an ECM motor from manufacturer M1 was labeled ECM_S12C-M1.

RESULTS AND MODELS

One of the goals of this study was to develop semi-empirical models for ECM series FPTUs similar to those previously developed for SCR series FPTUs by Furr et al. (2008a). These models had to provide sufficient characterization of the FPTUs so they could be used in building simulation models.

During testing, there were several operational problems with some FPTUs. For example, it was observed that under some conditions, the terminal unit fan would stop and run

backward. It was also observed that when the ECM controller was turned to its highest setting for some FPTUs, the fan sometimes pulsed or cycled on and off. Because these operational problems were typically outside the manufacturer's recommended operating range, the data collected for these conditions were not used for any of the data analysis. However, these problems could be experienced in a field application if the installer and/or operator did not stay within the recommended operating range of static pressure or fan speed specified by the manufacturer.

Terminal Unit Airflow

Series terminal units require that the fan operate continuously to supply air to the conditioned space. If the primary airflow is lower than the air being supplied by the terminal unit fan, additional air can be drawn in from the plenum. Both the primary airflow delivered to the FPTU and the air delivered by the FPTU fan are variables that needed to be quantified.

Primary Airflow

The primary air supplied to the FPTU was modeled as a function of the pressure differential (DP) across the FPTU and the air inlet damper position. In this study, the differential pressure is defined as the difference in the upstream (primary air) static pressure and the downstream (supply air) static pressure of the terminal unit.

Manufacturers who provided units for this study used either butterfly or opposing blade designs for their primary air inlet dampers. During testing, both types of dampers were set at 100% open, 75% open, 50% open, and 25% open. Manufacturer C used an opposed blade damper for both brands of motors. In this case, 0° indicated a fully open damper, while 45° represented a fully closed damper. Both manufacturers A and B used a butterfly damper. In that case, 0° indicated a fully open damper, while 90° represented a fully closed damper.

Figure 3 shows the plot of primary air versus the differential pressure for the 8 in. (203 mm) series FPTU from manufacturer C, using motor M2. Figure 4 shows a similar plot for the 12 in. (304 mm) series FPTU from manufacturer A. The curves in both figures were generated from a best fit of the data to Equation 1. In this equation, C_1 , C_2 , and C_3 were constants determined from the regression analysis, S was the damper position (in degrees), and DP was the differential pressure defined earlier. The form of Equation 1 was originally developed by

Table 1. Series Fan-Powered Terminal Unit Test Matrix

Independent Variable	Test Points	Value Range
D , damper position	4	100%, 75%, 50%, 25% open
V_{fan} , fan input voltage (ECM)	4	100%, 75%, 50%, 25% full scale
P_{up} , upstream static	6	0.0–2.0 in. w.g. (0–498 Pa)
P_{down} , downstream static	1	0.25 in. w.g. (62 Pa)

Furr et al. (2008a). The primary airflow delivered to the FPTU was proportional to the square root of the differential pressure across the terminal unit at a given damper setting. Because the downstream static pressure was maintained at 0.25 in. w.g. (62.3 Pa) for all of the tests, the DP required an offset to keep the value inside the square root positive. Furr et al. (2008a) determined that an offset of 0.27 in. w.g. (67.3 Pa) best fit the empirical data, and the same offset was used in this study to maintain model consistency. If the static pressure internal to the FPTU were measured and used in the model, it is likely that no offset would be needed. While it might also improve the series FPTU primary air model, no FPTU manufacturers provide static pressure taps at this location.

$$Q_{primary} = C_1 \cdot (1 + C_2 \cdot S + C_3 \cdot S^2) \cdot \sqrt{DP + 0.27} \quad (1)$$

The coefficients of the model for the different terminal units tested, as well as the R^2 values, are presented in Table 2.

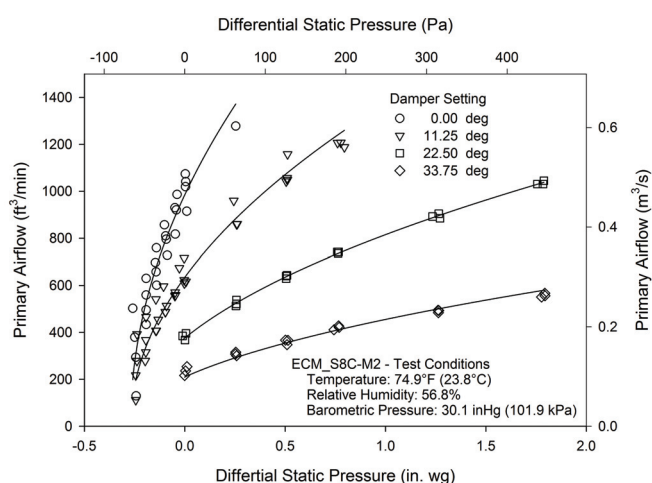


Figure 3 Primary airflow as a function of upstream minus downstream differential static pressure for ECM_S8C-M2.

The results for FPTU ECM_S8C-M1 were measured by Cramlet (2008). The measured data correlated well with Equation 1. The R^2 values for the ECM-controlled FPTUs ranged from 0.895 to 0.977 and were comparable to those reported by Furr et al. (2008a) for SCR series FPTUs.

Fan Airflow

The airflow provided by the fan in an ECM series FPTU is mainly a function of the ECM input setting. Figures 5 and 6 show fan airflow versus inlet velocity pressure for FPTUs ECM_S8B and ECM_S12C-M2, respectively. As seen in both figures, the FPTUs also showed a slight dependence on inlet air velocity pressure, P_{iav} .

These results were similar to those obtained by Furr et al. (2008a) who found that fan airflow was primarily dependent on the SCR voltage which controlled fan speed and showed a much smaller dependence on P_{iav} .

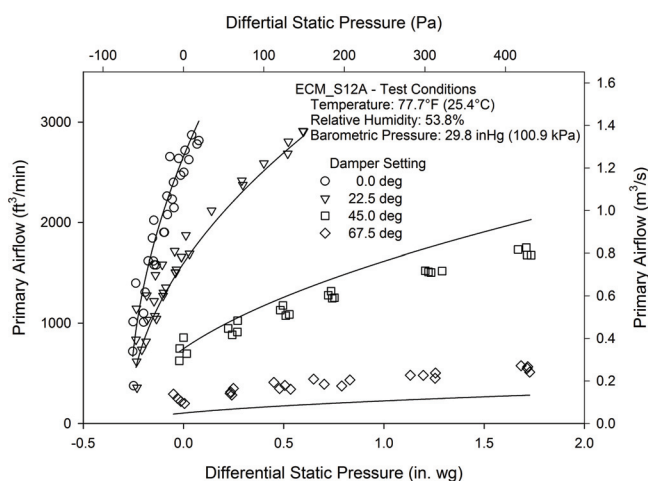


Figure 4 Primary airflow as a function of upstream minus downstream differential static pressure for ECM_S12A.

Table 2. Model Coefficients for ECM-Controlled Series FPTUs

FPTU	C_1	C_2	C_3	R^2
ECM_S8A	1637	-1.95E-02	7.80E-05	0.955
ECM_S12A	5109	-2.15E-02	1.14E-04	0.946
ECM_S8B	2094	-2.83E-02	2.06E-04	0.962
ECM_S12B	5886	-3.17E-02	2.54E-04	0.895
ECM_S8C-M1	2344	-3.84E-02	4.15E-04	0.977
ECM_S8C-M2	1895	-3.58E-02	3.70E-04	0.951
ECM_S12C-M1	5125	-3.09E-02	1.28E-04	0.927
ECM_S12C-M2	4561	-1.86E-02	-1.71E-04	0.909

One reason for the similar results was the design of the series terminal units. Because upstream airflow and pressure have little effect on the internal static pressure, the fan operates with approximately the same pressure differential over a wide range of operating conditions. In addition, for ECM units, the electronically commutated motor was designed to maintain constant airflow for a given ECM input setting despite changes in operating conditions. Results for the other ECM series FPTUs were similar to those shown in Figures 5 and 6.

The model used to fit the fan airflow data is shown in Equation 2 and was similar to that used by Furr et al. (2008a). The results for all the ECM series units are shown in Table 3. Overall, the model correlated well with the data, with the lowest R^2 value being 0.987 for ECM_S8A.

$$Q_{fan} = C_1 + C_2 \cdot V_{fan}^2 + C_3 \cdot V_{fan} + C_4 \cdot P_{iav} \quad (2)$$

For both the SCR and ECM units, the fan airflow was dependent on the inlet air velocity pressure, P_{iav} . However,

there was a major difference between the SCR and ECM correlations concerning the definition of the fan voltage. For the SCR correlations presented by Furr et al. (2008a), the fan voltage was the AC voltage provided by the SCR to the fan motor. In the ECM models, the fan voltage was the percentage of the voltage between the minimum and maximum ECM settings on the controller.

The reason for using percentages for the ECM units instead of DC voltages was because manufacturers had different ways of specifying the input to the ECM controllers. For example, manufacturer A provided a controller that was adjusted by turning a set screw to change the setting from 0 to 100%, so settings of 25%, 50%, 75%, and 100% were used. FPTUs from manufacturer B had a 2 to 10 VDC input, so settings of 4 VDC (25%), 6 VDC (50%), 8 VDC (75%), and 10 VDC (100%) were used when varying the speed of the fan with the controller. Manufacturer C provided a controller that

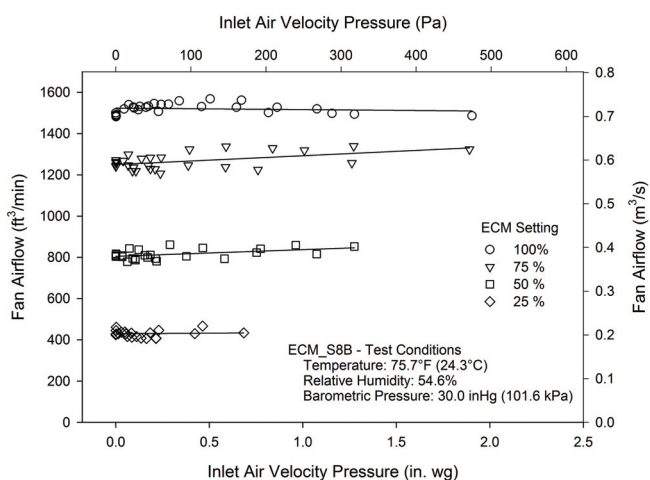


Figure 5 Terminal unit fan airflow versus $P_{ia,z}$ for ECM_S8B.

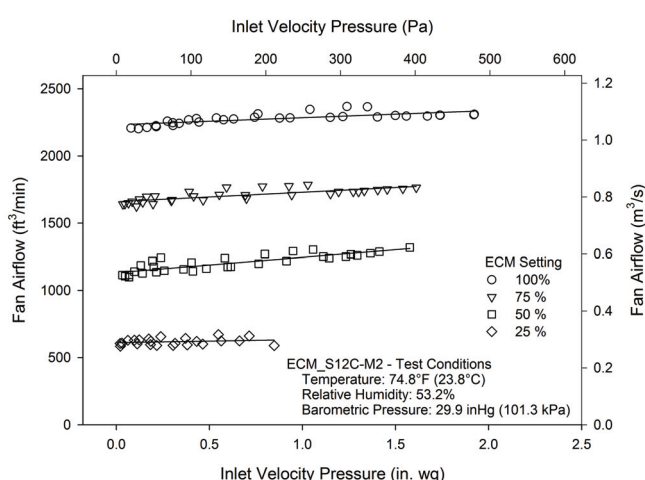


Figure 6 Terminal unit fan airflow versus $P_{ia,z}$ for ECM_S12C-M2.

Table 3. Coefficients for Fan Airflow Model for ECM-Controlled Series FPTUs

FPTU	C_1	C_2	C_3	C_4	R^2
ECM_S8A	58.92	0.016	8.50	6.60	0.987
ECM_S12A	148.92	0.025	20.24	43.50	0.996
ECM_S8B	-90.80	-0.052	21.41	20.12	0.991
ECM_S12B	375.12	0.015	11.59	-32.31	0.993
ECM_S8C-M1	108.30	0.0113	12.30	12.44	0.997
ECM_S8C-M2	-82.18	-0.043	18.18	34.25	0.992
ECM_S12C-M1	467.40	0.025	15.48	26.10	0.995
ECM_S12C-M2	67.43	-0.000787	21.47	75.60	0.997

Table 4. Summary of ECM Settings for the Three Manufacturers

FPTU Manufacturer	ECM Settings			
	25%	50%	75%	100%
A	25%	50%	75%	100%
B	4 VDC	6 VDC	8 VDC	10 VDC
C	2.5 VDC	5 VDC	7.5 VDC	10 VDC

was adjusted using a 0 to 10 VDC signal, so settings of 2.5 VDC (25%), 5 VDC (50%), 7.5 VDC (75%), and 10 VDC (100%) were used. Table 4 contains a summary of the ECM settings for each manufacturer.

Terminal Unit Power Performance

Both power consumption and power factor were measured. A model was developed for the power consumption as a function of ECM setting and inlet air velocity pressure, P_{iav} . Because the fan airflow was mainly controlled by the fan speed, which, in turn, was controlled by the ECM setting, the model used the ECM setting rather than fan airflow as an input. Power consumption was also influenced by downstream static pressure and the primary airflow. Because downstream pressure remained constant, it was not used in the model. The impact of primary airflow on the power consumption was modeled by including P_{iav} .

The power consumption of the VAV fan was mainly dependent on the airflow it produced. The airflow was almost entirely dependent on the ECM setting, and because the ECM setting was an input into the system, it was used for modeling rather than the airflow. It also showed a small dependence on primary airflow, which was represented by P_{iav} . Figure 7 shows the fan power versus the airflow of the fan for terminal unit ECM_S8C-M2, while Figure 8 shows these data for terminal unit ECM_S12C-M1.

The power curves for all the ECM series terminal units were similar in form to those shown in Figures 7 and 8. Power varied approximately with the square of the airflow. The main difference between the data in Figures 7 and 8 and the power data obtained by Furr et al. (2008a) for SCR series units was that the power was nearly linear with respect to the SCR fan airflow, while it was quadratic for the ECM series units. Figure 9 shows a comparison of power consumption for SCR_S12A from Furr et al. (2008a) and ECM_S12A from this study. At the lowest flow rate for the SCR unit, which was about 850 ft³/min (0.40 m³/s), it consumed approximately 370 W of power. In contrast, the ECM unit at the same airflow consumed approximately 70 W. Thus, at low flow conditions, the SCR unit used over five times as much power as the ECM unit. As the fan airflow rates increased, as shown in Figure 9, the difference in power consumption between the SCR and ECM units narrowed. However, when the SCR unit is initially installed in a building, its speed would be set by the installer

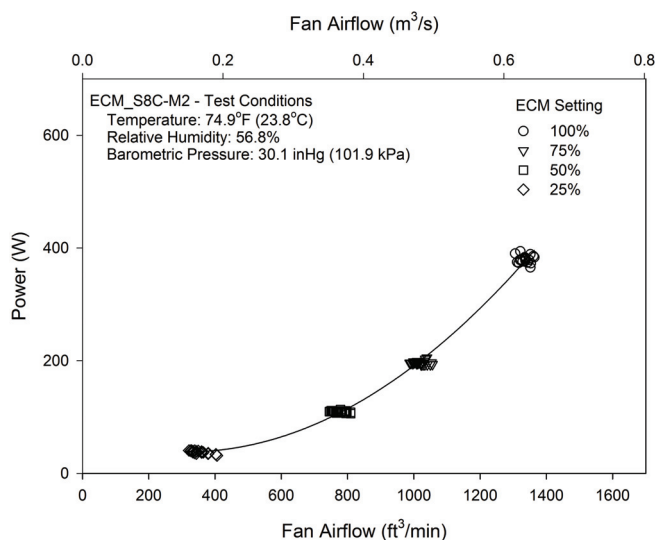


Figure 7 FPTU power versus fan airflow for ECM_S8C-M2.

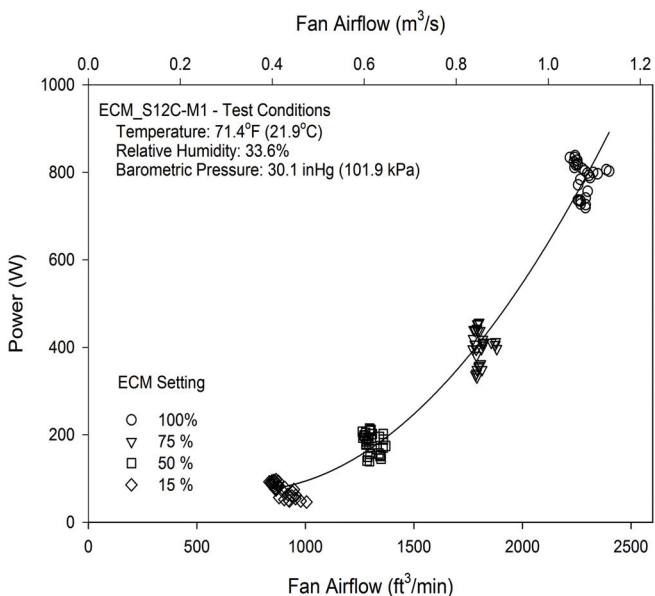


Figure 8 FPTU power versus fan airflow for ECM_S12C-M1.

to meet the maximum (or design) load conditions in the space. It would then run continuously at that speed whenever the HVAC system is operating even though load conditions in the space may be light compared to the maximum conditions. In contrast, the ECM unit would vary its speed to meet lighter (or heavier) load conditions. As a consequence, the savings in fan power with the ECM FPTU can be potentially higher than in the example discussed above. A building simulation model would have to be used to estimate the savings with an ECM or a SCR series unit.

The fan power model used for the ECM-controlled fans was similar to that used for the SCR-controlled units (Equation 3) except for the definition of the fan voltages. For the SCR units, the fan voltage represented the AC voltage measured after the SCR controller. For the ECM units, the fan voltage represented the percent of maximum ECM setting. Table 5 presents the coefficients for the ECM terminal units. The model produced satisfactory results for the ECM units, with the lowest R^2 being 0.968. Overall, the model from Furr et al.

(2008a), with the appropriate modifications for the definition of fan voltage, appeared to correlate the power consumption of the ECM motors as well as it did the SCR motors reported by Furr et al. (2008a).

$$Power_{fan} = C_1 + C_2 \cdot V_{fan}^2 + C_3 \cdot V_{fan} + C_4 \cdot P_{iav} \quad (3)$$

For the ECM-controlled FPTUs, the power factor typically varied between 0.4 and 0.6, regardless of the ECM setting. Each individual motor seemed to react differently to increasing ECM settings, with no consistent trend. Table 6 shows how the power factor varied for ECM_S8B and ECM_S12C-M1. For ECM_S8B, the power factor increased with ECM setting, while it decreased for ECM_S12C-M1. For each of the FPTUs, the power factors were averaged over the whole range of ECM settings. The results are shown in Table 7. With the exception of ECM_S8C_M2, the 8 in. (203 mm) FPTUs generally had smaller power factors than the 12 in. (304 mm) units. Motor manufacturer M2 had slightly higher power factors than the same FPTU with motor/controllers from manufacturer M1. While the ECM units measured here had lower power factors than those of the SCR units, the overall impact on the building power factor may still be smaller for ECM units because of the significantly reduced overall power consumption during off-peak conditions. The detailed comparison would require use of a building simulation program, which was beyond the scope of this paper.

SUMMARY AND CONCLUSION

An integral part of every VAV system is the terminal unit. Some applications use fan-powered terminal units, which come in either series or parallel configurations. Furr et al. (2008a) developed detailed performance models for fan power terminal units that had SCR-controlled motors. This study extended the work of Furr et al. (2008a) to eight series ECM-controlled fan-powered terminal units from three terminal unit and two motor manufacturers. The overall trends in performance of the ECM-controlled FPTUs were similar among the

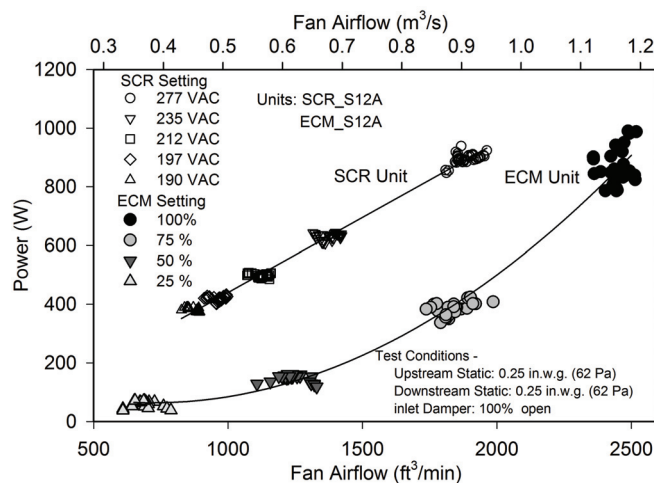


Figure 9 Comparison of FPTU power as a function of fan airflow for SCR-S12A and ECM_S12A.

Table 5. Fan Power Model Coefficients for ECM Series Terminal Units

FPTU	C_1	C_2	C_3	C_4	R^2
ECM_S8A	70.34	0.049	-2.602	2.34	0.968
ECM_S12A	197.65	0.161	-9.589	24.38	0.989
ECM_S8B	8.89	0.061	-0.221	21.26	0.985
ECM_S12B	112.28	0.074	-3.657	-31.92	0.978
ECM_S8C-M1	79.00	0.0705	-3.150	-12.99	0.998
ECM_S8C-M2	46.61	0.045	-1.165	-4.71	0.993
ECM_S12C-M1	145.83	0.111	-4.310	-45.40	0.998
ECM_S12C-M2	179.66	0.131	-7.303	-18.47	0.996

Table 6. Power Factors for ECM_S8B and ECM_P12A for Different ECM Settings

ECM Setting	Power Factor	
	ECM_S8B	ECM_S12C-M1
25%	0.40	0.51
50%	0.42	0.52
75%	0.42	0.49
100%	0.43	0.48

units evaluated. Semi-empirical models of the same form used by Furr et al. (2008a) were applied in this study to satisfactorily represent the different performance characteristics of the ECM-controlled FPTUs.

Each series unit needed three models to characterize its performance. The first was the primary air performance, which was independent of fan voltage. This model had R^2 values that ranged from 0.895 to 0.962 for the ECM units. The series model could possibly be improved by using the internal FPTU static pressure to calculate the differential pressure used in the model instead of the static pressure downstream of the fan.

The second model developed for the series fan-powered terminal units was the airflow provided by the terminal unit fan. For the ECM-controlled units, the R^2 values of this model ranged from 0.987 to 0.997. Furr et al. (2008a) reported that the model also correlated highly for the SCR-controlled units, with R^2 values ranging from 0.989 to 0.997 for properly functioning SCR controllers. The exceptionally high R^2 values for this form of the model demonstrate that it explains most of the variability in the data.

The third model developed for the series units was that of fan power consumption. This was an important model because ECM-controlled fans are expected to perform much better than their SCR counterparts. This model also correlated well with the data for the ECM units. R^2 values ranged from 0.968 to 0.988. These R^2 values were similar to those reported by Furr et al. (2008a) for SCR series FPTUs. This model can be used in conjunction with the fan airflow model to compare the power consumption of ECM- and SCR-controlled units at different operating conditions.

The data and models provided in this study should also allow an engineer to determine if an ECM series FPTU would be more energy efficient than an SCR series or parallel FPTU for a given application. These models should allow development of better air system models in building simulation programs. The actual implementation or integration of these models into one of the popular building simulation programs is left to the engineers and scientists who maintain and upgrade those programs.

Table 7. Average Power Factors for Each of the ECM Fan-Powered Terminal Units

Unit	Average Power Factor
ECM_S8A	0.40
ECM_S8B	0.42
ECM_S8C_M1	0.44
ECM_S8C_M2	0.54
ECM_S12A	0.51
ECM_S12B	0.43
ECM_S12C-M1	0.50
ECM_P12C-M2	0.54

ACKNOWLEDGMENTS

The authors wish to thank the following individuals and organizations who provided support and advice for this project: Gus Faris of Nailor Industries, David John of Metal Industries, Inc., Dan Int-Hout of Krueger Manufacturing Co., Ron Jordan and Doug Fetters of A.O. Smith Electrical Products Company, Floyd Blackwell of Regal Beloit Corporation, Gaylon Richardson of Engineered Air Balance Co., Inc., and Jack Stegall of Energetics Laboratory.

NOMENCLATURE

- DP = Pressure differential across the terminal unit, in. w.g. (Pa)
- P_{down} = Downstream (supply air) static pressure, in. w.g. (Pa)
- P_{iav} = Pressure across inlet air differential (velocity) flow sensor, in. w.g. (Pa)
- P_{unit} = Static pressure inside terminal unit, in. w.g. (Pa)
- P_{up} = Upstream (primary air) static pressure, in. w.g. (Pa)
- $Power_{fan}$ = Power consumption of terminal unit fan, W
- Q_{fan} = Amount of airflow through terminal unit fan, ft³/min (m³/s)
- $Q_{induced}$ = Amount of airflow induced from plenum, ft³/min (m³/s)
- Q_{supply} = Amount of parallel terminal unit airflow output, ft³/min (m³/s)
- $Q_{primary}$ = Amount of primary airflow, ft³/min (m³/s)
- S = Damper setting, degrees
- V_{rms} = RMS average of AC voltage used by the terminal unit, V
- V_{fan} = Input voltage (in percentage of full scale) for ECM units, %

REFERENCES

- AMCA. 1999. ANSI/AMCA Standard 210-99. *Laboratory Methods of Testing Fans for Aerodynamic Performance*

Rating. Arlington Heights, IL: Air Movement and Control Association.

ASHRAE. 2006. ANSI/ASHRAE Standard 130-1996 (RA 2006). *Methods of Testing for Rating Ducted Air Terminal Units*. Atlanta: American Society of Heating, Refrigerating and Air-Conditioning Engineers, Inc.

ASHRAE. 2008. Room air distribution equipment. In *ASHRAE Handbook—HVAC Systems and Equipment*. Atlanta: American Society of Heating, Refrigerating and Air-Conditioning Engineers, Inc.

Cramlet, A. 2008. Performance of ECM controlled VAV fan powered terminal units. M. Sc. Thesis, Texas A&M University, College Station, TX.

Davis, M., J. Bryant, and D.L. O'Neal. 2009. Modeling the performance of single-duct VAV systems that use fan powered terminal units. *ASHRAE Transactions: Symposium* 115(1).

Furr, J., D.L. O'Neal, M. Davis, J.A. Bryant, and A. Cramlet. 2008a. Performance of VAV fan powered terminal units: Experimental results and models for series units. *ASHRAE Transactions* 114(1).

Furr, J., D.L. O'Neal, M. Davis, J.A. Bryant, and A. Cramlet. 2008b. Performance of VAV fan powered terminal units:

Experimental results and models for parallel units. *ASHRAE Transactions* 114(1).

Furr, J., D.L. O'Neal, M. Davis, J. Bryant, and A. Cramlet. 2008c. Performance of VAV fan powered terminal units: Experimental setup and methodology. *ASHRAE Transactions* 114(1).

DISCUSSION

Kenneth Elovitz, Professional Engineer, Energy Economics, Inc., Foxboro, MA: How did you coordinate the ECM speed with the downstream airflow chamber so only the downstream chamber measured and did not affect the ECM fan airflow?

Dennis O'Neal: Both the upstream and downstream airflow chambers had booster fans with variable speed drives. The speed of these fans could be adjusted during tests to compensate for either more or less pressure loss through the chamber nozzles, screens, etc. For most tests, the static pressure downstream of the fan-powered terminal unit was fixed at a certain value. As the airflow setting on the fan-powered terminal unit was adjusted, the speed of the booster fan would be adjusted, so the downstream static pressure remained at the specified value for the tests. In this way, the fan-powered terminal unit always sensed the same downstream static pressure over its range of airflow settings.

ML-11-037

Performance of Parallel Fan-Powered Terminal Units with Electronically Commutated Motors

Jacob L. Edmondson
Associate Member ASHRAE

John A. Bryant, PhD, PE
Member ASHRAE

Dennis L. O'Neal, PhD, PE
Fellow ASHRAE

Michael A. Davis, PhD
Member ASHRAE

ABSTRACT

Measurements were made on eight fan-powered terminal units that used electronically commutated fan motors. Semi-empirical models were developed for fan airflow output, fan power consumption, and primary airflow for parallel fan-powered variable-air-volume terminal units with electronically commutated motors. Units with both 8 in. (203 mm) and 12 in. (304 mm) primary inlets from three different manufacturers were tested.

Fan power and airflow data were collected at downstream static pressures ranging from 0.1 to 0.5 in. w.g. (25 to 125 Pa). Upstream static pressures were varied from 0.0 to 2.0 in. w.g. (0 to 498 Pa). Data were collected at four different primary inlet damper positions and at four different control input voltage settings to the electronically commutated motors. Model variables included primary air inlet damper position, input voltage setting, the air inlet differential sensor pressure, and the upstream (primary air) and downstream (supply air) static pressures. Each terminal unit was also tested with the fan off to characterize any leakage from the unit.

Most of the resulting fan power and airflow models, except leakage, had R^2 values greater than 0.90. The models for terminal unit leakage had R^2 values that ranged from 0.826 to 0.972. These models could be used in HVAC simulation programs to estimate the performance of parallel fan-powered terminal units with electronically commutated motors. In addition, the potential savings of using EMC- versus SCR-controlled motors could be explored.

INTRODUCTION

Variable-air-volume (VAV) systems maintain space conditions by varying the volume of conditioned air delivered

to a space. A VAV system often consists of a central air handler unit (AHU), where cooling coils cool and dehumidify the primary air. This conditioned air, referred to as "primary air," is delivered by the AHU central supply fan through a single duct supply system to VAV terminal units. These terminal units are ducted to air outlets usually serving two or more offices or open areas. Terminal units with a fan are called fan-powered terminal units (FPTU) and offer several advantages over terminal units without fans (ASHRAE 2008). FPTUs provide better mixing of the air induced from the plenum space with the primary air and allow the downstream air pressure to be increased to service rooms that might be short of air. Because the fan in the FPTU can be operated independently of the primary air handler, perimeter zones can be heated during unoccupied hours (ASHRAE 2008).

When the fan in a VAV fan-powered terminal unit operates in parallel with the primary air, the unit is referred to as a parallel fan-powered terminal unit. In parallel units, the terminal unit delivers air to the space whether or not the terminal unit fan is in operation. The primary air inlet damper modulates the amount of primary air delivered to the space to maintain the temperature setpoint while an inlet air velocity sensor provides data on the primary airflow supplied to the terminal unit. For a parallel terminal unit, the fan typically operates only after the primary air damper is partially or completely closed to maintain airflow into the zone or to moderate the temperature of air (reheat) supplied to the zone to maintain the zone temperature. The terminal unit fan is not operated in full-cooling mode (ASHRAE 2008). Electric resistance or hot water coils can also be used to provide supplemental terminal reheat.

Jacob L. Edmondson is a mechanical engineer with Goetting and Associates, San Antonio, TX. **Dennis L. O'Neal** is Holdredge/Paul Professor and head of the Department of Mechanical Engineering, Texas A&M University, College Station, TX. **John A. Bryant** is an associate professor at Texas A&M University at Qatar, Doha, Qatar. **Michael A. Davis** is the director of laboratories at New York University Abu Dhabi, Abu Dhabi, United Arab Emirates.

Furr et al. (2008a; 2008b) developed performance models for parallel and series fan-powered terminal units that had silicon-controlled rectifier (SCR) motors. Manufacturers also sell fan-powered terminal units with newer electronically commutated motors (ECMs), which are assumed to be more energy efficient than SCR-controlled models. For this paper, the overall performance of eight FPTUs from three manufacturers was measured. The data developed in this study can be used as input to building simulation programs to estimate the impact different FPTUs have on the overall energy use in a building.

EXPERIMENTAL SETUP AND PROCEDURE

Furr et al. (2008c) described in detail the experimental setup and methodology used to test and characterize the performance of series and parallel SCR-controlled fan-powered terminal units. A brief description of the setup and test procedure is provided here. The basic test setup used for airflow measurements in this study is shown in Figure 1. Airflow was controlled and measured using nozzle airflow chambers (AMCA 1999) located both upstream and downstream of the FPTU. Each chamber had a booster fan controlled by a variable speed drive (VSD). Nozzle combinations differed between each chamber and were selected by the operator. As the cumulative nozzle diameter was increased, less pressure was required to attain the same volumetric airflow.

The two airflow chambers and FPTU were connected with sheet-metal ductwork. The length of this duct followed the specifications outlined in ASHRAE Standard 130 (2006). Tests were also done with only ductwork connected between the two airflow chambers to compare the airflow measurements between the two chambers. For the airflow ranges used for this study, the two chambers agreed within $\pm 3\%$.

Airflow quantities were calculated using the techniques found in AMCA Standard 210 (1999). The upstream airflow

chamber was used to measure the primary air into the FPTU. Airflow values were adjusted to standard temperature and pressure conditions to compensate for environmental changes in the laboratory during the days of data collection. Induced airflow into the FPTU was calculated as the difference of the airflow measured with the upstream and downstream airflow chambers.

ASHRAE Standard 130 (2006) also dictated that the static pressure measurements be located specific distances (2.5 duct diameters downstream and 1 duct diameter upstream) from the FPTU. Static pressures were averaged across the respective cross sections both upstream and downstream of the terminal unit.

FPTUs typically share three common elements. Incoming primary air is received via an inlet duct with an inlet air velocity pressure (P_{iav}) sensor, which is a multipoint device that averages pressure over four locations across the duct. A second common element is a mechanical damper that regulates the flow rate of primary air and helps set the pressure differential across the entire terminal unit. Dampers typically come in either butterfly or opposing blade configurations. Modulation of these dampers is typically achieved using an electrically controlled actuator with a 0 to 10 VDC range that provides for operation from fully open to fully closed. The third common element is the fan, whose location inside the terminal unit varies by manufacturer. Parallel FPTUs also have a backdraft damper, which is used to prevent air from leaking in through the induction port when the FPTU fan is not running.

Electrical performance data were recorded with a power quality analyzer. Current probes rated for 0–5A were selected and had a $\pm 1\%$ full scale accuracy. The current clamps were applied to both the power and neutral wires of the single phase 277 VAC input. The simultaneously measured and recorded data included but were not limited to real and apparent power, RMS voltage (V_{RMS}) and current (I_{RMS}), associated harmon-

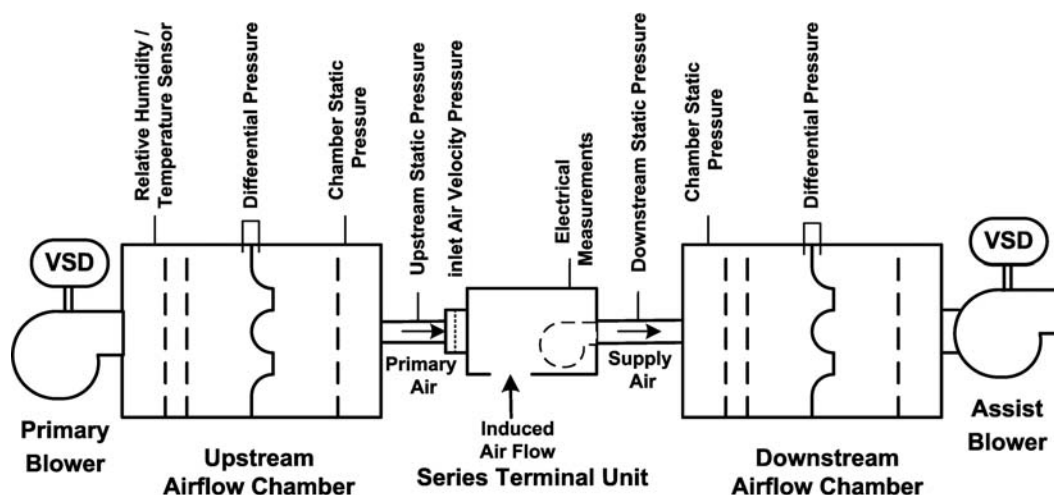


Figure 1 Airflow test apparatus including FPTU and airflow chambers.

Table 1. Parallel Fan-Powered Terminal Unit Test Levels

Independent Variable	Number of Test Points	Value Range
D , damper position	4	100%, 75%, 50%, 25% open
V , ECM setting	5	100%, 75%, 50%, 25%, 0% full scale
P_{up} , upstream static pressure	5	0.0–2.0 in. w.g. (0–498 Pa)
P_{down} , downstream static pressure	3	0.1–0.5 in. w.g. (25–125 Pa)

ics, and total harmonic distortion. The data files were cached in the power quality analyzer's internal memory and then transferred to a personal computer.

A factorial test matrix spanning several independent variables was established for the FPTU designs to adequately span the expected range of operation in the field. Table 1 shows the independent variables and their ranges for this study.

The damper position, D , varied for the respective FPTU designs. Orientation was controlled using a damper actuator with a 0 to 10 VDC input that could vary the damper position between 100% fully open and fully closed. The fully closed condition was not included in the test matrix because this damper position would have produced no primary airflow regardless of upstream pressure.

The three manufacturers' FPTUs were labeled A, B, and C. Each terminal unit was labeled according to the primary air inlet size and manufacturer. An 8 in. (203 mm) terminal unit from manufacturer A was labeled ECM_P8A. Manufacturer C provided units with ECM motors from two different manufacturers, so these terminal units are also differentiated by brand of ECM motor, either M1 or M2. A 12 in. (304 mm) model with an ECM motor from manufacturer C was labeled ECM_P12C-M1. Even though there were slight differences in the designs of the terminal units from the different manufacturers, the statistical analysis was still able to yield generalized models of each unit's performance.

RESULTS AND MODELS

Several aspects of the airflow performance of the FPTU were analyzed and modeled. It was important to quantify the primary airflow delivered to the FPTU as well as the air supplied by the FPTU. The primary airflow behaved similarly to that of the SCR units in that it depended on damper setting and the differential static pressure across the terminal unit. The air supplied by the terminal unit depended on primary airflow, the airflow induced by the terminal unit fan, and leakage from the terminal unit.

Primary Airflow Analysis and Model

The upstream (primary air) and downstream (supply air) static pressures were used to calculate the differential static pressure across the FPTU. There must be a positive pressure differential static pressure for there to be airflow through the FPTU for normal operating conditions.

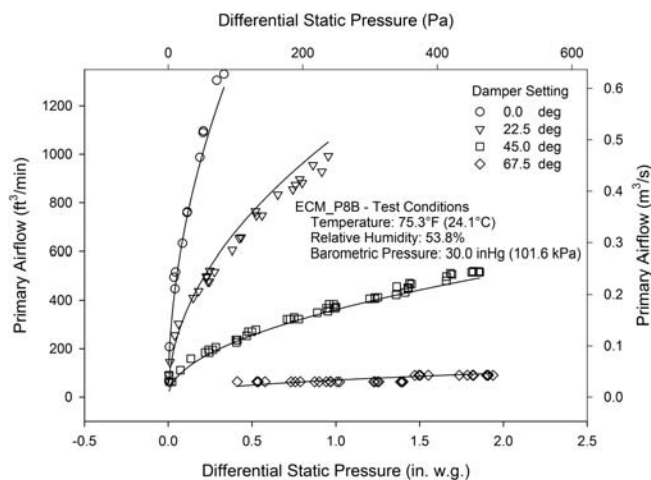


Figure 2 Primary airflow as a function of upstream minus downstream differential static pressure for ECM_P8B.

All of the manufacturers used butterfly dampers in the parallel units, so each FPTU was tested at settings of 0° (fully open), 22.5°, 45°, and 67.5°. Figure 2 shows the primary airflow ($Q_{primary}$) plotted against differential (upstream minus downstream) static pressure (DP) across the 8 in. (203 mm) unit from manufacturer B: ECM_P8B. Figure 3 shows the same data for the 12 in. (304 mm) terminal unit from manufacturer B with the second motor manufacturer: ECM_P12C-M2. The curves were generated using a fit of the data to Equation 1. In this equation, C_1 , C_2 , and C_3 were constants from the regression fit of the data, S was the damper setting (in degrees), and DP was the differential pressure (in. w.g.):

$$Q_{primary} = C_1 \cdot (1 + C_2 \cdot S + C_3 \cdot S^2) \cdot \sqrt{DP} \quad (1)$$

The values for the coefficients and R^2 values for each terminal unit are presented in Table 2. The data for ECM_P8C-M1 were from Cramlet (2008). The only differences in design between the ECM-controlled FPTUs from manufacturer C were the motors and controllers used to vary the fan speed.

This model generally correlated well with the primary airflow data. All of the FPTUs had R^2 values of 0.96 or above. The only exception to the higher R^2 was the 12 in. (304 mm) FPTU from manufacturer B, which was 0.872. It was difficult

to set the damper position correctly for ECM_P12B due to an inaccurate analog display that was used to set the damper position. The results for this unit could possibly be improved by further testing and calibration of the damper with the display. These results were generally higher than those obtained for the SCR units reported by Furr et al. (2008a).

Fan Airflow Analysis and Model

Figure 4 shows the fan airflow for terminal unit ECM_P8B plotted against the downstream (supply air) static pressure. For each ECM setting, the airflow showed a small dependence on downstream static pressure, but was primarily driven by the ECM setting. For some of the FPTUs (ECM_P8A, ECM_P8B, and ECM_P12B), the ECM controller performed erratically at the highest (100%) input setting.

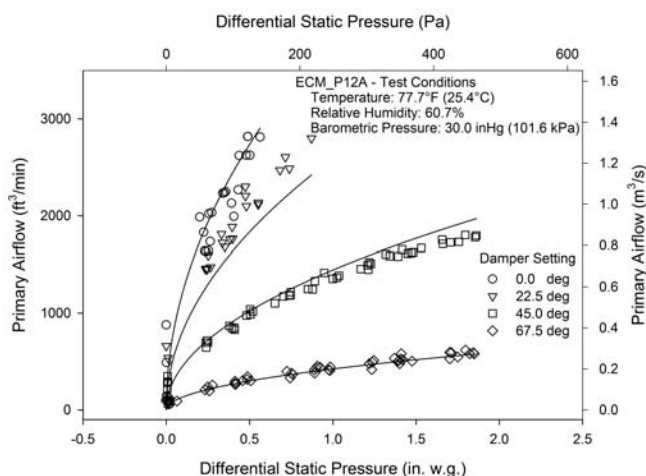


Figure 3 Primary airflow as a function of upstream minus downstream differential static pressure for ECM_P12A.

For each of the three units, the manufacturers did not recommend using the FPTU at the highest ECM setting. As a result, any data taken at the highest setting were not included in the data analysis or model development of that FPTU.

Figure 5 shows the fan airflow for terminal unit ECM_P12A. The airflow induced by the fan in a parallel unit was mainly a function of the ECM setting. This figure shows a nearly constant airflow for a given ECM setting across a wide range of downstream static pressures.

The model for fan airflow is shown in Equation 2. It was the same general form used by Furr et al. (2008a) except for the following changes. First, Furr included a term that was dependent on the inlet air velocity pressure (P_{iav}) at the inlet to the FPTU. In this study, one of the units had a backdraft damper whose performance was dependent on the primary air coming into the FPTU. All of the ECM FPTUs used in this study had gravity-operated backdraft dampers. As a consequence, the ECM fan airflow showed no dependence on P_{iav} , so it was not included for the ECM airflow model.

$$Q_{fan} = C_1 + C_2 \cdot V^2 + C_3 \cdot V + C_4 \cdot P_{down} \quad (2)$$

A second difference in Equation 2 from that of the model in Furr et al. (2008a) was the definition of the voltage (V). For the SCR units, V represented the AC voltage measured after the SCR controller. For the ECM units, V represented the ECM setting as a percentage of the maximum airflow setting. Manufacturer A provided a controller adjusted by turning a screw to choose a setting from zero to 100%, so it simply represented the ECM setting. Manufacturer B used a 2 to 10 VDC signal, so the settings used were 4 VDC (25%), 6 VDC (50%), 8 VDC (75%), and 10 VDC (100%). Manufacturer C used a control signal of 0 to 10 VDC, so settings of 2.5 VDC (25%), 5 VDC (50%), 7.5 VDC (75%), and 10 VDC (100%) were used. Table 3 contains a summary of the ECM settings used.

Table 2. Model Coefficients for ECM-Controlled Units

FPTU	C_1	C_2	C_3	R^2
ECM_P8A	1380	-2.03E-02	8.90E-05	0.982
ECM_P12A	3868	-1.54E-02	3.27E-05	0.961
ECM_P8B	2212	-2.71E-02	1.89E-04	0.988
ECM_P12B	6528	-2.84E-02	2.06E-04	0.872
ECM_P8C-M2	1469	-2.35E-02	1.38E-04	0.975
ECM_P8C-M1	1671	-2.53E-02	1.71E-04	0.978
ECM_P12C-M1	3380	-2.25E-02	1.22E-04	0.960
ECM_P12C-M2	3747	-2.98E-02	2.27E-04	0.969

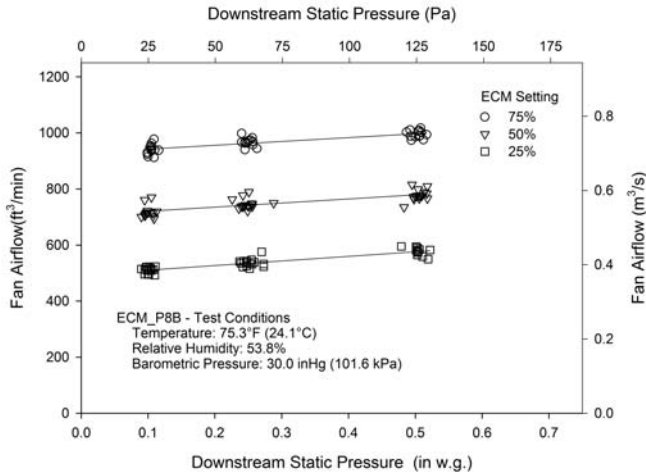


Figure 4 Terminal unit fan airflow versus downstream static pressure for ECM_P8B.

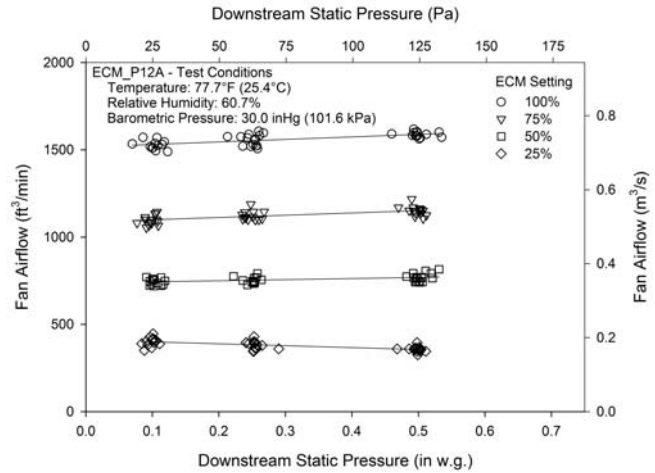


Figure 5 Terminal unit fan airflow versus downstream static pressure for ECM_P12A.

Table 3. Summary of ECM Controller Settings for the Units Tested

FPTU Manufacturer	ECM Settings			
	25%	50%	75%	100%
A	25%	50%	75%	100%
B	4 VDC	6 VDC	8 VDC	10 VDC
C	2.5 VDC	5 VDC	7.5 VDC	10 VDC

The coefficients and R^2 values for the ECM units are presented in Table 4. All models for the ECM-controlled FPTUs had R^2 values above 0.955, and most of them above 0.98.

FPTU Leakage Analysis

The fan airflows in the previous section were the net airflows induced by the terminal unit fan. The induced air provided by the terminal fan was equal to the difference between the supply air and the primary air supplied to the terminal unit plus the leakage (Equation 3). Because there was no easy way to directly measure the air induced by the fan with the laboratory setup, leakage was measured by turning off the terminal fan so that the induced air from the fan, Q_{fan} , would be equal to zero. This meant the leakage was simply the difference between the primary air and the supply air.

$$Q_{fan} = (Q_{supply} - Q_{primary}) + Q_{leakage} \quad (3)$$

Figures 6 and 7 show the leakage for ECM_P8B and ECM_P12A, respectively, versus the pressure downstream (P_{down}) of the FPTU. Leakage for both units was shown for three inlet air velocity pressures (P_{iav}) to illustrate the effect of increasing primary airflow (reflected as an increase in P_{iav}) on leakage from the terminal units. The leakage for ECM_P8B

varied almost linearly with downstream static pressure and showed little dependence on the inlet air velocity pressure, P_{iav} . The leakage for ECM_P8B was primarily dependent on the internal static pressure of the FPTU, regardless of the airflow. This variation was different from ECM_P12A where an increase in P_{iav} from 0.25 to 1.25 in. w.g. (62 to 311 Pa) resulted in an approximately 75 ft³/min (0.0354 m³/s) increase in leakage at a downstream static pressure of 0.1 in. w.g. (24.9 Pa). For the ECM units evaluated, both units from manufacturer A had much higher leakage and more dependence on P_{iav} than the most of the units from the other manufacturers. It appeared that the larger leakage with ECM_P12A was possibly due to three leaking punch-out tabs near the primary air inlet and lack of sealing between the grommet and the power/control cable bundle that penetrated the side of the unit. In addition, there may have been higher leakage around the backdraft damper. However, it was not possible to view the damper during these tests to verify it was also a source of leakage. Because one of the objectives of this study was to characterize off-the-shelf fan-powered terminal units, no attempt was made to seal or correct the leakage of any of the units.

Figure 7 shows that the leakage for unit ECM_P12A was four to five times higher than the leakage from terminal unit ECM_P8B. Comparing the leakage values in Figure 7 with the

Table 4. ECM Coefficients for Fan Airflow Model

FPTU	C_1	C_2	C_3	C_4	R^2
ECM_P8A	139.91	0.18	5.05	66.16	0.992
ECM_P12A	24.71	0.019	13.22	51.43	0.995
ECM_P8B	300.03	0.007	7.846	139.83	0.994
ECM_P12B	358.35	0.011	7.170	49.80	0.955
ECM_P8C-M1	-282.27	-0.138	25.80	-290.92	0.982
ECM_P8C-M2	40.27	-0.011	11.02	-111.87	0.979
ECM_P12C-M1	-206.12	-0.083	22.93	-122.0	0.99
ECM_P12C-M2	-53.47	-0.039	16.12	-272.66	0.987

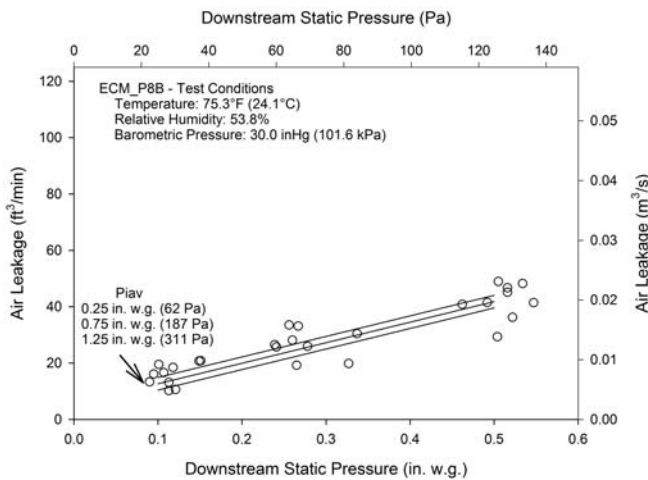


Figure 6 Measured air leakage from ECM_P8B.

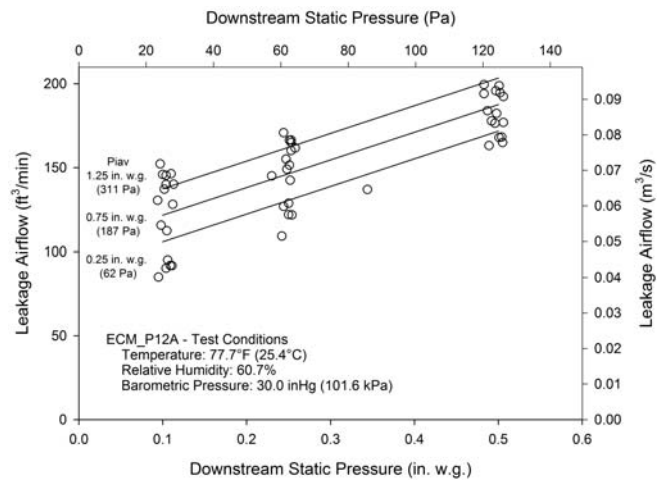


Figure 7 Measured air leakage from ECM_P12A.

fan airflow for ECM_P12A in Figure 5, it is possible to see that for this unit leakage could easily reach 20% to 40% of the fan airflow when the ECM setting was between 25% and 50%. Even at the highest ECM setting, the leakage for this unit could easily reach as high as 10% of the airflow produced by the fan. Air leakage from this FPTU would have a severe negative impact on its overall performance, because the air leakage would be directly into the return air plenum in a typical building application. The leakage would result in a lower supply airflow to the conditioned space and more power consumed by the FPTU fan in the application in the building (Davis et al. 2009; Faris 2009).

The equation used to model the air leakage was taken from the SCR model of Furr et al. (2008a) and is shown in Equation 4. The constant coefficients (C_1 , C_2 , and C_3) for the ECM-controlled terminal units are presented in Table 5. The data for ECM_P8C-M1 was taken from Cramlet (2008). The R^2 values ranged from 0.826 to 0.972 for the ECM FPTUs and were comparable to those reported for SCR units by Furr et al. (2008a). Both units from manufacturer A and one unit

from manufacturer B (ECM_P12B) had the highest coefficients for P_{iav} .

$$Q_{leakage} = C_1 + C_2 \cdot P_{down} + C_3 \cdot P_{iav} \quad (4)$$

Terminal Unit Power Performance. One of the main reasons for choosing an ECM-controlled FPTU over an SCR-controlled unit is that the fan speed of an ECM-controlled fan follows the airflow requirement of the space the FPTU is serving. Because fan power is related to the third power of fan speed, a reduction in airflow by 50% can be expected to produce as much as an 87.5% reduction in power, everything else (primary air pressure, downstream static pressure, etc.) being equal. To model the energy use of a FPTU, the power of the FPTU must be characterized over the whole range of operating conditions of each FPTU. The power use of each terminal unit was measured and a semi-empirical model developed. In addition to the real power, the power factor was also measured for each unit.

Table 5. Coefficients for Leakage Model for the ECM-Controlled FPTUs in This Study

FPTU	C_1	C_2	C_3	R^2
ECM_P8A	43.29	121.92	11.88	0.972
ECM_P12A	81.34	165.05	31.64	0.948
ECM_P8B	8.71	72.87	-4.47	0.887
ECM_P12B	16.00	78.83	-13.24	0.856
ECM_P8C-M1	37.87	119.98	3.21	0.918
ECM_P8C-M2	27.13	90.50	-4.99	0.895
ECM_P12C-M1	29.00	72.27	-6.63	0.927
ECM_P12C-M2	35.04	76.50	-4.95	0.826

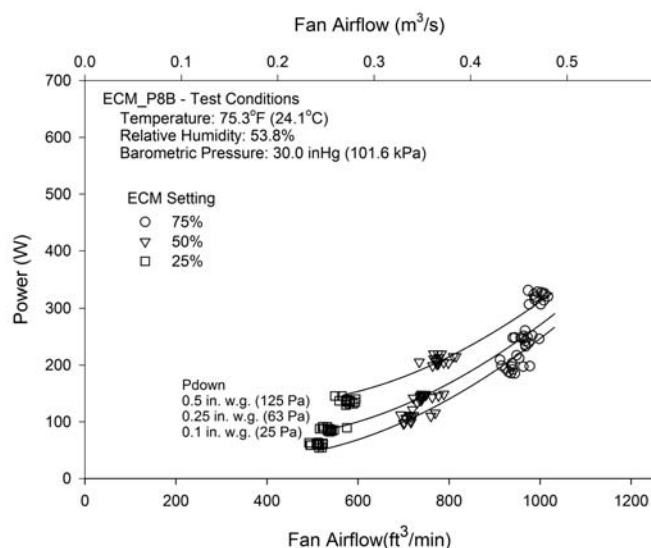


Figure 8 FPTU power versus fan airflow for ECM_P8B.

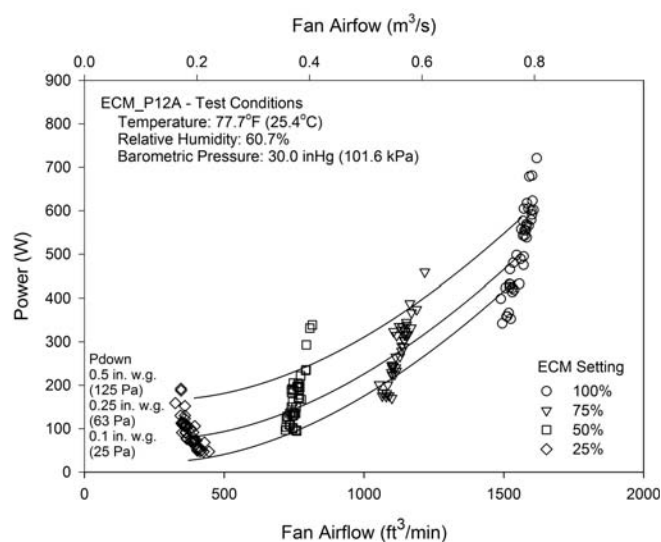


Figure 9 FPTU power versus fan airflow for ECM_P12A.

Fan Power Consumption Analysis and Model

The fan power in a parallel FPTU is dependent on the airflow produced and the downstream static pressure. Figures 8 and 9 show the power use of terminal units ECM_P8B and ECM_P12A, respectively, as a function of fan airflow (Q_{fan}) and downstream static pressure (P_{down}). As downstream pressure increased, power consumption also increased for both units. For ECM_P8B at an ECM setting of 25% (4 VDC), the fan was producing an airflow of between 500 and 600 ft³/min (0.236 to 0.283 m³/s). There were three distinct power consumption levels for this ECM setting: one at about 75 W, one at about 100 W, and the highest at about 150 W. These three power values corresponded directly with P_{down} levels of 0.1 in. w.g. (24.9 Pa), 0.25 in. w.g. (62.3 Pa), and 0.5 in. w.g. (124.5 Pa).

The results presented in Figures 8 and 9 were typical of the ECM terminal units tested in this study. One of the major

differences between the power consumption data of the SCR units from Furr et al. (2008a) and the data from the ECM units in this study was that the SCR power increased linearly with increasing airflow, while the increase was quadratic for the ECM units evaluated for this paper.

The form of the equation used to model power consumption was adopted from Furr et al. (2008a) and is shown in Equation 5. Furr et al. (2008a) required an additional term for SCR terminal unit P8A, which was the inlet air velocity pressure, P_{iav} . The term for P_{iav} was not used in the model for the power consumption of ECM-controlled units. Because each manufacturer's controller utilized a different control signal, it was determined that the best way to compare different ECM units was to use the percentage from minimum to maximum ECM setting rather than the voltage. The coefficients (C_1 , C_2 , C_3 , and C_4) for the ECM units are presented in Table 6. Each

Table 6. Coefficients for Fan Power Model for the ECM-Controlled FPTUs

FPTU	C_1	C_2	C_3	C_4	R^2
ECM_P8A	11.70	0.025	-0.92	203.92	0.953
ECM_P12A	3.35	0.060	-1.99	358.34	0.922
ECM_P8B	11.46	0.036	-0.35	245.19	0.990
ECM_P12B	29.07	0.042	-0.52	196.66	0.955
ECM_P8C-M1	-202.61	-0.041	9.99	-8.42	0.919
ECM_P8C-M2	55.74	0.074	-3.74	172.10	0.943
ECM_P12C-M1	-59.41	0.027	1.35	167.82	0.977
ECM_P12C-M2	22.52	0.043	-1.32	114.36	0.976

Table 7. Power Factors for ECM_P8B and ECM_P12A for Different ECM Settings

ECM Setting	Power Factor	
	ECM_P8B	ECM_P12A
25%	0.44	0.51
50%	0.45	0.52
75%	0.45	0.52
100%	n.a.	0.54

of the regressions for the ECM-controlled FPTUs had an R^2 above 0.919, indicating that the model correlated well with the measured performance.

$$Power_{fan} = C_1 + C_2 \cdot V_2 + C_3 \cdot V + C_4 \cdot P_{down} \quad (5)$$

Power Factor. Table 7 shows the average power factors for ECM_P8B and ECM_P12A as a function of ECM setting. Data were not included in Table 7 for ECM_P8B at the 100% setting because of erratic performance of the ECM. There was little variation of power factor with the ECM setting. The data from the other fan-powered units also showed little dependence on ECM setting. As a consequence, the power factors were averaged for each FPTU and are presented in Table 8. The power factors for the ECM-controlled parallel units ranged from 0.42 to 0.53. The power factor data reported by Furr et al. (2008a) for SCR units showed a low power factor at the lowest AC voltage setting, then increasing to near 1.0 for the highest setting (277 VAC). While the ECM units had lower power factors than those of the SCR units, the overall impact on the building power factor may still be smaller for ECM units because of the significantly reduced overall power consumption at off-peak conditions. The detailed comparison would require use of a building simulation program, which was beyond the scope of this paper.

Table 8. Average Power Factors for Each of the ECM Fan-Powered Terminal Units

Unit	Average Power Factor
ECM_P8A	0.42
ECM_P8B	0.45
ECM_P8C	0.50
ECM_P12A	0.52
ECM_P12B	0.45
ECM_P12C-M1	0.49
ECM_P12C-M2	0.53

SUMMARY AND CONCLUSION

This paper summarized detailed measurements made on eight parallel fan-powered units using electronically commutated motors. Three fan-powered unit manufacturers provided units for this study. In addition, two motor manufacturers provided ECMs that were used on one manufacturer's units. To provide some consistency with the previous work of Furr et al. (2008a), the same basic equations developed by them were used here, with minor modifications to accommodate the differences in input fan voltage (DC versus AC). Also, in some correlations the inlet air velocity pressure was not significant and thus was not used.

The parallel FPTUs in this study required four different models to characterize their performance. The first model was for the primary air supplied to the parallel terminal unit. All but one of the models had R^2 values between 0.960 and 0.988. One model had an R^2 value of 0.872, which could likely be improved by further testing of this unit. Overall, this primary air model provided excellent correlation of the data for both ECM and SCR units.

The second model developed for ECM units was that for fan airflow and represented the effective airflow induced by

the terminal fan. This model provided high correlation to the data, with R^2 values ranging from 0.955 to 0.995.

The third model developed for parallel units was for leakage. This model represented the amount of conditioned primary air lost to the return air plenum and was developed by testing the terminal unit with the FPTU fan switched off. The correlation to the data of this model varied widely, with R^2 values ranging from 0.826 to 0.972.

The final model developed was one for fan power consumption and is important in helping characterize the potential energy savings for ECM units over SCR units. With the exception of one SCR unit presented by Furr et al. (2008a), the model for the ECM units had the same basic form as the SCR units. This model correlated well to the data for ECM units, with R^2 values from 0.919 to 0.99.

These four models used to characterize the overall performance of parallel ECM FPTUs could be used in a building simulation model to allow building designers to estimate the annual or seasonal energy use of ECM FPTUs in a VAV system. This energy use data could then be compared to similar data from parallel SCR FPTUs to determine the potential savings parallel ECM FPTUs might have over parallel SCR FPTUs for a given VAV system design.

ACKNOWLEDGMENTS

The authors wish to thank the following individuals and organizations that provided support and advice for this project: Gus Faris of Nailor Industries, David John of Metal Industries, Inc., Dan Int-Hout of Krueger Manufacturing Co., Ron Jordan and Doug Fetters of A.O. Smith Electrical Products Company, Floyd Blackwell of Regal Beloit Corporation, Gaylon Richardson of Engineered Air Balance Co., Inc., and Jack Stegall of Energistics Laboratory.

NOMENCLATURE

DP	= Pressure differential across the terminal unit, in. w.g. (Pa)
P_{down}	= Downstream (supply air) static pressure, in. w.g. (Pa)
P_{iav}	= Pressure across inlet air differential (velocity) flow sensor, in. w.g. (Pa)
P_{unit}	= Static pressure inside terminal unit, in. w.g. (Pa)
P_{up}	= Upstream (primary air) static pressure, in. w.g. (Pa)
$Power_{fan}$	= Power consumption of terminal unit fan, W (hp)
Q_{fan}	= Amount of airflow through terminal unit fan, ft ³ /min (m ³ /s)
$Q_{induced}$	= Amount of airflow induced from plenum, ft ³ /min (m ³ /s)
$Q_{leakage}$	= Amount of airflow leaking from a terminal unit, ft ³ /min (m ³ /s)
Q_{supply}	= Amount of parallel terminal unit airflow output, ft ³ /min (m ³ /s)
$Q_{primary}$	= Amount of primary airflow, ft ³ /min (m ³ /s)

S = Damper setting, degrees

V = Input voltage (in % of full scale) for ECM units, %

REFERENCES

- AMCA. 1999. ANSI/AMCA Standard 210-99, *Laboratory Methods of Testing Fans for Aerodynamic Performance Rating*. Arlington Heights, IL: Air Movement and Control Association.
- ASHRAE. 2006. ANSI/ASHRAE Standard 130-1996 (RA 2006), *Methods of Testing for Rating Ducted Air Terminal Units*. Atlanta: American Society of Heating, Refrigerating and Air-Conditioning Engineers, Inc.
- ASHRAE. 2008. Room air distribution equipment. In *ASHRAE Handbook—HVAC Systems and Equipment*. Atlanta: American Society of Heating, Refrigerating and Air-Conditioning Engineers, Inc.
- Cramlet, A. 2008. Performance of ECM controlled VAV fan power terminal units. M. Sc. Thesis, Texas A&M University, College Station, TX.
- Davis, M., J. Bryant, and D.L. O'Neal. 2009. Modeling the performance of single-duct VAV systems that use fan powered terminal units. *ASHRAE Transactions: Symposium* 115(1).
- Faris, Eugene W. 2009. Reflections on ARI/ASHRAE Research Project RP-1292, comparison of the total energy consumption of series versus parallel fan powered VAV terminal units. *ASHRAE Transactions: Symposium* 115(1).
- Furr, J., D.L. O'Neal, M. Davis, J.A. Bryant, and A. Cramlet. 2008a. Performance of VAV fan powered terminal units: Experimental results and models for series units. *ASHRAE Transactions* 114(1).
- Furr, J., D.L. O'Neal, M.A. Davis, J.A. Bryant, and A. Cramlet. 2008b. Performance of VAV fan powered terminal units: Experimental results and models for parallel units. *ASHRAE Transactions* 114(1).
- Furr, J., D.L. O'Neal, M. Davis, J. Bryant, and A. Cramlet. 2008c. Performance of VAV fan powered terminal units: Experimental setup and methodology. *ASHRAE Transactions* 114(1).

DISCUSSION

Ken Fonstad, HVAC Application Engineering Manager, ABB, New Berlin, WI: What power factor were you measuring: displacement (fundamental) or total?

Dennis O'Neal: The power factor reported in this paper is the total power factor. The low power factor of ECM motors is caused by high current harmonics. The manufacturers who provided the ECM motors stated that the measured power factors were within the expected range.

CH-12-017

Modeling the Performance of ECM and SCR Series Fan-Powered Terminal Units in Single-Duct VAV Systems

Michael A. Davis, PhD
Member ASHRAE

John A. Bryant, PhD, PE
Member ASHRAE

Dennis L. O'Neal, PhD, PE
Fellow ASHRAE

ABSTRACT

Single-duct variable-air-volume systems often use series- and parallel-fan-powered terminal units to control the airflow in conditioned spaces. A laboratory-verified model of single-duct variable-air-volume systems was developed to simulate both series and parallel fan terminal units where the terminal unit fans are controlled by either silicon-controlled rectifiers or electronically commutated motors.

The paper provides the equation needed to simulate the performance of a fan-powered terminal unit. The simulation model developed here includes a five-zone office building whose performance was simulated in five cities in the United States: Houston, Phoenix, Chicago, New York, and San Francisco. The model includes total plant energy, total cooling plant energy, primary fan energy, terminal unit fan energy, and heat energy added.

The single-duct variable-air-volume simulation results showed that the reduction in the annual energy used by the office building with series-fan-powered terminal units having electronically commutated motors compared to series units having silicon-controlled rectifier-controlled motors varied by location. The largest energy savings for the building was in Phoenix (8.4%), while the smallest was in Chicago (5.9%). In all cases, the reduction in electricity used by the terminal unit fans with electronically commutated motors was near 65%. These results indicate that using fan-powered terminal units with electronically commutated motors offers the potential for sizable savings in energy compared to units with silicon-controlled rectifier-controlled motors.

INTRODUCTION

Figure 1 shows a typical three-zone, single-duct variable-air-volume (SDVAV) system that uses fan-powered terminal units (FPTUs) to control the flow of conditioned air to each zone. Fresh air is mixed with return air from the zones and run through a preheat coil (if needed). Air is then cooled and dehumidified in the cooling coil. The primary fan provides the needed pressurization upstream of the FPTUs. Each FPTU then induces air from the return air plenum, which is then mixed (or blended) with primary air before being discharged into the zone served by the FPTU. Each FPTU has a small fan that is mounted either in series or in parallel with the primary system fan. Figure 2 shows a schematic of a typical series FPTU. The unit is called a series FPTU because the airflow path of the terminal fan is in series with the airflow path of the primary fan.

First-generation FPTUs had constant-speed fans driven by permanent split capacitor (PSC) motors where the fan motor speed was regulated with a silicon-controlled rectifier (SCR) controller. With an SCR controlled motor, the fan speed would be set during the installation and commissioning process. Once set, it operated as a constant-speed, on/off device. For series FPTUs, when the air-conditioning system was operating, the fan was on continuously. In recent years, manufacturers have begun to integrate electronically commutated motors (ECMs) in FPTUs, which allow the speed of the fan to vary as the load in the zone changes. As a consequence, FPTUs with ECM fan motors require much less power over much of the airflow range compared to similar sized SCR-controlled motors (Edmondson et al., 2011). FPTUs with ECM motors do incur a higher cost than similarly sized SCR controlled motors. The series unit fan operates continuously

Michael A. Davis is Director of Laboratories at New York University Abu Dhabi, Abu Dhabi, United Arab Emirates; **John A. Bryant** is an associate professor at Texas A&M University at Qatar, Doha, Qatar; and **Dennis L. O'Neal** is the Holdredge/Paul Professor and Associate Dean of Engineering at Dwight Look College of Engineering, Texas A&M University, College Station, TX.

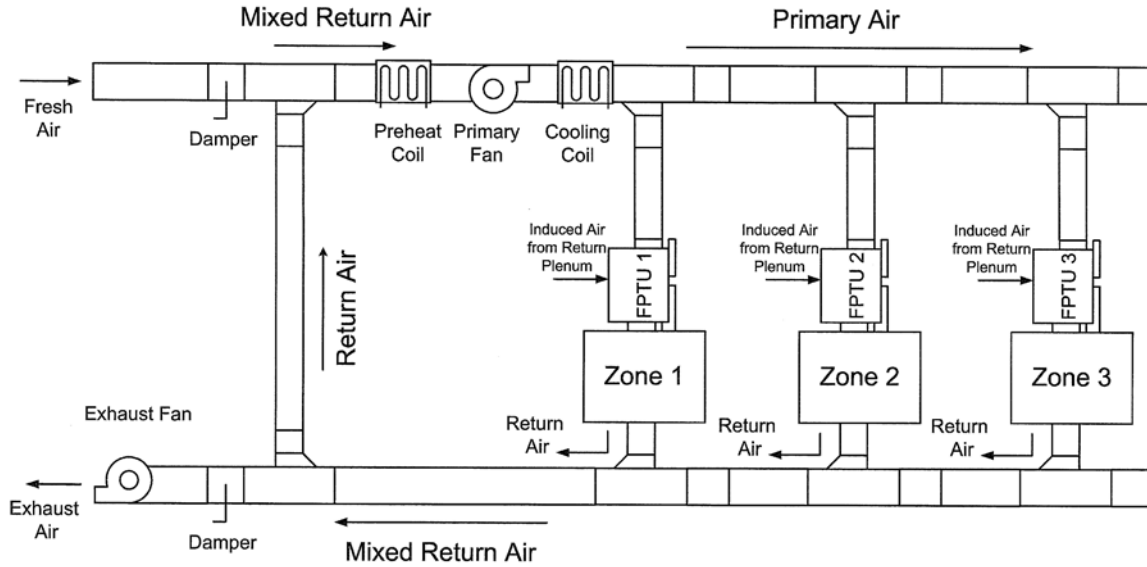


Figure 1 A typical multi-zone SDVAV system using fan-powered terminal units.

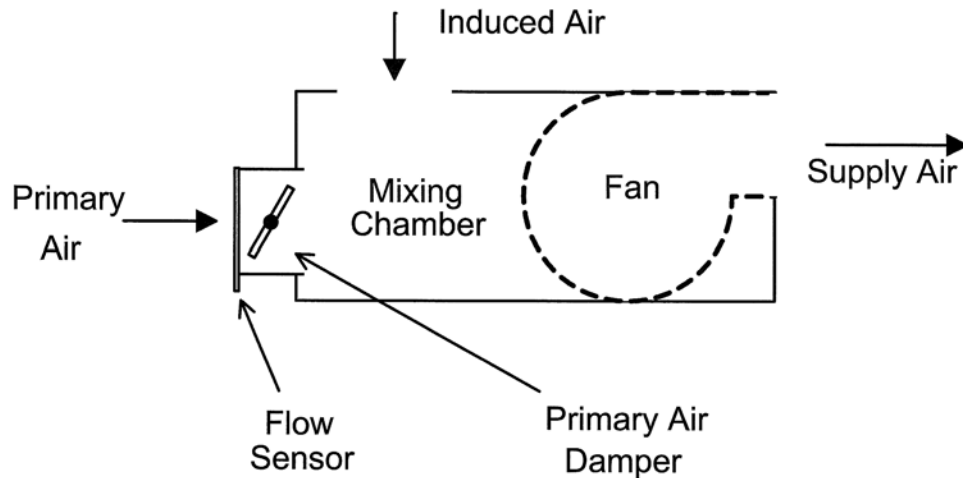


Figure 2 A typical series fan-powered terminal unit.

when the air-conditioning system is operating. In this study, the series ECM FPTUs were only operated in constant speed mode. A follow-up study is underway to investigate the operation of the system when the series ECM FPTU motor speed varies with the space loads. Air properties for the system were calculated as described in the next section.

This paper outlines the basic equations needed to simulate the annual performance of a five-zone VAV system that uses series-fan-powered terminal units. For this paper, when the term SCR is used, it will refer to a terminal unit where the fan is driven by a PSC motor with the speed of the motor controlled by an SCR. Both ECM and SCR units were simulated. The simulation model used experimental data generated by Furr et al. (2008) for SCR units and Edmondson et al. (2011) for ECM units.

SIMULATION MODEL

The simulation model included a number of equations that were used to calculate air properties, determine airflow and power, and account for the difference in operation when in either cooling or heating mode. The equations and the logic used in the simulation model are described below.

Calculating Changes in the Properties of Air

Simulating the air side of a VAV system requires a way to estimate basic air properties. For this model, air property calculations were simplified by assuming constant properties that, for the temperature ranges of interest to this project, resulted in less than a 0.2% error in the calculations (Cengal et al., 2005). Operating conditions for supply and return air

were assumed to be 55°F (12.8°C), 95% rh and 78°F (25.5°C), 50% rh, respectively. The density of air at 55°F (12.8°C), 95% rh was assumed to be 0.076 lb/ft³ (1.22 kg/m³). Given these basic assumptions, the sensible load (\dot{Q}_s) and latent load (\dot{Q}_l) can be calculated using Equations 1 and 2, respectively. Equation 1 was used throughout the simulations to model sensible heating and cooling of air as it passed through the cooling coil or when heat was added at the terminal as a result of the operation of the terminal unit fan motor or when heat was added to maintain space conditions.

$$\dot{Q}_s = C_{ps}\dot{Q}(\Delta T) \quad (1)$$

\dot{Q}_s was the heat energy transferred to or from the air, C_{ps} was the coefficient that accounted for the specific heat and density, and \dot{Q} was the volumetric flow rate (ft³/min [l/s]). Equation 2 was used throughout the simulations to model the energy change resulting from a change in the humidity ratio ($\omega_2 - \omega_1$), such as the latent heat removal at the cooling coil.

$$\dot{Q}_l = C_{pl}\dot{Q}(\omega_2 - \omega_1) \quad (2)$$

\dot{Q}_l was the energy transferred to or from the air due to an addition or removal of moisture. C_{pl} was the coefficient that accounted for the latent heat energy and density, and \dot{Q} was the volumetric flow rate of the air.

The model described in this paper was based on the verified calculation procedure that was implemented as described in Bryant et al., 2009. The program was developed to facilitate the incorporation of the model into existing commercially available programs.

The analysis of the operation of a zone required some of the variables to be set by the user. For the series FPTU, these variables consisted of the primary air temperature, T_p , primary air relative humidity, rh_p , the setpoint temperature of the space, T_{sp} , the downstream static pressure, P_{dwn} , and the minimum primary airflow rate, $\dot{Q}_{p,min}$, that must be delivered to the space. The user had to specify the fan flow settings, and once they were set, the fan speed, supply airflow, and fan power were constant.

The values used for this project were based on recommendations from the advisory board of an industry consortium that helped fund the work. For the model, the minimum primary airflow rate, $\dot{Q}_{p,min}$, was a variable, and for this project it was set at 20% of design flow.

The primary air temperature, T_p , and primary air relative humidity, rh_p , were set at 55°F and 95%, respectively. The setpoint temperature of the space, T_{sp} , was 78°F for both heating and cooling loads, and the downstream static pressure was a constant 0.25 in. w.g. for all operating conditions.

CAV Mode Setup and Operation

When a constant-air-volume (CAV) series FPTU is installed and set up by an HVAC contractor, the terminal unit fan speed is adjusted to the desired value and runs at a constant speed from that time forward whenever the fan is in operation.

It was shown by Furr et al. (2008), Cramlet (2008), and Edmondson et al. (2011) that when series FPTUs are operated at a constant speed they supply a constant volume of air to the space over the operating range of the terminal unit for both the speed of the motor and the range of damper settings used to control the supply temperature.

For cooling load operation, the temperature in the zone was maintained at the setpoint without adding supplemental heating by adjusting the primary airflow, which changes the supply air temperature. As the cooling load dropped, the primary airflow rate was reduced to match the space-sensible cooling load. The primary airflow rate can be reduced to a minimum flow rate that was determined by the need for fresh air to be supplied to the space.

Furr et al. (2008) demonstrated that the fan airflow for a series FPTU was a function of the fan motor speed and the flow rate of the primary air that entered the mixing chamber expressed as a velocity pressure, P_{iav} , across the inlet flow sensor. The speed of the motor was expressed as a function of the control voltage (V). For SCR-controlled motors, V varied from 0 to 277 V. For ECM motors, V typically varied from 0 to 10 VDC (Edmondson et al., 2011). For this model, the user input the fan speed as a percentage of the full speed, and the algorithms automatically adjusted the inputs to the equations as appropriate for the ECM- or the SCR-controlled FPTU used by the zone.

For the series FPTUs, the supply airflow, \dot{Q}_s , used in the model was the same as the fan airflow, \dot{Q}_f , that Furr et al. (2008) used in characterizing several ECM FPTUs under laboratory conditions. Furr et al. (2008) developed a correlation (Equation 3) with four empirical coefficients (C_1 through C_4) that related \dot{Q}_f for SCR units to the voltage setting, V , and the inlet air velocity pressure, P_{iav} . As mentioned above, the voltage for SCR units varied from 0 to 277 volts.

$$\dot{Q}_s = \dot{Q}_f = C_1 + C_2V^2 + C_3V + C_4P_{iav} \quad (3)$$

Edmondson et al. (2011) measured the performance of ECM units from three manufacturers and used the same equation to correlate the airflow performance of ECM units except that the voltages were the range of DC voltages (0 to 10 volts) for the ECM controller.

Calculations for the Series FPTU When in CAV Mode

Figure 3 shows a flow chart of the algorithm used to model operation of the series FPTU when operated in the CAV mode.

One of the energy-saving strategies for the series FPTU was to turn the unit off if the space was not actively controlled. The process diagram shown in Figure 3 applied when the zone was in an operating mode and the space conditions were actively controlled by the building energy management system.

Because the supply airflow was both fixed and known for all operating conditions, the first step in the analysis was to use

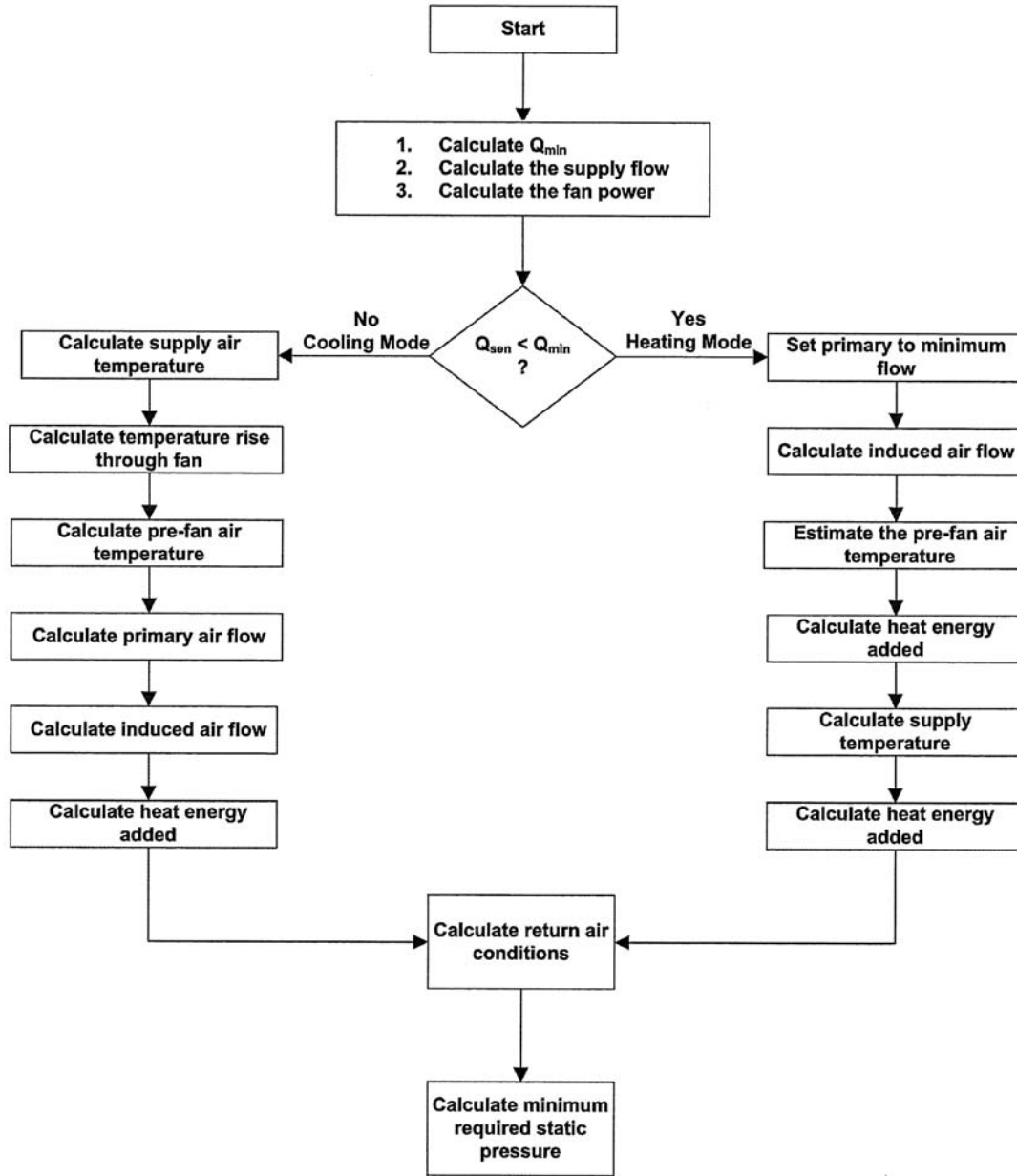


Figure 3 Flowchart of the series FPTU operation.

Equation 3 to calculate the supply flow rate from the user inputs and to use Equation 4 to calculate the power consumed by the fan, \dot{W}_f .

Equation 4 was developed by Furr et al. (2008). The coefficients for the SCR-controlled FPTUs were from Furr et al. (2008). The coefficients for the ECM-controlled FPTUs were from Edmondson (2011). As with Equation 3, V varied from 0 to 277 volts AC for the SCR-controlled FPTUs and 0 to 10 volts DC for the ECM-controlled FPTUs.

$$\dot{W}_f = C_1 + C_2 V^2 + C_3 V + C_4 P_{dwn} + C_5 P_{iav} \quad (4)$$

The next step in the analysis was to estimate the minimum amount of cooling, Q_{min} , that was supplied to the space at minimum primary flow, Q_{pmin} . The minimum primary flow was calculated by using the minimum flow setting that was input by the user of the simulation program. For this project, the minimum primary flow rate was 20% of the cooling design flow rate as per the recommendation from the industry advisory board. The design flow rate was also a user input and was based on the design cooling (primary flow rate) capacity of the FPTU as per the manufacturer's specifications for the FPTU. The minimum amount of cooling, Q_{min} , would then be given by Equation 5:

$$\dot{Q}_{min} = C_{ps}\dot{Q}_{pmin}(T_{sp} - T_p) \quad (5)$$

The sensible space load, \dot{Q}_{sens} , that was supplied by the building loads simulation (DOE2) was then compared to \dot{Q}_{min} ; if it was lower, then the zone was in heating mode, otherwise the zone was in cooling mode.

Calculations for the Series FPTU when in Heating Mode

When in heating mode, the primary airflow, \dot{Q}_p , was set to the minimum flow rate, and the induced airflow, \dot{Q}_{ind} , was calculated by subtracting the primary flow, \dot{Q}_p , from the supply flow rate, \dot{Q}_s . After the induced airflow was calculated, a mass and energy balance on the mixing chamber was done and the pre-fan mixed-air temperature was calculated using Equation 6.

$$T_{pfest} = \frac{\dot{Q}_p T_p + \dot{Q}_{ind} T_p}{\dot{Q}_s} \quad (6)$$

After the pre-fan temperature was calculated, the heat added to maintain space conditions was calculated using Equation 7.

$$\dot{Q}_{aux} = \dot{Q}_{min} - \dot{Q}_{sens} \quad (7)$$

The estimated supply temperature was then calculated using Equation 8:

$$T_s = T_{pfest} + \frac{\dot{Q}_{aux} + 3.412\dot{W}_f}{C_{ps}\dot{Q}_s} \quad (8)$$

The constant 3.412 was used to convert watts to BTUs per hour. The return air conditions were then calculated where the return air temperature was the same as the space setpoint temperature, and the return air humidity ratio was calculated using Equation 9:

$$\omega_r = \omega_p + \frac{\dot{Q}_{lat}}{C_{pl}\dot{Q}_p} \quad (9)$$

Calculations for the Series FPTU When in Cooling Mode

The first task in cooling mode was to calculate the required supply temperature using Equation 10.

$$T_s = T_{sp} - \frac{\dot{Q}_{sen}}{C_{ps}\dot{Q}_s} \quad (10)$$

The required pre-fan, mixed-air temperature was calculated using Equation 11.

$$T_{rpf} = T_s - \frac{3.412\dot{W}_f}{C_{ps}\dot{Q}_s} \quad (11)$$

After the required pre-fan mixed-air temperature was calculated, the amount of primary air that was required to obtain the correct pre-fan mixed-air temperature was calculated using Equation 12.

$$\dot{Q}_p = \left(\frac{T_{rpf} - T_{sp}}{T_p - T_{sp}} \right) \dot{Q}_s \quad (12)$$

When Equation 12 was derived, the temperature of the return air, T_r , was considered to be equal to the space temperature, T_{sp} , because in all operating cases the supply air temperature was adjusted to meet the space load for both heating and cooling modes, which resulted in a return air temperature that is the same as the space setpoint temperature.

After the primary airflow was calculated, the induced air was calculated by subtracting the primary airflow from the supply airflow. For the case where the zone was in cooling mode, the supply temperature and humidity conditions were known, and the return air humidity ratio, ω_r , was calculated using Equation 9; the return airflow was the same as the primary airflow.

Pressure Calculations: Minimum Static Pressure

One advantage of VAV systems is the ability to reduce fan power as a result of the reduced airflow requirements at part-load conditions. When the flow rate decreases, there is a related drop in the amount of static pressure required to move the primary air through the system and to deliver the air to the space. The static pressure requirement for the zone was defined as the static pressure required at the inlet of the primary air valve to move the air through the FPTU. To be able to optimize the operation of the system, it would be valuable to know the minimum static pressure requirement for each of the zones. With this information, the operator could reduce the primary fan speed to supply the proper airflow at the minimum pressure required by the system.

The procedure for estimating the minimum required static pressure consisted of using the previously described process to determine the required amount of primary airflow to meet the space loads. Once the primary airflow rate was known, the minimum static pressure could be calculated.

Furr et al. (2008) and Edmondson et al. (2011) developed correlations from experimental data on SCR and ECM FPTUs, respectively, that can be used to calculate the flow rate for the primary air for a given damper setting and differential pressure across the FPTU. The correlation required three constants (C_1 , C_2 , and C_3), shown in Equation 13, to fit the equation to the experimental data.

$$\dot{Q}_p = C_1(1 + C_2S + C_3S^2)\sqrt{\Delta P + 0.27} \quad (13)$$

The pressure differential was calculated by using a binary search algorithm for the ΔP needed to calculate the primary flow, \dot{Q}_p , required to meet space conditions. The minimum static pressure required that the damper be in a fully open position, so the value of S was zero (0) degrees for this calculation.

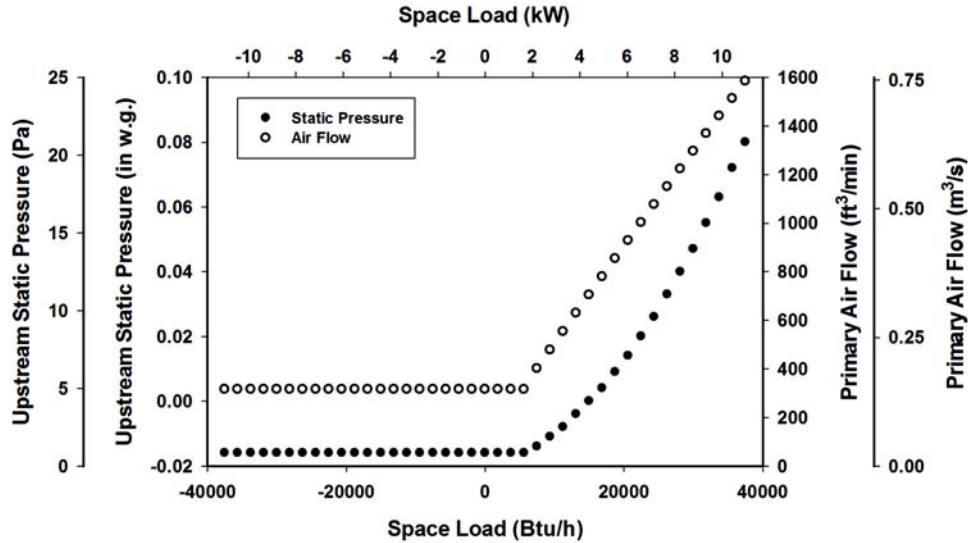


Figure 4 Graph of the series primary airflow rate and upstream static pressure as a function of space load.

Once ΔP was determined, the upstream static pressure was determined by adding ΔP to the downstream static pressure. For this research, the downstream static pressure was a constant 0.25 in. w.g., which meant that it was possible that the minimum upstream static pressure could be less than 0 in. w.g.

The performance of the system was a function of the operating characteristics of the zones. Figure 4 shows the primary airflow rate and the upstream static pressure as a function of the space load from maximum heating to maximum cooling for a series FPTU. The primary airflow rate is the amount of primary air that is required to provide the proper supply temperature to maintain space conditions.

Figure 4 shows that the upstream static pressure for the series terminal unit dropped with the space loads and that it stayed at the minimum value when the primary flow rate was at a minimum. The primary fan can be operated at minimal speeds to reduce system static pressure as the loads decreased to minimum values.

Calculations for the SDVAV System with Series FPTU

As shown in Figure 1, the components of the SDVAV system consisted of FPTUs that control the zones, return air ducts, exhaust and fresh air ducts, a pre-heat coil (PHC), the primary air fan (Fan), the primary air cooling coil (CC), and the primary air distribution ducts. Figure 5 shows a diagram that identifies the calculation sequence used in the simulation program.

Zone Calculations

The system control algorithm started at the first hour of the year and on an hourly basis executed the zone simulation procedure for the series FPTU illustrated in Figure 3. The hourly procedures provided information such as the required

primary flow, return airflow, minimum static pressure, heat energy added, and FPTU fan power that resulted from the operation of the zone. After all of the zone calculations were completed, the system return air properties were calculated.

Return Air

The return air mixed-air temperature is calculated from an energy and mass balance on the air returning from all the zones in the building. If the air-specific heat is assumed constant, then the mixed-air temperature and humidity ratio can be calculated using Equations 14 and 15, respectively, for n zones. For these simulations, n was five.

$$T_{ra} = \frac{\sum_i^n Q_i \times T_i}{\sum_i \dot{V}_i} \quad (14)$$

$$\omega_{ra} = \frac{\sum_i^n \omega_i \dot{Q}_i}{\sum_i \dot{V}_i} \quad (15)$$

Exhaust/Fresh Air

The temperature and humidity ratio of the air after the exhaust/fresh air intake was calculated by assuming an adiabatic mixing process. If X is the fraction of fresh air mixed with the return air, then the temperature (T_{rapf}) and humidity ratio (ω_{rapf}) of the air after the mixing process can easily be estimated using Equations 16 and 17. For this study, X was assumed to be 20% (0.20) in both equations.

$$T_{rapf} = XT_{oa} + (1 - X)T_{ra} \quad (16)$$

$$\omega_{rapf} = X\omega_{oa} + (1 - X)\omega_{ra} \quad (17)$$

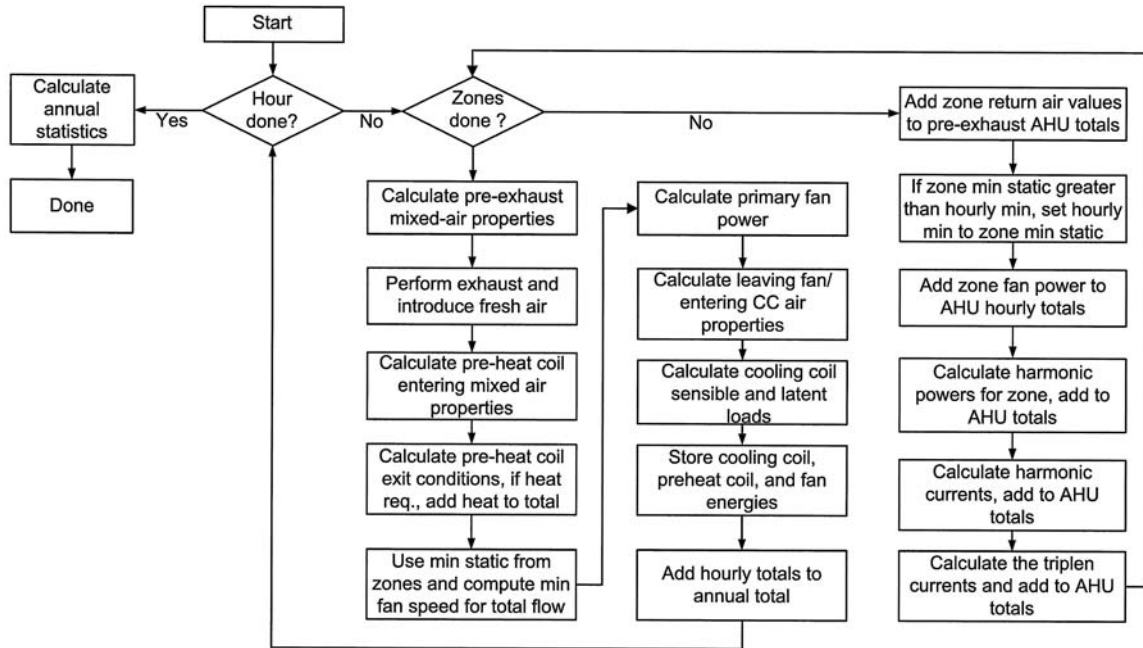


Figure 5 SDVAV system simulation flow chart.

Primary Fan

The primary airflow, \dot{Q}_p , developed by the primary fan can be correlated as a function of the fan speed, S , in revolutions per minute and static pressure, P , in in. w.g. Equation 18 shows the form of the equation used in this study. Equation 19 was used to calculate the fan power, \dot{W}_f , as a function of fan speed, S , in rpm. Equation 18 was a correlation developed using published data for a fan with an operating range that covered the simulations included in this study. Equation 19 was included in the published data provided by the fan manufacturer and was modified to include the efficiency of the fan motor, f_{an} , which was 85%.

$$\dot{Q}_p = a_1 + a_2P + a_3P^2 + a_4S + a_5S^2 + a_6PS + a_7P^2S^2 \quad (18)$$

$$\dot{W}_f = 746 \left(\frac{s}{1631} \right)^3 \left(\frac{1}{f_{an}} \right) \quad (19)$$

where $a_1 \dots a_7$ were constants that were inputs by the user of the model and f_{an} was the user-defined efficiency of the fan in percent. A binary search algorithm held the static pressure constant and searched for the fan speed that would produce the required amount of flow. The static pressure in Equation 18 was the maximum value of the minimum required static pressure for all of the zones.

Pre-Heat Coil

The return air entered the pre-heat coil after the fresh air was introduced into the system. If the temperature of the pre-fan return air, T_{rapf} , was below the pre-fan minimum temperature, T_{pfm} , then heat energy, Q_{ph} , was added so that the pre-

fan return air temperature was at the minimum. An energy balance was performed to develop Equation 20, which was used to calculate the amount of heat required to warm the return air to the minimum pre-fan temperature.

$$Q_{ph} = C_{ps} \dot{V}_{ra} (T_{pfm} - T_{rapf}) \quad (20)$$

The minimum entering fan temperature was calculated by subtracting the fan temperature rise from the cooling coil leaving air temperature. If the temperature of the return air was above the minimum entering air temperature for the fan, then no thermal energy was added, and the temperature of the air entering the fan was the pre-fan return air temperature, T_{rapf} .

The increase in the temperature of the air, ΔT_f , as it passed through the fan was calculated from an energy balance on the fan. The result was Equation 21, which used the power consumed by the fan, \dot{W}_f , which was calculated using Equation 19.

$$\Delta T_f = \frac{3.412 \dot{W}_f}{C_{ps} \dot{Q}_r} \quad (21)$$

The humidity ratio of the air entering the fan was the same as the humidity ratio of the mixed air after the fresh air was added to the air stream.

Primary Cooling Coil

The return air cooling coil entering temperature, T_{raec} , was calculated by adding the temperature rise across the fan to the pre-fan return air temperature, T_{rapf} . The sensible cooling

load, Q_{ccsen} , handled by the cooling coil was calculated using Equation 22.

$$Q_{ccsen} = C_{ps} \dot{Q}_p (T_{raec} - T_p) \quad (22)$$

The latent load, Q_{cclatt} , on the primary cooling coil was calculated using Equation 23.

$$Q_{cclatt} = C_{pl} \dot{Q}_p (\omega_{raec} - \omega_p) \quad (23)$$

The total load on the cooling coil was the sum of the sensible and latent loads.

SIMULATION RESULTS

The system model was used to predict the 24-hour operation of a commercial building for one year at five different geographical locations around the United States using TMY2 (NREL 1995) weather data. The base case operating conditions used Houston weather data for the analysis. Following the base case operation, a sensitivity analysis was done that investigated changes in the manufacturer and location.

The building model consisted of five zones with exterior exposures covering a range of loads resulting from weather and solar effects while the interior, or core zone, was dominated by internal thermal loads. The hourly space loads were normalized to the peak cooling capacity of the FPTUs and were based on the hourly loads generated by modeling a single-story rectangular structure with four perimeter zones and a single core zone.

This technique allowed modeling of the operation of the facility at various geographic weather locations while maintaining the peak cooling loads within the capacity of the selected FPTU. This method also eliminated any bias in the simulation results if the VAV terminal units were either over- or undersized when moved to different geographic locations. The procedure used to generate the normalized loads at each of the five weather locations was described by Bryant et al. (2009).

One of the objectives of the study was to isolate the interaction between the terminal unit fan and the primary fan, so some additional simplifications to the model were made that included using the same space setpoint temperature for the winter and summer operation, a 24-hour operation only, no return heat gains or losses, and no duct heat gains or losses. The impact of different operating schedules and return air heat gain and duct losses will be included in follow-on studies.

Base Case

The base case settings were intended to mimic the theoretical best case operating patterns of buildings that used fan-powered terminal units. The “theoretical best case” means that parallel terminal units did not leak primary air from the mixing chamber into the return air plenum. Laboratory tests showed that every parallel FPTU evaluated had some leakage. Some units had air leakage over 10%. Table 1 shows the annual totals for total plant energy, cooling plant energy, primary fan energy, terminal unit fan energy, heat added to maintain space

Table 1. Simulation Results Summary for the Base Case Houston Location*

	Fan-powered Terminal Unit			
	SCR_S12A	ECM_S12A	SCR_P12A	ECM_P12A
Total Plan Energy (MWh)	174	161	156	156
Total Cooling Plant (MWh)	61	58	56	56
Primary Fan Energy (MWh)	4	3	3	3
Terminal Unit Fan Energy (MWh)	33	11	9	3
Heat Energy Added (MWh)	77	89	87	93
Fan + Heat Energy (MWh)	109	100	96	96
Maximum Static, in. w.g. (Pa)	0.117 (29)	0.072 (18)	0.261 (65)	0.368 (92)
Minimum Static, in. w.g. (Pa)	0.000(0)	0.000(0)	0.026 (6)	0.036 (9)

* Note: SCR_P12A and ECM_P12A results assume no leakage by the FPTUs.

temperature, the maximum upstream static pressure required to supply air to the zones, and the minimum upstream static pressure required to supply air to the zones. The values shown in Table 1 do not include any leakage, and as a result, the operating energy shown is lower than the terminal units in operation in the field. The simulation used ECM_S12A and SCR_S12A terminal units.

The total plant energy was the summation of the cooling plant, primary fan energy, terminal unit fan energy, and heat added. The total cooling energy was the cooling MWhs supplied by the primary cooling coil over the entire year. Because the model developed during this project was intended to be used within commercially available simulation programs, neither detailed cooling nor heating plant simulations were done, and the energy quantities used by the mechanical systems were not estimated by the simulation.

The cooling plant energy was estimated using a system with an annual average energy efficiency ratio (EER) of 11.0, which was taken from the minimum efficiency standards for package rooftop air-conditioning units (Energy Star 2010). The heat energy added was treated as electric resistance heating and was the heating plant energy.

The total plant energy used by the ECM_S12A was 6.9% less than the total plant energy used by the SCR_S12A terminal unit. The drop in total plant energy consumption was due to the decreased terminal unit fan energy (64.9%), which resulted in a drop in cooling energy of 4.8% and was a net decrease after including the increased heat added (16.0%) during the winter operation.

Figure 4 shows the primary airflow rate as the normalized space load varies from heating to the maximum cooling load. Figure 6 shows that the primary airflow for the SCR_S12A system was higher than the primary airflow rates for ECM_S12A while handling the same space loads.

Figure 7 shows the upstream static pressure for both ideal case terminal units as a function of space load. From Figure 7, the upstream static pressure for the series terminal units decreased from 0.10 in. wg. (24.9 Pa) at peak flow to less than 0.0 in. wg. (0 Pa) at minimum flow. The peak primary airflow rate through the terminal units in Figure 7 was 1,575 CFM (units), which was the rated capacity of the unit.

Case 1: Sensitivity to Unit Manufacturer

Table 2 shows the simulation summary results for the base case simulation using series ECM FPTUs S12A, S12B, and S12C. The total plant energy consumed by the ECM_S12A system when replaced by the ECM-S12B and ECM-S12C increased by 2.2% and 0.9%, respectively. The terminal unit fan for the S12B and S12C was 56% and 28% higher, respectively, than the S12A.

Overall, the slight change in energy consumed by the system was due to the decreased amount of heat energy added during low load conditions. The combination of the heat added and the terminal unit fan energy for the S12B and S12C were 2.6% and 1.2% more than for the ECM_S12A.

With less than a 2.2% difference in total plant energy, cooling energy, total plant energy, and cooling plant energy, the impact of the selection of the unit from a particular manufacturer had a smaller impact on the performance of the system compared to the switch from SCR to ECM FPTUs. The sensitivity of the simulation to unit manufacturer for the SCR series units was previously documented in the final report for ASHRAE RP-1292 (Davis et. al., 2007) and also showed only small differences in the results among the three manufacturers' units evaluated.

Case 2: Base Case Operation at Five Locations in the United States

Table 3 shows the energy used by each system component at each weather location for SCR_S12A and ECM_S12A. Table 4 shows a summary of the change in energy consumption for all five locations when SCR_S12A was replaced with ECM_S12A.

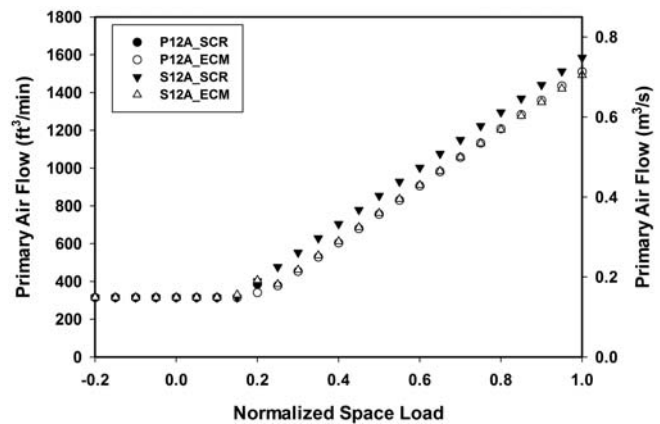


Figure 6 Primary airflow rate as function of the space load for the base FPTU.

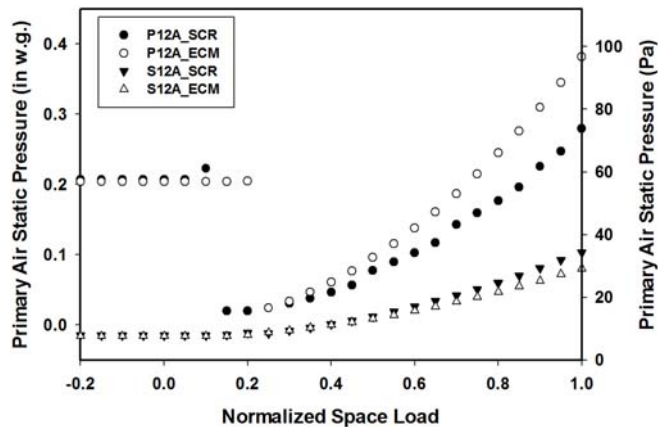


Figure 7 Primary static pressure as a function of space load for the base FPTU.

Table 2. Simulation Results for Three FPTUs

	Fan-Powered Terminal Unit		
	ECM_S12A	ECM_S12B	ECM_S12C
Total Energy (MWh)	161	165	163
Total Cooling (MWh)	58	59	58
Primary Fan Energy (MWh)	3	3	3
Terminal Unit Fan Energy (MWh)	11	18	15
Heat Added (MWh)	89	85	87
Fan + Heat (MWh)	100	103	102
Max Static, in w.g. (Pa)	0.072 (18)	0.053 (13)	0.075 (19)
Min Static, in w.g. (Pa)	0.00 (0)	0.00 (0)	0.00 (0)

Table 3. Energy Usage of SCR_S12A and ECM_S12A by Location for 24-hour Operation

City	Total Plant Energy, MWh		Total Cooling Plant, MWh		Primary Fan Energy, MWh		FPTU Fan Energy, MWh		Heat Added During Htg, MWh		Heat Added During Htg + FPTU Fan Energy, MWh	
	SCR	ECM	SCR	ECM	SCR	ECM	SCR	ECM	SCR	ECM	SCR	ECM
Houston	174	161	61	58	4	3	33	11	77	89	109	100
Phoenix	160	146	65	62	4	3	33	11	59	70	91	81
Chicago	165	155	46	45	3	2	33	11	83	97	116	109
New York	157	147	49	47	3	2	33	11	73	87	106	98
San Francisco	148	138	48	46	3	2	33	11	65	79	98	90

Table 4. Percentage Change in Energy Usage for ECM_S12A Compared to SCR_S12A by Location for 24-hour Operation

CITY	Total Plant Energy, %	Total Cooling Plant, %	Primary Fan Energy, %	FPTU Fan Energy, %	Heat Added During Htg, %	Heat Added During Htg + FPTU Fan Energy, %
Houston	-6.9	-4.8	-15.6	-64.9	16.0	-8.0
Phoenix	-8.4	-5.4	-15.3	-64.9	19.5	-10.9
Chicago	-5.9	-3.8	-14.6	-65.8	16.9	-6.1
New York	-6.5	-4.2	-14.1	-65.8	18.4	-7.2
San Francisco	-6.7	-4.3	-15.7	-65.8	21.2	-7.5

The change in energy consumption from the SCR_S12A unit to the ECM_S12A unit resulted in an average drop in total plant energy consumption of 7.0% for all locations. The drop in consumption was higher for locations that had a higher cooling load such as Houston (-7.0%) and Phoenix (-8.5%) when compared to cooler climates such as Chicago (-5.9%).

Table 4 shows a summary of the change in terminal unit fan energy consumption for all five locations when the SCR_S12A was replaced with the ECM_S12A, which resulted in an average drop of 65.4% for all locations. The drop in consumption was only slightly higher for locations that had higher heating requirements; San Francisco required only 0.9% more terminal unit fan energy than Phoenix.

Table 4 shows a summary of the change in primary fan energy consumption for all five locations when the SCR_S12A is replaced with the ECM_S12A, which resulted in an average drop of 14.9% for all locations. The drop in consumption was only slightly higher for locations that had higher cooling requirements; Phoenix required only 1.2% more primary fan energy than San Francisco. The change in primary fan energy was a direct result in the drop in primary air that resulted from the lower power consumption of the ECM motor.

Table 4 shows a summary of the change in primary heat energy added during heating for all five locations when the SCR_S12A is replaced with the ECM_S12A, which resulted in an average increase of 18.4% for all locations. The increase in heat added was higher for locations that had longer heating seasons; San Francisco required 5.2% more heat added than Houston.

The increased heat added was a direct result of the increased efficiency of the ECM motor, which added less heat to the space when the zone load was at or below the cooling load handled by the minimum primary flow setpoint. In most cases, even though the heat added increased by switching to a more efficient motor, the reduced load during cooling was more than the added heating loads during the winter, which resulted in an average net decrease in FPTU Fan + Heat Added of 7.9%.

Summary and Conclusions

A system model was developed that used the performance characteristics of ECM and SCR FPTUs that were measured by Furr et al. (2008), Cramlet (2008), and Edmondson et al. (2011). The measurements from laboratory experiments combined with the sensitivity analysis indicated that the ECM-controlled motor can have a substantial positive impact on the system performance as well as the overall energy consumption.

Consideration should also be given to what happens to the SDVAV system during low-load conditions when one of the terminal unit fans turns on: there is no change in the system static pressure.

The results from the simulation showed:

1. The systems with the series ECM FPTU used an average of 6.7% less total plant energy than the systems with the SCR-controlled FPTU.
2. The increased energy efficiency from the ECM motor reduced the heat load on the system enough that the primary airflow required to handle the motor load was small and a net decrease in primary fan energy was realized.
3. The average net decrease in heat added during heating and terminal unit fan energy was 7.9% and in Phoenix, the city with the greatest cooling load, the savings was over 10%.

The results of this study show that paying a premium cost for an ECM fan motor in a series terminal unit will provide significant cost reductions in energy use. Current conventional wisdom is to install this technology for both parallel and series FPTU applications and to prefer parallel FPTU over series FPTU. These results indicate that for the series FPTU application, the additional cost is warranted when the FPTU is operated as a CAV device and that there is a potential of over a 10% reduction in the total plant energy use of the systems that use ECM FPTU versus the SCR-controlled FPTU.

ACKNOWLEDGMENTS

The authors wish to thank the following individuals and organizations that provided support and advice for this project: Gus Faris of Nailor Industries, David John of Metal Industries, Inc., Dan Int-Hout of Krueger Manufacturing Co., Ron Jordan and Doug Fetters of A.O. Smith Electrical Products Company, Floyd Blackwell of Regal Beloit Corporation, Gaylon Richardson of Engineered Air Balance Co., Inc., and Jack Stegall of Energistics Laboratory. The authors would also like to acknowledge the Qatar Research Fund, which helped support the research of this project.

NOMENCLATURE

C_{pl}	latent heating/cooling specific heat
C_{ps}	sensible heating/cooling specific heat
$C_1 \dots C_n$	coefficients of an equation
in. w.g.	pressure inches of water
K	constant relating ΔP to \dot{Q}^2 (in w.g.-min ² /ft ⁶)
L_p	primary air leakage as decimal percent of primary flow
P_{dwn}	downstream static pressure
P_{iav}	primary air inlet valve entering air velocity differential pressure
ΔP	pressure drop
\dot{Q}	volumetric airflow rate
Q	heat energy transferred
Q_{aux}	auxiliary sensible heat added
Q_f	fan power
Q_f	flow rate of the terminal unit fan

\dot{Q}_{ind}	induced airflow rate
\dot{Q}_L	leakage flow rate
Q_{lat}	latent space load
Q_{min}	minimum sensible cooling supplied to a zone
\dot{Q}_p	primary airflow rate
\dot{Q}_{pmin}	primary minimum airflow rate
\dot{Q}_r	return airflow rate
\dot{Q}_s	supply airflow rate
Q_{sen}	Sensible space load
rh	relative humidity (%)
rh_p	primary air relative humidity (%)
S	damper position in degrees
T_L	leaked air temperature
T_p	primary air temperature
T_{pfeest}	estimated pre-fan mixed air temperature
T_{rpf}	required pre-fan mixed air temperature
T_r	return air temperature
T_s	supply air temperature
T_{sest}	supply temperature based on current conditions
T_{sreq}	supply temperature required to maintain T_{sp}
T_{sp}	setpoint temperature
V	FPTU fan control voltage
\dot{W}_f	fan power (watts)
ω_r	return air humidity ratio
ω_p	primary air humidity ratio
ρ	density of the air

REFERENCES

- Bryant, J., M. Davis, D. O'Neal, A. Cramlet. 2009. Experimental Verification of a Three Zone VAV System Model Operating with Fan Powered Terminal Units (RP-1292). *ASHRAE Transactions* 115(1).
- Cengal, Y.A., R.H. Turner. 2005. *Fundamentals of Thermal-Fluid Sciences*, 2nd Edition. New York, NY: McGraw-Hill.
- Cramlet, A. 2008. Performance of ECM controlled VAV fan powered terminal units. M.S. Thesis, Mechanical Engineering, Texas A&M University—College Station.
- Davis, M., J. Bryant, D. O'Neal, A. Cramlet. 2007. ASHRAE Project 1292-RP, Phase II Final Report. Energy Systems Laboratory, Texas A&M University—College Station.
- Edmondson, J., D.L. O'Neal, J.A. Bryant, and M.A. Davis. 2011. "Performance of Series Fan Powered Terminal Units with Electronically Commutated Motors." *ASHRAE Transactions* 117(2).
- Energy Star. 2010. Energy Star Building Manual, Table 9.3: Federal efficiency standards for commercial packaged air-cooled air conditioners and heat pumps. http://www.energystar.gov/ia/business/EPA_BUM_CH9_HVAC.pdf
- Furr, J., D. O'Neal, M.A. Davis, J.A. Bryant, and A. Cramlet. 2008. "Performance of VAV Fan Powered Terminal Units: Experimental Results and Models for Series Units." *ASHRAE Transactions* 114(1).
- National renewable Energy Laboratory (NREL). 1995. National Solar Radiation Data Base 1961–1990: Typical Meteorological Year 2. U.S. Department of Energy.

CH-12-018

Modeling the Performance of ECM and SCR Parallel Fan-Powered Terminal Units in Single-Duct VAV Systems

Michael A. Davis, PhD
Member ASHRAE

John A. Bryant, PhD, PE
Member ASHRAE

Dennis L. O'Neal, PhD, PE
Fellow ASHRAE

ABSTRACT

Single duct variable air volume systems often use series and parallel fan powered terminal units to control the air flow in conditioned spaces. A laboratory verified model of single duct variable air volume systems was developed that used series and parallel fan terminal units where the fan speeds were controlled by either silicon controlled rectifiers or electronically commutated motors.

The single duct variable air volume simulation results showed that there was no significant difference between the annual energy used by parallel systems with silicon controlled rectifier controlled motors when they were compared to parallel systems that used electronically commutated motors. The study included the simulation of the operation of the same facility at five weather locations around the United States.

INTRODUCTION

Figure 1 shows a typical single-duct variable air volume (SDVAV) system that uses fan-powered terminal units (FPTUs) to control the flow of conditioned air supplied by the primary fan. The FPTU has a small fan that is mounted either in series or in parallel with the primary system fan. Figure 2 shows a schematic of a typical parallel FPTU. The unit is called a parallel FPTU because the air flow path of the terminal fan is parallel to the air flow path of the primary fan.

In Figure 1 the terminal unit fan induces air from the return air plenum into the mixing chamber while primary air flows into the mixing chamber. The mixed air stream leaves the mixing chamber and is then supplied to the zone.

First generation FPTUs had constant speed fans where the fan motor speed was regulated with a silicon controlled rectifier (SCR) controller. Once the fan speed was set during the

installation and commissioning process, it was operated as a constant speed on or off device. Manufacturers have begun to make available electronically commutated motors (ECM) in FPTUs which allow the speed of the fan to vary as the load in the zone changes. ECM motors also use about one-third of the power of a similar sized SCR controlled motor but they cost more than conventional single speed motors (Edmondson et. al. 2011). The parallel unit fan only operates at low primary air flow conditions when heat is added to maintain space temperature set points. Air properties for the system were calculated as described in the next section.

SIMULATION MODEL

The simulation model included a number of equations that were used to calculate air properties, determine airflow, leakage, and power, and accounted for the difference in operation when in either cooling or heating mode. The equations and the logic used in the simulation model are described below.

Calculating Changes in the Properties of Air

Air property calculations were simplified by assuming constant properties which, for the temperature ranges of interest to this project, resulted in less than a 0.2% error in the calculations (Cengal et. al. 2005). Operating conditions for supply and return air were assumed to be 55° F (12.8° C), 95% RH and 78° F (25.5° C), 50% RH respectively. The density of air at 55° F (12.8° C), 95% RH was assumed to be 0.076 lb/ft³ (1.22 kg/m³) and was used to derive Equations 1 and 2. Equation 1 was used throughout the simulations to model sensible heating and cooling of air as it passed through the cooling coil or when heat was added at the terminal as a result of the operation of the

Michael A. Davis is director of laboratories at New York University Abu Dhabi, Abu Dhabi, United Arab Emirates. **John A. Bryant** is an associate professor at Texas A&M University at Qatar, Doha, Qatar. **Dennis L. O'Neal** is Holdredge/Paul Professor and associate dean of engineering at Dwight Look College of Engineering, Texas A&M University, College Station, TX.

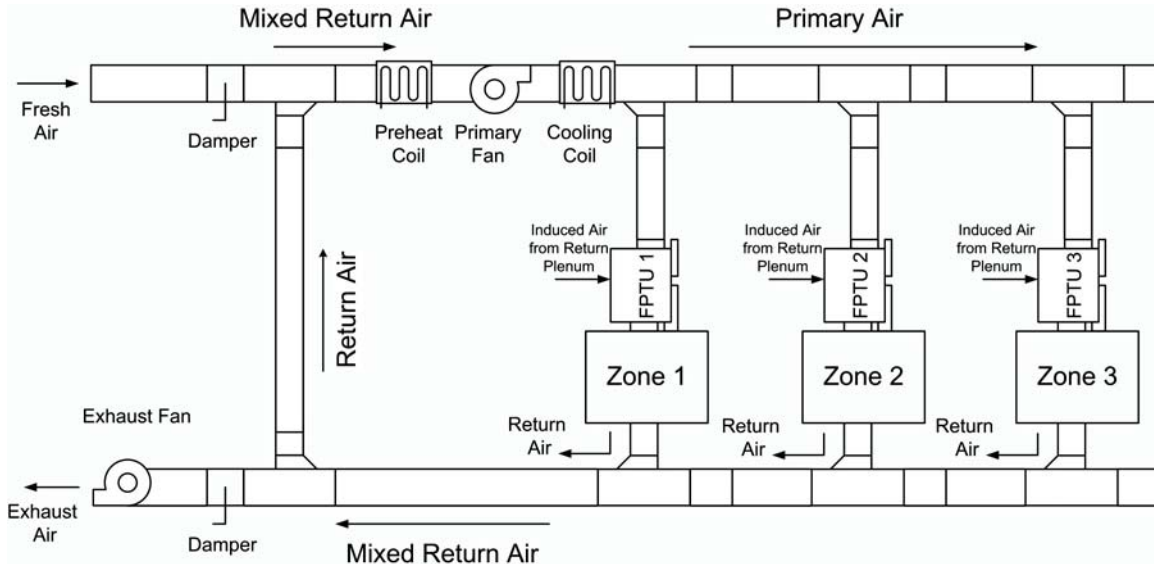


Figure 1 A typical multi-zone SDVAV system using fan-powered terminal units.

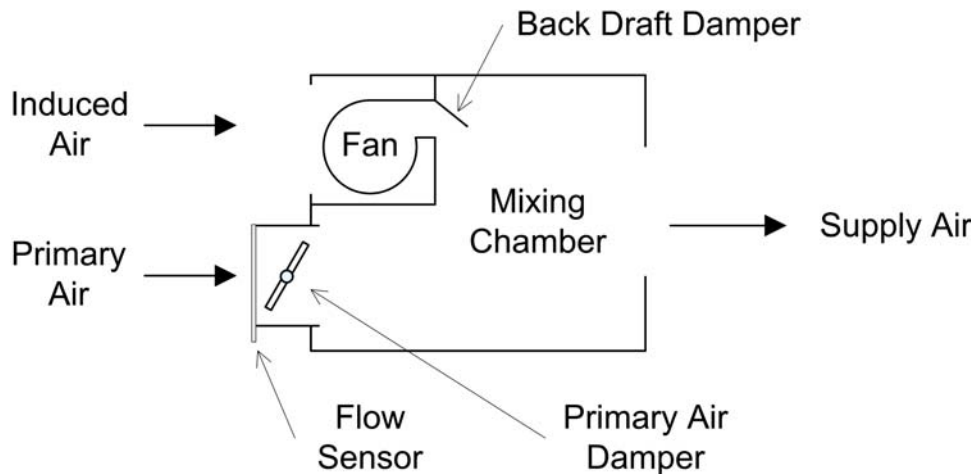


Figure 2 A typical parallel type fan powered terminal unit.

terminal unit fan motor or when heat was added to maintain space conditions.

$$Q = C_{ps} \dot{Q} (\Delta T) \quad (1)$$

Where Q was the heat energy transferred to or from the air, C_{ps} was the coefficient that accounted for the specific heat, density, and time, and \dot{Q} was the volumetric flow rate (ft³/min (l/s)). Equation 2 was used throughout the simulations to model the energy change resulting from a change in the humidity ratio (such as latent heat removal at the cooling coil.

$$Q = C_{pl} \dot{Q} (\omega_2 - \omega_1) \quad (2)$$

Where Q was the heat energy transferred to or from the air, C_{pl} was the coefficient that accounted for the latent heat, density, and time, and \dot{Q} was the volumetric flow rate.

The model described in this paper was based on the verified calculation procedure that was implemented as described in Bryant et al. 2009. The program was developed to facilitate the incorporation of the model into existing commercially available programs.

The parallel FPTU has two basic operating modes – fan-on and fan-off. Although the ECM control units can be used in a variable speed mode as an adjustable reheat mixing box, only the constant speed “on” or “off” fan operation was considered

in this model which means that when the fan was on, it operated at a constant speed.

The minimum primary air flow rate, $\dot{Q}_{p,min}$, for this project was 20% of design flow. When the fan was operational, the induced air flow rate was 50% of the design flow. The 20% minimum primary plus the 50% return air from the fan totaled 70% of the design flow rate when the fan was operating.

The primary air temperature T_p , and primary air relative humidity RH_p , were set at 55° F (12.8° C) and 95% respectively. The setpoint temperature of the space T_{sp} , was 78° F (25.5° C) for both heating and cooling loads. The primary air leakage rate L_p , was input during the simulation and was set at 5% (0.05), 10% (0.10) or 20% (0.20).

Terminal Unit Leakage

First documented by Furr, et al. (2008) and later confirmed by Cramlet (2008) and Edmondson et al. (2011), parallel terminal units leak during both fan-off and fan-on operation. Leakage is the air that passes through the primary air valve into the mixing chamber that does not pass through the supply port into the conditioned space. The source of this leakage includes seams, penetrations for electrical power into the terminal unit and the back draft damper. The effect on the air distribution system is to increase the amount of air that must be delivered by the primary fan.

The primary leakage rate, L_p , was input by the user as a decimal percent of the total primary flow rate as shown by Equation 3 and allowed the user to investigate the sensitivity of the system operation to leakage.

$$L_p = \frac{\dot{Q}_L}{\dot{Q}_s + \dot{Q}_L} = \frac{\dot{Q}_L}{\dot{Q}_p} \quad (3)$$

Calculations for the Parallel FPTU When the Fan Is Off

Figure 3 shows a flow chart of the algorithm used to model operation of the parallel variable-air-volume (VAV) terminal unit and the zone supplied by the terminal unit. The first step in the analysis was to determine whether or not the zone sensible space load was a cooling load. If the load was a cooling load, then the terminal unit fan was off and the supply air properties were the same as the primary air properties.

The supply air flow rate, \dot{Q}_s , required to meet the cooling load was calculated using Equation 4. When leakage was not included and the fan was off, the supply air flow was the same as the primary air flow. When leakage was included and the fan was on, the supply air flow was the primary air flow plus the induced air flow minus the leakage flow.

$$\dot{Q}_s = \frac{\dot{Q}_{sen}}{c_{ps}(T_{sp} - T_p)} \quad (4)$$

The properties for the return air were evaluated by performing an energy and mass balance on the return air duct. In all cases, the return air flow rate, \dot{Q}_r , was the same as the

primary air flow rate, \dot{Q}_p . Equation 5 was used to calculate the mixed return air temperature and was based on an energy balance of the return air stream.

$$T_r = T_{sp} + L_p(T_p - T_{sp}) \quad (5)$$

If the primary air leakage rate, L_p , was zero, the return air temperature, T_r , was the same as the set point temperature, T_{sp} , for the space; otherwise, the return air temperature was lower than the setpoint temperature.

The latent load of the space was combined with the humidity ratio of the supply air to calculate the humidity ratio of the return air. The zone return air humidity ratio, was calculated using Equation 6.

$$\omega_r = \omega_p + \frac{Q_{lat}}{C_{pl}\dot{Q}_p} \quad (6)$$

Calculations for the Parallel FPTU When the Fan Is On

For the case where the primary air flow rate was at or below the minimum, the analysis of the operation of FPTU proceeded along the path in Figure 3 as if the unit were not in cooling mode. If the sensible load for the zone was not a cooling load, then the terminal unit was in heating mode, the terminal unit fan was turned on, and the analysis followed the “fan-on” operation.

Once the fan was turned on and the primary flow delivered to the space was set to the minimum, the downstream static pressure was calculated using Equation 7.

$$P_{dwn} = K \left(\frac{\dot{Q}_s}{1000} \right)^2 \quad (7)$$

The “K” factor in Equation 7 is the loss coefficient for the duct system that connects the supply port of the FPTU to the conditioned space. The “K” for the zone was calculated with a user-defined downstream static pressure at design air flow with Equation 7 for each zone. The calculated “K” was then used at part load conditions to calculate the downstream static pressure, P_{dwn} .

Equation 8, developed by Furr et al. (2008), was used to calculate the flow rate of the fan. The coefficients for the SCR controlled motors were from Furr et al. (2008). The coefficients for the ECM motors were from Edmondson et al. (2011).

$$\dot{Q}_f = C_1 + C_2 V^2 + C_3 V + C_4 P_{dwn} + C_5 P_{dwn} \quad (8)$$

After the downstream static pressure was determined, the fan power was calculated using Equation 9 which was developed by Furr et al. (2008). The coefficients for the SCR controlled motors were from Furr et al. (2008). Coefficients for the ECM motors were from Edmondson et al. (2011).

$$\dot{W}_f = C_1 + C_2 V^2 + C_3 V + C_4 P_{dwn} + C_5 P_{iav} \quad (9)$$

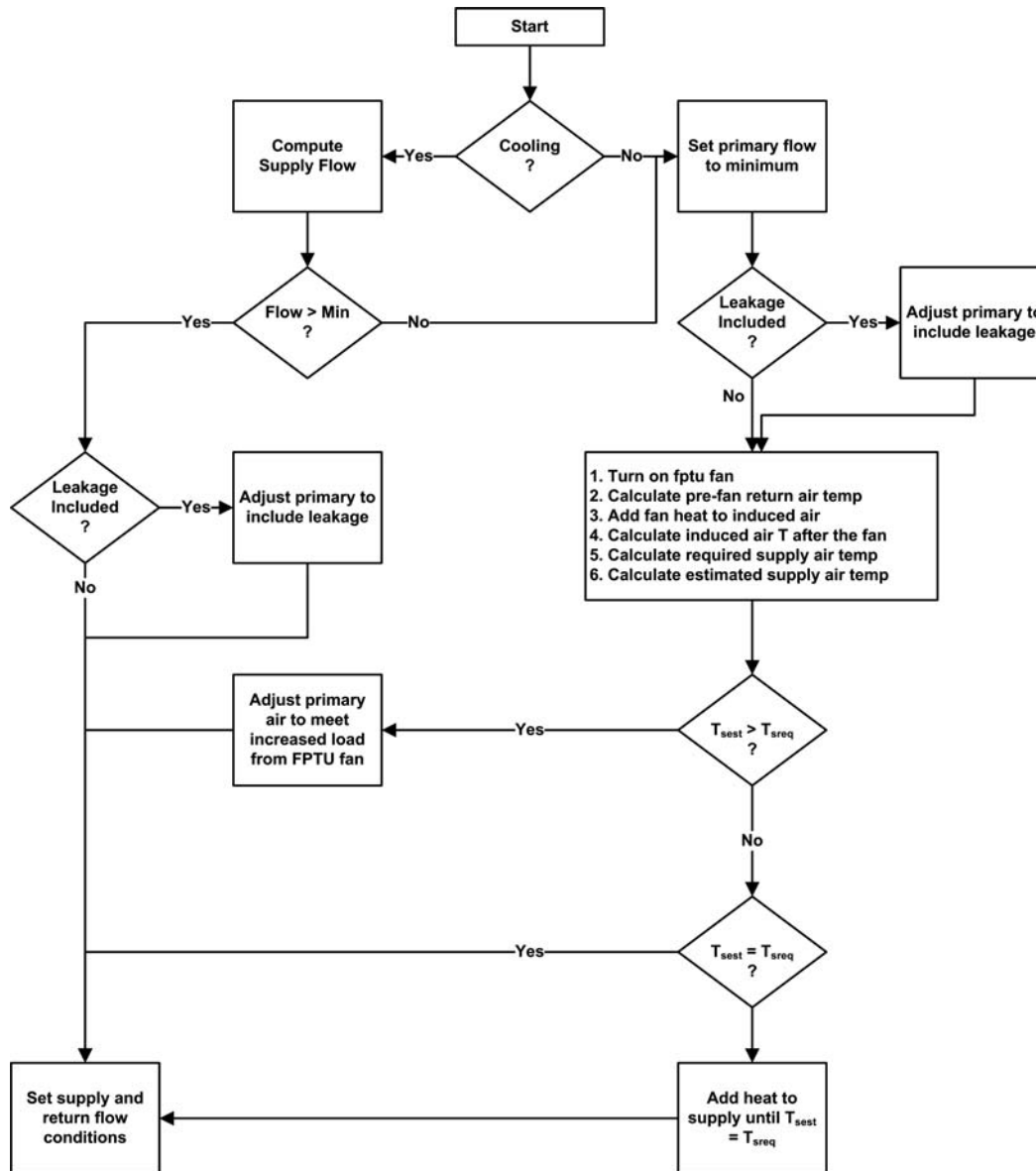


Figure 3 Flowchart of the parallel FPTU operation.

Equation 10 was developed by Furr et al. (2008) and was used to calculate the value of P_{iav} in Equation 9. As before, coefficients for the SCR parallel FPTUs were from Furr et al. (2008) and the coefficients for the ECM parallel FPTUs were from Edmondson et al. (2011).

$$P_{iav} = C_1 + C_2 \dot{Q}_p \quad (10)$$

In Equations 8 and 9 the term “V” refers to the “voltage” applied to control the terminal unit fan. In the case of the SCR controlled motors, “V” refers to the SCR output voltage which ranged from 0–277 VAC. For the ECM controlled motors “V” meant either a control voltage of 0–10 VDC or a controller setting of 0–100%. Edmondson et al (2011) detailed the vari-

ations in the use of the voltage (V) as it related to the equations. For the model, the user inputs a flow rate of 0–100% in the FPTU setup portion of the user interface and the software automatically converts to the proper “V” range for the calculations.

The fan power, \dot{W}_f , in Watts was added to the return air inducted into the fan and the temperature of the air supplied to the mixing chamber by the fan, T_f , was computed:

$$T_f = T_r + \frac{3.413 \dot{W}_f}{C_s \dot{Q}_f} \quad (11)$$

where 3.413 was the factor used to convert from Watts to BTU/hr. The supply air temperature, T_{sest} , calculated from an energy balance was:

$$T_{sest} = \frac{\dot{Q}_p T_p + \dot{Q}_f T_f}{\dot{Q}_p + \dot{Q}_f} \quad (12)$$

Equation 13 was used to estimate the temperature of the return air, for the zone. The temperature of the supply air and the temperature of the return air were estimated using a procedure that iterated through equations 12 and 13 until both the supply temperature and the return air temperature changed by less than 0.01° F between iterations.

$$T_r = \frac{\dot{Q}_1 T_m + \dot{Q}_s T_{sp}}{\dot{Q}_p + \dot{Q}_f} \quad (13)$$

Once the estimated supply air temperature, T_{sest} , was known it was compared to the supply air temperature required to maintain space conditions, T_{sreq} which was calculated using Equation 1. Here, the sensible heat transfer was the summation of the space load and the cooling delivered to the space by the minimum primary air setting supplied by the user.

If the estimated temperature differed from the required temperature, then the primary air flow rate was increased so that the extra heat energy provided by the terminal unit blower motor or heat energy was added to increase the supply temperature to the required value.

Static Pressure Calculations— Minimum Static Pressure

Equation 14, developed by Furr et al. (2008), was used to calculate the flow rate for the primary air for both the SCR and ECM FPTUs for a given damper setting and differential pressure. The coefficients for SCR parallel FPTUs were from Furr et al. (2008) and the coefficients for ECM parallel FPTUs were from Edmondson et al. (2011).

$$\dot{Q}_p = C_1(1 + C_2S + C_3S^2)\sqrt{\Delta P} \quad (14)$$

A binary search algorithm determined the differential pressure, required to produce a primary air flow \dot{Q}_p , needed to maintain zone conditions. The minimum static pressure required that the damper be in the fully open position so the value of “S” was zero (0) degrees for this calculation. Once ΔP was determined, the downstream static pressure was calculated using Equation 7. The upstream static pressure was determined by adding ΔP to the downstream static pressure.

Figure 4 shows that the upstream static pressure for the parallel terminal unit drops with the space loads but that it jumps to almost half of the full-load levels when the terminal unit fan is in operation. The increase in the upstream static pressure at low-load conditions causes a system-wide increase in the available upstream static pressure for all zones.

Calculations for the SDVAV System with Parallel FPTU

From Figure 1, the components of the SDVAV system consisted of FPTUs that control the zones, return air ducts, exhaust and fresh air ducts, a pre-heat coil (PHC), the primary air fan (Fan), the primary air cooling coil (CC), and the primary air distribution ducts. Figure 5 shows a diagram that identifies the calculation sequence used in the simulation program.

Zone Calculations

The system control algorithm started at the first hour of the year and on an hourly basis it executed the zone simulation procedure for the parallel FPTU illustrated in Figure 3. The hourly procedures provided information such as the required primary flow, return air flow, minimum static pressure, heat added, and FPTU fan power that resulted from the operation

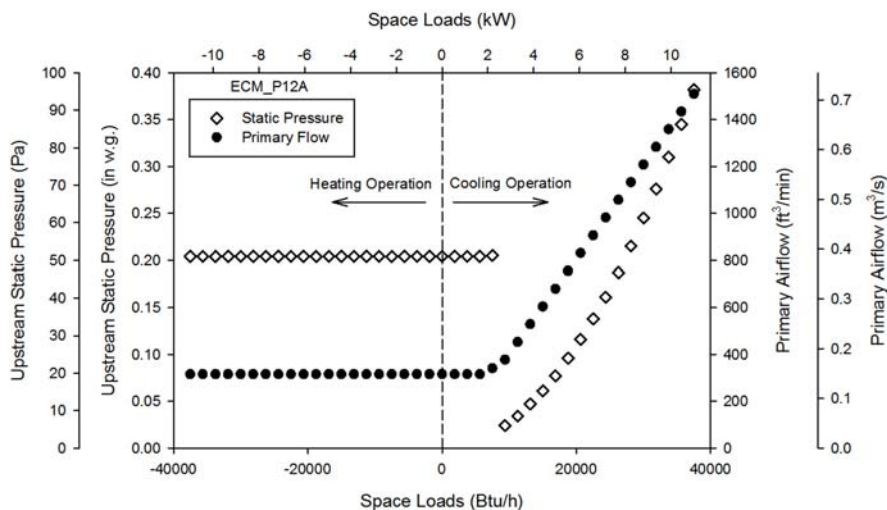


Figure 4 Parallel primary air flow and static pressure vs. space load.

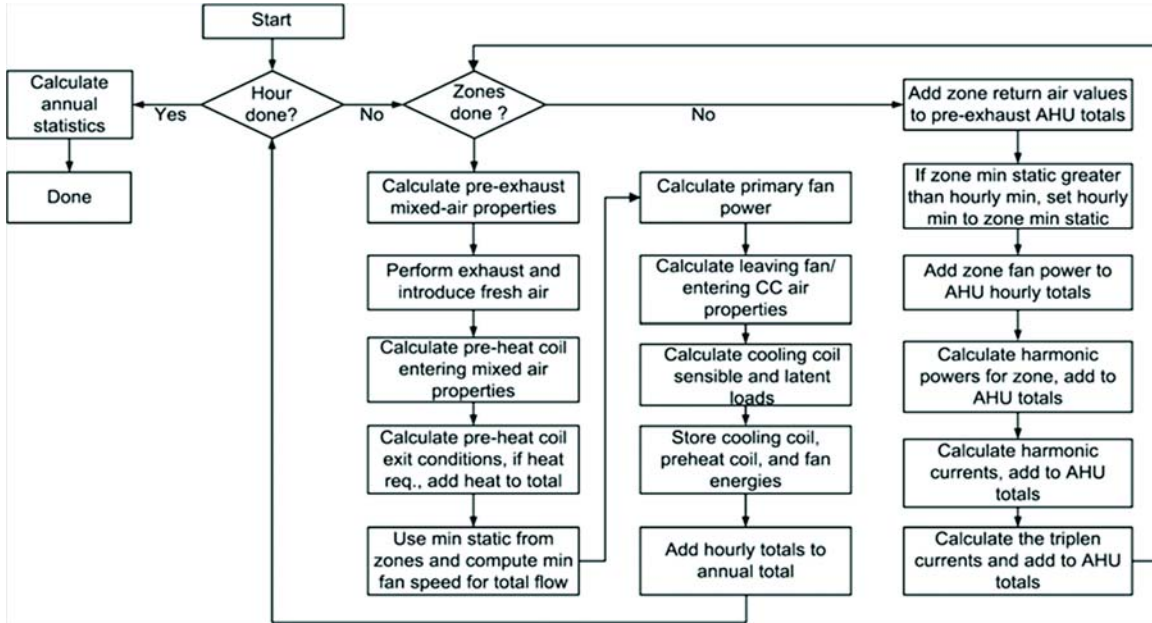


Figure 5 SDVAV system simulation flow chart.

of the zone. After all of the zone calculations were completed, the system return air properties were calculated.

Return Air

Equations 15 and 16 were used to calculate the return air mixed air temperature and humidity ratio.

$$T_{ra} = \frac{\sum_i^n \dot{Q}_i \times T_i}{\sum_i \dot{V}_i} \quad (15)$$

$$\omega_{ra} = \frac{\sum_i^n \omega_i \dot{Q}_i}{\sum_i \dot{V}_i} \quad (16)$$

Exhaust/ Fresh Air

The temperature and humidity ratio after the exhaust/fresh air intake was calculated using Equations 17 and 18 where X is the fraction of fresh/exhaust air introduced into the return air stream which was 20% (0.20).

$$T_{rapf} = XT_{oa} + (1 - X)T_{ra} \quad (17)$$

$$\omega_{rapf} = X\omega_{oa} + (1 - X)\omega_{ra} \quad (18)$$

Primary Fan

Equation 19 was used to calculate the primary air flow, \dot{Q}_p , as a function of the fan speed, S , in revolutions per minute and static pressure P , in inches of water (in. w.g.). Equation 20 was used to calculate the fan power as a function of fan speed, S , in rpm. Equation 19 was a correlation developed using published data for a fan with an operating range that covered the simulations included in this study. Equation 20 was

included in the published data provided by the fan manufacturer and was modified to include the efficiency of the fan motor, fan , which was 85%.

$$\dot{Q}_p = a_1 + a_2P + a_3P^2 + a_4S + a_5S^2 + a_6PS + a_7P^2S^2 \quad (19)$$

$$\dot{W}_f = 746 \left(\frac{S}{1631} \right)^3 \left(\frac{1}{fan} \right) \quad (20)$$

where $a_1 \dots a_7$ were constants that were inputs by the user and fan was the user defined efficiency of the fan motor in percent. The binary search algorithm held the static pressure constant and searched for the fan speed that would produce the required amount of flow. The static pressure used in Equation 19 was the maximum value of the minimum required static pressure for all of the zones.

Pre-Heat Coil

The return air entered the pre-heat coil after the fresh air was introduced into the system (Figure 1). If the temperature of the pre-fan return air, T_{rapf} , was below the pre-fan minimum temperature, T_{pfm} , then heat energy was added so that the pre-fan return air temperature was at the minimum. Equation 21 was used to calculate the amount heat energy, Q_{ph} , required to warm the return air to the minimum pre-fan temperature.

$$Q_{ph} = C_{ps} \dot{Q}_{ra} (T_{pfm} - T_{rapf}) \quad (21)$$

The minimum entering fan temperature was calculated by subtracting the fan temperature rise from the cooling coil leaving air temperature. If the temperature of the return air was

above the minimum entering air temperature for the fan, then no heat was added.

The increase in the temperature of the air, ΔT_f , as it passed through the fan was calculated with Equation 22 using the power consumed by the primary fan, \dot{W}_f .

$$\Delta T_f = \frac{3.412 \dot{W}_f}{C_s \dot{Q}_{ra}} \quad (22)$$

Primary Cooling Coil

The return air cooling coil entering temperature, T_{raec} , was determined by adding the temperature rise across the primary fan to the pre-fan return air temperature, T_{rapf} . The sensible cooling load, Q_{ccsen} , handled by the cooling coil was found using Equation 23.

$$Q_{ccsen} = C_s \dot{Q}_p (T_{raec} - T_p) \quad (23)$$

The latent load, Q_{cclatt} , on the primary cooling coil was calculated using Equation 24.

$$Q_{cclatt} = C_l \dot{Q}_p (\omega_{raec} - \omega_p) \quad (24)$$

SIMULATION RESULTS

The system model was used to predict the operation of a commercial building for one year at five different geographical locations around the United States using TMY2 (NREL 1995) weather data. The base case operating conditions used Houston weather data for the analysis. Following the base case operation, a sensitivity analysis was done that investigated changes in the air leakage and location.

The building model consisted of five zones with exterior exposures covering a range of loads resulting from weather and solar effects while the interior, or core zone, was dominated by internal thermal loads. The hourly space loads were normalized to the peak cooling capacity of the FPTUs and were based on the hourly loads generated by modeling a single

story rectangular structure with four perimeter zones and a single core zone.

This technique allowed modeling of the operation of the facility at various geographic weather locations while maintaining the peak cooling loads within the capacity of the selected FPTU. This method also eliminated any bias in the simulation results if the VAV terminal units were either over or undersized when moved to different geographic locations. The procedure used to generate the normalized loads at each of the five weather locations was described by Bryant et al. (2009).

Base Case

The base case settings were intended to mimic the theoretical best case operating patterns of buildings that used fan powered terminal units with no leakage. Table 1 shows the simulation results for the base case for systems with ECM_P12A, and SCR_P12A terminal units.

The total plant energy was the summation of the cooling plant, primary fan energy, terminal unit fan energy and heat added. The total cooling energy was the cooling energy supplied by the primary cooling coil over the entire year. Because the model developed was intended to be used within a building simulation program, neither detailed cooling nor heating plant simulations were done and the energy quantities used by the mechanical systems were not estimated by the simulation.

The cooling plant energy was estimated using an annual average Energy Efficiency Ratio (EER) of 11.0 which was taken from the minimum efficiency standards for package rooftop air-conditioning units (Energy Star 2010). The heat energy added was from the heating plant.

The ECM_P12A FPTU used 0.2% less total plant energy than the SCR_P12A unit. The annual operating hours were the same for both the SCR_P12A and the ECM_P12A but the ECM FPTUs used 65% less unit fan energy as a result of the more efficient ECM motor. However, because the terminal unit fan motors are in the air stream and parallel terminal unit fans operated only during heating mode, the fan heat energy

Table 1. Simulation Results Summary for the Base Case Houston Location (No Leakage Case)

Item	SCR_P12A	ECM_P12A	% Difference
Total Plant Energy (MWh)	156	156	0
Total Cooling Plant (MWh)	56	56	0
Primary Fan Energy (MWh)	3	3	4
Terminal Unit Fan Energy (MWh)	9	3	-66
Heat Added (MWh)	87	93	7
Fan + Heat Energy (MWh)	96	96	0
Maximum Static Pressure in. w.g. (Pa)	0.25 (65)	0.37 (92)	0.16 (41)
Minimum Static Pressure in. w.g. (Pa)	0.024 (6)	0.036 (9)	0.15 (38)

Table 2. Simulation Results for Three ECM Parallel FPTUs (No Leakage Case)

Item	Parallel FPTU		
	ECM_P12A	ECM_P12B	ECM_P12C
Total Plant Energy (MWh)	156	156	156
Total Cooling Plant (MWh)	57	56	57
Primary Fan Energy (MWh)	3	3	3
Terminal Unit Fan Energy (MWh)	3	4	3
Heat Added (MWh)	93	92	93
Fan + Heat Energy (MWh)	96	96	96
Maximum Static Pressure in. w.g. (Pa)	0.37 (92)	0.27 (68)	0.41 (103)
Minimum Static Pressure in. w.g. (Pa)	0.036 (9)	0.028 (7)	0.040 (10)

Table 3. Energy Usage of SCR_P12A and ECM_P12A by Location for 24 Hour Operation (No Leakage Case)

City	Total Plant Energy (MWh)		Total Cooling Plant (MWh)		Primary Fan Energy (MWh)		Terminal Unit Fan Energy (MWh)		Heat Added (MWh)		Heat Added + Fan Energy (MWh)	
	SCR	ECM	SCR	ECM	SCR	ECM	SCR	ECM	SCR	ECM	SCR	ECM
Houston	156	156	56	56	3	3	9	3	87	93	96	96
Phoenix	140	140	60	60	3	3	9	3	68	74	77	76
Chicago	152	151	44	44	3	3	11	4	95	102	105	105
New York	143	143	46	46	3	3	10	4	84	91	95	94
San Francisco	134	134	45	45	2	2	10	4	76	83	87	87

not added to the air stream from the more efficient ECM motor had to be offset by added space heating.

Case 1—Sensitivity to Unit Manufacturer

Table 2 shows the simulation summary results for the ideal case simulation using parallel ECM FPTUs P12A, P12B and P12C. The replacement of the ECM_P12A terminal unit with either of the other two manufacturer's units had no significant impact on the total cooling plant energy, total cooling energy or primary fan energy. ECM_P12B used more terminal unit fan energy than ECM_P12A or ECM_P12C but the additional energy was used during heating mode and was offset by the reduced amount of added heat required by the zone so there was no net increase in the energy consumed by the system as shown by the value of the "fan + heat" which was 96 MWh for all three units.

The sensitivity of the simulation to unit manufacturer for the SCR parallel units was previously documented in the report for ASHRAE RP 1292 (Davis et al. 2007) and showed

no difference in the results based on the selection of the manufacturer.

Case 2—Base Case Operation at Five Locations in the United States

Table 3 shows the energy used by each system component at each weather location for SCR_P12A and ECM_P12A. Table 4 shows a summary of the change in energy consumption for all five locations when SCR_P12A was replaced with ECM_P12A. Both tables show that there was no significant difference in the operation of the ECM_P12A and the SCR_P12A for the no leakage case.

Case 3—Impact of Leakage Rates of 5%, 10%, and 20%

Table 5 shows the results of the simulation when leakage was added to the base case (Houston) operation for the SCR_P12A and ECM_P12A. The total plant energy increased by 3.0%, 5.8% and 11.7% over the base case when leakage was 5%, 10% and 20%, respectively, for both the ECM_P12A

Table 4. Percentage Change in Energy Usage for ECM_P12A Compared to SCR_P12A by Location for 24 Hour Operations (No Leakage Case)

City	Total Plant Energy	Total Cooling Plant	Primary Fan Energy	Terminal Unit Fan Energy	Heat Added	Heat Added + Fan Energy
Houston	-0.1	-0.1	3.6	-65.7	6.7	-0.3
Phoenix	-0.2	-0.1	3.5	-66.7	8.2	-0.4
Chicago	-0.1	0.0	3.7	-66.7	7.1	-0.3
New York	-.02	0.0	3.7	-65.7	7.6	-0.3
San Francisco	0.0	-0.1	3.8	-65.7	8.8	0.0

Table 5. Simulation Results for P12A for 24 Hour Operation with 5%, 10%, and 20% Leakage Rates

Item	Leakage Rates							
	Base (0%)		5%		10%		20%	
	SCR	ECM	SCR	ECM	SCR	ECM	SCR	ECM
Total Plant Energy (MWh)	156	156	161	161	165	165	174	175
Total Cooling Plant (MWh)	56	56	58	58	59	59	61	61
Primary Fan Energy (MWh)	3	3	4	4	4	4	5	5
Terminal Unit Fan Energy (MWh)	9	3	9	3	9	3	9	3
Heat Added (MWh)	87	93	90	96	93	99	98	105
Fan + Heat Energy (MWh)	96	96	99	99	102	102	108	108
Max Static Pressure in. w.g. (Pa)	0.26 (65)	0.37 (92)	0.26 (66)	0.38 (96)	0.27 (67)	0.40 (99)	0.28 (69)	0.43 (108)
Min Static Pressure in. w.g. (Pa)	0.024 (6)	0.036 (9)	0.024 (6)	0.036 (9)	0.024 (6)	0.04 (10)	0.028 (7)	0.04 (10)

and SCR_P12A units. For both the ECM_P12A and SCR_P12A units, the cooling plant energy increased by 2.1%, 4.1% and 8.7% over the base case when leakage was 5%, 10% and 20%, respectively and the primary fan energy increased by approximately 13.0%, 25% and 55%, respectively. For the SCR_P12A unit, the heat added increased by 3.3%, 6.4% and 13.0% for 5%, 10% and 20% leakage rates, respectively. For the ECM_P12A unit, the heat added increased by 3.2%, 6.4% and 13.0% for 5%, 10% and 20% leakage rates, respectively.

SUMMARY AND CONCLUSIONS

A system model was developed that used the performance characteristics of ECM and SCR FPTUs that were measured by Furr et al. (2008), Cramlet (2008) and Edmondson et al. (2011). The measurements from laboratory experiments combined with the sensitivity analysis indicated that leakage can have a substantial impact on the system performance as well as the overall energy consumption.

Consideration should also be given to what happens to the SDVAV system during low-load conditions when one of the terminal unit fans turns on. The activation of the terminal unit

fan resulted in the increase in the pressure of the primary fan which increased the overall operating cost of the system. This was shown clearly in Figure 4. The large change in static pressure is quite evident upon fan activation resulting in an increase in static pressure at the primary fan with a coincident increase in operating energy.

The results from the simulation showed:

1. Terminal unit fan energy was reduced by approximately two thirds when ECM motors were used compared to SCR controlled motors.
2. Because the parallel unit fan motors operated only in heating mode, the heat energy that was added to the air stream from the fan motor was reduced and had to be made up by supplemental heating. If the supplemental heat energy is supplied by electric resistance heating then this is a one-for-one trade which resulted in no net energy savings.

The results of this study show that paying a premium cost for an ECM fan motor in a parallel terminal unit will provide

no significant cost reduction in energy use. The energy comparisons show virtually identical energy consumption for these two motor types regardless of operation or load. Current conventional wisdom is to install this technology for both parallel and series FPTU applications. These results indicate that for parallel FPTU application, the additional cost is not warranted. This study shows that paying a premium for an ECM motor in a parallel FPTU would not be cost effective.

ACKNOWLEDGMENTS

The authors wish to thank the following individuals and organizations that provided support and advice for this project: Gus Faris of Nailor Industries, David John of Metal Industries, Inc., Dan Int-Hout of Krueger Manufacturing Co., Ron Jordan and Doug Fetters of A.O. Smith Electrical Products Company, Floyd Blackwell of Regal Beloit Corporation, Gaylon Richardson of Engineered Air Balance Co., Inc., and Jack Stegall of Energistics Laboratory. The authors would like to acknowledge the Qatar National Research Fund, which helped support the research for this project.

NOMENCLATURE

C_{pl}	= latent heating/cooling specific heat
C_{ps}	= sensible heating/cooling specific heat
$C_1 \dots C_n$	= coefficients of an equation
K	= constant relating ΔP to \dot{Q}^2 (in w.g.-min ² / ft ⁶)
L_p	= primary air leakage as decimal percent of primary flow
P_{dwn}	= down stream static pressure
P_{iav}	= primary air inlet valve entering air velocity differential pressure
ΔP	= pressure drop
\dot{Q}	= volumetric air flow rate
Q	= heat energy transferred
Q_{aux}	= auxiliary sensible heat added
Q_f	= fan power
\dot{Q}_f	= flow rate of the terminal unit fan
\dot{Q}_{ind}	= induced air flow rate
\dot{Q}_L	= leakage flow rate
Q_{lat}	= latent space load
Q_{min}	= minimum sensible cooling supplied to a zone
\dot{Q}_p	= primary air flow rate
\dot{Q}_{pmin}	= primary minimum air flow rate
\dot{Q}_r	= return air flow rate
\dot{Q}_s	= supply air flow rate
Q_{sen}	= sensible space load

RH_p	= primary air relative humidity (%)
S	= damper position in degrees
T_L	= leaked air temperature
T_p	= primary air temperature
T_{pfest}	= estimated pre-fan mixed air temperature
T_{rpf}	= required pre-fan mixed air temperature
T_r	= return air temperature
T_s	= supply air temperature
T_{sest}	= supply temperature based on current conditions
T_{sreq}	= supply temperature required to maintain
T_{sp}	= set point temperature
V	= FPTU fan control voltage
\dot{W}_f	= fan power (Watts)
ω_r	= return air humidity ratio
ω_p	= primary air humidity ratio
ρ	= density of the air

REFERENCES

- Bryant, J. A., Davis, M. A., O'Neal, D. L., Cramlet, A. 2009. Experimental Verification of a Three Zone VAV System Model Operating with Fan Powered Terminal Units (RP-1292). ASHRAE Transactions 115(1).
- Cengel, Y. A., Turner, R. H. 2005. Fundamentals of Thermal-Fluid Sciences, 2nd Edition. New York, NY: McGraw-Hill.
- Cramlet, A. 2008. Performance of ECM controlled VAV fan powered terminal units. M. S. Thesis, Mechanical Engineering, Texas A&M University - College Station.
- Davis, M. A., Bryant, J. A., O'Neal, D. A., Cramlet, A. 2007. ASHRAE Project 1292-RP, Phase II Final Report. Energy Systems Laboratory, Texas A&M University - College Station.
- Edmondson, J., O'Neal, D.L., Bryant, J.A., and Davis, M.A., 2011, "Performance of Parallel Fan Powered Terminal Units with Electronically Commutated Motors", ASHRAE Transactions, 117(2).
- Energy Star. 2010. Energy Star Building Manual, Table 9.3: Federal efficiency standards for commercial packaged air-cooled air conditioners and heat pumps. http://www.energystar.gov/ia/business/EPA_BUM_CH9_HVAC.pdf
- Furr, J., O'Neal, D., Davis, M.A., Bryant, J.A., and Cramlet, A. 2008 "Performance of VAV Fan Powered Terminal Units: Experimental Results and Models for Parallel Units", ASHRAE Transactions, 114(1).
- National renewable Energy Laboratory (NREL). 1995. National Solar Radiation Data Base 1961 - 1990: Typical Meteorological Year 2. U.S. Department of Energy.

Comparison of performance characteristics of SCR and ECM controlled series fan powered terminal units

DENNIS L. O'NEAL^{1,*}, JACOB L. EDMONDSON², and PENG "SOLOMON" YIN³

¹*School of Engineering and Computer Science, One Bear Place #97356 Baylor University, Waco, TX 76798, USA*

²*Center for Science and Engineering, NYU Abu Dhabi, Mussafah, Abu Dhabi, UAE*

³*Energy Systems Laboratory, Texas A&M University, College Station, TX, USA*

Airflow, efficiency, power, and power quality characteristics were evaluated for two variable air volume series fan powered terminal units. The power and power quality data included real power, power/airflow, apparent power, harmonic frequencies, and total harmonic distortion. Each unit had the same sized primary air inlet and were provided by the same manufacturer. One unit had a motor controlled by a silicon controlled rectifier and the other had an electronically commutated motor. Data were collected at a fixed downstream static pressure and a range of upstream static pressures, primary inlet damper positions, and input controller voltages. Both controllers maintained a nearly constant fan airflow as the primary air was varied. Fan/motor efficiencies were low (below 35%) and increased with fan static pressures. The electronically commutated motor unit had efficiencies as much as four times higher than the silicon controlled rectifier controlled unit which was reflected in much lower power draws. The electronically commutated fan/motor unit had the lowest apparent power at airflows below approximately 1000 ft³/min (0.47 m³/s). For both units, the total power harmonic distortion was less than 1%. The performance data indicated a major advantage of units with electronically commutated motors.

Introduction

Variable air volume (VAV) systems maintain space conditions by varying the volume of conditioned air delivered to a space. The system usually includes a central air handler unit (AHU) and numerous VAV terminal units. The primary air is cooled and then delivered by the AHU central supply fan to VAV terminal units. The terminal units are ducted to air outlets usually serving two or more zones. Terminal units with a fan are called fan powered terminal units (FPTUs). These terminal units can draw in air from the plenum air and mix it with primary air to maintain conditions in the occupied space.

The fan in a FPTU can either be in series or parallel with the primary air. This article focuses on the performance of series FPTUs. In series units (Figure 1), the terminal unit fan must be in operation for air to be delivered to the space. The primary air inlet damper modulates the amount of primary air delivered to the space to maintain the temperature set point. An inlet differential pressure sensor allows the terminal unit to maintain appropriate primary air supply. Electric resistance or hot water coils can be used to provide supplemental terminal reheat.

It is important to be able to characterize both series and parallel terminal units because of their effect on the energy performance of VAV systems in buildings. Furr et al. (2008a, 2008b) developed performance models for series and parallel fan powered terminal units where the fans used silicon controlled rectifiers (SCRs). Davis et al. (2009) then used these FPTU models to evaluate the performance of VAV systems utilizing series and parallel FPTUs for different climates. Their results indicated that VAV systems with SCR controlled series units tended to use more energy than VAV systems with SCR controlled parallel units in them unless there was significant leakage (>10%) in the parallel units.

Manufacturers also sell fan powered terminal units with newer electronically commutated motors (ECM) that are expected to be more energy efficient than the older SCR controlled models. Edmondson et al. (2011a, 2011b, 2011c) developed airflow, pressure, and power data for a range of series and parallel ECM FPTUs. Davis et al. (2012) used these data to estimate the annual performance of ECM controlled FPTUs.

This article has two objectives. The first is to provide a comparison of the airflow performance and fan/motor efficiency of "off-the-shelf," similarly sized SCR and ECM controlled FPTUs. Both FPTUs were made by the same manufacturer. Characteristic equations for the fan airflow were established as a function of the primary airflow into the FPTU. Because the fan/motor efficiency is used as an input into building energy simulation programs (EnergyPlus 2012), this article also provides a comparison of the fan/motor efficiencies of the SCR and ECM controlled FPTU. The data presented should be

Received May 23, 2013; accepted September 5, 2013

Dennis L. O'Neal, PhD, PE, Fellow ASHRAE, is Dean. **Jacob L. Edmondson**, Associate Member ASHRAE, is Laboratory and Equipment Engineering Specialist. **Peng "Solomon" Yin**, Student Member ASHRAE, is Graduate Assistant.

*Corresponding author e-mail: dennis.oneal@baylor.edu

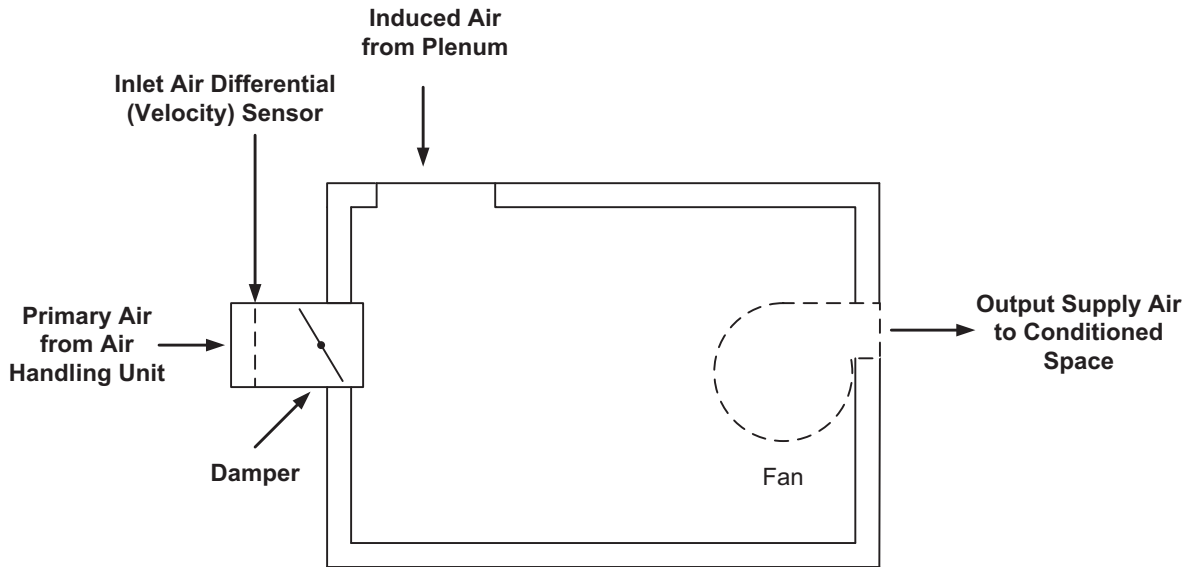


Fig. 1. Simplified schematic of a series FPTU.

usable as input for simulating FPTU performance in a typical building simulation program.

A second objective was to provide a detailed comparison of the power characteristics of SCR and ECM controlled series FPTUs. These characteristics included power, power factor, and harmonic data. The combined airflow, efficiency and data models provide a comprehensive comparison of SCR and ECM FPTUs.

Experimental setup and procedure

The two units evaluated had an 8 in. (203 mm) inlet and were both from the same manufacturer, designated as manufacturer C. The designation of the manufacturer was meant to be consistent with the designation used by Furr et al. (2008a, 2008b) and Edmondson et al. (2011a, 2011b).

The laboratory equipment included measurement of airflow and power. While a brief description is provided here, a more detailed description can be found in Furr (2006), Furr et al. (2008c), Cramlet (2008), and Edmondson et al. (2011c). Airflow was controlled and measured using nozzle airflow chambers (Air Movement and Control Association [AMCA] 1999) located both upstream and downstream of the FPTU (Figure 2). Each chamber had a booster fan controlled by a variable speed drive (VSD). Nozzle combinations differed between each chamber and were selected by the operator.

The two airflow chambers and FPTU were connected with sheet-metal ductwork which followed the specifications outlined in the ANSI/ASHRAE Standard 130 (ASHRAE 2006). The upstream duct diameter was 8 in. (203 mm). The downstream duct was 16 in. (406 mm) × 15 in. (381 mm). Tests were done with only ductwork between the two airflow chambers

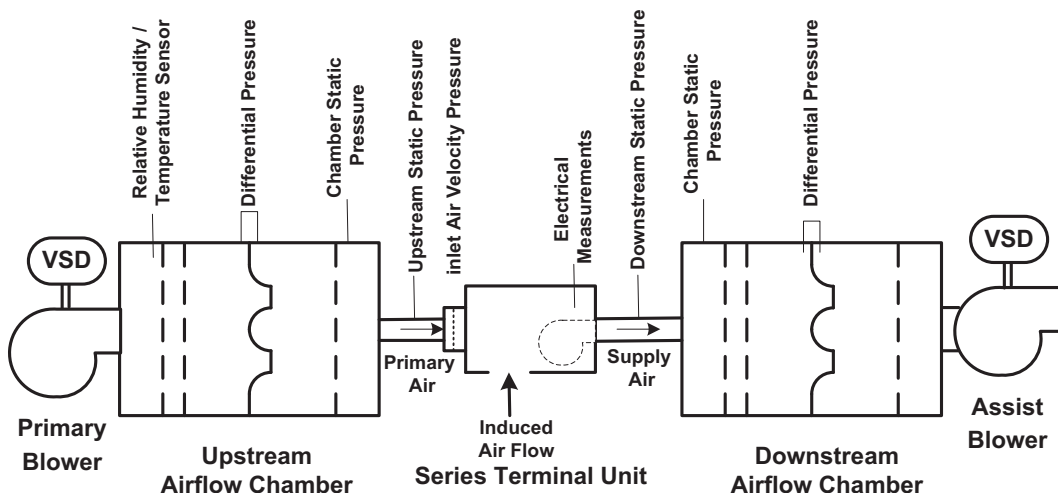


Fig. 2. Airflow test apparatus including FPTU and airflow chambers.

Table 1. Pressure transducer sizing.

Measurement point location	Transducer range, in. w.g. (kPa)
Upstream chamber differential pressure	0–6 (0–1.5)
Upstream chamber static pressure	0–10 (0–2.5)
Upstream static pressure	0–2 (0–0.5)
Inlet air velocity differential pressure	0–2 (0–0.5)
Downstream static pressure	0–2 (0–0.5)
Downstream chamber static pressure	0–10 (0–2.5)
Downstream chamber differential pressure	0–6 (0–1.5)

to compare the measured airflow measurements between the two chambers. For the airflow ranges used for this study, the two chambers agreed to within $\pm 3\%$.

Airflow quantities were calculated consistent with ANSI/AMCA Standard-210 (AMCA 1999). The upstream airflow chamber was used to measure the primary air into the FPTU. Airflow values were adjusted to standard temperature and pressure conditions to compensate for environmental changes in the laboratory during data collection. Induced airflow into the FPTU was calculated as the difference of the airflow measured with the upstream and downstream airflow chambers. Static pressures were averaged across the respective cross-sections both upstream and downstream of the terminal unit.

Both FPTUs had similar mechanical dampers used to regulate the primary airflow. The damper shaft was attached to a DC motor that could control the rotation angle of the damper. The motor had an electrically controlled actuator with a 0 to 10 VDC range that went from fully open to fully closed and allowed precise control of damper position.

The SCR and ECM controlled fan motors were both rated at 0.25 hp (373 W). The ECM controllers were matched to the unit's internal fan and preprogrammed by the supplier. The ECM motor could dynamically adjust fan torque and speed to maintain a preprogrammed airflow. The microprocessor and ECM motor controller were operated via a 0 to 10 VDC input signal.

Both static and differential pressures were measured with pressure transducers calibrated with a water manometer to within 0.01 in. w.g. (2.49 Pa) and had an accuracy of $\pm 0.25\%$ of full-scale output. All pressure transducers shown in Table 1 had an output of 4–20 mA proportional to the pressure across the device. Terminating resistors converted the output current into a voltage the data acquisition system could measure.

Both temperature and relative humidity values were taken with a dual purpose probe which had a $\pm 0.9^\circ\text{F}$ ($\pm 0.5^\circ\text{C}$) and a $\pm 3\%$ relative humidity (RH) accuracy. The location of this probe was near the opening in the FPTUs induction port, but placed so as not to interfere with airflow into the terminal fan. A redundant mercury thermometer was also placed near the transducer to allow for quick temperature verification.

The pressure, temperature, and RH voltage signals were collected using a computer-based multi-board data acquisition system. Two external input/output (I/O) boards were connected to the computer's internal controller cards via a proprietary serial connection.

Electrical performance data were recorded with a power quality analyzer. Current probes rated for 0–5A were selected and had a $\pm 1\%$ full scale accuracy. The current clamps were applied to both the power and neutral wires of the single phase 277 voltage alternating current (VAC) input. The simultaneously measured and recorded data included, but was not limited to, real and apparent power, root mean square (RMS) voltage (V_{RMS}) and current (I_{RMS}), associated harmonics and total harmonic distortion. The data files were cached in the power quality analyzer's internal memory then transferred to a personal computer.

A factorial test matrix spanning several independent variables was established for the fan powered terminal unit designs to adequately simulate the expected range of operation in the field. The interrelated variables listed in Table 2 outline the various input levels used to set the conditions for the study.

The damper position, D , was controlled using an actuator with a 0 to 10 VDC input that could vary the damper position between 100% fully open (0°) and fully closed (45°). The two series units had opposing-blade dampers with a 45° range of operation and four damper test points (0° , 11.25° , 22.5° , and 33.75°) were used. The fully closed condition was not included in the test matrix because this damper position would have produced no primary airflow.

For the ECM unit, the fan motor was controlled with a 0 to 10 VDC input signal, V_{fan} . This input voltage fed a logic circuit which controlled the speed of the ECM. The ECM controller voltage could be varied between 0 to 10 VDC to change fan speed (and airflow) in the test matrix. A 0 VDC condition was impractical because series fans must always be on. It should be noted that for applications in the field, the manufacturer did not recommend operating the ECM controller above 8 VDC. However, for these tests, the ECM controller was used at the 10VDC setting and operated without any problems at this higher voltage setting. This provided for a slightly wider range of data that are presented in this paper.

The fan/motor with the ECM controller was removed from the FPTU to conduct efficiency tests. For these tests, the fan airflow was measured with one of the airflow chambers shown in Figure 2. The fan inlet was open to the atmosphere and the fan discharged into the inlet of the airflow chamber. Fan discharge static pressure was measured and controlled by the airflow chamber.

For the SCR unit, the input voltage was controlled by a setscrew that could be manually adjusted from its minimum to maximum position. For this unit, the minimum voltage was 153 VAC and the maximum was 277 VAC. For a typical unit

Table 2. Series terminal unit test levels.

Independent variable	Test points	Value range
D , damper position	4	Full open–close
V_{fan} , fan input voltage (ECM), VDC	4	2.0–10
V_{fan} , fan input voltage (SCR), VAC	5	153–277
P_{up} , upstream static, in. w.g. (Pa)	6	0.0–2.0 (0–498)
P_{down} , downstream static, in. w.g. (Pa)	1	0.25 (62)

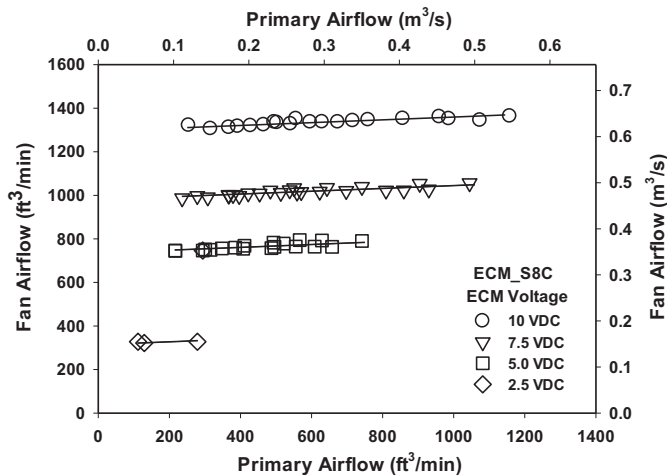


Fig. 3. Fan airflow for the ECM series terminal unit.

in the field, the setscrew would be used to adjust the FPTU fan to a specific setting only once as the VAV system was being initially balanced and then would not change during operation. For the SCR unit, fan/motor efficiency data was provided by the manufacturer of the FPTU.

In a building, both upstream static pressure, P_{up} , and downstream static pressure, P_{down} , depend on conditions in the building. These variables were also included in the test matrix. Pressure adjustments were made by use of the VSD controlling the assist blowers on the upstream and downstream airflow chambers. The data acquisition system allowed the user to manually adjust the VSD controlled blowers as needed to achieve the desired static pressures. Tests were performed with upstream static pressure reaching as high as 2.0 in. w.g. (498 Pa). Downstream static pressure was set at a constant 0.25 in w.g. (62 Pa).

Experimental data were collected in a test environment where the ambient space temperature varied between 60°F (15.5°C) to 80°F (26.7°C) and relative humidity varied between 40% and 70%. For this study, unconditioned laboratory air was used because the research was primarily concerned with FPTU airflow and power consumption. Temperature, RH, and pressure measurements were used to calculate the airflow rate (AMCA 1999). All volumetric airflow was adjusted to a standardized airflow with a reference air density of 0.075 lb/ft³ (1.20 kg/m³).

Airflow results

In a series terminal unit, the internal pressure is affected by variations in upstream duct static pressure, damper position, and primary airflow. Even with these variations, a series terminal unit typically provides a nearly constant airflow at a given fan setting.

The desired airflow model was developed to quantify both the induced and supply air delivered by the series FPTU. The fan speeds on both the ECM and SCR controllers could be varied. The ECM interface to the terminal unit used a 0 to 10 VDC user controlled input. ECM controlled FPTUs employ

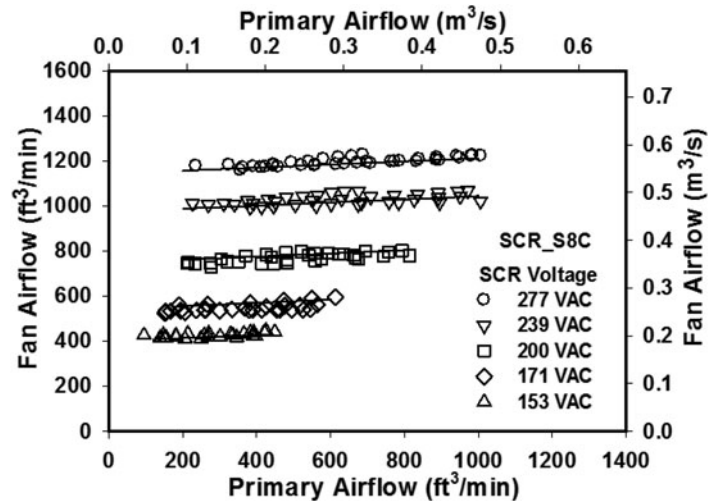


Fig. 4. Fan airflow for the SCR series terminal unit.

application-specific, programmable logic routines that allow the controller's internal microprocessor to dynamically adjust fan motor RPM and torque with the purpose of delivering constant airflow over a range of external conditions. The SCR controller allowed a reduction of the full scale 277 VAC down to 153 VAC. The SCR chopped the voltage sine wave twice every period and slowed the motor speed. The amount of voltage chop was determined by a setscrew located on the SCR. The full rotation of the setscrew fixed the minimum voltage that could be achieved by the SCR.

The variable with the greatest influence on fan airflow was the controller voltage of either the SCR or ECM unit. The ECM controlled unit with its 0 to 10 VDC input was compared against the SCR controlled units using a 153 to 277 VAC input range. The static pressure across the fan is normally a variable used in estimating the airflow produced by a fan. For a fan in a series terminal unit, the downstream static pressure is easily measured. However, the upstream static pressure immediately upstream of the fan is internal to the terminal unit. Because neither of the terminal units had pressure taps for measuring the static pressure internal to the unit, it was not measured. It would also not normally be measured in the field for the same reason (i.e., lack of pressure taps). During normal operation, the internal static pressure would need to be less than atmospheric pressure to induce air into the unit from the induction port.

Figures 3 and 4 show the results of the fan airflow, Q_{fan} , plotted as a function of the primary airflow, Q_{pri} , for the ECM and SCR FPTUs, respectively. As the primary air damper closes, less primary air enters the FPTU and more secondary air is induced into the FPTU. The fan airflow for both the ECM and SCR controlled FPTU fan motors show little variation with changes in the primary airflow into the FPTU. While both units were from the same manufacturer and had the same size primary air duct diameter, the ECM controlled fan was able to generate slightly higher airflows than the SCR unit. While the fan airflow was stable for both units, the ECM unit showed virtually no slope while the SCR did drop slightly

Table 3. Model coefficients for fan airflow in the series terminal units.

Motor control	C_1 , ft ³ /min	C_2 , (ft ³ /min)/V	C_3 , (ft ³ /min)/V ²	C_4 , (ft ³ /min)/V ³	C_5	R^2
ECM	-529.9	455.2	-53.59	2.632	0.0648	0.999
SCR	-1286.7	13.80	-0.01816	0	0.0698	0.999

as the damper closed and less primary air was available to the FPTU.

A simple model of the fan airflow as a function of the controller voltage and the primary airflow was developed and is shown in Equation 1. The coefficients for the ECM and SCR units for Equation 1 are shown in Table 3. As noted, the R -squared values for both models were 0.999:

$$Q_{fan} = C_1 + C_2 V_{fan} + C_3 V_{fan}^2 + C_4 V_{fan}^3 + C_5 Q_{pri} \quad (1)$$

where C_1 , C_2 , C_3 , C_4 , and C_5 are regression coefficients; V_{fan} is voltage input to the fan motor controller; and Q_{pri} is primary airflow.

Fan/motor efficiency results

Energy simulation programs often require input of fan and motor efficiency and pressure differential across the fan to simulate the performance of FPTUs (EnergyPlus 2012). Separate fan and motor efficiencies are rarely provided by the FPTU manufacturers for the fan/motor combinations in their FPTUs. For small fractional horsepower fan motors typically found in FPTUs, the fan and motor are usually evaluated as a unit rather than separately.

Figures 5 and 6 show the fan/motor total efficiency, η_{Tfm} , of the ECM and SCR fans plotted against the static pressure, ΔP_{stat} , of the fans. The total efficiency (McQuiston, Parker, and Spitler 2005) is defined as:

$$\eta_{Tfm} = \frac{Q_{fan} \Delta P_{tot}}{Pow_{fan}} \quad (2)$$

where Pow_{fan} is the power input to the fan motor; ΔP_{tot} is $\Delta P_{stat} + \Delta P_{vel}$; and ΔP_{vel} is change in velocity pressure across the fan.

For both fan/motor units, the efficiency was dependent on the static pressure. Both fans produced higher efficiencies at higher static pressures. The SCR controlled fan/motor could not operate at fan static pressures above about 0.6 in. w.g. (149.4 Pa), so both sets of data were plotted with 0.6 in. w.g. (149.4 Pa) as the maximum static pressure. For the ECM con-

trolled fan/motor, the highest efficiencies were generally at the lowest speed setting (4 VDC). For the efficiency tests with the ECM controlled motor, the voltage was dropped down to as low as 2 VDC; however, the controller did not operate properly at that low a voltage setting. At a static pressure differential of 0.25 in. w.g. (74.7 Pa), the fan efficiency varied from 36.4% for a 4 VDC controller input to a low of 27.3% for the 10 VDC controller input. For this controller, the efficiencies for the ECM controlled unit were typically lowest for the 10 VDC.

The total efficiency of the SCR controlled fan/motor was significantly less than that for the ECM controlled fan/motor across the range of static pressures evaluated for these two units. It was surprising that at fan static pressures below 0.2 in. w.g. (50 Pa), the fan/motor efficiencies for the SCR controlled unit were below 10%. At 0.25 in. w.g. (62.3 Pa) and lower operating fan speeds (4 VDC for the ECM and 208 VAC for the SCR), the ECM unit had an efficiency (36.4%) that was about four times greater than the efficiency (8.9%) for the SCR controlled unit. Thus, at lower static pressures and lower speeds, the ECM FPTUs have a significant efficiency advantage over the SCR controlled FPTUs. When the controllers were operated at full speed (10 VDC for the ECM and 277 VAC for the SCR), the efficiency advantage of the ECM over the SCR controlled unit decreased.

The efficiency, η_{Tfm} , for both the SCR and ECM controlled fan/motor combinations were fit to the static pressure (ΔP_{stat})

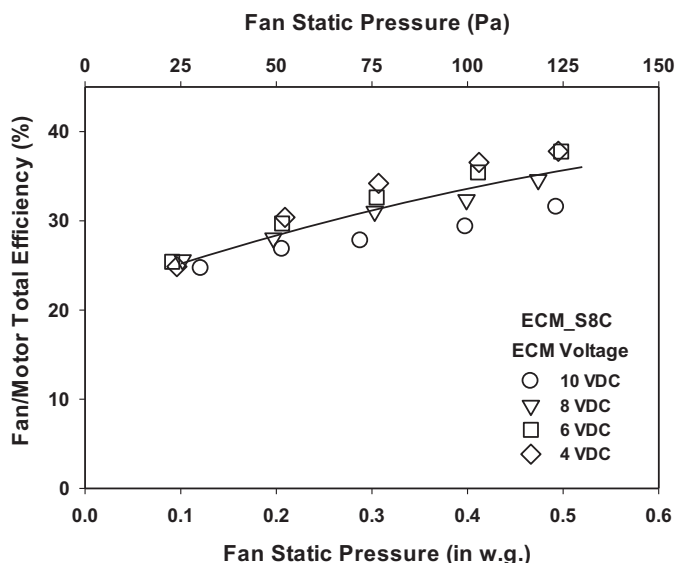


Fig. 5. Fan total efficiency as a function of fan static pressure for the ECM controlled unit.

Table 4. Regression coefficients for fan/motor total efficiency for the ECM and SCR controlled units.

Fan/motor	a_1	a_2	a_3	R^2
ECM	21.67	37.21	-18.43	0.873
SCR	0.438	49.95	-29.46	0.932

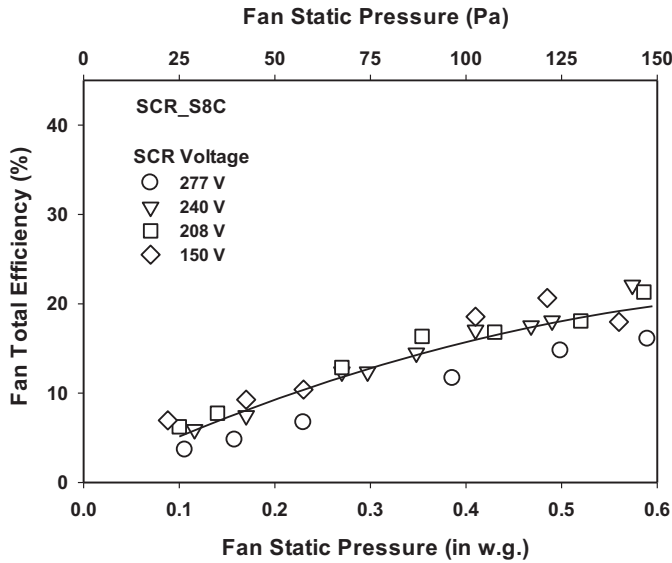


Fig. 6. Fan total efficiency as a function of fan static pressure for the SCR controlled unit.

data with the following equation:

$$\eta_{Tfm} = a_1 + a_2 * \Delta P_{stat} + a_3 * \Delta P_{stat}^2 \quad (3)$$

The constants a_1 , a_2 , and a_3 are regression coefficients. The coefficients for the ECM and SCR data are shown in Table 1. Note that range of static pressures in this table are limited to between 0.1 in w.g. (24.9 Pa) and 0.6 in w.g. (149.4 Pa).

In some building simulation programs, both the efficiency and pressure are required inputs when describing FPTUs. It is clear from the plots in Figures 5 and 6 that fan efficiency is not independent of the fan static pressure in either the SCR or ECM controlled units. Both plots indicate that caution should be exercised when inputting fan efficiencies and pressures independently into building simulation programs. Previously mentioned data were for fan motors with a nominal power of 1/4 hp (0.186 kW), which are some of the smaller motors found in FPTUs. Larger fans/motor combinations could be expected to have higher efficiencies (Cermak and Ivanovich 2013).

Terminal unit power

The fan in a series FPTU is required to operate continuously in a building application. As a consequence, the power consumption of both SCR and ECM controlled FPTUs is of particular interest. A comparison of real power consumption for both the ECM and SCR controlled FPTUs as a function of fan airflow is shown in Figure 7. The data were fit with a quadratic with respect to the controller voltage both the ECM and SCR controlled units. The ECM controlled unit showed significantly less power draw than the SCR controlled unit between 400 to 1000 ft³/min (0.19 to 0.47 m³/s) as might be expected with the higher efficiency of the ECM unit. The only time the ECM began to lose its advantage over the SCR unit was at the highest controller setting (10 VDC), which, in the

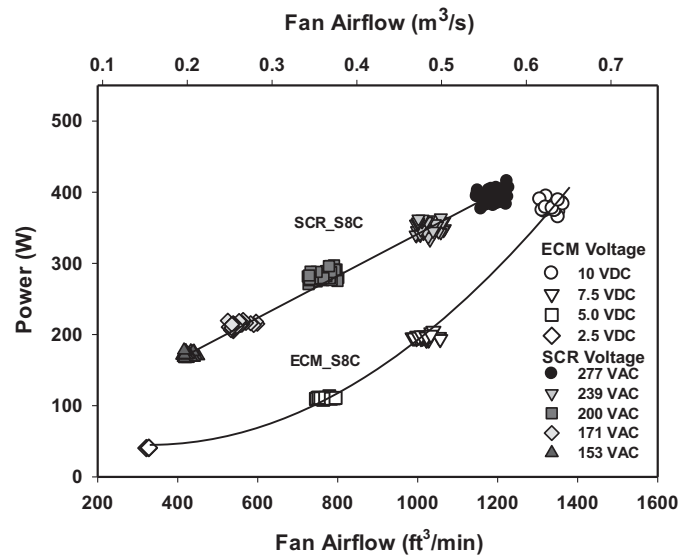


Fig. 7. Power consumption for ECM and SCR series terminal units.

field, would be outside the voltage setting recommended by the manufacturer of this unit. For off peak operating conditions in a building where the FPTU would be operating at lower airflows, the ECM controlled FPTU would have a significant energy and power advantage over the SCR controlled FPTU.

The data in Figure 7 can be fit using a simple quadratic fit for the ECM controlled unit and a linear fit for the SCR controlled unit. The general equation is given in Equation 4. For the SCR controlled unit, the constant, C_3 , is set to zero. In both cases the fit to the data had R -squared of over 0.99, indicating an excellent fit. The regression coefficients for the ECM and SCR units are listed in Table 5:

$$Pow_{fan} = C_1 + C_2 Q_{fan} + C_3 Q_{fan}^2 \quad (4)$$

A popular way of presenting a measure of the efficiency and power of fan/motor combinations in literature from manufacturers is to present the fan power divided by fan airflow. In the United States, the units are usually expressed in W/(ft³/min). Equation 2 can be rearranged to show how the power is divided by airflow is related to efficiency:

$$\frac{Pow_{fan}}{Q_{fan}} = \frac{\Delta P_{tot}}{\eta_{Tfm}} \quad (5)$$

Table 5. Model coefficients for the fan motor power consumption.

Motor control	C_1 , W	C_2 , W/(ft ³ /min)	C_3 , W/(ft ³ /min) ²	R^2
ECM	80.46	-0.2164	0.00033	0.997
SCR	54.5	0.288	0	0.993

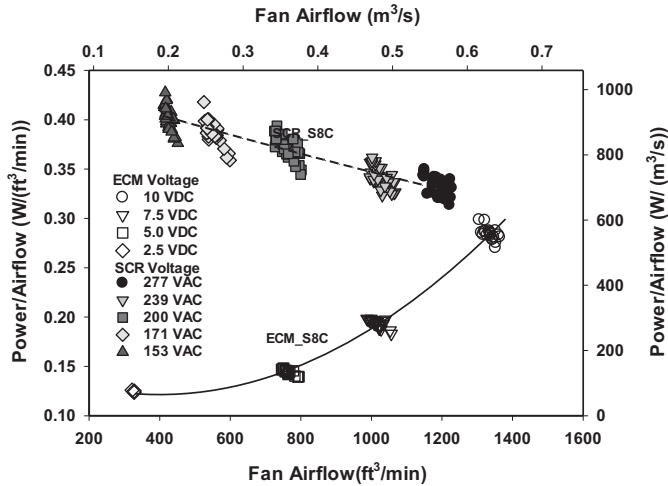


Fig. 8. Fan power/airflow for both ECM and SCR series terminal units.

The fan power divided by fan airflow could be considered an inverse efficiency if the total pressure is held constant. Thus, higher efficiency fans should have a lower fan power to airflow value. However, the fan efficiency is not independent of fan total pressure. Thus, one should be cautious about using this measure by itself when considering fan performance.

Figure 8 shows a plot of the fan power divided by fan airflow for the ECM and SCR controlled FPTUs. The ECM controlled unit displayed better fan power-to-airflow ratios over the entire range compared to the SCR controlled terminal unit. It was particularly better at lower airflow rates. The difference between the SCR and ECM controlled units decreased dramatically as the SCR output voltage approached the ideal 277 VAC input signal and the ECM unit approached its maximum controller voltage of 10 VDC. The SCR controller was much more efficient when it was not required to do distort the input sine wave at the higher AC voltages. Thus, the slope of the SCR unit was negative.

Power quality results

The power quality analysis of the series VAV terminal unit focuses on power factor and total harmonic distortion. Figure 9 show the difference in power factors for the ECM and SCR units. The ECM power factors never exceed 0.45 and maintain a nearly horizontal over the whole range of airflows while the SCR power factor increased with airflow. The increasing power factor for the SCR occurred because of the reduction in the distortion of the sine wave as the input voltage increased to the fan motor. At the full setting of the SCR controller, the 277 VAC signal was not modified and the power factor was nearly equal to 1.

Figure 10 compares the apparent power of the two series units. The SCR apparent power curve peaked at near 800 ft³/min (0.378 m³/s) then decreased at higher fan speeds. Because the ECM controller’s power factor was nearly constant, the shape of the apparent power closely matched that of the

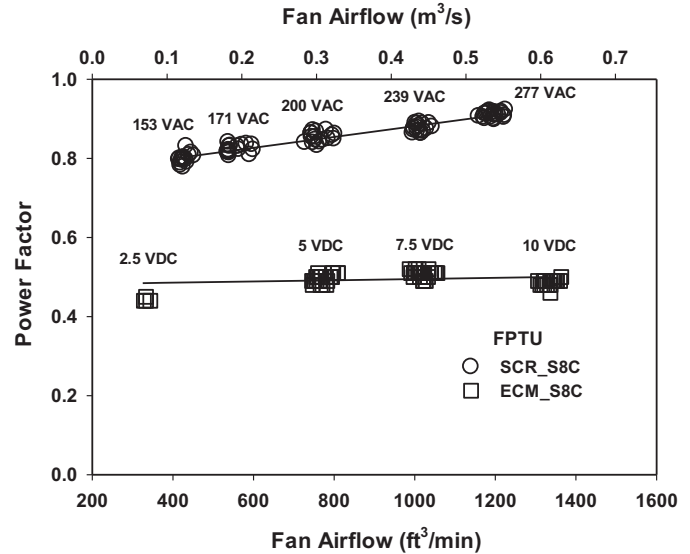


Fig. 9. Comparison of power factors for the SCR and ECM series terminal units.

real power. While the SCR controlled unit had an advantage over the ECM unit for airflows above approximately 1000 ft³/min (0.47 m³/s), the higher airflow corresponded to the 10 VDC setting, which was outside the voltage recommended by the manufacturer for field applications.

Figures 11 and 12 show each of power harmonics of the ECM and SCR units as a percentage of the fundamental (60 Hz) harmonic out to the 25th harmonic. The power harmonics were relatively small in magnitude and represented only a small fraction of the real power consumed. The negative harmonic values were attributed to that part of the cycle where energy is actually transferred from the inductor (load) back into the voltage source. These plots are useful for getting a “visual” observation of where the largest harmonic contributions to the power may be.

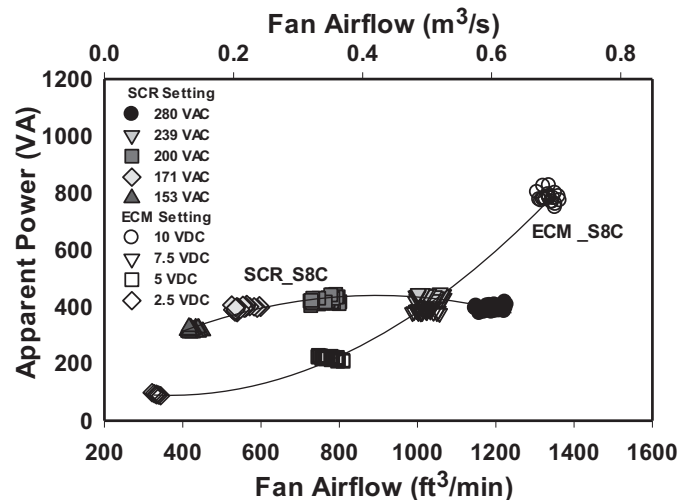


Fig. 10. Apparent power for the ECM and SCR series terminal units.

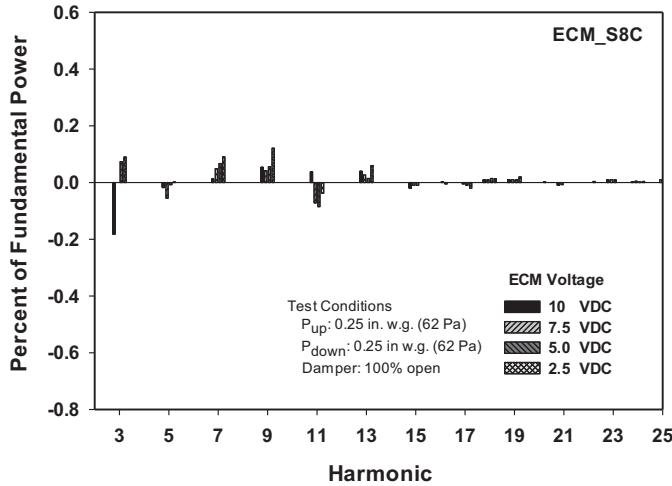


Fig. 11. ECM series FPTU power harmonics.

For the ECM controlled motor, there was power (though small) distributed all the way to the 25th harmonic. By contrast, the harmonic distortion in the SCR unit was concentrated in the first seven harmonics with nothing measureable beyond the 13th harmonic. At the full 277 VAC, the SCR control motor had nearly negligible power in the harmonics because the SCR did not have to chop the alternating current sine wave.

Total harmonic distortion (THD) is a term often used to evaluate the total impact of an electrical component on the electrical system in a system. The THD for real power is defined as (Kennedy 2000):

$$THD = \frac{\sum \text{harmonic powers}}{\text{fundamental frequency power}} \quad (6)$$

Power THD is often expressed as a percentage of the fundamental frequency (60 Hz) power.

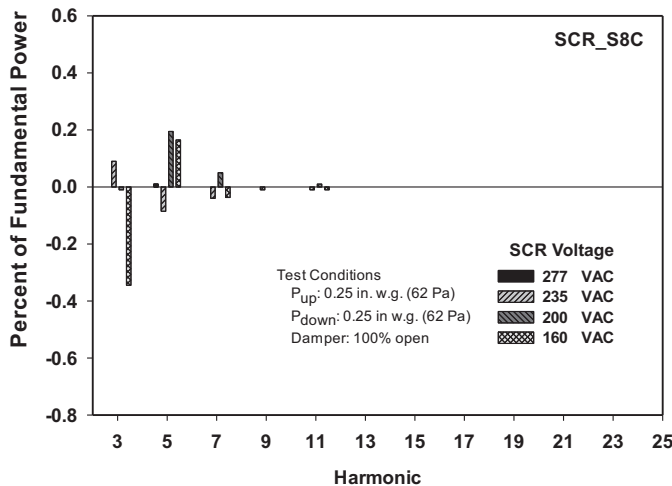


Fig. 12. SCR series FPTU power harmonic.

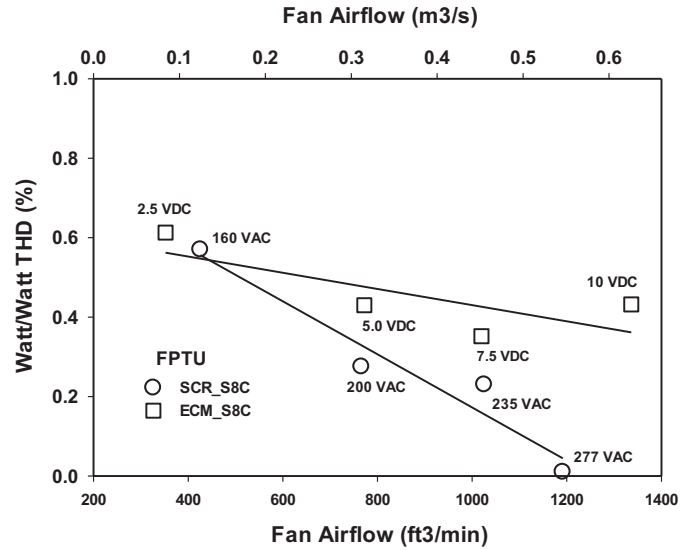


Fig. 13. Real power THD for series terminal units.

Figure 13 presents both the ECM and SCR controlled FPTU's power THD (expressed as a percentage) over their respective control input ranges. The SCR unit approached 0% total harmonic distortion as fan speed was increased while the ECM controlled unit ranged from 0.35% to 0.61%. What is significant for both the SCR and ECM units are that with the exception of the very low airflow cases, the percentage THD was less than 0.5%. Even at the lowest airflow case, only the ECM was above 0.6%.

The percentage harmonic distortion was higher for the ECM unit at most airflows. However, because the overall power for the ECM unit over most of the airflow range was significantly lower than that of the SCR unit (Figure 7), its absolute harmonic distortion (in Watts) would be less in a building.

Summary and conclusions

This article provided a detailed comparison of two similar “off-the-shelf” FPTUs from a single manufacturer. One of the units came with an SCR controlled motor and the other with an ECM controlled motor. Both provided excellent control of airflow over a wide range of primary airflows into the FPTUs indicating that either technology is suitable for controlling the fan airflow.

A major difference in the two units was in the fan/motor efficiencies and power requirements. The efficiency of the combined fan and motor were evaluated together rather than independently because both are an integrated system for the smaller sized fans and motors used in the FPTUs. The ECM controlled fan/motor provided a substantial advantage in efficiency compared to the SCR fan/motor. The efficiency data presented in this paper should provide users of building simulation programs with useful data to estimate actual performance of smaller sized FPTUs in commercial

buildings. The higher efficiencies of the ECM unit were reflected in the much lower power requirements of the ECM controlled FPTU. Given that series FPTUs fans must operate continuously whenever the HVAC system is on, ECM applications in FPTUs have the potential to save substantial energy over SCR units.

Power quality can be an issue in commercial building applications. The SCR unit had an advantage over the ECM unit in power factor over the whole range of airflows evaluated. The higher power factor in the SCR unit, particularly at high airflows (and high AC voltages) meant that its apparent power was less than the ECM unit at airflow above approximately 1000 ft³/min (0.47 m³/s). However, these higher airflows for the ECM unit occurred outside the normal operating range recommended by the manufacturer of the FPTU. These data would suggest that to take full advantage of an ECM controlled unit, it would be best to size the unit so that it operates in the middle of its range rather than near its maximum output. For this unit, if the unit were sized in an application so its controller were set at 6 VDC, it would have had an airflow of approximately 800 ft³/min (0.378 m³/s) versus a 200 VAC setting for the SCR. The ECU controlled unit would have used approximately 60% less power and 50% less apparent power than the SCR controlled unit for this airflow.

The overall harmonic distortion for both controllers was less than 1%. Harmonic distortion was highest at the lowest fan speeds (lowest airflows) for both controllers. At least with both of these controllers, it does not appear that either would generate enough harmonic distortion to be a consideration in many applications.

Acknowledgment

We acknowledge ASHRAE, which funded the SCR portion of this work under RP-1292 and a manufacturer's research consortium consisting of Nailor Industries, Metal Industries, Inc., Krueger Manufacturing Co., Regal Beloit Corporation, and A.O. Smith which funded the ECM portion of the work. We also thank the individuals from these companies that provided guidance to the research.

References

- Air Movement and Control Association. 1999. *ANSI/AMCA standard 210-99. Laboratory methods of testing fans for aerodynamic performance rating*. Arlington Heights, IL: Air Movement and Control Association.
- ASHRAE. 2006. *ANSI/ASHRAE standard 130-1996 (RA 2006), Methods of testing for rating ducted air terminal units*. Atlanta: ASHRAE.
- Cermak, J., and M. Ivanovich. 2013. Fan efficiency requirements for Standard 90.1-2013. *ASHRAE Journal* 55(4):24–30.
- Cramlet, A. 2008. Performance of ECM controlled VAV fan power terminal units. M. Sc. Thesis, Texas A&M University, College Station, TX.
- Davis, M., J. Bryant, and D.L. O'Neal. 2009. Modeling the performance of single-duct VAV systems that use fan powered terminal units. *ASHRAE Transactions: Symposia* 115(1):307–13.
- Davis, M.A., J.A. Bryant, and D.L. O'Neal. 2012. Modeling the performance of ECM and SCR parallel fan powered terminal units in single-duct VAV systems. *ASHRAE Transactions* 118(1):908–19.
- Edmondson, J., D.L. O'Neal, J.A. Bryant, and M.A. Davis. 2011a. Performance of series fan powered terminal units with electronically commutated motors. *ASHRAE Transactions* 117(2):876–84.
- Edmondson, J., D.L. O'Neal, J.A. Bryant, and M.A. Davis. 2011b. Performance of parallel fan powered terminal units with electronically commutated motors. *ASHRAE Transactions* 117(2):885–93.
- Edmondson, J., D.L. O'Neal, J.A. Bryant, and M.A. Davis. 2011c. Performance of ECM controlled fan-powered terminal units. VAVRC-R01. Energy Systems Laboratory, Texas A&M University, College Station, TX.
- EnergyPlus. 2012. EnergyPlus engineering reference. University of Illinois and Lawrence Berkeley National Laboratory, Berkeley, CA.
- Furr, J. 2006. Development of models for series and parallel fan variable air volume terminal units. M.Sc. Thesis, Texas A&M University, College Station, TX.
- Furr, J., D.L. O'Neal, M. Davis, J. Bryant, and A. Cramlet. 2008a. Performance of VAV Fan powered terminal units: Experimental results and models for series units. *ASHRAE Transactions* 114(1):91–7.
- Furr, J., D.L. O'Neal, M. Davis, J. Bryant, and A. Cramlet. 2008b. Performance of VAV fan powered terminal units: Experimental results and models for parallel units. *ASHRAE Transactions* 114(1):83–90.
- Furr, J., D.L. O'Neal, M. Davis, J. Bryant, and A. Cramlet. 2008c. Performance of VAV fan powered terminal units: Experimental setup and methodology. *ASHRAE Transactions* 114(1):76–82.
- Kennedy, B.W. 2000. *Power quality primer*. New York: McGraw-Hill Professional.
- McQuiston, F.C., J.D. Parker, and J.D. Spitler. 2005. *Heating, ventilating, and air conditioning analysis and design*, 6th Ed. Hoboken, NJ: Wiley.

SE-14-025

Characterizing Airflow and Power of VAV Series Fan-Powered Terminal Units from Component Data—Part I

Peng Yin

Student Member ASHRAE

Dennis L. O'Neal, PhD, PE

Fellow ASHRAE

ABSTRACT

Fan-powered terminal units (FPTUs) are composed of three main components: the fan/motor/controller, damper, and housing. These three components were experimentally characterized separately to determine if the overall system performance of series FPTU could be predicted by combining the models of the three components. Eight terminal units, from three manufacturers, with 8 in. (203 mm) and 12 in. (304 mm) primary air inlets were studied.

Fan airflow and power data were collected from eight fans with electronically commutated motors (ECMs) over a range of fan speeds and discharge static pressures. Semi-empirical models were developed from the experimental data. Model variables included the nondimensional fan speed and the discharge static pressure. The resulting models had a coefficient of determination (R^2) value greater than 0.99 for fan airflow model and 0.97 for power consumption model. These models can be applied to HVAC simulation programs to model variable-air-volume (VAV) systems with series FPTU.

INTRODUCTION

A key component in variable-air-volume (VAV) systems is the air terminal unit, which is used to control the amount of conditioned air introduced into a space. Figure 1 shows the airflow in a VAV system. Primary air is conditioned by a central air-handler unit (AHU) and delivered by a central supply fan through a single supply air duct system to terminal units. By mixing primary and plenum air within terminal units, supply air is produced and provided to different zones. Terminal units using fans to regulate airflow are called fan-powered terminal units (FPTUs). They are typically installed in return plenums and ducted to air outlets. Compared with terminal

units without fans, FPTUs offer several advantages, including reducing or eliminating reheat by mixing primary air with warmer plenum air, reducing central supply fan operating pressure and energy consumption in an air distribution system, and boosting downstream air pressure that allows the air to be delivered to the zones with insufficient airflow (ASHRAE 2012).

When a terminal unit fan is in series with primary air, this unit is referred to as a series FPTU. In a series FPTU, a terminal unit fan must be operating continuously whenever a central supply fan is on and all the air delivered to a conditioned zone passes through the terminal unit fan, as shown in Figure 2. When cooling load decreases, the inlet damper gradually closes to regulate primary air until it reaches its predetermined minimum position. At the same time, the fan induces more return air from the plenum to compensate for reduced primary air. By adjusting the amount of primary and plenum air, the temperature setpoint can be maintained without reducing the amount of supply air. An optional electric strip heater or hot-water coil can be used to provide supplemental heat.

Currently, the two types of motors used in series FPTUs are permanent-split capacitor (PSC) motors and electronically commutated motors (ECM). PSC motors are driven by alternating current (AC) and equipped with silicon-controlled rectifiers for motor speed control. ECM motors are brushless direct current (DC) motors with permanent magnet rotors and ball bearings (Roth et al. 2004). The torque-driven design of ECM motors allows them to maintain a relatively constant flow rate in an air terminal unit, regardless of downstream static pressures (Kenty 2007). The *Nonresidential Compliance Manual for California's 2005 Energy Efficiency Standards* has mandated the use of ECM motors in series FPTUs unless standard motors

Peng Yin is a PhD student in Mechanical Engineering at Texas A&M University, College Station, TX. **Dennis L. O'Neal** is a professor and dean of Engineering and Computer Science at Baylor University, Waco, TX.

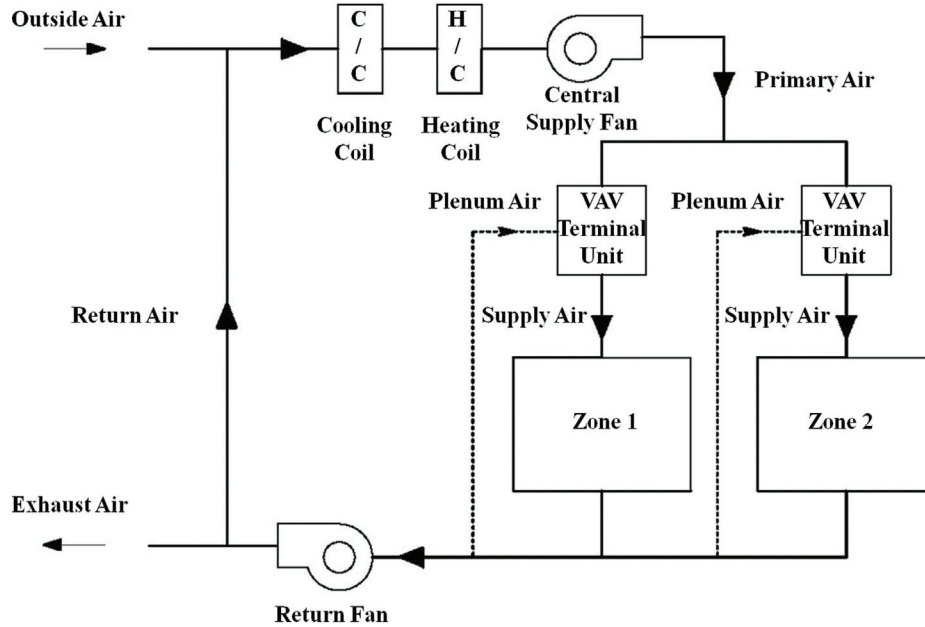


Figure 1 Airflow in a VAV system.

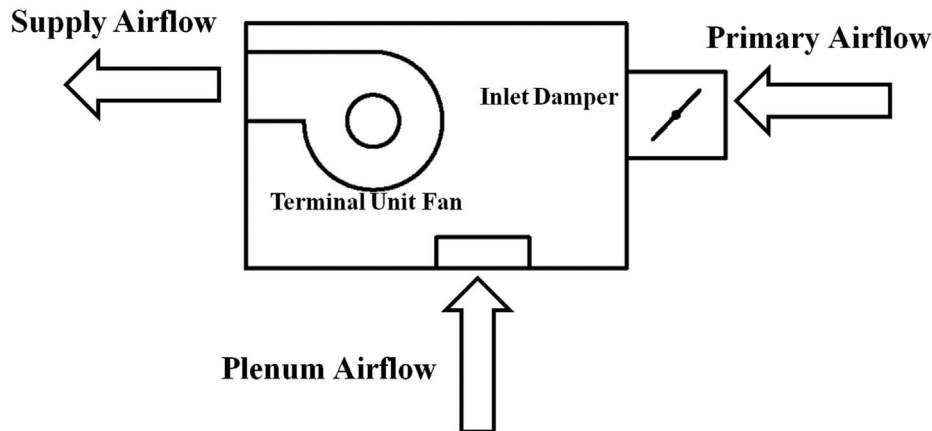


Figure 2 Simple schematic of a series FPTU.

that can be shown to be at least 70% efficient are used (CEC 2005). To model a VAV system properly, it is important to characterize the performance of terminal units.

Recently, Furr et al. (2008a, 2008b, and 2008c) and Edmondson et al. (2011a and 2011b) have experimentally studied FPTUs. They utilized a system-oriented model to estimate airflow, pressure, and power of FPTUs with PSC and ECM motors. Because of the complexity in aerodynamic conditions and airflow patterns within FPTUs, they treated FPTUs as “black boxes” and mainly focused on correlating the airflow and power measurement with peripheral pressure settings. In their experimental setup, FPTUs were connected to two airflow chambers for the measurement of primary and fan airflow under varying upstream static pressures from 0.1

to 2.0 in. wg (24.9 to 498.3 Pa) and fixed downstream static pressures at 0.25 in. wg (62.3 Pa). Their models were limited by the black box approach and required knowledge of pressure conditions upstream and downstream of an FPTU.

The public domain building energy simulation program, EnergyPlus, uses a simplified component approach to simulate the performance of series and parallel FPTUs. FPTUs are treated as compound components, including a zone mixer, a constant volume fan, and a heating coil, which can use hot water, electric, or gas as input (EnergyPlus 2012a). Figure 3 shows the schematic of series and parallel FPTUs simulated in EnergyPlus (EnergyPlus 2012b). The zone mixer receives airstreams from multiple inlets and mixes them together. The simulation of the mixer involves simple mass and energy

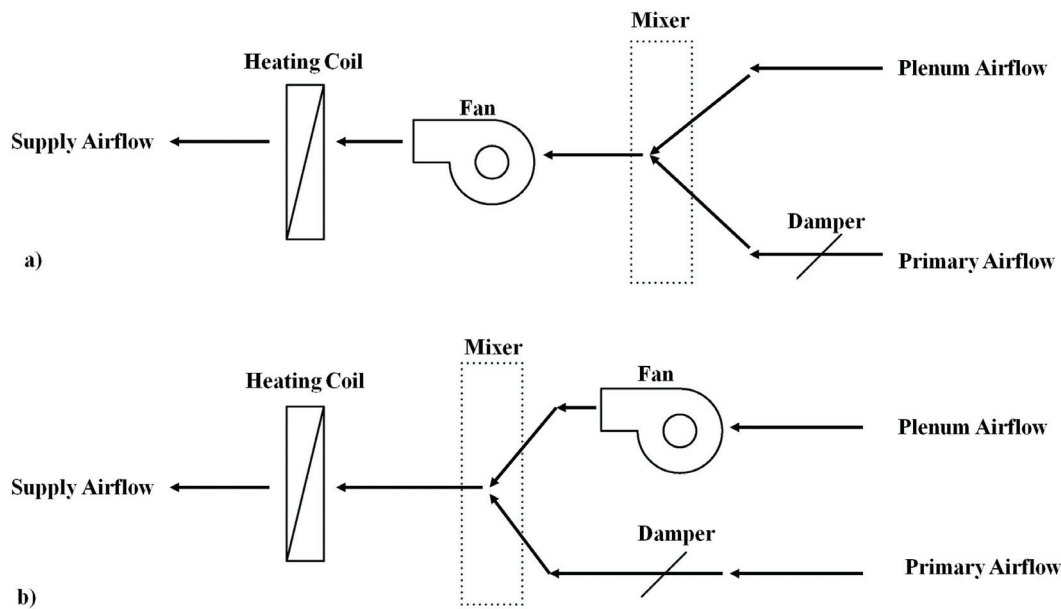


Figure 3 (a) Series FPTUs in EnergyPlus. (b) Parallel FPTUs in EnergyPlus.

balances of airstreams. The model of constant-volume fan assumes the fan operates continuously based on a time schedule. To appropriately characterize the fan performance, the knowledge of overall fan efficiency, pressure rise, maximum flow rate, and motor position are required. The heating coil is also modeled with a simple mass and energy balances to estimate the amount of sensible heating required. The overall performance of FPTUs is estimated by simulating the three subcomponents in sequence. From the zone simulation results, EnergyPlus calculates the heating/cooling demand on FPTUs. If a zone needs cooling and the terminal unit is not scheduled off, then it is available to serve the zone. The outlet air temperature required to meet the zone load is calculated, and then the primary and plenum airflow rates can be determined. The models of fan and heating coil are used to calculate the energy use for each component.

Compared with the experimentally determined empirical models developed by Furr et al. (2008b and 2008c) and Edmondson et al. (2011a and 2011b), the component-based approach can be generally applied on any FPTU. However, it fails to capture the effects caused by air pressures either on the primary or supply side of the system. For example, both Furr et al. (2008b) and Edmondson et al. (2011a) found significant leakage caused by pressure differentials across parallel FPTUs. This leakage could dramatically increase the energy use of parallel FPTUs. Because pressure input is not included in the EnergyPlus model, leakage is not explicitly modeled. Thus, EnergyPlus can be expected to underpredict the energy consumption of a VAV system using parallel FPTUs. In addition, fan efficiency and power consumption also vary with inlet and outlet pressures, but these inputs are currently constant in EnergyPlus.

An important question is whether piecing together the individual components of FPTUs will provide adequate representation of overall system performance. If the individual components, when combined, do not provide a good performance representation of FPTUs, then the energy use estimated by building energy simulation programs may not be accurate.

The objective of this study was to investigate how well the performance of a series FPTU could be modeled by combining the models of its individual components, namely fan/motor/controller, damper, and housing. The test procedure was developed and the experimental data for the individual components from eight series FPTUs were collected. Component models were established from the collected data, and then a system model was built by assembling the component models. In addition, the model outputs were compared with the experimental results from previous study (Edmondson et al. 2011b) for model verification. Since the developed models only focused on the air side and power performance, the evaluation of heating performance was not included in the scope of this study and was not conducted.

This is Part I of this study. In this paper, the experimental setup for fan testing was described and the models of fan airflow and fan/motor/controller power consumption were developed from the measured data. Additionally, overall fan efficiency and power factor were measured and reported. Part II summarized the experimental results and empirical models of primary and plenum airflow. It also included the development of a system model of series FPTU and model verification.

EXPERIMENTAL SETUP AND PROCEDURE

Eight series FPTUs from three manufacturers; labeled as A, B, and C; were experimentally studied. They were the same units used by Edmondson et al. (2011b). All units were equipped with ECM motors. They differed in the size of primary air inlet. Four of the units had 8 in. (203 mm) inlets and the other four had 12 in. (304 mm) inlets. The terminal unit with an 8 in. (203 mm) inlet from Manufacturer A was designated as S8A, and likewise Manufacturer B's 12 in. (304 mm) terminal unit was S12B, etc. Fans were named after the corresponding terminal units. For example, F_S8A was the fan from terminal unit S8A, while F_S12B was the name of the fan from terminal unit S12B. Table 1 summarizes the key characteristics of series FPTUs and fans tested in this study.

The experimental apparatus included a fan/motor/controller from a series FPTU, a supply duct, and an airflow chamber, as shown in Figure 4. Fan/motor/controllers were removed from each series FPTU and directly connected to the airflow chamber through a rectangle sheet metal duct with a length of 3.5 hydraulic diameters. This duct had the same cross-sectional dimensions as the fan outlet and was constructed in accordance with ASHRAE Standard 130 (1996).

Table 1. Series FPTU and Fan Characteristics

Fan	Fan Motor Horsepower, hp (W)	Fan Airflow Range, ft ³ /min (m ³ /s)
F_S8A	1/2 (373)	300–1050 (0.14–0.50)
F_S12A	1 (746)	700–2500 (0.33–1.18)
F_S8B	1/2 (373)	200–900 (0.09–0.42)
F_S12B	1/2 (373)	400–1600 (0.19–0.76)
F_S8C_M1	1/2 (373)	200–1100 (0.09–0.52)
F_S8C_M2	1/2 (373)	200–1100 (0.09–0.52)
F_S12C_M1	3/4 (559)	500–2000 (0.24–0.94)
F_S12C_M2	3/4 (559)	500–2000 (0.24–0.94)

Airflow was measured by using the airflow chamber. This chamber had a nozzle board consisting of one 1 in. (25 mm), one 3 in. (76 mm), and four 5 in. (127 mm) nozzles. It was built to ASHRAE Standard 51 (ASHRAE 2007) requirements for an outlet chamber setup. An assist blower controlled by a variable-frequency drive (VFD) was attached to the chamber and was used to adjust discharge static pressure. Airflow through the known open nozzle areas was calculated based on the measurement of discharge static pressure and nozzle differential pressure. The calculation procedure was directly adopted from ASHRAE Standard 51 (ASHRAE 2007). Raw airflow data were adjusted to standard conditions of temperature and barometric pressure to compensate for environmental changes in the period of data collection.

A stand-alone psychrometric station was used to monitor the temperature and humidity of ambient air. Air density was calculated based on this measurement in conjunction with barometric pressure. Air pressures were measured by pressure transducers with 4–20 mA output. Fan electrical performance was evaluated using a power quality analyzer. The simultaneously measured and recorded data included real and apparent power, root mean square (RMS) voltage and current, as well as power factor. The data files were cached in the power quality analyzer's internal memory and then downloaded to a PC. The instrument specification is listed in Table 2.

The outlet airflow chamber was verified over a wide range of flow rates from 150 to 2000 ft³/min (0.07 to 0.94 m³/s) by using another airflow chamber which was set up as an inlet chamber in accordance with ASHRAE Standard 51 (ASHRAE 2007). The two chambers were directly connected via a piece of duct. The volumetric flow rate obtained by the outlet chamber was compared with the value measured by the inlet chamber. Various nozzle combinations were used, depending on the flow rate investigated. In all cases, the differences between the two chambers did not exceed ±3%.

Fan speed and discharge static pressure were key parameters influencing fan performance. Variable fan speed was realized by using the ECM controller that came with each fan/motor. Two types of controllers were encountered. Manufacturer A provided a controller that consisted of a LCD display and a potentiometer. It could be set to a numerical value

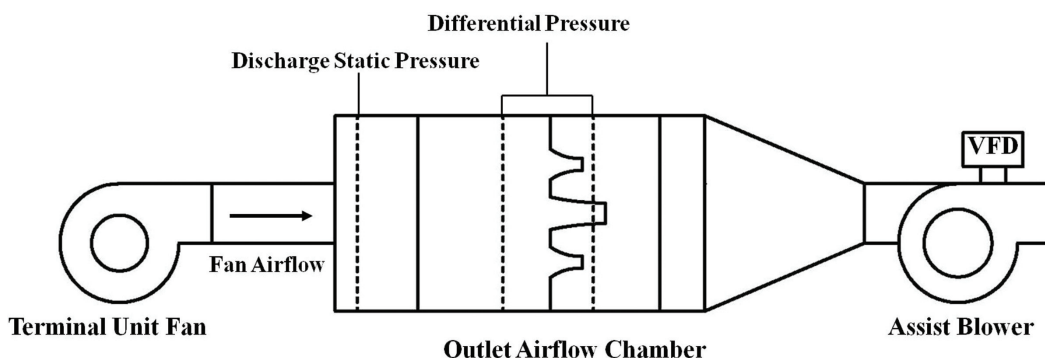


Figure 4 Fan testing apparatus, including airflow chamber and assist blower.

between 0 and 100 to represent fan speed. The other type of controller used DC voltage as input signal. Manufacturers B and C employed this design. Each manufacturer also had different design operating ranges for their series FPTUs. According to the catalog data provided by each manufacturer, a test matrix spanning these two independent variables was established to cover the expected operating ranges in the field. Table 3 shows the independent variables and their ranges for fan testing. At the specified ECM setting and discharge static pressure, the corresponding airflow and electrical performance were measured.

Table 2. Instrument Specification

Measurement Point	Sensor Specification
Ambient temperature	0°F–100°F (–17.8°C–37.8°C), ±0.7°F (±0.39°C)
Ambient relative humidity	0–100%, ±2%
Chamber static pressure	0–10 in. wg (0–2492 Pa), ±0.25% full scale
Chamber differential pressure	0–6 in. wg (0–1495 Pa), ±0.25% full scale
Voltage	±0.1% of reading
Current	±1% of reading
Power	±1% of reading

RESULTS AND MODELS

Experimental data were collected on airflow and power consumption over a range of fan speeds and discharge static pressures. The corresponding models were developed from the measurement.

Fan Airflow

Figure 5 shows the airflow plotted against ECM setting for F_S8A. At a given ECM setting, the airflow obtained at different discharge static pressures were almost the same. These data indicated that the fans with ECMs were able to provide relatively constant airflow regardless of changes in discharge static pressure. ECMs were designed to sense the motor's torque changes and automatically match the output torque to the torque required to maintain motor's setpoint. Thus, variations in discharge static pressures would not significantly impact the fan airflow. Moreover, Figure 5 also demonstrated that fan airflow was mainly a function of ECM setting

Table 3. Fan Test Matrix

FPTU Manufacturer	ECM Settings	Discharge Static Pressure
A	20%, 40%, 60%, 80%, 100% full scale	0.1–0.6 in. wg (24.9–149.5 Pa)
B	4V, 6V, 8V, 10V	0.1–0.5 in. wg (24.9–124.6 Pa)
C	2V, 4V, 6V, 8V, 10V	0.0–0.5 in. wg (0–124.6 Pa)

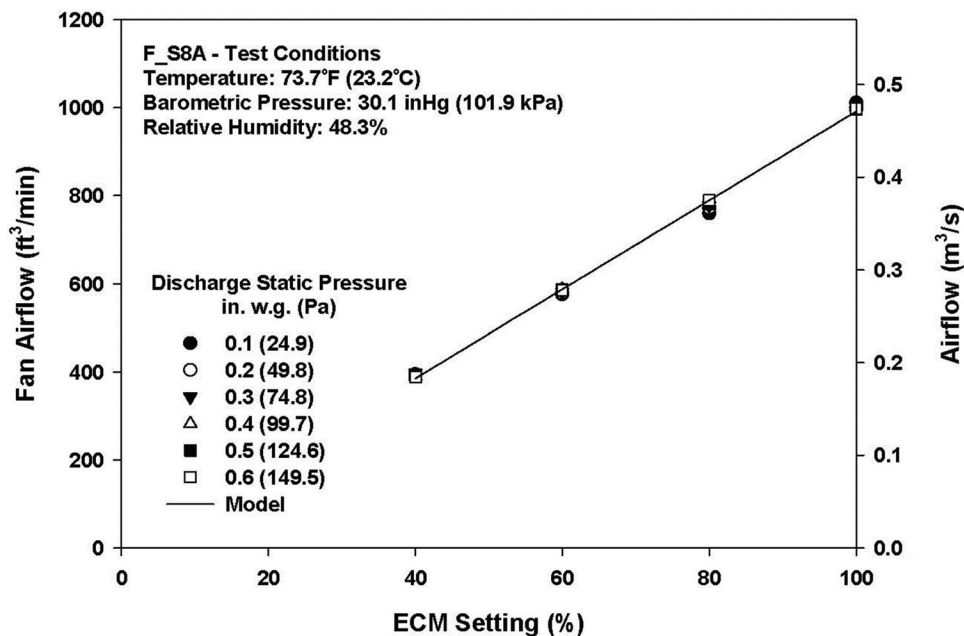


Figure 5 Fan airflow versus ECM setting for F_S8A.

and a linear relationship existed between these two variables. This observation confirmed the result reported by Edmondson et al. (2011b), who found that airflow delivered by ECM fans was primarily dependent on fan speed control signal and showed less dependence on inlet air velocity pressure.

ECM setting was chosen as the only input variable for the fan airflow model. Considering the variety in ECM controller input, a single variable was needed to describe the ECM setting for all the fans from different manufacturers. A dimensionless variable η was defined. It represented the percentage of input signal to the controller over the whole operating range.

A linear regression was conducted and Equation 1 was used to fit the experimental data.

$$\dot{Q}_{fan} = C_1 + C_2 \times \eta \quad (1)$$

C_1 and C_2 are empirical parameters estimated from the experimental data. They varied by terminal units. Figure 6 compares the model prediction with experimental measurement for fan airflow. The predicted and measured values were in close agreement with each other. The error was bounded within $\pm 10\%$ of measurement.

The empirical parameters and coefficient of determination (R^2) for developed model were reported in Table 4. All R^2 values were above 0.99. The agreement shown in Figure 6 and high R^2 values listed in Table 4 provided evidence that the model was adequate to characterize the fan airflow performance.

Fan Power

Figure 7 shows the fan-power consumption plotted against discharge static pressure for F_S8A. At a given ECM setting, fan power increased linearly when discharge static pressure was increased. At a given discharge static pressure, an increase in ECM setting always led to an increase in fan-power draw. The similar trend was also observed for the other fans. The two most important factors affecting fan power were ECM setting and discharge static pressure. So these two variables were used as the input variables for the fan-power model. The format of this model is shown in Equation 2.

$$\text{Power}_{fan} = C_1 \times \eta + C_2 \times \eta^2 + C_3 \times P_{discharge} \quad (2)$$

C_1 , C_2 , and C_3 are empirical parameters determined from the experimental data. A comparison between estimated and measured fan-power consumption for all the eight fans was shown in Figure 8. The prediction from the developed model closely matched the experimental data. The empirical parameters and R^2 values for developed fan-power model were listed in Table 5.

Fan/Motor Efficiency

The total and static efficiencies of each fan/motor combination were calculated from the experimental data. The total efficiency is defined as the ratio of fan/motor output to the fan/motor power input, as shown in Equation 3. The fan/motor static efficiency was determined from the total efficiency and the ratio of static pressure to total pressure using Equation 4.

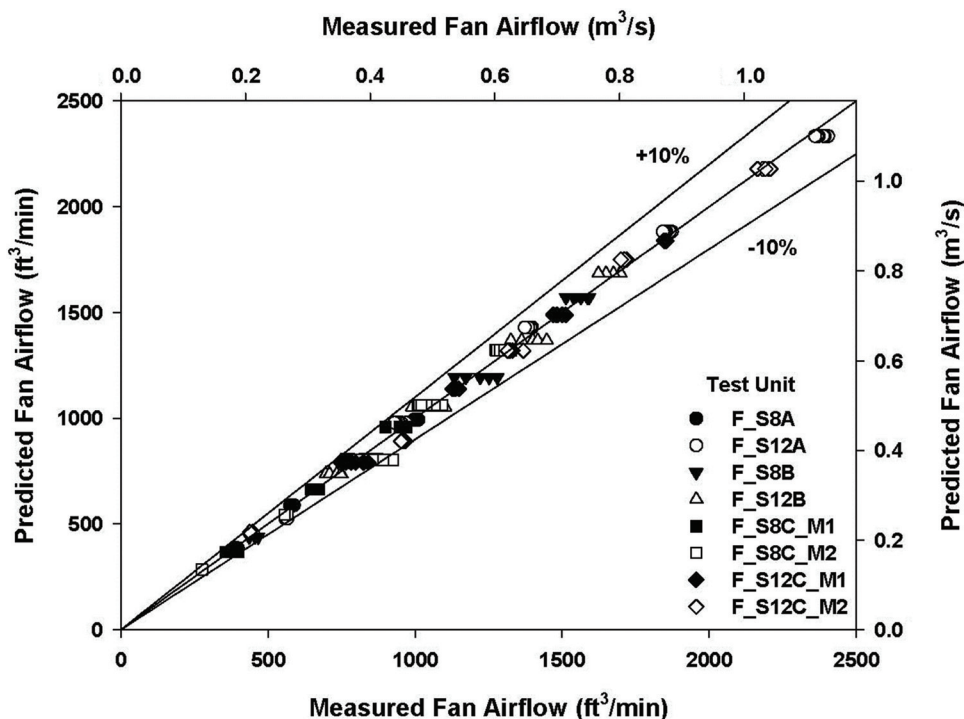


Figure 6 Comparison between measured and predicted fan airflow for all units.

Table 4. Empirical Parameters and R^2 Value for Fan Airflow Model

Fan	C_1	C_2	R^2
F_S8A	-19.258	10.110	0.998
F_S12A	73.093	22.607	0.996
F_S8B	60.233	15.119	0.994
F_S12B	420.260	12.639	0.994
F_S8C_M1	70.961	14.810	0.998
F_S8C_M2	24.375	12.974	0.990
F_S12C_M1	441.522	17.467	0.994
F_S12C_M2	32.695	21.458	0.995

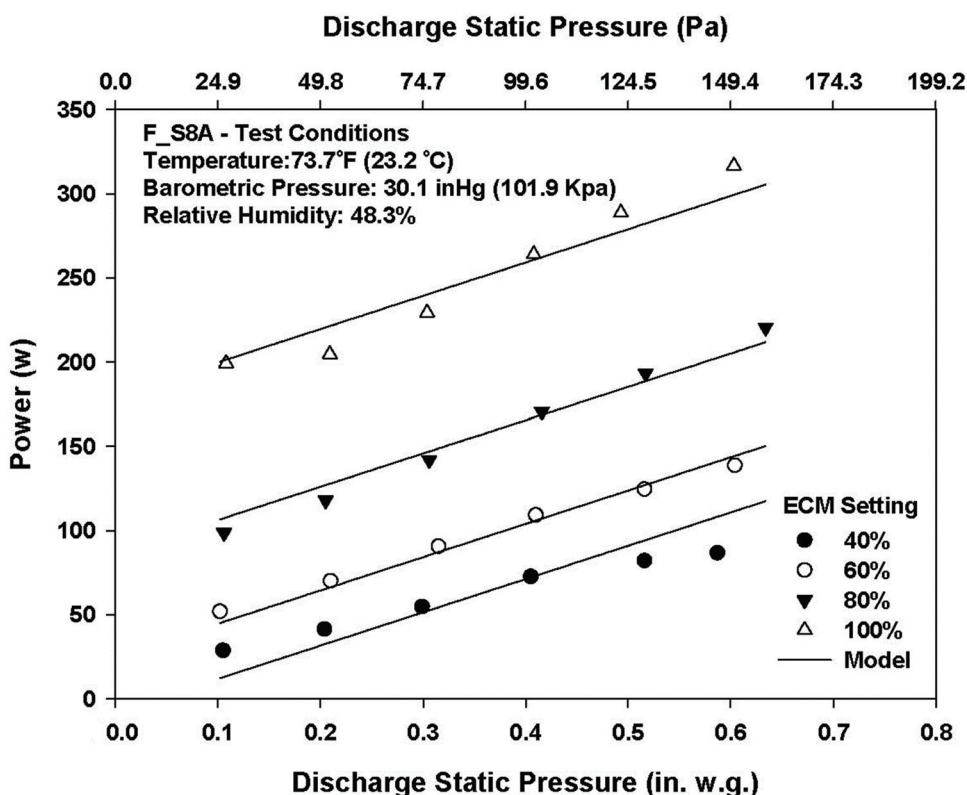


Figure 7 Fan-power performance at various ECM settings versus discharge static pressure for F_S8A.

Both equations were adopted from ASHRAE Standard 51 (ASHRAE 2007). In these equations, P_t and P_s are the total and static pressure changes across a fan. Since fans were tested in the configuration of open inlet in this study, the total pressure at the fan inlet was considered equal to 0. The fan total pressure change was numerically equal to the total pressure at the fan outlet, which is calculated from Equation 5. P_v is velocity pressure and calculated from Equation 6.

$$\eta_t = \frac{Q_{fan} P_t}{Power_{fan}} \quad (3)$$

$$\eta_s = \eta_t \left(\frac{P_s}{P_t} \right) \quad (4)$$

$$P_t = P_v + P_s \quad (5)$$

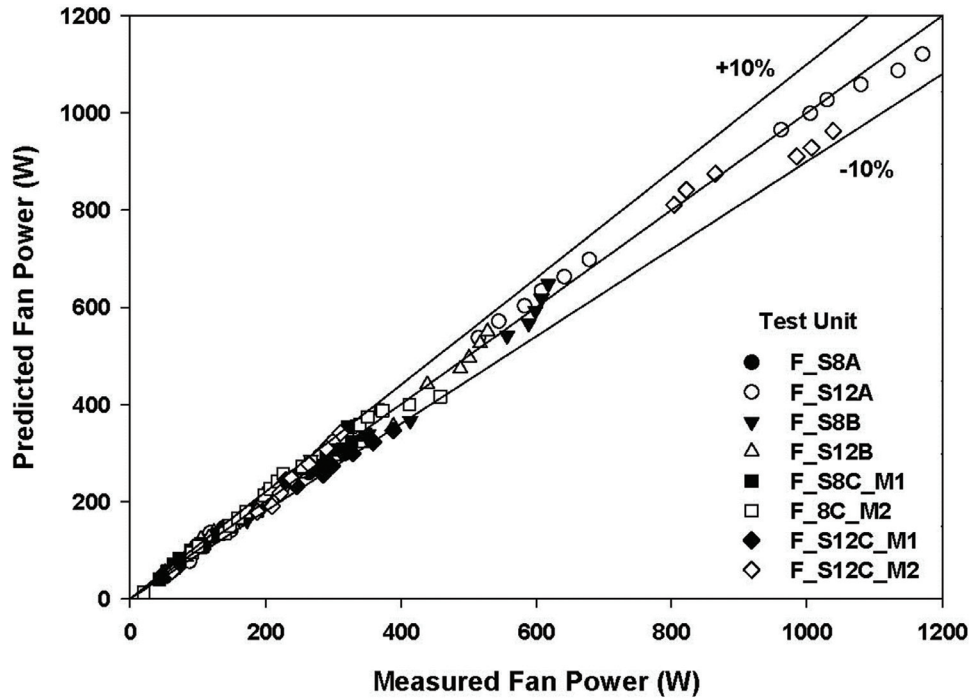


Figure 8 Comparison between measured and predicted fan power for all units.

Table 5. Empirical Parameter and R^2 Value for the Fan-Power Model

Fan	C_1	C_2	C_3	R^2
F_S8A	-1.631	0.0341	199.283	0.985
F_S12A	-5.760	0.151	316.009	0.995
F_S8B	-3.041	0.0814	275.299	0.990
F_S12B	-1.181	0.0533	272.298	0.993
F_S8C_M1	-1.673	0.104	160.150	0.995
F_S8C_M2	-1.035	0.0459	152.260	0.976
F_S12C_M1	2.102	0.0289	229.583	0.977
F_S12C_M2	-4.391	0.125	306.752	0.980

$$P_v = \frac{\rho}{2} \times \left(\frac{Q_{fan}}{A} \right)^2 \quad (6)$$

Although fan/motor combinations from different series FPTUs did not perform the same, they did share some common characteristics. Figure 9 shows the fan/motor total efficiency for F_S8A. For a given discharge static pressure, the total efficiency increased following an increase in airflow. At 0.1 in. wg (24.9 Pa), total efficiency increased from 28% to 33% when the airflow increased from 390 to 1000 ft³/min (0.18 to 0.47 m³/s). The same trend was also observed in the other pressure settings. For a given airflow rate, the increase in

discharge static pressure has a positive impact on total efficiency. For example, at the airflow of 1000 ft³/min (0.47 m³/s), the total efficiency increased from 33% to 39% as the pressure was increased from 0.1 in. wg to 0.6 in. wg (24.9 to 149.5 Pa).

Figure 10 shows the fan/motor static efficiency for F_S8A. The static efficiency increased with increasing discharge static pressure and decreased with increasing airflow. For a given airflow rate, both fan/motor total and static efficiency increased with increasing discharge static pressure. However, for a given static pressure, the fan/motor static efficiency decreased dramatically when fan airflow rate

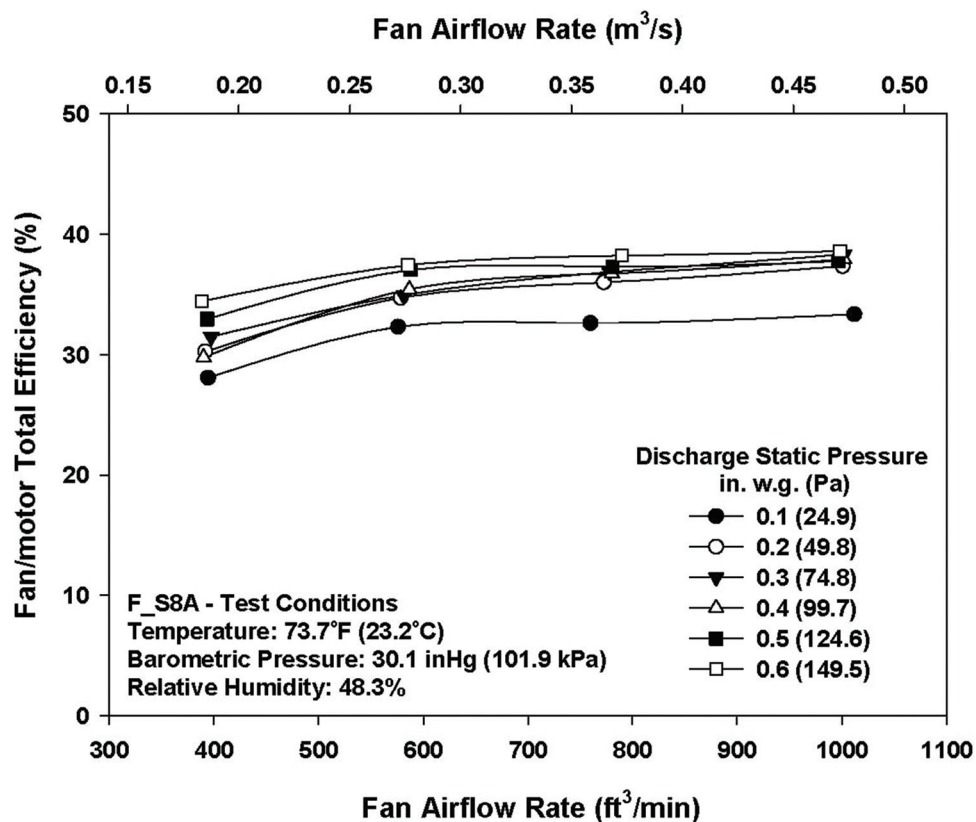


Figure 9 Fan/motor total efficiency for F_S8A.

increased. Overall, the eight fan/motor combinations had total efficiencies ranging from 11% to 50% and static efficiencies ranging from 1% to 22% at their maximum speed.

Both Figures 9 and 10 show that fan/motor efficiencies vary significantly with discharge static pressure and airflow rate. The data for all eight fan/motor combinations showed an even wider variation. These plots and data for the remaining fan/motor combinations show the difficulty of picking a single value to represent the fan efficiency, as required in EnergyPlus (2012a, 2012b).

Power Factor

Power factor is defined as the ratio of the real to apparent power. Figure 11 shows the power factor for F_S8A. The power factor increased responding to increasing discharge static pressure. Also, when the fan was operating at higher speeds, the power factor tended to increase. From the test results of the eight fan/motor combinations, the power factor varied between 0.27 and 0.56, which was consistent with the previous measurement (Edmondson et al. 2011b)

SUMMARY AND CONCLUSIONS

In the previous studies of Furr et al. (2008c) and Edmondson et al. (2011b), they developed detailed semi-empirical performance models for series FPTUs with PSC and ECM motors, respectively. However, due to the complexity in aero-

dynamic conditions and flow patterns within series FPTUs, they applied the black box approach and simply correlated the airflow and power performance with the measurement of peripheral pressures. This approach limited their models that were only applicable to certain units at specific working conditions. In this study, the component approach was taken. The ultimate goal of this research is to characterize the performance of series FPTUs by combining the models of individual components, namely fan/motor/controller, damper, and housing.

Eight fan/motor/controllers were removed from the series FPTUs used by Edmondson et al. (2011b) and tested as stand-alone units. The models of airflow and power consumption were generated from the measured data. In the airflow model, the nondimensional ECM setting was taken as the single input since the ECM fan was able to provide constant airflow regardless of pressure changes. The R^2 values of this model were all above 0.99. The fan/motor power consumption model also correlated well with measured data and had R^2 values ranging from 0.976 to 0.995. Comparisons were made between predicted and measured data in airflow and power consumption. The results indicated that the prediction using developed models can be as accurate as $\pm 10\%$ of measurement.

Estimations of fan airflow and power consumption are required to characterize the performance of series FPTUs in the

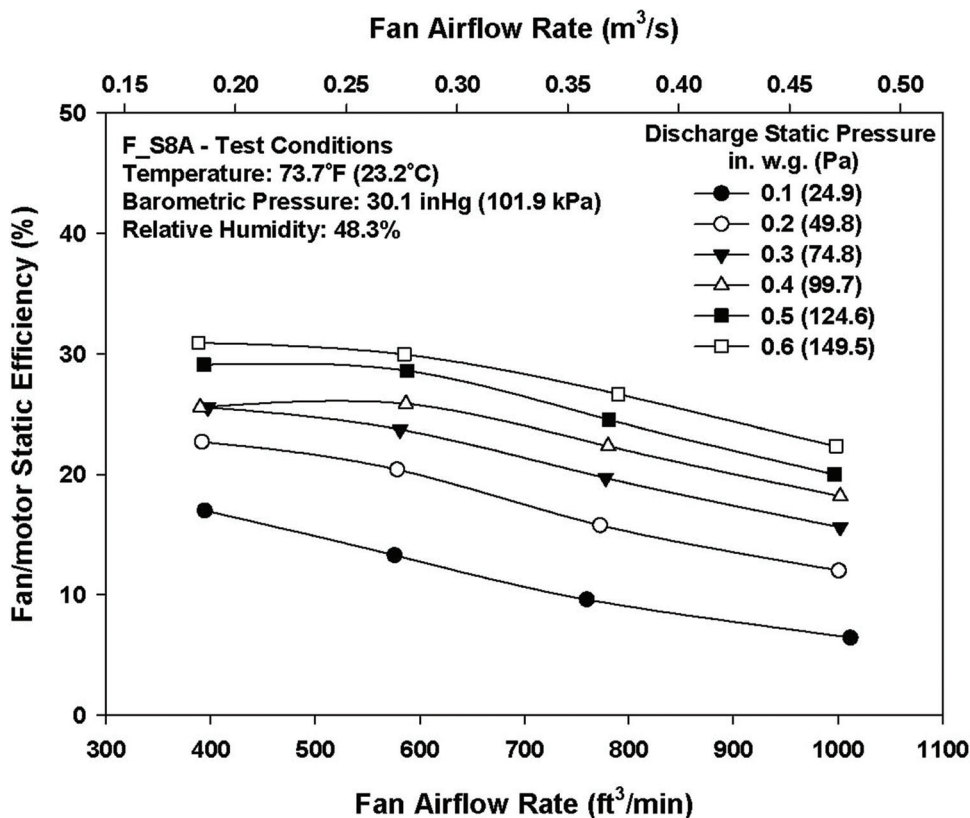


Figure 10 Fan/motor static efficiency for F_S8A.

component-based modeling approach. Models produced in this paper can be used to predict the airflow and power performance of fans with ECM motors in series FPTUs, and thus can be used as the submodels to evaluate the whole terminal unit performance. This is the first part of this study. In Part II, the experimental results and empirical models of primary and plenum airflow will be introduced. In addition, the development of a system model of series FPTU using component-based modeling approach will be discussed. Model validation against experimental data will also be presented.

NOMENCLATURE

A	= cross-sectional area of duct at fan outlet, ft ² (m ²)
$P_{\text{discharge}}$	= discharge static pressure, in. wg (Pa)
$\text{Power}_{\text{fan}}$	= power consumption of terminal unit fan/motor, W
P_s	= fan static pressure, in. wg (Pa)
P_t	= fan total pressure, in. wg (Pa)
P_v	= fan velocity pressure, in. wg (Pa)
Q_{fan}	= amount of airflow through terminal unit fan, ft ³ /min (m ³ /s)
η	= percentage of the controller voltage over the whole operating range
η_t	= fan/motor total efficiency, %

η_s	= fan/motor static efficiency, %
ρ	= air density, lb _m /ft ³ (kg/m ³)

REFERENCES

- ASHRAE. 1996. ANSI/ASHRAE Standard 130-1996, *Methods of Testing Air Terminal Units*. Atlanta: ASHRAE.
- ASHRAE. 2007. ANSI/ASHRAE Standard 51-2007, *Laboratory Methods of Testing Fans for Certified Aerodynamic Performance Rating*. Atlanta: ASHRAE.
- ASHRAE. 2012. *ASHRAE Handbook—HVAC Systems and Equipment*. Atlanta: ASHRAE.
- CEC. 2005. *Nonresidential Compliance Manual for California's 2005 Energy Efficiency Standards*. Sacramento: California Energy Commission.
- Edmondson, J., D.L. O'Neal, J.A. Bryant, and M.A. Davis. 2011a. Performance of parallel fan-powered terminal units with electronically commutated motors. *ASHRAE Transactions* 117(2):885–93.
- Edmondson, J., D.L. O'Neal, J.A. Bryant, and M.A. Davis. 2011b. Performance of series fan-powered terminal units with electronically commutated motors. *ASHRAE Transactions* 117(2):876–84.
- EnergyPlus. 2012a. *EnergyPlus Engineering Reference: The Reference to EnergyPlus Calculations*. Berkeley: Lawrence Berkeley National Laboratory.

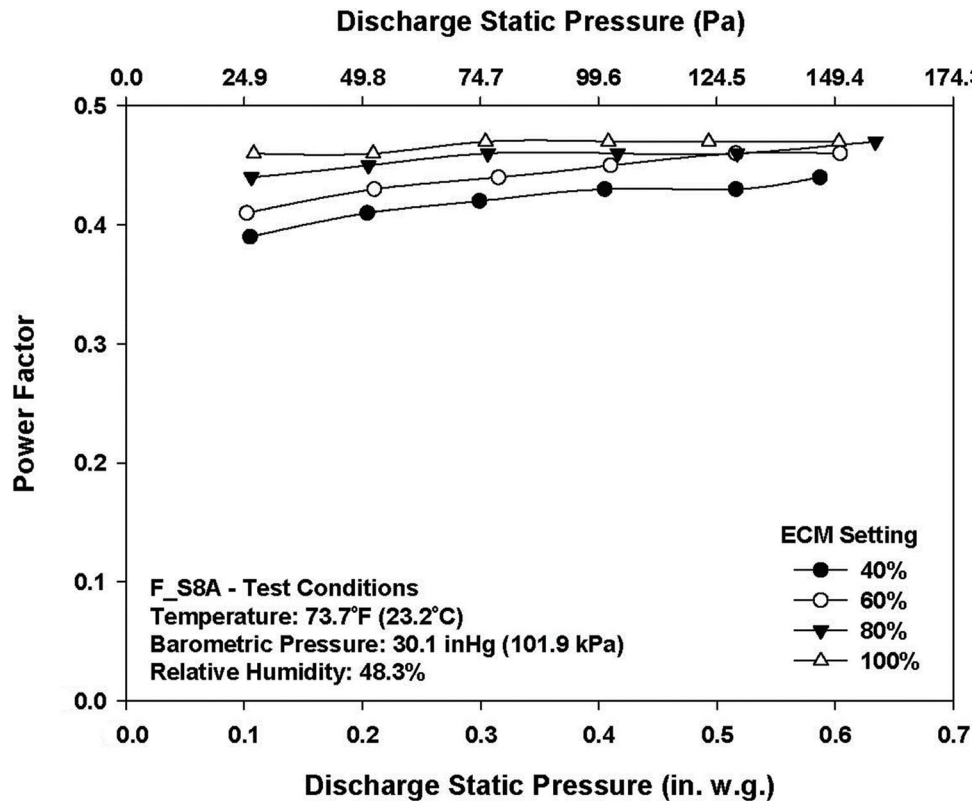


Figure 11 Power factor for F_S8A.

EnergyPlus. 2012b. *Input Output Reference: The Encyclopedic Reference to EnergyPlus Input and Output*. Berkeley: Lawrence Berkeley National Laboratory.

Furr, J., D.L. O'Neal, M. Davis, J.A. Bryant, and A. Cramlet. 2008a. Performance of VAV fan-powered terminal units: Experimental setup and methodology. *ASHRAE Transactions* 114(1):75–82.

Furr, J., D.L. O'Neal, M. Davis, J.A. Bryant, and A. Cramlet. 2008b. Performance of VAV parallel fan-powered terminal units: Experimental results and models. *ASHRAE Transactions* 114(1):83–90.

Furr, J., D.L. O'Neal, M. Davis, J.A. Bryant, and A. Cramlet. 2008c. Performance of VAV series fan-powered terminal units: Experimental results and models. *ASHRAE Transactions* 114(1):91–7.

Kenty, K.L. 2007. Use of electronically commutated motors (ECMs) in air terminal unit. *ASHRAE Transactions* 113(1):334–41.

Roth, K.W., A. Chertok, J. Dieckmann, and J. Brodrick. 2004. Electronically commutated permanent magnet motors. *ASHRAE Journal* 46(3):75–76.

SE-14-026

Characterizing Airflow and Power of VAV Series Fan-Powered Terminal Units from Component Data—Part II

Peng Yin

Student Member ASHRAE

Dennis L. O'Neal, PhD, PE

Fellow ASHRAE

ABSTRACT

The goal of this study was to investigate how well the performance of a series fan-powered terminal unit (FPTU) could be predicted by combining the models of its individual components, namely fan/motor/controller, damper, and housing. Eight series FPTUs, from three manufacturers, with electronically commutated motors (ECMs) were investigated. In Part I of this paper, the fan airflow and power performance were experimentally studied. The corresponding empirical models were established from the measured data. Part II of this paper described the development of primary and plenum airflow models by testing dampers and housings. The primary airflow model predicted the airflow through dampers as a function of damper angles and damper differential pressures. The plenum airflow model estimated the amount of air induced into housings by using the housing differential pressures and plenum air inlet areas. The overall performance of a series FPTU was evaluated by systematically assembling its component models.

Comparisons were made between model outputs and experimental data from previous studies. While the predicted airflows were in agreement with measurements, the component-based model underestimated fan-power consumptions for some units. This discrepancy may be caused by fan-system effects that occur as a consequence of flow mixing and swirl inside housings. These flow distortions create a condition that is different from the condition used in the laboratory fan tests.

INTRODUCTION

Series fan-powered terminal units (FPTUs) are designed to provide a constant airflow to a thermal zone by mixing primary and plenum air. An FPTU consists of a fan, a damper, and a

housing. The fan is driven by a small motor and acts to draw the air in the plenum space into the housing. The damper at the primary air inlet is used to modulate the conditioned air. For example, the damper is completely open when the maximum cooling capacity is required. As the cooling load decreases, the damper gradually closes to throttle the primary air until it reaches its preset minimum stop position. At the same time, the fan draws more air from the plenum space to compensate for the primary air reduction. By adjusting the ratio of primary and plenum air, the temperature setpoint can be maintained without reducing the amount of supply air. In addition, an optional heating coil can be employed for supplemental heat.

To properly simulate variable-air-volume (VAV) systems with FPTUs, it is important to be able to characterize the performance of individual terminal units. Furr et al. (2008a, 2008b, and 2008c) and Edmondson et al. (2011a and 2011b) measured airflows, pressures, and power consumption of FPTUs with permanent-split capacitor (PSC) motors and electronically commutated motors (ECMs), respectively. They developed empirical models of airflows and power consumption by fitting the experimental data to second-order polynomials. Because of the complexity in aerodynamic conditions and airflow patterns within FPTUs, both Furr et al. (2008a, 2008b, and 2008c) and Edmondson et al. (2011a and 2011b) treated FPTUs as “black boxes.” They mainly focused on correlating the airflow and power data with peripheral pressure measurements. This approach limited the application of their models to specific terminal units that operated over a set of specific pressure conditions.

Because all series FPTUs have the same components and share a similar structure, the question was raised whether the overall performance of a series FPTU could be predicted by its component models. Figure 1 shows an idealized static pres-

Peng Yin is a PhD student in Mechanical Engineering at Texas A&M University, College Station, TX. **Dennis L. O'Neal** is a professor and dean of Engineering and Computer Science at Baylor University, Waco, TX.

sure change with gradients referenced to atmospheric pressure in a series FPTU and its adjacent ducts. The fan's continuous operation creates a negative pressure, P_{internal} , inside the housing. The plenum airflow is driven by the pressure difference between the P_{internal} and ambient pressure. The primary airflow is affected by the upstream differential pressure, which is the difference between upstream static pressure, P_{upstream} , and the P_{internal} . The fan performance is also influenced by the downstream differential pressure, which is the difference between the downstream static pressure, $P_{\text{downstream}}$, and the P_{internal} . As can be seen, the P_{internal} is important in modeling the overall performance of series FPTUs in the component-based approach because it affects all three airstreams entering and leaving a series FPTU. Edmondson et al. (2011b) pointed out that his primary airflow model could be improved if the P_{internal} were measured and used in the model development, but this pressure was not monitored in previous studies.

As an extension of previous work conducted by Furr et al. (2008a, 2008b, and 2008c) and Edmondson et al. (2011a and 2011b), this study examines how well the performance of a series FPTU could be evaluated by combining the models of its individual components, namely fan/motor/controller, damper, and housing. In Part I of this paper, fan airflow and power performance were experimentally studied. The corresponding empirical models were established from the measured data. Part II of this paper describes the development of primary and plenum airflow models by testing dampers and housings. The overall performance of a series FPTU was evaluated by systematically assembling its component models. Moreover, the model verification was made by comparing model outputs with the experimental data.

EXPERIMENTAL SETUPS AND PROCEDURES

Eight series FPTUs from three manufacturers were investigated. These units are the same FPTUs that were used by Edmondson (2011b) in his study, which provides a more detailed description of the units. All units were equipped with ECM motors. The three manufacturers who provided units for this study were designated as manufacturers A, B, and C. Two primary inlet sizes were encountered: 8 in. (203 mm) and 12 in. (304 mm). Each terminal unit was labelled according to inlet sizes and manufacturer. For example, a 12 in. (304 mm) terminal unit from Manufacturer B was labelled as S12B. Two types of primary air inlet dampers were provided: butterfly (BF) and opposed-blade (OB). Each damper was labelled by the type and size. For example, an 8 in. (203 mm) butterfly damper was designated as BF8 whereas, OB12 was assigned to a 12 in. (304 mm) opposed-blade damper. This section introduces the experimental setup and the test matrix for the determination of damper and housing characteristics.

Apparatus for the Damper Testing

A damper is used to modulate the amount of conditioned air delivered to a series FPTU. Damper characteristics were experimentally determined for the development of the primary airflow model. Legg (1984 and 1986) established a series of empirical correlations between damper angles and damper pressure loss coefficients. The same correlations were used in this study for the development of primary airflow model.

Figure 2 shows the experimental setup for the damper testing in this study. It consisted of a damper, a supply duct,

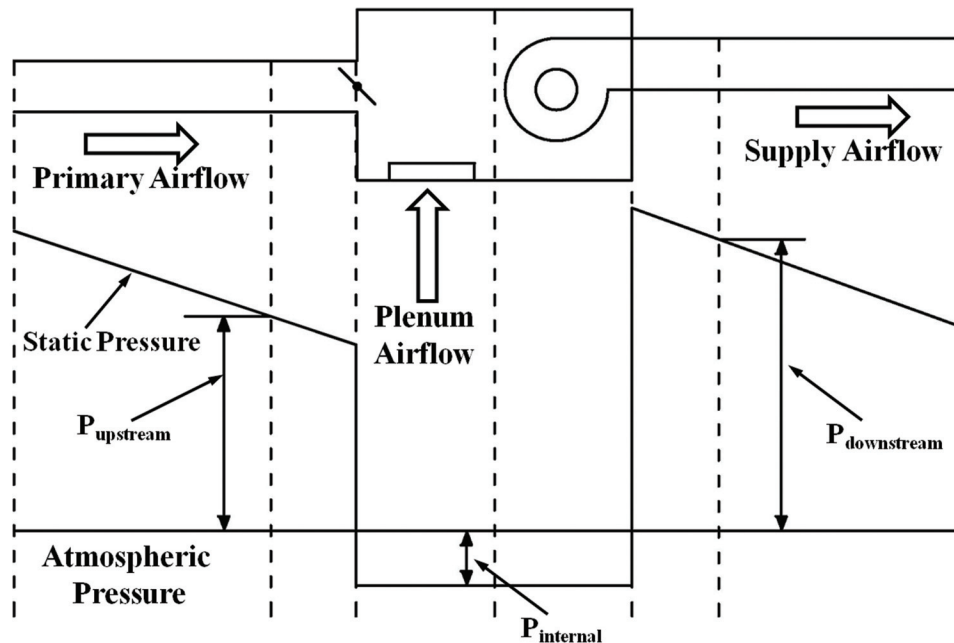


Figure 1 Static pressure change in series FPTUs and its adjacent ducts.

and an airflow chamber. Dampers were removed from series FPTUs and directly connected to the airflow chamber through a circular sheet metal duct with a length of 2.5 hydraulic diameters. This duct had the same cross-sectional dimensions as the damper and was constructed in accordance with ASHRAE Standard 120 (ASHRAE 2008).

Airflow measurements were taken by using the inlet airflow chamber, which was built following the requirements of ASHRAE Standard 51 (ASHRAE 2007). It had a nozzle board consisting of two 3 in. (76 mm), two 4 in. (102 mm), two 6 in. (152 mm), and one 7 in. (178 mm) nozzles. An assist blower equipped with a variable-frequency drive (VFD) was attached to the chamber. It was used to vary the $P_{upstream}$ by adjusting the rotational speed.

Two control variables were the damper positions and the $P_{upstream}$. Damper position was described in terms of the damper tilt angle, which was defined as the degree of the angle formed by the blade relative to the duct axis. For a BF configuration, 0° indicated a fully open damper, while 90° represented a fully closed damper. For an OB configuration, 0° indicated a fully open damper, while 45° represented a fully closed damper. Damper angles were controlled by an actuator which took direct current (DC) voltage as a control signal. During the testing, both types of dampers were set at 100% open in the beginning, and then gradually closed by 10% of their operating range until they reached the preset minimum stop position. It was set at 72° for the BF dampers and 40.5° for the OB dampers in this study due to the limitation of minimum measurable airflow rate caused by using the damper test-

ing setup. Table 1 shows the variable ranges for the damper testing. Tilt angle above these limits were not studied because dampers in series FPTUs are seldom in fully closed position because a minimum primary air is needed for ventilation requirements. In addition, it is hard to obtain an accurate measurement in the nearly closed region given the fact that only an extremely small amount of air was allowed to pass through the damper at these positions. The nozzle differential pressures generated from this small airflow were too low to be accurately measured. The $P_{upstream}$ was varied from 0.25 to 1.5 in. w.g. (62 to 374 Pa) by using 0.25 in. w.g. (62 Pa) increments at each damper position.

Apparatus for Housing Testing

The plenum airflow is driven by the pressure differential across the FPTU housings. The experimental setup for the housing testing is shown in Figure 3. It was similar to the setup that was used in the damper testing except that an outlet chamber was used, rather than an inlet chamber. This outlet cham-

Table 1. Damper Test Variable Ranges

Damper Type	Operating Range (Degree)	Control Voltage (Volt)	Voltage Increment (Volt)	Test Point
BF	0–72	0–8	1	9
OB	0–40.5	0–4.5	0.5	10

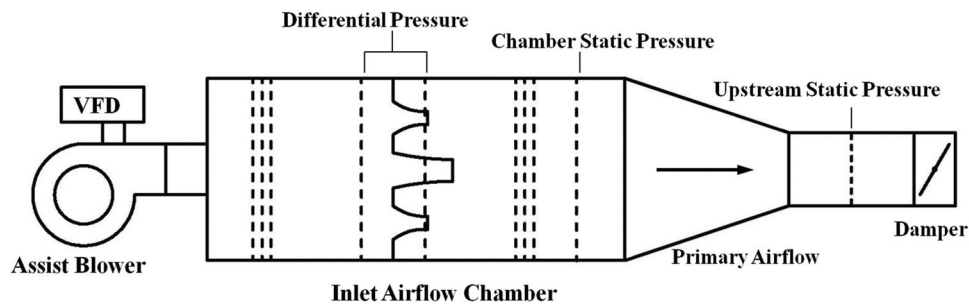


Figure 2 Primary airflow test apparatus, including chamber and assist blower.

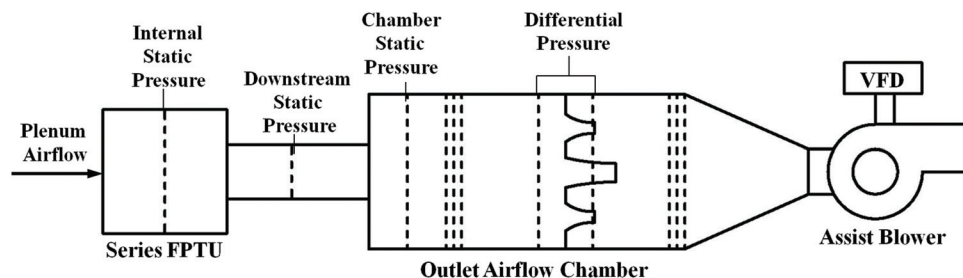


Figure 3 Plenum airflow test apparatus, including chamber and assist blower.

ber was constructed according to ASHRAE Standard 51 (ASHRAE 2007). It came with one 1 in. (25 mm), one 3 in. (76 mm), and four 5 in. (127 mm) nozzles.

The housings of series FPTUs were connected to the airflow chamber through a rectangular sheet metal duct. The fan was removed and the primary air inlet was blocked to eliminate the interference from the other airstreams. By adjusting the speed of the assist blower, the P_{internal} was varied from -0.01 to -0.2 in. w.g. (-2.5 to -50.0 Pa) by using 0.01 in. w.g. (2.5 Pa) decrements.

In both damper and housing testing, the air density was calculated from the measurements of ambient temperature and relative humidity that were monitored by a stand-alone psychrometric station. Air pressures were measured by using pressure transducers with a 4–20 mA output. The airflow rate through the known open-nozzle areas was calculated following the procedure directly adopted from ASHRAE Standard 51 (ASHRAE 2007) by measuring the nozzle differential pressure and chamber static pressure. Raw airflow data were adjusted to the standard temperature and barometric pressure to compensate for environmental changes during the period of data collection. Table 2 shows the specifications for the instruments that were used in both tests.

The uncertainty in calculated airflow rate was the result of using various measurements, including temperature, relative humidity, and air pressures. Each of the measurements was associated with an uncertainty. Generally, the combined uncertainty for calculated airflow rates was within 1% when the nozzle differential pressures were maintained above 1 in. w.g. (249 Pa). The combined uncertainty increased in response to the decrease in nozzle differential pressures. When the differential pressure decreased from 1 to 0.05 in. w.g. (249 to 12.5 Pa), the combined uncertainty increased from 1% to 15% of the calculated airflow rate. This significant increase in

combined uncertainty imposed a limit on the minimum measurable airflow rate for both damper and housing testing. The limit was $40 \text{ ft}^3/\text{min}$ ($0.019 \text{ m}^3/\text{s}$) for the damper testing and $4.5 \text{ ft}^3/\text{min}$ ($0.002 \text{ m}^3/\text{s}$) for the housing testing, both of which were calculated at the nozzle differential pressure of 0.05 in. w.g. (12.5 Pa) by using the smallest nozzle. Since the measured plenum airflow rate was way above $4.5 \text{ ft}^3/\text{min}$ ($0.002 \text{ m}^3/\text{s}$), the housing testing was not affected by this limit. However, a restriction on damper angles had to be made to prevent the measured airflow rate from dropping below $40 \text{ ft}^3/\text{min}$ ($0.019 \text{ m}^3/\text{s}$). It was set at 72° for the BF dampers and 40.5° for the OB dampers.

EXPERIMENTAL RESULTS AND MODELS

Experimental data were collected to characterize dampers and housings from series FPTUs. Regression analysis was applied to the measured data for the development of primary and plenum airflow models.

Primary Airflow Model

The primary airflow was modeled as a function of the differential pressure across the damper $P_{\text{diff, damper}}$, the damper tilt angle θ , and damper sizes and types. The pressure loss coefficient of the dampers at a specific damper angle K_θ was calculated from Equation 1.

$$K_\theta = \frac{P_{\text{diff, damper}}}{\dot{Q}_{\text{primary}}^2} \times \frac{2A_\theta^2}{\rho_a} \quad (1)$$

The relationship between θ and K_θ was described by Equation 2.

$$\ln K_\theta = a_1 + b_1 \times \theta \quad (2)$$

The empirical constants a_1 and b_1 were determined from statistical fits of the data. Both Equation 1 and 2 were from Legg's correlations (1986). The damper open area at a specific damper tilt angle A_θ , is also a function of the θ . For BF and OB dampers, A_θ was calculated according to Equations 3 and 4.

$$A_\theta = (1 - \sin\theta) \times A_0 \quad (3)$$

$$A_\theta = (1 - \sqrt{2} \times \sin\theta) \times A_0 \quad (4)$$

The A_0 was the damper open area at the damper tilt angle of zero. After the K_θ was calculated from the measurements of pressure and airflow rate, it was fitted into Equation 2 for the estimation of empirical parameters. Tables 3 and 4 show these parameters for BF and OB dampers, respectively.

Figure 4 shows the primary airflow for OB8 plotted against the damper angle over a range of damper differential pressures. The curves in Figure 4 were generated from the model by using Equations 1 to 4. It can be seen that the flow rate through the damper was highly nonlinear with respect to damper angles and differential pressures. When the damper angle was in the region

Table 2. Instrument Specifications

Measurement	Sensor Specification
Ambient temperature	0°F–100°F (–17.8°C–37.8°C), ±0.7°F (±0.39°C)
Ambient relative humidity	0%–100%, ±2%
Chamber static pressure	0–10 in. w.g. (0–2492 Pa), ±0.25% full scale
Nozzle differential pressure	0–6 in. w.g. (0–1495 Pa), ±0.25% full scale
Upstream static pressure	0–2 in. w.g. (0–498 Pa), ±0.25% full scale
Internal static pressure	0–1 in. w.g. (0–249 Pa), ±0.25% full scale
Downstream static pressure	0–2 in. w.g. (0–498 Pa), ±0.25% full scale

below 10°, a small change in the damper angle would cause a significant change in airflows. In addition, the volumetric flow rate through the dampers increased in response to an increase in differential pressures. The results for the other dampers were similar to the plots shown in Figure 4. Good agreement was observed between measurements of primary airflow and model outputs. The current model fits the measured data well and can

be used to characterize the primary airflow over the range of operating conditions studied in this paper.

Plenum Airflow Model

The plenum airflow \dot{Q}_{plenum} was modeled as a function of two variables: the plenum differential pressure, P_d , and the plenum air inlet area, γ . The P_d was defined as the static pressure difference between the P_{internal} and the air gauge pressure in the plenum space, which is assumed to be zero. The γ was used to represent the nondimensional plenum air inlet area. It was defined as the ratio of the plenum air inlet area A_p to a constant, A_{max} , with a value of 252 in² (0.16 m²), as shown in Equation 5.

$$\gamma = \frac{A_p}{A_{\text{max}}} \quad (5)$$

There are two configurations for the plenum airflow. They differed in flow directions. When the flow direction of the plenum air was parallel to the primary air, this configuration was designated as the parallel arrangement. Manufacturers A and B employed this design. If the flow direction of the plenum air was perpendicular to the primary air, it was labelled as the perpendicular arrangement. Manufacturer C adopted this design.

Empirical models for both airflow arrangements shared the same format with different empirical parameters. Equation 6 was used to fit the experimental data. Two empirical parameters, a_2 and b_2 , were determined from the regression analysis. The estimated parameters and R^2 values for both airflow arrangements are listed in the Table 5.

$$\dot{Q}_{\text{plenum}} = \sqrt{P_d} \times (a_2 + b_2 \times \gamma^2) \quad (6)$$

Table 3. Empirical Parameter for Primary Airflow Model with Butterfly Damper

Damper Angle	BF8 ($R^2 = 0.992$)		BF12 ($R^2 = 0.956$)	
	a_1	b_1	a_1	b_1
0° to 9°	-14.1	0.0129	-15.06	-0.0065
9° to 54°	-14.295	0.0461	-14.963	0.0535
54° to 72°	-8.0979	-0.066	-13.992	0.0328

Table 4. Empirical Parameter for Primary Airflow Model with Opposed-Blade Damper

Damper Angle	OB8 ($R^2 = 0.990$)		OB12 ($R^2 = 0.926$)	
	a_1	b_1	a_1	b_1
0° to 4.5°	-14.186	0.0141	-14.976	-0.0527
4.5° to 27°	-14.187	0.0423	-14.815	0.0393
27° to 40.5°	-14.989	0.0724	-15.817	0.0704

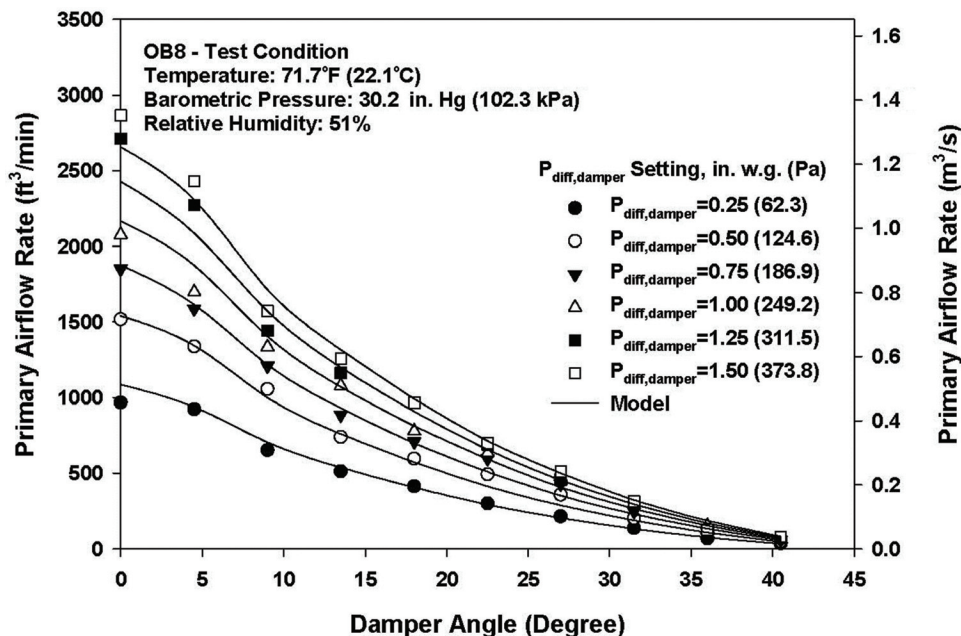


Figure 4 Primary airflow as a function of damper differential pressure and damper angle for OB8.

Table 5. Empirical Parameter and R^2 Value for Plenum Airflow Model

Configuration	a_2	b_2	R^2
Parallel arrangement	1530.113	3064.358	0.996
Perpendicular arrangement	4538.701	-943.824	0.997

As can be seen in Figure 5, the model outputs were consistent with the measured data of plenum airflow, which indicated that the developed model was capable of providing an accurate description of the plenum airflow.

SERIES FPTU MODEL

Figure 6 shows the mass balance of a series FPTU. There are four airstreams entering and exiting the terminal units. They are the primary, plenum, leakage, and fan airflows. The

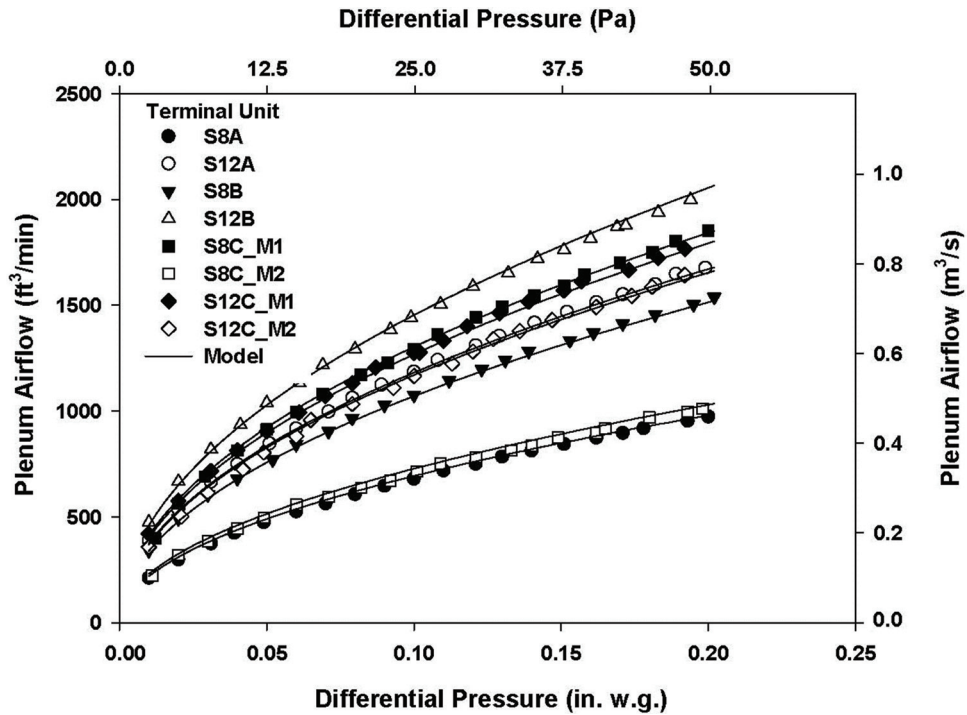


Figure 5 Plenum airflow under varying differential pressures.

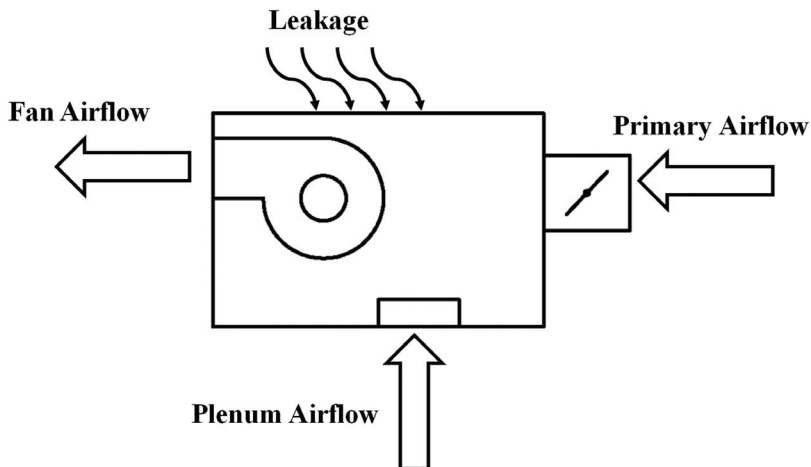


Figure 6 Volumetric balance for series FPTU.

fan airflow model was developed in Part I of this paper and is shown in Equation 7.

$$\dot{Q}_{fan} = C_1 + C_2 \times \eta \quad (7)$$

The primary and plenum airflows were modeled empirically by correlating the airflow data with pressure measurements. The leakage is not an issue because the air that is drawn into series FPTUs by leakages has the same properties as the plenum air due to the fact that they are induced from the same plenum space. Leakages in series FPTUs just offset the amount of air that would have been drawn into housings through plenum air inlets.

Equation 8 was developed by applying the mass conservation equation on series FPTUs.

$$\frac{dm}{dt} = \sum \dot{m}_{in} - \sum \dot{m}_{out} \quad (8)$$

Three assumptions were made to simplify this equation. First, this model was only applicable to series FPTUs that were operating in the steady-state condition, which implies the term on the left hand side of Equation 8 is zero. Second, the air density was assumed constant given the fact that the unconditioned laboratory air was used in all experiments. In addition, previous results indicated that the effect on density changes due to heat gains from terminal unit fans was less than 1% (Cramlet 2008). The third assumption was that leakages were negligible. Based on these three assumptions, Equation 8 was simplified into Equation 9.

$$\dot{Q}_{primary} + \dot{Q}_{plenup} = \dot{Q}_{fan} \quad (9)$$

The overall airflow performance of series FPTUs was estimated by solving Equations 1, 2, 6, 7, and 9 simultaneously. It should be noted that the $P_{internal}$ was unknown and required by both the primary and plenum airflow models. In this group of equations, the variables γ , η , θ , and $P_{upstream}$ were known for a given operating condition. The variable γ was constant for a specific terminal unit, the variable η was available from ECM settings, and the variable θ could be calculated from the damper control voltage. The $P_{upstream}$ could be measured directly. The $\dot{Q}_{primary}$, \dot{Q}_{plenup} , \dot{Q}_{fan} , and $P_{internal}$ were variables to be solved.

Once the $P_{internal}$ was available, the fan pressure rise could be determined by subtracting the $P_{internal}$ from $P_{downstream}$, and then the fan power could be evaluated by applying Equation 10.

$$Power_{fan} = a_4 \times \eta + b_4 \times \eta^2 + c_4 \times (P_{downstream} - P_{internal}) \quad (10)$$

A program using iteration procedures was developed to solve the group of equations. Figure 7 shows the flow chart of the algorithm used to determine the overall performance of series FPTUs.

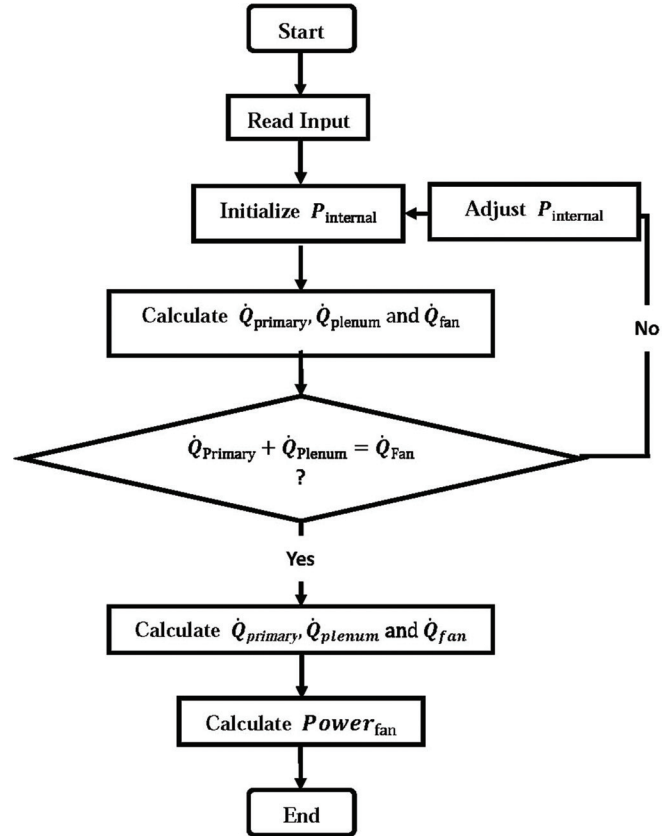


Figure 7 Flowchart of series FPTU operation.

COMPARISONS OF MODEL OUTPUTS AND EXPERIMENTAL DATA

Results from the developed model of series FPTUs were compared with the experimental data previously published by Edmondson et al. (2011b). The prior data included airflow and power measurements from eight series FPTUs that operated at various combined conditions of pressures, fan speeds, and damper settings (Edmondson et al. 2011b). The same operating conditions used by Edmondson were inputted into the component-based model of series FPTUs. Model outputs and experimental data were plotted in Figures 8–12 for comparison.

Figure 8 shows the comparison of plenum airflow for terminal unit S8A. The experimental data were inferred from the published data of Edmondson et al. (2011b) because there was no direct measurement on the plenum airflow. The plenum airflow increased in response to increasing differential pressures. The model output was capable of capturing this trend and agreed with the experimental data.

Comparisons of fan airflows and power consumptions are shown in Figures 9 and 10. Due to discrete ECM settings in the

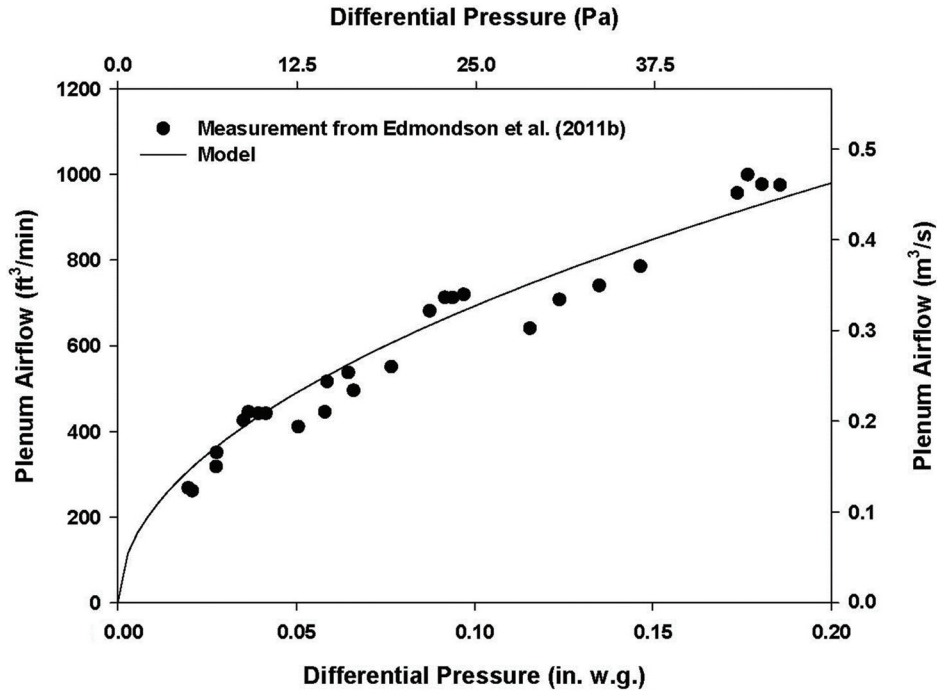


Figure 8 Measured and predicted plenum airflow for terminal unit S8A.

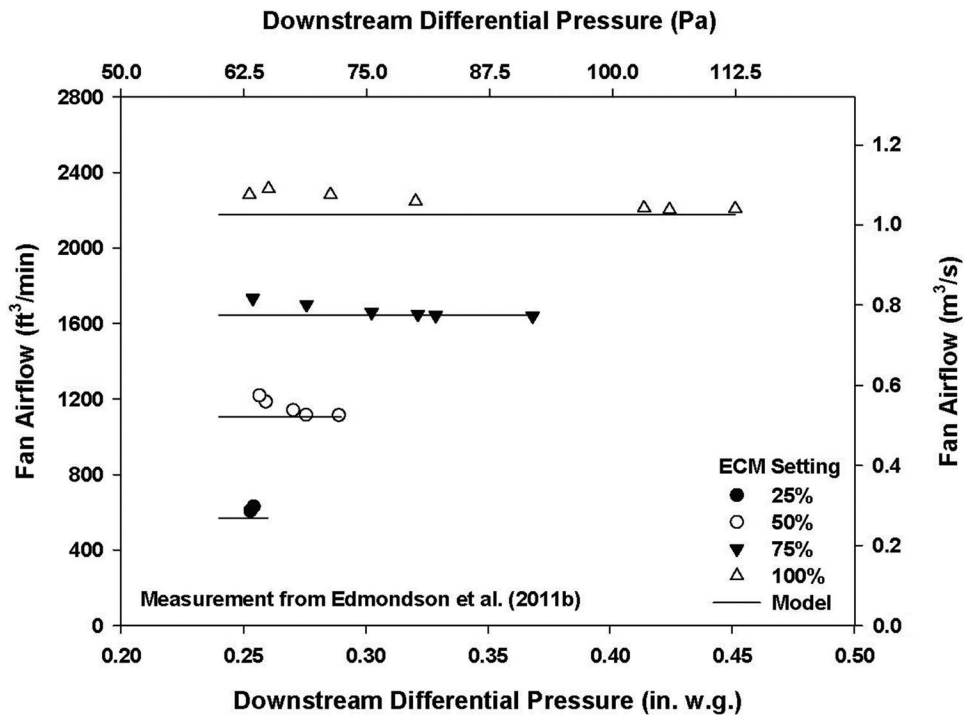


Figure 9 Measured and predicted fan airflow for terminal unit S12C_M2.

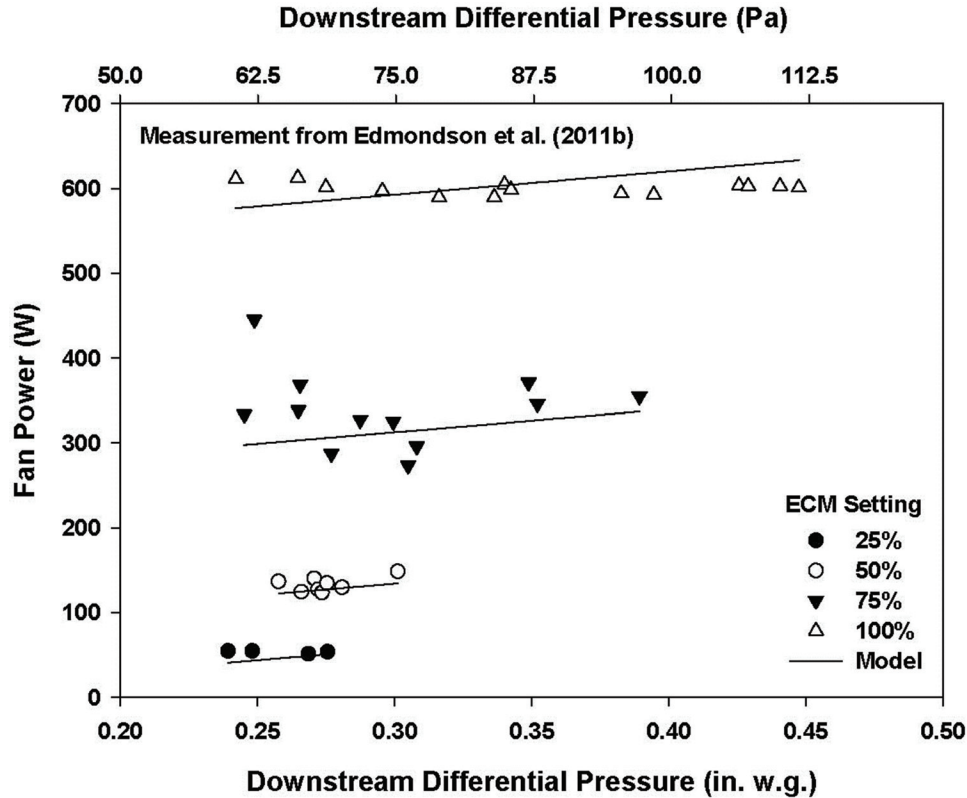


Figure 10 Measured and predicted fan-power consumption for terminal unit S8B.

previous tests, measured data in both figures fell into four separated groups. Because fans with ECMs were able to maintain a constant airflow rate regardless of pressure changes, the measured fan airflow data were nearly constant over the pressure range shown in Figure 9. The model used a series of nearly horizontal lines to represent this characteristic of ECM fans. Fan-power consumption was primarily dependent on airflow, which was controlled by the ECM setting. When ECM settings were increased, more air was delivered by ECM fans, and thus more power was consumed. In both figures, model outputs were in agreement with the experimental data.

Figure 11 shows the primary airflow over a range of damper settings for terminal unit S8B. Edmondson et al. (2011b) measured the primary airflow at four damper settings for a range of P_{upstream} from 0.1 to 2.0 in. w.g. (25 to 498 Pa). For a given damper setting, airflows increased with increasing differential pressures. The model output was consistent with the trends in the experimental data, but generally underpredicted the primary airflow. One possible reason for this discrepancy was the difference between approaches in the model development and terminal unit configurations. In a real system, the damper is located in the housing of an FPTU. While in the model development, the damper was removed from the housing and tested separately. It is possible that the flow mechanics within the housing were different enough to affect the performance of the damper, compared with the conditions at which the damper was tested as an individual component.

The model underpredicted the fan-power consumption for some terminal units. Figure 12 shows the fan-power consumption of terminal unit S8A. For each ECM setting, the estimated power from the model was lower than measured data. This discrepancy was also observed for terminal units S12A, S12C_M1, and S8C_M1. It could have been caused by fan-system effects within the housings. These were not captured when fans were removed from housings and tested as stand-alone components in the laboratory testing. The fan-power consumption model was developed by testing fans without housings under the condition of a free inlet with a ducted outlet. This test configuration did not include the effect of obstructions in the fan inlet, such as influences from swirl flows created by the primary damper or distorted flows created by mixing the primary and plenum air. For some units, the induced plenum air comes into housings at a 90° angle from the primary air. The mixing process would tend to distort the flow to the side of the housing opposite the plenum air inlet. This distortion should provide a fan-system effect that would result in different fan performance from the measurements that were taken for the model development. It would appear that when the fans are installed inside housings, there is a negative impact on fan performance. It leads to an increase in fan-power consumptions for delivering the same amount of air compared to the stand-alone configuration.

Kenty (2007) examined the impact of the plenum air inlet size on the power draw of a PSC motor in a series FPTU by

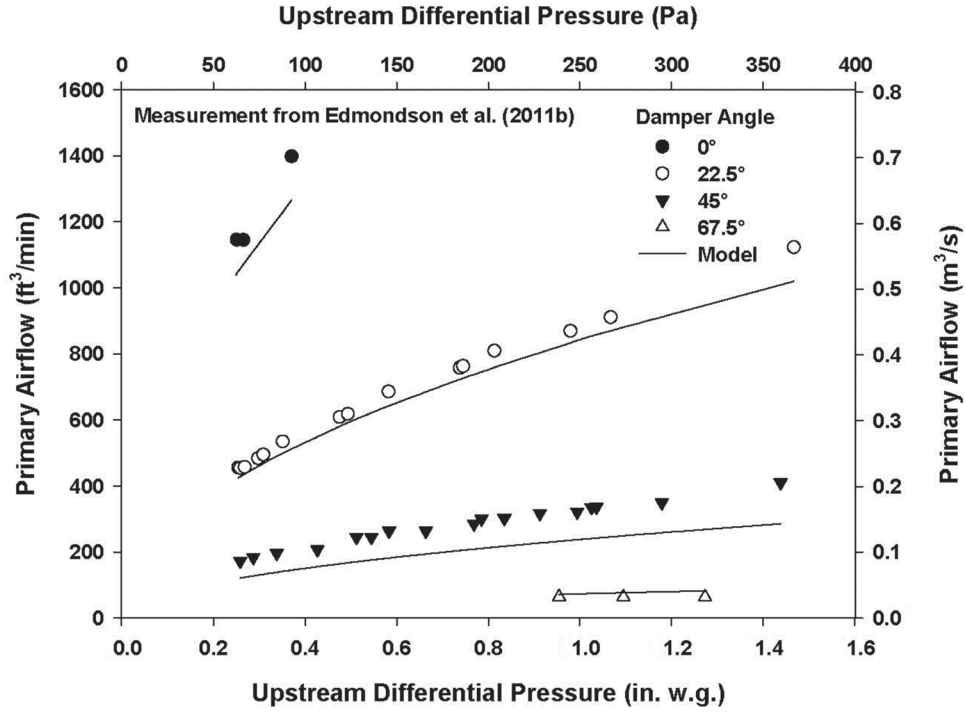


Figure 11 Measured and predicted primary airflow for terminal unit S8B.

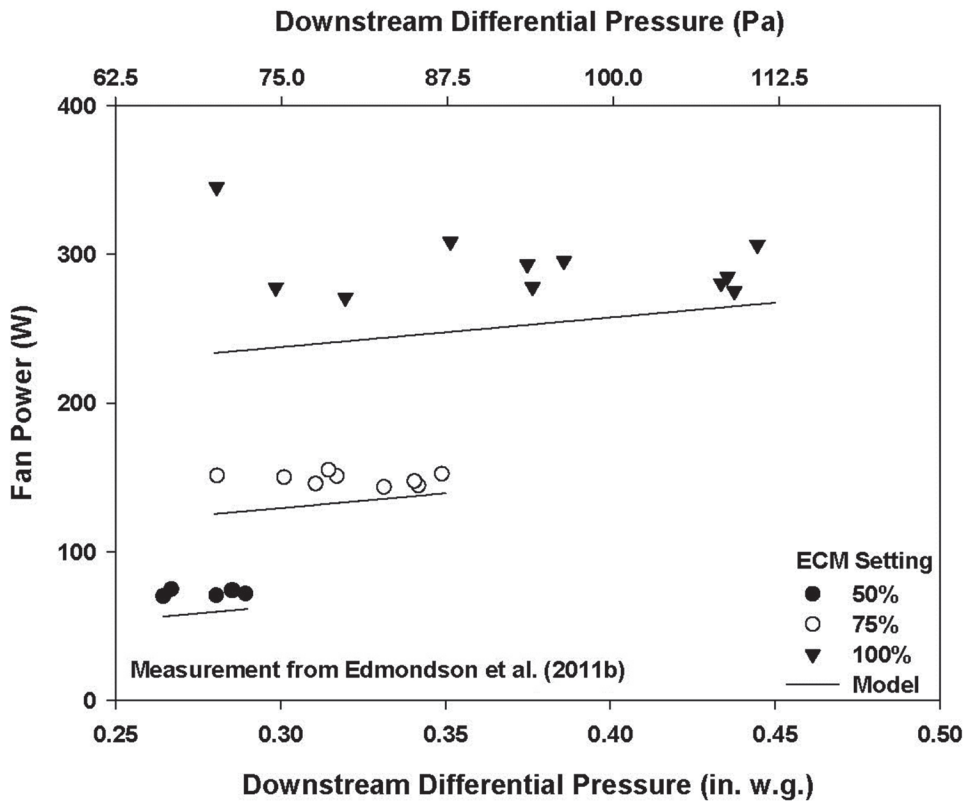


Figure 12 Measured and predicted fan-power consumption for terminal unit S8A.

partially blocking the plenum air inlet. The result indicated that both the power draw and fan airflow decreased when the terminal unit's plenum air inlet was blocked off 50%. This was a result of a static pressure load added to the fan inlet. Thus, housings may also apply an extra pressure load to ECM fans, compared to the stand-alone configuration. Unlike PSC fans, ECM fans should be able to sense and automatically compensate for the external load changes by adjusting the rotational speed to maintain the constant airflow. In this process, more power would be required to overcome the additional pressure load. However, this additional pressure load caused by housings was not considered in the model development, and thus resulted in a possible systematic bias to predict fan-power consumptions from the component-based model.

SUMMARY AND CONCLUSION

The series FPTU is an important component in many VAV systems. An empirical model was developed to investigate how well the performance of a series FPTU could be evaluated by combining the component models of the fan/motor/controller, damper, and housing.

Each series FPTU required three airflow and one power consumption models to characterize its performance. The fan airflow and power consumption models were previously reported in Part I of this paper. In Part II, the primary and plenum airflows were experimentally characterized and corresponding models were developed. The primary airflow was modeled as a function of pressure differential across the damper and the damper tilt angle. This model had an R^2 value that ranged from 0.926 to 0.992.

The plenum airflow was simulated as a function of differential pressure and air inlet area. Depending on the flow direction, two airflow configurations were encountered: parallel and perpendicular. The model for both configurations shared the same format but with different empirical parameters. The R^2 values of this model for parallel and perpendicular arrangements were 0.996 and 0.997.

The overall performance of series FPTUs was evaluated by solving the mathematical models of each component simultaneously. Model outputs were compared with the experimental data. Results from the comparisons indicated that the developed model was capable of characterizing the overall performance of series FPTUs, but it had a tendency to underestimate fan-power consumptions for some units. This discrepancy may be caused by fan-system effects, which were attributable to the difference between model development approaches and unit configurations.

This study provides a generic approach to predict the overall performance of a series FPTU based on the knowledge of its component characteristics. Due to the black box approach, the empirical models developed by Furr et al. (2008a, 2008b, and 2008c) and Edmondson et al. (2011a and 2011b) are only applicable to certain terminal units that operate at a specific pressure condition. Compared with their models, the component-based modeling approach can gener-

ally be applied to any series FPTU as long as the performance of fan/motor/controller, damper, and housing is known. Since the component-based model captured the relationship between airflows and pressure differentials, it also enables engineers to achieve a better airflow control over series FPTUs. Future work needs to focus on the flow patterns within housings and the impact of system effects on fan performance in order to eliminate the system bias in fan-power predictions.

NOMENCLATURE

A_0	= damper fully open area, in. ² (m ²)
A_{\max}	= 252 in. ² (0.16 m ²)
A_p	= plenum air inlet area, in. ² (m ²)
A_θ	= damper open area, in. ² (m ²)
K_θ	= pressure loss coefficient
P_d	= differential pressure across the FPTU housing, in. w.g. (Pa)
$P_{\text{diff, damper}}$	= differential pressure across damper, in. w.g. (Pa)
$P_{\text{downstream}}$	= downstream static pressure, in. w.g. (Pa)
P_{internal}	= internal static pressure, in. w.g. (Pa)
P_{upstream}	= upstream static pressure, in. w.g. (Pa)
\dot{Q}_{fan}	= fan airflow rate, ft ³ /min (m ³ /s)
\dot{Q}_{plenum}	= plenum airflow rate, ft ³ /min (m ³ /s)
\dot{Q}_{primary}	= primary airflow rate, ft ³ /min (m ³ /s)
R^2	= coefficient of determination
γ	= nondimensional plenum air inlet area
η	= nondimensional ECM setting
θ	= damper angle, degree
ρ_a	= air density, lb _m /ft ³ (kg/m ³)

REFERENCES

- ASHRAE. 2007. ANSI/ASHRAE Standard 51-2007, *Laboratory Methods of Testing Fans for Certified Aerodynamic Performance Rating*. Atlanta: ASHRAE.
- ASHRAE. 2008. ANSI/ASHRAE Standard 120-2008, *Method of Testing to Determine Flow Resistance of HVAC Ducts and Fittings*. Atlanta: ASHRAE.
- Cramlet, A. 2008. Performance of ECM controlled VAV fan powered terminal units. Master's of Science Thesis, Texas A&M University, College Station, TX.
- Edmondson, J., D.L. O'Neal, J.A. Bryant, and M.A. Davis. 2011a. Performance of parallel fan-powered terminal units with electronically commutated motors. *ASHRAE Transactions* 117(2):885–93.
- Edmondson, J., D.L. O'Neal, J.A. Bryant, and M.A. Davis. 2011b. Performance of series fan-powered terminal units with electronically commutated motors. *ASHRAE Transactions* 117(2):879–84.
- Furr, J., D.L. O'Neal, M. Davis, J.A. Bryant, and A. Cramlet. 2008a. Performance of VAV fan-powered terminal units:

- Experimental setup and methodology. *ASHRAE Transactions* 114(1):75–82.
- Furr, J., D.L. O'Neal, M. Davis, J.A. Bryant, and A. Cramlet. 2008b. Performance of VAV parallel fan-powered terminal units: Experimental results and models. *ASHRAE Transactions* 114(1):83–90.
- Furr, J., D.L. O'Neal, M. Davis, J.A. Bryant, and A. Cramlet. 2008c. Performance of VAV series fan-powered terminal units: Experimental results and models. *ASHRAE Transactions* 114(1):91–97.
- Kenty, K.L. 2007. Use of electronically commutated motors (ECMs) in air terminal unit. *ASHRAE Transactions* 113(1):334–41.
- Legg, R.C. 1984. Multi-blade dampers for ducted air systems. *Proceedings of the Installation Effects in Ducted Fan Systems Conference*, 67–80. UK: London.
- Legg, R.C. 1986. Characteristic of single and multi-blade dampers for ducted air system. *BSERT Journal* 7(4):129–45.

AT-15-028

Modeling Fan-Powered Terminal Unit Fan/Motor Combinations Controlled by Silicon Controlled Rectifiers

Dennis L. O'Neal, PhD, PE
Fellow ASHRAE

Douglas D. Ingram

Carl L. Reid
Student Member ASHRAE

ABSTRACT

Data on the performance of fan/motor combinations used in fan-powered terminal units (FPTUs) were evaluated, and relationships were developed between fan/motor efficiency and fan total pressure as well as fan motor power and fan airflow. All fan motors were permanent split capacitor, with the speed of the motors being altered with silicon-controlled rectifiers (SCRs). Three manufacturers provided detailed experimental data on 12 fan/motor combinations employed in commercially available FPTUs. The fan motors ranged in size from 1/8 hp (93 W) to 1 hp (746 W). The maximum fan airflows ranged from 690 to 4524 ft³/min (0.33 to 2.14 m³/s). Data were collected by each manufacturer and provided to the authors. The performance data included SCR voltage, discharge static pressure, airflow, volts, amps, volt-amps, power factor, power, motor speed, motor size, and power divided by airflow. Data were also provided on fan discharge area and motor size. A linear relationship between fan/motor total efficiency and fan total pressure was inferred for the units evaluated. By use of the definition of "fan efficiency," it was also shown that the relationship between fan motor power and fan airflow should also be linear. The correlations developed should be in a form that can be readily used in energy simulation programs to better estimate the performance of FPTUs.

INTRODUCTION

Variable-air-volume (VAV) systems are designed to vary the amount of conditioned air delivered to a zone to maintain space comfort. Conditioned air from an air-handling unit (AHU) is delivered by the central primary (supply) fan through the duct system to VAV terminal units. These terminal units provide air to each zone. Terminal units with fans are

called "fan-powered terminal units" (FPTUs). FPTUs mix secondary air with primary air and provide additional pressurization and supplemental heat (when needed) to the air before the air is delivered to the zone the FPTU serves. They also make it possible to reduce the central supply fan operating pressure and reduce the air distribution system's energy consumption (ASHRAE 2012).

FPTUs come in two configurations: series and parallel. When the fan in the FPTU is in series with the primary supply fan, the configuration is called a "series" FPTU. In a series FPTU, all primary and secondary (induced) air passes through the FPTU blower, which operates continuously during normal operating hours of the HVAC system. In a parallel FPTU, the fan operates intermittently. The fan is located in the secondary airstream and operates in parallel with the primary airstream. It is used to induce air into the FPTU during heating and dead-band operations.

FPTU manufacturers utilize permanent split capacitor (PSC) motors and electronically commutated motors (ECM) to drive the fans in the units. The speed of a PSC motor can be controlled by a silicon-controlled rectifier (SCR). ECM motors' speed can be varied with the use of a controller that provides a DC voltage to the motor. In traditional applications, the field technician sets the speed of the motor to supply the design airflow into the zone served by the FPTU. Once the speed of the fan is set during installation and/or commissioning of the FPTU, the controller setting of the motor typically is not changed. With ECMs, the motor can either be set at a fixed setting or can be integrated into an energy management control system so that the speed of the motor (and fan) can be varied to meet the load within the zone served by the FPTU.

Dennis L. O'Neal is Dean of Engineering and Computer Science, **Douglas D. Ingram** is an undergraduate research assistant in the Department of Electrical and Computer Engineering, and **Carl L. Reid** is a graduate research assistant in the Department of Mechanical Engineering, Baylor University, Waco, TX.

Unlike large central AHUs, the fan motors in FPTUs are matched with FPTU fans and come as a working pair. The fan motors in FPTUs are small—typically 1 hp (746 W) or less. It is not unusual in large commercial buildings to have dozens or even hundreds of FPTUs installed, depending on the size of the building. Such large numbers of FPTU fan/motors in a building means that the sum of the FPTUs can make a significant contribution to the energy use of a commercial building.

The purpose of this paper is to develop performance data and models for a wide range of SCR-controlled PSC fan/motor combinations used in FPTUs. The models generated in this paper should allow an energy modeler to more accurately estimate the annual performance of FPTUs in building energy simulation programs.

BACKGROUND

Recent studies by Furr et al. (2007, 2008a, and 2008b), Cramlet (2008), Edmondson et al. (2011a and 2011b) and Yin and O'Neal (2014a and 2014b) have done much to characterize the steady-state and part-load performance of FPTUs. Furr et al. conducted laboratory characterization of the power, power factor, pressure, and airflow performance of SCR-controlled FPTUs from three manufacturers and included two primary inlet diameter sizes. Cramlet extended the work of Furr et al. by including power quality measurements and developing a set of equations for characterizing the performance of an ECM-controlled FPTU. Edmondson et al. further extended Cramlet's work by conducting extensive measurements of ECM-controlled FPTUs from three manufacturers. The experimental studies by Furr et al., Cramlet, and Edmondson et al. treated the FPTU as a system. Semiempirical relationships were developed from the experimental data that could be used to estimate the electrical, pressure, and airflow performance of FPTUs. As demonstrated by Davis et al. (2012), the models developed from the prior experimental work allowed a modeler to use the sets of equations to simulate hourly performance of a particular FPTU in a building if the static pressures inside the duct system were known. Some building energy simulation programs use a much simpler model of FPTUs that relies on energy and mass balances of the FPTU to estimate performance. Directly utilizing the data from the above studies would require a different approach to modeling the air-side systems than is commonly found in some building simulation programs.

Recently, Yin and O'Neal measured the performance of the individual components (fan/motor combination, the damper, and cabinet) of ECM-controlled FPTUs. Their strategy was to determine if the individual component models could be combined together to predict overall system performance. The system performance predicted with this approach was compared to the measured system performance of the FPTU collected by Edmondson et al. (2011a). There was general agreement in the trends and the comparison demonstrated that a component approach could be used if the performance of the fan/motor/controller, damper, and housing were

known. Some of the differences in performance between the component and measured system performance focused on the airflow effect on fan performance within the FPTU. Specifically, when the fan/motor combination was tested outside the FPTU it was not possible to reproduce the changes in performance caused by fan system effects that occur because of the constrained space within housing of the FPTU.

BACKGROUND—ENERGYPLUS

EnergyPlus is a widely used building simulation program that can estimate the annual energy use of a wide range of buildings and their systems. Both series and parallel FPTUs can be modeled. The description below is drawn from the EnergyPlus engineering reference (2013), which discusses the calculation procedures used to model FPTUs. In EnergyPlus, an FPTU is called a “powered induction unit” (PIU). This paper uses the more generic term (FPTU).

EnergyPlus uses a simple component approach to simulate the performance of FPTUs. EnergyPlus makes the assumption that both series and parallel FPTU systems can be modeled as a combination of three major components: a mixer, a constant-volume fan, and a heating coil. Figure 1 shows the placement of the components used to model series FPTUs in EnergyPlus.

EnergyPlus assumes there is no pressure interaction between the components in an FPTU. Each component has a submodel that is connected via mass and energy balances to the other components. Once the zone loads are determined, then the mass and energy balances can be used to determine the energy use and airflow requirements of the FPTU. While the damper is not explicitly modeled in EnergyPlus, the program does use an energy and mass balance calculation to estimate the distribution of airflows between the primary and secondary air streams. This calculation mimics the main function of the damper (i.e., control the amount of airflow).

Before a simulation is started for the series FPTU, the user can specify a number of design flow rates (maximum total airflow rate, maximum primary air flow rate, and minimum primary airflow fraction) or these values can also be autosized by the program.

The user is required to input the fan properties shown in Table 1. The fan calculation submodel assumes a constant speed fan for both series and parallel FPTU fans. Though the fan motor controller can vary the speed of the FPTU fan, the controller voltage is typically set during installation of the unit or during commissioning of the building to meet airflow requirements in the zone, and it stays at that value unless manually adjusted later. The assumption that the fan is at a constant speed is only true if the pressure differential across the fan remains constant. If the pressure differential varies, then the controller will adjust fan speed in an attempt to keep the fan airflow constant.

The user inputs the fan total efficiency η_{tot} and the fan motor efficiency η_{mot} separately, and a design air-pressure rise across the fan, ΔP . It is assumed that the pressure rise is the

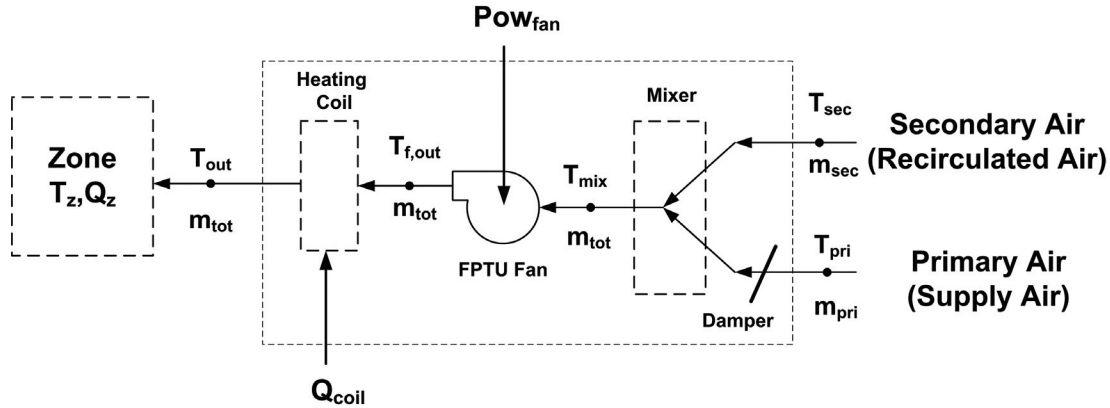


Figure 1 Components and energy and mass flows in the simulation of a series fan-powered terminal unit in EnergyPlus.

Table 1. Fan Characteristics Used for Series FPTUs in EnergyPlus

EnergyPlus Fan Input Characteristics
Design air pressure rise across the fan, ΔP
Design volumetric flow rate, m_{design}
Fan total efficiency, η_{fan}
Fan motor efficiency, η_{mot}
Fraction of fan waste heat that enters airstream, Q_{toair}

total pressure rise across the fan. The static pressure rise could be used, but the definition of the fan efficiency would require use of fan static efficiency rather than fan total efficiency. Typically, pressure differentials should be substantially less than 1 in. wg (250 Pa) for fans in FPTUs. The FPTU test procedure (ASHRAE 2006) requires testing at downstream static pressures of 0.25 in wg (62 Pa). The fan efficiency is assumed to be associated with the total pressure across the fan rather than the static pressure, but the Energy Plus documentation was not clear. The individual fan and motor efficiencies are rarely provided separately by the FPTU manufacturers. For the small fans and fan motors used in FPTUs, the fan and motor are usually tested as a unit rather than individually.

EnergyPlus has a default fan efficiency of 70%, which is a value more appropriate for a central air handler but not for the smaller fan/motor combinations used in FPTUs. O’Neal et al. (2014) recently published efficiency data for an SCR-controlled FPTU fan/motor combination where the SCR-controlled motor used 400 W at the 277 VAC rating point. The total efficiency of this fan/motor combination varied from 5% to 20% for fan static pressures ranging from 0.2 to 0.6 in. wg (25 to 149 Pa). While these data were for just one FPTU fan/motor combination, they illustrated that the fan/motor efficiencies for these smaller fans were less than the default fan efficiency used in EnergyPlus. Better performance data for FPTUs are needed for use in building simulation programs to

help building professionals better evaluate the energy use in buildings that utilize FPTUs.

DATA COLLECTION

Three FPTU manufacturers, identified as manufacturers A, B, and C in tables and figures, provided data for this study. The data covered a wide range of fan motor sizes, from 1/8 hp (93 W) to 1 hp (746 W). Table 2 shows the fan motor sizes provided by each manufacturer. Overall, 12 fan/motor combinations were evaluated. These units cover much of the range of FPTU fans and motors expected to be used in the field. Manufacturers apply these fan/motor combinations in a wide range of cabinet sizes (underfloor or overhead) and styles (“low” and “standard” profile). Each cabinet design will potentially produce different flow conditions entering the FPTU fan, which could generate differing air system effects that impact the overall performance of the fan.

Data on fan/motor combinations were collected by manufacturers in their own laboratories and provided to the authors through a representative of the Air-Conditioning, Heating, and Refrigeration Institute (AHRI) so that the identity of the manufacturers remained anonymous. All FPTUs were designed for 277-V applications. Manufacturers were asked to provide both descriptive and performance data (Tables 3 and 4, respectively) on the fan/motor combinations. Table 5 summarizes the range in SCR voltage settings and discharge static pressures in the data sets provided by each manufacturer. The SCR voltage settings ranged from a low of 110 V in one of manufacturer B’s units to a high of 277 V in all of manufacturer A’s units. The discharge static pressures were set at anywhere from 0 to 0.75 in. wg (0 to 187 Pa).

An identification procedure was developed for reporting each fan/motor combination. Because all of the fan motors in this paper were SCR controlled, all designations started with “SCR”. Fan motor sizes ranged from 1/8 to 1 hp (93 to 746 W). The fan motor size in horsepower was converted to its decimal equivalent ($1/2 = 0.50$) and multiplied by 1000. For example, a 1/2 hp (373 W) fan’s decimal equivalent was 0.500.

Table 2. FPTU Fan/Motor Data Provided by the Manufacturers

Fan Motor Size, hp (W)	Manufacturer A	Manufacturer B	Manufacturer C
1/8 (93)		X	
1/6 (125)	X		
1/4 (187)	X		
1/3(248)	X	XX*	
1/2 (373)	X	XX*	XX
1 (746)		X	

*Multiple "Xs" in an entry indicate the manufacturer provided more than one unit at that size.

Table 3. Descriptive Data for FPTU and Fan/Motor Combinations

Item
Fan model number
Series or parallel FPTU application
Primary inlet diameter
Design range of airflow of FPTU
Recommended operating pressures
Maximum recommended airflow
Minimum recommended airflow
Fan manufacturer
Motor manufacturer
Motor size
Fan discharge dimensions

$$\eta_{fm} = \frac{Q_{flow} \times \Delta P_{tot}}{Pow_{fan}} \quad (1)$$

where

ΔP_{tot} = fan total pressure, in. wg (Pa)

Pow_{fan} = power of the fan motor, W

ρ_{air} = density of the air at standard temperature and pressure, lb/ft³ (kg/m³)

Q_{flow} = volumetric airflow, ft³/min (m³/s)

Figures 2 and 3 show sample data for the fan/motor total efficiency versus fan total pressure for the 1/4 hp (187 W) and 1/2 hp (373 W) fan/motor combinations from manufacturers A and B, respectively. The fan/motor efficiency showed a direct dependence on the fan total pressure.

Four observations can be made from the data in Figures 2 and 3. First, there was an almost linear relationship between fan/motor efficiency and fan total pressure. The r^2 values for the regressions in Figures 2 and 3 were 0.99 for both SCR fan/motor combinations. In building simulation programs such as EnergyPlus, the fan efficiency and fan total pressure are treated as independent variables. Figures 2 and 3 show that they should not be treated independently for SCR-controlled PSC motors applied to FPTUs. If the total pressure is specified, then the fan/motor efficiency is also known within the uncertainty of the correlation. A second observation is that both Figures 2 and 3 show there is not a single efficiency for a particular fan/motor combination. The fan/motor efficiency depends on the total fan pressure. If there were variations in total fan pressure during the operation of an FPTU over the course of a day, week, or year, then the efficiency would also vary. Unfortunately, there are little data on the operating total pressures across the fan within a FPTU over the range of operating conditions found in the field. A third observation from these figures is that the fan/motor efficiencies of small SCR fan/motor combinations are relatively low. For SCR-250A, the fan/motor efficiencies ranged from low single digits up to 22%, while for SCR-500B they ranged from about 5% to 32%. A fourth observation from these plots is the relatively low total pressures these fans can produce. For SCR-250A, the maxi-

Multiplying by 1000 gave a value of 500. Combining the SCR designation, motor size, and manufacturer provided the identifier used in this paper. A 1/2 hp (373 W) fan/motor from manufacturer A was identified as SCR-500A. If a manufacturer had more than one fan/motor combination of the same size, a number was added after the manufacturer's identifier to differentiate units. For example, manufacturer B had two fan/motor combinations for 1/2 hp (373 W), which were identified as SCR-500B1 and SCR-500B2.

DATA ANALYSIS

Each manufacturer provided its data in spreadsheets. With the discharge area of the fans provided, it was possible to calculate the exit air velocity from the discharge area and measured airflow. With the exit velocity known, the velocity pressure was calculated and added to the measured static pressure differential across the fan to obtain a fan total pressure. The fan/motor total efficiency (η_{fm}) was calculated using fan total pressure, mass flow of the air, and fan power:

Table 4. Detailed Measured Performance Data on Each FPTU Fan/Motor Combination

Item	Units
SCR voltage	Volts*
Discharge static pressure	in. wg (Pa)
Airflow	ft ³ /min (m ³ /s)
Current	Amps
Volt-amperes	Volt-amperes
Power factor	—
Power	W
Motor speed	rpm
Power/airflow	W/(ft ³ /min) (W/[m ³ /s])

Table 5. SCR and Discharge Static Pressure Ranges Provided by Each Manufacturer

Quantity	Range of Values		
	Manufacturer A	Manufacturer B	Manufacturer C
SCR Voltage	140 to 277 V	110 to 276 V	Low to High*
Discharge Static Pressure	0 to 0.62 in. wg (0 to 154 Pa)	0.1 to 0.75 in. wg (25 to 187 Pa)	0.1 to 0.6 in. wg (25 to 149 Pa)

*Manufacturer C provided low, mid-low, mid-high, and high for the SCR voltage settings.

imum total pressure was 0.66 in. wg (164 Pa), while for SCR-500B it was 0.99 in. wg (247 Pa). The discharge static pressures at which the two fans in Figure 2 and 3 operated varied from 0 to 0.75 in. wg (0 to 187 Pa). These total pressures are a fraction of those expected to be produced by a large central air handler in a commercial building.

Because the fan/motor total efficiency data appears to be nearly linear with respect to total pressure, the data were fit with a simple line that passed through the origin. This meant that the total efficiency and total pressure were related by a simple constant, α_η :

$$\eta_{fm} = \alpha_n \times \Delta P_{tot} \quad (2)$$

α_η had units of %/(in. wg) in the I-P system and %/Pa in the SI system of units. The fan/motor total efficiency in Equation 2 was substituted back into Equation 1 and rearranged to solve for the fan power. The result showed that the fan airflow and fan motor power should also be linearly related since α_η was a constant:

$$\text{Pow}_{fan} = \frac{Q_{flow}}{\alpha_n} \quad (3)$$

If the airflow was in ft³/min (m³/s) and the power was in W, then the constant, α_η , would need to be multiplied by the proper unit conversions to make the units in Equation 3 to come out correctly. Equation 3 can be rewritten with a new constant α_p that includes the unit conversions:

$$\text{Pow}_{fan} = \alpha_p \times Q_{flow} \quad (4)$$

Equation 4 was a surprising result. It was completely unexpected that the fan power would be simply related to the airflow by a constant. However, Equation 4 was derived directly from the definition of fan efficiency and the experimental data that showed the linear relationship between fan/motor total efficiency and fan total pressure. Figures 4 and 5 show the power and airflow plots for the same two fan/motor combinations in Figures 2 and 3, respectively. While there was scatter in the data, the plots showed the same general linear trends that would be predicted from Equation 4. Some of the scatter in Figure 4 occurs at specific SCR voltages. For example, at 208 V, the airflow varied over a very narrow range of 762 to 774 ft³/min (0.36 to 0.37 m³/s), while the power varied from a low of 257 to 324 W. This resulted in some horizontal compression of data in the plots around a narrow range of flows for some of the units.

The general linear trend in the plots was powerful because it implied that efficiency and pressures did not need to be known or specified explicitly for the FPTU when modeling SCR-controlled PSC motors in FPTUs. Instead, for the modeler, if the airflow is known, then the power consumed by the fan motor can be estimated from relationships similar to what is found in Figures 4 and 5. The constant, α_p , is a familiar term in that it is the power divided by airflow. In the I-P system, it is W/(ft³/min), and in the SI system, it is W/(m³/s). Essen-

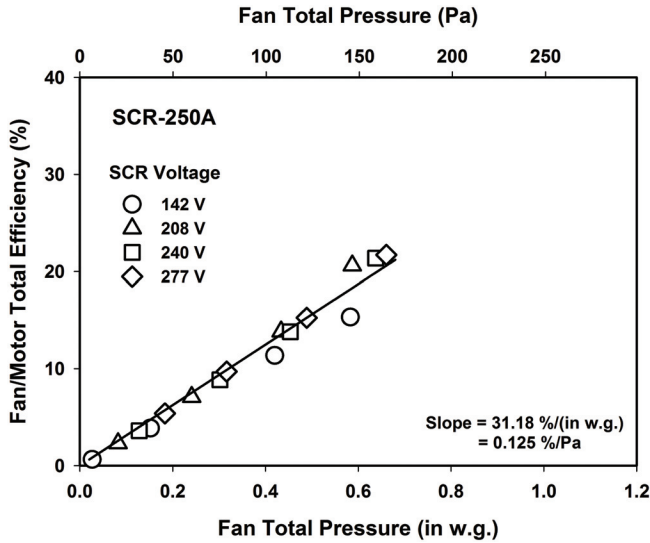


Figure 2 Fan/motor performance data for SCR-250A.

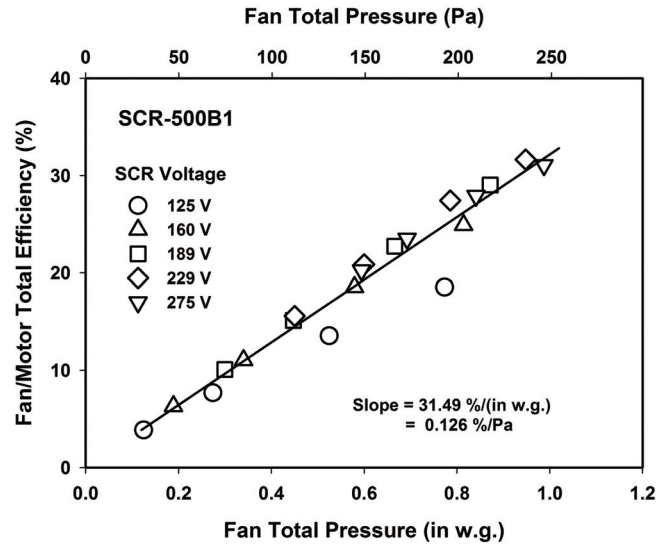


Figure 3 Fan/motor performance data for SCR-500B1.

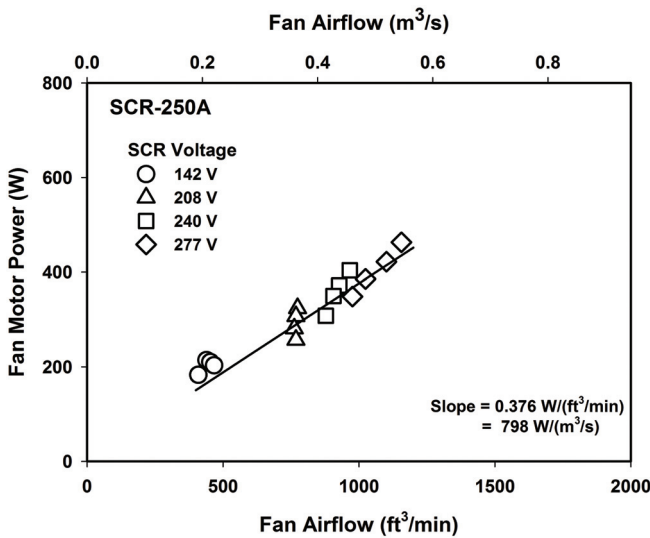


Figure 4 Fan motor power versus fan airflow for SCR-250A.

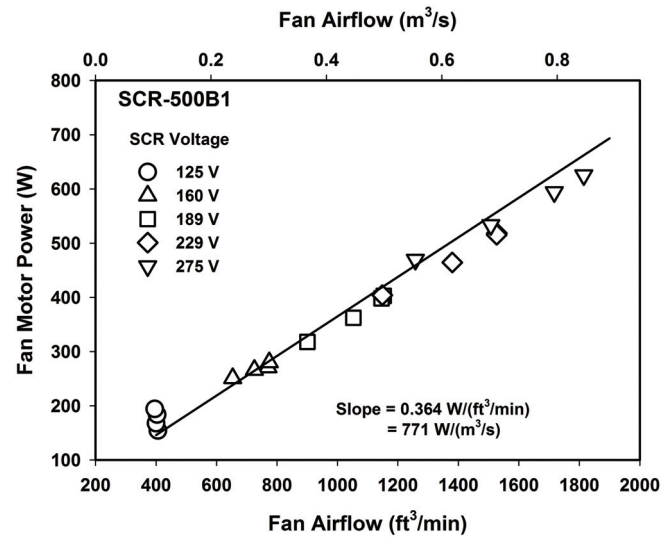


Figure 5 Fan motor power versus fan airflow for SCR-500B1.

tially, Equation 4 implies that for modeling purposes the power divided by airflow can be treated as a constant for SCR-controlled PSC motors. While there was scatter around the average slope α_p , it would appear a constant can be used for relating the power and airflow of SCR-controlled PSC fan/motor combinations in building simulation programs. If building simulation programs do not have this simple option of modeling SCR-controlled fan motors, then they should be modified. This relationship provides realistic performance information based on experimental data. Manufacturers typically have data on power/airflow for their specific units. Such data combined with the model in Equation 4 could provide the energy modeler with the capability to quickly estimate the power used by specific FPTUs that had SCR-controlled fan

motors. With the absence of specific data, then the more generic numbers developed below could be used.

As mentioned, the constant α_p had units of $W/(ft^3/min)$ in the I-P system, then α_p was related numerically to α_η by the following:

$$\alpha_p = \frac{11.75}{\alpha_\eta} \quad (5)$$

For the SI system, α_p had units of $W/(m^3/s)$ and α_η had units of $\%/(Pa)$, then α_p was related numerically to α_η by the following:

$$\alpha_p = \frac{100}{\alpha_\eta} \quad (6)$$

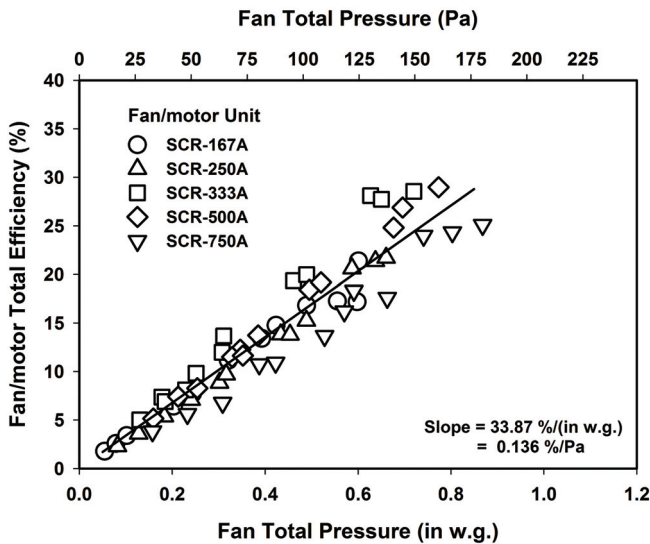


Figure 6 Fan/motor total efficiency versus fan total pressure for all fan/motors from manufacturer A.

For both fan/motor combinations, the data for the lower SCR voltages showed a lower efficiency as compared to the rest of the data at higher total pressures. This drop off showed up more in data from manufacturer B than in data from either manufacturer A or C. In previous work performed on SCR fan/motor combinations, Furr et al. (2007) found it was difficult to make the SCRs consistently operate below about 160 V. In communicating with engineers for two manufacturers who provided data to this study, they indicated that the efficiency decreased at the lower voltages (and speeds) for an SCR-controlled PSC motor. They also indicated they did not like to see the speed of the motor operate below about 600 rpm. Furr et al. (2007) measured the speed of three SCR-controlled fan motors. One of the motors was 1/4 hp (187 W). It operated below 600 rpm when SCR voltages were below 190 V. Based on the data from Furr et al. and communications with engineers from the companies providing the data, it was decided to exclude all performance data below 160 V from the analysis presented below.

Figures 2 through 5 show the results for two fan/motor combinations from two different manufacturers. To answer the question of whether linear relationships shown in these figures hold for other fan/motor combinations, data from all manufacturers were plotted. Figures 6 and 7 show the fan/motor total efficiencies plotted against total pressure for all of the fans provided by manufacturers A and B. Because manufacturer C only provided data for two fan/motor combinations and both had the same motor size, their data were only included in the final two plots discussed further below. While there was scatter in the data from both manufacturers, it was surprising how well the efficiency/pressure data fell along roughly the same slopes for the two manufacturers. The r^2 for the data in Figure 6 was 0.979, while that for the data in Figure 7 was 0.994. As implied above, if the efficiency-versus-total-pressure relationship is

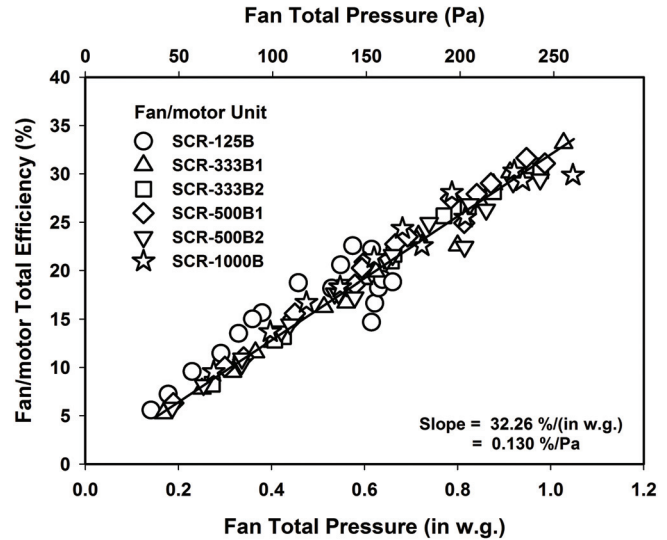


Figure 7 Fan/motor total efficiency versus fan total pressure for all fan/motors from manufacturer B.

linear, then the fan-motor-power-versus-airflow relationship is also linear. Figures 8 and 9 again show that fan motor power can be correlated linearly with fan airflow. The data from manufacturer A showed more scatter than that from manufacturer B. The r^2 for manufacturer A's data was lower (0.971 vs 0.997) compared to manufacturer B's data. However, given the wide range in fan motor sizes, from 1/8 hp (92 W) to 1 hp (746 W), both the efficiency/total pressure data and the power/airflow data showed high correlation.

In modeling energy use in buildings, the modeler often may not be interested in a specific manufacturer's line of FPTUs, but is looking for more generic relationships for the performance of the fan/motors in the FPTUs. To get to more generic or averaged values of the fan/motor efficiency and power, the data from all manufacturers were combined into the same plots. Figure 10 shows the fan/motor efficiencies plotted versus fan total pressure for the three manufacturers. As with the individual manufacturer's data, there continued to be a strong correlation between fan/motor efficiency and fan total pressure. The line fit to the data in Figure 10 had an r^2 of 0.983. Figure 11 shows the fan motor power versus fan airflow for all manufacturers. The regression showed an r^2 of 0.978. Even with the great r^2 values, there was still significant scatter in the data. For example, in Figure 10, the fan/motor efficiency could vary from as low as 10.5% to as high as 28% for a fan total pressure of 0.6 in. wg (149 Pa). Likewise, in Figure 11, the fan motor power varied from about 750 W to over 1200 W for an airflow of about 2300 ft³/min (1.09 m³/s). The slopes for both figures represent the average relationships between the two variables in each plot. For building modelers attempting to simulate a generic SCR-controlled FPTU, the values of the slopes in either Figures 10 or 11 can provide average input performance characteristics for the fan/motor. To model a specific manufacturer's FPTU, the above methodology could

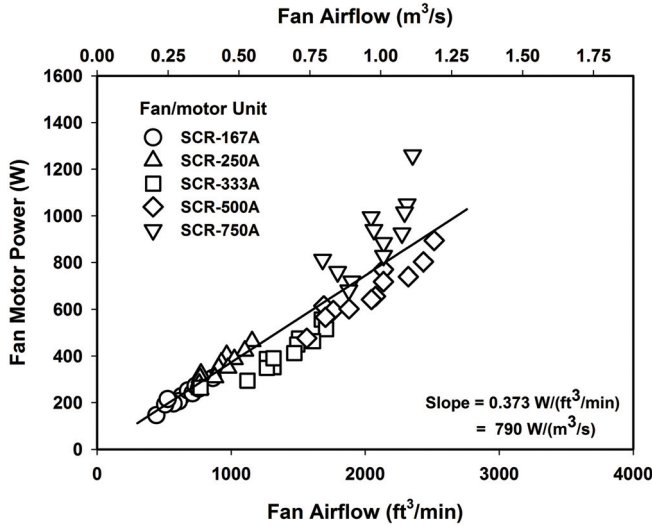


Figure 8 Fan motor power versus fan airflow for all fan/motors from manufacturer A.

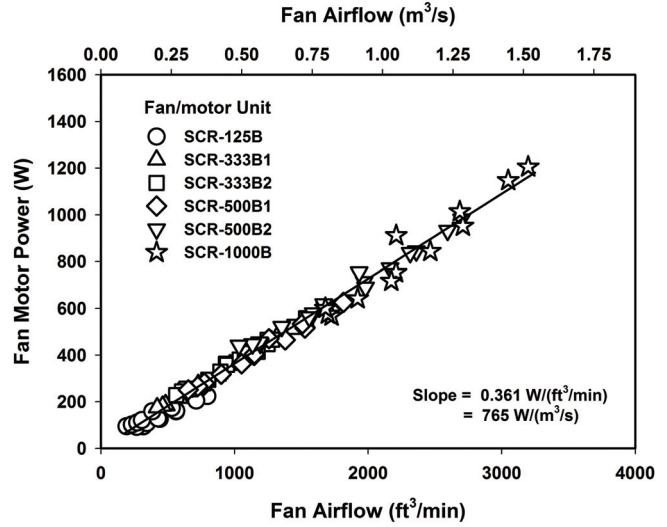


Figure 9 Fan motor power versus fan airflow for all fan/motors from manufacturer B.

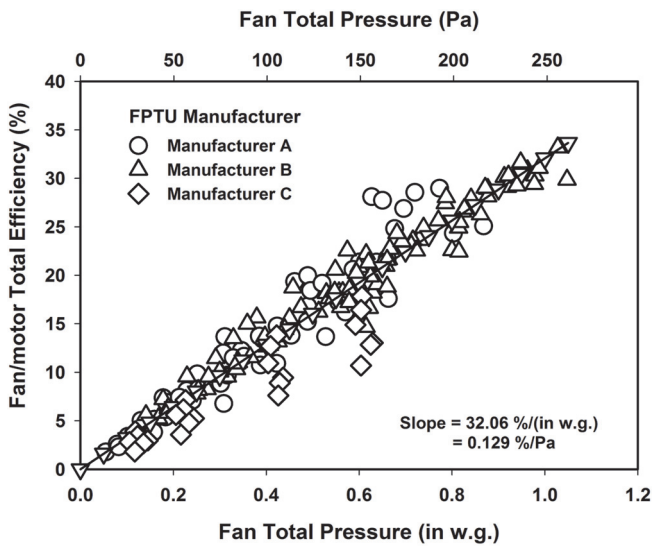


Figure 10 Fan/motor total efficiency versus fan total pressure for all fan/motors from all manufacturers.

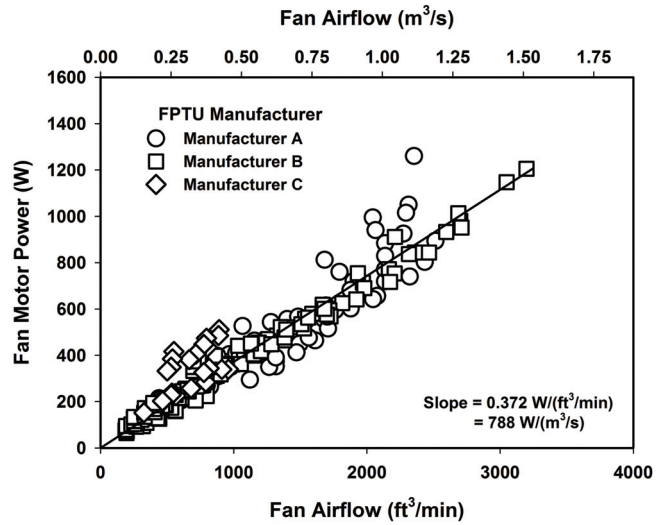


Figure 11 Fan motor power versus fan airflow for all fan/motor manufacturers.

be used along with the appropriate power/airflow values for the fan/motor used in the FPTU.

CONCLUSIONS

FPTUs employing SCR-controlled fan motors continue to be used in new and existing buildings. This study sought to fill a gap in performance data and models for SCR-controlled fan/motors used in FPTUs. Three manufacturers provided detailed experimental data on 12 fan/motor combinations employed in commercially available FPTUs. The fan motors ranged in size from 1/8 hp (93 W) to 1 hp (746 W). The fan

maximum airflows ranged from 690 to 4524 ft³/min (0.33 to 2.14 m³/s).

The models developed from the data were simple linear relationships between fan/motor efficiency and fan total pressure and between fan motor power and fan airflow. These relationships should provide a user of building energy simulation programs with the input and models needed to provide reliable estimates of the hourly and annual performance of SCR-controlled fan motors used in FPTUs. As discussed, there was still too significant scatter in the data to use these relationships to model a particular manufacturer's specific FPTU. However, in modeling a generic FPTU, the fan/motor relationships

should provide the modeler with data that would provide estimates near the average of the SCR-controlled fan/motor combinations that are currently in use in FPTUs.

ACKNOWLEDGMENT

The authors wish to thank the Air-Conditioning, Heating, and Refrigeration Institute (AHRI) for their support of this project. In particular, we wish to thank all the members of the Air Control and Distribution Devices Committee for their input and advice.

REFERENCES

- ASHRAE. 2006. ANSI/ASHRAE Standard 130-1996 (RA 2006), *Methods of Testing for Rating Ducted Air Terminal Units*. Atlanta: ASHRAE.
- ASHRAE. 2012. *ASHRAE Handbook—HVAC Systems and Equipment*, Chapter 20, “Room air distribution equipment.” Atlanta: ASHRAE.
- Cramlet, A. 2008. Performance of ECM Controlled VAV Fan Power Terminal Units. M. Sc. Thesis, Texas A&M University, College Station, TX.
- Davis, M., J. Bryant, and D.L. O’Neal. 2012. Modeling the performance of ECM and SCR series fan-powered terminal units in single-duct VAV systems. *ASHRAE Transactions* 118(1):908–18.
- Edmondson, J.L., D.L. O’Neal, J.A. Bryant, and M.A. Davis. 2011a. Performance of series fan-powered terminal units with electronically commutated motors. *ASHRAE Transactions* 117(2):876–84.
- Edmondson, J.L., D.L. O’Neal, J.A. Bryant, and M.A. Davis. 2011b. Performance of parallel fan-powered terminal units with electronically commutated motors. *ASHRAE Transactions* 117(2):885–93.
- EnergyPlus. 2013a. “Air system distribution terminals.” In *EnergyPlus Energy Simulation Software—EnergyPlus Documentation—Engineering Reference*. Berkeley: Lawrence Berkeley National Laboratory.
- Furr, J., D.L. O’Neal, M. Davis, J. Bryant, and A. Cramlet. 2007. Comparison of the total energy consumption of series versus parallel fan-powered VAV terminal units. RP-1292 Phase I Final Report. Atlanta: ASHRAE.
- Furr, J., D.L. O’Neal, M. Davis, J. Bryant, and A. Cramlet. 2008a. Performance of VAV fan-powered terminal units: Experimental setup and methodology (RP-1292). *ASHRAE Transactions* 114(1):75–82.
- Furr, J., D.L. O’Neal, M. Davis, J. Bryant, and A. Cramlet. 2008b. Performance of VAV series fan-powered terminal units: Experimental results and models (RP-1292). *ASHRAE Transactions* 114(1):91–97.
- O’Neal, D.L., J.L. Edmondson, and P. Yin. 2014. Comparison of performance characteristics of SCR and ECM controlled series fan powered terminal units. *HVAC&R Research* 20(2):194–202.
- Yin, P., and D.L. O’Neal. 2014a, Characterizing airflow and power of VAV series fan-powered terminal units from component data—Part I. *ASHRAE Transactions* 120(1).
- Yin, P., and D.L. O’Neal. 2014b. Characterizing airflow and power of VAV series fan-powered terminal units from component data—Part II. *ASHRAE Transactions* 120(1).

AT-15-025

A Simplified Model of the Fan/Motor Performance of Fan-Powered Terminal Units that Use Electronically Commutated Motors

Dennis L. O'Neal, PhD, PE
Fellow ASHRAE

Carl L. Reid
Student Member ASHRAE

Douglas D. Ingram

ABSTRACT

Four manufacturers provided detailed performance data on 36 fan/motor combinations applied in commercially available series and parallel fan-powered terminal units. The fan motors ranged in size from 0.33 to 1 hp (249 to 746 W). Data were provided for fan static discharge pressures ranging from 0.1 to 0.75 in. w.g. (25 to 187 Pa). All of the fan motors were electronically commutated motors. The performance data were analyzed to develop a generalized performance model that would be suitable for use in building energy simulation programs. The model developed had two components. First, the data for static discharge pressures ranging from 0.1 to 0.5 in. w.g. (25 to 125 Pa) were used to develop a correlation between the full-load power and the maximum airflow of the fan/motor combinations. These data were fit with a simple linear regression model. Second, part-load power and airflow data were evaluated over a wide range of controller settings for each fan/motor combination. The data were normalized to the airflow and power corresponding to the maximum controller setting for each static pressure. It was found that the normalized data for those fan motors whose full maximum power operations were less than 80% of the rating of the motor were problematic and were not used in the part-load evaluation. The normalized power and airflow were fit with a third-degree polynomial. The resulting full-load power correlation along with the part-load correlation can be used together in a building simulation program to estimate the part-load energy use of fan/motor combinations used in fan-powered terminal units that use electronically commutated motors.

INTRODUCTION

Variable air volume (VAV) systems vary the amount of conditioned air delivered to a zone to maintain space comfort. Conditioned air from an air-handling unit (AHU) is delivered through the duct system to VAV terminal units that provide air to each zone. Terminal units containing a fan are called fan-powered terminal units (FPTUs). FPTUs mix secondary air from the plenum space with the primary air, provide additional pressurization to the air, and provide supplemental heat (when needed) to the air before it is delivered to the conditioned zone (ASHRAE 2012).

FPTUs come in both series and parallel configurations. If the FPTU fan is in line with the primary supply fan, the configuration is called a *series FPTU*. All primary and secondary (induced) air passes through the FPTU fan, which operates continuously during the normal operating hours of the HVAC system. For a parallel FPTU, the fan is located in the secondary airstream, operates in parallel to the primary air stream, and is on only during heating or dead band modes.

Manufacturers use permanent split capacitor (PSC) motors and electronically commutated motors (ECM) to drive the fans in FPTUs. While the speed of both PSC motors and ECMs can be varied, PSC motors are applied in situations where the airflow provided by the FPTU fan is fixed. A silicon-controlled rectifier (SCR) is used to control the speed of a PSC motor. For FPTU applications, the airflow for a SCR-controlled PSC motor is set by a technician in the field and typically not changed after installation or commissioning. The speed of ECMs is varied with the use of a DC voltage controller. ECMs in series FPTUs can be used to either run the fan at a fixed airflow or their speed can be varied so the airflow from the FPTU matches the required load in the

Dennis L. O'Neal is the dean of engineering and computer science, **Carl L. Reid** is a graduate research assistant in the department of mechanical engineering, and **Douglas D. Ingram** is an undergraduate research assistant in the department of electrical and computer engineering at Baylor University, Waco, TX.

zone. For a fixed airflow application, the field technician sets the ECM controller to supply the design airflow during installation and/or commissioning of the FPTU, similar to what is done with a PSC fan motor controlled by a SCR. For a variable airflow application, the ECM can be tied into an energy management control system and the airflow varied to provide the desired amount of airflow to meet the thermal load requirement of the zone.

The fan motors in FPTUs are matched with FPTU fans and come as an integrated assembly. While the fan motors in FPTUs are small, typically 1 hp (746 W) or less, there may be many of these in a building, so their contribution to the total energy use may be significant.

The purpose of this paper is to develop a simplified performance model that could be applied to a wide range of ECM controlled fan/motor combinations used in FPTUs. The model is based on detailed ECM fan/motor performance data provided by four manufacturers. The model developed in this paper should allow an energy modeler to more accurately estimate the annual performance of FPTUs in building energy simulation programs. This paper complements a prior paper (O'Neal et al. 2015) that focused on modeling SCR-controlled PSC fan/motor combinations used in FPTUs.

BACKGROUND

Studies by Cramlet (2008), Edmondson et al. (2011a, 2011b), and Yin and O'Neal (2014a, 2014b) have done much to characterize the steady-state and part-load performance of FPTUs using ECMs. Cramlet developed a set of equations to characterize the performance of a single ECM FPTU. Edmondson et al. conducted detailed measurements and developed performance models of ECM-controlled FPTUs from three manufacturers. The experimental studies of Cramlet and Edmondson et al. treated the FPTU as a system. Semiempirical relationships were developed from the experimental data that could be used to estimate the electrical, pressure, and airflow performance of FPTUs. As demonstrated by Davis et al. (2012), the models developed from the prior experimental work allowed a modeler to use the sets of equations to simulate the hourly performance of a particular FPTU in a building if the static pressures inside the duct system were known. Some building energy simulation programs utilize a much simpler model of FPTUs that rely on energy and mass balances of the FPTU to estimate performance. Utilizing the data from Cramlet (2008) and Edmondson et al. (2011a, 2011b) would require a different approach to modeling air-side systems than is commonly found in building simulation programs.

Yin and O'Neal (2014a, 2014b) measured the performance of the individual components (fan/motor combination, damper, and cabinet) of ECM-controlled FPTUs. Their strategy was to determine if the individual component models could be combined to predict overall system performance. The system performance predicted with this approach was compared to the measured system performance of the FPTU

collected by Edmondson et al. (2011a). There was general agreement in the trends, and it demonstrated that a component approach could be used if the performance of the fan/motor/controller, damper, and housing were known. Some of the differences in performance between the component and measured system performance focused on the airflow effects on the fan performance within the FPTU. Specifically, Yin and O'Neal (2014b) found that when the fan/motor combination was tested outside the FPTU, it was not possible to reproduce the changes in performance caused by fan system effects occurring because of the constrained space within the housing of the FPTU.

SIMPLIFIED ENERGY MODELS

Because ECM fan motors in FPTUs can be used in a constant airflow or variable airflow mode, any model of ECM fan motors needs to be able to capture both types of applications. The public domain building simulation program, EnergyPlus, models both series and parallel FPTUs (LBNL 2014). It treats the fan in FPTUs as operating at constant airflow. The user is required to input the fan properties shown in Table 1. EnergyPlus calculates the power of the fan motor shown in Equation 1 based on the variables defined in Table 1.

$$Pow_{fan} = \frac{Q_{flow} \Delta P_{fan}}{\eta_{fan} \eta_{mot}} \quad (1)$$

Manufacturers typically provide FPTU data in their literature so that engineers can correctly apply FPTUs in the field. These data are typically at an FPTU system level and not at the level of the components that make up an FPTU. Thus, some of the data needed in Equation 1 are not available to the energy modeler. One example is the fan/motor assembly. The fan/motor in an FPTU is a matched assembly and tested as a unit. If manufacturers were to publish efficiency data, it would be a combined fan/motor efficiency, not the individual efficiencies of the fan and motor. Another example is the design air-pressure rise across the fan. Fans in an FPTU (whether a series or parallel unit) are installed inside the FPTU. Determining the pressure rise across the fan would require installation of a pressure tap in the FPTU housing to measure the static pressure inside the FPTU housing. The pressure rise across fans inside an FPTU is not measured, even though this information is an

Table 1. Fan Characteristics Used for Series FPTUs in EnergyPlus

Design air-pressure rise across the fan, ΔP_{fan}
Design volumetric flow rate, Q_{flow}
Fan total efficiency, η_{fan}
Fan motor efficiency, η_{mot}
Fraction of fan waste heat that enters airstream, Q_{toair}

input required by EnergyPlus. Bryant and Bryant (2015) reported some limited pressure differential measurements across a fan inside of a single series FPTU.

If the ECM in the FPTU is programmed to follow the load in the zone, then the fan is operating as a variable-speed fan. LBNL (2014) has an option for modeling variable speed fans, though not directly in an FPTU (or *powered induction unit*, as they are called in EnergyPlus) because the FPTU is assumed to operate at a fixed airflow. For a variable-speed fan, the power required by the fan, Pow_{fan} , at a particular airflow is determined by

$$Pow_{fan} = f_{pl} \frac{Q_{fan_design} \Delta P_{fan}}{\eta_{fan}} \quad (2)$$

where

f_{pl} = part-load power fraction of fan/motor unit operating at a specific airflow

Q_{fan_design} = design airflow for the fan, ft³/min (m³/s)

Because building simulation programs often separate the fan and motor performance in their input, Equation 2 is usually written solely in terms of the power requirement of the fan. To calculate the power to the fan motor would require dividing the fan power by the fan motor efficiency.

The fan part-load power fraction (PLPF) f_{pl} is defined as the power of the fan at a given airflow divided by the power at design airflow.

$$f_{pl} = \frac{Pow_{fan}}{Pow_{fan_design}} \quad (3)$$

The fan part-load power fraction is determined by a fourth-degree polynomial (LBNL 2014).

$$f_{pl} = c_1 + c_2 f_{flow} + c_3 f_{flow}^2 + c_4 f_{flow}^3 + c_5 f_{flow}^4 \quad (4)$$

The part-load airflow fraction (PLAF) f_{flow} in Equation 4 is defined as the airflow produced by the fan at a given speed to the design airflow produced by the fan.

$$f_{flow} = \frac{Q_{fan}}{Q_{fan_design}} \quad (5)$$

Applying this equation requires detailed flow and power information from a manufacturer for the particular fan. Specifically, to fit a fourth-degree polynomial, a minimum of five data points are needed over the range of flow and power of the fan. Some of the manufacturers who provided data for this study only tested at three or four part-load settings for the ECM controller. Thus, for the ECM-controlled fans used in FPTUs, there may be limited data available at part-load conditions, which may make it difficult to get a fit for the fourth-degree polynomial in Equation 4. A second issue with the fourth-degree polynomial fit is that it is a higher-degree polynomial than what is normally expected for a relationship

between fan power and airflow. With the fan affinity laws, one would generally expect the fan power to vary with the cube of the airflow, because the airflow is proportional to the speed of the fan at a given pressure differential across the fan.

$$f_{pl} = \frac{Pow_{fan}}{Pow_{fan_design}} \alpha \left(\frac{Q_{fan}}{Q_{fan_design}} \right)^3 \quad (6)$$

A third-degree polynomial approach to modeling variable-speed fans was used in other building simulation programs (Knebel 1983; BLAST 1986) to estimate f_{pl} .

$$f_{pl} = a_1 + a_2 f_{flow} + a_3 f_{flow}^2 + a_4 f_{flow}^3 \quad (7)$$

Variables $a_1 \dots a_4$ are constants and are given in Table 2. This variable-speed fan model was also in the ASHRAE toolkit of models put together by Brandemuehl (1993). The original figure from which the third-degree polynomial model used by Knebel (1983) and others was first presented by Janisse (1969). Spitler et al. (1986) made the following comments about Janisse's figure:

"The performance data used for comparison were given by Janisse (1969) ... The origin of these curves is undocumented ... However, a comprehensive on-line literature search revealed no documented data on the effect of different methods of modulation on fan performance."

While it is probable that there were original data used by Janisse (1969) to develop the part-load performance model of variable speed fans, it was never documented. This leaves the user of the model in Equation 7 and Table 2 on questionable grounds when trying to defend energy calculations for variable speed fans in building simulation programs that utilize this model. The lack of substantive data indicated there was a need for data than could be used to justify a better part-load performance model of variable speed fans.

Knebel (1983) reported the coefficients (see Table 2) to fit the curves in Janisse (1969). As a consequence, the model in Equation 7 and Table 2 is called the Knebel model in this paper.

Both the third- and fourth-degree polynomial fits are used to estimate the normalized part-load performance of only the fan in building simulation programs. As has been mentioned previously, for FPTU applications, the fan performance cannot be separated from the motor because they are a matched assembly. While the form of Equations 4 or 7 could be used for ECM

Table 2. Values of Constants in Equation 7 (Knebel 1983; BLAST 1986)

Constant	Value
a_1	0.00153
a_2	0.005208
a_3	1.1086
a_4	-0.11636

FPTUs fan/motor assemblies, the part-load power fraction f_{pl} in Equations 4 and 7 would have to be redefined to include the combined fan and motor. If the fan motor efficiency varied with speed, then the shape of the polynomial describing part-load performance may vary from a part-load performance curve that was developed for just the fan alone.

The models represented in either Equations 4 or 7 describe the fraction of airflow and power based off a given design condition. For a model to be complete, the user must know the full-load design airflow and power requirements of the fan/motor assembly. With the full-load design performance, the part-load performance could be estimated with the part-load models developed from Equations 4 or 7.

DATA COLLECTION

Four FPTU manufacturers provided data on their units for this study. The manufacturers are identified as Manufacturers A, B, C, and D in the tables and figures below. The data covered a range in nominal fan motor sizes from 0.33 hp (249 W) to 1 hp (746 W) and included data from both series and parallel terminal units. Table 3 shows the fan motor sizes provided by each manufacturer. Overall, data were provided on 36 fan/motor combinations. Six of the combinations were from parallel and 30 were from series terminal units. Data were also provided on two dual fan/motor assemblies that had 0.33 hp (249 W) and 0.75 hp (560 W) motors. Manufacturer A provided data on 24 of the 36 units in Table 3. The units should cover much of the range of fans and motors expected to be found in FPTUs used in the field. Manufactures apply these fan/motor combinations in a wide range of cabinet sizes and cabinet styles (underfloor or overhead) and cabinet profiles (low and standard). Each cabinet design potentially

produces different flow conditions entering the FPTU fan, which could generate differing air system effects that impact the overall performance of the fan.

Data were collected on fan/motor combinations by manufacturers in their own laboratories and provided to the authors through a representative of the Air-Conditioning, Heating and Refrigeration Institute (AHRI) so that the identity of the manufacturer remained anonymous. Manufactures were asked to provide both descriptive (see Table 4) and performance data (see Table 5) on the fan/motor combinations. In Table 5, the settings on the controllers were specified in DC voltages (typically from 0 to 10 V) or from 0% to 100%.

An identification procedure was developed for reporting each fan/motor combination. Because all of the fan motors in this paper were ECMs, all designations start with "ECM." This designation distinguishes these units from the SCR units evaluated in a complementary paper by the authors (O'Neal et al. 2015). The rated fan motor size, in horsepower, was converted to its decimal equivalent and multiplied by 1000. For example, the identification of a 0.5 hp (373 W) unit would be 0.500 multiplied by 1000 to give a value of 500. The four manufacturers were each given a letter designation of either A, B, C, or D. A 0.5 hp (373 W) fan/motor from Manufacturer A was identified as ECM-500A. If a manufacturer had more than one fan/motor combination of the same size, such as Manufacturer B had for 0.5 hp (373 W), then the first fan/motor was identified as ECM-1000B1 and the second as ECM-1000B2. For cases where there were dual fan/motors in an FPTU, the unit was identified with a 2x before the unit size. For example, the first 0.75 hp (560 W) from Manufacturer A would be designated as ECM-2x750A1.

Table 3. ECM FPTU Fan/Motor Data Provided by Manufacturers

Nominal Fan/Motor Size, hp (W)	Manufacturer A	Manufacturer B	Manufacturer C	Manufacturer D
0.33 (249)	XXXXXXXXXXXX*	X	—	XXX*
2 × 0.33 (249)	XX*	—	—	—
0.50 (373)	XXX*	X	X	—
0.75 (560)	XXXXX*	—	—	X
2 x 0.75 (560)	XX*	—	—	X
1.0 (746)	—	XX	—	XX

*Multiple Xs indicate the manufacturer provided more than one unit's data at that size.

DATA ANALYSIS

Each manufacturer provided their data in spreadsheets. With the discharge area of the fans provided, it was possible to calculate the exit air velocity from the discharge area and measured airflow. With the exit air velocity known, the velocity pressure was calculated and added to the measured static pressure differential across the fan to obtain a fan total pressure. The fan/motor total efficiency η_{fm} was calculated using fan total pressure, mass flow of the air, and fan power

$$\eta_{fm} = \frac{Q_{fan} \Delta P_{tot}}{Pow_{fan}} \quad (8)$$

where

Table 4. Descriptive Data for FPTU and Fan/Motor Combinations

Item
Fan model number
Series or parallel FPTU application
Primary inlet diameter
Design range of airflow of FPTU
Recommended operating pressures
Maximum recommended airflow
Minimum recommended airflow
Fan manufacturer
Motor manufacturer
Motor size
Fan discharge dimensions

Table 5. Detailed Measured Performance Data on Each FPTU Fan/Motor Combination

Item	Units
ECM setting	voltage or value
discharge static pressure	in. w.g. (Pa)
airflow	ft ³ /min (m ³ /s)
current	amps
volt-amps	volt-amps
power factor	—
power	W
motor speed	rpm
power/airflow	W/(ft ³ /min) W/(m ³ /s)

ΔP_{tot} = fan total pressure, in. w.g. (Pa)

Pow_{fan} = power of the fan motor, W

Q_{fan} = fan volumetric airflow, ft³/min (m³/s)

Figure 1 shows sample data for the fan/motor total efficiency versus fan total pressure for the 1 hp (746 W) fan/motor combination from Manufacturer B. The fan/motor total efficiency showed an increase as the fan total pressure was increased. As the ECM setting was increased, the fan and motor rotated faster and the data showed a consistent decrease in efficiency. This figure illustrates the difficulty in attempting to use a single efficiency to describe the efficiency of the ECM fan/motor combination. The efficiency increased with fan total pressure, but the ECM setting (i.e., airflow) also had a large influence. For example, at a total pressure of 0.3 in. w.g. (75 Pa), the fan/motor efficiencies ranged from about 11% at an ECM setting of 100 to 28% at the lowest setting of 1. These wide ranges in efficiency were also found at both higher and lower fan total pressures. Manufacturers typically do not provide the detailed data on efficiencies found in Figure 1 in their product literature. Even if they did, the energy modeler would be left with a large range of efficiencies from which to choose. Unless modelers knew the ECM setting and total pressure for the FPTU, they would only be guessing at a value that might correspond with the actual performance of the FPTU fan/motor. If the ECM in the FPTU were programmed to follow the load in the zone, the ECM would be varying the airflow (and ECM setting) in response to changes in the loads in the zone. Figure 1 would also imply that a single efficiency should not be used to model the FPTU in a variable airflow application.

The fan/motor behavior in Figure 1 shows that the efficiency increases with pressure and decreases with increased

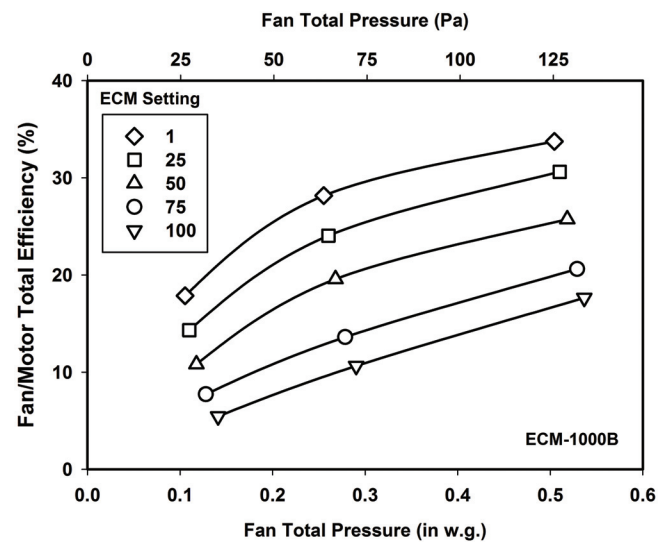


Figure 1 Sample data for total efficiency versus fan total pressure for ECM-1000B, which had a nominal-sized 1 hp (746 W) motor.

ECM setting. Many of the fan/motor combinations at 0.5 hp (373 W) and above had plots similar to Figure 1. If there were deviations from Figure 1, it was generally in the data at the lowest ECM power setting, which was at 2 V or 20% of full scale.

Figure 2 shows the plot of ECM-750A3. While there are differing slopes to the lines for each ECM setting, the trend of lower efficiencies at higher ECM settings was consistent with ECM-1000B in Figure 1.

A substantial number of the 0.33 hp (249 W) fan/motor combinations showed a large variance from the more predictable behavior shown in Figure 1. Figure 3 shows a sample efficiency plot for ECM-333A3. In this case, the lowest efficiencies occurred at the lowest ECM setting (2 V). The efficiency peaked at the 7 V setting, and then decreased at the highest ECM setting (10 V). The efficiency at the 10 V setting initially started near the efficiency of the 2 V setting at the lowest total pressure. It then increased as the total pressure increased, crossing the 5 V efficiency at about 0.4 in. w.g. (100 Pa), and finally intersecting the line for the 7 V setting at nearly 0.8 in. w.g. (200 Pa). While the efficiencies generally increased with increasing total pressure, the increase in efficiency with increasing total pressure at 10 V was much larger than at the other settings.

Building a model that accounted for efficiency as a function of ECM settings and total pressure could potentially be done for individual units such as ECM-1000B and ECM-750A3. However, the behavior of ECM-333A3 and some of the other 0.33 hp (249 W) units were so different, that it would not be possible to develop a generalized model relating fan/motor efficiency to fan total pressure and power settings for all the ECM units evaluated. As discussed later in this section, some of the unusual behavior may be the result of the relative

size of the motor to the maximum power required for the airflow application. Even with the more predictable performance behavior of the larger-sized ECMs, like those in Figures 1 and 2, the wide variation in fan/motor efficiencies would make it difficult for a building modeler to choose a single value of efficiency to input into a building simulation program. These considerations led to the conclusion that an alternative approach should be evaluated. Specifically, it was decided to consider whether the simpler third- or fourth-degree polynomial models for part-load performance, such as those used by Knebel (1983) or LBNL (2014), could be used.

Manufacturers collected data for discharge static pressures ranging from 0.1 to 0.75 in. w.g. (25 to 187 Pa). Table 6 shows the discharge static pressures that each manufacturer used in their data collection. Three manufacturers (A, C, and D) took data at four settings while one (B) took data at three settings. All manufacturers reported data for 0.10 in. w.g. (25 Pa) discharge static pressure. Three manufacturers (A, B, and C) reported data at 0.5 in. w.g. (125 Pa). The top discharge static pressure reported ranged from 0.5 to 0.75 in. w.g. (125 to 187 Pa).

Figure 4 shows sample data from ECM-1000B of the measured fan/motor power versus fan airflow for a range of ECM settings and discharge static pressures. The relationship between fan/motor power and fan airflow was nonlinear for a given discharge static pressure. As the discharge static pressure was increased, the power increased. The general shape of these curves shown in Figure 4 was similar to those of the other units evaluated. In some instances, the differences between the curves over the range in static pressures was small and in some cases, there was overlap in the power versus flow curves at different discharge static pressures. However, all showed the

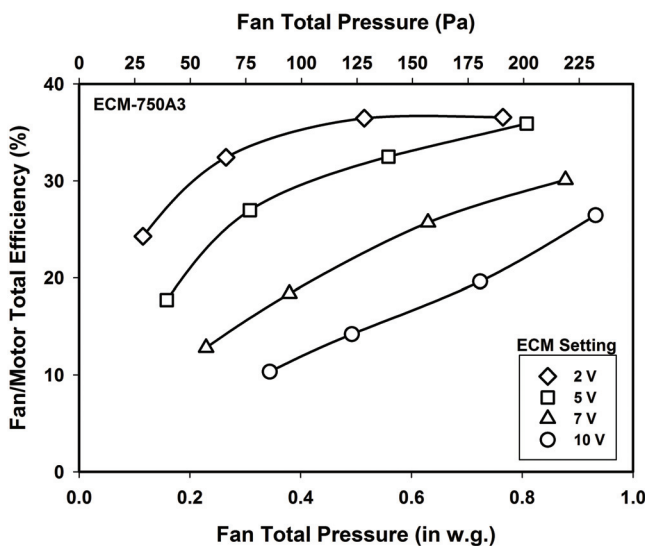


Figure 2 Sample data for total efficiency versus fan total pressure for ECM-750A3, which had a nominal-sized 0.75 hp (560 W) motor.

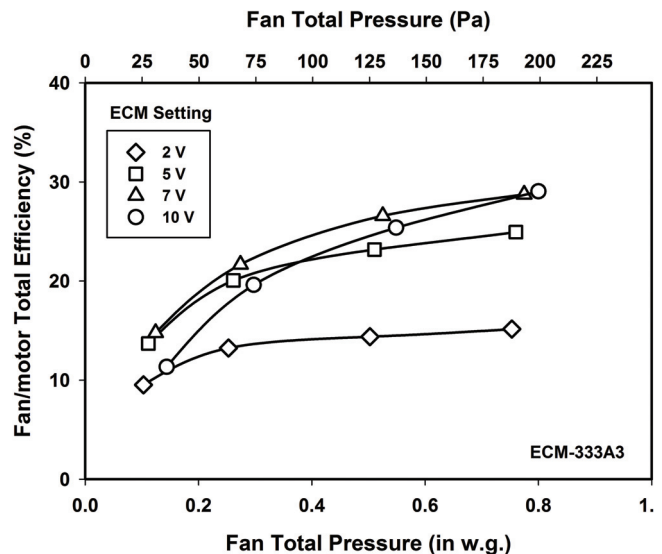


Figure 3 Sample data for total efficiency versus fan total pressure for ECM-333A3, which had a nominal 0.33 hp (249 W) motor.

Table 6. ECM FPTU Fan/Motor Discharge Static Pressure Tests Conducted by Each Manufacturer

Discharge Pressure Setting	Discharge Static Pressure – in w.g. (Pa)			
	Manufacturer A	Manufacturer B	Manufacturer C	Manufacturer D
Lowest	0.10 (25)	0.10 (25)	0.10 (25)	0.10 (25)
Mid-Low	0.25 (63)	0.25 (63)	0.20 (50)	0.30 (75)
Mid-High	0.50 (125)	n.a.	0.40 (100)	0.50 (125)
Highest	0.75 (187)	0.50 (125)	0.60 (150)	0.70 (174)

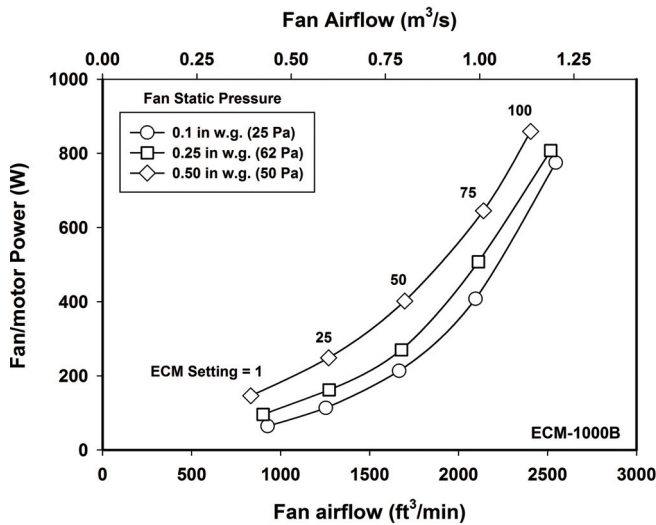


Figure 4 Fan/motor power versus fan airflow as a function of ECM setting and discharge static pressure.

same nonlinear trend for power versus airflow along a specific static pressure line. The shape of the curves in Figure 4 should be similar if the data were normalized to the airflow and power at the maximum ECM setting for a given discharge static pressure. The data should also lend itself to a polynomial fit.

In the prior experimental studies of FPTUs by Edmondson et al. (2011a and 2011b), significant data were taken at 0.25 in. w.g. (63 Pa) static pressure because FPTUs are rated at this discharge pressure (AHRI 2011; ASHRAE 2006). It was decided to focus on the data collected for discharge static pressures ranging from 0.1 to 0.5 in. w.g. (25 to 125 Pa) for the part-load airflow and power analysis. This discharge pressure range bracketed the 0.25 in. w.g. (63 Pa) in the FPTU test procedure and should cover a wide range of FPTU applications in buildings.

PART-LOAD POWER FRACTION MODEL

Figure 5 shows the PLPF f_{pl} versus PLAF f_{flow} at a discharge static pressure of 0.5 in. w.g. (125 Pa) for the 0.33 hp (249 W) fan/motor combinations provided by the manufacturers. Fan/motor combinations ECM-333A9 and ECM-333A10

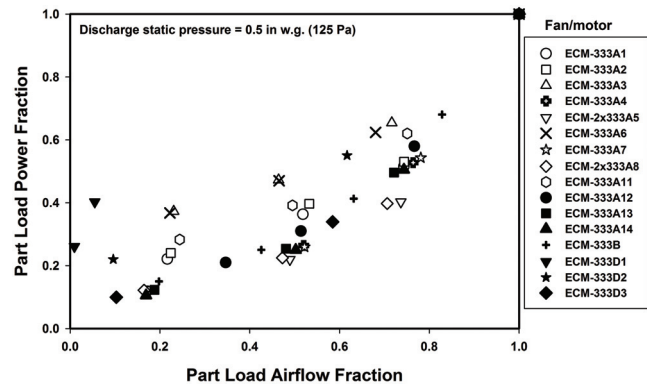


Figure 5 Fan part-load power fraction versus part-load airflow fraction at 0.5 in. w.g. (125 Pa) for the 0.33 hp (249 W) fan/motor combinations.

were omitted from the plot because they did not have enough data to plot the part-load power fraction.

The definitions of f_{pl} and f_{flow} are modified in Equations 9 and 10 so the denominator is the redefined to mean the power and airflow of the fan/motor at the maximum ECM setting rather than the design power and airflow.

$$f_{pl} = \frac{Pow_{fan}}{Pow_{maxECM}} \tag{9}$$

$$f_{flow} = \frac{Q_{flow}}{q_{maxECM}} \tag{10}$$

where

Pow_{maxECM} = fan motor power at the maximum ECM setting at a specified discharge pressure

Q_{maxECM} = fan airflow at the maximum ECM setting at a specified discharge pressure

For most of the ECM controllers, the maximum setting was 10 V or 100%. As can be seen in Figure 5, there was a large spread in the data, which was also typical of the plots at other discharge static pressures. A closer look at the data indicated a possible explanation for some of the scatter shown in Figure 5. Table 7 lists the nominal motor size, the maximum fan power draw, the power ratio, and maximum airflow for each of the 0.33 hp (249 W) fan/motor combinations at 0.5 in.

Table 7. Maximum FPTU Power Application, Power Ratio, and Airflow for the 0.33 hp (249 W) Units Operating at 0.5 in. w.g. (125 Pa) Discharge Static Pressure

Fan/Motor	Nominal Motor Size, W	Maximum FPTU Application, W	Power Ratio	Max Airflow, ft ³ /min (m ³ /s)
ECM-333A1	249	190	0.765	480 (0.23)
ECM-333A2	249	179	0.721	477 (0.23)
ECM-333A3	249	110	0.443	433 (0.20)
ECM-333A4	249	360	1.449	884 (0.42)
ECM-2x333A5	2×249	720	1.448	1732 (0.82)
ECM-333A6	249	117	0.471	454 (0.21)
ECM-333A7	249	370	1.489	861 (0.41)
ECM-2x333A8	2×249	730	1.468	1816 (0.86)
ECM-333A9	249	210	0.843	459 (0.22)
ECM-333A10	249	440	1.767	915 (0.43)
ECM-333A11	249	166	0.668	625 (0.30)
ECM-333A12	249	300	1.208	882 (0.42)
ECM-333A13	249	260	1.047	519 (0.24)
ECM-333A14	249	380	1.530	907 (0.43)
ECM-333B1	249	349	1.405	1140 (0.54)
ECM-333D1	249	111	0.447	452 (0.21)
ECM-333D2	249	195	0.785	755 (0.36)
ECM-333D3	249	497	2.001	1427 (0.67)

w.g. (125 Pa). The power ratio was the maximum fan motor power at 0.5 in. w.g. (125 Pa) used by the ECM fan motor at the maximum ECM setting divided by the nominal motor size. Each of the fan motors was nominally rated at 249 W. Comparing the fan/motor combinations in Table 7 with the data in Figure 5, a trend emerges. Those ECMs with a power ratio less than 0.8 tend to have the poorer part-load performance (i.e., higher part-load power fraction for a given part-load airflow fraction). Without detailed design characteristics and performance data on each of the individual fans and motors, it would be difficult to pinpoint the exact reasons why the part-load performance was so different for those with power ratios below 0.8. One possible factor may have to do with the power used by the ECM controller. This controller probably uses a fixed amount of power even at low settings and this power, while perhaps “in the noise” at high ECM settings, may be significant at lower settings. For example, ECM-333D1 at its lowest ECM setting (2 V) used only 28.9 W at 0.5 in. w.g. (125 Pa). If the controller only used 10 W, then one-third of the power at the low setting would be due to the controller.

Another factor may be the performance of the motors at very low loads. The 28.9 W for ECM-333D1 was less than 12% of the nominal power rating of the motor. The authors were not aware of any study showing the part-load efficiency of ECM motors. If there was any efficiency drop in the motor at extremely low loadings, then it would potentially create a smaller overall power savings at the lower settings than those fan/motor combinations with higher power ratios. In either case, neither the amount of controller power or ECM motor efficiency were separately measured or provided in the data we evaluated. It may be worthwhile in a future study to obtain and analyze more detailed information on the units that could shed some insights into the differences in part-load performance for these units with the low power ratios.

Even though those units with power ratios less than 0.8 did not achieve as large a drop in part-load power fraction, their full-load power performance was typically better than the units with power ratios above 0.8. Those units with power ratios below 0.8 had an average full-load power to airflow ratio

of 0.29 W/ft³/min (615 W/m³/s) compared to 0.38 W/ft³/min (805 W/m³/s) for the units with a power ratio above 0.8.

Seven of the 0.33 hp (249 W) fan/motor combinations had power ratios less than 0.8. These were separated from the rest of the fan/motor combinations along with two of the larger units. None of these were used for the analysis below. After removal of the units with the low power ratios from the population of the 0.33 hp (249 W) units in Figure 5, the remaining units were plotted in Figure 6 for static discharge pressures ranging from 0.1 to 0.5 in. w.g. (25 to 125 Pa). While there was some scatter in the data, the data tended to group together along a nonlinear curve that could be fit with the third-degree polynomial shown in Equation 7, except that the definitions in Equations 9 and 10 would be substituted for the PLPF f_{pl} and the PLAF f_{low} .

The PLPF versus PLAF data for the ECM-500, 750, and 1000 were added to the ECM-333 units and all were plotted together in Figure 7. Besides the units with low power ratios, there were four fan/motor combinations (ECM-333A9, ECM-333A10, ECM-750A5, and ECM-750A6) with only partial data sets available that were also not used in the analysis. All four of these were from parallel terminal units. A regression analysis was performed and the data fit to the third-degree polynomial of Equation 7. The regression coefficients are shown in Table 8. The r^2 was 0.981, which indicated an excellent fit for the third-degree polynomial. Because the lowest data for PLAF only went down to about 0.10, the regression should be used with caution below this value. The PLPF for the third-degree polynomial leveled off to a value of 0.062 for values of PLAF below 0.1. The nonzero value of PLPF at low values of PLAF may be due to the presence of the controller, which requires a small amount of power even when the controller is operating at low values.

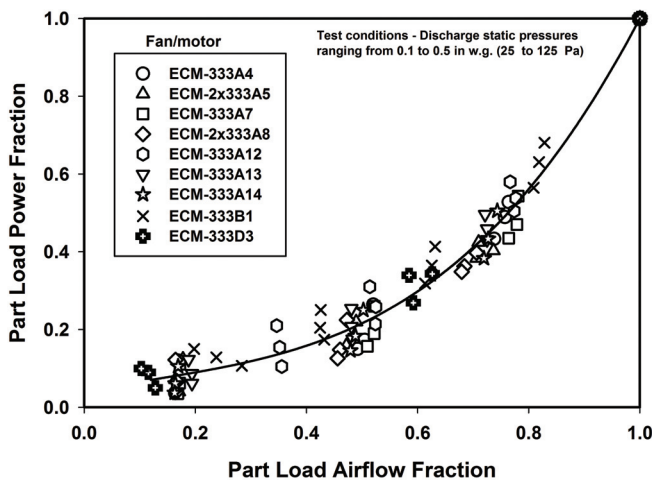


Figure 6 Fan part-load power fraction versus part-load airflow fraction at discharge pressures ranging from 0.1 to 0.5 in. w.g. (50 to 125 Pa) for the 0.33 hp (249 W) fan/motor combinations.

Because EnergyPlus uses a fourth-degree polynomial fit to characterize part-load performance of fans, a fourth-degree polynomial was also fit to the same data. The coefficients for a fourth-degree polynomial are provided in Table 9.

The third- and fourth-degree polynomials are plotted in Figure 8, along with the Knebel model and the curve for the

Table 8. Values of Coefficients in Equation 7 for the Best-Fit Curve to the Data in Figure 7

Coefficients	Value
a_1	0.061715
a_2	0.093022
a_3	-0.11627
a_4	0.961538

Table 9. Values of Coefficients in Equation 4 for Fourth-Degree Polynomial Fit Curve for the Data in Figure 7

Coefficient	Value
c_1	0.116008
c_2	-0.46192
c_3	1.679005
c_4	-1.31496
c_5	0.982138

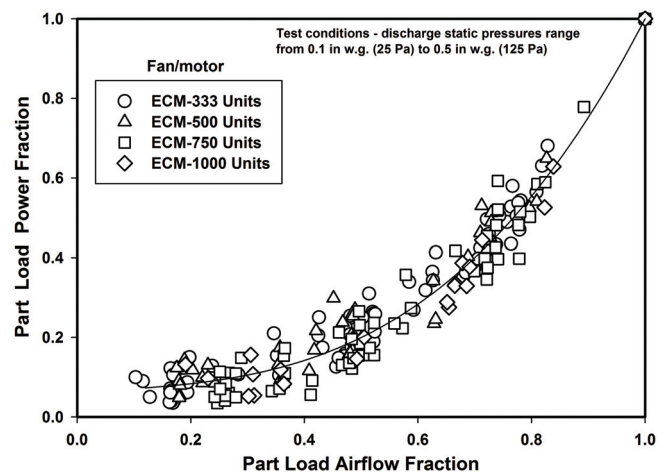


Figure 7 Fan part-load power fraction versus part-load airflow fraction at discharge pressures ranging from 0.1 to 0.5 in. w.g. (25 to 125 Pa) for the range of fan/motor combinations in this study.

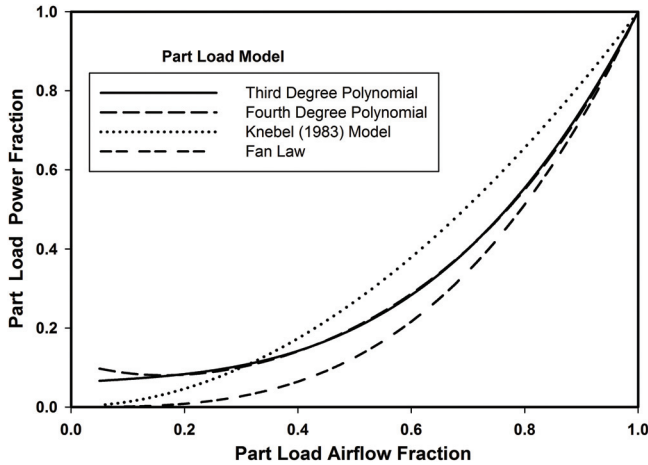


Figure 8 Plots of the third- and fourth-degree polynomial fits of the data shown in Figure 7, along with the Knebel (1983) model and the fan power law.

traditional fan law relating fan airflow and power. Both the polynomial fits generally fell nearly on top of each other. The only exception was at values of the PLAF below 0.17 where the PLPF estimated by the fourth-degree polynomial increased with decreasing values of PLAF. At 0 PLAF, the fourth-degree polynomial had a PLPF of 0.116. While the fourth-degree polynomial fit the data closely for most of the range of data, the third-degree polynomial did not have the upward trend in the values of PLPF at low PLAFs. For these data, there was no advantage to using the more complicated fourth-degree polynomial fit. The Knebel model estimated higher PLPFs for all PLAFs down to about 0.3, then it predicted lower values of PLPFs down to zero PLAF. At a PLAF of 0.6, the third-degree polynomial fit estimated a PLPF of 0.28 while the Knebel model estimated a PLPF of 0.39—nearly 40% more power fraction for the same airflow fraction. When modeling an ECM fan/motor on an FPTU operating between 30% and 100% of design airflow, the current third-degree polynomial fit estimated significantly less energy use than would the Knebel model. The curve for the fan law estimated lower power load fractions than all the other curves. The fan laws apply to the power input to the fan only and not the power input to the motor driving the fan. The fan motor introduced additional losses in efficiency not present in just the fan alone. Thus, it should not be surprising that the fan law curve estimated a more optimistic reduction in power fraction than did the regression for the fan/motor combinations.

One potential problem with the fourth-degree polynomial fit was encountered when first analyzing some of the fan data from Manufacturer A. Data from six units operating at 0.50 in. w.g. (125 Pa) were initially plotted at ECM settings of 2, 5, 7, and 10 V, with 10 V being full scale.

The surprising result of the best fit is shown in Figure 9. Having only a small amount of data with most of it clumped near the same PLAFs did not provide a wide enough scatter in

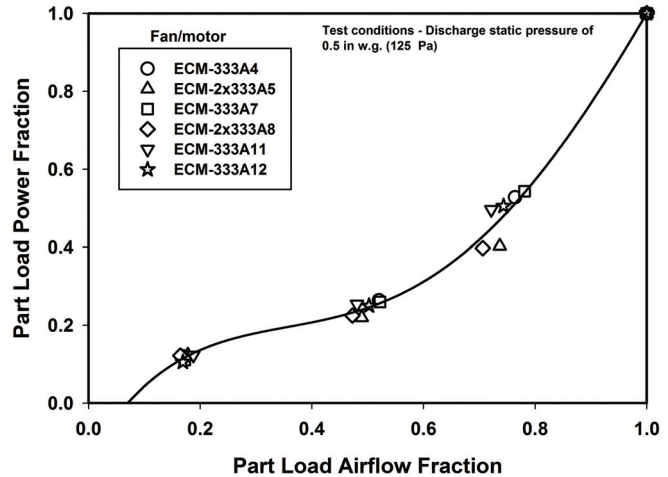


Figure 9 Plot of the fourth-degree polynomial fit of the data shown for six units from Manufacturer A.

data to allow a fourth-degree polynomial to provide a curve with a physically realistic shape. Rather than having a fit where the fractional power continually decreased with decreasing fractional flow, the curve began to assume a very shallow slope at a PLAF of about 0.4, and then dropped quickly as the PLAF decreased below 0.2. The curve went negative at a PLAF of 0.07. Clearly, negative values of the fractional power would be unacceptable. This figure illustrates one danger in using a fourth-degree polynomial with limited part-load data.

POWER AND AIRFLOW AT MAXIMUM ECM SETTING

The PLPF versus PLAF curve shown in Figure 7 was generated with the power and airflows normalized to their respective values at the maximum settings of the ECMs. To calculate the power and airflow at part-load conditions in a building simulation model, the values of power and airflow at the maximum ECM settings need to be known.

The airflow and power data at the maximum ECM settings for the units used in Figure 7 were plotted and shown in Figure 10. There was significant scatter in the data, particularly near an airflow of 1500 ft³/min (0.71 m³/s) for two units. One was a 0.5 hp (373 W) unit and the other was a 0.75 hp (560 W) unit. All of the data were fit with a linear regression that went through the origin. The relationship between the power of the fan and the fan airflow at maximum ECM is given by Equation 11.

$$P_{ow_{maxECM}} = C_1 Q_{maxECM} \quad (11)$$

where

$$C_1 = 0.380 \text{ W}/(\text{ft}^3/\text{min}) \quad (805 \text{ W}/[\text{m}^3/\text{s}])$$

A second-degree polynomial was also fit to the data, but only provided a marginally improved r^2 over a linear model. It was decided to use the simpler linear model.

The slope of the line in Figure 10 was surprisingly close to the 0.372 W/ft³/min (788 W/m³/s) slope for the SCR units from the same group of manufacturers (O'Neal et al. 2015). This result would suggest that at full load, there was not a significant difference in performance, as measured by W/ft³/min (W/m³/s), between the SCR and ECM fan/motor units evaluated in this study. However, as discussed in the next section, there was a large reduction in W/ft³/min (W/m³/s) of the ECM-controlled units if they were run at part load rather than at the maximum ECM setting. This performance improvement was not reflected in the linear regression shown in Figure 10. The improvement in part-load performance is discussed in the following paragraphs.

With the power and airflow at the maximum ECM settings (Figure 10) and the part-load performance curve (Figure 7), it was now possible to calculate the power requirement for a given airflow at part-load conditions. The part-load performance curves of Figure 7 and Equation 7 were integrated into the plot of the power and airflow performance at the maximum ECM settings (see Figure 10). This integration resulted in a set of part-load curves that dropped down from the line representing the power and airflow at the maximum ECM setting (see Figure 11).

The part-load curves illustrated in Figure 11 started at 1500, 2000, 2500, 3000, and 3500 ft³/min (0.71, 0.94, 1.18, 1.42, and 1.66 m³/s). These were created by multiplying the third-degree polynomial of Equation 7 (having the coefficients of Table 8) with the values of power at the maximum ECM settings for the respective airflows calculated from Equation 11. For example, at 2000 ft³/min (0.94 m³/s), the power at maximum ECM setting was 760 W. For the curve that dropped down from 2000 ft³/min (0.94 m³/s), the PLAF at a partial airflow value was calculated, then used to determine the PLPF. The PLPF was then multiplied by the full-load power (760 W)

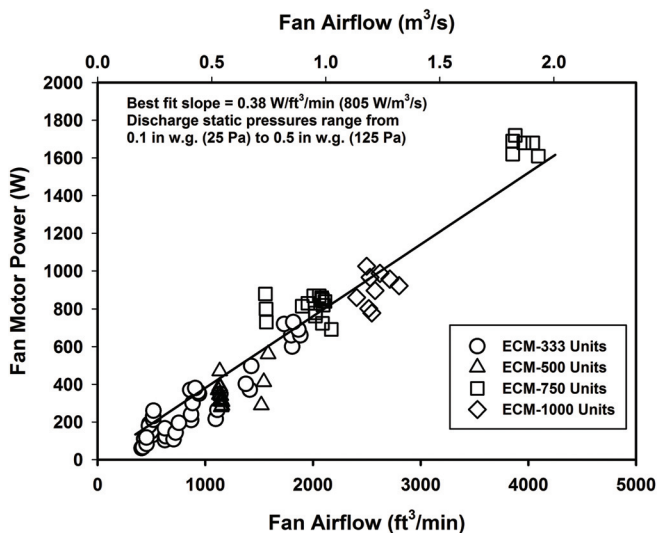


Figure 10 Full-load fan motor power and fan airflow at the maximum ECM setting for the units in this study.

to determine the power the fan motor would use at the lower airflows. This process was repeated over a range of partial airflows to estimate reduction in power as the airflow decreased. The results for the PLPFs are shown in Table 10 for a unit having 2000 ft³/min (0.94 m³/s) airflow at the maximum

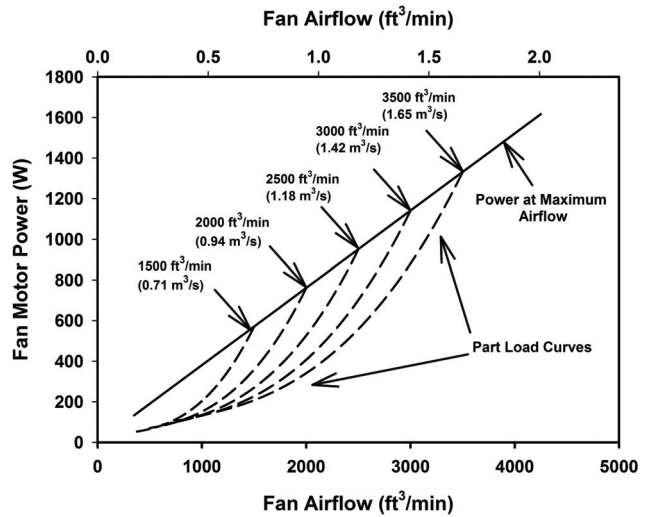


Figure 11 Relationship between the part-load curves to the airflow and power curve at maximum ECM setting.

Table 10. Sample Value of Part-Load Airflows and Power for a Unit with a Maximum Airflow of 2000 ft³/min (0.94 m³/s) and Power of 760 W

Airflow ft ³ /min (m ³ /s)	PLAF	PLPF	Power (W)	Power/Airflow W/ft ³ /min (W/m ³ /s)
2000 (0.94)	1.00	1.00	760	0.38 (805)
1900 (0.90)	0.95	0.870	661	0.35 (737)
1800 (0.85)	0.90	0.752	572	0.32 (673)
1700 (0.80)	0.85	0.647	492	0.29 (613)
1600 (0.76)	0.80	0.554	421	0.26 (558)
1500 (0.71)	0.75	0.472	358	0.24 (506)
1400 (0.66)	0.70	0.400	303	0.22 (459)
1300 (0.61)	0.65	0.337	256	0.20 (417)
1200 (0.56)	0.60	0.283	215	0.18 (380)
1100 (0.52)	0.55	0.238	181	0.16 (349)
1000 (0.47)	0.50	0.199	152	0.15 (322)
900 (0.43)	0.45	0.168	127	0.14 (299)
800 (0.38)	0.40	0.142	108	0.14 (286)

ECM setting. This table also demonstrates how rapidly the power/airflow drops under part-load operation. At the maximum ECM setting, where the PLAR and PLPR are both one, the fan/motor unit had an estimated 0.38 W/ft³/min (805 W/m³/s) while at a PLAR of 0.5, it had improved to 0.15 W/ft³/min (322 W/m³/s). The combination of the part-load curve (Equation 7) and the power/airflow at the maximum ECM setting (Equation 11) give the modeler the tools necessary to estimate the part-load power for a given airflow.

APPLICATION OF ECM FPTUS WITH FIXED AIRFLOW SETTING

A traditional approach to applying ECM FPTUs is to set the airflow of the ECM to a fixed value to satisfy the design load in the space. For this type of application, a modeler might be tempted to use the relationship in Equation 11 with the design airflow to calculate the required power. However, the data plotted in Figure 11 would suggest that if a modeler used such a simple approach, their estimate of the power (and energy use) for the ECM FPTU would be larger than might be obtained if a slightly larger airflow capacity ECM FPTU were installed. The curves that drop down from the higher airflow capacity units tended to provide lower power consumption than a unit with airflow at the maximum ECM setting that just matched the design airflow requirements.

To illustrate the potential benefit of using the part-load performance of a higher-capacity ECM unit, consider the following example. Assume that a space calls for 2000 ft³/min (0.94 m³/s) of air to satisfy the design load and an FPTU with an ECM fan/motor is specified that can produce 2000 ft³/min (0.94 m³/s) at the maximum ECM setting. Using Equation 11, the expected power used by the ECM fan would be calculated to be 760 W. This value of power is shown in Figure 12 where the 2000 ft³/min (0.94 m³/s) airflow intersects the line for fan power at the maximum ECM setting.

If a slightly larger FPTU was chosen which had a capacity of 2500 ft³/min (1.18 m³/s) at its maximum ECM setting, but was set at a lower airflow so that it produced the required 2000 ft³/min (0.94 m³/s), then its PLAF would be 2000/2500 = 0.8. Using Equation 7 and the coefficients in Table 8, the PLPF would be 0.554 for a PLAF of 0.8. The power at the maximum ECM setting for the 2500 ft³/min (1.18 m³/s) unit was 950 W from Equation 11. The expected power at 2000 ft³/min (0.94 m³/s) would be the full-load power (950 W) multiplied by the PLPF (0.554), which would be 526 W (See Figure 12). This power usage represented a savings of 30.8% over the unit that was sized to just meet the thermal load requirements of the zone at the maximum ECM setting. Figure 12 illustrates the savings for several other oversized units. If a unit with a larger capacity of 3000 ft³/min (1.42 m³/s) were chosen and only run at the required 2000 ft³/min (0.94 m³/s) airflow, then the models developed from the data would suggest that the power usage would drop to 407 W. If the application were in a series FPTU where the fan was on continuously, then the lower power usage could represent a significant annual

savings in energy use. Whether an engineer should take advantage of the oversizing would depend on variables such as the incremental cost of the larger FPTUs, noise requirements, and size of the cabinet. Because FPTUs are installed in plenum and underfloor areas, there may not be enough physical space to install a larger unit that has a higher airflow capacity than what is required to meet the design airflow. These considerations go beyond the scope of this paper, but are important considerations in the application of an FPTU.

This sample problem illustrates that an energy modeler has some leeway in a FPTU for the particular application. The documentation of some of the building simulation programs provided little guidance on sizing FPTUs to best fit the application. The sample problem shows that the choice of sizing of the FPTU relative to the design load can potentially have a profound impact on the estimated energy use of FPTU in a particular application. With the data and correlations available previously stated, it should be possible to determine a strategy to provide an optimum sized FPTU for a particular application.

The discussion relative to Figure 12 is based on the combination of the power and airflow at the maximum ECM setting and the third-degree polynomial part-load curve. One could legitimately ask how realistic are the reductions in power and power/airflow shown in Figure 12. To try to answer that question, a simple test from the data supplied by the manufacturers was evaluated. Unit ECM-333A11 had an airflow and power at a maximum ECM setting of 517 ft³/min (0.24 m³/s) and 231 W, respectively, at 0.25 in. w.g. (62 Pa) static pressure. If the design requirement for a space were 517 ft³/min (0.24 m³/s), then this unit would just match the load at its maximum ECM setting. We then considered three other units that had higher airflow rates at their maximum ECM settings:

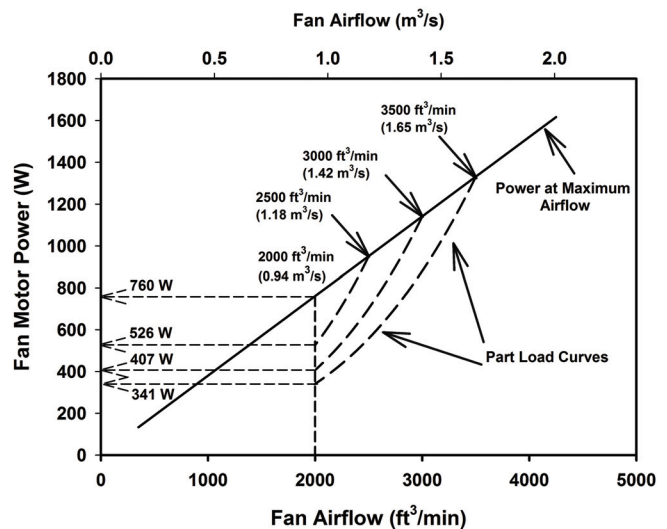


Figure 12 Illustration of how larger ECM fan/motor units can be used to reduce power at 2000 ft³/min (0.94 m³/s).

ECM-333A4, ECM-500A2, and ECM-750A1. The airflow at maximum ECM setting for all four are listed in Table 11.

If the three alternative units were used to provide the design airflow then each would be set at 517 ft³/min (0.24 m³/s). The power consumption at that airflow could be calculated for each of the units based on the data provided by the manufacturers for those units. Table 12 shows the PLAF, the power, and the power/airflow for the base unit (ECM-333A11) and the three alternative ECM units. The trend in Table 12 with decreasing power and power/airflow with increasing capacity was consistent with that shown in Figure 12. Table 12 suggests that it is possible to have considerable savings in power by using an oversized ECM FPTU that operates at a reduced speed to meet the design airflow requirements. Table 12 does not say whether some of the larger units would be practical due to economics or physical constraints, but the data support the trends shown in Figure 12.

APPLICATION OF ECM FPTU TO FOLLOW THE THERMAL LOAD OF THE ZONE

If the ECM FPTU is programmed to vary airflow to meet the thermal load in the zone, then both the performance of the FPTU at the maximum ECM setting (Equation 11 and Figure 10) and the part-load performance (Equation 7, Table 8, and Figure 7) would be needed to estimate the required power and energy used by the fan motor in the FPTU. If a building energy modeler has manufacturer's performance data available

Table 11. Four ECM units with Their Capacity and Power Ratings at the Maximum ECM Setting at 0.25 in. w.g. (62 Pa) Static Pressure

Unit	Capacity, ft ³ /min (m ³ /s)	Power, W
ECM-333A11	517 (0.24)	231
ECM-333A4	892 (42)	370
ECM-500A2	1144 (0.54)	710
ECM-750A1	2086 (0.85)	850

Table 12. PLAF, Power, and Power/Airflow for Four ECM Units Operating at 517 ft³/min (0.24 m³/s)

Unit	PLAF	Power (W)	Power/Airflow, W/ft ³ /min (W/m ³ /s)
ECM-333A11	1.00	231	0.449 (951)
ECM-333A4	0.58	89	0.172 (364)
ECM-500A2	0.45	66	0.128 (271)
ECM-750A1	0.25	50	0.096 (203)

for the maximum ECM setting, then these data should be used to provide the power at the design airflow at the maximum ECM setting. Likewise, if the modeler had access to part-load data from a manufacturer, then it would be possible to develop a third-degree polynomial fit to get the coefficients in Equation 7. Lacking manufacturer's data, the coefficients in Table 8 for part-load performance should be used.

If no manufacturer's data are available, then Equation 11 can be used to calculate the power for design airflow if the FPTU is sized so that the airflow at the maximum ECM setting just equals the airflow needed to meet the design thermal load in the zone (i.e., $Q_{maxECM} = Q_d$). As the thermal load requirements in the zone change, the airflow (Q_f) needed to satisfy that load can be calculated and used to estimate the part-load airflow fraction.

$$f_{flow}\left(\frac{Q_f}{Q_d}\right) = \frac{Q_f}{Q_d} \quad (12)$$

With the PLAF known, it can be substituted into Equation 7 to calculate the expected part-load power fraction, $f_{pl}(Q_f/Q_d)$. The fan motor power, Pow_{fan} , would then be calculated from Equation 13.

$$Pow_{fan} = f_{pl}\left(\frac{Q_f}{Q_d}\right) Pow_{maxECM} \quad (13)$$

In building simulation programs, the load varies each hour, so the part-load airflow fraction would be recalculated each hour, and then used to estimate the new part-load power fraction and fan power.

The procedure above assumes that the airflow at the maximum ECM setting just meets the design airflow requirements for the zone. If the FPTU is oversized, then the airflow needed to satisfy the design thermal load in the zone would be less than the airflow at the maximum ECM setting for the FPTU. In this situation, the ECM setting at design airflow for the FPTU would be lower than the airflow at the maximum ECM setting for this unit. Because the PLPF and PLAF are normalized to the maximum ECM setting, installing a slightly larger fan/motor than required would mean that at design conditions, the unit would not be operating at a PLAF and PLPF of 1.0, but would be operating at some point down the curve in Figure 7.

Consider the following example. Assume a zone had a design airflow requirement of 1500 ft³/min (0.71 m³/s). If an FPTU were installed with an airflow at a maximum ECM setting that just met the design load, its power would be 570 W according to Equation 11. If the thermal load in the zone were to drop so the airflow needed was 1000 ft³/min (0.47 m³/s), then the PLAF would be 1000/1500 or 0.667. Using Equation 7 for part-load operation would yield a PLPF of 0.357 and power requirement of 570 W × 0.357 = 203 W. Similar calculations were made at lower airflows and are shown in Table 13. If instead of a 1500 ft³/min (0.71 m³/s) capacity unit, an oversized unit with 2000 ft³/min (0.94 m³/s) capacity was

installed, then at the maximum ECM setting, it would use 760 W according to Equation 11. However, this unit was installed in an application where the design airflow requirement was 1500 ft³/min (0.71 m³/s) which corresponded to a PLAF of 1500/2000 or 0.75. Applying Equation 7, a PLAF of 0.75 yielded a PLPF of 0.47 or a power of 0.47 × 760 W = 357 W at the design airflow of 1500 ft³/min (0.71 m³/s). This oversized unit used only 357 W at the design airflow compared to 570 W for the unit that just met the design load. At the part-load condition of 1000 ft³/min (0.47 m³/s), the oversized unit would be at a PLAF of 0.5 which would yield a PLPF of 0.20 or a power requirement of 0.20 × 760 W = 152 W. The oversized ECM unit still used less power (152 W versus 203 W) at 1000 ft³/min (0.47 m³/s) than the unit whose maximum capacity just matched the design airflow. The calculations for the lower airflows for the oversized unit are shown alongside the 1000 ft³/min (0.47 m³/s) unit in Table 13. The oversized unit used less power at all airflows down to about 500 ft³/min (0.24 m³/s) where the 1000 ft³/min (0.47 m³/s) unit began to have comparable or less power consumption. While the larger unit used lower power at the design airflow, its power advantage did not persist at the lower airflows. Thus, a slightly oversized unit may be preferable in applications where much of the airflow over the course of the year was near the design airflow. In contrast, a unit that provides just the needed airflow to meet the design thermal load may be preferable if the zone spends a considerable amount of time at low loads. Trying to determine an optimal selection would require knowledge of the hourly loads in a space over the course of a year as well as energy and installation costs.

SUMMARY AND CONCLUSIONS

Electronically commutated motors are now widely applied in fan powered terminal units. This paper presented an analysis of a wide range of ECM fan/motor combinations

Table 13. Comparison of the Part-Load Performance of the Base Unit That Is Just Sized to Meet the Thermal Load and One Oversized Unit That Has 33.3% More Airflow Capacity

Zone Airflow ft ³ /min (m ³ /s)	Base Unit, 1000 ft ³ /min (0.47 m ³ /s) Capacity		Oversized Unit, 2000 ft ³ /min (0.94 m ³ /s) Capacity	
	PLAF	Power, W	PLAF	Power, W
1500 (0.71)	1.000	570	0.750	357
1000 (0.47)	0.667	203	0.500	152
750 (0.35)	0.500	113	0.375	100
500 (0.24)	0.333	65	0.250	70
250 (0.12)	0.167	45	0.125	56

provided by four FPTU manufacturers. The data showed scatter, which could be expected to occur because each manufacturer used different fans and motor combinations as well as their own design strategies for each unit. Even with the scatter, it was possible to develop a third-degree polynomial fit to the part-load data in the general format used by prior building energy simulation models. Unlike models in prior building energy simulation programs that focused solely on the fan, the part-load model developed here included the fan/motor assembly. While the data showed the same general shape as the third-degree polynomial of Knebel (1983), the drop in power was much steeper for higher part-load airflows. Unlike the Knebel (1983) model that went to zero PLPF at zero PLAF, the model for the ECM fan/motor units leveled off near 0.062 for PLAF values less 0.1. The non-zero value of PLPF may correspond to a small amount of power required by the controller in the ECM even where there is little or no airflow.

The analysis of the data also provided estimates of the power/airflow relationship for ECM fan/motors operating at their maximum ECM setting. An energy modeler should be able to directly use this relationship along with the third-degree polynomial regression to estimate the hourly performance of ECM fan/motors in FPTUs.

There was an issue with the data for the fan/motor units whose power ratios were less than 80%. The issue showed up primarily in some of the 0.33 hp (249 W) units where the part-load power fraction did not drop as much with lower airflow fractions as did the ECM fan/motor units that had higher power ratios. While the data on the lower power ratio units was not used in this analysis, it may be worthwhile to examine additional information on these units that could help provide more insights into the differences in performance of these units.

In looking at the application of the part-load and full-load models to estimating ECM FPTU performance both for constant airflow and variable airflow applications, the analysis suggested that there is a benefit to oversizing FPTUs relative to design airflow requirements for the zone. The analysis also suggested that it might be possible to determine an optimal amount of oversizing for a particular application if the part-load model were coupled with a building simulation program and fuel and installation costs factored into an evaluation. This matter appeared to warrant further study.

ACKNOWLEDGMENT

We wish to thank the AHRI for its support of this project. In particular, we wish to thank all the members of the Air Control and Distribution Devices Committee for their input and advice.

REFERENCES

- AHRI. 2011. ANSI/AHRI Standard 880 (I-P) with addendum 1, *Performance rating of air terminals*. Arlington, VA: Air-Conditioning, Heating, and Refrigeration Institute.

- ASHRAE. 2006. ANSI/ASHRAE Standard 130-1996, *Methods of testing for rating ducted air terminal units*. Atlanta: ASHRAE.
- ASHRAE. 2012. Room air distribution equipment. Ch. 20, *ASHRAE Handbook—HVAC Systems and Equipment*. Atlanta: ASHRAE.
- BLAST. 1986. *Building loads analysis and system thermodynamics programs: Users manual*, Version 3.0, Army Construction Engineering Research Laboratory. Champaign, Illinois: Building Loads Analysis and System Thermodynamics.
- Brandemuehl, M.J. 1993. *HVAC 2 toolkit*. Atlanta: ASHRAE.
- Bryant, J., and Bryant, S., 2015. In situ fan differential pressure rise for a series VAV fan power terminal unit with SCR control. *ASHRAE Transactions* 121(2): in press.
- Cramlet, A. 2008. Performance of ECM controlled VAV fan power terminal units. Master's Thesis, Texas A&M University, College Station, TX.
- Davis, M., J. Bryant, and D.L. O'Neal. 2012. Modeling the performance of ECM and SCR series fan-powered terminal units in single-duct VAV systems. *ASHRAE Transactions* 118(1).
- Edmondson, J., D.L. O'Neal, J.A. Bryant, and M.A. Davis. 2011a. Performance of series fan powered terminal units with electronically commutated motors. *ASHRAE Transactions* 117(2).
- Edmondson, J., D.L. O'Neal, J.A. Bryant, and M.A. Davis. 2011b. Performance of parallel fan powered terminal units with electronically commutated motors. *ASHRAE Transactions*. 117(2).
- Janisse, N. 1969. How to control air systems. *Heating, Piping and Air Conditioning* 41(4):129–136.
- Knebel, D. E., 1983. *Simplified energy analysis using the modified bin method*. Atlanta: ASHRAE.
- LBNL. 2014. Air system distribution terminals. In *Energy-Plus engineering reference—The reference to Energy-Plus calculations*. Berkeley, CA: Lawrence Berkeley National Laboratory.
- O'Neal, D.L., D. Ingram, and C. Reid. 2015. Modeling fan-power terminal unit fan/motor combinations controlled by silicon-controlled rectifiers. *ASHRAE Transactions* 121(2): in press.
- Spitler, J.D., D.C. Hittle, D.L. Johnson, and C.O. Pedersen. 1986. Fan electricity consumption for variable air volume. *ASHRAE Transactions* 92(2):5–18.
- Yin, P. and D.L. O'Neal. 2014a. Characterizing airflow and power of VAV series fan-powered terminal units from component data—Part I. *ASHRAE Transactions* 120(1).
- Yin, P. and D.L. O'Neal. 2014b. Characterizing airflow and power of VAV series fan-powered terminal units from component data—Part II. *ASHRAE Transactions* 120(1).

AT-15-026

Development of Models to Simulate the Part-Load Performance of Oversized ECM Fan-Powered Terminal Units

Dennis L. O'Neal, PhD, PE
Fellow ASHRAE

ABSTRACT

Mathematical models were developed for estimating the performance of oversized fan-powered terminal units with electronically commutated motors in both constant and variable airflow applications. These models can be readily implemented in building energy simulation programs to estimate the annual energy use of fan-powered terminal units. The models were developed from data from 36 fan/motor combinations used in commercially available fan-powered terminal units with fan motors ranging from 0.33 to 1 hp (249 to 746 W) and fan static discharge pressures ranging from 0.1 to 0.50 in. w.g. (25 to 125 Pa). Data from six of the 36 fan/motor combinations were from parallel fan-powered terminal units. The required inputs for the constant airflow model included only the design airflow for the space and fraction oversizing relative to the design airflow to estimate the power and energy use of the fan-powered terminal unit. For the variable airflow model, the operating airflow rate was required in addition to the design airflow and fraction oversizing. The model developed for fixed airflow operations was used to analyze the impact of using fan-powered terminal units with electronically commutated motors in applications where the capacity of the unit is oversized relative to the design airflow but the unit is operated at the design airflow. The analysis showed a reduction in power (and energy use) of approximately 30% for a unit whose capacity was 25% larger than the design airflow but was operated at the design airflow. A more general model was also developed for oversized fan-powered units in variable airflow applications. This general model could be programmed into building simulation programs to estimate power and energy savings of fan power terminal units used in variable airflow applications.

INTRODUCTION

Electronically commutated motors (ECMs) are increasingly being used as the motors of choice to drive the fans in fan-powered terminal units (FPTUs). As a consequence, it is important that accurate and simple-to-use models be developed for ECM FPTUs that can be implemented in building simulation programs. One approach to modeling FPTUs is to break the FPTU into its components (fan, motor, mixer, and heating coil) and utilize energy and mass balances of each component (EnergyPlus 2013). The user inputs on the fan include efficiency and pressure drop across the fan. The fan motor efficiency is input separately from the fan efficiency. As noted in O'Neal et al. (2015a), manufacturers test the FPTU fan/motor combinations together rather than separately. Thus, efficiency should be specified for the fan/motor combination, not the individual components in these models. That same paper showed that the fan/motor efficiency was dependent on the total pressure produced by the fan. Thus, the fan/motor efficiency cannot be treated as an independent variable from the total pressure of the fan, as is done in some building simulation programs (EnergyPlus 2013).

In a paper on ECM fan/motors used in FPTUs, O'Neal et al. (2015b) presented data showing fan/motor efficiency was dependent on both the fan total pressure and the ECM setting (or fan airflow). In one of the fan/motors units, the efficiency varied from below 10% to over 30%, depending on the fan total pressure and ECM setting. Manufacturers typically do not provide fan/motor efficiency data in their engineering data sheets for FPTUs. The user of building simulation programs requiring input of fan efficiency and total pressure is left to estimate these values and hope those estimates were reasonable. It would be useful to have an alternative approach to

Dennis L. O'Neal is dean of engineering and computer science at Baylor University, Waco, TX.

modeling ECM FPTUs that did not require knowledge of fan efficiency and total pressure. Ideally, the alternative modeling approach would utilize data that manufacturers are already providing in their engineering data sheets and would provide a reasonably accurate way to model ECM FPTUs.

Another aspect of the performance of series ECM FPTUs relates to their oversizing relative to the design cooling or heating loads (and airflows) in the zone the FPTU serves. There are two ways in which an engineer is encouraged (or required) to oversize FPTUs relative to the design loads and airflows. The first is found in ASHRAE Standard 90.1-2013, section G3.1.2.2, where for simulating the baseline annual energy use in a building, equipment capacities are required to be oversized by 15% for cooling and 25% for heating. Assuming that the airflow is proportional to the amount of oversizing of the equipment, then if the modeler simply oversized a series ECM FPTU by 15% and ran it at the oversized airflow, then this FPTU would be expected to have a larger energy use than one sized to just meet the design load. The amount of the overestimate of energy use would depend on whether the FPTU was in a fixed or variable airflow application.

For the modeler, ASHRAE Standard's 90.1-2013 requirement that equipment (including FPTUs) must have a capacity that is oversized with respect to the design airflow by the 15% to 25% ensures that the energy used by a fixed airflow series FPTU in the building simulation model will be much higher than that for a series FPTU that is just sized to the design load. For a fixed airflow application, an ECM FPTU set at the design airflow would use less fan energy than if that same ECM FPTU were set at the 15% to 25% oversized airflow requirement. Because the reduction in power is related to the airflow by a cubic equation (O'Neal et al. 2015b) for an ECM FPTU, there is a potential for significant savings in power for a specific FPTU operating at the design airflow versus the oversized airflow requirement. If the ECM is operating in a variable airflow mode where it tracks the load, then the potential for savings is even larger than for a fixed airflow application. What would be useful to the modeler is a way to estimate the savings of an oversized ECM FPTU operating in either fixed or variable airflow modes.

The second factor encouraging the oversizing of series FPTUs is the desire to reduce the noise produced in the air distribution system. To reduce noise levels from series FPTUs, some manufacturers in their engineering and application guides encourage "upsizing" (or oversizing) series FPTUs fan relative to the design airflow and then operating the FPTU at a reduced airflow to meet the design airflow requirements (Nailor 2014; Trane 2014). While the motivation (noise reduction) is different from the ASHRAE Standard 90.1-2013 requirements, the outcome is the same: the installed FPTU has an airflow capacity that is oversized relative to the design airflow requirement for the zone. If the oversized unit is then operated at a lower airflow than its full rated capacity, it would have the potential for reduced power and energy use, whether the ECM FPTU was operated in fixed or variable airflow

mode. The application procedures for FPTUs related to noise reduction lead to a similar need to be able to estimate the performance of ECM FPTUs when they have more capacity than the design airflow, but operate at or below the design airflow. Having a definitive procedure for estimating the power and energy savings from operating an oversized ECM FPTU unit at lower airflows would provide a modeler with a way to more realistically model ECM FPTUs.

Having models that can estimate the performance of oversized ECM units is essential for understanding the potential power and energy reduction that ECM units can provide. The purpose of this paper is to develop simplified models of ECM fan/motor units used in FPTUs that allow the user to easily model the ECM FPTU when it is either oversized or sized to match the design airflow. The models are based on data from four manufacturers of ECM FPTUs. It is the intent that these ECM models can be incorporated into building energy simulation models so more accurate estimates of the annual energy use of ECM FPTUs can be calculated.

BACKGROUND

O'Neal et al. (2015b) analyzed 36 fan-powered terminal units (FPTUs) from four manufacturers that used electronically commutated motors (ECMs) to drive the fans in the FPTUs. These FPTUs had motors ranging from 0.33 to 1 hp (249 to 746 W). Six of the units were parallel FPTUs and the other 30 were series FPTUs. The units included a variety of fan diameters, fan widths, and several units that had dual fan/motor combinations. In their analysis, they developed an approach to modeling the part-load performance of fan/motor combinations with two submodels that did not require the use of fan or motor efficiencies or fan differential pressures required in some public domain building simulation models (EnergyPlus 2013). The models were developed from fan discharge static data ranging from 0.1 to 0.5 in w.g. (25 to 125 Pa). These data points bracketed the 0.25 in w.g. (63 Pa) data point in the FPTU test procedure and provided a range of downstream static pressures that should cover many applications (ASHRAE 2006; AHRI 2011). Manufacturers typically provided two to three data point in the static pressure ranging from 0.1 to 0.5 in w.g. (25 to 125 Pa). The first submodel was used to estimate the fan power as a function of airflow when the ECM was at its maximum setting. A linear regression was used to fit the performance of the power Pow_{max} to the airflow Q_{max} at the maximum ECM setting of the FPTU (see Figure 1). The data in Figure 1 also include ECM units evaluated by Edmondson et al. (2011) in an earlier study. The equation representing the line in Figure 1 was given as

$$Pow_{max}(Q_{max}) = C_1 \times Q_{max} \quad (1)$$

where $C_1 = 0.380 \text{ W}/(\text{ft}^3/\text{min})$ [$805 \text{ W}/(\text{m}^3/\text{s})$].

In Figure 1, units designated 333, 500, 750, and 1000 had fan motors that were nominally rated at 0.33, 0.50, 0.75, and 1 hp (249, 373, 560, and 746 W), respectively.

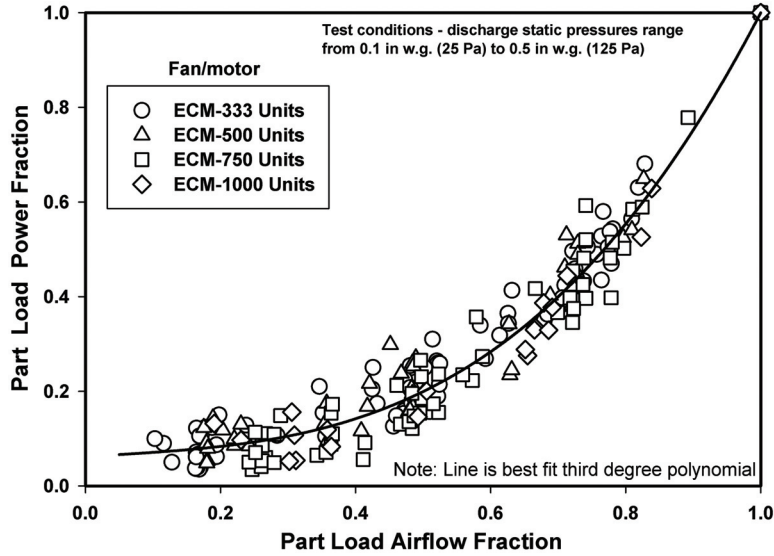


Figure 2 Part-load power fraction as a function of part-load airflow fraction from units in O’Neal et al. (2015b).

Table 1. Values of Coefficients in Equation 4 for ECM Fan/Motor Combinations

Coefficient	Value
a_1	0.061715
a_2	0.093022
a_3	-0.11627
a_4	0.961538

The second sub model developed by O’Neal et al. (2015b) was one that related the part-load power to the part-load airflow of the fan/motor combination. Previous modelers (Knebel 1983; Brandemuehl 1993) and models (BLAST 1986; EnergyPlus 2013) have utilized part-load models for simulating fan performance at part-load conditions. Typically, the airflow and power were normalized to their respective values at full load conditions. In the part-load model developed by O’Neal et al. (2015b), the power and airflow were normalized to the power and airflow at the maximum ECM setting for static discharge pressures P_{stat} ranging from 0.1 to 0.5 in w.g. (25 to 125 Pa). The model was different from the prior models in that the part-load performance was for the fan/motor combination not just the fan. The discharge pressures bracketed the typical 0.25 in w.g. (62 Pa) static discharge pressure required in fan power terminal unit test procedures (AHRI 2011; ASHRAE 2006). The normalized power was designated as the part-load power fraction f_{pl} while the normalized airflow was designated as the part-load airflow fraction f_{flow} . These can be written in equation form as

$$f_{pl} = \frac{Pow_{fan}(Q_{flow})}{Pow_{max}(Q_{max})} \quad (2)$$

$$f_{flow} = \frac{Q_{flow}}{Q_{max}} \quad (3)$$

where

Pow_{fan} = power of the fan motor at a given airflow rate Q_{flow} and static discharge pressure, W

Q_{flow} = airflow rate at a given ECM setting and static discharge pressure, ft^3/min (m^3/s)

The relationship between the part-load power fraction and the part-load airflow fraction was fit with a third degree polynomial in the form shown in Equation 4. The coefficients a_1 through a_4 were developed from a regression fit of the performance data from the four manufacturers. The values of the coefficients are shown in Table 1. A plot of Equation 4 with the original data from the four manufacturers is shown in Figure 2.

$$f_{pl}(f_{flow}) = a_1 + a_2 f_{flow} + a_3 f_{flow}^2 + a_4 f_{flow}^3 \quad (4)$$

Both f_{pl} and f_{flow} were 1.0 at the maximum ECM setting and decreased as ECM setting (and consequently airflow) decreased. Typically manufacturers provided power and airflow data from 20% to 100% of the maximum ECM setting. The fan power at a given flow rate Q_{flow} can be calculated with the knowledge of the part-load power fraction, $f_{pl}(f_{flow})$, and the power at the maximum ECM setting.

$$Pow_{fan}(Q_{flow}) = f_{pl}(f_{flow}) \times Pow_{max}(Q_{max}) \quad (5)$$

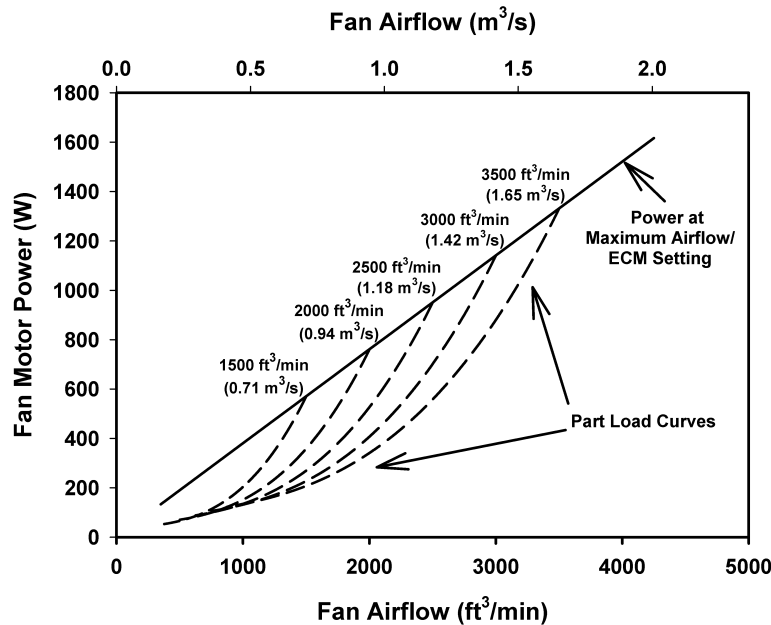


Figure 3 Part-load curves related to the airflow and power curve at maximum ECM setting.

Equation 5 can be combined with Equation 1:

$$Pow_{fan}(Q_{flow}) = f_{pl}(f_{flow}) \times C_1 \times Q_{max} \quad (6)$$

Equation 6 provides a way to calculate the fan power at a given part-load setting. Figure 3 shows a plot of fan power as a function of airflow for both the maximum ECM setting (line) and part load for five different airflows calculated from Equation 6. The part-load curves drop down below the maximum ECM line and look something like tentacles below a jellyfish that is ascending in water. The part-load curves (i.e., the “tentacles”) eventually cross over each other at low airflow rates.

While Equation 6 provides a way to calculate directly the part-load power of the fan from the maximum ECM setting and part-load power fraction, the application of ECM FPTUs is complicated in that they are often oversized relative to the design load so that they operate at airflows that are less than the maximum ECM setting. As discussed by O’Neal et al. (2015b), the ECM units provided by the manufacturers had a performance (as measured by the power divided by the airflow) at their maximum ECM setting that was comparable to the performance of permanent split capacitor (PSC) motors controlled by silicon controlled rectifiers (SCRs). The real benefit to applying ECM units is that they can take advantage of their part-load performance. While O’Neal et al. (2015b) showed tangible benefits to oversizing ECM units, there was no systemic way presented on how to quantify the benefit of oversizing.

MATHEMATICALLY MODELING OVERSIZING

There are two applications of ECM FPTUs. In the first, when the ECM unit is installed, the airflow is set at a specific

value, and the unit attempts to maintain that fixed airflow whenever the FPTU fan motor is on. For the second application the ECM controller is integrated into the building energy management control systems so the airflow of the FPTU can be varied to meet the load as the load changes. While the two cases were described briefly in the prior paper by O’Neal et al. (2015b), the mathematical models needed to fully integrate ECM fan/motors into building simulation models was not. These are discussed below for both the fixed and variable airflow cases.

Fixed Airflow Case

For a building energy simulation program to estimate the power and energy used by an ECM FPTU, it is necessary to develop mathematical relationships between power, airflow, and oversizing. Figure 4 shows the line relating the power to the airflow at maximum ECM setting along with the part-load curves for several ECM units of different capacities. If the airflow needed to satisfy the design load of the space is assumed to be Q_d , then at that design airflow, an ECM FPTU could be selected that had an airflow at its maximum ECM setting that would just match the design airflow. In that case, the power demand for the unit, given as $Pow_{max}(Q_d)$ in Figure 3, would be on the straight line that related the power and airflow at the maximum ECM setting. The calculation of the power for this unit would be accomplished by using Equation 1 and substituting Q_d for Q_{max} in that equation.

$$Pow_{max}(Q_d) = C_1 \times Q_d \quad (7)$$

While a unit could be selected whose airflow at its maximum ECM setting just matched the design airflow, it can be

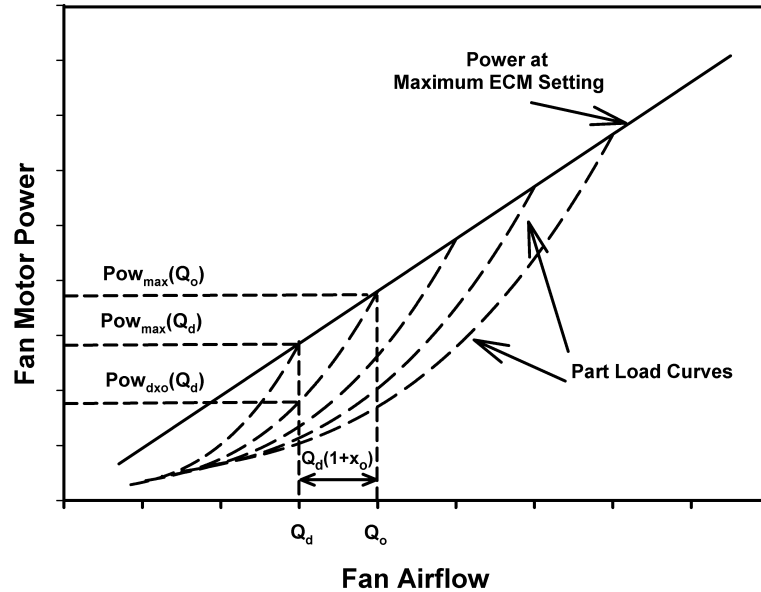


Figure 4 Representation of the power used by different sized units at the design airflow (Q_d) and an oversized unit having an airflow of Q_o at its maximum ECM setting.

observed in Figure 4 that a unit with a larger capacity should use less power than that from the unit that was just sized to meet the design load at its maximum ECM setting. If an oversized unit was considered whose airflow capacity was some arbitrary amount q_o above the capacity of the design load, then the total capacity Q_o of the oversized unit would be given by

$$Q_o = Q_d + q_o \quad (8)$$

If x_o was defined as the fraction of oversizing that q_o was above the design load, then q_o can be written as

$$q_o = x_o Q_d \quad (9)$$

Equation 9 can be substituted into Equation 8 and simplified to obtain

$$Q_o = Q_d + x_o Q_d = Q_d(1 + x_o) \quad (10)$$

Equation 10 shows that capacity of the oversized unit can be written in terms of the fractional oversizing and the design capacity.

Assuming an oversized unit of capacity Q_o was run at its maximum ECM setting, then its power, $Pow_{max}(Q_o)$, could be calculated from Equation 1 if the airflow for the oversized unit, Q_o , was substituted for Q_{max} :

$$Pow_{max}(Q_o) = C_1 \times Q_o \quad (11)$$

In Figure 4, the power of the oversized unit operating at the design airflow is given by $Pow_{dx0}(Q_d)$. This operating point can be calculated from the product of the part-load power frac-

tion of the oversized unit at the design airflow, $f_{pl}(f_{flow_do})$ and power at the maximum ECM setting for that unit:

$$Pow_{dx0}(Q_d) = f_{pl}(f_{flow_do}) \times Pow_{max}(Q_o) \quad (12)$$

In the above equation, f_{flow_do} is the part-load airflow fraction for the oversized unit operating at the design airflow. The part-load power fraction would be given by

$$f_{pl}(f_{flow_do}) = a_1 + a_2 \times f_{flow_do} + a_3 \times f_{flow_do}^2 + a_4 \times f_{flow_do}^3 \quad (13)$$

The part-load airflow fraction f_{flow_do} would be

$$f_{flow_do} = \frac{Q_d}{Q_o} \quad (14)$$

The constants $a_1 \dots a_4$ in Equation 13 were given in Table 1. For the continued mathematical derivation of the model, it would be more convenient to use the ratio of Q_d/Q_o rather than f_{flow_do} . Equation 13 can then be rewritten as

$$f_{pl}(f_{flow_do}) = a_1 + a_2 \times \left(\frac{Q_d}{Q_o}\right) + a_3 \times \left(\frac{Q_d}{Q_o}\right)^2 + a_4 \times \left(\frac{Q_d}{Q_o}\right)^3 \quad (15)$$

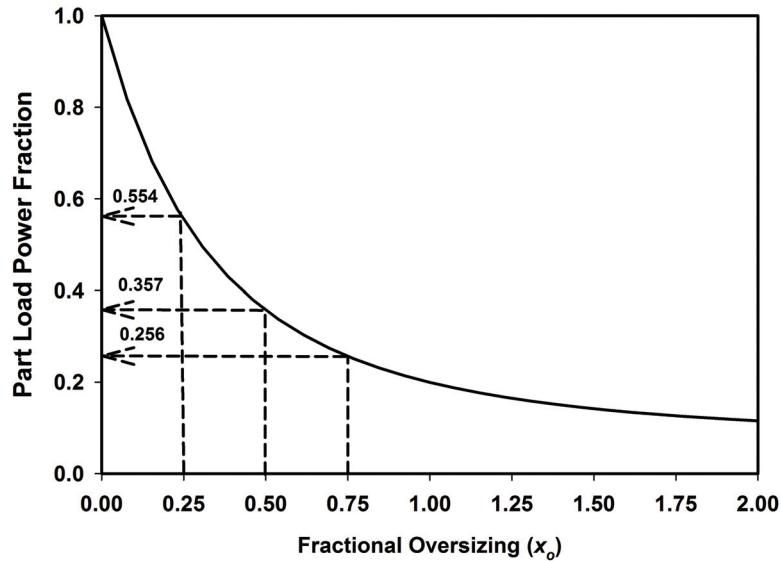


Figure 5 Part-load power fraction as a function of ECM fan/motor fractional oversizing.

Equation 10 relates Q_d , Q_o , and the fraction oversizing x_o . The equation for the part-load power fraction, $f_{pl}(Q_{do})$, can be rewritten as

$$f_{pl}(f_{flow_do}) = a_1 + a_2 \times \left(\frac{Q_d}{Q_d(1+x_o)} \right) + a_3 \times \left(\frac{Q_d}{Q_d(1+x_o)} \right)^2 + a_4 \times \left(\frac{Q_d}{Q_d(1+x_o)} \right)^3 \quad (16)$$

Simplifying the above yields

$$f_{pl}(f_{flow_do}) = a_1 + a_2 \times \left(\frac{1}{1+x_o} \right) + a_3 \times \left(\frac{1}{1+x_o} \right)^2 + a_4 \times \left(\frac{1}{1+x_o} \right)^3 \quad (17)$$

Equation 17 is an important result because the capacities, Q_d and Q_o , disappeared with the simplification and the only variable remaining on the right-hand side of the equation was the fractional amount of oversizing x_o of the unit. Therefore, the part-load power fraction for an oversized unit only depended on the amount of oversizing and not the specific capacity of the unit. It would not matter for the calculation of the part-load power fraction, $f_{pl}(f_{flow_do})$, if the design airflow was 500 ft³/min (0.24 m³/s) or 2500 ft³/min (1.18 m³/s). As long as the fraction oversizing (x_o) was known, then the part-load power fraction could be calculated for an oversized unit that was operating at the design load using Equation 17.

Figure 5 shows a graphical representation of Equation 17 for fractional oversizing ranging from 0 to 2. A value of 1.0 for

the fractional oversizing represents installing a unit with twice the capacity of the design airflow, or 100% oversized. The dashed lines in Figure 4 show the decreasing benefit for increasingly oversizing the ECM fan/motor to the design airflow. Oversizing by 0.25 (or 25%) reduced the part-load power fraction from by 44.6% to a value of 0.554. Oversizing by another increment of 0.25 to a value of 0.50 reduced the part-load power fraction to 0.375, or a reduction of 35.5% over the case for 25% oversizing.

While the behavior of the part-load power fraction is important in the calculation of power, it is not the only variable that must be considered. As shown in Equation 12, the calculation of the power used by the ECM fan/motor unit required both the part-load power fraction and the power used by the fan motor at the maximum ECM setting for the oversized unit, $Pow_{max}(Q_o)$. As shown in Figure 1, the power of the ECM units was linearly related to the airflow capacity at their maximum ECM settings. The part-load power fraction, $f_{pl}(f_{flow_do})$, the first term on the right-hand side of Equation 12, was shown to be dependent on only the fractional oversizing x_o of the ECM unit. The second term on the right-hand side of Equation 12 is the power at the maximum ECM setting for the oversized unit, $Pow_{max}(Q_o)$. It can be divided by power at the maximum ECM setting for a unit that just satisfied the design capacity, $Pow_{max}(Q_d)$, to obtain

$$\frac{Pow_{max}(Q_o)}{Pow_{max}(Q_d)} = \frac{C_1 \times Q_o}{C_1 \times Q_d} = \frac{Q_o}{Q_d} = \frac{Q_d(1+x_o)}{Q_d} = (1+x_o) \quad (18)$$

As shown in the above equation, it was possible to simplify this ratio to show that it was only dependent on the

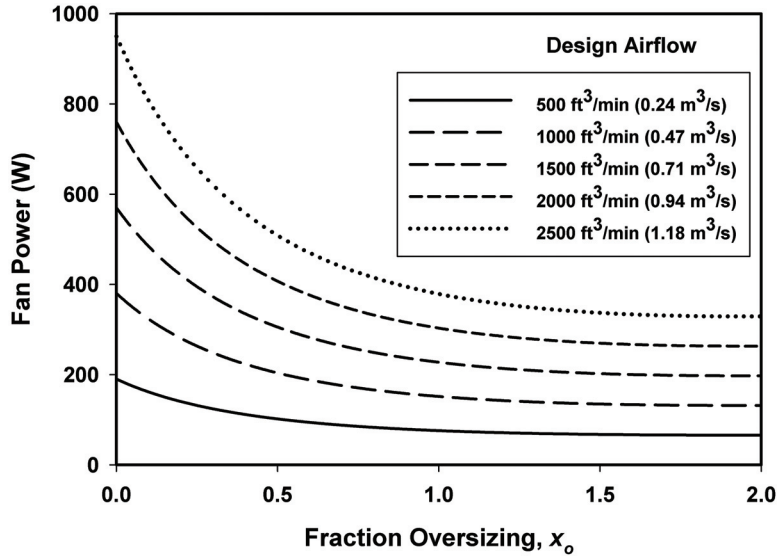


Figure 6 Fan power variation with fractional oversizing and design airflow.

fractional oversizing, x_o . Equation 18 can also be rearranged to solve for the power used by the oversized unit at its maximum ECM setting:

$$Pow_{max}(Q_o) = Pow_{max}(Q_d) \times (1 + x_o) \quad (19)$$

Referring back to Equation 12, both the power at the maximum ECM setting for the oversized unit and the part-load power fraction for the oversized unit operating at the design airflow must be known to be able to calculate the power of the oversized unit operating at the design airflow, $Pow_{dxo}(Q_d)$. Equation 19 can be substituted into Equation 12 to get the following:

$$Pow_{dxo}(Q_d) = f_{pl}(f_{flow_do}) \times Pow_{max}(Q_d) \times (1 + x_o) \quad (20)$$

In Equation 20, the power for the fan operating at the maximum ECM for the design airflow, $Pow_{max}(Q_d)$ can be calculated from Equation 7 and substituted into Equation 20, which results in

$$Pow_{dxo}(Q_d) = f_{pl}(f_{flow_do}) \times C_1 \times Q_d \times (1 + x_o) \quad (21)$$

Looking at Equation 21, the only variables an energy modeler would need to estimate the power of an oversized ECM unit operating at the design airflow would be the design airflow Q_d and the fraction of oversizing x_o . The power/airflow slope, C_1 , was given in Equation 1. The coefficients, $a_1 \dots a_4$ were given in Table 1 for calculating the part-load power fraction. There was no requirement in Equation 21 for specifying motor efficiencies, fan efficiencies, fan pressure differentials, etc. as is currently required by some building energy simulation models. The above result was based on fits of data from

dozens of currently produced units from four manufacturers. A modeler could use a different value of C_1 if manufacturer's data were available. For example, should future units be shown to be more efficient than those used by O'Neal et al. (2015b), then C_1 should decrease, which would be reflected in a drop in power requirements for a given design airflow and amount of oversizing. Likewise, should more data be analyzed that provide a different part-load curve, the coefficients a_1 through a_4 could be recalculated and modified to calculate a new part-load power fraction.

Figure 6 shows a plot of the power calculated using Equation 21 for design airflows ranging from 500 to 2500 ft³/min (0.24 to 1.18 m³/s) and for fractional oversizing ranging from 0 to 2. In all cases, the maximum power is at zero oversizing and then rapidly drops as the oversizing is increased then begins to level off for oversizing above about 1.5 or 150% larger than the design airflow.

Equation 21 can be used to calculate the power used by either a parallel or series ECM FPTU. However, it may be useful to pose the question, "Is there a mathematical limit to how much a system should be oversized to reduce power used at a given design airflow?" The power used by an oversized unit in Equation 21 was the product of the part-load power fraction (a cubic equation) that decreased with increased oversizing and a second term on the right-hand side of Equation 21, which was a linear term that increased with increased oversizing. With one term increasing and the other decreasing, it would be possible that multiplying the two together could produce a minimum value for power. Thus, there may be an amount of oversizing where the power no longer decreased.

To investigate this possibility, it would be useful to normalize the power used by any oversized unit at the design airflow to the maximum power that would be used at the same

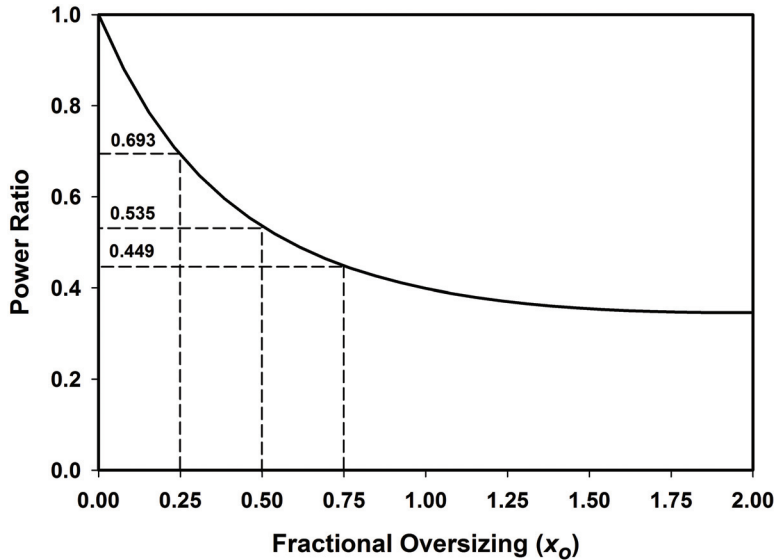


Figure 7 Power ratio as a function of fractional oversizing.

design airflow. The maximum power would be that used by a unit whose airflow capacity at its maximum ECM setting would just meet the design airflow. This power would be given by $Pow_{max}(Q_d)$ in Equation 7. Both sides of Equation 21 can be divided by $Pow_{max}(Q_d)$ to normalize the power for the oversized units to $Pow_{max}(Q_d)$.

$$\frac{Pow_{dxo}(Q_d)}{Pow_{max}(Q_d)} = \frac{f_{pl}(f_{flow_do}) \times C_1 \times Q_d \times (1 + x_o)}{Pow_{max}(Q_d)} \quad (22)$$

Because $Pow_{max}(Q_d)$ is equal to $C_1 \times Q_d$, it can be substituted into right-hand side of Equation 22 to produce

$$\begin{aligned} Pow_{Rat} &= \frac{Pow_{dxo}(Q_d)}{Pow_{max}(Q_d)} \\ &= f_{pl}(f_{flow_do}) \times (1 + x_o) \end{aligned} \quad (23)$$

For convenience, the ratio of the power of the oversized unit operating at the design airflow divided by the power of the unit sized to just meet the design airflow was defined with the symbol Pow_{Rat} . Looking at the right-hand side of Equation 23, the part-load power ratio was only dependent on x_o . The second term on the right-hand side only contained x_o as a variable, so the power ratio was only dependent on the fraction oversizing x_o and not the capacity of the unit.

A plot of Equation 23 is shown in Figure 7. The power ratio ranged from 1.0 for a unit with no oversizing ($x_o = 0$) to a low of about 0.35 for a unit with oversizing of 2.0. An oversizing of 2.0 would correspond to a unit with a capacity that was 200% or three times larger than the design airflow. Above

an oversizing of 2.0, the power ratio began to increase indicating the units should never be oversized beyond 2.0.

Another way of presenting the data in Figure 7 was to calculate the fractional power savings that would result from oversizing. The fractional power savings can be calculated from Equation 19 by subtracting the power ratio from one:

$$Pow_{sav} = 1 - Pow_{Rat} \quad (24)$$

Table 2 shows the percentage power savings as a function of percentage oversizing when the oversized FPTU is operated at design airflow. The calculations show that a modestly oversized unit of 25% that was operated at the design airflow should produce a power savings of about 30% over a unit that was just matched in size to the design airflow. These numbers showed that the recommendations of manufacturers to “upsized” or oversize FPTUs and then reduce the operating airflow to the design airflow to reduce noise can also provide a significant energy savings for ECM FPTUs. Table 2 shows that there was essentially little power savings benefit for applying a unit that was oversized more than 100%. Implementing the equations that provided the curves for Figure 7 and data in Table 2 in a building simulation program would allow an energy modeler to choose from infinite possibilities of oversized FPTUs along the continuous curve of Figure 7. In contrast, the applications engineer operating in the field would be faced with a discrete number of ECM FPTUs with capacities larger than the design airflow because manufacturers only offer a limited number of FPTUs in their product offerings. However, an applications engineer should be able to use either Figure 7 or Table 2 to get a quick estimate of the savings from applying an oversized ECM FPTU and operating it in a fixed airflow mode at the design airflow.

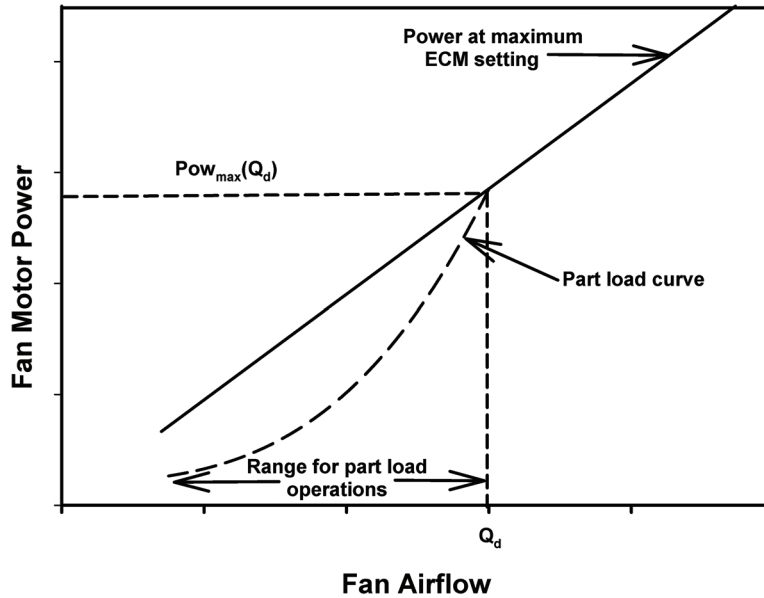


Figure 8 Power at part-load operations for an ECM unit sized to just meet the design load.

Table 2. Calculated Percentage Power Savings from Operating an Oversized ECM FPTU at the Design Airflow Using Equation 20

Percentage Oversizing	Percentage Power Savings
5	8.1
10	15.0
15	21.0
20	26.2
25	30.1
30	34.7
35	38.2
40	41.3
45	44.0
50	46.5
100	60.1
150	64.5
200	65.4

Varying Airflow to Track the Load

An ECM FPTU can be integrated into an energy management control system so that the ECM can vary the airflow to match the load requirements in the zone. There were two

scenarios that were considered. The first was when the ECM FPTU was sized to just meet the design airflow requirement for the space. The second case was when the capacity of the FPTU was oversized relative to the design airflow requirement for the space. Each is discussed below.

Figure 8 presents an ECM unit that is sized to just meet the design airflow Q_d requirements of the space. The ECM can operate over its complete design range as shown in the curved dotted line (marked “part-load curve”) below the solid line representing the power at the maximum ECM setting. The unit would operate along the dashed line in response to changes in load in the space.

The part-load curve in Figure 8 at a given airflow is the power used by the ECM fan/motor, $Pow_{fan}(Q_{flow})$. This power was given in a general form in Equation 5. For use here, the design airflow, Q_d , was substituted for Q_{max} , and the part-load airflow fraction is given the symbol f_{flowd} rather than f_{flow} because the reference for the part-load airflow fraction was the design airflow. These changes are shown in Equations 25 through 27.

$$Pow_{fan}(Q_{flow}) = f_{pl}(f_{flowd}) \times Pow_{max}(Q_d) \quad (25)$$

For Equation 25, the part-load power fraction, $f_{pl}(f_{flowd})$ and part-load airflow fraction are given by

$$f_{pl}(f_{flowd}) = a_1 + a_2 \times (f_{flowd}) + a_3 \times (f_{flowd})^2 + a_4 \times (f_{flowd})^3 \quad (26)$$

and

$$f_{flowd} = \frac{Q_{flow}}{Q_d} \quad (27)$$

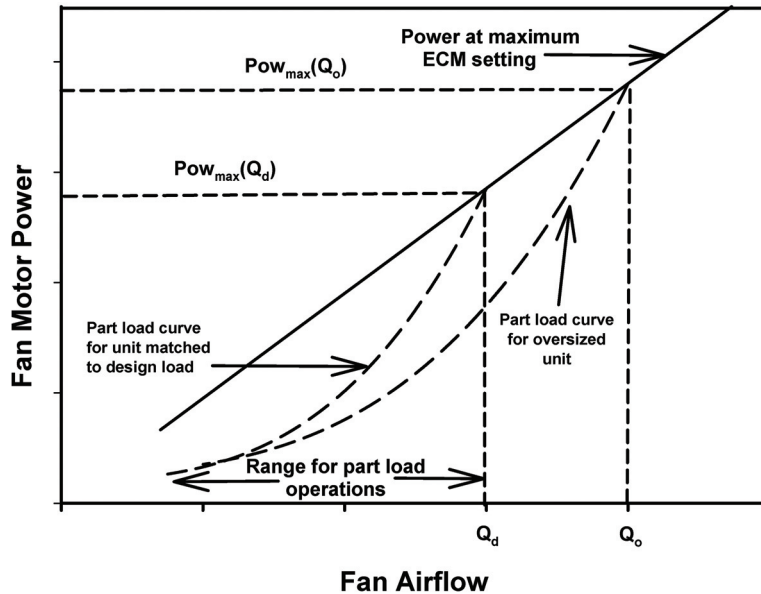


Figure 9 Power of an ECM unit with an oversized capacity (Q_o) that meets the design load (Q_d) and the range of part-load operations where speed is varied to meet the airflow requirements of the space.

The constants, $a_1...a_4$ were the same as those listed in Table 1. The ratio of Q_{flow}/Q_d is the part-load airflow fraction for an ECM unit whose capacity at its maximum ECM setting would just equal the design airflow for the zone served by the ECM FPTU. The part-load power ratio would be 1.0 when the airflow was at the design airflow rate and would decrease for lower values of the airflow.

The second term on the right-hand side of Equation 25 is the power for the fan motor operating at the maximum ECM setting to just satisfy the design airflow. For a unit operating at its maximum ECM setting, the power is related to the airflow by a constant, C_1 , as shown in Equation 1. Thus, Equation 25 can be rewritten in terms of this constant and the design airflow.

$$Pow_{fan}(Q_{flow}) = f_{pl}(f_{flowd}) \times C_1 \times Q_d \quad (28)$$

If the FPTU was sized to just meeting the design airflow when the ECM was at its maximum setting, then Equation 28 can be used to calculate the power at any airflow that was less than the design value. It should be straightforward to implement Equation 28 into a building energy simulation program. The design load would either be specified by the user or calculated by the program. At any given airflow requirement, the part-load airflow fraction Q_{flow}/Q_d , the part-load power fraction, and the power would be calculated.

The example above was for the simple case where there was no oversizing of the ECM FPTU to the design airflow requirements. As discussed in the previous section for the fixed airflow case, there was the potential for significant power and energy savings if the ECM FPTU was oversized relative

to the design airflow requirements. For the case where the ECM would be at a fixed airflow, the analysis showed that calculating the power only required knowledge of the fraction oversizing and the design airflow. Figure 9 shows the power versus airflow for two ECM units. One was sized to the design load Q_d and the other was oversized and had a capacity of Q_o at its maximum ECM setting. These plots were made from utilizing Equations 1 and 4 which were developed from manufacturer's data. The part-load curve for the oversized unit started at a higher power requirement at its maximum ECM setting than did the unit that was just matched to the design airflow. However, the power of the oversized unit rapidly dropped as the airflow requirements decreased. When its airflow capacity crossed the design airflow Q_d the oversized unit had a lower power requirement than the unit sized to match the design airflow. As the airflow was further decreased, the oversized unit continued to have a lower power requirement until the part-load curves for the unit matched to the design load and the oversized unit eventually crossed at very low airflows. The plots in Figure 9 would indicate that oversizing should provide additional benefits over a unit matched to the design load for varying airflows below the design airflow.

Developing a mathematical model to describe the part-load performance for an oversized unit followed a similar strategy to what was used for the unit matched to the design load. The general equation for power used by the ECM fan motor along the part-load curve for the oversized unit was the same as for Equation 25 except the maximum airflow was not at the design airflow but at the airflow Q_o of the oversized unit operating at its maximum ECM setting. Likewise the part-load

airflow and power fractions were referenced to Q_o rather than Q_d . With these changes, Equations 25 through 27 became

$$Pow_{fan}(Q_{flow}) = f_{pl}(f_{flowo}) \times Pow_{max}(Q_o) \quad (29)$$

$$f_{pl}(f_{flowo}) = a_1 + a_2 \times (f_{flowo}) + a_3 \times (f_{flowo})^2 + a_4 \times (f_{flowo})^3 \quad (30)$$

$$f_{flowo} = \frac{Q_{flow}}{Q_o} \quad (31)$$

Equations 29 through 31 also had the restriction that the airflow Q_{flow} must be less than the design airflow, Q_d . In Figure 9, $Q_{flow} < Q_d$ was represented by the airflow that was labeled “range for part-load operations.” If the design load represented the maximum airflow the zone should need, then all part-load operations would be below that airflow. Figure 9 showed that the oversized unit used a “truncated” portion of the part-load curve because the airflow would never go above Q_d . In contrast, the ECM unit in Figure 9 that was sized to match the design airflow would use the full range of its part-load curve. Even though the matched unit used the full part-load curve, it still used more power over most of the range than the oversized unit.

Equation 19 related the fan power for the maximum ECM setting for the oversized unit to the unit that just matched the design load. Equation 29 can be rewritten with the relationship from Equation 19 to obtain

$$Pow_{fan}(Q_{flow}) = f_{pl}(f_{flowo}) \times Pow_{max}(Q_d) \times (1 + x_o) \quad (32)$$

The only term left in Equation 32 that still directly had the oversizing capacity embedded in it was the part-load power fraction, $f_{pl}(f_{flowo})$. The oversized capacity could be eliminated from the part-load power fraction by utilizing Equation 10 which related the oversized capacity to the design capacity and oversizing fraction. The relationship in Equation 10 could be substituted into the expression for the part-load airflow fraction (Equation 31) and substituted into the part-load power fraction (Equation 30) to get

$$f_{pl}(f_{flowo}) = a_1 + a_2 \times \left(\frac{Q_{flow}}{Q_d(1 + x_o)} \right) + a_3 \times \left(\frac{Q_{flow}}{Q_d(1 + x_o)} \right)^2 + a_4 \times \left(\frac{Q_{flow}}{Q_d(1 + x_o)} \right)^3 \quad (33)$$

Once an ECM FPTU unit was selected by a modeler for a simulation, the fraction oversizing would be known. Equa-

tion 33 could be simplified by incorporating the $(1 + x_o)$ terms into the constants and redefining the constants in the following way:

$$a'_2 = \frac{a_2}{(1 + x_o)} \quad a'_3 = \frac{a_3}{(1 + x_o)^2} \quad a'_4 = \frac{a_4}{(1 + x_o)^3} \quad (34)$$

The constant a_1 did not require any changes. Substituting the new constants into Equation 29 gave the following:

$$f_{pl}(f_{flowo}) = a_1 + a'_2 \times \left(\frac{Q_{flow}}{Q_d} \right) + a'_3 \times \left(\frac{Q_{flow}}{Q_d} \right)^2 + a'_4 \times \left(\frac{Q_{flow}}{Q_d} \right)^3 \quad (35)$$

The ratio Q_{flow}/Q_d in Equation 35 was already defined as the part-load airflow fraction f_{flowd} in Equation 27. This substitution can be made into Equation 35 to obtain

$$f_{pl}(f_{flowo}) = a_1 + a'_2 \times (f_{flowd}) + a'_3 \times (f_{flowd})^2 + a'_4 \times (f_{flowd})^3 \quad (36)$$

The redefined constants in Equation 36 would vary depending on the fraction of oversizing and would need to be calculated for each application of an ECM FPTU in a model. The above expression in Equation 36 for the part-load power fraction for the oversized unit can be compared to the one in Equation 26 for the case where the unit just matched the design airflow. The two expressions were very similar except for the definition of the constants. However, if a unit was just sized to match the design load, then the amount of oversizing would be zero. In that case, x_o would equal zero and the term, $1 + x_o$, would be equal to one and each of the redefined constants would drop back down to the original values:

$$a'_2 = a_2 \quad a'_3 = a_3 \quad a'_4 = a_4 \quad (37)$$

The part-load power fraction calculated from Equation 36 for the case where $x_o = 0$ would equal to the part-load power fraction of Equation 26. Thus, Equation 36 could be viewed as the “general” case and could be applied to both situations where the unit was oversized to the design airflow and when it was sized to just match the design airflow.

In Equation 32, there was also a term for the fan power at the maximum ECM setting for the unit that just matched the design load. By using Equation 11, this power term can be written in terms of the design airflow and the constant C_1 .

$$Pow_{fan}(Q_{flow}) = f_{pl}(f_{flowo}) \times C_1 \times Q_d \times (1 + x_o) \quad (38)$$

The fan power at a given airflow Q_{flow} can easily be calculated since all of the terms on the right-hand side of Equation 38 only depended on Q_{flow} , Q_d , and x_o . There was no requirement for fan or motor efficiencies or pressure differentials across the fan. Equation 35 could be implemented into a building simulation program to estimate the power used by an ECM fan as the airflow was varied to meet the thermal load in the space and should apply to both heating and cooling applications.

SUMMARY AND CONCLUSIONS

Electronically commutated motors are increasingly being used as the motors of choice to drive the fans in fan-powered terminal units. As a consequence, it is important that accurate and simple-to-use models be developed for ECM FPTUs that can be used in building simulation programs. Both ASHRAE Standard 90.1-2013 and manufacturer's recommendations for noise reduction both are pushing ECM FPTUs to be oversized relative to the design airflows. As a consequence, building simulation models need to include ECM FPTU models that capture the energy and power savings of operating these FPTUs at either the design airflow (fixed airflow applications) or below design airflow where the FPTU tracks the load.

The part-load methodology used here and in the previous paper (O'Neal et al. 2015b) provided simple models that can be used to estimate the performance of ECM units either sized or oversized to the design airflow requirements for the space. The models can be used in applications where the airflow is fixed or varies to meet the load requirement in the space.

The models developed here rely on data that can be readily obtained from manufacturers of ECM FPTUs in contrast to current models that require the user to input fan and motor efficiency and fan pressure differential (EnergyPlus 2013). These data are typically not provided by manufacturers. They are either guessed or not known by the modeler in current building simulations. In addition, none of the current building energy simulation models explicitly incorporate oversizing into the modeling of ECM FPTUs.

The model developed here for fixed airflow applications needed only the design airflow and fraction oversizing to estimate the power used by the ECM unit. The model was used to analyze how effective oversizing could be for fixed airflow applications. Based on the analysis, applying a unit that was 25% oversized relative to the design airflow but operating it at the design airflow would produce over a 30% power reduction compared to a unit that was just sized to match the design airflow. There appeared to be little benefit in power reduction for a unit that was oversized by more than 100% larger than the design airflow. The analysis produced a continuous curve for the power savings for oversized units operating at the design airflow. In reality, units offered by manufacturers are in discrete sizes, so an engineer may be able to choose only a select number of units that are oversized relative to the design airflow. The discrete options will limit the potential savings with an oversized unit. While costs were not included in the

analysis, the choice of an oversized unit will depend on whether the savings it provides offset its additional costs. There may also be other factors that constrain the application of a larger unit. For example, an oversized unit may require choosing a larger cabinet size, which may not fit the specific application. Another factor is how low a speed an ECM can be run. Most of the data provided by the manufacturers typically covered a range that went from 15% to 20% of the maximum setting on the controller. An oversized ECM may be required to operate below the data collected by the manufacturer. Manufacturers typically have their reasons for not operating below these lower limits and an engineer needs to verify with the manufacturer that the ECM can operate below these limits. Another practical concern that may limit the selection of an oversized unit is noise requirements.

For a variable airflow application, the actual airflow required for a specific load in the space would be the only additional input needed beyond the fraction oversizing and design airflow for the space. This model should be straightforward to incorporate into a building simulation program because the hourly thermal and airflow requirements are calculated in the program.

Both the fixed and variable airflow models capture the power used by the fan motor. Assuming all the fan power is expended in the airstream, a reduction in fan power with an ECM fan/motor unit would reduce the calculated cooling energy since less heat energy would be added to the airstream in an FPTU. However, the opposite would occur with heating. The exact annual benefits in cooling or penalty in heating would need to be calculated with a building simulation program and goes beyond the scope of this paper.

ACKNOWLEDGEMENT

I wish to thank the Air Conditioning, Heating, and Refrigeration Institute (AHRI) for their support of this project. In particular, thanks go to all the members of the Air Control and Distribution Devices Committee for their input and advice.

TERMINOLOGY

- f_{flow} = part-load airflow fraction (dimensionless)
- f_{flow_do} = part-load airflow fraction for the oversized unit at the design airflow (dimensionless)
- f_{flowd} = part-load airflow fraction for a unit just sized to meet the design airflow (dimensionless)
- f_{flowo} = part-load airflow fraction for the oversized unit at a given airflow (dimensionless)
- f_{pl} = part-load power fraction (dimensionless)
- $QPow_{dco}$ = fan motor power for the oversized unit at the design airflow, W
- Pow_{fan} = fan motor power at a given airflow, W
- Pow_{max} = fan motor power at maximum ECM setting, W
- Pow_{Rat} = ratio of the power of an oversized unit operating at the design airflow to the power of a unit operating at

- maximum ECM setting to meet the design airflow (dimensionless)
- Pow_{sav} = fractional savings in power of an oversized unit operating at the design airflow compared to a unit operating at maximum ECM setting to meet the design airflow (dimensionless)
- Q_d = fan airflow at the design airflow, ft³/min (m³/s)
- Q_o = fan airflow capacity for the oversized unit, ft³/min (m³/s)
- q_o = incremental airflow capacity above the design airflow, ft³/min (m³/s)
- Q_{flow} = fan airflow at a given ECM setting, ft³/min (m³/s)
- Q_{max} = fan airflow at maximum ECM setting, ft³/min (m³/s)
- x_o = fractional oversizing above the design airflow (dimensionless)

REFERENCES

- AHRI. 2011. Performance rating of air terminals. ANSI/AHRI Standard 880 (I-P) with addendum 1. Arlington, VA: Air-Conditioning, Heating, and Refrigeration Institute.
- ASHRAE. 2006. Methods of testing for rating ducted air terminal units. ANSI/ASHRAE Standard 130-1996 (RA 2006). Atlanta: ASHRAE.
- ASHRAE. 2013. Energy standards for buildings except low-rise residential buildings. ANSI/ASHRAE/IES Standard 90.1-2013. Atlanta: ASHRAE.
- BLAST. 1986. *Building load analysis and stem thermodynamic programs: User's manual*, Version 3.0. Champaign, IL: Army Construction Engineering Research Laboratory.
- Brandemuehl, M.J. 1993. *HVAC 2 toolkit*. Atlanta, GA: ASHRAE.
- Edmondson, J., D.L. O'Neal, J.A. Bryant, and M.A. Davis. 2011. Performance of series fan powered terminal units with electronically commutated motors. *ASHRAE Transactions* 117(2).
- EnergyPlus. 2013. Air system distribution terminals. In *EnergyPlus engineering reference: The reference to EnergyPlus calculations*. Berkeley, CA: Lawrence Berkeley National Laboratory.
- Knebel, D.E. 1983. *Simplified energy analysis using the modified bin method*. Atlanta: ASHRAE.
- Nailor Industries, Inc. 2014. Sizing fan powered terminals. In *Engineering guide and index*. Houston, TX.
- O'Neal, D.L., D. Ingram, and C. Reid. 2015a. Modeling fan power terminal unit fan/motor combinations controlled by silicon controlled rectifiers. *ASHRAE Transactions* 121(2).
- O'Neal, D.L., D. Ingram, and C.L. Reid. 2015b. Simplified model of the fan/motor performance of fan powered terminal units that utilize electronically commutated motors. *ASHRAE Transactions* 121(2).
- Trane, Inc. 2014. *Selection procedure in fan-powered series*. VAV-PROC008-EN, La Crosse, WI.

AT-15-027

In-Situ Fan Differential Pressure Rise for a Series VAV-Fan-Powered Terminal Unit with SCR Control

John A. Bryant, PhD, PE
Member ASHRAE

Stephen J. Bryant

ABSTRACT

Open-source and commercial energy simulation programs require differential pressure rise as an input when simulating variable air volume (VAV) HVAC systems using fan-powered terminal units. Typically, these data are generated by the fan/motor manufacturer under standard testing protocols. The fan/motor set is then installed into the finished series fan-powered terminal unit and the ensemble is tested as a unitary piece of equipment by the terminal unit manufacturer. Some blogs recommend values as high as 2.5 or greater in. w.g. (622.7 Pa) of differential pressure rise across the fan. Differential static pressure data were collected for fan airflow rates ranging from 500 to 1,300 ft³/min (0.236 to 0.613 m³/s) while holding a constant downstream static pressure of 0.25 in. w.g. (62.3 Pa) using an 8 in. (203 mm) VAV series fan-powered terminal unit. The differential static pressure rise for this fan ranged from 0.128 to 0.246 in. w.g. (31.9 to 61.3 Pa). From these data, a linear relationship between total airflow and series fan differential static pressure could be inferred. The results show that the low static pressure rise across the fan can be linearly related to total fan airflow. This work will lead to improved input values for use in energy simulation programs and better estimates for energy performance for VAV systems using fan-powered terminal units.

INTRODUCTION

The energy savings in variable air volume (VAV) systems result from their ability to vary the amount of conditioned air delivered to a zone to maintain space comfort. Conceptually, primary (supply) air from the fan in an air-handling unit (AHU) is delivered to VAV terminal units via supply air ductwork. These VAV terminal units then respond to zone load

requirements and modulate that primary supply air to the zone. Typically, this modulation varies from some minimal airflow (normally around 20% of maximum) to the rated maximum flow for the given terminal unit. A common designation for terminal units with internal fans is *fan-powered terminal units* or FPTUs. FPTUs operate in a similar way as non-fan-powered terminal units in that they respond to load requirements in the zone that they serve. However, the operation is different in that internal fans are used. These units blend air induced from the plenum (secondary air) with primary air, can provide additional pressurization to the supplied airflow stream, and can add supplemental heat (when needed) to the supply air before air delivery to the conditioned zone.

There are two commonly available FPTU configurations: series and parallel. A fan that is located in series with the primary AHU fan is referred to as a *series FPTU*. In a series FPTU, both primary and secondary or induced air passes through the FPTU fan. Series FPTU fans normally operate continuously and provide a constant volume of air to the zone that they serve. The fan in these FPTUs is located such that it operates in series with the primary AHU fan. Some “free” heating is available through an induction port that induces warm return plenum air to be drawn into the air stream. *Parallel FPTUs*, on the other hand, have an internal fan that operates only when there is a call for supplemental heating from the conditioned zone. The fan is located in the induction or secondary air inlet for the FPTU and operates in parallel with the primary airstream. For either system, if supplemental heating energy is called for in the conditioned space, an optional heating coil using hot water, electrical energy, steam, or direct-fired with natural gas can be added to the FPTU.

John A. Bryant is an associate professor in the department of construction science, Texas A&M university, College Station, TX. **Stephen J. Bryant** is a project manager intern with Dynamic Systems, Inc., Austin, TX.

Fan motors for either of the FPTU types can be supplied with a permanent split capacitor (PSC) motor or an electronically commutated motor (ECM) to drive the fans in the units. PSC motor speed is controlled with a silicon controlled rectifier (SCR). The SCR “chops” the alternating current (AC) voltage being supplied to the motor, and it allows AC motors to be speed controlled as if they were direct current (DC) motors. ECM motor speed is controlled through the use of circuitry that provides a DC voltage to the motor. In most FPTUs with PSC motors, a field technician would set the speed (supply voltage) of the motor to meet the design airflow into the zone served by that FPTU. Once set during the installation and/or commissioning of the FPTU, the speed of the motor typically would not be changed for the life of the FPTU. ECM motors, on the other hand, can either be set for a fixed operational airflow delivery or the ECM controller can be integrated into a building's energy management control system so the speed of the motor (and fan) can be varied to meet the load within the conditioned zone served by the FPTU.

Unlike the fans used in medium to large central AHUs, fan motors in FPTUs are matched with FPTU fans and come as a pair. Fan motors in FPTUs are typically of fractional power size, around 1.0 hp (746 W) or less. In large commercial office buildings, it would not be unusual to have dozens or even hundreds of FPTUs installed, depending on the size of the building. With such large quantities of FPTU fan/motors in a building, the total power consumption of these units can be a significant portion of the energy use in a commercial building.

The purpose of this paper is to report on the results of in-situ static differential pressure measurements taken for the fan/motor combination in a series FPTU. A range of primary airflow and induced airflow was used to characterize the differential pressure performance of this fan. Results show that a correlation can be developed for this performance that is linear with total airflow as the dependent variable. The velocity differential pressures for these same flow ranges were also calculated and show similar promising correlations. Models suggested for pressure rise for series FPTUs should allow an energy modeler to more accurately estimate the annual performance of FPTUs in building energy simulation programs.

BACKGROUND

Recent studies by Furr et al., Cramlet, Edmondson et al., and Peng and O'Neal (2014a, 2014b) have done much to characterize the steady state and part-load performance of FPTUs. Furr et al. (2007, 2008a, 2008b) conducted laboratory characterization of the power, power factor, pressure, and airflow performance of SCR controlled FPTUs from three manufacturers and two primary inlet diameter sizes. Cramlet (2008) extended the work of Furr et al. by including power quality measurements and developing a set of equations for characterizing the performance of an ECM controlled FPTU. Edmondson et al. (2011a and 2011b) further extended Cram-

let's work by conducting extensive measurements of ECM controlled FPTUs from three manufacturers. The experimental studies by Furr, Cramlet, and Edmondson, treated the FPTU as a system. Semiempirical relationships were developed from the experimental data that could be used to estimate the electrical, pressure, and airflow performance of FPTUs. As demonstrated by Davis et al. (2012), the models developed from the prior experimental work allowed a modeler to use the sets of equations to simulate the hourly performance of a particular FPTU in a building if the static pressures inside the duct system were known. Some building energy simulation programs use a much simpler model of FPTUs that rely on energy and mass balances of the FPTU to estimate performance. Directly using the data from the abovementioned studies would require a different approach to modeling the air-side systems than is commonly found in some building simulation programs.

Recently, Peng and O'Neal (2014a, 2014b) measured the performance of the individual components (fan/motor combination, the damper, and cabinet) of ECM-controlled FPTUs. Their strategy was to determine if the individual component models could be combined together to predict overall system performance. The system performance predicted with this approach was compared to the measured system performance of the FPTU collected by Edmondson et al. (2011a). There was general agreement in the trends and it demonstrated that a component approach could be used if the performance of the fan/motor/controller, damper, and housing were known. Some of the differences in performance between the component and measured system performance focused on the airflow effect on fan performance within the FPTU. Specifically, when the fan/motor combination was tested outside the FPTU, it was not possible to reproduce the changes in performance caused by fan system effects that occur because of the constrained space within the housing of the FPTU.

Background—EnergyPlus

EnergyPlus is a powerful and popular building simulation program that can be used to estimate the annual energy usage of a wide range of buildings including by type of HVAC and other energy consuming systems in the building. Within the program, VAV systems using series or parallel FPTUs can be modeled. Following is a description of the modeling process taken from the *EnergyPlus Engineering Reference* (EnergyPlus 2013), which discusses the procedures used to model FPTUs. EnergyPlus describes a FPTU as powered induction unit (PIU) in the document. To avoid confusion, the more generic FPTU term will be used in the remainder of this paper.

The input submodels for a single-duct, series FPTU with supplemental heat, or for the single-duct, parallel FPTU with supplemental heat, provide models for constant volume FPTUs that occur in a variety of configurations. EnergyPlus models two types: series (sometimes called constant) and parallel (sometimes called intermittent). The series unit

provides a constant flow of air to the zone (the fan is always on at a constant flow) with a variable proportion of primary and secondary or induced airflow. The parallel FPTU has an intermittent fan: the fan is off at maximum cooling and does not operate until primary airflow is significantly reduced from the maximum and there is still need for heating in the zone being served by that FPTU. Once on, the FPTU provides a constant flow of secondary air with coincident minimal primary airflow. If the zone conditions still call for heating, the FPTU can add supplemental heat as needed. Both units induce air from the zone or plenum (secondary air) and mix it with centrally conditioned supply air (primary air) to raise the temperature of the air supplied to the conditioned zone before adding supplemental heat. Both units are variable volume: the supply airflow (primary air) rate is varied to match zone conditioning requirements.

Model

Both of these FPTUs are modeled as compound components. The series unit, in order from the primary air inlet port, consists of an air mixer, a constant volume fan, and a supplemental heating coil. In terms of EnergyPlus models, these are as follows:

- A zone mixer
- A constant volume fan
- A supplemental heating coil that can be one of the following; hot water, electric, gas, or steam

The parallel unit contains a fan that is located in the secondary air stream, an air mixer, and a supplemental heating coil. In terms of EnergyPlus models these are:

- A constant volume fan
- A zone mixer
- A supplemental heating coil that can be one of the following; hot water, electric, gas, or steam

Both units are forward models, that is, their inputs are defined by the state of their inlets—namely the air inlet and the supplemental heating coil inlet. The outputs of the models are the conditions of the outlet air stream: flow rate, temperature, and humidity ratio (EnergyPlus 2013).

EnergyPlus uses a simplified component approach to simulate the performance of FPTUs. The program makes the assumption that both series and parallel FPTU systems can be modeled as a combination of three major components as described above: a mixer, a constant volume fan, and a supplemental heating coil. Figure 1 shows the placement of the components used to model series FPTUs in EnergyPlus.

EnergyPlus assumes there is no pressure interaction between the components in a FPTU. Each component has a submodel that is connected via only mass and energy balances to the other components. Once the zone loads are determined, then the mass and energy balances can be used to determine the energy use and airflow requirements of the FPTU. While

the primary air (inlet) damper is not explicitly modeled in EnergyPlus, the program does use an energy and mass balance calculation to estimate the distribution of airflows between the primary and secondary air (induced) streams. This calculation mimics the main function of the damper (i.e., control of the amount of airflow).

As part of the data input process for simulation of a VAV system with FPTUs, the user must specify a number of design flow rates (maximum total airflow rate, maximum primary airflow rate, and minimum primary airflow fraction) or these values can also be autosized by the program.

The user is required to input the fan properties as shown in Table 1. The fan calculation, as used in EnergyPlus for

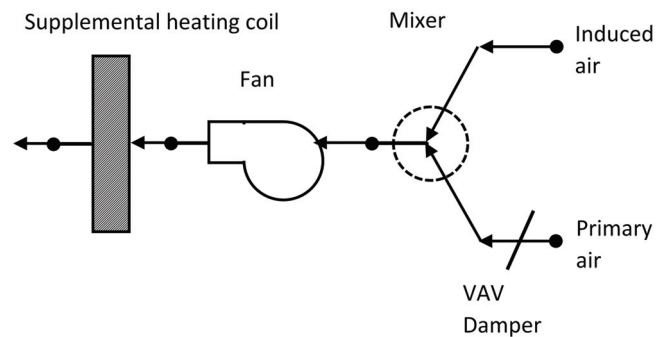


Figure 1 Components used in EnergyPlus for the simulation of a series FPTU (FPTU).

Table 1. Fan Characteristic Inputs Required for Series FPTUs in EnergyPlus

Field	Description
Name	Unique user-assigned name for referenced FPTU
Availability	Schedule that allows fan to run during a given time period
Fan Efficiency	Fan total efficiency, η_{fan} , default is 0.7
Maximum Flow Rate	Design volumetric flow rate, m_{design}
Motor Efficiency	Fan motor efficiency, η_{mot} , default is 0.9
Motor in Airstream Fraction	Fraction of fan heat that enters airstream, Q_{toair}
Air Inlet Node	Name of HVAC supply node
Air Outlet Node	Name of HVAC node receiving outlet air
End-Use Subcategory	User specified name/report created for Output:Meter object
Pressure Rise	Design air pressure rise across the fan, ΔP

FPTU systems, is called a constant volume fan submodel and assumes a constant speed fan for either the series or parallel FPTU fans. The fan motor controller in FPTUs is capable of varying the speed of the FPTU fan. However, the controller voltage (SCR for PSC and DC voltage for ECM) of the FPTU fan is typically set during installation of the unit or commissioning of the building to meet airflow requirements in the zone and remains fixed unless manually adjusted at some later time. The assumption that the fan is at a constant speed is only true if the pressure differential across the fan remains constant. If the pressure differential varies, then the ECM controller will adjust fan speed in an attempt to keep the fan airflow constant.

In the constant volume fan submodel of EnergyPlus, the user is also required to provide inputs for fan total efficiency (η_{tot}), fan motor efficiency (η_{mot}), and a “design air pressure rise across the fan,” ΔP . This last input is a vague term at best. It is assumed that the pressure rise is the total pressure rise across the fan and this is because the definition of fan efficiency normally uses total pressure. Fan static differential pressure rise could be used, and there is not a significant difference for the small diameter fans typically used in FPTUs. But, it is not clearly stated in the EnergyPlus documentation which differential pressure rise is appropriate. Individual fan and motor efficiencies are rarely provided separately by the FPTU manufacturers. For the small-diameter fans and fan motors used in FPTUs, the fan and motor are usually tested as a unit rather than individually. After a motor/fan combination has been tested and accepted for use in a particular manufacturer's FPTU, the system is tested as a whole unit. So again, individual fan or motor efficiencies are not available.

Regardless of definition used, the small fan/motor sets used in FPTUs should generate either static or total differential pressure rises substantially less than 1.0 in. w.g. (250 Pa). This is because static pressures downstream of the FPTU are usually less than 0.5 in. w.g. (125 Pa), with 0.25 in. w.g. (62.5 Pa) being a very common engineering design point.

Since the differential pressure rise is one of the fundamental fan inputs to the EnergyPlus simulation of a VAV HVAC system using FPTUs, actual fan performance data are needed for these units. Accepting “default” or using inappropriate values for the fan inputs can have a major impact on the validity of simulation models using FPTUs, especially series types, in VAV systems. Modeling of FPTU VAV systems using correlations based upon actual fan pressure rise data should result in better energy used models and allow building professionals to make better system application decisions.

EXPERIMENT

The experimental apparatus that was used to generate the static differential pressure rise was constructed from equipment remaining from previous research projects (Peng et al. 2013). Care was taken to adhere to good engineering design to minimize error in the experimental data. The basic apparatus is shown schematically in Figure 2. The system consisted of a fan (primary air), straight duct section, 8 in. (200 mm) inlet

diameter series FPTU, straight duct section, and a suction (assist) fan. The series FPTU was a unit that had been used in a previous research project (Furr et al. 2008a) and in that study had been assigned the designation of S8C. This designation indicated that the motor was a PSC type, controlled by an SCR, with an 8 in. (200 mm) primary inlet diameter and supplied by manufacturer C.

The two fans and FPTU were connected to each other with rectangular, uninsulated sheet-metal ductwork. The length of this duct (Figure 2) followed specifications outlined in ANSI/ASHRAE *Standard-130* (2006).

The upstream duct was a 16 in. \times 15 in. (406 mm \times 381 mm) rectangular duct and the downstream rectangular duct was 8 in. \times 9 in. (203 mm \times 230 mm). All of the fans in this system were nominal 277 Vac type, single-phase motors. The series S8C FPTU was supplied with a 0.5 hp (373 W) motor and on-board-diagnostic-type inlet dampers. The setup is shown in Figures 3 and 4.

Testing Sequence

Tests were run under as wide a range of values as supported by the S8C FPTU. The units were each turned on in a sequence of primary fan, S8C FPTU fan, then assist fan. The primary fan was set to maximum airflow through its controller. The SCR controller on the S8C was started at a minimal setting with the assist fan then modulated to maintain the desired static pressure in the discharge duct immediately downstream of the S8C FPTU. Discharge static pressure was set at 0.25 in. w.g. (62.3 Pa) because this value is set forth for FPTU testing under ANSI/AHRI *Standard 880* (AHRI 2011).

As the system came to steady state, the discharge static pressure would be adjusted to 0.25 in. w.g. (62.3 Pa) through adjustment of the assist fan or the opposed blade damper in the discharge duct. Once the desired setpoint had settled to an acceptable level, the static differential pressure across the FPTU fan would be measured. Specialty static pressure probes with a magnetic base were used for these measurements. Finally, velocity pressure was measured in the discharge duct and primary air duct. These velocity pressure measurements allowed for calculation of the total airflow from the FPTU, total airflow supplied to the FPTU and the difference between these would be the airflow induced through the FPTU induction port. Once a data point set was completed, the flows would be reset for the FPTU, primary fan and discharge static subsequently set back to 0.25 in. w.g. (62.3 Pa), and the process

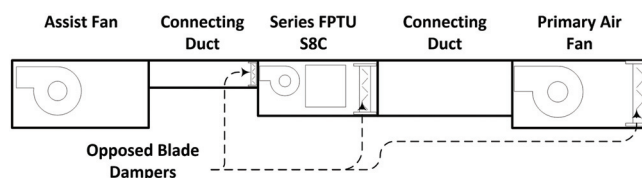


Figure 2 Schematic of test apparatus used to measure differential pressure rise at FPTU.

repeated for the next data point. Table 2 shows the primary data collected and applicable ranges.

Instrumentation used for data collection included micro-manometers to measure duct static, velocity pressure, and static differential pressure increase across the S8C FPTU fan and a pitot tube to measure total and induction port airflow. S8C FPTU fan power was measured with an industrial power

quality meter. Differential pressure measurements were taken continuously for one minute and averaged for each data point.

RESULTS

Static pressure probe placement was an important part of this study. Two positions were evaluated at the discharge of the S8C FPTU and a series of positions upstream of the FPTU fan were also investigated. Because of the chaotic nature of the flow field entering through the FPTU and into the FPTU fan, it was felt that there might be significant issues with measurement stability or other measurement issues. The centerline of the FPTU fan (transverse to the FPTU cabinet) was chosen as a datum, and static pressure tap holes were placed along the centerline of the longitudinal axis of the FPTU cabinet at 4 in. (100 mm) on center towards the inlet port of the FPTU. Figure 5 shows a photo of this arrangement. Testing revealed that what was referred to as position +2,-3 provided the most stable and consistent measurements of differential static pressure rise across the S8C FPTU fan. All subsequent testing was completed for static differential pressure rise using these measuring positions.

Power data for the S8C FPTU was taken as a function of airflow in a previous research project (Cramlet 2008). Data from this study was compared to the data taken in that project to ensure reliable measurement techniques and that the fan was still performing consistently. These data are shown in Figure 6. The original data from the Cramlet study were taken under slightly different ambient conditions. To ensure a proper

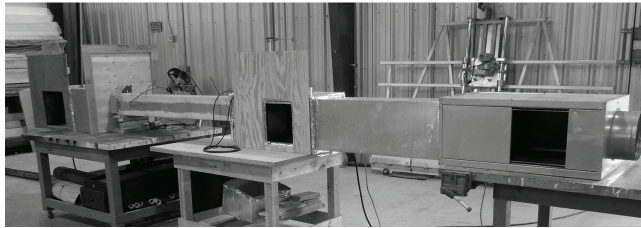


Figure 3 Side view of experimental apparatus. Right-Left: Primary fan, duct section, S8C FPTU, duct section, assist fan.

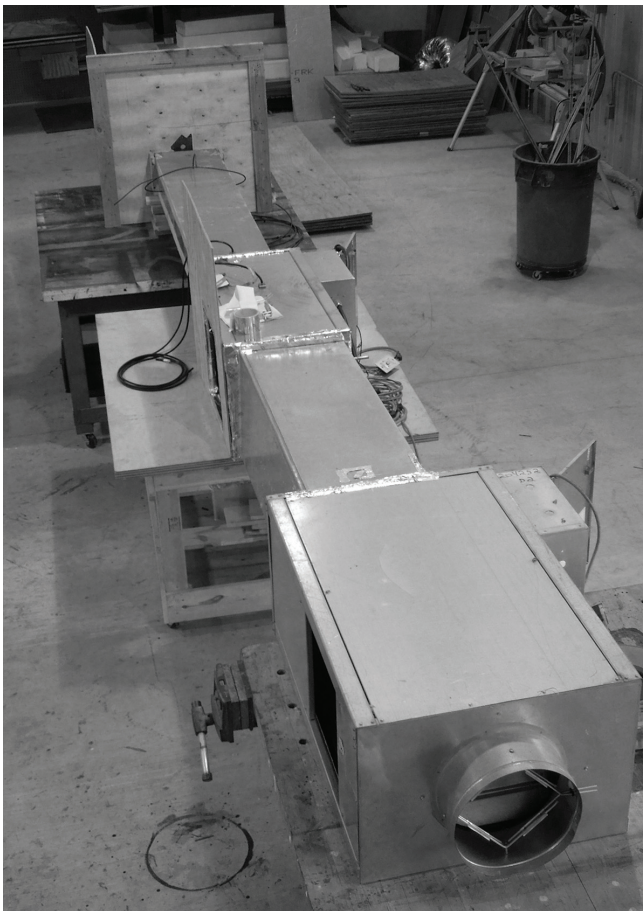


Figure 4 Overhead view of experimental apparatus. Bottom-Top: Primary fan, duct section, S8C FPTU, duct section, assist fan.

Table 2. S8C FPTU Test Points

Independent Variable	Range of Values
Fan Power	220–400 W
Primary Airflow	0–1,400 ft ³ /min (0–0.66 m ³ /s)
Induced Airflow	0–850 ft ³ /min (0–0.40 m ³ /s)

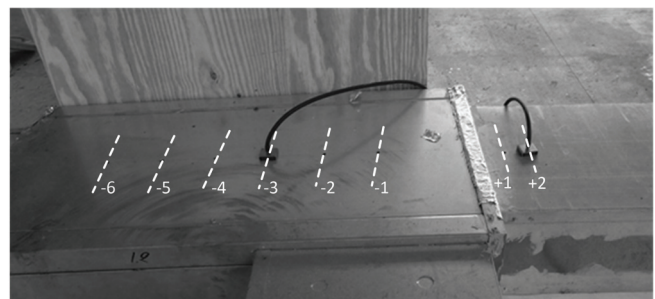


Figure 5 View of static pressure tap points in S8C FPTU cabinet (left) and discharge static pressure points (right).

comparison, data from that study were adjusted for air temperature as shown in Equation 1.

$$q_{current} = q_{Cramlet} \left(\frac{273.1 + T_{current}}{273.1 + T_{Cramlet}} \right) \quad (1)$$

where

$q_{current}$ = airflow for S8C FPTU in the current study, ft³/min (m³/s)

$q_{Cramlet}$ = airflow for S8C FPTU in the Cramlet study, ft³/min (m³/s)

$T_{current}$ = air temperature at FPTU inlet for the current study, °C

$T_{Cramlet}$ = air temperature at FPTU inlet for the Cramlet (2008) study, °C

After the adjustment for temperature (air density), the data for both studies agree within 2%. This demonstrated that the power/flow measurements were reliable and consistent with those taken in work done several years ago on this S8C FPTU and that the measurement technique for this study could replicate that earlier data.

Figure 7 shows a nearly linear relationship between total airflow through the FPTU and static differential pressure rise across the FPTU fan. The data ranged from about 0.10–0.25 in. w.g. (24.9–62.3 Pa) over the airflow range of 600–1300 ft³/min (0.283–0.613 m³/s).

The relationship between airflow and velocity pressure was also investigated. It was not possible to measure velocity pressure directly because of the extreme nonuniform airflow through the FPTU. The average velocity through the FPTU was determined from Equation 2

$$q = \bar{V}A \quad (2)$$

where

q = airflow in ft³/min (m³/s)

\bar{V} = average airflow velocity through test section in ft/s (m/s)

A = cross-sectional area for airflow, ft² (m²)

For the apparatus shown in Figure 3, the cross-sectional area was measured and found to be 1.67 ft² (0.155 m²) for the FPTU case and 0.72 ft² (0.067 m²) in the discharge duct immediately following the FPTU. Airflow was measured for each test run from data taken with a pitot tube reading at the inlet to the FPTU and in the discharge duct downstream from the FPTU. Once the average velocity was obtained from Equation 2, then the velocity pressure could be found as shown in Equation 3 (3a for I-P units, 3b for SI units),

$$V_p = \left(\frac{\bar{V}}{1096.2} \right)^2 \rho \quad (3a)$$

$$V_p = \frac{\rho \bar{V}^2}{2} \quad (3b)$$

where

V_p = velocity pressure, in. w.g. (Pa)

\bar{V} = average airflow velocity through test section in ft/s (m/s)

ρ = density of air at test conditions (temperature and humidity), lb/ft³ (kg/m³)

Figure 8 shows the resulting data for the flow range tested with the S8C FPTU. As with static pressure rise and total airflow, Figure 8 shows that there is a generally linear trend that allows one to predict static pressure rise with velocity pressure in this FPTU.

DISCUSSION

The power versus flow comparisons for this study and the work done by Cramlet showed very good agreement. The values were within 2% when the Cramlet (2008) data were

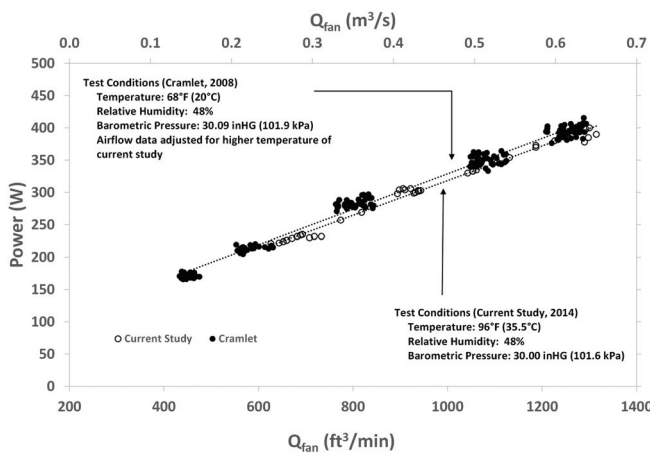


Figure 6 Airflow performance versus power for S8C compared to the Cramlet study (2008).

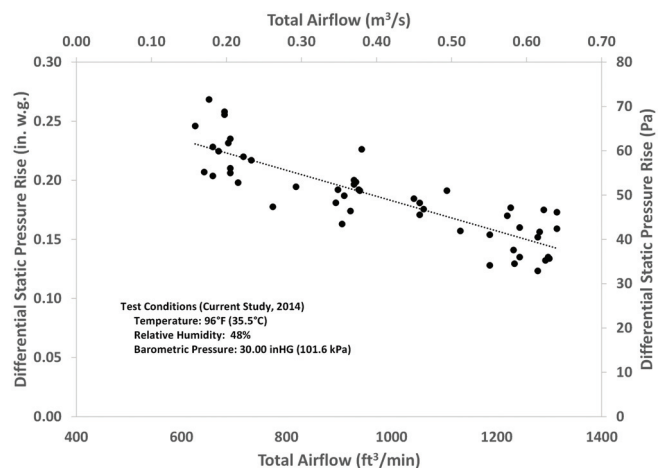


Figure 7 Differential pressure rise for S8C FPTU fan as a function of total airflow.

adjusted for the high temperature conditions of this study. Most gratifying were that measurements taken in this study could replicate data taken in a much more sophisticated laboratory setting. The current study is actually the first in a multi-part project. This first phase was intended to demonstrate an experimental approach to gather differential static pressure data for FPTU fans. The data presented here are a result of that first effort. The next phase will consist of obtaining a much wider sample of FPTU differential pressure data from a variety of manufacturers at their research facilities. There are no known sources of such data available to those using EnergyPlus to model VAV systems using series or parallel FPTUs. In fact, an online reference for EnergyPlus suggested a pressure rise of 1.5 in. w.g. (373 Pa) as a common value when modeling constant volume fans (DesignBuilder 2014). These values are actually not unexpected. The documentation for the constant volume fan model in EnergyPlus is clearly written for larger (AHU) fans and not as applicable for smaller fans such as those found in FPTUs. The examples given in these online forums would be very acceptable for the larger fans found in central AHUs. In those applications, one would expect to see fan/motor efficiencies close to those recommended in the EnergyPlus defaults as shown in Table 1. From Figure 7 it is obvious that the in-situ measured static differential was much less than the pressure rise as suggested in the modeling forums. Values for the range of airflow for the S8C FPTU of 0.25–0.10 in. w.g. (62.3–25.0 Pa) for the range of 1300–500 ft³/min (0.613–0.236 m³/s) are easily an order of magnitude less than what would be expected at the primary AHU fan of a typical HVAC system. The error on FPTU fan power when over-estimating the fan pressure rise as described above is quite clear, as shown in Equation 4 (4a for I-P units, 4b for SI units).

$$Power_{fan} = \Delta P_{rise}q/6356 \quad (4a)$$

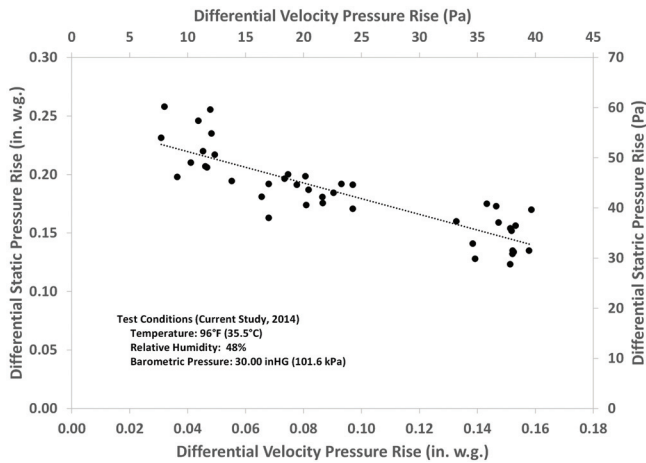


Figure 8 Differential static fan pressure rise for S8C FPTU versus differential velocity pressure.

$$Power_{fan} = \Delta P_{rise}q \quad (4b)$$

where

- $Power_{fan}$ = ideal power consumed by FPTU fan, hp (W)
- ΔP_{rise} = differential total pressure rise across fan, in. w.g. (Pa)
- q = airflow delivered by the fan, ft³/min (m³/s)

In Equation 4, the differential pressure rise is for total pressure. The EnergyPlus documentation is not clear on which pressure rise is to be used in the FPTU submodel. The documentation of the constant volume fan model describes how fan power is estimated from the user inputs and uses a form of Equation 4. This would indicate that EnergyPlus might be looking for total differential pressure as the input. It is not clear in the FPTU model documentation. It is of note that the static and total differential pressure rises are similar in magnitude for the small diameter fans typically found in FPTUs. The intent with showing Equation 4 is to highlight the problem with using overly large differential pressure values that can be as much as an order of magnitude too high. The results shown in Figure 7 seem to indicate that the static differential pressure rise for a series FPTU can be determined with a simple linear relationship with total FPTU airflow. Similarly, if differential velocity pressure for an FPTU is known, Figure 8 indicates that a linear relationship again will predict the static differential pressure rise for a series FPTU. With additional data for a wider range of series and FPTU models and from different manufacturers, it appears that solid linear relationships will be able to be developed for wider use in modeling programs such as EnergyPlus.

CONCLUSIONS

FPTUs employing SCR-controlled fan motors continue to be used in new and existing buildings. This initial work has shown that in-situ static fan differential pressure rise is significantly less than many sources recommend. These differences are as much as an order of magnitude and bring into question any modeling effort that might have been commissioned with such values for series or parallel FPTUs. The actual range for static differential pressure rise was measured in the range of 0.25–0.10 in. w.g. (62.3–25.0 Pa) for the range of 1300–500 ft³/min (0.613–0.236 m³/s) for an 8 in. (200 mm) inlet series FPTU supplied with a PSC motor and SCR controller. Similar low values for differential pressure rise are expected to be the case as additional FPTU models and manufacturers are tested.

The models developed from the data indicate that simple linear relationships exist between total airflow and fan differential static pressure. These relationships should provide a user of building energy simulation programs with the input and models needed to provide reliable estimates of the hourly and annual performance of SCR controlled fan motors used in FPTUs. There is significant scatter in the data found in this study and that would make it difficult to use these relationships

to model a particular manufacturer's specific FPTU. However, for the modeler desiring to model a generic VAV FPTU, the data presented here are quite an improvement over anecdotal information available from Internet sources.

ACKNOWLEDGMENT

We wish to thank the Air Conditioning, Heating, and Refrigeration Institute (AHRI) for their support of this project. In particular, we wish to thank all the members of the Air Control and Distribution Devices Committee for their input and advice.

REFERENCES

- AHRI. 2011. ANSI/AHRI Standard 880 (I-P). *Standard for performance rating of air terminals*. Air Conditioning, Heating, and Refrigeration Institute.
- ASHRAE. 2006. ANSI/ASHRAE Standard 130-1996 (RA 2006), *Methods of testing for rating ducted air terminal units*. Atlanta: ASHRAE.
- Cramlet, A. 2008. *Performance of ECM controlled VAV fan power terminal units*. Master's thesis, Texas A&M University, College Station, TX.
- Davis, M., J. Bryant, and D.L. O'Neal. 2012. Modeling the performance of ECM and SCR series fan-powered terminal units in single-duct VAV systems. *ASHRAE Transactions* 118 (1).
- DesignBuilder, 2014. http://www.designbuilder.co.uk/help/v3.1/Content/Fan_-_Constant_Volume.htm, referenced September 20, 2014.
- Edmondson, J., D.L. O'Neal, J.A. Bryant, and M.A. Davis. 2011a. Performance of parallel fan powered terminal units with electronically commutated motors—Part 1. *ASHRAE Transactions* 117(2).
- Edmondson, J., D.L. O'Neal, J.A. Bryant, and M.A. Davis. 2011b. Performance of parallel fan powered terminal units with electronically commutated motors—Part 2. *ASHRAE Transactions* 117(2).
- EnergyPlus. 2013. Air system distribution terminals. *EnergyPlus engineering reference: The reference to EnergyPlus calculations*. Berkeley: Lawrence Berkeley National Laboratory.
- Furr, J. D.L. O'Neal, M. Davis, J. Bryant, J., and A. Cramlet. 2007. ASHRAE Research Project 1292: *Comparison of the total energy consumption of series versus parallel fan powered VAV terminal units*, Phase I Final Report, Atlanta: ASHRAE.
- Furr, J., D.L. O'Neal, M. Davis, J. Bryant, and A. Cramlet. 2008a. Performance of VAV fan powered terminal units: Experimental setup and methodology. *ASHRAE Transactions* 114(1).
- Furr, J., D.L. O'Neal, M. Davis, J.A. Bryant, and A. Cramlet. 2008b. Performance of VAV fan powered terminal units: Experimental results and models for series units. *ASHRAE Transactions* 114(1).
- O'Neal, D. L., J.L. Edmondson, and Y. Peng. 2014. Comparison of performance characteristics of SCR and ECM controlled series fan powered terminal units. *HVAC&R Research (now Science and Technology for the Built Environment)* 20(2):194–202.
- Yin, P., and D.L. O'Neal. 2014a. Characterizing airflow and power of VAV series fan-powered terminal units from component data—Part I. *ASHRAE Transactions* 120(1).
- Yin, P., and D.L. O'Neal. 2014b. Characterizing airflow and power of VAV series fan-powered terminal units from component data—Part II. *ASHRAE Transactions* 120(1).

ST-16-025

Characterizing the Performance of Fixed-Airflow Series Fan-Powered Terminal Units Using a Mass and Energy Balance Approach

Carl L. Reid
Student Member ASHRAE

Dennis L. O'Neal, PhD, PE
Fellow ASHRAE

Peng Yin
Student Member ASHRAE

ABSTRACT

A traditional mass and energy balance component approach was used to characterize the performance of fixed-airflow series fan-powered terminal units for applications in building simulation programs. The approach included developing relevant energy and mass balance equations for the components in a fan-powered terminal unit—heating coil, fan/motor combination, and mixer. Fan motors that included permanent-split-capacitor motors controlled by silicon-controlled rectifiers or electronically commutated motors were included in the model development. The paper demonstrates how to incorporate the fan/motor combination performance models for both permanent-split-capacitor and electronically commutated motors into the mass and energy balance approach. The fan models were developed from performance data that were provided by multiple fan-powered terminal unit manufacturers. The fan/motor performance data included a fan airflow range from 250 to 3500 ft³/min (0.118 to 1.65 m³/s) and a motor size range from 0.333 to 1 hp (248.6 to 745.7 W).

INTRODUCTION

A common heating, ventilating, and air-conditioning (HVAC) system used in commercial buildings is the single-duct variable-air-volume (VAV) system (ASHRAE 2012). A VAV system varies the amount of air delivered to a conditioned zone to ensure the desired thermal comfort level. The supply air to each zone is modulated by using a single terminal unit based on the sensible load sensed by a thermostat in the zone.

If a terminal unit includes a fan, it is called a fan-powered terminal unit (FPTU) or powered induction unit (PIU). The more general term *FPTU* is used in this paper. FPTUs mix the primary air with induced recirculated (secondary) air. The FPTU may provide supplemental heating to the air depending

on whether the FPTU is in heating or cooling mode. Supplemental heating can be provided with either a hot-water coil (heat exchanger) or electric resistance (ASHRAE 2012).

One configuration of an FPTU is shown in Figure 1. In this case, the FPTU fan and the primary air fan are in series. Both primary and secondary air pass through the FPTU fan, which operates continuously while the system is on. Secondary air is induced into the FPTU from the return air plenum by the FPTU fan.

Two different motors are commonly used in FPTUs: a permanent-split-capacitor (PSC) motor controlled by a silicon-controlled rectifier (SCR) and an electronically commutated motor (ECM). PSC motors are commonly used in those applications where the airflow from the FPTU fan is expected to be constant. The SCR chops the voltage supplied to the PSC motor to lower the speed of the motor and allows an installer to match the airflow from the FPTU to the airflow requirements of the zone. Once the voltage is set, the FPTU fan should operate at a nearly constant airflow rate. A PSC motor operates at maximum efficiency when it is at full load.

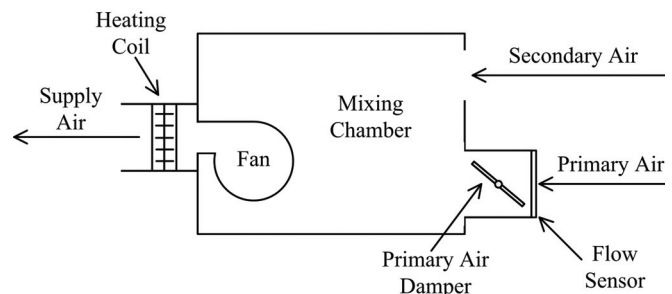


Figure 1 Series configuration for FPTU.

Carl L. Reid is staff engineer at Bee in Austin, TX. Dennis L. O'Neal is dean of Engineering and Computer Science, and Peng Yin is a post-doctoral research associate in the Department of Mechanical Engineering at Baylor University, Waco, TX.

ECMs provide an advantage over PSC motors in FPTU applications because ECMs can be used where the airflow from the FPTU is either fixed or allowed to vary to match the airflow requirements in the zone. An ECM converts alternating current (AC) to direct current (DC) to operate the motor. An ECM provides direct control over the voltage, which allows for more precise speed control. An ECM should operate at a higher efficiency than the SCR-controlled PSC motors (Int-Hout 2015).

Modeling work by Davis et al. (2012) showed that series FPTUs with fixed-airflow ECM fan motors outperformed series FPTUs with SCR-controlled PSC fan motors in five different cities: Houston, Phoenix, Chicago, New York, and San Francisco. The annual total plant energy savings ranged from 5.9% to 8.4% in Chicago for a small, five-zone office building. Davis et al. (2012) based his FPTU models on the power, pressure, and airflow data collected and analyzed by Furr et al. (2008) and Edmondson et al. (2011). While the analysis by Davis et al. (2012) was useful in estimating savings of ECM FPTUs, it required detailed knowledge of the pressures upstream and downstream of the FPTU. This approach was not directly compatible with the mass and energy balance (MEB) modeling approach often used in building energy simulation programs such as EnergyPlus (2013). As a consequence, it is difficult to use the modeling work of Davis et al. (2012) and the data from Furr et al. (2008) and Edmondson et al. (2011) directly in building simulation programs. O'Neal et al. (2015a, 2015b) and O'Neal (2015) analyzed performance data on both PSC/SCR and ECM fan/motor data from four FPTU manufacturers and developed performance models that were compatible with a mass and energy balance system modeling approach found in some building simulation programs.

The purpose of this paper was to demonstrate how to combine the PSC/SCR and ECM performance data developed by O'Neal et al. (2015a and 2015b) with the mass and energy balance modeling approach used in EnergyPlus (2013). The models can be integrated into building energy simulations to predict the annual energy consumption in a VAV system using

fixed-airflow series FPTUs. Ongoing work is being done that extends the mass and energy balance modeling approach to variable-airflow applications with ECM fan motors applied in series FPTUs to match the thermal load in the zone.

MASS AND ENERGY BALANCE APPROACH

The mass and energy balance approach is commonly used to model components in the HVAC system of a building (Knebel 1983). This approach is currently used in EnergyPlus (2013). The MEB approach treats each subsystem in an HVAC system, such as an FPTU, as a set of equations to describe the mass and energy flows into and out of each subsystem. A series FPTU can then be decomposed into its major components: mixer, fan/motor, and heating coil. Figure 2 shows a control volume around the whole FPTU. With the MEB approach, an analysis can be performed on each component to estimate overall airflows into and out of the FPTU as well as the energy used by the FPTU fan/motor for each time step of a simulation. The large dashed box is the overall control volume for the FPTU. Each FPTU component can be treated with a smaller control volume with mass and energy inputs and outputs. Figure 2 represents one FPTU. However, a building could include dozens of these in a VAV system.

Series FPTU Model

Looking at the overall control volume around the series FPTU, energy is input to the FPTU via electrical energy to the fan, heat energy to the heating coil, and energy associated with the primary and secondary airstreams. The only mass and energy leaving the series FPTU is with the airstream at the discharge of the FPTU.

The series FPTU consists of three major components: mixer, fan, and heating coil. A mass and energy balance needs to be performed on each of the components and the conditioned zone to estimate temperatures and airflows to determine the performance of the FPTU. The approach outlined below incorporates empirical models for the FPTU fan/motor to calculate the fan power.

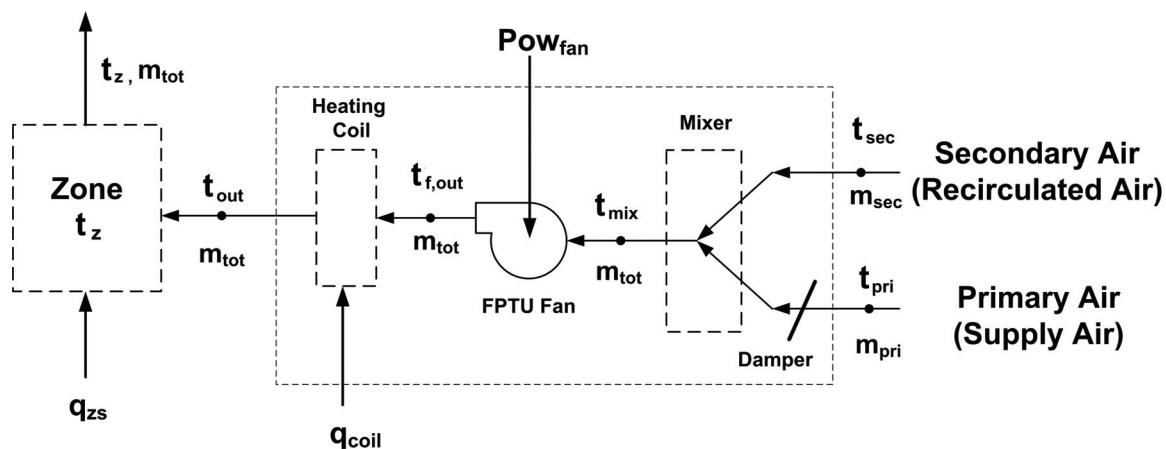


Figure 2 Mass and energy flows into and out of a series FPTU.

Before starting an analysis, it is important to outline some basic assumptions we used in developing the MEB model. First, the system in Figure 2 is assumed to operate at quasi-steady state during each time step. During a particular time-step, the temperature and airflows remain constant and are averaged over the time step. Given that the typical time step is an hour, this type of analysis cannot capture rapid transients occurring in a control system at smaller time steps. We also assume that the thermophysical properties are constant. This allows the specific heat and density of the air to be treated as constants. Given the small temperature differences in the airstreams, constant specific heats and density should introduce small errors (less than a 1%) in the analysis. Third, the energy input to the fan motor is assumed to be completely converted into the heat energy in the airstream. For a series FPTU, the fan/motor combination is located completely in the airstream. Thus, all of the heat energy for the fan should be dissipated in the airstream. This assumption is discussed in more detail later in the paper. Fourth, the FPTU must always operate with a minimum amount of primary air to ensure enough fresh air is introduced into the zone. Thus, even when the zone calls for heating or a very low amount of cooling, there will always be a minimum amount of primary air provided to the FPTU.

The mass and energy balances for a general control volume at steady state are given by Equations 1 and 2, respectively.

Mass balance is as follows:

$$\{\text{Airflow out of FPTU}\} = \{\text{Airflow into FPTU}\} \quad (1)$$

Energy balance is as follows:

$$\{\text{Energy out of FPTU}\} = \{\text{Energy into FPTU}\} \quad (2)$$

For the FPTU control volume shown in Figure 2, the mass flow into the control volume includes the primary, m_{pri} , and secondary, m_{sec} , airstreams. The only mass out of the control volume is the total airflow, m_{tot} . Application of the mass balance in Equation 1 to the control volume yields the mass balance shown in Equation 3:

$$m_{tot} = m_{pri} + m_{sec} \quad (3)$$

The value of m_{pri} is often an unknown that must be estimated using the analysis discussed below. The only exceptions are when the series FPTU is operating under minimum or maximum primary flow conditions.

The energy transfer into the control volume includes the energy carried by the two airstreams, the rate of energy input in the heating coil (q_{coil}), and the power input to the fan (POW_{fan}). The energy into and out of the control volume can be substituted into Equation 2 to obtain the general energy balance for the control volume given in Equation 4.

$$m_{tot} h_{out} = q_{coil} + POW_{fan} + m_{pri} h_{pri} + m_{sec} h_{sec} \quad (4)$$

Equations 3 and 4 provide the foundation for the analysis of the FPTU. The unknowns in these equations vary depending on the mode of operation (heating, cooling, or dead band) of the FPTU. Solving for the unknowns requires applying mass and energy balances to each of the components in the FPTU. The process typically starts from the left at the FPTU discharge to the zone and moves to the right to the primary and secondary air inlets.

For the case of a fixed airflow with either a PSC/SCR or ECM fan/motor, the total airflow, m_{tot} , in the above equations is a fixed value. With constant air properties, Equation 4 can be rewritten in terms of temperatures and specific heats.

$$m_{tot} c_p t_{out} = q_{coil} + POW_{fan} + m_{pri} c_p T_{pri} + m_{sec} c_p t_{sec} \quad (5)$$

Proceeding with the analysis requires decomposing the FPTU into its components and performing mass and energy balances on each component as described below.

Zone Analysis

Figure 3 shows the mass and energy flows into and out of the conditioned zone. Energy is carried into and out of the zone via the total airflow, m_{tot} . The load in the zone due to people, equipment, solar gain, infiltration, etc., is represented by q_{zs} .

The value of the FPTU discharge temperature, t_{out} , must be calculated. This is done with an energy and mass balance on the zone in Figure 3. During heating operations, t_{out} is not allowed to drift above 90°F (32.2°C). The rationale for this assumption is provided in the "Heating Coil Analysis" section. During cooling operations, this value cannot drop below the sum of the primary air temperature plus temperature increase due to the FPTU fan. An energy balance is performed on the zone to yield Equation 6, which is used to

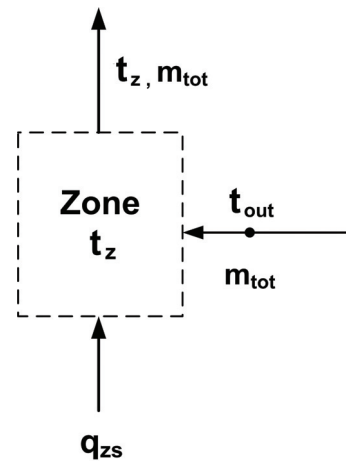


Figure 3 Energy and mass flows into and out of the zone control volume.

determine the discharge temperature of the air at the outlet of the FPTU unless the heating coil is engaged. The assumption for constant properties is used throughout the system.

$$q_{zs} = m_{tot}c_p(t_z - t_{out}) \quad (6)$$

The way that Equation 6 is used in an analysis depends on whether the system is in heating or cooling mode. For example, for a fixed-airflow application, m_{tot} is known. In addition, the zone load q_{zs} , specific heat c_p , and zone setpoint temperature t_z , are also known. For cooling applications, Equation 6 can be rewritten and solved for the discharge outlet temperature t_{out} for the FPTU:

$$t_{out} = \frac{q_{zs}}{m_{tot}c_p} + t_z \quad (7)$$

For heating calculations, t_{out} is calculated from Equation 7 but typically has an upper limit of 15°F (8.3°C) above the zone setpoint temperature or a fixed value of 90°F (32.2°C) to help reduce temperature stratification in the zone (Hydeman and Eubanks 2014). Procedures are provided later in the paper for the calculation of t_{out} for heating and cooling applications.

Heating Coil Analysis

Figure 4 shows the mass and energy flows into and out of the heating coil. It is assumed the system is operating at a quasi-steady state and the mass flow of air entering the coil is equal to the mass flow of air exiting the coil in a given time step. The energy entering the coil is the heating energy input, q_{coil} , and is equal to the energy absorbed by the air flowing through the coil. Heating energy is often provided by electric resistance or hot water. The energy exiting the coil is carried by air leaving the coil and supplied to the zone. Applying an energy balance to the heating coil yields the following:

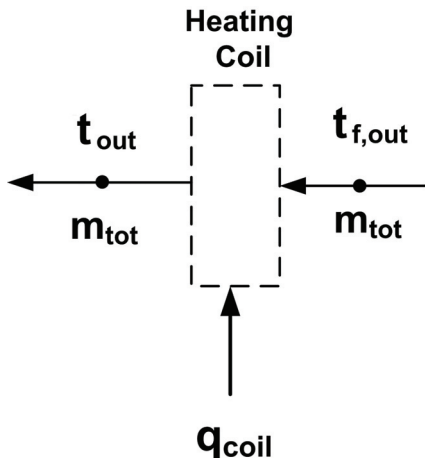


Figure 4 Energy and mass flows for the heating coil.

$$m_{tot}c_p t_{out} = q_{coil} + m_{tot}c_p t_{f, out} \quad (8)$$

Many times, the variable of interest is q_{coil} , the heating energy input, so the above equation can be rearranged to solve for q_{coil} :

$$q_{coil} = m_{tot}c_p(t_{out} - t_{f, out}) \quad (9)$$

FPTU Fan Analysis

The mass and energy flows into and out of the FPTU fan are shown in Figure 5. It was assumed that all of the fan motor and controller power is converted to heat energy in the airstream. This fraction of electric power dissipating into airstreams as heat energy can be varied by the user in Energy-Plus (2013). With a series FPTU, the electric motor is located in the primary airstream. With an ECM, the controller is also in the airstream, so for an ECM it should be expected that all the energy converted for the fan motor and controller goes into the airstream. With an SCR-controlled fan motor, the SCR controller is typically not located in the primary airstream but in the plenum airstream. Estimates of the power dissipated by an SCR controller are 1.5 W/amp of current flowing through the controller (Roman and Heiligenstein 2002). Table 1 shows the estimated percentage of total power that an SCR controller consumes for a 0.5 hp (373 W) PSC fan motor from one manufacturer. The power used by the SCR controller ranged between 0.57% to 0.83% of the total power of the motor. Calculations were run for fan motors ranging from 0.167 to 1.0 hp (124 to 746 W) with a similar range in percentages of the total power. Thus, with SCR-controlled fan motors, assuming that all the fan power is dissipated into the primary airstream introduces less than a 1% error in the heat energy added by the fan.

The airflow out of the fan is assumed to be equal to the airflow into the fan and both are equal to m_{tot} . For constant properties, an energy balance on the fan yields the following:

$$m_{tot}c_p t_{f, out} = m_{tot}c_p t_{mix} + POW_{fan} \quad (10)$$

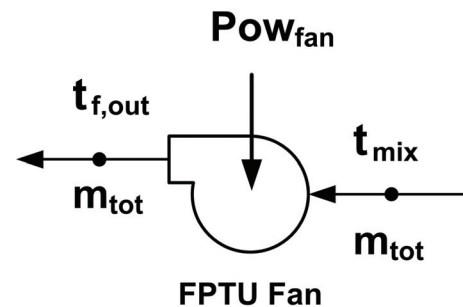


Figure 5 Mass and energy balance on the series FPTU fan.

Table 1. SCR Power Consumption for a 0.5 hp (373 W) FPTU Series Fan Motor

SCR Voltage	Airflow, ft ³ /min (m ³ /s)	Current, Amps	Power, Watts	SCR Power, Watts	SCR Power/ Total Power
277	2515 (1.19)	3.28	894	4.92	0.55%
277	2435 (1.15)	2.89	803	4.335	0.54%
277	2322 (1.10)	2.66	740	3.99	0.54%
277	2047 (0.97)	2.27	642	3.405	0.53%
240	2136 (1.01)	3.32	770	4.98	0.65%
240	2136 (1.01)	3.07	719	4.605	0.64%
240	2077 (0.98)	2.78	656	4.17	0.64%
240	1879 (0.89)	2.45	602	3.675	0.61%
208	1691 (0.80)	3.1	615	4.65	0.76%
208	1762 (0.83)	2.95	595	4.425	0.74%
208	1703 (0.80)	2.71	566	4.065	0.72%
208	1564 (0.74)	2.25	476	3.375	0.71%
140	1019 (0.48)	2.17	409	3.255	0.80%
140	1079 (0.51)	2.14	409	3.21	0.78%
142	1098 (0.52)	2.06	407	3.09	0.76%
146	877 (0.41)	1.93	397	2.895	0.73%

The power of the fan, POW_{fan} , can be estimated using models from O'Neal et al. (2015a, 2015b) and O'Neal (2015) and is discussed below in a separate section. The procedure for estimating power depends on whether the fan has an SCR-controlled PSC motor or an ECM. The power multiplied by each time step and summed over the entire year of a simulation would yield the energy use of the FPTU fan.

The temperature increase of the air due to the fan Δt_{fan} , can be evaluated by rearranging Equation 10:

$$\Delta t_{fan} = t_{f, out} - t_{mix} = \frac{POW_{fan}}{m_{tot}c_p} \quad (11)$$

Equation 11 provides a means of quantifying the impact of the fan power on the temperature rise of the air.

Mixer

The remaining component in the FPTU is the mixer (see Figure 6). For an FPTU, mixing of the primary and secondary airstreams occurs in the main housing of the FPTU immediately prior to the air entering the series FPTU fan. As with the other components, an energy and mass balance can be applied to the mixing process. The result of the mass balance yields the same equation as Equation 3. The mixer is assumed to perform

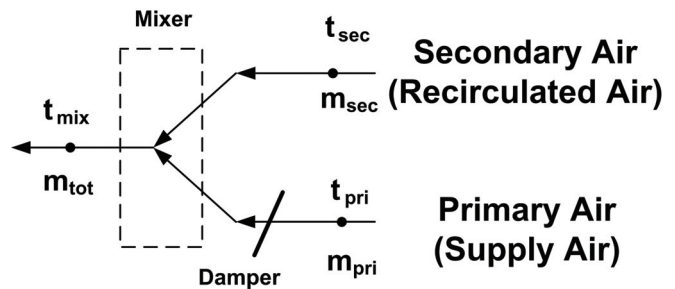


Figure 6 Energy and mass flows for the series FPTU mixer.

adiabatic mixing; therefore, no heat energy is lost to or gained from the surroundings. Applying an energy balance to the mixer yields the following:

$$m_{tot}c_p t_{mix} = m_{pri}c_p t_{pri} + m_{sec}c_p t_{sec} \quad (12)$$

The variables that would be calculated from Equation 12 depend on whether the FPTU is in cooling or heating mode. When the FPTU is in heating mode, the primary airflow would be set at a prescribed minimum needed to satisfy fresh air requirements (ASHRAE 2013). The minimum primary air is also used during dead band operations and when the estimated cooling load in the zone is smaller than the amount of cooling

provided by FPTU when the primary air is at its minimum value. Another time when the primary airflow is a fixed value is when the cooling load requirement in the zone is higher than the cooling provided by the FPTU when the primary airflow is at its maximum value. In this case, the FPTU would reach its maximum airflow and remain constant even if more cooling is required. In all other cooling cases, the primary airflows fall between these two values and the energy and mass balances on each component have to be utilized. The process is described later and depends on the operation mode of the FPTU.

ESTIMATING FAN POWER

Making an accurate estimate of the fan energy use in a series FPTU is important because the fan runs continuously and the fan power is used for estimating the temperature increase of the air across the fan. The fan energy requires estimating the fan power, POW_{fan} , which can be done with either measured field data or a model. For a fixed-airflow fan, some building simulation programs (EnergyPlus 2013) have a simple fan-power model that relates the power to the mass flow rate of the air through the fan m_{tot} , the pressure differential across the fan ΔP_{fan} , the fan/motor combined efficiency η_{tot} , and the density of the air ρ_{air} .

$$POW_{fan} = \frac{m_{tot} \Delta P_{fan}}{\eta_{tot} \rho_{air}} = \frac{Q_{tot} \Delta P_{fan}}{\eta_{tot}} \quad (13)$$

The quantity Q_{tot} in Equation 13 is the volumetric flow rate of the air, which is usually expressed in ft^3/min or m^3/s . This type of model requires knowledge of the pressure differential across the fan and the fan/motor efficiency, which are two quantities often not known to the modeler. In addition, analysis of fan/motor performance data from several manufacturers by O'Neal et al. (2015a, 2015b) and O'Neal (2015) demonstrated that these two variables cannot be treated independently for fans having either PSC motors with SCR controllers or ECMs. In contrast, some building simulation programs, such as EnergyPlus (2013), allow the user to independently input these two variables. Alternative approaches to characterizing fan/motor performance were developed and depended on whether the FPTU had a PSC fan motor controlled by an SCR (O'Neal et al. 2015a) or had an ECM (O'Neal et al. 2015b). Utilization of these models in the mass and energy balance approach is discussed below.

PSC Motor with an SCR Controller

With a PSC fan motor controlled by an SCR, O'Neal et al. (2015a) analyzed data from three manufacturers covering a range of FPTU fan motor sizes from 0.125 to 1 hp (93 to 746 W). The fan efficiency was dependent on the total pressure across the fan. They fit the data with a simple linear model:

$$\eta_{tot} = C_1 \cdot \Delta P_{fan} \quad (14)$$

where, C_1 was 32.06%/(in. w.g.) in I-P units or 0.129%/Pa in SI units. Equation 14 can be rearranged to show that the efficiency divided by the pressure differential across the fan can be treated as a constant for a PSC motor with SCR control.

$$\frac{\eta_{tot}}{\Delta P_{fan}} = C_1 \quad (15)$$

Equation 15 can be substituted into Equation 13 and simplified to give an expression for the power solely in terms of air mass flow m_{tot} , the density of the air ρ_{air} , and C_1 :

$$POW_{fan} = \frac{m_{tot}}{C_1 \rho_{air}} = \frac{Q_{tot}}{C_1} \quad (16)$$

The correct units for C_1 need to be used in the above expression and were different in the I-P or SI systems. If the power is desired in Watts, then Equation 16 can be rewritten with conversion constants to allow the user to input the volumetric flow and C_1 in ft^3/min and %/(in. w.g) in Equation 17 or in m^3/s and %/Pa in Equation 18, respectively, to get the power in Watts.

In I-P Units:

$$POW_{fan} = \frac{11.75 \cdot Q_{tot}}{C_1} \quad (17)$$

In SI Units:

$$POW_{fan} = \frac{100 \cdot Q_{tot}}{C_1} \quad (18)$$

Another approach was also developed by O'Neal et al. (2015a) to correlate airflow and power data. A simple linear best fit of the power versus airflow data provided the following (O'Neal et al. 2015a) is as follows:

$$POW_{fan} = C_2 \cdot Q_{tot} \quad (19)$$

where C_2 was 0.372 W/(ft^3/min) in I-P units and 788 W/(m^3/s) in SI units. Equations 16 through 19 provide a straightforward way for a building simulation user to estimate the power used by a PSC fan motor controlled with an SCR in a series FPTU.

To illustrate the use of Equations 16 through 19, consider a series FPTU fan that is producing 1000 ft^3/min (0.472 m^3/s). The value of C_1 would be either 32.06%/(in. w.g.) in I-P units or 0.129%/Pa in SI units. Using Equations 17 for I-P and 18 for SI units, we get the following fan power starting with airflow in I-P units,

$$POW_{fan} = \frac{11.75 \cdot (1000)}{32.06} = 366.5 \text{ W} \quad (20)$$

or starting with airflow in SI units,

$$\text{POW}_{fan} = \frac{100 \cdot (0.472)}{0.129} = 365.9 \text{ W} \quad (21)$$

The small differences between the two are due to round-off errors in the coefficients.

Using Equation 19 to calculate the fan motor power provides an estimate of 372 W for delivering an airflow rate of 1000 ft³/min (0.472 m³/s). While the coefficient C_1 in Equation 16 was developed from a fit of the fan/motor efficiency versus fan total pressure and the coefficient C_2 in Equation 19 was developed from a regression of the fan airflow versus fan/motor power (O'Neal et al. 2015a), all of the power calculations agreed to within about 1.5% of each other. As illustrated above, the calculation of fan motor power is very straightforward when the FPTU fan is powered by a PSC motor.

ECM Fan/Motor Analysis

For an ECM fan/motor combination, the simple approach of Equation 13 becomes problematic. The data for fan/motor total efficiency for an ECM fan motor showed dependence on both the pressure differential across the fan and fan speed. Thus, unless a modeler knows both the total pressure across the fan and the fan speed, it would be difficult to use Equation 13 directly. In addition, if the FPTU fan is set in a mode where the airflow is varied to meet the load requirements in the zone, then some building simulation programs (EnergyPlus 2013) do not allow application of a variable-speed fan motor in a series FPTU. Even for a fixed-airflow application with an ECM fan motor, O'Neal et al. (2015b) showed that the power is dependent on the amount of excess capacity the FPTU fan has relative to the design airflow requirements in the space. An ECM FPTU that was sized so that its maximum capacity just met the design airflow requirement in the space would use more power than one that had additional capacity but whose speed was lowered so the airflow would just meet the design airflow requirements. Thus, the building simulation user should know something about the maximum airflow output of an ECM FPTU relative to the size of the design requirements in the space.

Calculation of the fan power for an ECM fan operating at a fixed airflow requires several steps. First, the design airflow requirement for the space must be determined. Usually, this is calculated or estimated by a building simulation program. Second, the user must decide how large of an FPTU fan will be used in the zone. The airflow capacity of the FPTU fan Q_o divided by the design airflow requirements in the zone Q_d can be used to calculate the fraction of excess capacity x_o :

$$x_o = \frac{Q_o}{Q_d} - 1 \quad (22)$$

The power requirement $\text{POW}_{fan}(Q_d)$ for an ECM FPTU fan that has an excess capacity fraction, x_o , but operates at the design airflow Q_d can be calculated from the following (O'Neal et al. 2015b):

$$\text{POW}_{fan}(Q_d) = f_{pl} \cdot C_3 \cdot Q_d \cdot (1 + x_o) \quad (23)$$

The first term on the right hand side is the part-load power fraction and is given by a third-degree polynomial fit of part-load data from four manufacturers (O'Neal et al. 2015b):

$$f_{pl} = a_1 + a_2 \cdot \left(\frac{1}{1+x_o}\right) + a_3 \cdot \left(\frac{1}{1+x_o}\right)^2 + a_4 \cdot \left(\frac{1}{1+x_o}\right)^3 \quad (24)$$

The coefficients in Equation 24 are given in Table 2.

The constant C_3 was 0.38 W/(ft³/min) in I-P units or 805 W/(m³/s) in SI units and was based on a simple linear regression of ECM FPTU data from four manufacturers operating at maximum airflow (O'Neal et al. 2015b). Equations 22 through 24 can be used to estimate the power of an ECM FPTU operating at a fixed airflow. It is important for a modeler to estimate the amount of excess capacity of the ECM FPTU relative to the design airflow requirements of the space. Discussions with manufacturers indicate that a typical ECM FPTU field installation could be expected to have 25% or more excess capacity.

To illustrate the use of these equations, the same example design airflow requirement for the zone used for the SCR case can be used for an ECM FPTU application. While the design airflow requirement is 1000 ft³/min (0.472 m³/s), the modeler needs to decide what size ECM FPTU to install in the zone. Table 3 illustrates the decreasing power requirements in FPTU fan energy use calculated with Equations 22 through 26 as ECM FPTUs with maximum capacities larger than the design airflow of 1000 ft³/min(0.472 m³/s) are used. If a modeler uses a default size for the ECM FPTU that is equal to the design airflow requirement, then the fan power will be little different from the SCR unit used in the example above. The major savings comes from ECM units when they have higher airflow capacity than the design requirement and their airflow is reduced so their airflow just meets the design requirement of the space.

Table 2. Part-Load Power Fraction Coefficients for Equation 24 (O'Neal et al. 2015b)

Coefficients	Value
a_1	0.061715
a_2	0.093022
a_3	-0.11627
a_4	0.961538

Table 3. Effect of Excess Capacity on the Power Requirements for ECM FPTUs Operating at the Design Airflow

FPTU Maximum Capacity, ft ³ /min (m ³ /s)	Excess Capacity, <i>x</i>	Part Load Power Fraction, <i>f_{pl}</i>	Fan Power, W
1000 (0.472)	0.00	1.000	380.0
1100 (0.519)	0.10	0.773	322.9
1200 (0.566)	0.20	0.615	280.4
1300 (0.613)	0.30	0.502	248.1
1400 (0.661)	0.40	0.419	223.0
1500 (0.708)	0.50	0.357	203.5

SYSTEM LEVEL CALCULATION PROCEDURE

Figure 7 shows the basic logic or flow of the calculation procedure for estimating the energy use of a fixed-airflow series FPTU. The system operates with the zone being maintained at a certain setpoint temperature t_z and with a sensible load q_{zs} and latent load q_{zl} . These data are provided for every hour of the year. The total airflow out of the FPTU, m_{tot} , is maintained at a constant level for operations in heating, cooling, and dead band modes. When the system is in heating mode, the primary airflow is set to its minimum airflow, which may vary from 10% to 30% of the design airflow (Zhang et al. 2014). The amount of secondary airflow that is required to maintain the constant airflow out of the FPTU is then calculated, along with the supplemental heating energy from the heating coil for satisfying the zone heating load. The solution continues throughout the FPTU. In cooling mode, the primary airflow is calculated to match the sensible load in the zone. The primary airflow is limited by the minimum airflow at minimum cooling requirements and the design airflow of the FPTU at maximum cooling requirements. The secondary airflow is used in cooling mode to make up the remainder of air needed to maintain constant total airflow when the system is on. The solution then proceeds throughout the FPTU. A dead band is defined to account for the transition between heating and cooling modes. The operation in dead band is similar to the operation in heating mode, except for the heating coil. When the system is in dead band, the primary airflow is set to its minimum value, and the secondary airflow is calculated from the difference between the total airflow and the primary airflow. Unlike the operation in heating mode, however, the heating coil is off in the dead band region. Operations in heating, cooling, and dead band modes merge in solving for the return air loop of the complete VAV system. The temperature of the return air mix with outdoor air is used to determine whether or not preheating is required. If the temperature is below the primary air temperature then the preheating coil is used to heat the mixed air to the primary air temperature. The procedure then calculates the power consumption of the primary fan and proceeds to calculate the cooling energy required at the primary cooling coil. If there is another hour in the simulation then the procedure loops back to the start; otherwise the procedure is completed.

Series FPTUs can be applied in systems where the primary airflow can be as low as 45°F (7.2°C), such as that provided by some chilled-water coils, and as high as 55°F (12.8°C). The variation in primary air temperatures often requires inclusion of secondary airflow at the maximum cooling. If the primary air temperature is in the 45°F to 48°F (7.2°C to 8.9°C) range, then at maximum cooling the discharge temperature from the FPTU might be set to at least 51°F (10.6°C) to prevent condensation on the registers or drafts from overly cold air discharging into the zone. If the cooling coil produces primary air temperatures at or near 55°F (12.8°C), then no mixing of secondary air is required at maximum cooling because the discharge temperature is high enough for that condition. While EnergyPlus (2013) allows the user to input a maximum airflow that is greater than the maximum primary airflow, it provides no guidance to the user on the minimum discharge temperatures needed for the FPTU, nor does it provide a check to ensure discharge temperatures are high enough to prevent condensation at the registers.

The total airflow rate m_{tot} from a fixed-airflow series FPTU is determined by using the zone design load q_{z_design} and the difference between the zone setpoint temperature t_z and the minimum discharge temperature t_{out} at design conditions:

$$m_{tot} = \frac{q_{z_design}}{c_p \cdot (t_z - t_{out})} \quad (25)$$

The selection of the minimum discharge temperature is dependent on the temperature of the air provided in the primary airstream. For example, in systems with a primary air temperature at or close to 55°F (12.8°C), the minimum discharge temperature at the design condition is equal to the primary air temperature if the heating effect caused by the FPTU fan is not considered. With the heating effect, the difference between the FPTU outlet discharge temperature t_{out} and the mixed air temperature t_{mix} in Figure 2 should be less than 1°F (0.6°C). If a primary air temperature in the range of 45°F to 48°F (7.2°C to 8.9°C) is used, the minimum discharge temperature from the FPTU needs to be at a value that ensures there is no condensation on the supply registers and grilles. The minimum discharge temperature at the design cooling

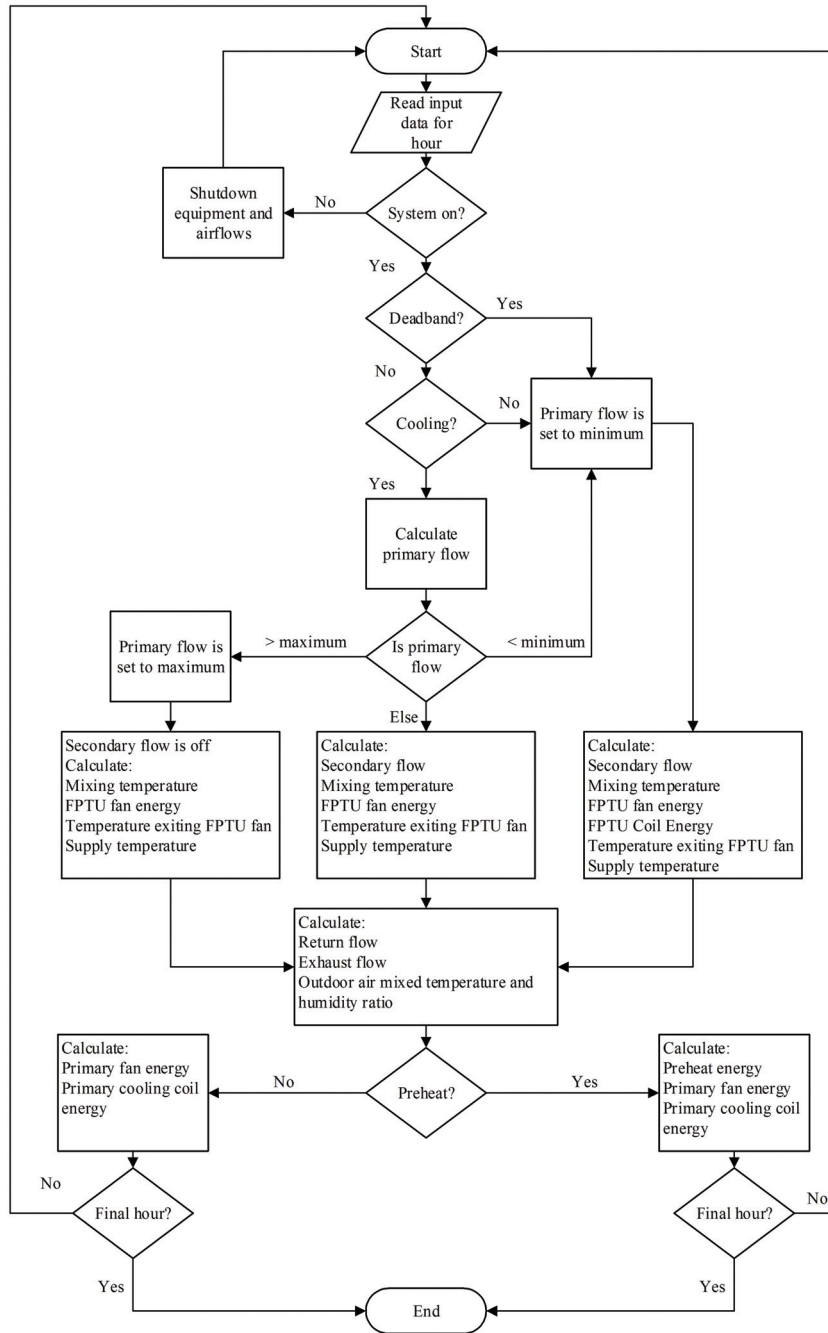


Figure 7 Series fixed airflow FPTU controller routine.

condition should be equal to or greater than 51°F (10.6°C) when a primary air temperature lower than 48°F (8.9°C) is used in a VAV system with series FPTUs.

If desired, the volumetric flow rate (often in ft³/min or m³/s) can be determined from the air mass flow rate and density ρ_{air} :

$$Q_{tot} = \frac{m_{tot}}{\rho_{air}} \quad (26)$$

It should be noted that once the total airflow rate is sized for a fixed-airflow series FPTU, the airflow remains constant and independent of the zone thermal load.

For demonstration purposes, the performance of a series FPTU was estimated by using the mass and energy balance approach discussed earlier and the empirical curves for ECM fan/motor power consumption developed by O’Neal et al. (2015b). As a first step, input data were created, including zone sensible loads, zone setpoint temperature, and primary air temperature. To demonstrate the operation in all modes of

heating, cooling, and dead band, the zone sensible load was allowed to range from $-40,000$ to $40,000$ Btu/h (-11.73 to 11.73 kW) by using an arbitrary incremental change of 479 Btu/h (0.14 kW), with negative values indicating heating loads and positive values indicating cooling loads. At each zone sensible load, a constant zone setpoint temperature of 78°F (25.6°C) was maintained. Also, two primary air temperatures of 55°F and 45°F (12.8°C and 7.2°C) were used for the series FPTU performance prediction. The higher primary air temperature of 55°F (12.8°C) represents a VAV system that uses a direct-expansion (DX) coil as the primary cooling coil, while the lower primary air temperature of 45°F (7.2°C) would represent a VAV system that uses a chilled-water coil as the primary cooling coil. In addition, a dead band ranging from -4000 to 4000 Btu/h was arbitrarily defined and used to help illustrate series FPTU operation in the dead band region. If the zone sensible load falls into the dead band range, the series FPTU was then considered to be operating in the dead band mode. It should be noted that the above input parameters, namely zone sensible loads, zone setpoint temperature, primary air temperature, and dead band range, are user-defined parameters and can be modified for different applications.

The airflow, discharge temperature, and supplemental heating energy for a fixed-airflow series FPTU were plotted against the zone sensible load and are shown in Figures 8 to 10, respectively. Figure 8 shows the primary and secondary air variations with the zone sensible load for cases with 55°F and 45°F (12.8°C and 7.2°C) primary air. In both cases, the primary airflow was allowed to decrease to a minimum of 20% of the design primary airflow rate when in the heating and dead band modes; secondary air makes up the remainder of the total airflow rate. While in cooling mode, the primary airflow was increased with the increasing zone sensible cooling load until the design airflow rate was reached for the 55°F (12.8°C) primary air case. For this case, the secondary airflow was decreased based on mass and energy balances until reaching zero at maximum cooling because constant total airflow was maintained over the entire range of the zone sensible cooling load.

Lowering the primary air temperature to 45°F (7.2°C) resulted in lower total airflow rates in both primary and secondary air for both heating and cooling. Rather than continuously increasing the primary airflow to the design airflow rate at maximum cooling, the primary air at 45°F (7.2°C) required mixing of secondary air at maximum cooling to maintain high enough air discharge temperatures from the FPTU to avoid condensate on the air registers when the primary air temperatures are in the lower temperature range for chilled-water coils—typically from 45°F to 48°F (7.2°C to 8.9°C). For the example of 45°F (7.2°C) primary air in Figures 8 to 10, the minimum discharge temperature was assumed to be 51°F (10.6°C), which was obtained by blending enough secondary air with primary air to achieve the mixed temperature.

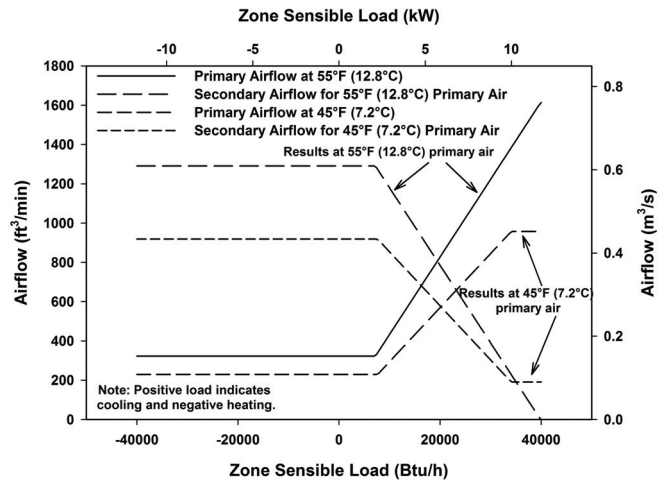


Figure 8 Primary and secondary airflows for a fixed-airflow series FPTU.

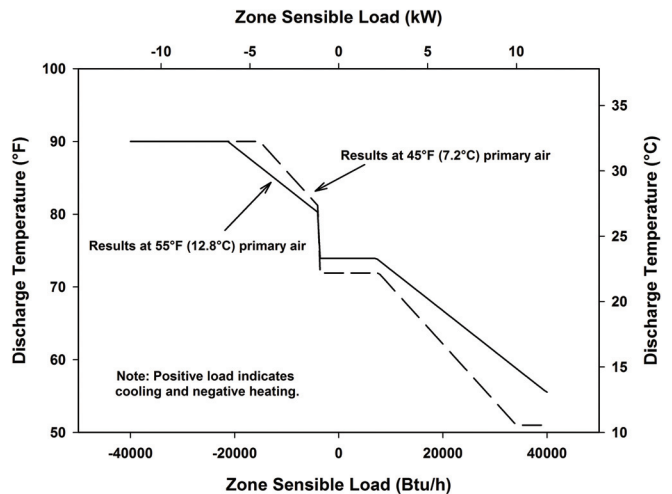


Figure 9 Discharge temperature for a fixed-airflow series.

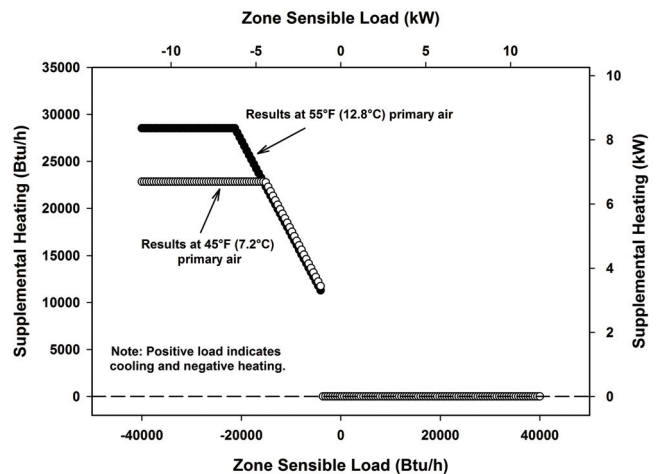


Figure 10 Supplemental heating energy for a fixed-airflow series FPTU.

Figure 9 shows the discharge temperature resulting from using 55°F and 45°F (12.8°C and 7.2°C) primary air over the entire range of zone sensible load. At the high end of the heating load, the discharge temperature was limited to 90°F (32.2°C) because a higher discharge temperature could increase the zone temperature stratification (Hydeman and Eubanks 2014). As the heating load decreased, the discharge temperature was decreased proportionally. A sharp temperature drop occurred at the lower limit of the dead band due to switching off the heating coil. The discharge temperature was maintained constant in the dead band and then decreased as zone cooling load increased. Figure 9 shows that at any given zone sensible load, the discharge temperature resulting from using 45°F (7.2°C) primary air was higher in heating mode and lower in cooling mode compared with a discharge temperature with 55°F (12.8°C) primary air. The use of lower primary air temperature resulted in a lower design airflow rate, as was shown earlier in Figure 8. To deliver the same amount of heating or cooling energy to the zone with a lower airflow rate, the discharge temperature has to be increased in heating mode and decreased in cooling mode with the zone setpoint temperature being a constant.

Figure 10 shows the supplemental heating energy use for 55°F and 45°F (12.8°C and 7.2°C) primary air. The heating coil only operates in heating mode and remains off in dead band and cooling modes. At the high end of the heating load, the supplemental heating energy was constant because the maximum discharge temperature of 90°F was reached. The system using 55°F (12.8°C) primary air provided a higher supplemental heating capacity than the system using 45°F (7.2°C) primary air due to a higher airflow rate. As the heating load decreased, the supplemental heating energy continuously decreased until reaching the lower limit of the dead band.

The logic for the FPTU performance calculations depends on which mode of operation it is in and what primary air temperature is provided to the FPTU. There are four distinct modes of operation: off, heating, cooling, and dead band. The logic for each is described in the following list.

1. The entire system is not operating. For this mode the primary and secondary airflows, the fan, and the central air handler are not running. Temperatures throughout the system are set to the zone setpoint temperature.
2. The system is operating in heating mode.
 - a. The discharge temperature that is required to satisfy the zone load is calculated based on the energy balance performed on the zone using Equation 27:

$$t_{out} = t_z - \frac{q_{zs}}{m_{tot}c_p} \quad (27)$$

If the calculated discharge temperature is greater than 90°F (32.2°C), then the discharge temperature is set to 90°F (32.2°C).

- b. The primary airflow is set to the minimum ventilation level (20% of design):

$$m_{pri} = m_{min} \quad (28)$$

- c. The secondary airflow is calculated from the mass balance performed on the mixer:

$$m_{sec} = m_{tot} - m_{pri} \quad (29)$$

- d. The temperature of the air leaving the mixer is calculated based on the energy balance performed on the mixer. Equation 12 is rearranged to solve for T_{mix} :

$$t_{mix} = \frac{m_{pri}c_p t_{pri} + m_{sec}c_p t_{sec}}{m_{tot}c_p} \quad (30)$$

- e. The temperature of the air leaving the fan is calculated based on the energy balance performed on the fan as shown in Equation 11, which can be rearranged into Equation 31:

$$t_{f, out} = \frac{POW_{fan}}{m_{tot}c_p} + t_{mix} \quad (31)$$

- f. The energy input into the heating coil is calculated from the energy balance performed on the heating coil as shown in Equation 32:

$$q_{coil} = m_{tot}c_p(t_{out} - t_{f, out}) \quad (32)$$

3. The system is operating in cooling mode. The operation in cooling mode is similar to the operation in heating mode except for the calculation of primary airflow m_{pri} . As a first step, the discharge temperature that is required to satisfy the zone load is calculated according to Equation 27. Then, the primary airflow m_{pri} in cooling mode is determined by substituting secondary airflow m_{sec} from Equation 3 into Equation 5 and rearranging to solve for m_{pri} , as shown in Equation 33. Note that because the system is in cooling mode, the energy use of the heating coil is zero ($q_{coil} = 0$):

$$m_{pri} = m_{tot} \frac{t_{out} - t_{sec}}{t_{pri} - t_{sec}} - \frac{POW_{fan}}{c_p(t_{pri} - t_{sec})} \quad (33)$$

Once the primary airflow m_{pri} is quantified, the logic for the performance calculation in cooling mode is the same as the steps from (c) to (e) in the heating mode.

It is important to recognize that the calculated primary airflow m_{pri} is constrained between its minimum, which typically ranges from 10% to 30% of the design primary airflow and its maximum (or design) amount. The total airflow from the FPTU will depend on the temperature of the primary air provided to the FPTU. For the case of higher primary air temperatures, such as 55°F

(12.8°C), the maximum amount of primary air can be 100% of the design airflow m_{tot} . In this case, the secondary air is set to zero at the design cooling load in the zone as shown in Figure 8. If the calculation of primary airflow results in a value smaller than the minimum or larger than the maximum, the logic needs to reset the primary airflow to the minimum or maximum accordingly and then proceed with the calculations in steps from (c) to (e) in the heating mode.

When lower primary air temperatures are provided to the FPTU, then secondary air needs to be blended in with the primary air to provide a high enough outlet (or discharge) temperatures to eliminate condensation on registers. The amount of secondary air needed will depend on the temperature and amount of the primary air. The desired discharge air temperature will allow for calculation of the total amount of airflow m_{tot} from the FPTU using Equation 33. The amount of secondary air can then be calculated using the mass balance from the mixing equation of Equation 3. The minimum limit on the primary air remains the same as with the case with a higher primary air temperatures.

4. System is operating in dead band mode. If the zone sensible load is within the prescribed dead band range, then the system is in dead band operation. For Figures 8 through 10, the dead band was assumed to vary from -4000 to 4000 Btu/h (-1.2 to 1.2 kW). In the dead band mode, the logic for the performance calculation is similar to the operation in heating mode except for the heating coil being switched off. Unlike the operations in heating and cooling modes where the purpose of the FPTU was to satisfy the zone load by maintaining a specific discharge temperature, the discharge temperature in dead band is not controlled and is a direct result of mixing the minimum primary air and maximum secondary air. In a simulation program, the dead band is often specified by the user. Thus, no method of calculating the dead band is provided here.

SUMMARY AND CONCLUSIONS

This paper has provided the basic equations needed to characterize a fixed-airflow series FPTU using a mass and energy balance approach. The approach follows closely that used in EnergyPlus (2013) for series FPTUs. A step-by-step process of how the basic equations should be used for each FPTU mode of operation was provided.

The current model for series FPTUs in EnergyPlus (2013) includes only constant airflow fans and bases fan power calculations on fan pressure and efficiency inputs typically not provided by the manufacturers of these units. A simplified approach was used to allow estimation of fan power based on correlations developed in earlier studies for both constant airflow fans (O'Neal et al. 2015a, 2015b). The constant airflow fans included both PSC motors controlled by SCRs and ECMs. The ECM model allows the user to include FPTUs

with excess capacity relative to the design load on the zone, which would provide for reduced energy and power use by the FPTU fan.

The methodology developed in this paper can be implemented into building simulation models that use an energy and mass balance approach. Given the widespread use of ECMs in series FPTUs, it is vital that future versions of building simulation models include variable-airflow-series FPTUs to allow energy professionals an opportunity to accurately characterize the energy use of FPTU technologies that are actually installed in buildings. The authors are currently working on a variable-airflow-series FPTU model that would include the variable-airflow ECM model developed by O'Neal (2015).

REFERENCES

- ASHRAE. 2012. Chapter 20, Room air distribution equipment, *ASHRAE Handbook—HVAC Systems and Equipment*. Atlanta: ASHRAE.
- Davis, M., J. Bryant, and D.L. O'Neal. 2012. Modeling the performance of ECM and SCR series fan-powered terminal units in single-duct VAV systems. *ASHRAE Transactions* 118(1).
- Edmondson, J., D.L. O'Neal, J.A. Bryant, and M.A. Davis. 2011. Performance of series fan-powered terminal units with electronically commutated motors. *ASHRAE Transactions* 117(2).
- EnergyPlus. 2013. Air system distribution terminals. In *EnergyPlus™ documentation: Engineering reference: The reference to EnergyPlus calculations*. Berkeley: Lawrence Berkeley National Laboratory.
- Furr, J., D. O'Neal, M.A. Davis, J.A. Bryant, and A. Cramlet. 2008. Performance of VAV fan-powered terminal units: Experimental results and models for series units. *ASHRAE Transactions* 114(1).
- Hydeman, M. and B. Eubanks. 2014. *Advanced control sequences for HVAC Systems—Phase I air distribution and terminal systems*. ASHRAE Research Project Report RP-1455. Atlanta: ASHRAE.
- Int-Hout, D. 2015. ECM Motors in fan powered terminal units. https://www.krueger-hvac.com/files/white%20papers/white_paper_ecm.pdf
- Knebel, D.E., 1983. *Simplified energy analysis using the modified bin method*. Atlanta: ASHRAE.
- O'Neal, D.L., D. Ingram, and C.L. Reid. 2015a. Modeling fan powered terminal unit fan/motor combinations controlled by silicon-controlled rectifiers. *ASHRAE Transactions* 121(2).
- O'Neal, D.L., D. Ingram, and C.L. Reid. 2015b. Simplified model of the fan/motor performance of fan powered terminal units that utilize electronically commutated motors. *ASHRAE Transactions* 121(2).
- O'Neal, D.L. 2015. Development of models to simulate the part-load performance of oversized ECM fan-powered terminal units. *ASHRAE Transactions* 121(2).

Roman, A. and A. Heiligenstein. 2002. *SCR power theory training manual*. PK501-1. LaVergne, TN: Chromalox Inc.

Zhang, H., T. Hoyt, S. Kaam, J. Goins, F. Bauman, Y. Zhai, T. Webster, B. West, G. Paliaga, J. Stein, R. Seidl, J. Tullym B. Rimmer, and J. Torftum. 2014. *Thermal and air quality acceptability in buildings that reduce energy by reducing minimum airflow from overhead diffusers*. ASHRAE Research Project Report RP-1515. Atlanta: ASHRAE.

DISCUSSION

Matthew Boss, Sales Manager, L.R. Gorrell Co., Raleigh, NC: Confirm that the power usage of PSC motors was essentially constant over range of airflow at 0.372 W/cfm.

Dennis L. O'Neal: We looked at PSC motors from three manufacturers in the *ASHRAE Transactions* paper "Modeling Fan-Powered Terminal Unit Fan/Motor Combinations Controlled by Silicon Controlled Rectifiers" (AT-15-028). For voltages above about 160 V, the PSC fan motor power usage was relatively flat at an average value of 0.372 W/cfm for units

ranging from 1/8 to 1 hp. There was scatter in the data, which could be expected because of the different designs from different manufacturers.

Louis Starr, Engineer, Northwest Energy Efficiency Alliance, Portland, OR: 1) Does the modeling you did for PSC motors include part-load operation of motors? 2) Does oversizing fan-powered boxes result in lack of control of airflow at low airflows?

O'Neal: 1) The part-load modeling for this paper only included ECMs. The PSC motors we evaluated had an average 0.372 W/cfm, which was relatively constant for SCR voltages down to about 160 V.

2) The scope of this study did not look at "lack of control" at low airflows for the ECMs. However, what I remember from our discussions with the manufacturers who provided data to us was that they typically didn't like to see the speed of the ECMs go below about 20% of the maximum setting on the controller. I would expect an engineer to follow the manufacturer's recommendation on minimum speed (or airflow) from the fan/motor combination, which would limit how much oversizing could be done with an ECM FPTU.

ST-16-026

Using a Mass and Energy Balance Approach to Model the Performance of Parallel Fan-Powered Terminal Units with Fixed-Airflow Fans

Peng Yin, PhD
Student Member, ASHRAE

Carl L. Reid
Student Member, ASHRAE

Dennis L. O'Neal, PhD, PE
Fellow ASHRAE

ABSTRACT

A mass and energy balance approach was used to characterize the performance of parallel fan-powered terminal units (FPTUs) with fixed airflow for applications in building simulation programs. The approach included developing relevant mass and energy balance equations for each component—*heating coil, fan/motor combination, and mixer*—in a parallel fan-powered terminal unit. Two locations of the heating coil were considered. One location, designated as the traditional configuration, was at the discharge of the unit. The second location, designated as the alternative configuration, was at the secondary air inlet. Fixed-airflow parallel fan-powered terminal units use fan motors that include either permanent split capacitor motors controlled by silicon controlled rectifiers or electronically commutated motors. This paper demonstrates how to incorporate fan/motor combination performance models for both permanent split capacitor and electronically commutated motors into the mass and energy balance approach. These fan models were developed from performance data provided by multiple FPTU manufacturers. The fan/motor performance data included an FPTU, a fan airflow range from 250 to 3500 ft³/min (0.118 to 1.65 m³/s), and a motor size range from 0.333 to 1 hp (249 to 746 W). Leakage was included in the models. The system was implemented in Engineering Equation Solver (EES) and results provided to illustrate the effect of leakage in both cooling and heating operations.

INTRODUCTION

The single-duct variable-air-volume (VAV) system is a common heating, ventilating, and air-conditioning (HVAC) system used in commercial buildings (ASHRAE 2012). VAV systems vary the amount of air delivered to a conditioned zone

to ensure a desired comfort level. The conditioned air is supplied to each zone by a single terminal unit based on the sensible load as sensed by a thermostat in the zone.

If a terminal unit includes a fan, it is called a *fan-powered terminal unit* (FPTU) or *powered induction unit* (PIU). FPTUs provide conditioned air to a zone that may include a mixture of the primary air with induced recirculated (secondary) air. The FPTU may provide supplemental heating to the air depending on whether the FPTU is in heating or cooling mode. The supplemental heating is typically provided with either a hot-water coil (heat exchanger) or electric resistance (ASHRAE 2012).

If the FPTU fan and the primary air fan are in parallel, as shown in Figure 1, then the FPTU is called a *parallel FPTU*. The fan is used to induce secondary air from the plenum space into the FPTU. For a parallel system, the fan is off during cooling operations. Primary air can be supplied to the zone without the fan being used. When the fan is off, the back draft damper closes to prevent air from escaping through the secondary air inlet. The primary air damper is located at the FPTU inlet and is used to

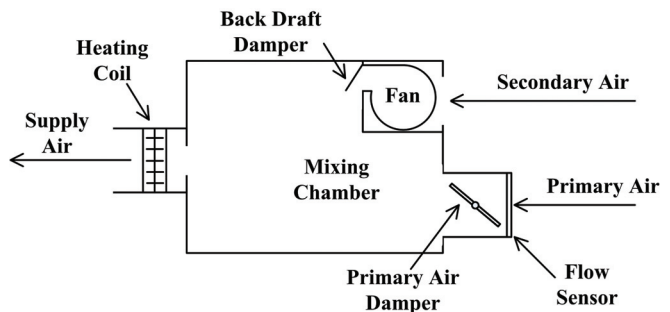


Figure 1 Parallel configuration for FPTU.

Peng Yin is an assistant professor in the Department of Mechanical Engineering, University of Louisiana at Lafayette, Lafayette, LA. Carl L. Reid is a staff engineer at BEE, Austin, TX. Dennis L. O'Neal is dean of Engineering and Computer Science, Baylor University, Waco, TX.

adjust the supply air entering the FPTU. When the fan is on, it adds recirculated (secondary) air to help control the temperature of the air supplied to the zone. An electric or hot-water heating coil can be used to provide supplemental heat to the airstream. The heating coil can be located at the discharge of the FPTU as shown in Figure 1 for a traditional configuration. The heating coil can also be located before the FPTU fan at the secondary air inlet.

Both permanent-split capacitor (PSC) motors controlled by silicon controlled rectifiers (SCRs) and electronically commutated motors (ECMs) have been applied in parallel FPTUs. PSC motors are only used in those applications where the airflow from the FPTU fan is expected to be constant. The SCR chops the voltage supplied to the PSC motor to lower the speed of the motor and allows an installer to match the airflow from the FPTU to the required airflow requirements of the zone. ECM motors can be used for either fixed or variable airflow. An ECM converts alternating current (AC) to direct current (DC) and allows for control of the motor speed.

Modeling work by Davis et al. (2012) shows that parallel FPTUs with fixed-airflow ECM fan motors performed similarly to parallel FPTUs with SCR-controlled PSC fan motors in five different cities: Houston, Phoenix, Chicago, New York, and San Francisco. Davis et al. were also able to show that air leaking from the FPTU cabinet could have a significant impact on the annual energy use of the HVAC system. Davis et al. (2012) based their FPTU models on the power, pressure, and airflow data collected and analyzed by Furr et al. (2008) and Edmondson et al. (2011). While the analysis by Davis et al. (2012) was useful in estimating savings of ECM FPTUs, it required detailed knowledge of the pressures upstream and downstream of the FPTU. This approach was not directly compatible with the mass and energy balance (MEB) modeling approach often used in building energy simulation programs such as EnergyPlus (2013). Given the difficulties of using the modeling work of Davis et al. (2012) and the data from Furr et al. (2008) and Edmondson et al. (2012), O'Neal

et al. (2015a, 2015b) and O'Neal (2015) analyzed performance data on both PSC/SCR and ECM fan/motor data from four FPTU manufacturers and developed performance models that could be used with an MEB modeling approach.

The purpose of this paper was to combine the PSC/SCR and ECM models developed by O'Neal et al. (2015a, 2015b) with a mass and energy balance modeling approach to develop parallel FPTU models that can be directly implemented in building simulation programs such as EnergyPlus (2013). The FPTU models included leakage and configurations for the heating coil at either the discharge of the FPTU or at the inlet to the secondary air. The authors are also working on a model on variable-airflow parallel FPTUs to complement this paper.

MASS AND ENERGY BALANCE APPROACH

Mass and energy balances have been a common approach used to model HVAC systems in building simulation programs (Knebel 1983). The MEB approach treats each subsystem in a HVAC system, such as an FPTU, as a set of equations that describe the mass and energy flows into and out of each subsystem. A parallel FPTU can then be decomposed into its major components: mixer, fan/motor, and heating coil. Figure 2 shows a control volume around a traditional parallel FPTU. An analysis can be performed on each component in the FPTU to estimate overall airflows (or mass flows) into and out of the FPTU as well as the energy used by the FPTU fan/motor for each time step of a simulation. The large dashed box in the right two thirds of the figure is the control volume for the FPTU. Each FPTU component can be treated as a smaller control volume with mass and energy inputs and outputs.

An alternate configuration of the traditional parallel FPTU moves the heating coil to the secondary air inlet as shown in Figure 3. One advantage this configuration provides over the traditional configuration of Figure 2 is that the heating coil is outside the primary airstream where it would add to the pressure drop of the primary airstream whenever the primary

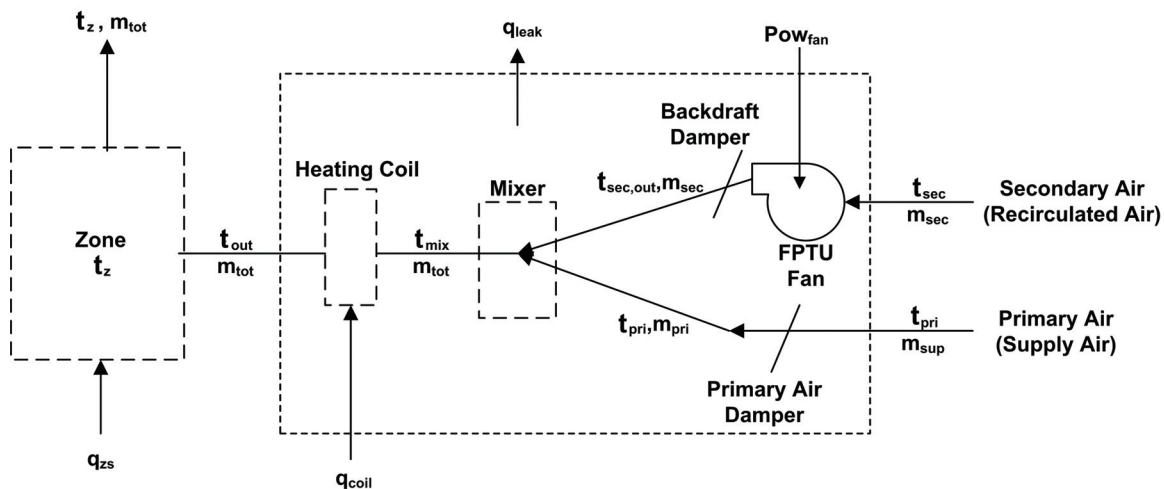


Figure 2 Traditional parallel FPTU with heating coil located after the mixing of the primary and secondary airflows.

air handler is operating. This pressure drop would have to be overcome by an increase in static pressure of the central air-handling unit. One potential disadvantage of the alternative configuration is that the fan motor is located downstream of the heating coil and would be subjected to higher air temperatures than in the traditional configuration in the heating mode.

Parallel FPTU Model

For the control volume around the entire FPTU in Figures 2 or 3, energy is input to the FPTU via electrical energy to the fan, heat energy to the heating coil, and energy associated with the supply and secondary airstreams. The only mass and energy leaving the FPTU is with the airstream at the discharge of the FPTU and leakage from the housing. Unlike series FPTUs that operate at a negative pressure with respect to the plenum, parallel FPTUs operate at a positive pressure. The primary air provided to the parallel FPTU has already been conditioned by the central cooling coil. Thus, air leaking from the parallel FPTU operating in the cooling mode is colder than the return air in the plenum and will reduce the temperature of the plenum air. Edmondson et al. (2011) found that parallel units can leak conditioned air from the housing through seams, penetrations, and the back draft damper.

The FPTU consists of three major components: mixer, fan, and heating coil. A mass and energy balance must be performed on each of the components to estimate temperatures and airflows to determine the performance of the FPTU.

There are some basic assumptions we used in developing the MEB models of parallel FPTUs. First, the system in either Figure 2 or 3 is assumed to operate at quasi-steady state during each time step. During a particular time step, the temperature and airflows remain constant and are averaged over the time step. Given that the typical time step is an hour, this type of analysis cannot capture rapid transients occurring at smaller time steps. Another assumption in the analysis below is that the thermophysical properties are constant. This allows the specific heat and density of the air to be treated as constants.

With the small temperature differences in the airstreams of an FPTU, constant specific heats and densities should introduce less than a 1% error in the analysis. Third, the energy input to the fan motor is assumed to be completely converted into the heat energy in the airstream. For a parallel FPTU, the fan/motor combination is located in the secondary airstream and is only on during heating operation. SCR fan motors typically have the controller outside of the airstream where the fan and motor are located. However, based on calculations of power consumption of SCR controllers, the controller should consume less than 1% of the total energy of the fan motor if the controllers use the typical 1.5 W/amp of supplied current to the fan motor (Roman and Heiligenstein 2002). ECM controllers are typically located in the same airstream as the fan/motor to ensure cooling of the electronic components in the controller. Thus, assuming all of the energy of the fan and motor being dissipated in the secondary airstream should introduce minimal error into the analysis. Fourth, the FPTU operates with a minimum amount of primary air to ensure enough fresh air into the zone. When the zone calls for heating or a very low amount of cooling, there will always be a minimum amount of primary air provided by the FPTU to the zone.

The mass and energy balances for a general control volume at steady state are given by Equations 1 and 2, respectively.

The mass balance is as follows:

$$\{\text{Airflow out of FPTU}\} = \{\text{Airflow into FPTU}\} \quad (1)$$

The energy balance is as follows:

$$\{\text{Energy out of FPTU}\} = \{\text{Energy into FPTU}\} \quad (2)$$

For the control volumes shown in Figures 2 or 3, the mass entering the system include the primary (supply) air m_{pri} from the central air handler and the secondary airstream m_{sec} . The mass exiting the control volume is total airflow m_{tot} and leakage m_{leak} . Applying Equation 1 to the control volume yields the mass balance shown below.

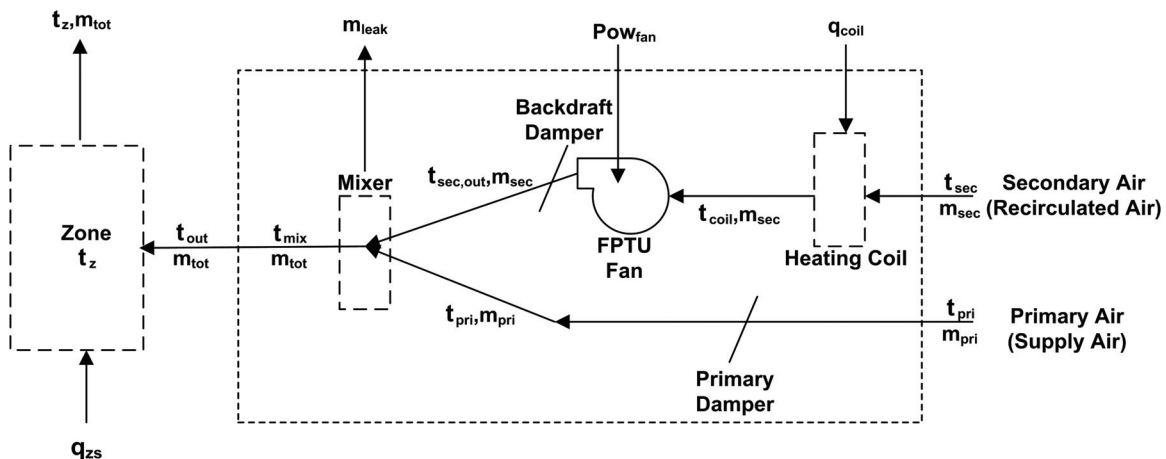


Figure 3 Parallel FPTU in alternate configuration where the heating coil is located in the secondary airstream.

$$m_{tot} + m_{leak} = m_{pri} + m_{sec} \quad (3)$$

Leakage is included in the modeling of parallel units because the housing is at a positive pressure with respect to the plenum air pressure. Characterizing leakage and its impact on parallel FPTUs is discussed later in this paper. The energy transfer into the control volume includes the energy provided by the supply and secondary airstreams, energy input into the heating coil, the energy leaving by leakage, and the power input into the fan. When these are substituted into Equation 2, it yields the following:

$$m_{tot}h_{out} + m_{leak}h_{leak} = q_{coil} + POW_{fan} + m_{pri}h_{pri} + m_{sec}h_{sec} \quad (4)$$

Equations 3 and 4 provide the basic equations that describe the overall mass and energy balance for the parallel FPTU. The unknowns in these equations vary depending on the mode of operation (heating, cooling, or deadband) of the FPTU. Solving for the unknowns in these equations requires applying mass and energy balances to each of the components in the FPTU. The process typically starts from the left at the FPTU discharge to the zone and moves to the right to the primary and secondary air inlets.

With a parallel FPTU, the fan is on when the FPTU is in the heating mode. During the heating mode, the fan operates at a fixed speed if the fan motor is a PSC, or can operate in fixed or variable speed if the fan motor is an ECM. The analysis provided in this paper is focused on fixed-airflow fans in the secondary airstream. The authors are developing a separate model for variable-airflow fans in parallel FPTUs.

For cooling operation, the FPTU fan is off and the primary air damper is used to vary the amount of supply air that flows through the FPTU. The term m_{tot} , shown in Equations 3 and 4, is the total airflow delivered to the space. In heating operations, the total airflow is the sum of the supply and secondary airflows minus leakage. In cooling operations, the total airflow is just the primary airflow minus the leakage. The total airflow is a fixed value in heating mode if the secondary airflow is fixed. In cooling mode, the total airflow is determined from the load in the zone and equals the primary airflow minus the leakage airflow in either Figure 2 or 3. Additional primary air must be provided that is equal to the amount of air leaking out of the FPTU cabinet to ensure the proper amount of discharge air m_{tot} is delivered to the zone to satisfy the cooling load. The primary airflow in the FPTU should not drop below a certain percentage (typically 20% to 30%) of the airflow needed at the design cooling load (ASHRAE 2013). This minimum amount of primary air is used to maintain fresh air requirements in the zone. A recent study found that minimum primary airflows as low as 10% might still provide acceptable indoor air quality in some applications in California (Zhang et al. 2014).

The terms in the left hand side of Equation 4 represent the energy leaving the FPTU in the airstream either carried by the discharge airflow or by the leakage airflow. The energy input

into the FPTU includes heat energy input in the heating coil, power input to the fan (which is assumed to be converted into heat energy in the airstream), and energy being carried into the FPTU by both the supply and secondary airstreams. If the temperature differences between the entering and exiting airstreams are small enough, then the air properties can be assumed to be constant and the enthalpies h can be rewritten as the product of specific heat c_p and temperature t . Equation 4 can be rewritten as shown below. Because the assumption of constant density is used throughout the project, all airflow rates are considered to be mass flows unless otherwise stated.

$$m_{tot}c_p t_{out} + m_{leak}c_p t_{mix} = q_{coil} + POW_{fan} + m_{pri}c_p t_{pri} + m_{sec}c_p t_{sec} \quad (5)$$

Both sides can be divided by the specific heat, c_p

$$m_{tot}t_{out} + m_{leak}t_{mix} = m_{sec}t_{sec} + m_{pri}t_{pri} + \frac{POW_{fan}}{c_p} + \frac{q_{coil}}{c_p} \quad (6)$$

Comparing the Energy Balance of the Alternate Configuration

In the alternate FPTU configuration in Figure 3, the heating coil location changes from the FPTU outlet to the secondary airstream inlet. A mass balance on the control volume in Figure 3 yields the same result as was derived for the traditional configuration as shown in Equation 3. An energy balance on the control volume also yields the same result as the traditional configuration as shown in Equation 6. From a simple mass and energy balance on the FPTU alone, the change in the location of the heating coil provides no change in the basic equations.

There are some differences between the two configurations. First, from a larger system standpoint, moving the heating coil out of the primary airstream will reduce the static pressure required by the central air handler to provide the required supply airflow to the FPTU. The additional pressure drop across the heating coil will depend on the characteristics of the coil (number of rows of the coil, airflow, fin density, etc.) and the amount of airflow through the coil. This pressure drop will require additional work by the central air handler and must be included in a simulation to properly handle the traditional configuration. A second difference is the temperature of the air leaking into the plenum. Because the supplemental heating for the alternative configuration is located upstream of any leakage locations in the FPTU, heated air can leak from the FPTU into the plenum. The leakage of this heated air will also reduce the overall heating provided to the zone once the heating coil discharge temperature reaches its maximum value. For the alternative configuration, the pressure drop of the heating coil in the secondary airstream must be included in heating operations when the FPTU fan is on.

Zone Analysis

Analysis of an FPTU often starts at the zone. Typically, the zone load is known and either the discharge temperature t_{out} or the total airflow m_{tot} needs to be calculated. Either requires an energy and mass balance on the zone. The zone control volume is represented by the control volume on the far left side of either Figures 2 or 3. The control volume is identical in both figures. An energy and mass balance on the zone yields the following:

$$q_{zs} = m_{tot}c_p(t_z - t_{out}) \quad (7)$$

In cooling mode, the outlet temperature is known and the total airflow needs to be calculated. There is no secondary air and all air is provided by the primary airstream at the primary air temperature. Thus, t_{out} is equal to t_{pri} in Figures 2 or 3. Equation 7 can be rewritten to calculate the required airflow to satisfy the zone load:

$$m_{tot} = \frac{q_{zs}}{c_p(t_z - t_{out})} \quad (8)$$

In heating mode, the airflow is fixed because the airflow is constant from the fan in the secondary airstream and the primary air is fixed at its minimum value. For this case, the outlet air temperature can be calculated from Equation 9:

$$t_{out} = \frac{q_{zs}}{m_{tot}c_p} + t_z \quad (9)$$

Heating Coil

An energy balance can be applied to the heating coil in the traditional location in Figure 2. The energy entering the coil is the energy input q_{coil} , either from electric resistance or hot water, and the energy from the air entering the coil from the discharge of the FPTU fan. The energy exiting the coil is carried by the air leaving the coil and is used to condition the zone. The variable of interest is the heating energy input. An energy balance yields

$$q_{coil} = m_{tot}c_p(t_{out} - t_{mix}) \quad (10)$$

The analysis for the heating coil for the alternative configuration is very similar to that for the traditional configuration. However, the airflow in and out of the heating coil is just the secondary airflow for the alternative configuration and not the total airflow. The temperature into the coil is the secondary air temperature t_{sec} and the outlet temperature from the coil is t_{coil} (see Figure 3). The coil energy balance yields:

$$q_{coil} = m_{sec}c_p(t_{coil} - t_{sec}) \quad (11)$$

These two equations represent the energy balance on the heating coil for either the traditional or alternate configurations.

Fan

The FPTU fan is located in the same place for both the traditional and alternative configurations. However, because of the presence of the heating coil in the airstream before the fan in the alternate configuration, the terminology will be slightly different. The amount of electrical energy input to the fan for a given time step is represented by POW_{fan} . In addition, energy is being carried into the fan from the secondary airstream. For the traditional configuration (Figure 2), the airstream temperature of the air at the inlet of the fan is t_{sec} . For the alternative configuration, the airstream temperature of the air at the fan inlet is given by t_{coil} , which is the outlet temperature of the heating coil. The energy exiting the fan is carried by the air leaving the fan and entering the mixer. The exiting temperature is given by $t_{sec, out}$ for both configurations (Figures 2 and 3). It is assumed that all of the power input to the fan is converted into heat energy. This assumption would apply to both PSC motors controlled by SCR controllers and ECM motors. For constant properties, the temperature increase of the air due to the fan can be evaluated with a mass and energy balance. Performing an energy balance on the fan and solving for the power input yields the following for the traditional configuration:

$$POW_{fan} = m_{sec}c_p(t_{sec, out} - t_{sec}) \quad (12)$$

For the alternative configuration, the energy input to the fan is given by:

$$POW_{fan} = m_{sec}c_p(t_{sec, out} - t_{coil}) \quad (13)$$

Mixer

An important variable needed in the modeling of the FPTU is the mixing temperature, t_{mix} , of the secondary and primary airflows. To solve for the mixing temperature, a mass and energy balance can be performed on the mixer shown in Figure 4. Mass flows into the mixer include the primary and secondary airflows. If the leakage is assumed to occur in the

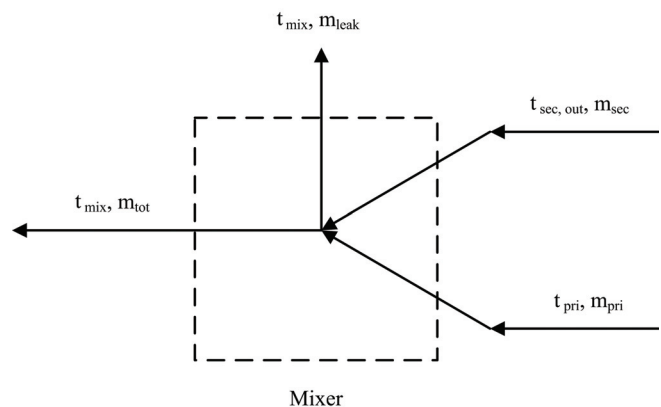


Figure 4 Mixer in a parallel FPTU.

region of the mixing in the main chamber of the FPTU, then the total airflow leaving the FPTU is just the sum of the total airflow in minus the leakage out of the FPTU.

$$m_{tot} = m_{pri} + m_{sec} - m_{leak} \quad (14)$$

The relationship between the primary airflow and the supply airflow from the air handler depends on the amount of leakage in the FPTU, which is discussed in the next section, "Leakage." The energy entering the mixer is from the primary and secondary airstreams when in heating mode. In cooling operations, there is no secondary airflow; therefore, the mixing temperature is equal to the primary air temperature. The energy exits the mixer in the total airstream and moves to the heating coil. The mixer is assumed to perform adiabatic mixing; no heat energy is lost to the surroundings. Performing an energy balance on the mixer to solve for the energy in the airstream leaving the mixer yields the following:

$$m_{tot} c_p t_{mix} = m_{pri} c_p t_{pri} + m_{sec} c_p t_{sec, out} - m_{leak} c_p t_{mix} \quad (15)$$

Leakage from the FPTU is assumed to occur at the mixed temperature of the primary and secondary airstreams. In cooling, there is no secondary airstream, so the mixed air temperature would be the same as the primary air temperature. With the mass and energy equations, we should have two equations and two unknowns that can be solved to give values for m_{pri} and t_{mix} as long as we know the amount of leakage, which is discussed in the next section on leakage. The solution can proceed for the contribution of the fan. There are multiple fan models that allow for direct calculation of fan power. These are described in a later section on estimating fan power. With the fan power calculated, Equation 12 or 13 can be solved for the temperature leaving the fan and entering the mixer, $t_{sec, out}$. The final step is to solve for the energy input of the heating coil in either Equation 10 or 11. All other variables in the equation have been calculated so the value of q_{coil} can be calculated.

Leakage

In modeling parallel FPTUs, both the direct and indirect effects of leakage on the performance of an FPTU should be considered. When supply air is provided by the central air handler to an FPTU, the cabinet operates at a higher pressure than the air surrounding the FPTU in the plenum. As a consequence, there is the potential for air to leak from the FPTU to the surrounding plenum space.

Both Furr et al. (2008) and Edmondson et al. (2011) measured leakage in parallel FPTUs. Furr et al. (2008) focused on units with PSC motors controlled by SCRs, and Edmondson et al. (2011) focused on FPTUs with ECM fan motors. They tested FPTUs over a range of downstream static pressures, upstream static pressures, and supply airflows. In all of their tests, the FPTU fan in the secondary airstream was off and only primary air was flowing through the FPTUs. The biggest determinant in leakage was downstream static pres-

ures, which ranged from 0.1 to 0.5 in. w.g. (24.9 to 124.5 Pa) in their tests. O'Neal and Edmondson (2016) reanalyzed the data of Edmondson et al. (2011) and presented leakage as a percentage (or fraction) of the primary airflow (see Figure 5).

$$f_{leak\ c} = \frac{m_{leak}}{m_{pri}} \quad (16)$$

The leakage fraction term has a *c* designation to indicate that this is a cooling leakage. As discussed later, the leakage in heating may be different than that for cooling. The FPTUs tested were divided into three leakage classifications: low, medium, and high. The percentage leakage was relatively flat for the high leakage case and slightly increased for the low and medium leakage cases.

The data in Figure 5 were collected under conditions when the FPTU fan was off, the back draft damper was closed, and only primary air was used in the FPTU. This condition simulated cooling operations for a parallel FPTU. Thus, these data are directly applicable to the cooling mode operation when simulating an FPTU. With the secondary airflow equal to zero, the cooling leakage fraction in Equation 16 can be substituted into the mass balance for the FPTU in Equation 14 to yield the following:

$$m_{tot} = m_{pri} - m_{leak} = m_{pri}(1 - f_{leak\ c}) \quad (17)$$

The total airflow m_{tot} is calculated from the cooling load on the zone. Equation 17 can be rearranged to provide an estimate of the amount of primary air needed when there is leakage:

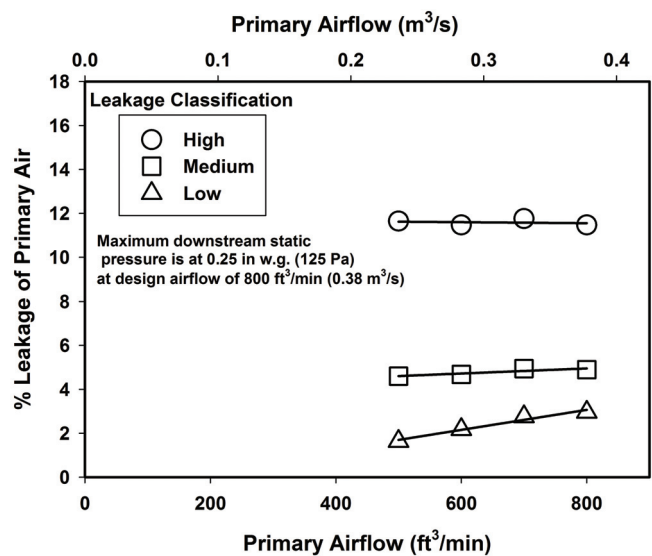


Figure 5 Percentage leakage as a function of primary airflow for three leakage classifications (O'Neal and Edmondson 2016).

$$m_{pri} = \frac{m_{tot}}{1 - f_{leak c}} \quad (18)$$

The above equation clearly shows that additional primary air is needed in cooling operations to provide the same amount of total airflow m_{tot} to the zone when there is leakage from the FPTU. This additional air has to be provided by the main air handler and means leakage creates a direct energy penalty on the air handler because it has to provide the additional air to the FPTU.

Besides the direct energy impact of leakage in cooling mode on the air handler, there are also indirect impacts. Leakage from the FPTU in cooling mode introduces cold primary air into the return airstream and will decrease the air temperature in the plenum. If the FPTU shares a common plenum with other FPTUs and some of those are in heating or deadband operations, then the colder plenum air will reduce the heating benefit from blending plenum (secondary) air with the primary air and will require additional heating when supplemental heating is used. Most of the return air is eventually mixed with outdoor air that is then sent to though the air handler and primary cooling coil. Because leakage during cooling operation reduces the return air temperature, it should reduce the temperature of the air that is returned to the primary cooling coil. This could reduce the load on the cooling coil. With the alternative FPTU configuration where the heating coil is located at the secondary inlet, leakage during heating operations would provide warm air to the plenum space. Quantifying the penalty or benefit of these indirect impacts of leakage requires a full air-conditioning system model that goes beyond the scope of this paper.

While Edmondson et al. (2011) identified three potential leakage paths (back draft damper, seams, and cabinet penetrations), they made no attempt to quantify the contributions from each of these sources. If the largest contributor for leakage is the back draft damper, then the data from either Edmondson et al. (2011) or Furr et al. (2008) would overestimate the leakage when the parallel FPTU is in the heating mode. Likewise, if building codes require taping all seams on the FPTU, then leakage from seams might be minimal. If the major leakage contributors in an FPTU are at the seams and/or penetrations, then the percentage (or fraction) leakage might remain relatively constant whether the FPTU is in the heating or cooling mode. Without definitive leakage data during heating operation, we are proposing use of a simple fraction (or percentage) $f_{leak h}$ to describe the leakage in a way similar to what was used for cooling.

$$f_{leak h} = \frac{m_{leak}}{m_{pri} + m_{sec}} \quad (19)$$

Equation 19 includes the primary and secondary airflows in the denominator because both flows are active during heating operations. This equation can be substituted back into the mass balance (Equation 14) for the mixing to yield the following:

$$m_{tot} = m_{pri} + m_{sec} - m_{leak} = (m_{pri} + m_{sec})(1 - f_{leak h}) \quad (20)$$

If the leakage is due to seams and penetrations, then the fraction of leakage for heating could be assumed to be the same as that used for cooling. However, if the leakage is due entirely to the back draft damper, then the fraction leakage in heating should be set to zero or have a smaller value than that for cooling.

Estimating Fan Power

Making an accurate estimate of the fan energy use in a parallel FPTU is still important even if the fan is only operating during heating operations. In cooler climates the fan will still be used significantly in some zones. Thus, the fan energy consumption needs to be captured in any model and needs to include the fan power and the temperature increase of the air across the fan/motor. The fan motor energy requires estimating the fan motor power POW_{fan} , either with measured data or a model. For a fixed-airflow fan, some building simulation programs (EnergyPlus 2013) have a simple fan power model that relates the power to the mass flow rate of the air through the fan m_{tot} , the pressure change across the fan ΔP_{fan} , the fan/motor combined efficiency η_{tot} , and the density of the air ρ_{air} .

$$POW_{fan} = \frac{m_{tot} \Delta P_{fan}}{\eta_{tot} \rho_{air}} = \frac{V_{tot} \Delta P_{fan}}{\eta_{tot}} \quad (21)$$

The quantity V_{tot} is the volumetric flow rate of the air, which is usually expressed in ft^3/min or m^3/s . This type of model requires knowledge of the pressure change across the fan and the fan/motor efficiency, which are two quantities often not known to the modeler. In addition, the analysis by O'Neal et al. (2015a, 2015b) and O'Neal (2015) of fan/motor performance data from several manufacturers demonstrated that these two variables cannot be treated independently for fans having either PSC motors with SCR controllers or ECM motors. In contrast, some building simulation programs, such as EnergyPlus (2013), allow the user to independently input these two variables. Alternative approaches to characterizing fan/motor performance were developed and depended on whether the FPTU had a PSC fan motor controlled by an SCR (O'Neal et al. 2015a) or had an ECM fan motor (O'Neal et al. 2015b; O'Neal 2015).

With a PSC fan motor controlled by an SCR, O'Neal et al. (2015a) analyzed data from three manufacturers covering a range of FPTU fan motor sizes from 1/8 to 1 hp (93 to 746 W). The fan efficiency was dependent on the total pressure across the fan. They fit the data with a simple linear model:

$$\eta_{tot} = C_1 \times \Delta P_{fan} \quad (22)$$

where, C_1 was 32.06%/(in. w.g.) in I-P units or 0.129%/Pa in SI units. Equation 22 can be rearranged to show that the efficiency divided by the pressure drop across the fan can be treated as a constant for a PSC motor with SCR control.

$$\frac{\eta_{tot}}{\Delta P_{fan}} = C_1 \quad (23)$$

Equation 23 can be substituted into Equation 21 and simplified to give an expression for the power solely in terms of air mass flow m_{tot} , the density of the air ρ_{air} , and C_1 :

$$POW_{fan} = \frac{m_{tot}}{C_1 \rho_{air}} = \frac{V_{tot}}{C_1} \quad (24)$$

The correct units for C_1 would need to be used in the above expression and were different in the I-P or SI system. If the power is desired in Watts, then Equation 24 can be rewritten with conversion constants to allow the user to input the volumetric flow and C_1 in ft³/min and %/(in. w.g.) in Equation 24 or in m³/s and %/Pa in Equation 26, respectively, to get the power in Watts.

In I-P Units, use the following:

$$POW_{fan} = \frac{11.75 \times V_{tot}}{C_1} \quad (25)$$

In SI Units, use the following:

$$POW_{fan} = \frac{100 \times V_{tot}}{C_1} \quad (26)$$

Another approach was also developed by O'Neal et al. (2015a) and that was to correlate airflow and power data. A simple linear best fit of the power versus airflow data provided the following:

$$POW_{fan} = C_2 \times V_{tot} \quad (27)$$

where C_2 was 0.372 W/(ft³/min) in I-P units and 788 W/(m³/s) in SI units. Equations 25 through 27 provide a straightforward way for a building simulation user to estimate the power used by a PSC fan motor controlled with an SCR in a parallel FPTU.

The simple approach for estimating power in Equation 21 is problematic when applied to an ECM fan/motor combination. The data for fan/motor total efficiency for an ECM fan motor is dependent on both total pressure and fan speed. Unless a modeler knows both the total pressure across the fan and the fan speed, it would be difficult to apply Equation 21 directly. For a fixed-airflow application with an ECM fan motor, O'Neal et al. (2015b) showed that the power was dependent on the amount of excess capacity the FPTU fan had relative to the design airflow requirements in the space. An ECM FPTU that was sized so that its maximum capacity just met the design airflow requirement in the space would use more power than one that had additional capacity but whose airflow was lowered so the airflow would just meet the design airflow requirements. Thus, the building simulation user should know something about the maximum airflow output of an ECM FPTU relative to the size of the design requirements in the space.

Calculation of the fan power for an ECM fan operating at a fixed airflow requires several steps. First, the design airflow requirement for the space must be determined. Usually, this is calculated or estimated by a building simulation or loads program. Second, the user must decide how large an FPTU fan will be used in the zone. The airflow capacity of the FPTU fan V_o , divided by the design airflow requirements in the zone V_d can be used to calculate the fraction of oversizing or excess capacity x_o :

$$x_o = \frac{Q_o}{Q_d} - 1 \quad (28)$$

The power requirement $POW_{fan}(V_d)$ for an ECM FPTU fan that has an excess capacity fraction x_o but operates at the design airflow V_d can be calculated from the following (O'Neal et al. 2015b):

$$POW_{fan}(V_d) = f_{pl} \times C_3 \times V_d \times (1 + x_o) \quad (29)$$

The first term on the right hand side is the part-load power fraction and is given by a third-degree polynomial fit of part-load data from four manufacturers (O'Neal et al. 2015b):

$$f_{pl} = a_1 + a_2 \left(\frac{1}{1+x_o} \right) + a_3 \left(\frac{1}{1+x_o} \right)^2 + a_4 \left(\frac{1}{1+x_o} \right)^3 \quad (30)$$

The coefficients in Equation 30 are given in Table 1.

The constant, C_3 , was 0.38 W/(ft³/min) in I-P units or 805 W/(m³/s) in SI units and was based on a simple linear regression of ECM FPTUs from four manufacturers operating at maximum airflow (O'Neal et al. 2015b). Equations 28 through 30 can be used to estimate the power of an ECM FPTU operating at a fixed airflow. The modeler needs to estimate the amount of excess capacity the FPTU has relative to the design airflow requirements of the space.

To illustrate the use of these equations, consider a zone with a design airflow requirement of 500 ft³/min (0.236 m³/s); the modeler needs to decide what size ECM FPTU to install in the zone. Table 2 illustrates the decreasing power requirements in FPTU fan energy calculated with Equations 28 through 30 as ECM FPTUs with capacities larger than the design airflow of 500 ft³/min (0.236 m³/s) design requirement are used. If a modeler uses a default size for the ECM FPTU that is equal to the design airflow requirement, then the fan

Table 1. Part-Load Power Fraction Coefficients for Equation 30 (O'Neal et al. 2015b)

Coefficients	Value
a_1	0.061715
a_2	0.093022
a_3	-0.11627
a_4	0.961538

power will be little different from the SCR unit used in the example above. The major savings come from ECM units when they have higher airflow capacity than the design requirement and their airflow is reduced so their airflow just meets the design requirement of the space.

SYSTEM LEVEL CALCULATION

For demonstration purposes, the performance of a parallel FPTU was estimated by using the mass and energy balance approach discussed earlier and the empirical curves for ECM fan/motor power consumption developed by O'Neal et al. (2015b). As a first step, a series of input data were created, including zone sensible loads, zone setpoint temperature, primary air temperature, secondary air temperature, and primary air leakage fraction. To show the operation in all modes of heating, cooling, and deadband, the zone sensible load was allowed to vary from $-40,000$ to $40,000$ Btu/h (-11.73 to 11.73 kW) by using an arbitrary incremental change of 479 Btu/h (0.14 kW), with negative values indicating heating loads and positive values indicating cooling loads. At each zone sensible load, a constant zone setpoint temperature of 78°F (25.6°C) was maintained with a primary air temperature of 55°F (12.8°C) and secondary air temperature of 78°F (25.6°C), both of which were assumed to be constant throughout the calculation. Also, a deadband sensible load ranging from -4000 to 4000 Btu/h was assumed and used to illustrate deadband operation with the parallel FPTU. In addition, four primary air leakage fractions of 0% , 2.5% , 5% , and 12% were used in the performance prediction of the parallel FPTU. While these percentages were applied to both cooling and heating operations, if the primary source of air leakage is through the back draft damper, then the heating leakage will be much smaller than the leakage for cooling operations. At each leakage level, the amount of supply air that was required to satisfy the zone load was determined. The performance impact of primary air leakage was evaluated by comparing the amount of supply air at different leakage levels. It should be noted that the above input parameters, namely zone sensible loads, zone setpoint temperature, primary air

temperature, secondary air temperature, and primary air leakage fraction, are user-defined parameters and can be modified for different applications and systems. For example, the secondary air temperature t_{sec} is defined based on the zone setpoint temperature t_z and a temperature differential, Δt , as shown in Equation 31.

$$t_{sec} = t_z + \Delta t \quad (31)$$

The value of Δt could be negative or positive. In cooling operation, leakage of cold air into the plenum should reduce the secondary air temperature for either the traditional or alternative parallel FPTU configuration. In that case, Δt would be negative. In heating mode for the alternative FPTU, leakage of warm conditioned air could make Δt a positive value. Ultimately, the overall air-conditioning system model in a building simulation program would have to be used to estimate Δt . We would anticipate that Δt might vary from a range of -4°F to 4°F (-2°C to 2°C).

Figure 6 shows the basic logic or flow of the calculation procedure for modeling the performance of a parallel FPTU. The calculation begins with reading the input data, then determines the operating mode based on the zone sensible load and control sequence. There are four different operating modes:

1. If the FPTU is off, all temperatures throughout the system are set at the zone setpoint temperature with no primary or secondary airflows.
2. If the zone sensible load is in the deadband range (assumed to vary from -4000 to 4000 Btu/h [-1.2 to 1.2 kW]), the FPTU is assumed to operate with the primary air set to its minimum value. For this paper, a minimum value of 20% was assumed with the secondary air making up the rest of the total airflow. The heating coil is turned off in deadband mode.
3. In heating mode, the primary and secondary air setting is the same as the operation in deadband mode except for the heating coil control. The heating coil is active in heating mode to provide supplemental heating to the zone.

Table 2. Effect of Excess Capacity on the Power Requirements for ECM FPTUs Operating at the Design Airflow

FPTU Maximum Capacity, ft^3/min (m^3/s)	Excess Capacity, x_o	Part-Load Power Fraction, f_{pl}	Fan Power, W
500 (0.236)	0.00	1.000	190.0
550 (0.260)	0.10	0.773	161.5
600 (0.283)	0.20	0.615	140.2
650 (0.306)	0.30	0.502	124.1
700 (0.331)	0.40	0.419	111.5
750 (0.354)	0.50	0.357	101.8

4. In cooling mode, the zone sensible load is satisfied by varying the amount of primary air that is delivered to the zone without providing secondary air. The amount of primary air is constrained between the minimum (assumed to be 20% of the design airflow) and the maximum (which is 100% of the design airflow). The FPTU fan is turned off as well as the heating coil.

A portion of the return air from the zone and plenum space is exhausted to the outdoors. The remaining air is mixed with outdoor air. The temperature of this mixture is used to determine whether or not preheating is required. If the temperature is below the primary air temperature, then the preheating coil is used to heat the mixed air to the primary air temperature. The power consumption of the primary fan is then calculated based on the primary airflow through the fan and the fan static (or total) pressure. The cooling energy required at the primary cooling coil is then calculated. The process then loops back to the start for the next time step until the simulation is completed.

Sample Results

The calculation procedure shown in Figure 6 was implemented in Engineering Equation Solver (EES) to perform the system scale calculation. Results of airflow, discharge temperature, and supplemental heating rate from a traditional FPTU were calculated and plotted against the zone sensible load as shown in Figures 7 to 9, respectively. The results for the alternative parallel FPTU configuration are the same as those for a traditional configuration except for the supplemental heating operations, which are shown in Figure 10.

Figure 7 shows the variation in primary and secondary airflows with changes in the zone sensible load for a traditional parallel FPTU at four leakage levels of 0%, 2.5%, 5%, and 12%. The zero leakage represents an ideal condition. The leakage levels of 2.5%, 5%, and 12% were based on the results reported by O'Neal and Edmondson (2016) and represented the scenarios with low, medium, and high leakages. The same leakage ratios were applied in heating, cooling, and deadband modes even though the measurements made by O'Neal and Edmondson (2016) were for conditions that simulated cooling operations of parallel FPTUs. Currently, there are no data available on leakage for heating operations when the FPTU fan is on. Thus, these figures show how leakage may affect heating operations should there be leakage during heating. More data are needed to confirm if leakages in heating operations are nearly as large as those in cooling.

In Figure 7, the primary airflow was set at a minimum of 20% of the total design airflow when operating in either heating or deadband modes with the secondary air making up the remainder of the total airflow rate. At the upper limit of the deadband, the FPTU fan was switched off, which resulted in the sharp decrease in the secondary airflow. In cooling mode, the FPTU fan remained off and no secondary air was provided. After the deadband region, the primary air maintained its mini-

um value at the low end of the cooling load range because the amount of cooling required by the zone was smaller than the cooling that could be provided at the minimum primary airflow. The primary airflow was constrained by its minimum (assumed to be 20% of design for this example) for ventilation purposes. In this case, the required amount of primary air for satisfying the zone load was lower than this minimum value. As the zone cooling load increased, the primary airflow increased proportionally until the total design airflow rate was reached at the maximum cooling load.

Figure 7 also shows that the impact of leakage differs in heating and cooling modes for the traditionally configured parallel FPTU. For example, the primary and secondary air remained the same regardless of leakage levels in heating mode. In contrast, the primary air supplied to the FPTU needed to be increased with increasing leakage rates in cooling mode to compensate for leakage airflow from the FPTU to meet the necessary cooling requirement of the zone. In heating mode, the FPTU fan provided a constant amount of secondary airflow and was independent of leakage. Likewise, in heating, the primary was set at a prescribed level and should not change with leakage. However, the heating provided to the zone was dependent on the amount of total airflow to the zone. With leakage, the total amount of airflow to the zone was smaller than it would be without leakage. Thus, even though leakage did not directly affect the primary and secondary airflows in heating mode, it did decrease the amount of air delivered to the zone. Consequently, with leakage, the discharge temperature from the FPTU reached its maximum temperature of 90°F (32.2°C) at smaller zone heating loads. Once this maximum temperature was reached, the maximum heating capacity of the FPTU was attained. As the heating requirements of the zone increased, the FPTU would be unable to meet the load.

Rather than maintaining airflow by varying discharge temperature in heating mode, the zone cooling load was satisfied by varying the primary airflow rate with a fixed temperature. In the ideal case of zero leakage, the primary airflow rate was equal to the amount of airflow that was required to match the zone cooling load. However, in scenarios with leakage, higher primary airflow rates were required at the same zone cooling load to compensate for the air loss due to leakage from the FPTU to the plenum space. For example, at the zone sensible load of 20,000 Btu/h, Figure 7 shows that the supply airflow rate was increased by 2.6% from 786 to 806 ft³/min (0.37 to 0.38 m³/s) relative to the no-leakage case as a result of introducing 2.5% primary leakage. The increases in supply airflow rate at the same zone sensible load were even greater at higher leakage levels of 5% and 12%, showing 5.3% and 13.6% increases, respectively, relative to the supply airflow rate without leakage.

Figure 8 shows the FPTU discharge air temperature with 55°F (12.8°C) primary air over a range of zone loads. At higher heating loads, the discharge temperature was limited at 90°F (32.2°C), because a higher discharge temperature could increase the zone temperature stratification (Hydeman and

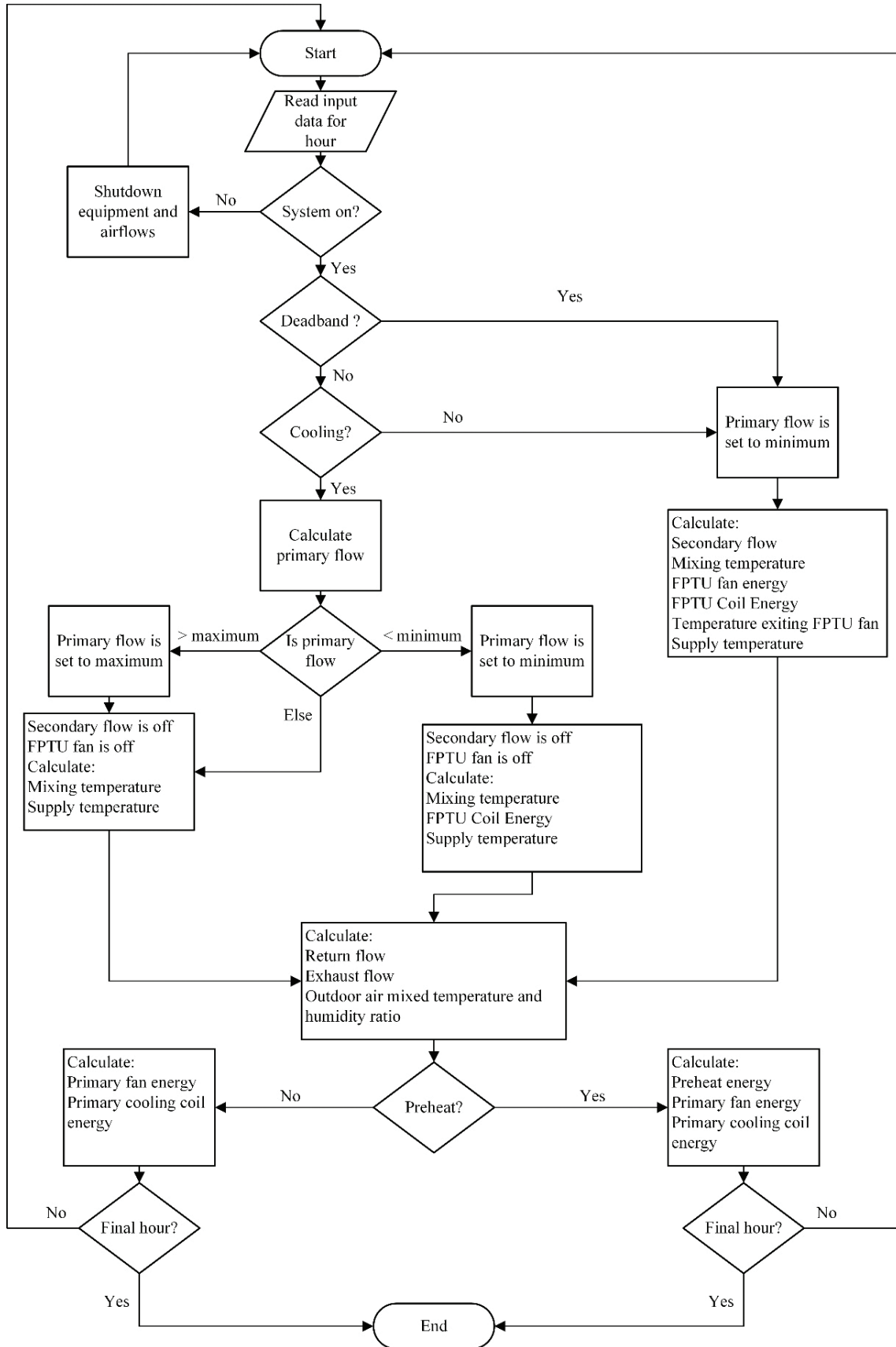


Figure 6 Parallel FPTU controller routine.

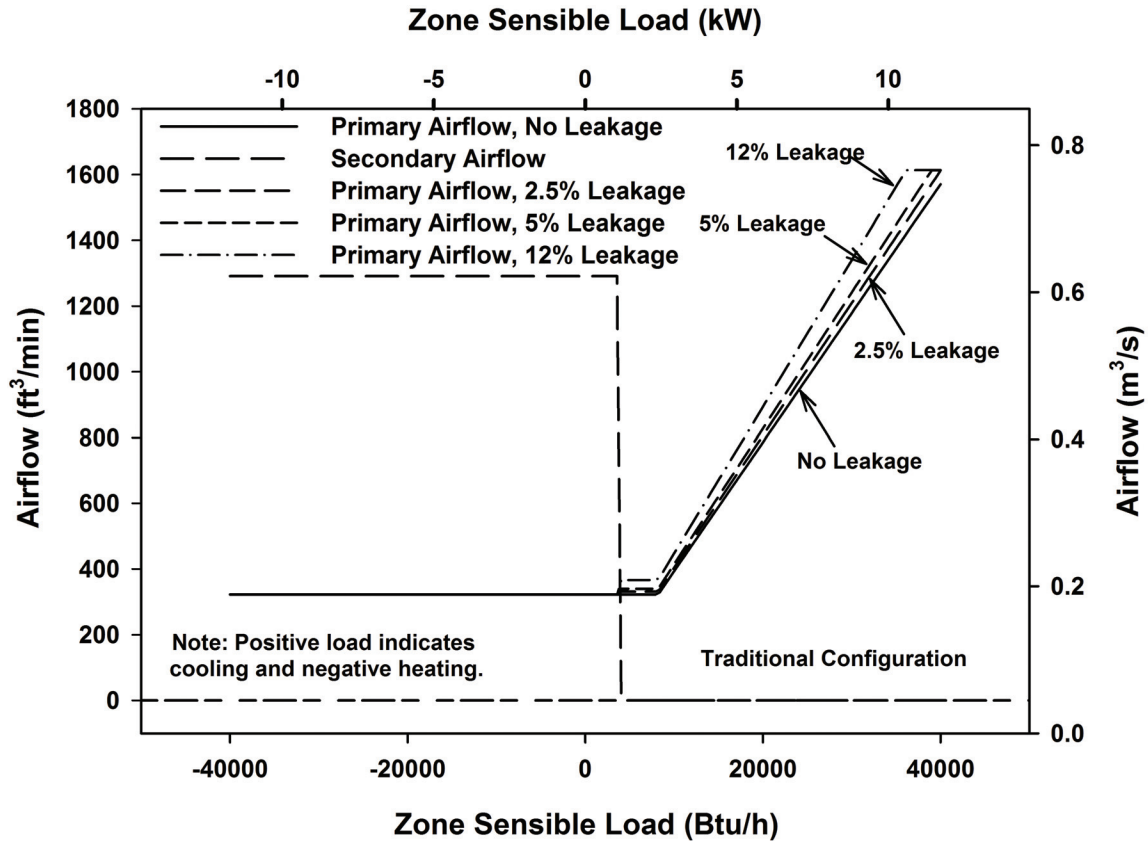


Figure 7 Primary and secondary airflows for a traditional parallel FPTU with different levels of leakage.

Eubanks 2014). As the heating load decreased, the discharge temperature was decreased proportionally. A sharp temperature drop occurred at the lower limit of the deadband due to switching off the heating coil. The discharge temperature was maintained at a constant of 74°F (23.3°C) in the deadband region. In cooling mode, the discharge temperature was the same as the primary air temperature given the fact that the FPTU fan was turned off, and, consequently, no secondary air was provided. In addition, the performance impact of leakage from the FPTU to the plenum space in heating mode was reflected in terms of discharge temperature, showing higher discharge temperatures at greater leakage levels for the same heating load. For example, Figure 8 shows that at the heating load of 10,000 Btu/h (2.93 kW), the discharge temperature increased by 0.8°F (0.4°C) from 83.6°F to 84.4°F (28.7°C to 29.1°C) as a result of increasing the leakage ratio from 0% to 12%. The increase in discharge temperature was the result of the lower total airflows to the space from increased leakage. With lower airflows, the discharge temperatures had to be elevated to meet the heating load in the zone.

Figure 9 shows the supplemental heating rate for a traditional FPTU as a function of the zone heating load. Leakage reduced the maximum supplemental heating provided by the FPTU at higher heating loads. This reduction occurred because there was reduced airflow through the heating coil.

With a reduced airflow, a fixed maximum discharge temperature of 90°F (32.2°C), and a fixed zone temperature, q_{coil} in Equation 10 had to decrease. At lower heating loads, the supplemental heating rate decreased proportionally with decreasing heating load until reaching the deadband region. At that point, the heating coil was turned off, and the supplemental heating rate became zero. The heating coil only operated in heating mode and remained off in the deadband and cooling modes. In addition to increasing the discharge temperature as shown in Figure 8, Figure 9 shows that the leakage in heating mode decreased the supplemental heating rate for the same zone load. For instance, at the zone heating load of 10,000 Btu/h (2.93 kW), a decrease of 5.1% in the supplemental heating rate from 17,375 to 16,490 Btu/h (5.09 to 4.83 kW) was observed as a result of increasing the leakage from 0% to 12%.

The decrease in supplemental heating rate became even greater and was in the same proportion as the air leakage when the zone was calling for maximum heating. For example, the maximum supplemental heating rate (or heating capacity) decreased by 717 Btu/h (0.21 kW) from 28,685 to 27,968 Btu/h (8.41 to 8.20 kW) with a 2.5% leakage rate. Greater decreases in the heating capacity occurred at higher leakage ratios. At 12% leakage, the reduction was 3442 Btu/h (1.01 kW) compared to the zero leakage case. At lower zone heating loads, the

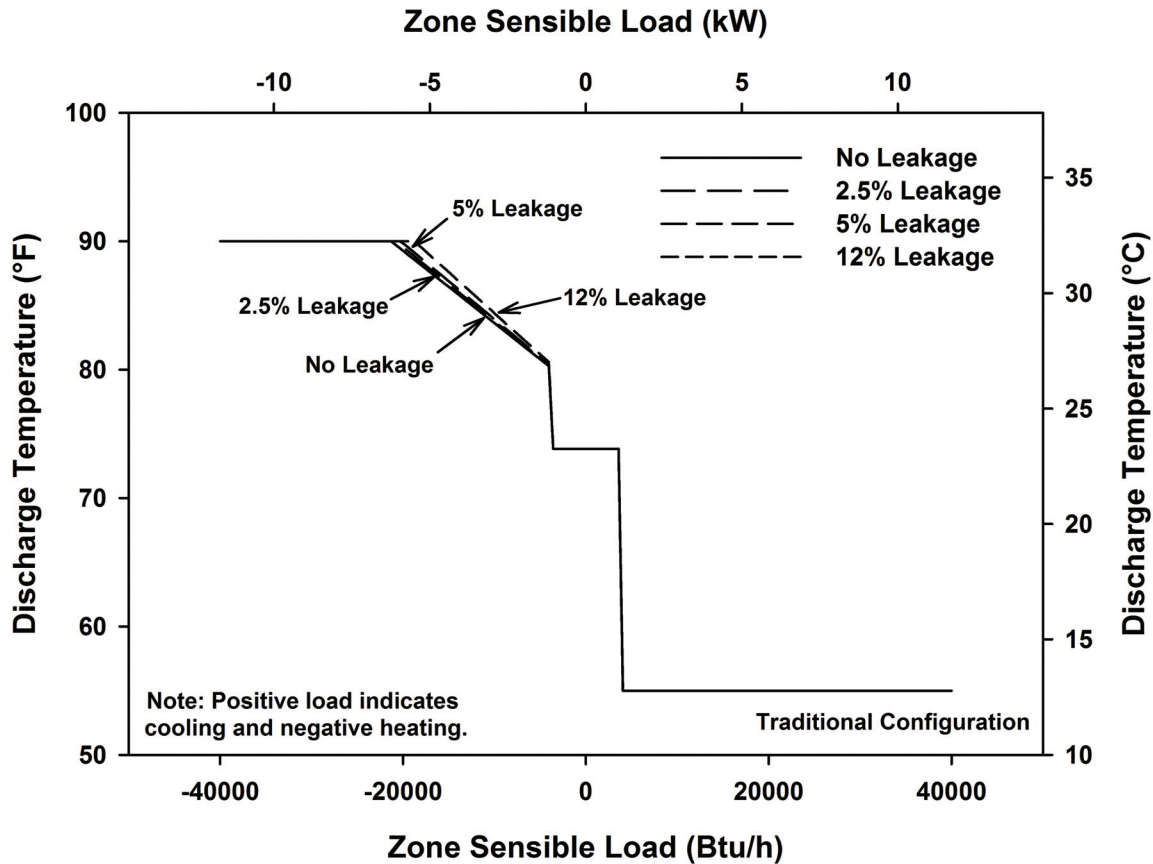


Figure 8 Discharge air temperature for a traditional parallel FPTU with different levels of leakage.

discharge temperature and supplemental heating varied proportionally with the zone heating load.

As discussed above, the impact of leakage on the cooling performance of the alternative configuration was the same as that for the traditional configuration. However, there was a difference in heating operations. Figure 10 shows the supplemental heating rate for a parallel FPTU with the alternate configuration where the heating coil was located at the secondary inlet (see Figure 3). Figure 10 indicates the leakage impact on the supplemental heating rate for an alternate FPTU was different from that for a traditional FPTU shown in Figure 9. Comparisons of the two figures shows that the maximum supplemental heating (or heating capacity) provided by the alternative configuration remained the same regardless of the leakage. Figure 10 shows the supplemental heating at the coil, which was different than the actual heating provided to the zone. For the zero leakage case, these two values would be same in Figure 10. However, with leakage, some of the heated air from the supplemental airstream leaks out of the FPTU and does not make it to the zone. Leakage decreased the maximum supplemental heating that was used by a traditionally configured FPTU. For the traditionally configured FPTU, the amount of supplemental heating would equal to the heating provided to the zone because leakage occurred upstream of the

heating coil. For the alternative configuration, increases in leakage increased the amount of supplemental heating, but the heating provided to the zone was less than the energy input to the heating coil because a portion of that conditioned air leaked from the FPTU into plenum. The differences in supplemental heating at the same heating load can be illustrated for the two configurations. At a zone heating load of 10,000 Btu/h (2.93 kW), the supplemental heating rate increased by 7.8% from 17,375 to 18,738 Btu/h (5.09 to 5.49 kW) as the leakage was increased from 0% to 12% for the alternative configuration. In contrast, for the same zone load and range in leakage levels, the supplemental heating rate for a traditional FPTU decreased 5.1%, as shown in Figure 9.

The difference in supplemental heating rate responding to various levels of leakage was caused by the different heating coil locations between the traditional and alternate FPTUs. For the traditional FPTU where the heating coil was located at the total airflow outlet, 100% of the energy input into the heating coil was used to satisfy the zone load because the leakage occurred before the air flowed through the heating coil. However, for the alternate FPTU where the heating coil was located at the secondary airflow, a portion of the energy input into the heating coil was lost to the plenum space because the leakage occurred downstream of the heating coil. Therefore,

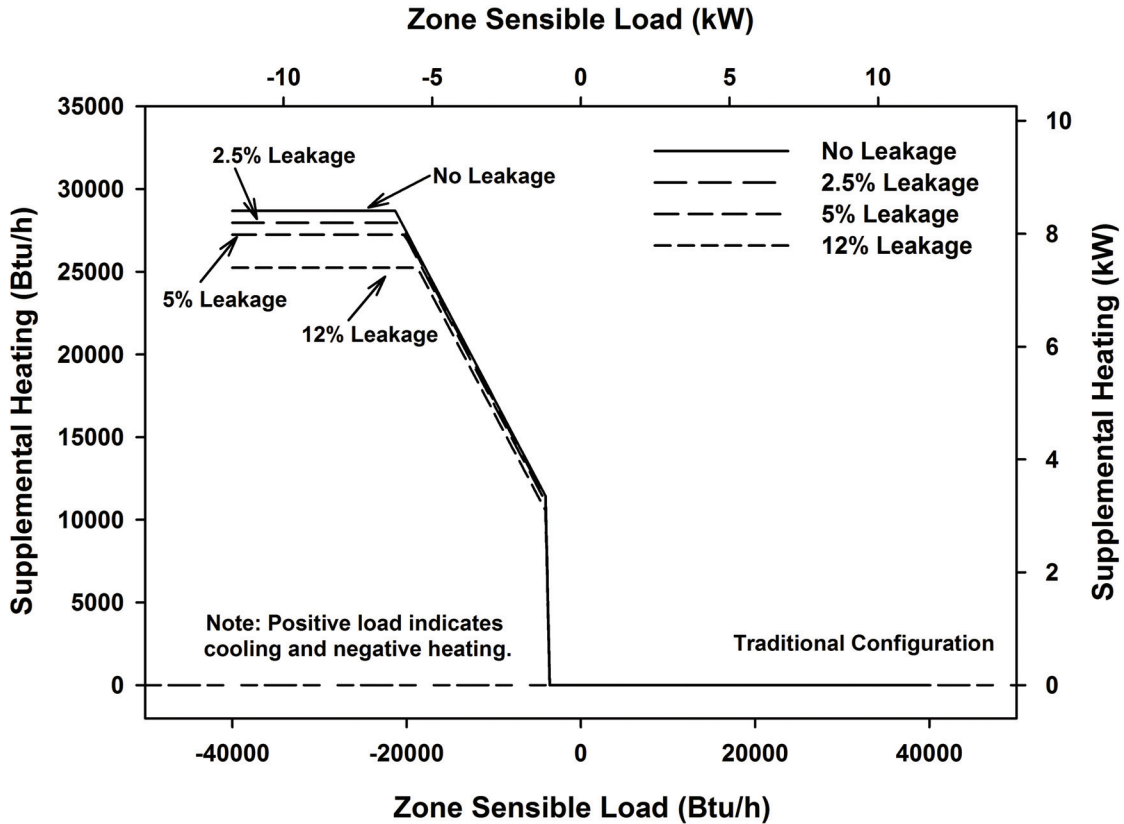


Figure 9 Supplemental heating energy for a traditional parallel FPTU with different levels of leakage.

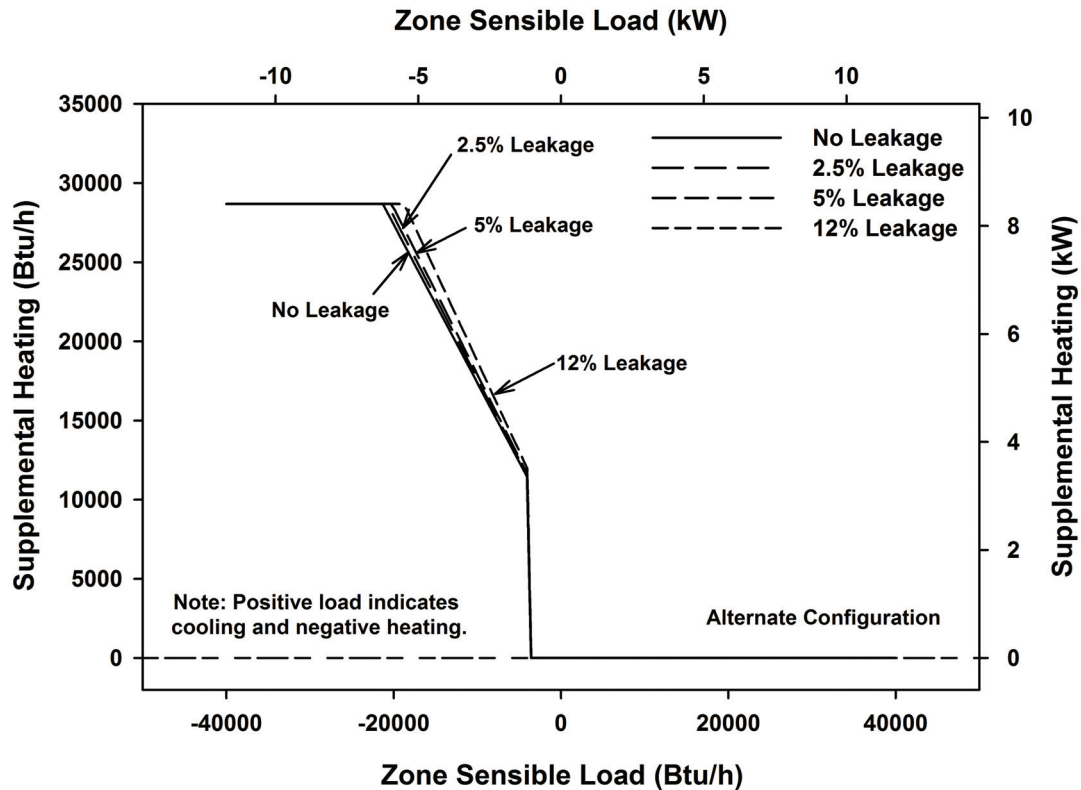


Figure 10 Supplemental heating energy for an alternate parallel FPTU with different levels of leakage.

greater energy was required to meet the zone heating load as the leakage was increased.

The logic for the FPTU performance calculations begins with sizing a parallel FPTU. The total volumetric flow rate from a parallel FPTU is estimated by using the zone design load q_{design} and the difference between the zone setpoint temperature t_z and the primary air temperature t_{pri} at the design condition. Based on the assumption of constant air density throughout the system in this study, the mass flow rate was used instead of volumetric flow rate, as shown in Equation 32:

$$m_{design} = \frac{q_{design}}{c_p(t_z - t_{pri})} \quad (32)$$

It should be noted that this design mass flow rate is the sum of primary and secondary airflow rates without considering the leakage airflow, as shown in Equation 33:

$$m_{design} = m_{pri} + m_{sec} \quad (33)$$

If desired, the volumetric flow rate (often in ft³/min or m³/s) can be determined from the air mass flow rate and density ρ_{air} :

$$m_{design} = \rho_{air} \cdot V_{design} \quad (34)$$

Once the design airflow rate is determined, it remains a constant throughout the calculation.

The FPTU performance calculations depend on which mode of operation it is in and whether FPTU is in the traditional or alternate configuration. There are four distinct modes of operation: off, heating, cooling, and deadband. The logic for each mode is described in the following list. The difference in calculations between traditional and alternate configurations is only in the heating mode because the heating coil remains off in both cooling and deadband mode.

1. System is off. For this mode the primary and secondary airflows, the FPTU fan, the heating coil, and the central air handler are not running, and temperatures throughout the system are set to the zone setpoint temperature.
2. System is in heating mode:

- a. Set the primary airflow to the minimum ventilation level:

$$m_{pri} = m_{min} \quad (35)$$

- b. Calculate the secondary airflow:

$$m_{sec} = m_{design} - m_{pri} \quad (36)$$

- c. As shown earlier in Equation 19, this study uses a fraction of primary and secondary airflow to quantify the leakage airflow. After both primary and secondary airflows being determined, the leakage airflow in heating mode can be calculated by rearranging Equation 19:

$$m_{leak} = (m_{pri} + m_{sec}) \cdot f_{leak h} \quad (37)$$

- d. Then, the actual amount of air delivered to the zone is the sum of primary and secondary airflow with the subtraction of leakage airflow:

$$m_{tot} = m_{pri} + m_{sec} - m_{leak} \quad (38)$$

- e. Calculate the outlet temperature that is required to meet the zone load by using the actual amount of air delivered to the zone. If the calculated temperature is greater than 90°F (32.2°C) then the system is at maximum heating. Set the outlet temperature to 90°F (32.2°C):

$$t_{out} = t_z - \frac{q_{zs}}{m_{tot}c_p} \quad (39)$$

The following calculation procedures vary with traditional and alternate configurations. For a parallel FPTU with traditional configuration do the following:

- f. Calculate the secondary air temperature at the FPTU fan outlet and the mixer inlet:

$$t_{sec, out} = \frac{POW_{fan}}{m_{sec}c_p} + t_{sec} \quad (40)$$

- g. Calculate the temperature of the mixed air:

$$t_{mix} = \frac{m_{pri}c_p t_{pri} + m_{sec}c_p t_{sec, out}}{m_{design}c_p} \quad (41)$$

- h. Calculate the heating energy input into the coil:

$$q_{coil} = m_{tot}c_p(t_{out} - t_{mix}) \quad (42)$$

For a parallel FPTU with alternate configuration do the following:

- f. Calculate the temperature of the mixed air:

$$t_{mix} = t_{out} \quad (43)$$

- g. Calculate the secondary air temperature at the FPTU fan outlet and the mixer inlet:

$$t_{sec, out} = \frac{m_{design}c_p t_{mix} - m_{pri}c_p t_{pri}}{m_{sec}c_p} \quad (44)$$

- h. Calculate the heating coil outlet temperature:

$$t_{coil} = t_{sec, out} - \frac{POW_{fan}}{m_{sec}c_p} \quad (45)$$

- i. Calculate the heating input from the coil:

$$q_{coil} = m_{sec}c_p(t_{coil} - t_{sec}) \quad (46)$$

3. System is in cooling mode.

- a. The heating coil is shut off:

$$q_{coil} = 0 \quad (47)$$

- b. Set the secondary air to zero:

$$m_{sec} = 0 \quad (48)$$

- c. Calculate the actual amount of primary air that is delivered to the zone to match the zone load:

$$m_{tot} = \frac{q_{zs}}{c_p \cdot (t_z - t_{pri})} \quad (49)$$

- d. Due to the leakage effect, the amount of primary air delivered to the parallel FPTU should be higher than the amount of primary air required for satisfying the zone load, as shown previously in Equation 18. Therefore, the amount of primary air that is required to compensate for the leakage effect can be calculated from rearranging Equation 18:

$$m_{pri} = m_{tot} / (1 - f_{leakc}) \quad (50)$$

It is important to recognize that the calculated primary airflow m_{pri} is constrained between the minimum, which typically ranges from 10% to 30% of the design total airflow and is assumed to be 20% in this study, and the maximum, which is 100% of the design total airflow. If the calculation of primary airflow results in a value smaller than the minimum or larger than the maximum, the logic resets the primary airflow to the minimum or maximum accordingly.

4. System is in deadband mode. In the deadband mode, the logic for the performance calculation is similar to the operation in heating mode except for the heating coil being switched off. Unlike the operations in heating and cooling modes where the purpose of the FPTU was to satisfy the zone load, the discharge temperature in deadband is not controlled and is a direct result of mixing the minimum primary air and maximum secondary air. In a simulation program, the deadband is often specified by the user. Thus, no method of calculating the range of the deadband is provided here.

SUMMARY AND CONCLUSIONS

This paper has provided the basic equations needed to characterize the performance of a fixed-airflow parallel fan-powered terminal unit using a mass and energy balance approach. Because heating coils can be located either at the discharge of the FPTU (traditional configuration) or at the inlet of the secondary air stream (alternative configuration), both locations were included in the modeling. In addition, a simple method of including leakage was included in the modeling. The overall approach follows closely that used in EnergyPlus (2013) for parallel FPTUs. A step-by-step process

on how the basic equations should be used for each FPTU mode of operation was also provided.

The impact of leakage on two parallel configurations was included for both cooling and heating operations. All available data on leakage in parallel FPTUs was based on cooling operations when the FPTU fan is off and the back draft damper is closed. If the primary source of leakage in parallel FPTUs is through the back draft damper, then leakage in heating mode will be significantly less than in cooling mode. Data needs to be developed for leakage in heating mode for parallel FPTUs. The methodology used in this paper could then be used with the new data to better estimate parallel FPTU heating performance with leakage.

The current model for parallel FPTUs in EnergyPlus bases fan power calculations on fan pressure and efficiency inputs typically not provided by the manufacturers of these units and does not include leakage from the FPTU cabinet. A simplified approach was used to allow estimation of fan power based on correlations developed in earlier studies for constant airflow fans (O'Neal et al. 2015a and 2015b). The constant airflow fans included both PSC motors controlled by SCRs and ECM motors.

The methodology developed in this paper can be implemented into building simulation models that use a mass and energy balance approach. Given the exclusion of leakage from the FPTU cabinet, there is a bias in favor of parallel FPTUs. It is vital that future versions of building simulations models include leakage in parallel FPTUs to allow energy professionals an opportunity to accurately characterize the energy use of FPTU technologies that are installed in buildings.

ACKNOWLEDGMENT

We wish to thank the Air-Conditioning, Heating, and Refrigeration Institute (AHRI) for their support of this project. In particular, we wish to thank all the members of the Air Control and Distribution Devices Committee for their input and advice.

REFERENCES

- ASHRAE. 2001. ASHRAE Standard 62-2001, *Ventilation for Acceptable Indoor Air Quality*. Atlanta: ASHRAE.
- ASHRAE. 2012. Chapter 20, Room air distribution equipment, *ASHRAE Handbook—HVAC Systems and Equipment*. Atlanta: ASHRAE.
- ASHRAE. 2013. ANSI/ASHRAE/IES Standard 90.1, *Energy Standards for Buildings Except Low-Rise Residential Building*. Atlanta: ASHRAE.
- CBSC. 2010. *California Energy Code, California Code of Regulations, Title 24, Part 6*. Sacramento: California Building Standards Commission.
- Davis, M., J. Bryant, and D.L. O'Neal. 2012. Modeling the performance of ECM and SCR parallel fan-powered terminal units in single-duct VAV systems. *ASHRAE Transactions* 118(1).
- Edmondson, J., D.L. O'Neal, J.A. Bryant, and M.A. Davis. 2011. Performance of parallel fan powered terminal

- units with electronically commutated motors. *ASHRAE Transactions* 117(2).
- EnergyPlus. 2013. Air system distribution terminals. In *EnergyPlus energy simulation software—EnergyPlus documentation—Engineering reference*. Berkeley: Lawrence Berkeley National Laboratory.
- Furr, J., D. O’Neal, M.A. Davis, J.A. Bryant, and A. Cramlet. 2008. Performance of VAV parallel fan powered terminal units: Experimental results and models. *ASHRAE Transactions* 114(1).
- Hydeman, M. and B. Eubanks. 2014. *Advanced control sequences for HVAC systems—Phase I air distribution and terminal systems*. ASHRAE Research Project Report 1455-RP. Atlanta: ASHRAE.
- Int-Hout, D. 2015. ECM motors in fan powered terminal units. www.krueger-hvac.com/files/white%20papers/white_paper_ecm.pdf.
- Knebel, D. E. 1983. *Simplified energy analysis using the modified bin method*. Atlanta: ASHRAE.
- O’Neal, D.L., D. Ingram, and C.L. Reid. 2015a. Modeling fan-power terminal unit fan/motor combinations controlled by silicon-controlled rectifiers. *ASHRAE Transactions* 121(2).
- O’Neal, D.L., D. Ingram, and C.L. Reid. 2015b. Simplified model of the fan/motor performance of fan powered terminal units that utilize electronically commutated motors. *ASHRAE Transactions* 121(2).
- O’Neal, D.L. 2015. Development of models to simulate the part-load performance of oversized ECM fan-powered terminal units. *ASHRAE Transactions* 121(2).
- O’Neal, D.L., and J.L. Edmondson. 2016. Characterizing air leakage in parallel fan-powered terminal units. *ASHRAE Transactions* 122(1).
- Roman, A., and A. Heiligenstein. 2002. *SCR power theory training manual*. Chromalox® Inc. PK501-1. LaVergne, TN: Chromalox Inc.
- Zhang, H., T. Hoyt, S., Kaam, J. Goins, F. Bauman, Y. Zhai, T. Webster, B. West, G. Paliaga, J. Stein, R. Seidl, J. Tullym B. Rimmer, and J. Torftum. 2014. *Thermal and air quality acceptability in buildings that reduce energy by reducing minimum airflow from overhead diffusers*. ASHRAE Research Project Report 1515-RP. Atlanta: ASHRAE.



© 2014, 2015, 2016 ASHRAE
1791 Tullie Circle, NE
Atlanta, GA 30329
www.ashrae.org

Product Code: D-MECP16